UNIVERSITÉ DE STRASBOURG

ÉCOLE DOCTORALE ED 222 Sciences Chimiques

UMR 7042 LIMA CNRS – Université de Strasbourg

THÈSE présentée par :

Baptiste DUPOUY

soutenue le : **5 Novembre 2024**

pour obtenir le grade de : **Docteur de l'université de Strasbourg**

Discipline/ Spécialité : Chimie – Chimie Organique/Médicinale

Optimisation de dérivés 3-benzylménadiones antiparasitaires rédox-actifs et conception de sondes moléculaires cliquables et/ou photoréactives

THÈSE dirigée par :

Dr. DAVIOUD-CHARVET Elisabeth	Directrice de recherche CNRS, Université de Strasbourg
Dr. ELHABIRI Mourad	Directeur de recherche CNRS, Université de Strasbourg

RAPPORTEURS :

Dr. AUDISIO Davide	Responsable de laboratoire, Commissariat à l'énergie atomique, Paris-Saclay
Dr. ANDRAUD Chantal	Directrice de recherche CNRS Emérite, Ecole normal supérieur de Lyon

---

AUTRES MEMBRES DU JURY :

Dr. SPECHT Alexandre	Directeur de recherche CNRS, Université de Strasbourg
Dr. PEYROTTES Suzanne	Directrice de recherche CNRS, Université de Montpellier

Remerciements

Je tiens à remercier les membres de mon jury pour avoir accepté d'évaluer mon travail et de participer à ma soutenance de thèse : Dr. Chantal Andraud, Dr. Suzanne Peyrottes, Dr. Davide Audisio et Dr. Alexandre Specht. Je remercie également mes deux encadrants de thèse, le Dr. Elisabeth Davioud-Charvet (directrice de thèse) et le Dr. Mourad Elhabiri (co-directeur de thèse).

Elisabeth, merci de m'avoir fait confiance et d'avoir cru en moi dès le début des candidatures ParaFrap. J'ai eu la chance d'apprendre énormément à tes cotés pendant ces 3 années. J'ai pu découvrir de nouvelles thématiques et affirmer mon raisonnement scientifique pluridisciplinaire. Tu m'as accordé beaucoup d'autonomie dans ce projet, ce qui, avec tes conseils et ton expertise, a permis de grandement enrichir et diversifier mon travail.

Mourad, je te remercie de m'avoir fait découvrir la chimie des fluorophores et de m'avoir fait partager tes connaissances en photo/physicochimie. J'ai beaucoup apprécié de travailler avec toi sur le projet flavylium. J'admire ta positivité et ton expertise dans ces domaines, qui m'ont vraiment motivé. Enfin, merci à tous les deux de m'avoir soutenu tout au long de la thèse, de m'avoir encouragé à rester positif dans les moments difficiles et d'avoir contribué à la valorisation de mes résultats.

Je tiens également à remercier tous les membres de notre équipe, actuels et anciens. J'ai rencontré des personnes formidables qui m'ont aidé tout au long de cette aventure et avec qui j'ai partagé de très bons moments, tant sur le plan professionnel que personnel.

Je commence par Nathan, avec qui j'ai passé plus de la moitié de ma thèse. On a bien rigolé pendant ces années-là avec Matthieu et Lucie. Puis, sont arrivés Jimmy et Jérémy. J'ai beaucoup aimé travailler avec vous, entre notre cohésion, nos rigolades, nos gouters/barbecues. On a partagé plusieurs colloques et séminaires, j'en garde de très bons souvenirs ! Valérie, merci pour ton aide sur la partie physicochimie et pour m'avoir guidé dans l'utilisation des instruments de mesure. Ilaria et Victoria, nos deux biologistes, merci pour votre excellent travail. Antoine, je te souhaite beaucoup de succès dans ton projet de thèse.
L'ECPM m'a beaucoup apporté pendant cette thèse. J'ai eu la chance d'y encadrer des TP de chimie et plusieurs stagiaires sur différents projets. J'ai beaucoup apprécié l'enseignement et j'en garde d'excellents souvenirs. Merci au Dr. Barbara Ernst, Dr. Damien Hazelard et Dr. Sabine Chopin pour votre encadrement. Un grand merci à Alexandre Desthèves pour ton aide précieuse sur de nombreux aspects pratiques, tu m'as fait gagner un temps précieux.

Je voudrais remercier les membres du LIMA, tout particulièrement Mathieu Chessé et le Dr. Emeric Wasielewski pour votre aide et expertise dans vos domaines respectifs. Merci aux membres du secrétariat, à la direction, et à Didier pour ton aide sur tous les problèmes techniques et ta bonne humeur.

Merci à tous les stagiaires que j'ai eu la chance d'encadrer, de près ou de loin : Manon Aniel (M1), Juline Barcet (ECPM 2A), Quentin Rielh (M1) et Guillaume Deeford (ECPM 2A). Un grand merci à ParaFrap d'avoir financé cette thèse et de m'avoir permis de participer à de nombreux workshops et colloques enrichissants. Grâce à ParaFrap, j'ai rencontré des doctorants formidables avec qui j'ai partagé de bons moments, des galères, et j'ai énormément appris à travers les différents séminaires, formations et colloques.

Enfin, je tiens à remercier ma famille, ma compagne et mes amis. Sans leur soutien, nous ne sommes pas grand-chose. Une bonne partie de ce travail et de mon évolution leur est due.

UNIVERSITE DE STRASBOURG

ECOLE DOCTORALE DES SCIENCES CHIMIQUES

RESUME DE LA THESE DE DOCTORAT

Discipline : Chimie organique

Spécialité (facultative) : Chimie - organique et médicinale

Présentée par : Dupouy Baptiste

Titre : Optimisation de dérivés 3-benzylmenadiones antiparasitaires rédox-actifs et conception de sondes moléculaires cliquables et/ou photoréactives

Unité de Recherche : UMR 7042 Laboratoire d'Innovation Moléculaire et Applications

Directeur de Thèse : Davioud-Charvet Elisabeth – DRCE

Co-Directeur de Thèse (s'il y a lieu) : Elhabiri Mourad – DR1

Localisation : 25 rue Becquerel 67087 Strasbourg Cedex 2

Thèse confidentielle : ☒ NON ☐ OUI

1) Introduction

L'approche novatrice de mon équipe d'accueil consiste à développer des candidats-médicaments antiparasitaires capables d'augmenter le stress oxydant à l'intérieur du parasite. L'équipe a ainsi découvert la série 3-benzylménadione (bMD) aux propriétés anti-paludiques puissantes sur diverses souches du parasite *Plasmodium falciparum (P. falciparum ou Pf)*, responsable du paludisme. La molécule tête de série, la plasmodione, exerce une activité anti-paludique importante sur les stades asexués (anneaux) et sexués jeunes du *Pf*. La poursuite du développement de cette tête de série nécessite désormais d'identifier ses cibles biologiques au sein du globule rouge parasité afin de mieux comprendre les modes d'interactions avec ses protéines-cibles et ainsi poursuivre l'optimisation de ce candidat-médicament. Outre les nombreuses approches déjà menées au sein de mon équipe d'accueil, mon travail de thèse a reposé sur 2 objectifs principaux.

Le premier a consisté à développer des sondes chimiques originales basées sur le châssis moléculaire bMD, capables de réagir par chimie bioorthogonale avec un outil moléculaire (fluorophore, biotine), afin d'obtenir des informations précises sur le site d'action de la bMD au sein du parasite[1]. Ces informations cruciales permettront de développer nos connaissances sur cette série de composés afin de faire évoluer cette recherche en corrélation avec les cibles biologiques identifiées. Deux stratégies distinctes ont été choisies pour répondre à cette problématique. La première, déjà utilisée au sein de l'équipe, permet de « pêcher » les cibles biologiques fonctionnalisées à la sonde bMD, afin d'identifier les adduits créés, connu sous le nom de AfBPP (*Affinity-Based Protein Profiling*). La seconde, couramment utilisée en biologie, permet de visualiser par microcopie de fluorescence le site d'action d'une molécule bMD grâce à une sonde fluorescente liée à celle-ci. Pour mener à bien ces deux stratégies, nous avons développé plusieurs outils moléculaires : 1) des dérivés de plasmodione cliquables (en version alcyne et azoture) (**Figure 1**), 2) des sondes fluorescentes bioinspirés de la famille des ions flavyliums, fonctionnalisées par une fonction azoture ou cyclooctyne, disposant d'une réponse fluorogénique en réponse à une réaction de cycloaddition avec les sondes bMDs (**Figure 1**).

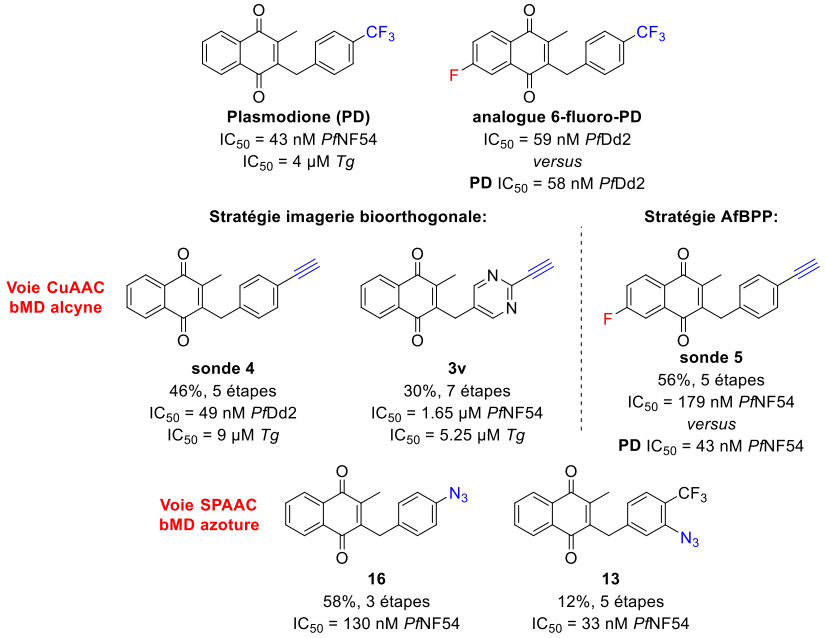

Figure 1: Sondes cliquables bMDs alcyne/azoture utilisables pour obtenir des informations clés sur les cibles biologiques des bMDs en imagerie par fluorescence et en utilisant la stratégie de photomarquage par affinité pour l'analyse protéomique (AfBPP). La synthèse de la sonde **4**, **5** et de la **6-fluoro-PD** sont décrites dans mon article publié dans *Chembiochem* 2024, e202400187. https://doi.org/10.1002/cbic.202400187. La synthèse de **3v**, **16** et

13 sont décrits dans dans l'article publié dans *ACS Infec. Dis*. 2024, accepted. https://doi.org/10.1021/acsinfecdis.4c00304.

Au cours de ce projet, nous avons utilisé deux types de réaction bioorthogonale, la CuAAC[2] (*Copper-catalyzed Azide-Alkyne Cyclo-addition*) et la SPAAC[3] (*Strain-Promoted Azide-Alkyne Cyclo-addition*). Mes objectifs ont ainsi été concentrés sur la synthèse des différentes sondes envisagées : 1) bMD-alcyne et flavylium-azoture (CuAAC) et 2) bMD-azoture et flavylium-cyclooctyne (SPAAC). L'étude approfondie de ces systèmes a permis la mise en place de stratégies ciblées en collaboration avec plusieurs équipes de biologistes pour valoriser ces nouveaux outils moléculaires et répondre à la principale problématique.
Le second objectif a consisté à poursuivre le développement des bMDs afin d'améliorer leurs propriétés pharmacocinétiques (PK) par variation de plusieurs propriétés physicochimiques-clés (PC) et optimiser leur activité antiparasitaire. En particulier, nous avons amélioré la solubilité aqueuse de nos composés bMD par l'introduction d'un motif hétéroaromatique azoté, ce qui permet également de les rendre moins lipophiles. Pour mener à bien cet objectif, il a été essentiel de disposer d'une large bibliothèque diversifiée de bMDs et d'évaluer leurs propriétés PC et ainsi converger vers des composés optimisés. Cette approche déjà initiée au sein de l'équipe avait permis de démontrer l'importance de certains groupements essentiels à l'activité antiparasitaire dans un modèle murin infecté par *P. berghei* après administration par voie orale. Notre approche a par ailleurs été fructueuse grâce au développement de plusieurs voies d'accès originales aux bMDs[4-8] et à leurs métabolites[9-12]. Pendant cette thèse, plusieurs séries de bMDs portant un motif *N*-hétéroaromatique ont été préparées (séries pyridine, pyrimidine et triazole), ainsi que l'introduction d'un méthyle angulaire au sein de la quinone, métabolisable afin d'apporter un nouveau mécanisme pro-drogue. L'étude de ces composés et de leurs activités antiparasitaires a permis d'établir de nouvelles stratégies de synthèse ainsi que des relations structures-activités (RSA) cohérentes.

2) Résultats et discussions

Comme indiqué précédemment, ce travail de thèse a eu pour premier objectif d'obtenir des informations sur les potentielles cibles biologiques des bMDs. La première stratégie (AfBPP) est basée sur la formation d'une liaison covalente entre la sonde bMD et une protéine environnante suivie de son extraction par un procédé d'enrichissement des adduits (*pull-down*). Dans notre cas, nous avons tiré profit de la présence d'une structure de type benzophénone présente au sein de la bMD réduite comme fonction photoréactive pour effectuer le marquage covalent sous UV. Une biotine azoturée est ensuite utilisée pour extraire l'adduit formé par réaction CuAAC avec la fonction alcyne présente au sein des bMDs. Une précédente étude AfBPP utilisant une première série de bMD-alcyne (**sonde 4**) avait déjà été mise en place au sein de mon équipe d'accueil.[10] Cette approche avait permis de valider cette stratégie à partir de protéines-modèles recombinantes pures: les glutathion réductases humaine et de *Pf*, deux protéines, purifiées au laboratoire, considérées comme cibles biologiques putatives des bMDs. Grâce aux travaux du Dr. Ilaria Iacobucci, postdoc et Victoria Monaco, doctorante au sein de notre équipe, nous avons pu approfondir cette première approche AfBPP en considérant des systèmes plus complexes, les protéomes de levure et du parasite *Pf*, permettant d'identifier 11 et 44 cibles potentielles chez la levure et *Pf*, respectivement. Ce projet a débuté avec la première sonde bMD-alcyne publiée (**sonde 4**, **Figure 3**), dont la synthèse a été optimisée dans le cadre de mon travail de thèse, par augmentation de son rendement global. Néanmoins, la cinétique et le rendement de photoalkylation étaient jugés trop faibles, ne permettant pas la détection des adduits produits en trop faible rendement lors de l'étape d'irradiation. J'ai donc synthétisé une sonde photoréactive optimisée plus oxydante afin d'améliorer la cinétique de photoréduction et par conséquent le rendement de photoalkylation. Cette nouvelle sonde bMD-alcyne comporte un atome de fluor en position C-6 (**sonde 5**), l'effet électroattracteur de cet élément permettant de rendre la fonction carbonyle plus réactive lors de la photoalkylation, augmentant son rendement de réaction et rendant cette stratégie plus effective (**Figure 1**).

La deuxième stratégie reposant sur la localisation de nos bMDs par imagerie de fluorescence a pu être ensuite mise en place. Un premier criblage des analogues hétéroaromatiques de la plasmodione sur deux parasites de l'ordre des Apicomplexes, *Pf* et *Toxoplasma gondii (T. gondii* ou *Tg)*, avaient permis d'identifier quelques dérivés pyrimidines actifs sur *Tg*. Nous avons débuté par la préparation d'une nouvelle sonde bMD-alcyne contenant un motif pyrimidine (**3v**, **Figure 3**). Cette dernière devait permettre d'augmenter la solubilité aqueuse afin d'obtenir des résultats d'imagerie plus pertinents[13]. Malheureusement, ce composé s'est avéré inactif contre *Pf* rendant son utilisation non pertinente avec ce parasite. Plus actif sur *Tg*, nous avons réalisé une étude d'imagerie cellulaire sur celui-ci, révélant une localisation au sein de l'apicoplaste par immunofluorescence grâce à un marqueur biologique spécifique. La même étude menée sur une sonde bMD-alcyne non-hétéroaromatique (**sonde 4**) dans le parasite *Pf* a révélé des résultats comparables, confirmant cette cible biologique et l'activité antiparasitaire. Les parasites apicomplexes *Pf* et *Tg* sont en effet considérés comme voisins disposant tous deux d'une organelle – l'apicoplaste – essentielle à leur viabilité. Cette organelle étant désignée comme un compartiment-cible potentiel de nos bMDs, nous avons alors décidé de réaliser une étude complémentaire d'imagerie cellulaire en utilisant les bMD-alcynes dans les parasites *Pf* et *Tg*. La **sonde 5** précédemment utilisée dans la stratégie AfBPP a permis de démontrer son internalisation au sein du parasite *Pf* justifiant son activité antiparasitaire. En tenant compte de ces premiers résultats encourageants, nous pouvons désormais envisager de nouvelles cibles biologiques et ainsi corréler leurs activités sur les parasites *Pf* et *Tg* (**Figure 1**).

En parallèle à cette première approche, nous avons proposé une alternative en termes de prix, d'accès et de modifications chimiques aux fluorophores organiques commerciaux tels que par exemple la rhodamine azoture utilisée dans le cadre de l'étude d'imagerie cellulaire décrite précédemment. Des fluorophores azoturés originaux dérivés d'ions flavyliums rigidifiés[14] et utilisables en chimie bioorthogonale[15] ont donc été préparés. Ces nouveaux fluorophores possèdent plusieurs avantages comme une voie d'accès en un minimum d'étapes simples, une bonne solubilité aqueuse, des possibilités de (post)fonctionnalisation et de modulation de leurs propriétés d'émission ainsi que des propriétés photophysiques intéressantes (forte brillance, photostabilité, émission dans le proche infrarouge PIR). Suite à des résultats peu satisfaisants pour des fonctions azotures directement substituées sur le système conjugué, nous avons décidé d'introduire un espaceur PEG afin de séparer le fluorophore de la fonction réactive azoturée. Au moyen d'une approche originale de « criblage/sélection » réalisée au moyen d'un lecteur de plaque hybride absorption-émission, le meilleur candidat en termes de propriétés optiques a été identifié. Sa synthèse a été réalisée et les mesures photophysiques ont démontré une émission dans le rouge-PIR, un rendement quantique absolu de près de 30 % et une brillance très satisfaisante dans un milieu tamponné aqueux contenant un électrolyte support (0,1 M NaCl) rendant son utilisation en imagerie cellulaire parfaitement pertinente (**F2**, **Figure 2**). De manière intéressante, lorsque ce dernier est engagé dans une réaction CuAAC avec une sonde bMD-alcyne, une inhibition de fluorescence significative a été observée (13 fois moins émissif) due à un transfert d'électron photoinduit (PeT) entre l'ion flavylium (donneur d'électron) et l'unité bMD (accepteur d'électron). Cette inhibition de fluorescence est intimement liée à l'activité rédox de l'électrophore bMD puisque lorsque ce dernier est réduit (par photoréduction ou en présence de bioréducteurs tels que le glutathion GSH ou la cystéine), l'émission de fluorescence de l'adduit est restaurée rendant ce système fluorogénique et dépendant de l'état rédox de l'unité bMD. Dans nos systèmes, nous disposons donc d'un transfert PeT intramoléculaire justifiant l'importance de la distance entre l'accepteur et le donneur. Sur ce principe, nous avons donc modifié la longueur de l'espaceur avec une chaine plus longue pour diminuer le processus PeT et plus courte pour l'augmenter accentuant davantage la fluorogénicité de la sonde correspondante. Ces modifications ont permis l'étude photophysique et électrochimique de ces trois systèmes distincts (sonde courte **F1** avec PEG-1, sonde normale **F2** avec PEG-2, sonde allongée **F3** avec PEG-3) afin de comparer l'émission des adduits flavylium-bMD suivant l'état rédox du squelette bMD (**Figure 2**). Comme l'activité antiparasitaire des bMDs est basée sur ses propriétés rédox, l'utilisation de ce système fluorogénique pourra être pertinente en imagerie ou pour la mesure de l'état

rédox d'un milieu ou d'une cellule vivante dans le futur. Afin de valoriser cette nouvelle famille de fluorophores utilisables en chimie bioorthogonale, nous collaborons aussi avec une équipe de biologistes de l'IBMP (Dr. Hubert Schaller) afin de suivre par imagerie de fluorescence le métabolisme de dérivés de phytostérols-alcynes au sein de cellule de tabac.

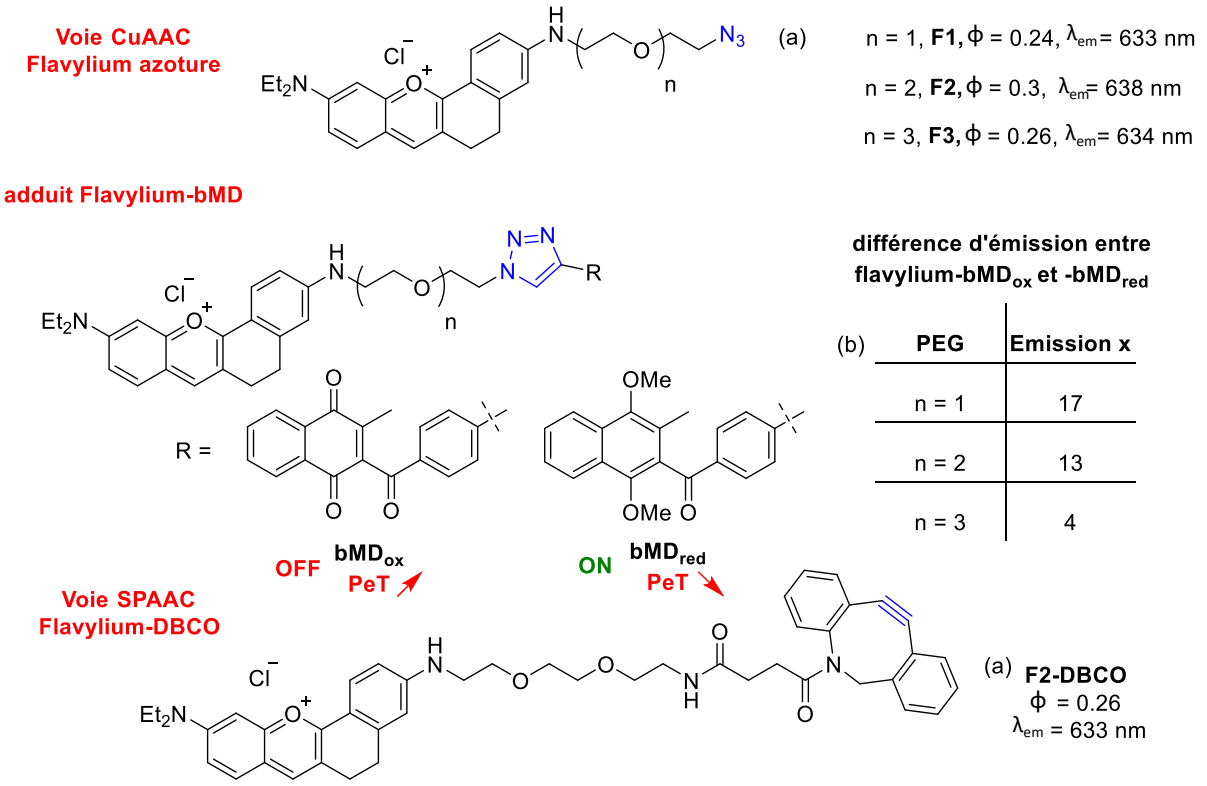

Figure 2: Sondes cliquables Flavylium azoture **F1**, **F2**, **F3** et **F2-DBCO** utilisable en imagerie bioorthogonale ainsi que les différences d'émission observées des adduits Flavylium-bMD suivant l'état rédox du bMD (a) tampon aqueux à pH 7.41 (0.1 M NaCl) (b) tampon aqueux à pH 7.41 (0.1 M NaCl) + 15% DMSO (dû à la faible solubilité de l'unité bMD).

Afin de diversifier les possibilités d'application en imagerie cellulaire, une cycloaddition sans cuivre basée sur une réaction de type SPAAC a été développée. Nous avons initié ce projet par la synthèse de deux sondes bMDs azoturés originales (**16** et **13**, **Figure 1** et **Figure 3**), ces dernières s'avérant être très actives à l'échelle du nM contre *Pf*. Concernant la sonde fluorescente cliquable, nous avons décidé de conserver le meilleur « scaffold » flavylium pour la partie fluorophore que nous avons combiné à une unité cyclooctyne (DBCO) pour l'alcyne contraint (**Figure 2**). La sonde **F2-DBCO** a été ainsi obtenue avec des propriétés photophysiques comparables à celles des flavyliums azoturés déjà synthétisés.

Le second objectif de mon travail de thèse a été centré sur la chimie médicinale des bMDs. Il s'agissait d'accroître l'activité antiparasitaire des bMDs par variation des paramètres PK et PC, comme par exemple la solubilité aqueuse ou la surface polaire de la molécule. Notre série étant très lipophile (valeur clog P), peu soluble dans l'eau et donc dans des conditions biologiques, nous avons tout d'abord choisi d'introduire des motifs hétéroaromatiques azotés. Des modifications similaires sur la partie ménadione (5-*N* ou 8-*N*) avaient déjà été réalisées antérieurement au sein de mon équipe d'accueil et avaient conduit à des activités antiplasmodiales inférieures à celle de la plasmodione, et une toxicité accrue.[5] C'est l'une des raisons pour laquelle l'introduction de motifs hétéroaromatiques azotés sur la partie benzylique a été privilégiée. Ces motifs sont bien connus en chimie médicinale car ils permettent de faire varier plusieurs paramètres simultanément au sein d'une molécule comme la solubilité aqueuse, la lipophilicité, la biodisponibilité, les valeurs de pK_a ou la surface polaire grâce à l'azote et à son doublet non liant pouvant être engagé dans des liaisons hydrogènes avec sa

cible biologique[13]. Les dérivés α-pyrimidine et α-pyridine (par rapport au groupement trifluorométhyle) étant déjà très prometteurs contre *Pf* et *Tg*, l'objectif premier était donc de synthétiser leurs régioisomères β (**Figure 4**). Les stratégies classiquement utilisées comme la réaction de Kochi-Anderson, la photoréduction ou le couplage de Suzuki ne sont cependant pas compatibles avec ce type de substrat. Il a donc fallu modifier la stratégie de synthèse (**Figure 3**). Une stratégie publiée basée sur un couplage de Negishi avait été préalablement choisie. Le Dr. Matthieu Roignant avait en effet initié ce projet au sein de l'équipe, mais les synthèses ne conduisaient qu'à des rendements globaux relativement faibles. Nous avons donc voulu revisiter cette stratégie afin d'améliorer leurs accessibilités et avons proposé une nouvelle voie d'accès permettant l'introduction de nombreux nouveaux motifs. Comme la réaction de Suzuki utilisant un substrat boré β-*N*-hétéroaromatique ne fonctionne pas, l'objectif a été d'inverser les fonctions réactives afin d'aboutir à un synthon boré sur la partie ménadione. Plusieurs composés ménadiones borés ont ainsi été synthétisés afin d'être engagés dans un couplage de Suzuki avec des synthons *N*-hétéroaromatiques commerciaux. Malheureusement des limitations souvent observées au cours de ce couplage ont conduit à un échec, notamment la faible stabilité de nos dérivés borés conduisant majoritairement au produit protodéborylé[16]. Néanmoins, la voie de synthèse initiale proposée fut optimisée rendant ces dérivés hétéroaromatiques plus accessibles et multipliant par deux leurs rendements globaux (**Figure 3**).

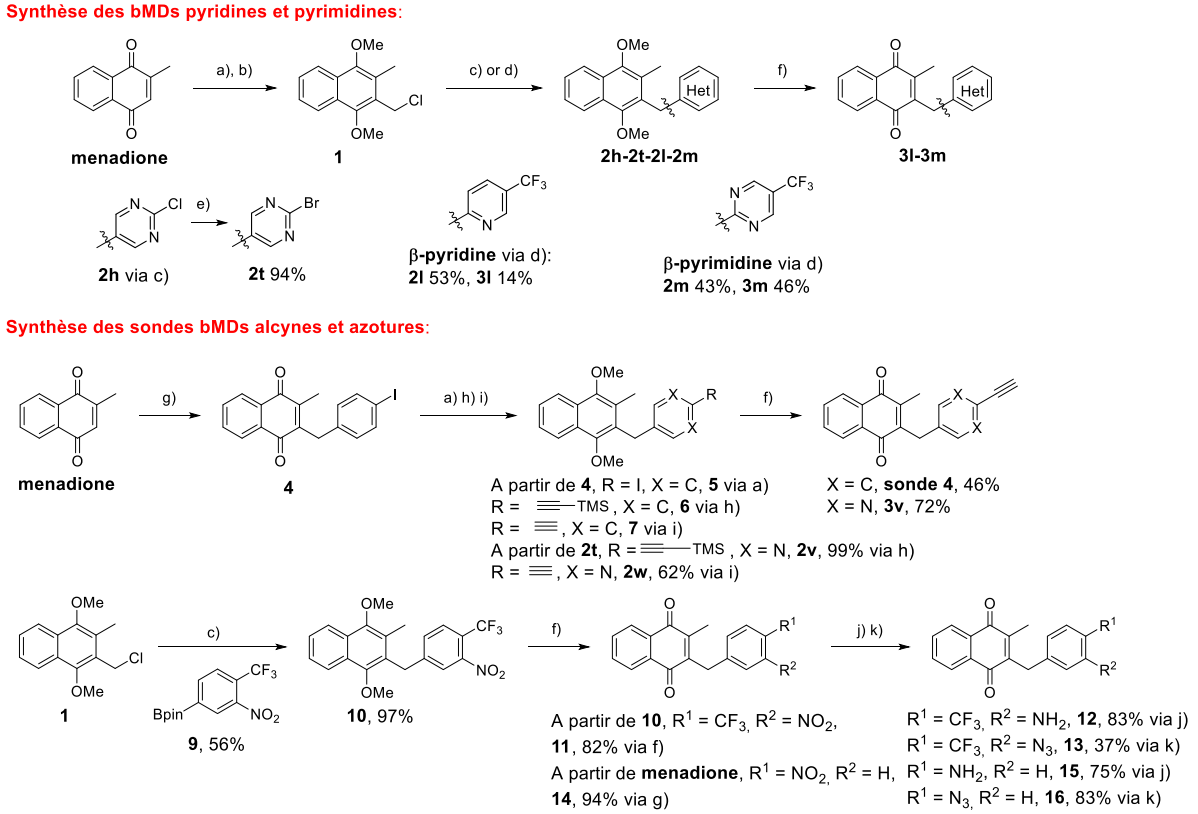

Figure 3: Synthèse des sondes bMDs alcynes et azotures ainsi que des dérivés bMDs pyridines et pyrimidines. Conditions : a) 1. $SnCl_2$, HCl, EtOH, rt, 2h, 2. Me_2SO_4, acétone, KOH, MeOH, 60°C, 4h; b) CH_2O, HCl, 80°C, 2h, 81%; c) $Pd(PPh_3)_4$, Na_2CO_3, DME:H_2O, 100°C, 1h; d) 1. Mg, LiCl, $ZnCl_2$, THF, rt, 2h, 2. $Pd(PPh_3)_4$, THF, 80°C, 24h; e) TMSBr, propionitrile, 100°C, 5h; f) CAN, CH_3CN:H_2O, rt, 1h; g) 4-iodophenylacetic acid or 4-nitrophenylacetic acid, $AgNO_3$, $(NH_4)_2S_2O_8$, CH_3CN:H_2O, reflux, 4h; h) ethynyltrimethylsilane, CuI, $Pd(PPh_3)_2Cl_2$, NEt_3, 70°C, 20h; i) TBAF, THF, rt, 1.5h; j) 1. Pd/C, EtOH, EtOAc, rt, 16h, 2. Acétone, rt, 72h; k) $NaNO_2$, NaN_3, H_2O:ionic liq., 30 min.

L'introduction d'un ou deux azotes aromatiques a ainsi pu être expérimentée et a conduit à des résultats très prometteurs. Sur la base de l'expertise acquise dans le domaine de la chimie clique de type CuAAC, nous avons choisi d'introduire un troisième azote grâce à la formation d'un groupement 1,2,3-triazole. Ce triazole devrait permettre d'améliorer la plupart des propriétés PC décrites précédemment. Par ailleurs, ce groupement triazole est connu

comme étant un bioisostère de groupement aromatique et sa stabilité biologique nous a donc conduit à étudier l'effet de ce motif sur l'activité de notre série bMD[17]. Deux séries d'une quinzaine de triazole-méthyle-ménadione chacune ont été ainsi préparées, la première disposant d'un α-triazole (par rapport au carbone benzylique), la seconde d'un β-triazole (**Figure 4**). Nous avons également apporté de la diversité structurale en faisant varier les groupements à l'extrémité *est* de la molécule (groupement électrodonneur/attracteur ou cycle aliphatique), afin d'obtenir des RSA suffisantes pour valider cette série. La série α s'est révélée peu active sur *Pf* probablement dû à la proximité du triazole par rapport au carbone benzylique, rendant moins favorable sa bioactivation en carbonyle nécessaire à l'activité de nos bMDs au sein de ce parasite. La seconde série basée sur un β-triazole s'est avérée en revanche plus active sur *Pf,* mais l'introduction d'une unité triazole n'a pas conduit à une augmentation significative de l'activité antiplasmodiale par rapport à la plasmodione, tête de série anti-paludique. Par ailleurs, de très bons résultats d'activités ont été obtenu sur son parasite voisin hématophage *Schistosoma mansoni*.

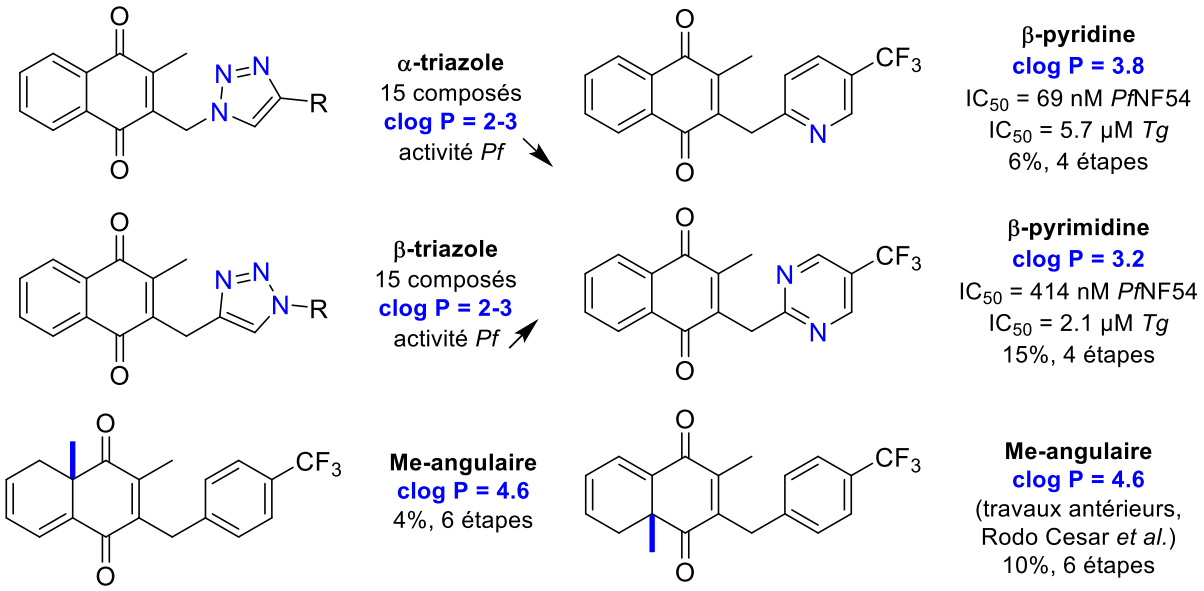

Figure 4: Introduction de groupement *N*-hétéroaromatique de type pyridine, pyrimidine ou triazole, ainsi que d'un méthyl angulaire dans le but d'améliorer les propriétés PK de la série bMD. clog P = moyenne logarithmique de cinq prédictions du coefficient de partage entre un milieu n-octanol et eau du composé.

Enfin, toujours dans le domaine de la chimie médicinale, nous avons décidé de synthétiser le régioisomère nécessaire pour compléter une approche initiée par le Dr. Elena Cesar Rodo et centré sur la synthèse de pro-drogues de la plasmodione possédant un méthyl angulaire sur la partie ménadione[18,19]. L'introduction d'un méthyl angulaire permettrait en effet de rompre l'aromaticité de la molécule et donc sa planéité, ces modifications étant connues pour améliorer la solubilité aqueuse et la biodisponibilité d'une molécule[20]. Par ailleurs, en se basant sur le mécanisme de l'aromatase, nous avons envisagé que ce méthyl angulaire pouvait subir une oxydation *in vivo* conduisant à son élimination et à la ré-aromatisation de la molécule en générant la plasmodione. Cet effet pro-drogue permettrait de développer une molécule distincte d'une naphtoquinone, un motif qui effraie toujours les industriels (**Figure 4**).

3) Conclusion générale

Plusieurs objectifs ont été abordés lors de ce travail de thèse et ont permis d'obtenir des résultats essentiels pour la suite des recherches menées sur cette série de composés de type bMD. Nos collaborations établies au niveau (inter)national ont permis d'apporter des informations-clés et des perspectives aussi bien en ingénierie de nouvelles sondes fluorescentes (chimie bioorthogonale, rédox) qu'en chimie médicinale antiparasitaire.

L'ensemble des résultats obtenus ont permis la rédaction de six articles, dont cinq ont été soumis récemment (deux articles ont été accepté). En ce qui concerne l'identification des cibles biologiques des bMDs chez les globules rouges parasités, nous avons pu établir, grâce à une stratégie AfBPP et à la synthèse d'une nouvelle sonde 'cliquable' optimisée, une première liste de 44 cibles biologiques potentielles chez *Pf*. La stratégie d'imagerie cellulaire basée sur la chimie bioorthogonale a permis, en outre, la synthèse de nouvelles sondes 'cliquables' et a validé l'apicoplaste et le mitochondrion du parasite comme organelles-cible des bMDs chez le parasite *Pf*. Le nouveau projet centré sur la famille de fluorophores 'cliquables' basés sur des ions flavyliums rigidifiés a permis d'étendre les capacités d'analyse en imagerie, de diversifier les thématiques abordées au sein de l'équipe et d'acquérir des expertises précieuses en chimie des fluorophores et en photophysique. Elle a notamment conduit à la mise en évidence d'une corrélation entre émissivité du fluorophore et état rédox de la bMD, ainsi qu'à la préparation de manière convergente de nouvelles sondes 'cliquables' pour des réactions CuAAC et SPAAC. Le second objectif de mon travail de thèse a été d'améliorer les propriétés PC/PK de la série bMD avec notamment l'introduction de groupements *N*-hétéroaromatiques. La synthèse de composés portant un groupement pyridine ou pyrimidine a été réalisée en expérimentant une nouvelle stratégie qui s'est avérée malheureusement non fructueuse. L'étude d'une nouvelle série basée sur un motif triazole (en version α ou β) a permis d'étendre la chimiothèque des bMDs sans pour autant améliorer significativement leur activité antiplasmodiale. De plus, nous avons poursuivi le développement de pro-drogues de la plasmodione en ajoutant un méthyle angulaire cassant l'aromaticité de la quinone, par une cycloaddition de Diels-Alder régiosélective. Les données obtenues dans le cadre de mon travail de thèse ouvrent des perspectives très intéressantes pour mon équipe d'accueil en approche AfBPP, chimie clique et bioorthogonale ou chimie médicinale rédox. Elles m'ont également apporté des connaissances et une formation en chimie à l'interface de la biologie.

4) Références

(1) Porte, K.; Riberaud, M.; Châtre, R.; Audisio, D.; Papot, S.; Taran, F. Bioorthogonal Reactions in Animals. *ChemBioChem* **2021**, *22* (1), 100–113. https://doi.org/10.1002/cbic.202000525.

(2) Meldal, M.; Tornøe, C. W. Cu-Catalyzed Azide−Alkyne Cycloaddition. *Chem. Rev.* **2008**, *108* (8), 2952–3015. https://doi.org/10.1021/cr0783479.

(3) Agard, N. J.; Prescher, J. A.; Bertozzi, C. R. A Strain-Promoted [3 + 2] Azide−Alkyne Cycloaddition for Covalent Modification of Biomolecules in Living Systems. *J. Am. Chem. Soc.* **2004**, *126* (46), 15046–15047. https://doi.org/10.1021/ja044996f.

(4) Müller, T.; Johann, L.; Jannack, B.; Brückner, M.; Lanfranchi, D. A.; Bauer, H.; Sanchez, C.; Yardley, V.; Deregnaucourt, C.; Schrével, J.; Lanzer, M.; Schirmer, R. H.; Davioud-Charvet, E. Glutathione Reductase-Catalyzed Cascade of Redox Reactions To Bioactivate Potent Antimalarial 1,4-Naphthoquinones – A New Strategy to Combat Malarial Parasites. *J. Am. Chem. Soc.* **2011**, *133* (30), 11557–11571. https://doi.org/10.1021/ja201729z.

(5) Lanfranchi, D. A.; Cesar-Rodo, E.; Bertrand, B.; Huang, H.-H.; Day, L.; Johann, L.; Elhabiri, M.; Becker, K.; Williams, D. L.; Davioud-Charvet, E. Synthesis and Biological Evaluation of 1,4-Naphthoquinones and Quinoline-5,8-Diones as Antimalarial and Schistosomicidal Agents. *Org. Biomol. Chem.* **2012**, *10* (31), 6375. https://doi.org/10.1039/c2ob25812a.

(6) Urgin, K.; Jida, M.; Ehrhardt, K.; Müller, T.; Lanzer, M.; Maes, L.; Elhabiri, M.; Davioud-Charvet, E. Pharmacomodulation of the Antimalarial Plasmodione: Synthesis of Biaryl- and N-Arylalkylamine Analogues, Antimalarial Activities and Physicochemical Properties. *Molecules* **2017**, *22* (1), 161. https://doi.org/10.3390/molecules22010161.

(7) Donzel, M.; Elhabiri, M.; Davioud-Charvet, E. Bioinspired Photoredox Benzylation of Quinones. *J. Org. Chem.* **2021**, *86* (15), 10055–10066. https://doi.org/10.1021/acs.joc.1c00814.

(8) Rodo, E. C.; Feng, L.; Jida, M.; Ehrhardt, K.; Bielitza, M.; Boilevin, J.; Lanzer, M.; Williams, D. L.; Lanfranchi, D. A.; Davioud-Charvet, E. A Platform of Regioselective Methodologies to Access Polysubstituted 2-Methyl-1,4-Naphthoquinone Derivatives: Scope and Limitations. *Eur. J. Org. Chem.* **2016**, *2016* (11), 1982–1993. https://doi.org/10.1002/ejoc.201600144.

(9) Bielitza, M.; Belorgey, D.; Ehrhardt, K.; Johann, L.; Lanfranchi, D. A.; Gallo, V.; Schwarzer, E.; Mohring, F.; Jortzik, E.; Williams, D. L.; Becker, K.; Arese, P.; Elhabiri, M.; Davioud-Charvet, E. Antimalarial NADPH-Consuming Redox-Cyclers As Superior Glucose-6-Phosphate Dehydrogenase Deficiency Copycats. *Antioxid. Redox Signal.* **2015**, *22* (15), 1337–1351. https://doi.org/10.1089/ars.2014.6047.

(10) Cichocki, B. A.; Khobragade, V.; Donzel, M.; Cotos, L.; Blandin, S.; Schaeffer-Reiss, C.; Cianférani, S.; Strub, J.-M.; Elhabiri, M.; Davioud-Charvet, E. A Class of Valuable (Pro-)Activity-Based Protein Profiling Probes: Application to the Redox-Active Antiplasmodial Agent, Plasmodione. *JACS Au* **2021**, *1* (5), 669–689. https://doi.org/10.1021/jacsau.1c00025.
(11) Cotos, L.; Donzel, M.; Elhabiri, M.; Davioud-Charvet, E. A Mild and Versatile Friedel–Crafts Methodology for the Diversity-Oriented Synthesis of Redox-Active 3-Benzoylmenadiones with Tunable Redox Potentials. *Chem. – Eur. J.* **2020**, *26* (15), 3314–3325. https://doi.org/10.1002/chem.201904220.
(12) Feng, L.; Lanfranchi, D. A.; Cotos, L.; Cesar-Rodo, E.; Ehrhardt, K.; Goetz, A.-A.; Zimmermann, H.; Fenaille, F.; Blandin, S. A.; Davioud-Charvet, E. Synthesis of Plasmodione Metabolites and 13C-Enriched Plasmodione as Chemical Tools for Drug Metabolism Investigation. *Org. Biomol. Chem.* **2018**, *16* (15), 2647–2665. https://doi.org/10.1039/C8OB00227D.
(13) Meanwell, N. A. Chapter Five - A Synopsis of the Properties and Applications of Heteroaromatic Rings in Medicinal Chemistry. In *Advances in Heterocyclic Chemistry*; Scriven, E. F. V., Ramsden, C. A., Eds.; Academic Press, 2017; Vol. 123, pp 245–361. https://doi.org/10.1016/bs.aihch.2016.11.002.
(14) Sun, Y.; Sun, P.; Li, Z.; Qu, L.; Guo, W. Natural Flavylium-Inspired Far-Red to NIR-II Dyes and Their Applications as Fluorescent Probes for Biomedical Sensing. *Chem. Soc. Rev.* **2022**, *51* (16), 7170–7205. https://doi.org/10.1039/D2CS00179A.
(15) Cruz, L.; Basílio, N.; Mateus, N.; de Freitas, V.; Pina, F. Natural and Synthetic Flavylium-Based Dyes: The Chemistry Behind the Color. *Chem. Rev.* **2022**, *122* (1), 1416–1481. https://doi.org/10.1021/acs.chemrev.1c00399.
(16) *Protodeboronation of Heteroaromatic, Vinyl, and Cyclopropyl Boronic Acids: pH–Rate Profiles, Autocatalysis, and Disproportionation*. https://doi.org/10.1021/jacs.6b03283.
(17) Dheer, D.; Singh, V.; Shankar, R. Medicinal Attributes of 1,2,3-Triazoles: Current Developments. *Bioorganic Chem.* **2017**, *71*, 30–54. https://doi.org/10.1016/j.bioorg.2017.01.010.
(18) Redondo, M. C.; Veguillas, M.; Ribagorda, M.; Carreño, M. C. Control of the Regio- and Stereoselectivity in Diels–Alder Reactions with Quinone Boronic Acids. *Angew. Chem. Int. Ed.* **2009**, *48* (2), 370–374. https://doi.org/10.1002/anie.200803428.
(19) Carreño, M. C.; Urbano, A.; Fischer, J. Enantioselective Diels–Alder Approach to Angucyclinones from (S)-2-(p-Tolylsulfinyl)-1,4-Naphthoquinone and Substituted Racemic Vinylcyclohexenes. *Angew. Chem. Int. Ed. Engl.* **1997**, *36* (15), 1621–1623. https://doi.org/10.1002/anie.199716211.
(20) Ishikawa, M.; Hashimoto, Y. Improvement in Aqueous Solubility in Small Molecule Drug Discovery Programs by Disruption of Molecular Planarity and Symmetry. *J. Med. Chem.* **2011**, *54* (6), 1539–1554. https://doi.org/10.1021/jm101356p.

LISTE DES PRESENTATIONS

Conférences nationales et internationales :
New frontiers in host-parasite interactions, from cell to organism, EMBO (European Molecular Biology Organisation) Workshop-LabEx ParaFrap Conference, Ile des Embiez, 04/10/22, Baptiste Dupouy, Elisabeth Davioud-Charvet, Mourad Elhabiri, affiche
REGIO Symposium, Freiburg, 28/08/23, Baptiste Dupouy, Elisabeth Davioud-Charvet, Mourad Elhabiri, communication orale
GDR (groupe de recherche) ChemBio, Illkirch, 09/06/23, Baptiste Dupouy, Elisabeth Davioud-Charvet, Mourad Elhabiri, communication orale
Autres presentations:
LIMA (Laboratoire d'Innovation Moléculaire et Applications) Spring Day, Mulhouse, 21/06/23, Baptiste Dupouy, Elisabeth Davioud-Charvet, Mourad Elhabiri, communication orale

---

LISTE DES PUBLICATIONS (format JACS)

Iacobucci, I.; Monaco, V.; Hovasse, A.; Dupouy, B.; Keumoe, R.; Cichocki, B.; Elhabiri, M.; Meunier, B.; Strub, J.-M.; Monti, M.; Cianférani, S.; Blandin, S. A.; Schaeffer-Reiss, C.; Davioud-Charvet, E. Proteomic Profiling of Antimalarial Plasmodione Using 3-Benz(o)Ylmenadione Affinity-Based Probes. *Chembiochem* **2024**, e202400187. https://doi.org/10.1002/cbic.202400
Dupouy, B.; Donzel, M.; Roignant, M.; Charital, S.; Keumoe, R.; Yamaryo-Botté, Y.; Feckler, A.; Bundschuh, M.; Bordat, Y.; Rottmann, M.; Mäser, P.; Botté, C. Y.; Blandin, S. A.; Besteiro,

S.; Davioud-Charvet, E. 3-Benzylmenadiones and Their Heteroaromatic Analogues Target the Apicoplast of Apicomplexa Parasites: Synthesis and Bioimaging Studies. *ACS Infect. Dis.* **2024**. https://doi.org/10.1021/acsinfecdis.4c00304.
Cesar-Rodo, E.; Dupouy, B.; Häberli, C.; Strub, J.-M.; Williams, D.L.; Mäser, P.; Rottmann, M.; Keiser, J.; Lanfranchi, D.A.; Davioud-Charvet, E. Regioselective Synthesis of Potential Non-Quinonoid Prodrugs of Plasmodione: Antiparasitic Properties Against Two Hemoglobin-Feeding Parasites and Drug Metabolism Studies. *Molecules* **2024**, 29, 5268. https://doi.org/10.3390/molecules29225268.

Table des matières

Liste des abréviations

2P	Deux photons
AfBPP	Profilage de protéines par affinité
AQ	Amodiaquine
ART	Artémisinine
bMD	3-benzylménadione
CAN	Nitrate de cérium et ammonium
CC_{50}	Concentration de cytotoxicité médiane
CHX	Cyclohexane
CQ	Chloroquine
CTA	Combinaison thérapeutique à base d'artémisinine
CuAAC	Copper(I)-Catalyzed Alkyne-Azide Cycloaddition
DCM	Dichlorométhane
DDQ	2,3-dichloro-5,6-dicyano-1,4-benzoquinone
DHA	Dihydroartémisinine
DME	Diméthoxyéthane
DMF	Diméthylformamide
DMSO	Diméthylsulfoxyde
ESIPT	Transfert de proton intramoléculaire à l'état excité
EtOAc	Acétate d'éthyle
FQ	Ferroquine
FRET	Transfert d'énergie par résonance de fluorescence
G6PD	Glucose-6-phosphate déshydrogénase
GR	Glutathion réductase (humaine *h*GR, *P. falciparum Pf*GR)
GSH	Glutathion
GSSG	Glutathion disulfure
H_2SO_4	Acide sulfurique
HBr	Acide bromhydrique
HCl	Acide chlorhydrique
HCQ	Hydroxychloroquine
***h*GR**	Glutathion réductase humaine
HRMS	Spectroscopie de masse à haute résolution
IC_{50}	Concentration inhibitrice médiane
ICT	Transfert de charge intramoléculaire
IEDDA	Inverse Electron Demand Diels–Alder
MB	Bleu de méthylène
MeCN	Acétonitrile
MetHb	Méthémoglobine
MFQ	Méfloquine
NADPH	Nicotinamide adénine dinucléotide phosphate réduite

NO	Monoxyde d'azote
NQ	1,4-naphtoquinone
OMS	Organisation mondiale de la santé
OxyHb	Oxyhémoglobine
PC	Propriétés physicochimiques
PD	Plasmodione
PDO	PD-Oxyde
PeT	Transfert d'électron photoinduit
Pf	*Plasmodium falciparum*
***Pf*GR**	Glutathion réductase du *P. falciparum*
PIDA	Diacétate d'iodobenzène
PIR	Proche infrarouge
PK	Propriétés pharmacocinétiques
PPQ	Pipéraquine
PQ	Primaquine
RMN	Résonance magnétique nucléaire
ROS	Espèces réactives de l'oxygène
RSA	Relations structure-activité
RSP	Relations structure-propriété
S. mansoni	*Schistosoma mansoni*
SN_2	Substitutionnucléophile
SN_{Ar}	Substitution nucléophile aromatique
SOD	Superoxyde dismutase
SP	Sulfadoxine-Pyriméthamine
SPAAC	Strain-Promoted Azide-Alkyne Cycloaddition
T	Toluène
T. cruzi	*Trypanosoma cruzi*
T. gondii	*Toxoplasma gondii*
TBAF	Fluorure de tétra-*n*-butylammonium
TBET	Through Bond Energy Transfer
Tf_2O	Anhydride trifluorométhanesulfonique
TFAA	Anhydride trifluoroacétique
TFAT	Triflate de trifluoroacétyle
TfOH	Acide triflique
THF	Tétrahydrofurane
TICT	Transfert de charge intramoléculaire twisté
TMS	Triméthylsilane
TrxR	Thiorédoxine réductase
UV	Ultraviolet

Chapitre I : Introduction sur le paludisme, les 3-benzylménadiones et les fluorophores cliquables

1.1 Maladies parasitaires

Les maladies parasitaires représentent une catégorie significative de pathologies infectieuses. Elles sont causées par divers parasites vivant sur ou dans un autre organisme, appelé hôte (humain ou animal ou plante), dont ils tirent profit au détriment de ce dernier. Ces maladies sont fréquentes dans les régions tropicales et subtropicales, ainsi que chez les personnes immunodéprimées. Elles ont un impact dévastateur sur la santé publique mondiale, affectant des millions de personnes chaque année et entraînant des pertes économiques importantes dues à leur morbidité et leur mortalité.

Les biologistes et les médecins utilisent le terme « parasites » pour désigner :

- **Les Protozoaires** : organismes unicellulaires qui se reproduisent par division cellulaire à l'intérieur de l'hôte. Parmi les plus notoires, on retrouve les agents pathogènes responsables du paludisme, de la leishmaniose, de la toxoplasmose et de la trypanosomiase (maladie du sommeil et maladie de Chagas).
- **Les Helminthes (vers)** : organismes pluricellulaires de plus grande taille, dotés d'organes internes. La plupart excrètent des œufs ou des larves qui se développent dans leurs hôtes. Ces vers induisent des maladies comme l'ascaridiose ou encore la schistosomiase.
- **Les Ectoparasites** : organismes vivant à la surface de leur hôte, pouvant causer des maladies directes ou être des vecteurs de pathogènes, comme par exemples les poux, puces et acariens.

Ces parasites peuvent se transmettre par voie orale (eau, objets ou nourriture contaminés), par lésion cutanée ou encore par piqûre. En général, un diagnostic rapide est possible après une étude des symptômes et une analyse de sang, de selles ou d'urines, conduisant la plupart du temps à un traitement antiparasitaire spécifique.

Pour prévenir l'infection, certaines mesures sont recommandées : une bonne hygiène personnelle, l'utilisation d'insecticides ou de moustiquaires, et éviter tout contact avec de l'eau contaminée. La prévention et l'éducation jouent également un rôle crucial. À l'heure actuelle, ces maladies représentent toujours un défi majeur dans le domaine de la santé publique et de la recherche.

1.1.1 Le Paludisme

Le Paludisme (ou Malaria pour les pays anglophones) est une maladie parasitaire causée par des parasites du genre *Plasmodium*. Les enfants de moins de 5 ans constituent la population en Afrique la plus touchée, représentant environ 80 % des décès en raison de leur système immunitaire encore immature. Cette maladie provoque d'abord des cycles de forte

fièvre importante, des maux de tête et de la fatigue, puis, si elle n'est pas traitée, elle entraine des complications graves telles que l'anémie, le paludisme cérébral ou une défaillance de certains organes, pouvant conduire à la mort dans les cas les plus graves. Les femmes enceintes présentent également un risque accru de développer une forme grave de l'infection car elles perdent une partie de leur immunité protectrice pendant la grossesse. Selon l'Organisme Mondial de la Santé[1] (OMS), en 2022, on estime à 249 millions le nombre de cas de paludisme et 608 000 décès dans 85 pays endémiques, avec 95% des cas et décès provenant d'Afrique sub-saharienne.

Le parasite *Plasmodium*, appartenant à l'embranchement des *Apicomplexa*, comprend plusieurs espèces capables d'infecter l'homme : *P. falciparum* (*Pf*), *P. vivax*, *P. ovale*, *P. malariae* et *P. knowlesi*. Chacune de ces espèces est réparties différemment dans les zones touchées et possèdent des caractéristiques cliniques, biologiques et morphologiques distinctes. Le parasite majoritaire et le plus virulent est *P. falciparum*, transmis à l'Homme par une piqûre de moustique femelle du genre *Anophèles* (vecteur). Ces moustiques apparaissent généralement en grande quantité de manière saisonnière, principalement dans les régions tropicales et subtropicales, pendant la saison des pluies.

1.1.2 Le parasite *Plasmodium falciparum*

L'espèce *P. falciparum* est responsable de la quasi-totalité du nombre des cas et des décès de paludisme[2], ce qui explique pourquoi la plupart des recherches biologiques et pharmaceutiques se concentrent sur cette espèce. *P. falciparum* a un cycle de vie bien défini, à la fois chez le moustique, où il suit un cycle sexué dit sporogonique, et chez l'homme, où il développe un cycle asexué dit schizogonique. Chez l'homme, on distingue deux phases distinctes : la phase hépatique (ou pré-érythrocytaire) et la phase sanguine (ou érythrocytaire) (Figure 1).

Le cycle de vie de *P. falciparum* commence par la piqûre d'un moustique infecté lors de son repas sanguin. Le moustique injecte alors une dizaine de parasites sous la forme de sporozoïtes mobiles, qui sont rapidement captés par la circulation sanguine et rejoignent le foie pour commencer la phase hépatique de la maladie. Pendant cette première phase, les parasites se multiplient rapidement pour atteindre une population de l'ordre du million, formant des schizontes. Cette phase est asymptomatique et dure généralement une semaine après l'infection. Cependant, pour d'autres espèces de *Plasmodium,* comme *P. vivax,* elle peut durer des mois, voire des années, avec des parasites restant au stade dormant, appelés hypnozoïtes[3], pouvant se réactiver et provoquer une nouvelle infection sanguine. À maturité, les cellules hépatiques perdent leur intégrité membranaire et libérèrent des mérozoïtes dans

la circulation sanguine. Ces mérozoïtes envahissent alors les globules rouges, déclenchant la phase symptomatique de la maladie (Figure 1).

Au cours de cette phase, les parasites suivent des cycles de 48 heures pendant lesquels les symptômes cliniques de la maladie se manifestent. La particularité de ce parasite est sa capacité à dégrader l'hémoglobine du globule rouge de l'hôte pour en faire une source de protéines et d'acides aminés indispensables à sa croissance, ce qui le catégorise comme hématophage. Les parasites passent par différents stades intra-érythrocytaires caractéristiques : d'abord le stade anneau (jusqu'à 26 heures), puis le stade trophozoïte (jusqu'à 38 heures), et enfin le stade schizonte (jusqu'à 48 heures) (Figure 1). À ce stade, la rupture de la membrane du globule rouge (lyse) libère dans la circulation sanguine une trentaine de mérozoïtes capables d'infecter de nouveaux globules rouges. Le nombre de parasites augmente ainsi très rapidement, atteignant plusieurs milliards en circulation libre dans le sang.

De plus, une petite proportion de parasite se différencie en gamétocytes sexués mâles ou femelles[4], qui se développent en cinq stades successifs dans la moelle osseuse. Une fois matures (stade cinq, 8-12 jours), ils rejoignent la circulation sanguine et peuvent alors infecter un moustique lors de son repas sanguin par piqûre de l'hôte. Ainsi commence le cycle de vie sexué chez le moustique, lequel, une fois complété, pourra infecter un nouvel hôte humain, perpétuant ainsi le cycle (Figure 1).

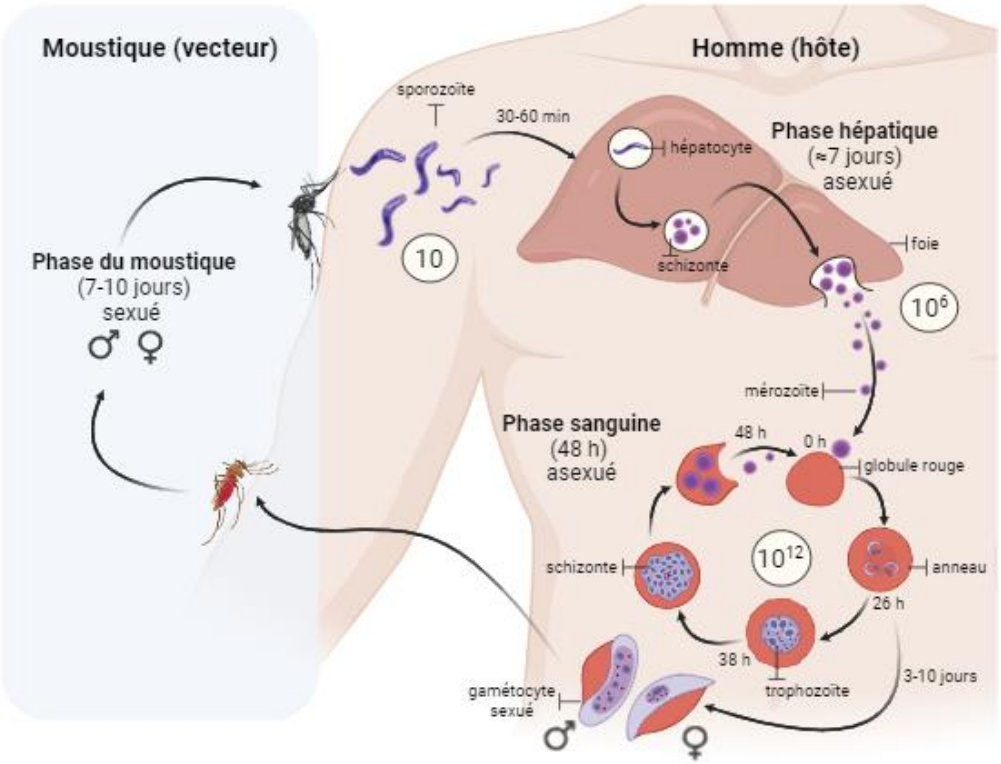

Figure 1: Cycle de vie simplifié du parasite *Plasmodium falciparum* chez son hôte l'Homme.

Chaque stade parasitaire présente des différences morphologiques, ainsi qu'une expression spécifique de leurs protéines et de leurs gènes, leur conférant des propriétés distinctes[5]. En raison de la complexité biologique et des conséquences provoquées par ce parasite, son étude a été très détaillée au cours des 30 dernières années. De nombreuses approches se basent sur l'analyse de souches de référence de *P. falciparum*, correspondant à des clones adaptés à la culture et pouvant subir des modifications génétiques. La souche la plus étudiée est *Pf*3D7. Grâce à d'importantes avancées technologiques en matière de séquençage et d'analyse, son génome a pu être élucidé pour la première fois en 2002[6]. Environ 5400 gènes codant pour les protéines ont été identifiés, dont 60% ne présentent pas de similarités suffisantes avec les protéines d'autres organismes vivants pour en justifier la fonction et leur rôle. Cela démontre l'importance du travail de recherche qu'il reste à mener sur ce parasite afin de mieux traiter cette maladie.

1.1.3 Traitements et prévention du Paludisme

Pour lutter contre cette maladie, d'importants moyens de recherche en matière de traitements antipaludiques ainsi que de prévention ont été mis en place.

Lutte contre le vecteur

La lutte contre le moustique, vecteur de la maladie, est essentielle pour éviter ou réduire sa transmission. Parmi les actions mises en œuvre, on retrouve l'utilisation de moustiquaires imprégnées d'insecticides et l'utilisation directe d'insecticides de type pyréthrinoïde[7]. Cependant, certains pays ont rapporté des résistances aux principales classes d'insecticides couramment utilisées, y compris les pyréthrinoïdes[8,9].

Vaccination

Un autre moyen de prévention envisageable est la vaccination. Bien que l'immunité contre parasite soit encore mal comprise, les populations vivant dans les zones endémiques développent parfois une défense efficace contre le parasite *P. falciparum*. Cette protection immunitaire pourrait permettre le développement d'un vaccin efficace[10,11]. Les vaccins ciblent généralement un stade parasitaire spécifique comme par exemples :

- Un vaccin pré-érythrocytaire qui empêche l'infection ou attaquera la cellule hépatique infectée.
- Un vaccin agissant sur le stade sanguin qui réduit le nombre de parasites et leur prolifération, diminuant ainsi la gravité des symptômes.

L'objectif d'un vaccin n'est pas de fournir une solution immédiate comme le fait un traitement pharmaceutique, mais de renforcer la défense immunitaire de l'individu contre certaines formes du parasite, interrompant ainsi son cycle de vie.

Après des décennies de recherche, en 2021, un premier vaccin a été approuvé par l'OMS : le vaccin RTS,S/AS01 ou Mosquirix™ [12], qui cible le stade hépatique et est élaboré à partir d'un antigène parasitaire recombinant impliqué dans l'invasion des hépatocytes par les sporozoïtes. Malheureusement, en raison des variations génétiques de la protéine codante ciblée, ce vaccin perd en efficacité globale[13]. Néanmoins, il est aujourd'hui utilisé et recommandé par l'OMS car il permet de réduire les formes graves du paludisme chez les jeunes enfants de 30-35% après quatre doses. L'amélioration de ce vaccin est en cours de développement, et d'autres vaccins prometteurs sont en développement, comme le R21 actuellement en phase IIb, ainsi que des vaccins nous protégeant du stade pré-érythrocytaire entier comme le *Pf*SPZ ou le *Pf*SPZ-CVac[10].

Chimiothérapie

Cette maladie peut être également traitée par chimiothérapie grâce au développement de molécules actives. Aujourd'hui, il existe environ cinq médicaments antipaludiques couramment utilisés, ainsi qu'un grand nombre de molécules en développement clinique. L'OMS recommande aujourd'hui d'utiliser des combinaisons thérapeutiques à base d'artémisinine (CTA) contre le parasite *P. falciparum*, la chloroquine (CQ) contre l'infection à *P. vivax*, et la primaquine (PQ) pour prévenir des rechutes d'infection face à *P. vivax* et à *P. ovale*.

Dans la suite de cette introduction, nous allons nous intéresser aux familles de molécules les plus actives, à leur mode d'action, à leurs cibles et à leur activité.

Les endopéroxydes :

Parmi cette classe de molécules, on retrouve l'artémisinine (ART), extraite de la plante chinoise *Artemisia annua*[14], découverte dans les années 70 par le Dr. Tu Youyou (prix Nobel de médecine 2015 pour cette découverte). D'un point de vue chimique, elle possède une lactone sesquiterpénique et un groupement endopéroxyde et a été synthétisé pour la première fois en 1983[15]. Elle est active dans le bas nanomolaire contre plusieurs souches de *P. falciparum* au stade érythrocytaire (sexué et asexué) et présente une toxicité moindre pour les cellules humaines saines. Cependant, plutôt que d'adopter la molécule chinoise, l'OMS a initialement décidé de synthétiser ses propres molécules plus actives. Ainsi, des analogues de l'artémisinine ont été développés, comme l'artémether, l'artésunate ou la dihydroartémisinine (DHA) (Figure 2). Ces analogues sont aujourd'hui largement utilisés car ils sont plus solubles et possèdent une meilleure biodisponibilité que l'artémisinine.

Initialement, l'ART était utilisé en monothérapie. Étant donné que l'artémisinine et ses analogues ont une demi-vie courte (1 à 2 heures chez l'Homme), une molécule partenaire avec une demi-vie plus longue et un mode d'action différent est utilisée. Plus tard, des bithérapies nommées CTA ont vu le jour.

Mode d'action

Le mode d'action de l'ART n'a pas encore été totalement élucidé. Ces molécules semblent cibler principalement la *Pf*ATPase 6[16]. L'ART et ses dérivés sont d'abord métabolisés en DHA[17], le métabolite actif sur le parasite.

L'oxyhémoglobine (OxyHb-Fe(II)) présente dans le globule rouge est séquestrée dans le compartiment du parasite à pH acide appelée vacuole digestive subit une oxydation produisant de la méthémoglobine (MetHb-Fe(III)). Cette méthémoglobine est digérée par différentes classes de protéases du parasite, dans la vacuole digestive, libérant des acides aminés qui servent de nutriments pour sa croissance. Ce processus génère également de l'hème Fe(III) libre dans le cytosol et la membrane du parasite. Comme cette espèce est toxique pour le parasite, elle est soit détoxifiée sous forme d'hémozoïne (non toxique) par biocristallisation, ou soit détruite par des espèces réactives de l'oxygène (ROS) générées par la réaction de Fenton, impliquant la réduction continue de Fe(III) en Fe(II) de l'hème en présence de glutathion (GSH). Une petite fraction d'hème Fe(II) libre produit plusieurs métabolites de l'ART sous forme radicalaire très réactifs (DHA*, réduction du pont endopéroxyde), capables d'alkyler les protéines, l'hème ou les lipides environnants, provoquant des dommages irréversibles ainsi que la génération de ROS (Figure 2).

Les endopéroxydes

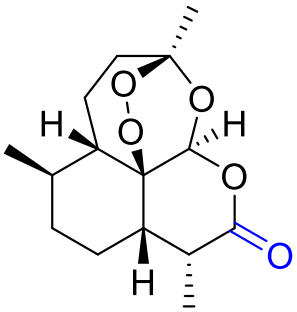

Artémisinine (**ART**)

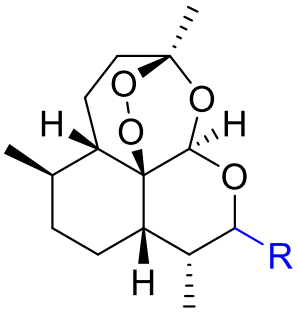

R = (-OH), Dihydroartémisinine (**DHA**)
R = (-OMe), Artéméther
R = (-O(C(O)(CH_2)$_2$COOH), Artésunate

Mode d'action simplifié:

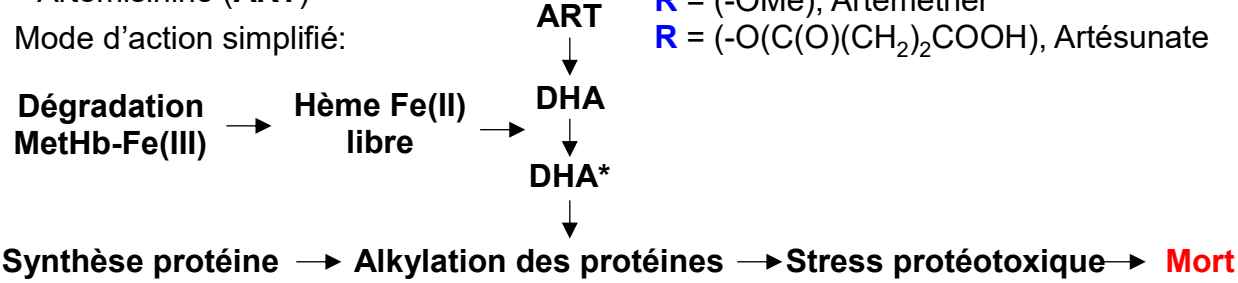

Figure 2: Structure de l'artémisinine et de ses analogues. Mode d'action simplifié : l'artémisinine et ses analogues sont d'abord réduits en **DHA**. Puis **l'hème Fe(II) libre** libéré lors de la digestion de la **MetHb-Fe(III)** va générer des métabolites radicalaires **DHA***, qui vont conduire à des dommages irréversibles sur les protéines du parasite, ce qui entrainent un stress protéotoxique et la mort du parasite.

Deux principales conséquences de ce traitement vont être observées : une réduction rapide de la parasitémie grâce à une très bonne activité sur le stade jeunes anneaux et une réduction considérable du nombre de parasites arrivant à maturité, ce qui diminue les symptômes et la transmission de la maladie.

Problèmes de résistance et de coût

Malgré ce traitement, la morbidité et la mortalité causées par le paludisme continuent d'augmenter. Deux facteurs sont en cause : le prix du médicament et les résistances développées par le parasite face à ces composés thérapeutiques.

Cette maladie affecte les pays les plus pauvres du monde, c'est pourquoi le coût du médicament détermine son utilisation dans les zones endémiques. Ainsi, des traitements plus anciens et moins chers comme la chloroquine (CQ) ou la sulfadoxine-pyriméthamine (SP) ont été largement utilisés au 20^{e} siècle jusqu'à l'apparition de souches résistantes à la CQ et à la SP, ce qui a conduit à l'introduction des CTA. Les CTA traitent la maladie en 3 jours par voie orale (une dose par jour) en combinaison avec d'autres molécules comme la luméfantrine (LMF), la SP, la méfloquine (MFQ) ou l'amodiaquine (AQ).

L'utilisation massive d'antipaludiques a entraîné l'apparition systématique de résistances, souvent dues à des modifications spécifiques des cibles antipaludiques, comme un changement d'acides aminés ou une mutation d'enzymes, conduisant à une perte d'affinité du composé pour sa cible. En 2008, les premiers cas de résistances à l'ART ont été signalés au Cambodge[18], puis dans toute l'Indonésie[19], et aujourd'hui en Afrique[20] et en Inde[21].

<u>Les aminoquinoléines :</u>

Cette famille d'antipaludiques fait partie des plus anciennes. La quinine, l'une des premières molécules utilisées, a été extraite dans les années 1820 de l'écorce d'un arbre d'Amérique du Sud (quinquina, *Cinchona officinalis*), puis synthétisée pour la première fois dans les années 1945[22] (Figure 3). Elle a été largement utilisée jusqu'en 1920 avant d'être remplacée par d'autres molécules de synthèse de la même famille, moins coûteuses à produire et non dépendantes de leur source naturelle. Parmi ces nouvelles molécules, on trouve : la chloroquine (CQ), l'amodiaquine (AQ), la méfloquine (MFQ), la pipéraquine (PPQ) ou encore la primaquine (PQ) (Figure 3).

Mode d'action

Cette famille de composés cible principalement le stade érythrocytaire du parasite. La CQ est la plus connue, ayant été massivement utilisée après la seconde guerre mondiale comme médicament de première intention en raison de son efficacité et de son faible coût de production. Comme pour les endopéroxydes, le mode d'action de la CQ et des aminoquinoléines en général n'est pas encore parfaitement élucidé. L'hypothèse la plus probable serait que les aminoquinoléines s'accumulent dans la vacuole digestive acide du parasite, bloquant la détoxification de l'hème Fe(II) libre en hèmozoïne[23]. L'accumulation d'hème toxique entraîne ainsi la mort du parasite et une augmentation du stress oxydant (Figure 3).

Résistance et développement de nouvelles molécules

À partir des années 1950, des souches résistantes à la CQ ont été détectées[24], atteignant la plupart des pays d'Asie et d'Afrique dans les années 1980. La toxicité de la CQ à forte dose a également posé problème, conduisant au développement de composés moins toxiques. D'autres molécules plus récentes, telles que la PQ, possèdent un mode d'action différent de celui de la CQ. De plus, certaines de ces molécules, comme l'AQ, la PPQ et la MFQ, sont utilisées dans des CTAs en tant que molécules partenaires. Ces composés sont actifs contre les souches résistantes à la CQ, et la MFQ, par exemple, est utilisée comme molécule préventive par les voyageurs se rendant dans des zones endémiques.

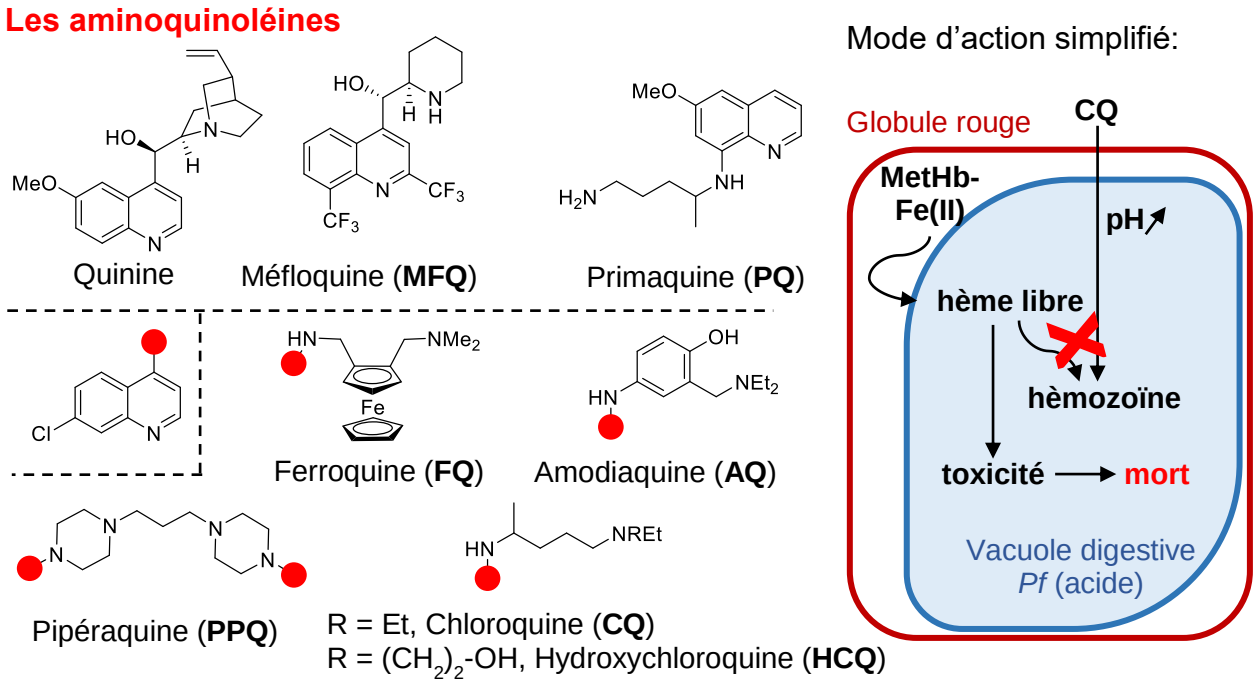

Figure 3: Structure des dérivés aminoquinoléines. Mode d'action simplifié : la **CQ** va s'accumuler dans la vacuole digestive acide et s'intercaler avec le dimère d'hème, inhibant ainsi le cristal d'hémozoïne se former. L'**OxyHb-Fe(II)** de l'hôte va être séquestré et oxydé par le parasite en **MetHb-Fe(III)** puis dégradé produisant de **l'hème Fe(III) libre** et des nutriments pour le parasite (protéines, acides aminées). La **CQ** va se lier à l'**hème libre**, bloquant ainsi sa détoxification en **hèmozoïne**, produisant une forte toxicité et conduisant à la mort du parasite.

La ferroquine

Une nouvelle molécule dans cette classe des antipaludiques est la ferroquine (FQ) (Figure 3). Elle est composée d'un groupement ferrocényle et a été développée par J. Brocart et C. Biot *et al.* en 1997. Actuellement en phase clinique II, elle est active contre les souches résistantes à la CQ. Ses propriétés pharmacocinétiques diffèrent de celles de la CQ, notamment grâce à la présence du ferrocène qui la rend moins flexible et moins basique. Son mode d'action n'est pas fondamentalement différent de celui de la CQ[25]. Cependant, l'accumulation d'hème Fe(II) libre conduit également à la libération de ROS, dont le radical hydroxyle (HO•). Ce radical très réactif et toxique est beaucoup plus présent lorsque la FQ est utilisée par rapport à la CQ, suggérant son implication dans la production de HO•. Pour confirmer cela, le Dr. C. Biot a développé une sonde fluorescente ratiométrique capable de détecter la présence de HO• après traitement d'un globule rouge parasité par la FQ[26].

L'atovaquone :

Cette molécule est le fruit de plus de 50 années de développement, elle fait partie de la classe des 2-hydroxynaphtoquinones et a été synthétisée pour la première fois en 1991[27] (Figure 4).

Mode d'action

Cette molécule cible le stade sanguin du parasite, en agissant plus précisément sur le complexe bc_1 de la chaine de transfert électronique mitochondriale du parasite. La mitochondrie joue un rôle crucial dans la croissance du parasite, notamment en produisant des orotates nécessaires à la biosynthèse des pyrimidines ou purines, composants essentiels des acides nucléiques du parasite[27]. L'atovaquone empêche la réoxydation du cofacteur ubiquinone, indispensable pour ce mécanisme, ce qui entraîne un arrêt de la biosynthèse d'orotate (Figure 4).

Efficacité et résistance

L'atovaquone est plus active que l'ART ou la CQ sur le stade sanguin et active contre leurs souches résistantes, bien que la mort du parasite soit observée plus lentement. Cette différence est due au fait que l'ART cible des stades jeunes comme le stade anneau, tandis que l'atovaquone agit sur des stades plus anciens (les trophozoïtes).

Lorsqu'elle est utilisée seule, des mutations du complexe bc_1 apparaissent, provoquant des résistances. Aucune résistance croisée avec d'autres antipaludiques n'a été observée, permettant ainsi le développement de combinaisons thérapeutiques. Pour surmonter les résistances associées à l'utilisation de l'atovaquone seule, elle a été combinée avec la

proguanil, un autre antipaludique. La proguanil agit en synergie parfaite avec l'atovaquone, contournant les mutations du complexe bc_1 (Figure 4). La combinaison atovaquone/proguanil est commercialisée sous le nom de Malarone et est aujourd'hui principalement utilisée en prophylaxie (prévention), comme la méfloquine (MFQ).

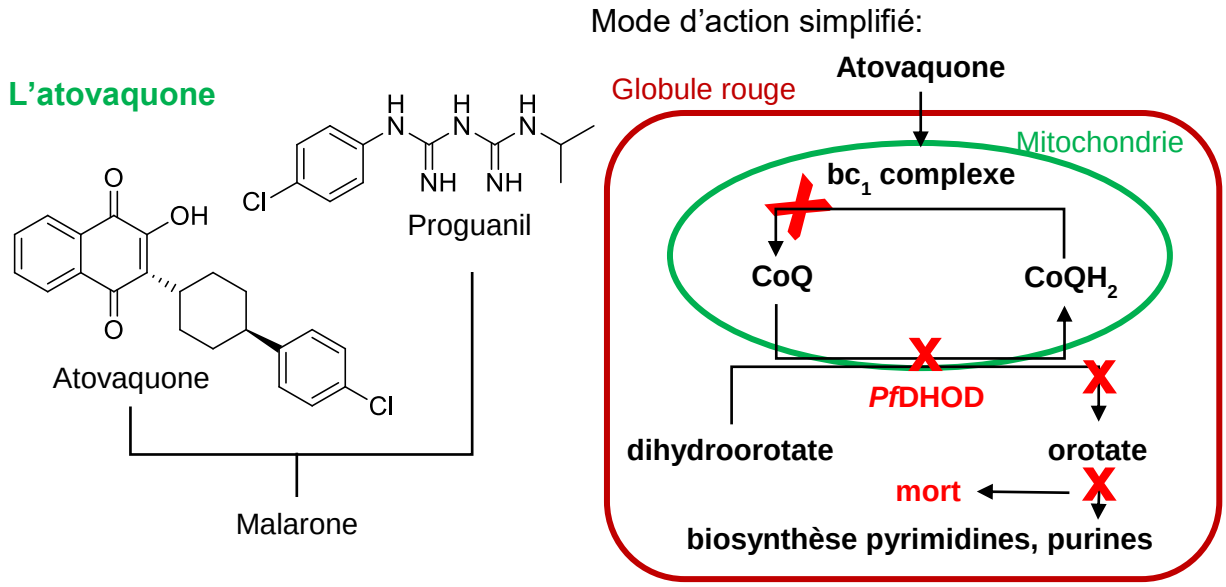

Figure 4: Structure de l'atovaquone et du proguanil. Mode d'action simplifié : le **complexe bc_1** va intervenir dans la chaine de transfert d'électrons mitochondriale du parasite en oxydant la coenzyme **$CoQH_2$** en ubiquinone (**CoQ**), nécessaire à la biosynthèse des pyrimidines et purines à partir de dihydroorotate converti en orotate par l'enzyme dihydroorotate déshydrogénase du parasite (***Pf*DHOD**). L'atovaquone va ainsi se lier au complexe bc_1 empêchant la réoxydation de **$CoQH_2$** et bloquant toute la chaine de transfert d'électron et la chaine de biosynthèse d'acide nucléique.

Le bleu de méthylène :

Le bleu de méthylène (MB)[28], découvert en 1891 par Guttmann et Ehrlich, appartient à la famille des phénothiazines. Il a été utilisé comme antipaludique avant la découverte et le développement de la CQ, mais a progressivement été remplacé par cette dernière en raison de son efficacité moindre *in vivo*. C'est une molécule dite « *redox-cycler* » car elle va agir comme substrat pour la glutathion réductase humaine (*h*GR) ou celle de *P. falciparum* (*Pf*GR). Les deux réductases sont des flavoprotéines dépendantes du NADPH, cofacteur essentiel dans de nombreux processus biologiques, fournissant des électrons (couple rédox $NADPH/NADP^+$).

MB va dans un premier temps être réduit en leucométhylène bleu (leucoMB) grâce à la réductase, puis se réoxyder en réduisant la MetHb-Fe(III) ou l'hème Fe(III) en Hb-Fe(II) ou en hème Fe(II)[29,30]. Ainsi, la croissance du parasite va diminuer (car moins de MetHb-Fe(III) à digérer ; l'OxyHb-Fe(II) n'est pas digérée par les protéases du parasite), la toxicité va augmenter (davantage d'hème libre) et la détoxification de l'hème libre en hémozoïne va être inhibée. Le MB réduit, ou leucoMB, pourra également réduire le dioxygène environnant, produisant des ROS. Cette molécule est utilisée pour traiter la méthémoglobinémie, une

condition congénitale caractérisée par un taux anormal de MetHb-Fe(III) dans le sang. La MetHb-Fe(III) ne pouvant se lier à l'oxygène, le transport de l'oxygène est compromis. Le leucoMB, en tant que *redox-cycler*, réduit le Fe(III) en Fe(II), rétablissant ainsi la capacité de l'hémoglobine à transporter l'oxygène.

1.1.4 Cibler l'équilibre rédox du parasite

La plupart des modes d'actions des antipaludiques actuels se basent sur l'altération de la balance rédox au sein du parasite. L'homéostasie rédox est cruciale pour éviter l'accumulation d'espèces réactives oxydantes, qui rendraient le parasite particulièrement vulnérable, notamment au stade sanguin[31]. Évoluant dans un environnement pro-oxydant riche en fer et en oxygène, le parasite est déjà soumis à un stress oxydant naturel. Ce stress est particulièrement dévastateur pour les jeunes parasites (stade anneaux) qui possèdent peu de défenses métaboliques contre une forte charge oxydante, permettant ainsi de réduire rapidement leur croissance et de limiter le développement de résistances.

Méthodes d'induction du stress oxydant :

- Action directe via des *redox-cyclers* : comme le MB et les 3-benzylménadiones (bMDs voir ci-dessous), agissant comme substrats subversifs, et donc inhibiteurs d'enzymes oxydoréductases-clés. Ces molécules peuvent altérer directement la balance rédox en détruisant l'homéostasie rédox du parasite.
- Action indirecte via la génération de ROS : comme la FQ, la PQ ou l'ART et ses analogues, induisant un stress oxydant en générant des ROS, surchargeant ainsi le système antioxydant du parasite.

La principale modification de la balance rédox est induite par le stress oxydant lié au flux de ROS générés (Figure 5). Le parasite produit naturellement des ROS de diverses manières, principalement via la séquestration de l'OxyHb-Fe(II) de l'hôte dans sa vacuole digestive, conduisant à son oxydation spontanée en MetHb-Fe(III) libérant le dioxygène qui prend l'électron du Fe(II), produisant des anions superoxyde (O_2•-). Ces anions vont être soit détoxifiés pour former du peroxyde d'hydrogène (H_2O_2), soit vont réagir avec le H_2O_2 déjà présent, produisant des HO•. Les HO• sont générés en présence de l'hème Fe(II) libre via la réaction de Fenton (Figure 5). Ces ROS provoquent des dommages irréversibles aux protéines, lipides et acides nucléiques du parasite, contribuant ainsi à sa destruction.

Production de ROS dans *Pf*:

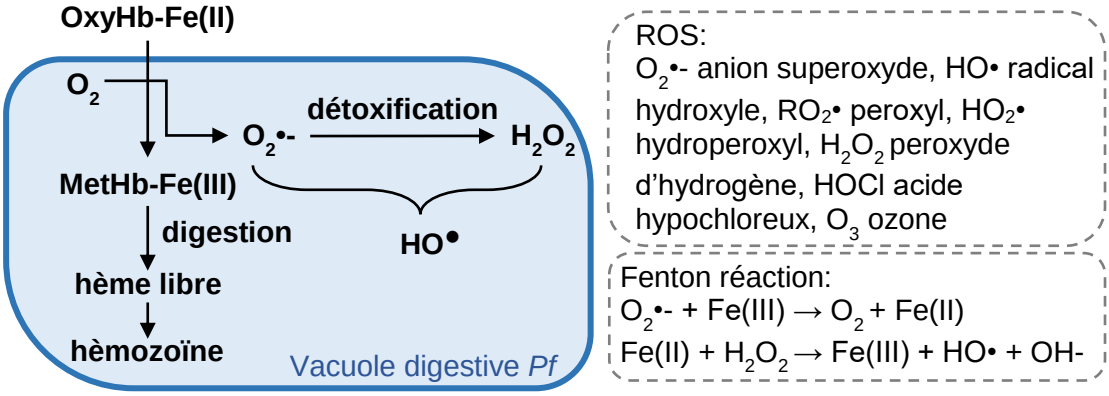

Figure 5: Production d'espèces réactives de l'oxygène (**ROS**) dans *P. falciparum*. Production simplifiée : l'**OxyHb-Fe(II)** est capté par le parasite dans sa vacuole digestive. Il va être oxydé en **MetHb-Fe(III)** par le dioxygène environnant formant l'anion superoxyde **O_2•-**. La majorité de la **MetHb-Fe(III)** est digérée par le parasite produisant notamment de **l'hème Fe(II)** et **Fe(III) libre** qui peut conduire à la production de radicaux hydroxyles **HO•** avec la réaction de Fenton. Le radical **O_2•-** formé peut être détoxifié en peroxyde d'hydrogène **H_2O_2** ou peut réagir avec de l'**H_2O_2** afin de former des **HO•**.

Pour se protéger contre cette suroxydation, le parasite *Plasmodium* dispose de mécanismes enzymatiques et non-enzymatiques dans le cytosol et différentes organelles, comme la mitochondrie.

- **La superoxyde dismutase (SOD)** : Cette enzyme convertit les O_2•- en H_2O_2 et O_2, H_2O_2 pouvant ensuite être éliminé par des péroxydases, réduisant ainsi la toxicité des anions superoxydes.
- **La glutathion réductase (GR)** : Utilisant le couple GSH/GSSG, cette enzyme maintient le glutathion sous sa forme réduite (GSH), essentielle pour neutraliser les ROS.
- **La thiorédoxine réductase (TrxR)** : Utilisant le couple $Trx(SH)_2$/$Trx(S)_2$, cette enzyme régule l'état rédox comme la GR.
- **Les antioxydants** : Des biomolécules comme l'ascorbate de sodium (vitamine C) et le tocophérol (vitamine E) neutralisent les ROS, limitant les dommages oxydatifs.

Les réductases GR et TrxR catalysent les réactions générant ces espèces réductrices, utilisant le NADPH comme source d'électrons. Inhiber ces enzymes ou dépléter leurs cofacteur NADPH pourrait augmenter le stress oxydant dans le parasite[31].

Points clés sur le paludisme, son parasite et les traitements antipaludiques :

i. **Problème persistant** : Le paludisme reste une menace majeure, causant un grand nombre de cas et de décès, ayant un impact économique considérable sur les pays endémiques, et posant des défis de traitement en raison des résistances vaccinales et thérapeutiques.

ii. **Efforts considérables** : De grands efforts sont déployés pour combattre le paludisme, incluant le développement de vaccins, d'insecticides, de mesures préventives (hygiène, éducation), de molécules préventives pour les voyageurs, et de nouveaux traitements thérapeutiques.

iii. **Développement de nouvelles molécules** : Les problèmes de résistance ont conduit au développement de nombreux antipaludiques avec divers modes d'action, l'altération de l'homéostasie rédox du parasite étant une cible privilégiée.

iv. **Résistances aux traitements** : L'utilisation prolongée des mêmes antipaludiques comme les CTAs a favorisé l'émergence de résistances, limitant l'efficacité des traitements.

v. **Recherche continue** : Une recherche constante en biologie et chimie médicinale est cruciale pour améliorer les traitements existants, découvrir de nouvelles molécules actives, et identifier de nouvelles cibles biologiques pour combattre le paludisme de manière plus efficace.

1.2 La plasmodione, les 3-benzylménadiones et leurs synthèses.

Préambule

Dans cette section, nous examinerons le développement et la synthèse de la famille de composés des 3-benzylménadiones (bMDs). Plusieurs points clés ont influencé le choix de cette stratégie antipaludique conduisant à ces composés :

i. **Ciblage du système antioxydant du parasite** : Utiliser une molécule *redox-cycler* comme le MB est une stratégie efficace contre le paludisme. Ces molécules peuvent perturber l'équilibre rédox du parasite, rendant son environnement toxique.

ii. **Inhibition de la *Pf*GR** : Inhiber la *Pf*GR et modifier la production de GSH tout en déplétant le stock cellulaire de NADPH pourrait mener à des molécules efficaces contre les souches résistantes à la CQ.

iii. **Génération des ROS** : La production de ROS et la diminution d'espèces réductrices ou l'altération de systèmes antioxydants sont des moyens efficaces de rendre l'environnement du parasite intolérable, menant à sa mort.

iv. **Élimination rapide du parasite** : En basant le développement d'antipaludiques sur cette stratégie, l'objectif est d'éliminer rapidement le parasite, en ciblant principalement le stade des jeunes anneaux, comme l'atteste le travail déjà réalisé avec la plasmodione[32].

v. **Mutation du gène G6PD** : Les mutations du gène de la glucose-6-phosphate déshydrogénase (G6PD) dans les pays endémiques sont associées à une protection des porteurs vis-à-vis des épisodes de paludisme sévères. L'enzyme G6PD est responsable de la régénération du NADPH à partir de $NADP^+$ et du glucose-6-phosphate. Les mutations

conduisent à un flux diminué du NADPH dans les globules rouges. Comme le NADPH est le principal cofacteur des GRs du globule rouge parasité (*h*GR et *Pf*GR), ces mutations protègent l'hôte en créant un flux continu de ROS chez le porteur des mutations. Ces dernières ne sont pas létales, et n'entraînent pas un pronostic défavorable en terme de longévité du porteur, ni ne sont associées à des comorbidités (cancers, …). Mimer l'effet de ces mutations par des petites molécules qui consomment en continu le NADPH, appelées substrats subversifs d'oxido-réductases ou *redox-cyclers*, a été la stratégie suivie par mon équipe d'accueil. Cette observation a encouragé l'exploration de stratégies augmentant le stress oxydant chez le parasite[33].

1.2.1 L'origine

Les 3-benzylménadiones antipaludiques, découvertes en développant la chimie de la ménadione (vitamine K_3), peuvent être divisés en deux parties bien distinctes : la partie « ouest » correspondant à la ménadione et la partie « est » correspondant au groupement benzylique (Figure 6). La ménadione est composée d'un motif 1,4-naphtoquinone (NQ) et possède des propriétés rédox dues à la présence de la quinone. Les quinones constituent une classe importante de composés retrouvés dans les plantes, champignons, bactéries, ainsi que dans de nombreuses vitamines (vitamine K_1, K_2, K_3), anticancéreux[34], antibactériens[35], antifongiques, ou encore colorants[36]. C'est un motif très répandu en chimie, offrant une réactivité variée pour diverses réactions d'addition de Michael ou de cycloaddition, et est également utilisé pour ses propriétés rédox. En effet, la NQ peut subir deux réductions réversibles à un électron, formant d'abord la semi-NQ• puis la dihydro-NQ dans un milieu protique (Figure 6). La partie « est » benzylique confère, quant à elle, un certain poids moléculaire, une rigidité et des propriétés physicochimiques et pharmacologiques (PC/PK) nécessaires à son activité biologique. Elle apporte également une stabilité métabolique supplémentaire en bloquant l'un des sites réactifs électrophile de l'électrophore quinone, par exemple vis-à-vis de l'addition de Michael par le glutathion.

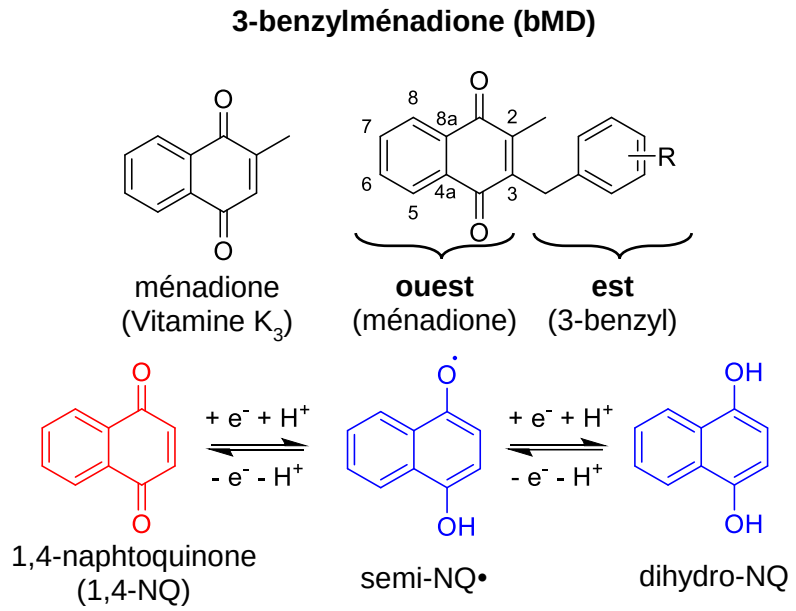

Figure 6: Structure de 3-benzylménadione dérivé de la ménadione ainsi que l'équilibre rédox en condition protique de la NQ.

C'est dans les années 1980 que le motif NQ a commencé à être introduit dans des molécules antiparasitaires[37]. Par exemple, on retrouve le lapachol[38] et ses dérivés communs pinnatal[39], isopinnatal, sterekunthal A ou B, ainsi que la plumbagone (plumbagin), la juglone, la lawsone et l'atovaquone.

- L'une des propriétés intéressantes de la ménadione est son potentiel à inhiber la réduction de la glutathion disulfure (GSSG) en GSH catalysée par la *Pf*GR[40] **(1)** (Figure 7).
- Tout comme le MB, les dérivés de la ménadione agissent comme des substrats de cette enzyme et sont donc des *redox-cyclers*. En effet, ces substrats se réduisent à la place du GSSG (normalement réduit en GSH) **(2)** (Figure 7).
- De plus, ces substrats sont dits « subversifs » car ils peuvent être oxydés et réduits de manière catalytique, selon leur état réduit ou oxydé de départ, transformant ainsi le rôle initial de la réductase en une oxydase **(3)** (Figure 7) produisant en présence d'oxygène un flux continu de ROS.
- Surtout, cette réoxydation peut s'effectuer grâce à la réduction de la MetHb-Fe(III) en Hb-Fe(II), privant ainsi le parasite de ses nutriments et inhibant sa croissance **(4)** (Figure 7).
- L'hème Fe(III) libre peut également servir d'oxydant, produisant l'hème Fe(II) libre toxique, ce qui empêche sa détoxification en hèmozoïne **(5)** (Figure 7).

Pour résumer, ces composés peuvent être appelés « substrats subversifs » ou « *redox-cyclers* ». Ils consomment le NADPH et inhibent la *Pf*GR, créant une déperdition d'espèces réductrices et contribuant à la génération de stress oxydant. De plus, ils conduisent à deux problèmes majeurs : la séquestration des nutriments du parasite (arrêt de la croissance) et l'inhibition de la formation de l'hèmozoïne (accumulation d'espèces toxiques).

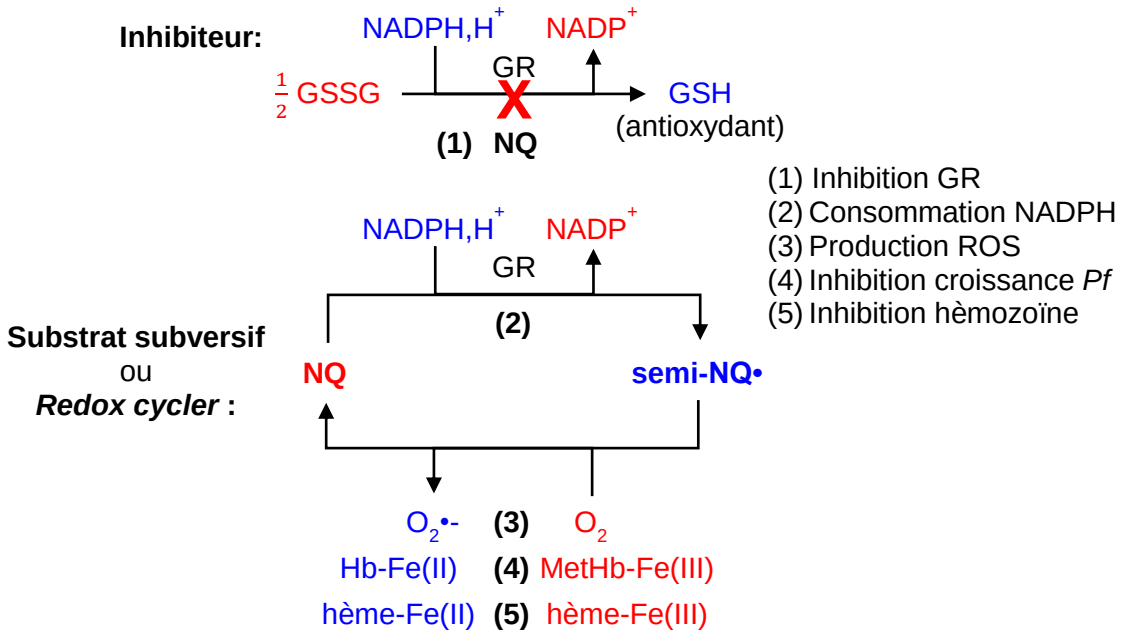

Figure 7: (1) la **NQ** (ou MB ou bMD) agit comme inhibiteur de la GR empêchant la production de GSH; **(2)** la **NQ** subit une réduction à un électron par le couple NADPH/NADP+ catalysé par le GR, consommant la NADPH; **(3)** la **semi-NQ•** peut subir une oxydation à un électron soit par le O_2 produisant des ROSs; **(4)** soit par la MetHb-Fe(III) inhibant la croissance du parasite; **(5)** soit par l'hème-Fe(III) inhibant sa détoxification en hèmozoïne.

- La plasmodione et les bMDs sont des pro-drogues, des benzoylménadiones qui agissent comme de très bons inhibiteurs de la *h*GR et de la *Pf*GR. Cependant, la bioactivation des bMDs a besoin de la présence du parasite qui produit de la MetHb, l'accepteur d'électrons pour la benzoylménadione réduite. Pour rappel, le globule rouge sain est quasiment dépourvu de MetHb. Par ailleurs, à la différence des autres cellules de l'hôte, la production de NADPH ne repose que sur l'expression de la voie des pentoses phosphates, dont la 1ère enzyme est la G6PD, dans les globules rouges. D'autres voies de production du NADPH sont exprimées dans toutes les cellules nucléées chez l'Homme.
- De plus, le stress oxydant est rapidement compensé dans un environnement sain grâce à d'autres mécanismes biologiques, alors que le parasite dans le globule rouge a peu de réponse face à ces conditions hostiles.
- Les mutations du gène G6PD dans les pays endémiques au paludisme illustrent parfaitement ce point[33]. Ce gène est responsable de la production de NADPH, et sa mutation entraine une forte diminution de la génération du NADPH en flux continu, conduisant à une inhibition de la *h*GR et à un stress oxydant accru. Les humains atteints

de cette mutation vivent parfaitement bien, cependant, ceux qui sont porteurs de mutation G6PD et atteints de paludisme sont beaucoup moins affectés par la maladie.

Pour conclure, ces mutations du gène G6PD affectent négativement la multiplication du parasite (par privation de son nutriment et par stress oxydant) et le maintien de l'infection, tandis que les globules sains continuent leur développement. C'est exactement l'effet produit par notre série de composés antipaludiques.

1.2.2 La plasmodione

C'est ainsi que mon équipe d'accueil, et plus particulièrement le Dr. Elisabeth Davioud-Charvet, a développé la première génération de bMDs antipaludiques agissant comme substrat subversif de la GR. Le composé nommé M_5 publié en 2001[40], est un *redox-cycler* portant une chaine grasse et un groupement acide carboxylique sur sa partie « est ». Ce composé étant trop polaire et trop lipophile, une stratégie de masquage « pro-drogue » de la fonction acide en un ester métabolisable a été mise en place. Beaucoup de dérivés du M_5 masquant cette fonction ont été décrits, tels que des esters, des tétrazoles[41], ainsi que des aminoquinoléines ayant un double effet d'inhibition grâce aux motifs ménadione et aminoquinoléine de type « CQ ». Les premiers résultats d'activité et d'inhibition ont apporté beaucoup d'espoir en cette stratégie antipaludique. Afin de valider la *Pf*GR comme cible biologique des dérivés ménadione, un substrat suicide a été développé. La présence d'un groupement partant (fluoro-M_5) en β du carbonyle de la quinone a servi de site d'attaque à un nucléophile biologique (par exemple un thiol). Ainsi, un adduit fluoro-M_5-GR irréversible a pu être obtenu et cristallisé, validant cette cible[42]. Cependant, ce composé étant peu actif contre *P. falciparum*, ces substrats-suicides n'ont pas été choisis pour de futurs développements antipaludiques, car en alkylant la GR, l'enzyme ne peut plus bioactiver la ménadione. Ces résultats suggèrent que les substrats-subversifs doivent rentrer dans des cascades rédox sans alkyler les oxydoréductases responsables de la production des ROS et des métabolites toxiques pour le parasite.

Quelques années de développement ont suivi, conduisant aux premiers 3-benzylménadiones (bMDs) développés par Müller T. *et al.* en 2011[29]. La plasmodione (PD) a ainsi été décrite pour la première fois. Elle est fonctionnalisée par un groupement trifluorométhyle (CF_3) en position para du benzyle et est toujours considérée comme la molécule de référence de cette famille de composés (Figure 8). Son activité est principalement due à l'ajout du groupement benzylique-CF_3 sur la ménadione. Il est également important de mentionner que le méthyle en position 2 de la NQ est indispensable à l'activité du composé. Ce composé a la particularité d'être actif dans le bas nanomolaire sur les souches résistantes à la CQ (*Pf*Dd2), tout en étant peu toxique sur les cellules saines humaines. Elle cible le stade

sanguin anneau du parasite mais aussi son stade sexué gamétocyte jeune, comme le MB, conduisant à une efficacité antipaludique rapide *in vitro*, diminuant la parasitémie aussi rapidement que l'ART. Cependant, elle présente une activité modérée *in vivo* sur le modèle murin *(P. berghei)*[43]. C'est pourquoi de futurs développements sont envisagés afin d'améliorer sa biodisponibilité ou de réduire sa métabolisation.

Mode d'action de la plasmodione

Très rapidement, la plasmodione (PD) a été considérée comme une molécule pro-drogue. L'effet pro-drogue, bien connu en chimie médicinale, permet à une molécule inactive d'être bioactivée en une molécule active. Ce phénomène est possible grâce à un mécanisme enzymatique apportant une modification structurale à la molécule initiale. Dans le cas de la PD et des bMDs en général, une fois internalisés dans le parasite, ces composés subissent une oxydation benzylique, produisant une 3-benzoylménadione (PD-Oxyde ou PDO si PD est utilisée) (Figure 8). Ce métabolite benzoyle est actif s'il est généré *in situ* dans le parasite, et plusieurs points importants ont confirmé ce mécanisme :

i. Si le carbone benzylique de la bMD est fonctionnalisé par un méthyle (bloquant ainsi l'oxydation benzylique) l'activité sur *P. falciparum* est perdue[29].
ii. Lorsque le métabolite benzoyle est directement utilisé comme molécule antipaludique, aucune activité n'est observée, probablement en raison d'une faible internalisation (justifiant une bioactivation uniquement dans le parasite)[29].
iii. Une étude *in tubo* utilisant la plasmodione enrichie en $^{13}C_{18}$ en présence de *Pf*FNR (férredoxine-NADP+, réductase de l'apicoplaste) et de G6PD (afin de générer de la NADPH) a montré, après une analyse de masse, la présence du métabolite 3-benzoylménadione formé[44].
iv. Les dérivés benzyliques sont de mauvais substrats de la *Pf*GR et de la *h*GR et leur capacité à réduire l'hémoglobine ou l'hématine est faible par rapport aux dérivés benzoyles[33,45].

En conclusion, cet effet est cohérent et permet de produire une molécule plus polaire et plus oxydante, améliorant son affinité pour la *Pf*GR et sa capacité à être réduite.

Le mode d'action détaillé de la PD et des bMDs en général sur *Pf* a donc pu être envisagé et démontré (Figure 8) :

- Une fois internalisée dans le globule rouge parasité, la **PD** subit une oxydation en position benzylique (**PDO_{ox}**) par un mécanisme rédox faisant intervenir la *Pf*FNR[45], le couple NADPH/$NADP^+$ et le dioxygène.
- La **PDO_{ox}** (métabolite I) est ainsi formée et entre dans la cascade rédox responsable de l'activité antipaludique.

- Étant très oxydante, **PDO_{ox}** est d'abord réduite par la *Pf*GR grâce au cofacteur NADPH/NADP+ (réduction à 1 électron) en **PDO_{red}** (métabolite II).
- La **PDO_{red}** va être réoxydée en **PDO_{ox}**, réduisant la MetHb-Fe(III) ou/et l'hème-Fe(III) en Hb-Fe(II) et/ou hème-Fe(II).
- Ces réductions entraînent deux conséquences : inhibition de la croissance du parasite en le privant de sa source de nutriments MetHb-Fe(III) et inhibition de la détoxification de l'hème-Fe(III) en hèmozoïne, créant un stress oxydant et une suroxydation des constituants membranaires en peroxydes, comme les lipides. De plus, les espèces Fe(II) peuvent se réoxyder, produisant des ROS augmentant le stress oxydant dans le parasite. Ainsi, on peut observer la formation de ferrylHb-Fe(IV)=O à partir de la MetHb-Fe(III) ou la dégradation totale de l'hème avec la réaction de Fenton. La ferrylHb peut se réduire en MetHb-Fe(III) ou se dégrader en formant une espèce insoluble, l'hémichrome[46].
- La forme **PDO_{red}** peut également subir un couplage oxydatif phénolique produisant la **benzoxanthone** (métabolite III), capable d'inhiber la formation d'hèmozoïne, comme peut le faire la CQ. Il est intéressant de noter que lorsque les sites en ortho du benzyle sont fonctionnalisés, le composé est moins actif (formation de la benzoxanthone bloquée).

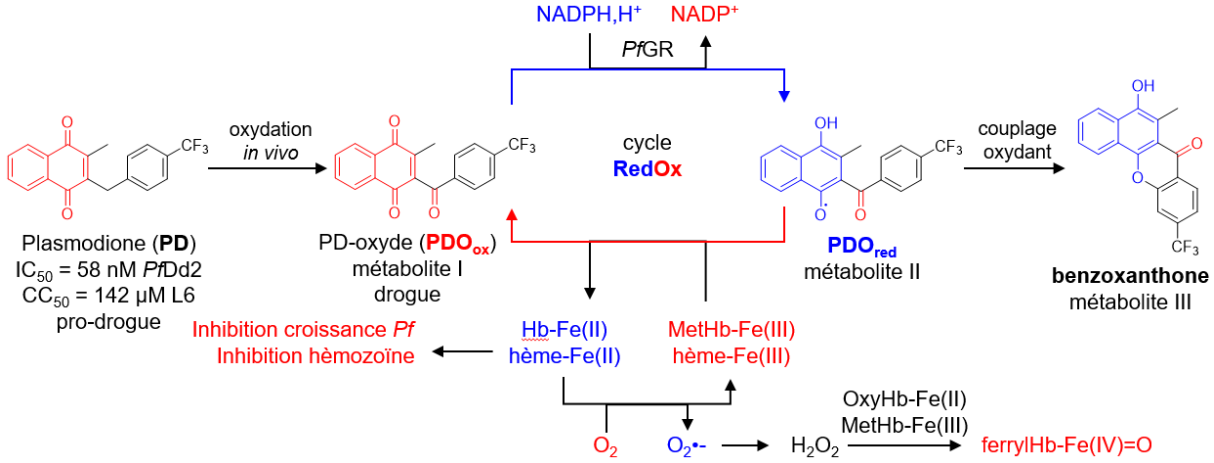

Figure 8: Mode d'action de la **PD** et des bMDs en général. CC_{50} (L6) = concentration requise du composé pour observer une diminution ou élimination de 50% de cellules saines L6 de rat. IC_{50} = concentration requise de l'inhibiteur pour observer une diminution ou élimination de 50% de l'antagoniste. IC_{50} obtenu avec l'essai SYBR® green.

Pour conclure, cela a permis de déterminer précisément son mode d'action ainsi que les métabolites formés. Cette famille de composés répond aux critères fixés dans le préambule, prouvant que les bMDs ont un fort potentiel de développement en tant que molécules antipaludiques/antiparasitaires. Cependant, la *Pf*GR n'est probablement pas la seule oxydoréductase cible du parasite impliquée, et davantage de recherches sont nécessaires pour toutes les identifier et les étudier.

1.2.3 La synthèse des 3-benzylménadiones

Préambule

Nous allons dans cette partie explorer les méthodes de synthèse permettant d'obtenir les 3-benzylménadiones et leurs dérivés. Lors du développement d'un composé bioactif, il est crucial pour un chimiste de trouver des solutions de synthèse afin de créer un large éventail de diversifications structurales. Ces diversifications, évaluées en fonction des résultats d'activité sur le pathogène, permettent de déterminer les bénéfices d'une fonction chimique par rapport à une autre. En chimie médicinale, ces relations sont appelées Relations Structure-Activité (RSA).

Dans notre cas, la PD est déjà active au nanomolaire *in vitro* sur les souches résistantes à la CQ, mais elle présente également des problèmes de solubilité, de lipophilicité et donc de biodisponibilité *in vivo*. Notre rôle de chimistes est de générer une librairie de composés bMDs avec diverses modifications structurales spécifiques. Ces modifications nous permettront de faire varier les propriétés PC/PK de la molécule. Le but est de rendre cette famille de composés plus active, moins toxique, moins métabolisable, tout en vérifiant et en investiguant ses cibles biologiques.

Partie « ouest » et RSA

Dans cette section, nous allons revenir sur les travaux antérieurs de synthèse concernant la partie « ouest » de la bMD et leurs RSAs. La NQ étant fonctionnalisable, de nombreuses modifications ont été apportées sur cette partie. Plusieurs voies de synthèse permettent d'obtenir diverses NQs, mais nous détaillerons ici uniquement les principales utilisées par notre équipe : la stratégie Diels-Alder et la stratégie naphtol.

La stratégie Diels-Alder :

Cette réaction de cycloaddition [4+2] utilise la quinone comme diénophile grâce à ses deux carbonyles électroattracteurs[47]. Elle est souvent employée comme synthon clé pour la synthèse de diverses molécules complexes. La complexité en chimie est souvent liée à la chiralité, c'est pourquoi de nombreuses de méthodologies de synthèse ont été développées pour contrôler la régio- et stéréosélectivité de cette réaction[48,49]. Plus d'informations concernant ce point seront traitées dans le chapitre quatre de cette thèse.

Cette stratégie de synthèse nous a permis d'introduire une grande diversité de substituants sur la ménadione[44,50–52], notamment des groupements méthyles et hydroxyles. Cinq dérivés ménadiones monométhyle ou diméthyles ont pu être obtenus en deux étapes grâce à la cycloaddition de Diels-Alder catalysée par l'acide de Lewis $ZnBr_2$ en présence de pyridine afin d'éliminer et de piéger le HBr formé *in-situ*. Ensuite, le DDQ permet de réaromatiser afin de restaurer les NQs ciblées avec des rendements modérés à bons (Figure 9).

Le diène de Danishefsky permet quant à lui d'obtenir deux NQs phénoliques en une seule étape. Le HBr généré permet de déprotéger le TMS, entraînant une cascade de réactions qui élimine le méthoxy, puis la réaromatisation permet d'obtenir les dérivés phénoliques en présence de pyridine (Figure 9). Ces dérivés peuvent ensuite subir diverses post-fonctionnalisations afin de produire des NQs ester, amide ou phosphate (Figure 9).

Enfin, une réaction aza-Diels-Alder est possible pour obtenir les aza-ménadiones souhaitées en une étape. Cette réaction domino génère, une fois le cyclo adduit formé, de l'HBr et de la Me_2NH, qui sera piégée par un excès de Ac_2O, donnant les dérivés voulues avec des rendements modérés (Figure 9).

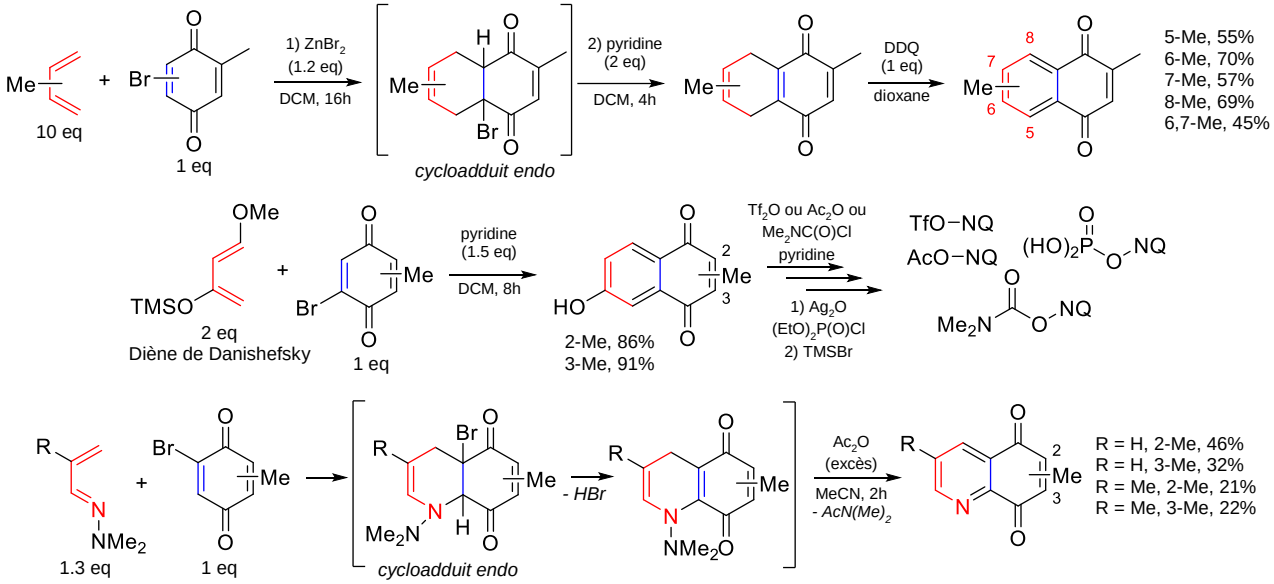

Figure 9: Synthèse de (di)méthyl-ménadiones, d'hydroxy-ménadione (et ses dérivés après post-fonctionnalisation) et d'aza-ménadiones par réaction de Diels-Alder ou aza-Diels-Alder.

Une fois la partie « est » benzylique fonctionnalisée, nous avons pu obtenir des RSAs indispensables à la compréhension des conséquences de ces modifications. En termes d'activité sur *P. falciparum* (IC_{50} sur *Pf*Dd2, SYBR green), la plupart des modifications conduisent à une perte d'activité antipaludique. Néanmoins, certains composés ont montré un potentiel notable : 6-Me/4'-CF_3 (215 nM); 6-Me/4'-Br (171 nM); 6-$P(O)_4(Et)_2$/4'-CF_3 (157 nM); 6-OH/4'-CF_3 (107 nM), indiquant que la position 6 est mieux tolérée que la position 7 (Figure 10).

Concernant les aza-bMDs, ils sont pour la plupart peu actifs, montrant que le *N*-hétérocycle sur la partie « ouest » est peu toléré. En termes de cytotoxicité, aucun changement significatif n'a été observé par rapport à la PD, sauf pour les aza-bMDs, qui sont pour la plupart plus toxiques. Les propriétés PC et PK doivent être évaluées au cas par cas. Les groupements hydroxyles, phosphates, amides et esters améliorent considérablement la solubilité et la polarité de la molécule. Introduire un groupement *N*-hétérocycle sur une molécule aromatique

bioactive est une méthode bien connue en chimie médicinale pour améliorer ses propriétés PC et PK[53], cet effet est donc observé pour les aza-bMDs.

Modifier le noyau NQ affecte les propriétés rédox du composé, un paramètre crucial pour l'activité antipaludique[54]. Seules les molécules fonctionnalisées par un groupement hydroxyle, phosphate et les aza-bMDs vont modifier les potentiels rédox de la quinone. Ces groupements, sont sensibles au pH et sont des donneurs de liaisons hydrogènes, altérant significativement les potentiels rédox. Les aza-bMDs, quant à elles, rendent généralement la molécule plus oxydante et sont donc plus facilement réductibles[52].

Le choix d'une fonctionnalisation en position 6 et 7 est aussi stratégique pour comprendre et améliorer la demi-vie et la biodisponibilité du composé. Des analyses (HPLC-MS) des urines de souris traitées avec de la PD ont révélé la présence des composés 6-OH/4'-CF_3, 7-OH/4'-CF_3, et benzoxanthone[44]. Bloquer ces voies métaboliques et synthétiser les métabolites formés est donc essentiel pour mieux comprendre ces mécanismes et améliorer l'activité des composés.

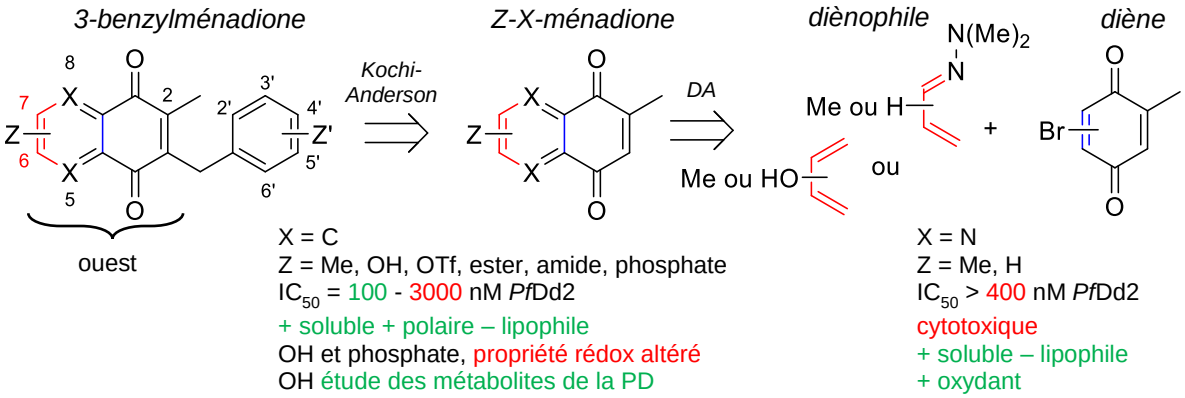

Figure 10: Stratégie utilisant la cycloaddition de Diels-Alder (DA), ainsi que les conséquences structurales sur l'activité antipaludique, la cytotoxicité, les propriétés PC/PK et les propriétés rédox. Kochi-Anderson: acide phénylacétique, $AgNO_3$, $(NH_4)_2S_2O_8$, CH_3CN:H_2O, 90°C, 4h.

La stratégie naphtol :

Cette voie de synthèse offre plus de possibilités de modifications structurales, mais elle est plus contraignante car plus longue et moins reproductible (rendement globale variant entre 20 et 40%) (Figure 11). Le naphtol peut être obtenu à partir de deux substrats différents : une α-tétralone ou une propiophénone[50,55]. À partir de la α-tétralone, trois étapes sont nécessaires pour synthétiser le naphtol. Il peut également être formé à partir de la propiophénone en quatre étapes. Enfin, la Z-ménadione peut être obtenue après oxydation du naphtol en présence de

PIDA[56], puis engagée dans une réaction de Kochi-Anderson afin de former la bMD souhaitée (Figure 11).

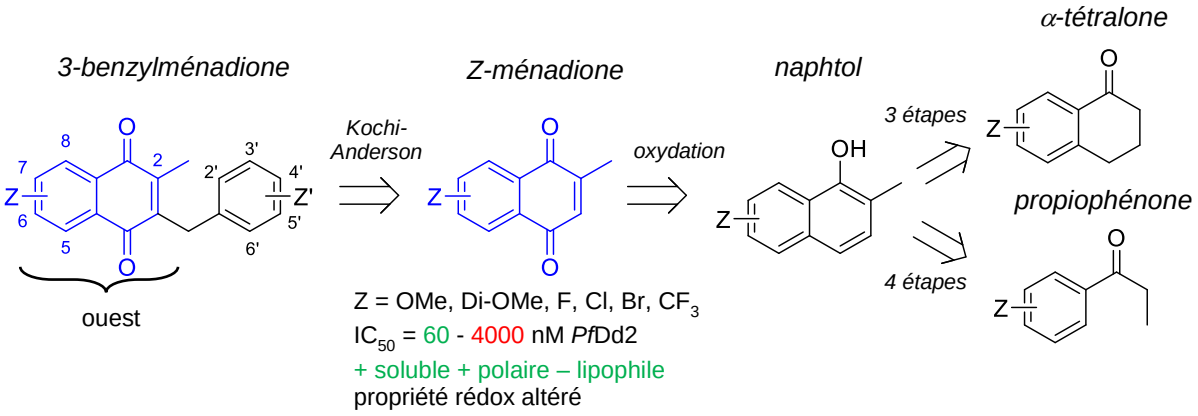

Figure 11: Stratégie basé sur la synthèse du naphtol, ainsi que les conséquences structurales sur l'activité antipaludique, les propriétés PC/PK et les propriétés rédox. Oxydation: PIDA, MeCN:H_2O, 0°C, 2h.

Des bMDs fonctionnalisées par des halogènes, des groupements méthoxy ou CF_3 ont ainsi été obtenues. L'activité de ces composés fonctionnalisés en position 6 (IC_{50} sur *Pf*Dd2, SYBR green) est très prometteuse : 6-OMe/4'-CF_3 (186 nM); 6-F/4'-CF_3 (59 nM); 7-F/4'-CF_3 (83 nM); 6-Cl/4'-CF_3 (242 nM); 6-CF_3/3'-OMe/6'-OMe (57 nM). Ces résultats confirment que bloquer la métabolisation de la PD en 6-OH/4'-CF_3 ou 7-OH/4'-CF_3 est une stratégie payante. De plus l'introduction d'un fluor permet de profiter de ces propriétés PC et PK bénéfiques (lipophilicité, pKa, polarité, accepteur de liaison H). Les propriétés rédox seront altérées par l'effet électroattracteur des halogènes, rendant la bMD plus oxydante.

Fonctionnalisation de la position 2 de la NQ :

La position 2 de la NQ peut également être fonctionnalisée. Cette position est nécessaire à l'activité du composé, le protégeant d'éventuelles attaques nucléophiles. Un fluor a déjà été fonctionnalisé sur ce méthyl (fluore-M_5) pour créer un adduit drogue-cible grâce au marquage covalent lors de la réduction de la NQ, mais cette modification n'a pas induit d'effet bénéfique sur l'activité[42].

Cependant, cette stratégie a été récemment revue plus en détails au sein de mon équipe d'accueil. Le composé PDO-CH_2-F en position 2 produit une fluorescence jaune importante dans les cellules de tabac BY-2 (modèle) après incubation. Grâce à l'ortho-quinone méthylène formée par réduction photochimique ou enzymatique, un nucléophile (thiol) peut attaquer cette ortho-quinone méthylène ou une réaction intramoléculaire peut former une anthrone. Les espèces réduites peuvent conduire à un mécanisme d'ESIPT (transfert de proton intramoléculaire à l'état excité) produisant une fluorescence intense jaune (570-580 nm)[57]. Ces

composés agissent ici comme pro-fluorophore après alkylation d'une protéine et réduction de la NQ.

La fonctionnalisation de cette position par un groupement partant ou un groupement électroattracteur rendra la NQ plus oxydante et renforcera le caractère électrophile du C-2, conduisant à une diminution de son activité antipaludique. Un groupement hydroxyle a aussi été introduit comme sur l'atovaquone, mais la molécule finale n'est pas active sur le parasite (2-OH/4'-CF_3 (3136 nM)).

Globalement, les modifications structurales apportées sur la partie « ouest » des bMDs ne permettent pas nécessairement d'améliorer l'activité antipaludique mais ont un effet bénéfique sur les propriétés PC et PK de nos composés. Ces modifications impactent les propriétés rédox de la molécule, principalement du fait de leur proximité avec l'électrophore NQ. Ces travaux nous ont permis de mieux comprendre le mode d'action de nos molécules grâce à la synthèse de métabolites de la PD ou de substrats subversifs.

Partie « est » et RSA

Pour apporter suffisamment de diversité structurale sur la partie « est » de la molécule, trois stratégies ont être mises en place :

La stratégie « tétralone express »[44] : Cette méthode, largement utilisée par le passé, a été remplacée par la deuxième stratégie car plus rapide et plus versatile.

- À partir d'une α-tétralone, une condensation avec un benzaldéhyde est réalisée en conditions basiques.
- Une aromatisation catalysée par du $RhCl_3$ permet d'obtenir le benzylnaphtol.
- Une oxydation au PIDA conduit au noyau NQ.
- La position 2 peut être fonctionnalisée par réaction de Kochi-Anderson avec l'acide correspondant afin d'obtenir la bMD en quatre étapes (Figure 12).

Cette voie permet d'introduire de la diversité structurale en position 2 de la NQ grâce aux différents acides utilisés. Elle a été utilisée avec l'acide acétique pour synthétiser la plasmodione enrichie en ^{13}C afin d'étudier les métabolites de la PD *in vivo* (rendement global 25%) mais cette dernière réaction est réalisée avec un faible rendement (Figure 12).

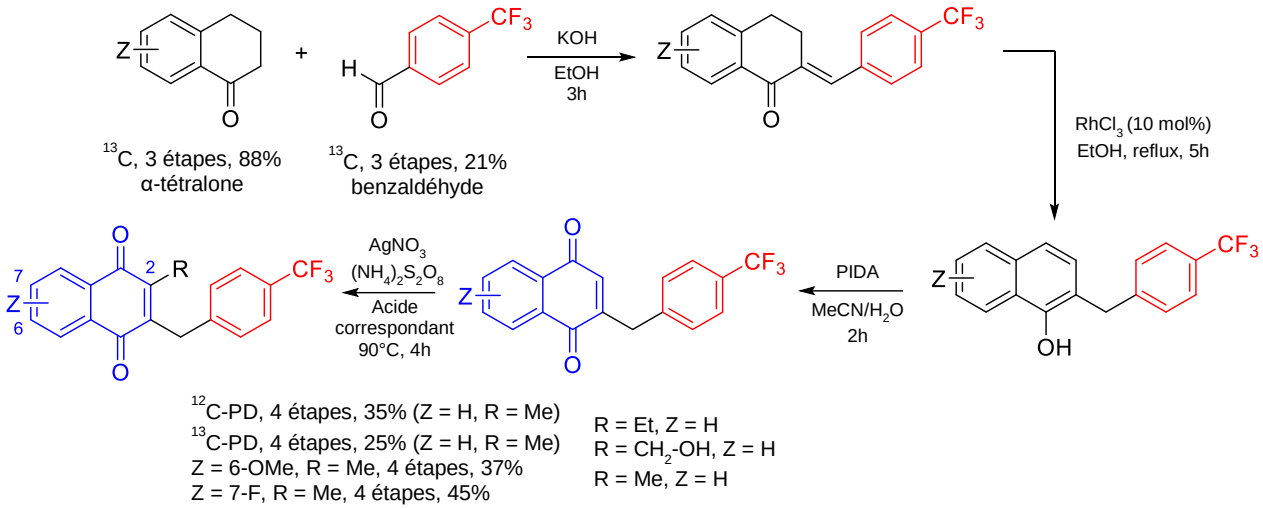

Figure 12: Synthèse de la plasmodione (PD), de la plasmodione enrichie en ^{13}C et de dérivés fonctionnalisés en position 2, 6, 7 utilisant la stratégie tétralone express.

La stratégie Kochi-Anderson : Elle offre un large choix de possibilités et dépendra des compatibilités réactionnelles par rapport aux substituants que l'on souhaite introduire. La réaction de Kochi-Anderson[58] est la plus utilisée par mon équipe d'accueil, car une grande variété de cycles aromatiques peut être introduite rapidement, avec dans la majorité des cas de très bons rendements.

- Cette réaction de décarboxylation radicalaire catalysée par l'argent (II) nécessite un acide phényle acétique souvent commercial et une quinone comme substrat (Figure 13).

Elle permet d'obtenir la plasmodione à partir de la ménadione et de l'acide trifluorométhyle-phénylacétique en une étape avec un rendement de 80%. Cependant, certains substrats comme les dérivés amides, aminés et *N*-hétéroaromatiques, sont incompatibles avec cette réaction[59].

Les couplages $C(sp^2)$-$C(sp^3)$[60] : Cette stratégie incluant le couplage de Suzuki-Miyaura[61], le couplage de Negishi ou d'autres couplages métallo-catalysés (Figure 13). Ces couplages ont l'avantage d'être extrêmement tolérants et ils offrent d'innombrables possibilités de fonctionnalisation et de post-fonctionnalisation. De plus, un large choix de substrats de départ est commercial.

- Si le substrat n'est pas commercial, les dérivés borés peuvent être obtenus grâce à la réaction de borylation de Miyaura[62].
- La ménadione étant sensible aux conditions basiques/nucléophiles, une protection des carbonyles est nécessaire pour les couplages ou post-fonctionnalisations problématiques, suivie d'une déprotection oxydante pour obtenir le produit final (Figure 13).

Plus de détails concernant l'introduction de dérivés *N*-hétéroaromatiques utilisant ces stratégies de couplage C-C seront donnés dans le chapitre 2 de cette thèse.

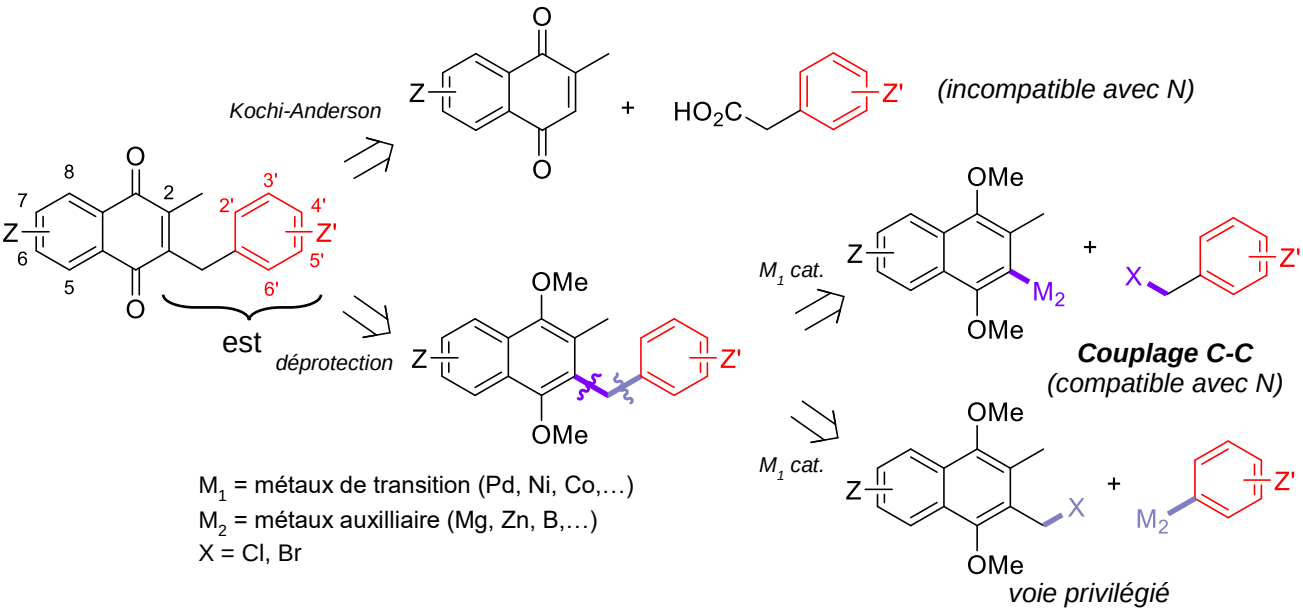

Figure 13: Stratégie de synthèse basé sur la réaction de Kochi-Anderson ou sur un couplage C-C. Déprotection: CAN, MeCN:H_2O, 1:1, 1h.

Ces deux dernières stratégies de synthèse ont permis d'obtenir la majeure partie des bMDs nécessaires pour compléter les RSAs, étudier leurs cibles biologiques, leurs métabolites, et leurs propriétés PC et PK.

<u>Autres possibilités de synthèse :</u>

D'autres possibilités de synthèse ont été étudiées au sein du laboratoire, notamment basées sur des alkylations C-H radicalaires. Ces méthodes ont été détaillées dans une revue publiée par Donzel M. *et al.*[63] en 2021, qui résume les différentes possibilités d'alkylation radicalaire, y compris la décarboxylation (comme la Kochi-Anderson), l'abstraction de protons, ou la réduction C-halogène. Mon équipe d'accueil a développé une nouvelle stratégie d'alkylation C-H sur la ménadione. À partir d'un bromure de benzyle, le fer(II) formé in situ à partir de fer (III) dans une cascade (photo)rédox catalyse la réduction de la liaison C-Br, créant un radical benzylique capable de s'additionner sur la ménadione sous irradiation visible (420 nm), produisant la bMD désirée[64].

D'un point de vue RSAs, plusieurs composés synthétisés présentent des activités similaires à la plasmodione PD[29,59] (IC_{50} sur *Pf*Dd2, SYBR green) comme 4'-Br (46 nM), 4'-F (79 nM), 4'-OH (55 nM), 4'-tBu (54 nM), 4'-NHBoc (42 nM), 4'-alcyne (49 nM), 4'-CF_3/5'-F (101 nM), 3'-OMe/6'-OMe (67 nM), 3'-Br/6'-Br (27 nM). Les amines primaires, secondaires et tertiaires ainsi que les groupements nitro, ester et cyano ne sont pas tolérées. Les substituants en position ortho sont moins tolérés que la position para 4'. Ces résultats sont en accord avec le blocage de la génération du métabolite (III), la benzoxanthone. De plus, une très bonne

activité a été observée pour les disubstitutions sur les positions 3' et 6' ou 5'. Toutefois, ajouter un autre groupement benzylique sur la partie « est » réduit considérablement l'activité antipaludique.

Concernant les propriétés PC et PK, elles vont être grandement affectées selon la nature des substituants introduits. Enfin, du fait de la distance plus importante entre la quinone et la partie benzylique, les propriétés rédox sont généralement peu altérées.

Nouvelles directions de recherche :

Afin d'améliorer la biodisponibilité des bMDs, de nouveaux projets ont été initiés pour introduire des modifications structurales plus complexes, apportant des effets bénéfiques. Ces modifications incluent :

- Di et tri-substitutions sur la partie benzylique (en position 3', 4', 5' ou 6') et la synthèse de régioisomères correspondants.
- Introduction de groupements spécifiques (en plus du CF_3 dans certain cas) : oxétane, boronique, CHF_2, SF_5.
- Substitution du groupement aromatique par des groupements hétéroaromatiques (azoté tout particulièrement), plus de détails sur ce point seront donnés dans le chapitre 2 et 4 de cette thèse.

Activité sur d'autres parasites :

En plus de leurs propriétés antipaludiques, les bMDs montrent des effets prometteurs contre d'autres parasites tels que *Toxoplasma gondii* (*T. gondii*) responsable de la toxoplasmose, *Trypanosomsa cruzi* (*T. cruzi*) responsable de la maladie de Chagas, et sur le vers *Schistosoma mansoni* (*S. mansoni*) responsable de la Schistosomiasis.

***Toxoplasma gondii* (*T. gondii*) :**

- *T. gondii* appartient, comme *P. falciparum*, à la famille des *Apicomplexa*, bien qu'il soit de taille plus importante (5-50 µm contre 1-2 µm pour *P. falciparum*).
- *T. gondii* dispose de plus d'organelles, d'une meilleure réponse immunitaire et de nombreux moyens de défense contre des composés bioactifs.
- *T. gondii* partage de nombreux points communs avec *P. falciparum* en termes d'expression génétique, de biologie, et de métabolisme. Il peut donc être utilisé comme parasite modèle.
- Certaines bMDs montrent une efficacité contre les deux parasites. Ces résultats seront détaillés dans le chapitre 2, en particulier leurs cibles biologiques voisines chez *P. falciparum* et *T. gondii*.

***Trypanosomsa cruzi* (*T. cruzi*) :**

- Des modifications structurales ont été apportées pour cibler spécifiquement *T. cruzi*.
- Les composés les plus actifs sur *T. cruzi* incluent une pipérazine fonctionnalisée avec un autre groupement aromatique sur le groupement benzylique[65].
- Ces molécules sont plus volumineuses, avec un poids moléculaire plus important, souvent tri-aromatiques.

***Schistosoma mansoni* (*S. mansoni*) :**

- Les bMDs sont parfois testées contre ces parasites. Le parasite *S. mansoni* est hématophage, comme *P. falciparum*, et partage avec le protozoaire les voies de détoxification de l'hème.
- Les aza-bMDs (*N*-hétéroaromatique sur la partie ouest) et la PD montrent des activités encourageantes sur *S. mansoni*.
- Des détails supplémentaires et résultats seront discutés dans le chapitre 4.

Ces résultats d'activité sur de nombreux parasites démontrent encore une fois le potentiel d'action antiparasitaire à large spectre de nos composés bMDs.

1.2.4 La synthèse des 3-benzoylménadiones

Comme évoqué précédemment, les 3-benzylménadiones (bMDs) sont métabolisés en 3-benzoylménadiones dans le parasite *P. falciparum*. Ces métabolites actifs sont essentiels pour l'activité antiparasitaire, ce qui rend crucial le développement de méthodes de synthèse efficaces afin d'obtenir ces composés. Voici un aperçu des méthodologies développées pour les synthétiser :

i. **Oxydation directe** de la position benzylique[29] :
- Utilisation de l'acide périodique et de trioxyde de chrome.
- Conditions oxydantes fortes, rendant certains substrats incompatibles.
- Limites : rendements modérés (Figure 14).

ii. Formation d'**organolithien** à partir d'une 3-bromoménadione protégée[66] :
- Génération d'un organolithien qui attaque sur un chlorure d'acyle benzylique.
- Après déprotection, la benzoylMD désirée est formé.
- Limites : disponibilité et stabilité des chlorures d'acyle benzylique commerciaux, génération d'un nucléophile aromatique pouvant poser des problèmes selon le substrat (Figure 14).

iii. **Photo-réduction** en présence de dioxygène dans un solvant protique[45,67] :
- Conditions permettant la photoréduction de la quinone puis l'oxydation de la position benzylique. Plus de détails concernant cette méthode seront disponible dans le chapitre 2 et 4.
- Limites : nécessite un photo-réacteur puissant, conduisant à des rendements modérés.

- Utile dans certaines conditions grâce à sa biocompatibilité (Figure 14).

iv. **Acylation** de Friedel-Crafts :

- Utilisation d'un système d'acide triflique et d'anhydride trifluoroacétique (TfOH/TFAA).
- Formation de triflate de trifluoroacétyle (TFAT), suivi de la génération d'un acyle trifluoroacétate réactif[68].
- L'acylium réagit par substitution électrophile aromatique avec la quinone protégée.
- Le dérivé 3-benzoylménadione est obtenu après déprotection ou engagé dans une post-fonctionnalisation (Figure 14).

Cette dernière méthode offre de nombreux avantages en termes de diversité de substrats et de reproductibilité. Cependant, des limitations incluent une faible tolérance aux substrats sensibles aux conditions acides, des rendements réduits pour les substrats encombrés en position ortho de l'acide, et la formation possible de régioisomères en positions 6 et 7 de la ménadione, diminuant l'accessibilité à ces composés.

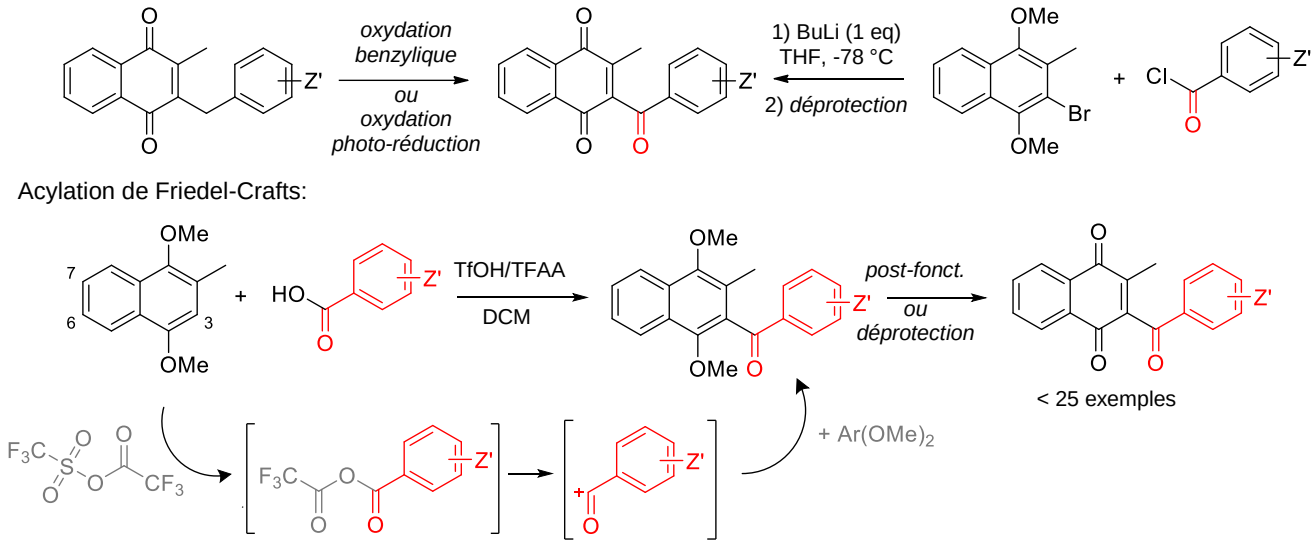

Figure 14: Stratégie de synthèse utilisant une oxydation benzylique chimique H_5IO_5 (7 equiv.), CrO_3 (20 mol%), MeCN, 16h ; ou des organolithiens ; ou une oxydation par photo-réduction à partir de bMDs: DCM:isopropanol, 1:1, O_2, irradiation 350 nm à 200W, 72h. Réaction d'acylation de Friedel-Crafts à partir d'acide benzoïque et du système TfOH/TFAA.

Les diverses méthodologies de synthèse, telles que la réaction de Kochi-Anderson, les couplages C-C, et les alkylations C-H radicalaires, permettent une grande diversité de modifications structurales sur la partie « est » des bMDs. Ces modifications ont un impact significatif sur : l'activité antiparasitaire, ainsi que sur leurs propriétés PC et PK, sans fortement affecter leurs propriétés rédox. C'est pourquoi dans l'optique d'améliorer notre molécule de référence, la PD, la plupart des projets en chimie médicinale vont être dirigés sur cette partie de la molécule.

1.3 Fluorophore cliquable pour l'imagerie

Préambule

L'un des principaux objectifs de ma thèse a été d'investiguer les cibles biologiques et les sites d'action des bMDs au sein du parasite. La glutathion réductase du parasite *P. falciparum* (*Pf*GR) semble être une cible privilégiée des bMDs. Cependant, plusieurs de nos études suggèrent que d'autres oxydoréductases pourraient être également ciblées par nos bMDs. L'oxydation de PD en son métabolite PDO est rendue possible grâce à la réductase (*Pf*FNR[45,69]) présente exclusivement dans l'apicoplaste du parasite. De plus, nous avons récemment montré que la PD induit un stress oxydant significatif dans l'apicoplaste, en utilisant une souche transgénique de *P. falciparum* contenant une protéine fluorescente rédox sensible[45].

L'apicoplaste est une organelle indispensable à la survie du parasite *P. falciparum* et est également présent chez son homologue, *T. gondii* [70]. Afin de guider notre recherche thérapeutique, nous cherchons à comprendre les modifications induites dans le parasite par notre famille de composés et à localiser ces cibles. Dans cet objectif, mon équipe d'accueil, sous la supervision du Dr. Mourad Elhabiri, s'intéresse à une famille de molécules fluorescentes originales et bioinspirée : les flavyliums.

Pour répondre au mieux aux objectifs ciblés, nous avons ainsi mis en place un projet d'imagerie par fluorescence (approches de chimie bioorthogonale avec les alcynes de phytostérol au niveau cellulaire (cellules BY-2) et au niveau d'organes de jeunes plants de tomate (*Solanum lycopersicum*)) permettant d'apporter une preuve de concept de notre approche. Cette partie servira donc d'introduction aux ions flavyliums ainsi qu'aux possibilités offertes par l'imagerie par fluorescence utilisant la chimie clique bioorthogonale.

1.3.1 Généralités sur l'imagerie par fluorescence et les fluorophores

L'imagerie est une technologie avancée permettant de visualiser le domaine du vivant dans plusieurs dimensions. Elle offre la possibilité de mesurer des paramètres physiques comme la quantification d'une espèce, les propriétés d'un tissu ou la surface d'un échantillon. Mais elle permet également, entre autres, le diagnostic d'une maladie et l'étude de la dynamique des protéines, de l'expression génétique ou de la temporalité de ces évènements.

Au cours de ces dernières années, plusieurs méthodes d'imagerie ont été mises au point, et nous allons nous focaliser sur l'imagerie par fluorescence. Le développement de petites molécules organiques fluorescentes permet de visualiser et de quantifier rapidement une multitude de mécanismes biologiques dynamiques ou statiques grâce à la grande sensibilité

et sélectivité de la technique de fluorescence. Plusieurs techniques microscopiques utilisant des chromophores organiques ont vu le jour ces dernières décennies :

- **La microscopie conventionnelle par fluorescence**[71] : C'est l'une des plus répandues car peu coûteuse à mettre en place. Certains microscopes (les moins coûteux) utilisent une source d'excitation polychromatique (par exemple éclairage par lampe à vapeur de mercure et utilisation de filtres d'excitation), donnant des images peu définies, notamment en raison du large domaine spectral d'excitation et d'une faible précision. Rapidement, la microscopie confocale est apparue (plus couteuse), avec l'avantage d'utiliser un laser comme source d'excitation monochromatique et un plan focal permettant une excitation et une détection précises sur un point fixe (précision ≈ 200 nm). Cette technique est particulièrement intéressante lorsque que l'on utilise des chromophores émettant dans le rouge/proche infrarouge (PIR) (≈ 600–1700 nm dont rouge lointain 600–700 nm, PIR-I, 700–900 nm, et PIR-II, 900–1700 nm)[72], puisque aucune espèce biologique n'absorbe à ces longueurs d'ondes. C'est ce type de microscopie que nous avons privilégié pendant cette thèse, grâce aux différentes collaborations mises en place. Plus particulièrement, en collaboration avec l'Institut de Biologie Moléculaire des Plantes (IBMP, CNRS, Strasbourg), nous avons également utilisé la spectro-imagerie de fluorescence (fluorescence SImaging ou FSI)[73]. La FSI est une technologie permettant l'acquisition d'un spectre d'émission continu en chaque point de l'image (défini par des pixels) avec un pas d'échantillonnage d'environ 10 nm. A chaque pas (λ_{em}), le système acquiert une image spécifique et chaque image enregistrée se comporte comme une matrice de pixels dont les valeurs dépendent de l'intensité de fluorescence de l'échantillon à la longueur d'onde d'émission. Cette approche permet ainsi de suivre par mesure d'un spectre d'émission de fluorescence continu en tout point d'une cellule les altérations (pH, rédox, métabolisme, stabilité, interaction…) d'un fluorophore.
- **Microscopie par absorption à deux photons (2P)**[74] : Cette technique permet d'exciter le chromophore avec deux photons d'énergie deux fois moins élevée chacun, donc de longueur d'onde deux fois plus élevée. Elle est plus coûteuse car nécessite un laser spécifique, mais permet une pénétration de l'échantillon plus profonde (≈ 3 cm) grâce à une longueur d'onde d'excitation plus élevé et une excitation sélective du chromophore à 2P. Les photo-dommages sont par la même occasion réduits, améliorant la biocompatibilité de cette technique et permettant des applications *in vivo*. Cependant, tous les chromophores ne disposent pas de propriétés d'absorption à 2P, cela dépendra en effet de leur capacité à absorber deux photons simultanément (sections d'absorption 2P)[75].
- **Imagerie en temps réel**[76] : Comme son nom l'indique, cette technologie permet l'imagerie d'un échantillon en temps réel, afin de suivre par exemple un marquage spécifique *in vitro*.

Cette technologie est également possible *in vivo* grâce à la chirurgie guidée par fluorescence. Elle sera fonction du temps de vie de la fluorescence du chromophore utilisé et dépendra d'une multitude de facteur interne ou externe.

- **Imagerie super-résolue par fluorescence**[77] : C'est à l'heure actuelle la technologie la plus avancée de toutes, puisqu'elle combine l'utilisation de fluorophore photo-switch ou photoactivable (fluorophore fluorogénique ou pro-fluorophore) et des techniques avancées de détection à l'échelle nanométrique. Cette technologie a notamment conduit au prix Nobel 2014 de physique.

Les fluorophores rouge-PIR

L'utilisation de chromophores émettant dans le rouge-PIR (≈ 600–1700 nm) en imagerie ou en spectroscopie par fluorescence est déterminée par plusieurs critères[78] :

i. **Solubilité aqueuse et cytotoxicité** : Si appliqué dans un milieu biologique, le chromophore doit être soluble dans l'eau et non cytotoxique.
ii. **Photostabilité** : Il doit maintenir une émission constante dans le temps sous photoexcitation pour des mesures fiables et reproductibles.
iii. **Longueur d'onde d'émission** : Elle doit évidemment se trouver dans la plage de longueur d'onde souhaitée.
iv. **Propriétés optiques** : Le rendement quantique, la brillance, le déplacement de Stockes, la durée de vie de fluorescence et le solvatochromisme doivent être adaptés à l'application mise en place.
v. **Perméabilité** : La perméabilité du chromophore est liée à ces propriétés physicochimiques.
vi. **Accessibilité chimique** : Elle influencera le coût final du fluorophore.
vii. **Stabilité** : Selon l'objectif recherché, le fluorophore doit être stable en solution aqueuse dans une large gamme de pH ou et doit être inerte électrochimiquement (c.-à-d. insensible aux réactions rédox par des oxydants ou réducteurs biologiques).

De nombreux fluorophores rouge-PIR ont été développés et commercialisés pour répondre à ces besoins. Les familles traditionnellement utilisées (naphthalimide, coumarine, oxazine, BODIPY, cyanine, xanthène [pyronine, rhodamine, fluorescéine, hémicyanine]) ont été largement appliquées avec ces différentes techniques microscopiques[79,80]. Cependant, elles souffrent souvent d'inconvénients limitant leurs propriétés telles que des absorption/émission souvent centrées dans le visible et de faibles brillance, solubilité, photo-stabilité et/ou déplacement de Stockes… C'est pourquoi le développement de fluorophores visant à améliorer certaines de ces propriétés est stratégique pour répondre à nos besoins de recherche ainsi qu'à d'autres applications.

1.3.2 La synthèse des flavyliums et leurs applications

Origine des flavyliums

Les flavyliums basés sur un chromophore de type 2-aryl-benzopyrylium appartiennent à la grande famille des anthocyanes (pigments naturels), responsables de la grande diversité chromatique chez les fleurs, fruits et feuilles[81]. Ces pigments reposent sur un squelette flavylium portant des fonctions hydroxyles, O-glycosyles, O-acyles et/ou O-méthyles, tandis que leurs homologues anthocyanidines (aglycones) sont dépourvus de groupements glycosylées et acylées (Figure 15). L'origine des flavyliums remonte à 1664, lorsque Robert Boyle observa pour la première fois un changement de couleur d'un extrait de fleurs après un traitement acide. Puis, en 1835, Ludwig Clamor Marquart utilisa pour la première fois l'appellation anthocyanine (en grec = fleur bleu). Enfin, grâce aux travaux de recherche de Richard Willstätter (prix Nobel de chimie 1915), cette famille de composés a pu être caractérisée et classifiée.

Depuis, l'étude de ces composés a permis la découverte de plus de 700 structures chimiques présentes dans la nature. Ils peuvent être utilisés dans diverse applications[82] : additifs, antioxydants, colorants, vins, nutrition... Ils ont la capacité à passer d'une espèce à une autre en fonction du pH du milieu (équilibres réversibles entre les formes quinonique neutre ou anionique ↔ cation flavylium ↔ hémiacétal ↔ chalcone *cis* et *trans* ↔ chalcones *cis* et *trans* ionisées) (Figure 15). Lorsque le pH augmente (à partir de 3-4), les positions électrophiles 2 et 4 peuvent en effet subir une attaque d'une molécule d'eau (l'hydrolyse en position 4 est minoritaire), formant ainsi des espèces ouvertes et incolores de type chalcone (*cis* ou *trans*), qui sont thermodynamiquement stables. Seules les espèces flavylium et quinonique (espèces minoritaires) sont colorées. La copigmentation (interactions non-covalentes) avec d'autres flavonoïdes et/ou l'interactions avec certains métaux de transition (Al^{3+}, Fe^{3+}), peuvent stabiliser voire améliorer la stabilité des espèces colorées en fonction du pH[83,84].

Comme attendu, l'introduction de divers substituants sur le squelette flavylium a des conséquences sur sa stabilité thermodynamique/cinétique, sur ses propriétés de protonation et sur ses propriétés photophysiques. Plusieurs études se sont intéressés aux relations structures-propriétés (RSP)[81,85], mais en raison du grand nombre de possibilités, les résultats doivent être traités au cas par cas. Par exemple, l'introduction d'une amine sur la position 4' ou 7 (substitution non rencontrée au sein des molécules naturelles) entraine un effet bathochrome important des bandes d'absorption et diminue l'acidité de la molécule grâce à l'effet donneur de l'amine[86] contribuant ainsi à augmenter le domaine de stabilité des formes colorées.

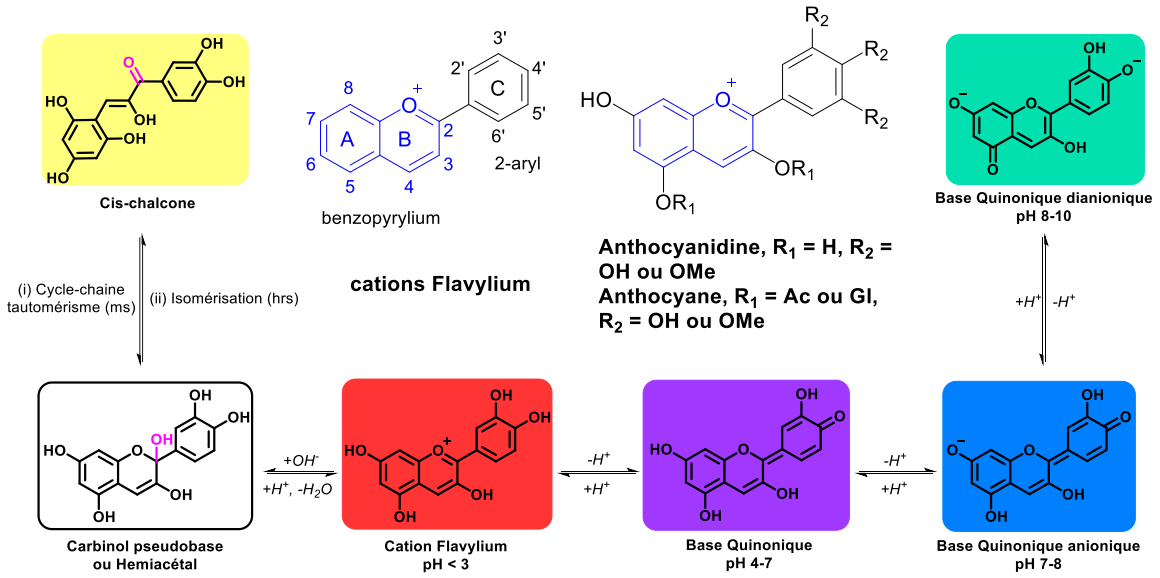

Figure 15: Le chromophore **flavylium** et la nomenclature des **antocyani(di)nes** (Ac = acyle, Gl = glycoside). Stabilité du **flavylium** en fonction du pH et l'équilibre des différentes espèces formées. Lorsque le pH augmente le **flavylium** peut subir soit i) une déprotonation conduisant à la forme **quinonique**, ou ii) subir une hydratation en position 2 suivie par un échange de proton avec le milieu pour conduire à la forme **hémiacétale**, puis le tautomère ***cis*-chalcone** se forme car plus stable (isomérisation en ***trans*-chalcone** possible).

Concernant la synthèse des ions flavyliums, elle est principalement basée sur la condensation acide entre une dicétone-aryle et un benzène-diol (résorcinol) pour les flavyliums substitués en position 4, ou sur une condensation entre une acétophénone et un salicylaldéhyde pour les flavyliums substitués en position 3. D'autres méthodologies spécifiques peuvent être utilisées, notamment à partir de flavones, et sont principalement décrites dans cette revue récente de L. Cruz *et al*[87].

Les flavyliums non-rigides :

La structure flavylium offre donc un grand potentiel de fonctionnalisation, ce qui ouvre la voie à une grande diversité d'applications. Cependant, peu de systèmes utilisent directement les flavyliums pour leurs propriétés de fluorescence, la plupart des systèmes étant conjugués avec un autre chromophore (composés hybrides)[88]. Des stratégies ratiométriques et/ou fluorogéniques ont été ainsi développées, basées sur ces systèmes hybrides (Figure 16). Ces chromophores, généralement fonctionnalisés en position 2, permettent de déplacer la longueur d'onde d'émission du système vers le rouge-PIR. De plus, le caractère électrophile du squelette flavylium peut conduire à l'attaque d'espèces nucléophiles (biomarqueurs ou analytes) ou à la réduction ou au clivage d'une fonction chimique produisant une réponse ratiométrique et/ou fluorogénique (Figure 16). Cette réponse, face à différentes espèces (réducteur, oxydant, ROS, enzyme, protéine, métal…), permet alors leur quantification ou leur détection, donnant lieu à de multiples applications dans le domaine biologique.

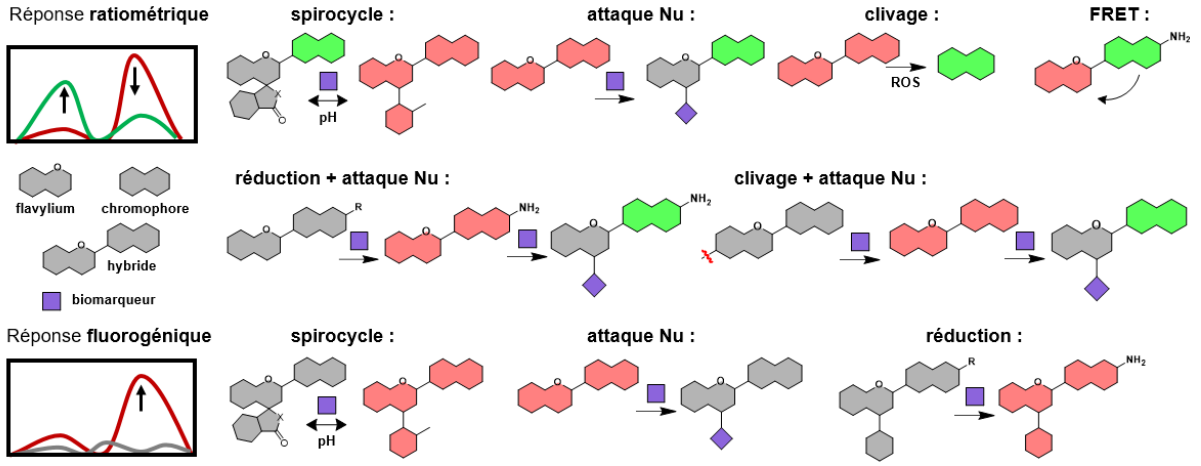

Figure 16: Exemple de système ratiométrique ou fluorogénique, basé sur le squelette flavylium, en présence de biomarqueur (ou analyte). Si la longueur d'onde d'émission du fluorophore donneur chevauche la longueur d'onde d'absorption du fluorophore accepteur, alors un transfert d'énergie par résonance Förster (**FRET**) peux être observé.

Par exemple, J. Liu *et al.*[89] ont décrit un modèle flavylium-coumarine (émission rouge-PIR) pouvant subir une attaque nucléophile de H_2S en position 4, bloquant ainsi la délocalisation des électrons π et conduisant à une émission dans le visible (émission de la coumarine). Ce système ratiométrique (émission rouge-PIR *versus* visible) permet une détection sélective de H_2S en solution et dans des cellules HeLa (cellule cancéreuse humain). En 2013[90], inspiré par les sondes xanthène spirocyclique, la même équipe a présenté un système flavylium-coumarine spirocyclique fonctionnalisé en position 4. Ce spirocycle permet, sous sa forme fermée (pH neutre-basique), d'inhiber la fluorescence rouge-PIR (émission de la coumarine seulement) grâce à une hybridation-sp_3-C-4. Une fois ouvert (pH acide), l'hybridation-sp_2-C-4 permet de retrouver une molécule fluorescente dans le rouge-PIR. Ce système ratiométrique leur a permis de détecter sélectivement du Hg^{2+} dans des cellules HeLa.

Si quelques exemples d'applications en imagerie cellulaire existent donc avec des ions flavylium, presqu'aucun exemple utilisant directement le flavylium pour ses propriétés fluorescentes n'a été décrit en raison de son instabilité en condition aqueuse face au changement de pH (hydrolyse des positions 2 et 4). Par ailleurs, la libre rotation des cycles aromatiques B et C induit un état TICT (Twisted Intramolecular Charge Transfer) conduisant à une désexcitation non-radiative et diminuant fortement la capacité du chromophore à fluorescer[91]. Cet inconvénient peut cependant devenir un atout. H. Li *et al.*[92] ont développé un flavylium-2-aryl qui, en fonction la viscosité du milieu, offre une réponse fluorogénique. Le passage à un environnement visqueux permet en effet de diminuer le TICT et conduit à un système fluorescent capable de sonder la viscosité d'un milieu.

Les flavyliums rigides :

L'introduction d'un pont éthylénique entre le cycle C et B permet d'améliorer grandement la rigidité[93], la stabilité (stable jusqu'à pH 9) et le rendement quantique de l'ion flavylium. De plus, la substitution des groupements hydroxyles par des groupements électrodonneurs de type amine, induit un déplacement bathochrome et hyperchrome de la longueur d'onde d'absorption maximale. Ces modifications structurales offrent ainsi un grand potentiel d'application en tant que fluorophores rouge-PIR.

Par exemple, en 2015, H. Chen *et al.*[93] ont mis au point un flavylium rigide fonctionnalisé en position 7 et 4' par des groupements hydroxyles. Selon le pH du niveau subcellulaire, différentes espèces peuvent être stabilisées (forme cationique, neutre ou anionique), induisant une modification de la longueur d'onde d'émission du chromophore et offrant une réponse ratiométrique à 3 canaux. Également, W. Jiang *et al.*[94] ont décrit un flavylium fonctionnalisé en position 4' par un groupement 2,4-dinitrobenzenesulfonate (électroattracteur) inhibant la fluorescence du composé à cause d'un transfert de charge intramoléculaire (ICT). Ce sulfonate peut être clivé sélectivement par des thiols (glutathion, cystéine), annulant ainsi le processus ICT et conduisant à une molécule fluorescente (réponse fluorogénique). Dans le même registre, L. Xu *et al*.[95] ont substitué le groupement sulfonate par un groupement phosphate capable de s'hydrolyser sélectivement en présence d'alcalines phosphatases, offrant également une réponse fluorogénique utilisable dans des cellules cancéreuses humaines (BEL-7402). Quelques exemples de systèmes flavyliums fonctionnalisés par un azoture[96–98] permettent également la détection sélective de H_2S par réduction de l'azoture (électroattracteur) en amine (électrodonneur). Cette réduction permet d'annuler le caractère ICT, restaurant l'émission du composé (réponse fluorogénique).

Plusieurs raisons nous ont donc poussés à développer davantage cette famille de chromophores rigides et à l'appliquer à nos projets afin de répondre à plusieurs de nos objectifs :

i. Leurs propriétés spectrales : Ces fluorophores possèdent des propriétés d'absorption et d'émission aussi intéressantes que celles des autres familles de fluorophores organiques conventionnels.
ii. Leurs propriétés physicochimiques : Bonne solubilité aqueuse, stabilité, polarité, lipophilicité, etc.
iii. Leurs bonnes perméabilités.
iv. Leurs accessibilités : Facilité d'obtention (en temps, coût et quantité).
v. Leurs grandes capacités de modulation structurale et spectrale.
vi. La facilité de fonctionnalisation ou post-fonctionnalisation.

vii. Leur fort potentiel d'applications et leur possible valorisation : Peu d'exemples de flavyliums rigides décrits à ce jour dans la littérature[88].

La synthèse des flavyliums rigides :

Mon équipe d'accueil a d'abord développé la chimie de ces chromophores en utilisant une stratégie de synthèse similaire à celle introduite précédemment : la condensation acide entre un salicylaldéhyde et une α-tétralone (au lieu de l'acétophénone pour les flavyliums non-rigides). Cette condensation en milieu acide offre une grande flexibilité en termes de substituants et de conditions réactionnelles. Les méthodes traditionnelles, décrites dans la littérature, utilisent généralement des combinaisons d'acides dangereux et très corrosifs (H_2SO_4 conc. + HCl conc. ou H_2SO_4 conc. + $HClO_4$). Nous avons donc décidé d'optimiser cette réaction pour la rendre plus accessible. Actuellement, nous utilisons principalement deux conditions différentes en fonction de la compatibilité avec les substrats utilisés (Figure 17) :

- HCl conc. (en excès) dans de l'acide formique (solvant) à 60°C pendant au moins 24 heures : Cette méthode a l'avantage de pouvoir solubiliser la majorité des substrats, mais reste dangereuse et nécessite d'être neutralisée puis extraite avant une purification sur colonne de silice.
- Chlorure d'acétyle et l'éthanol dans l'acétate d'éthyle: Cette méthode permet la formation contrôlée et quantifiée d'HCl (gazeux) *in situ* ainsi que de l'acétate d'éthyle qui constitue notre solvant. La solution est ensuite ajoutée aux deux substrats solubilisés dans l'acétate d'éthyle à température ambiante. Bien que beaucoup moins dangereuse, cette méthode peut présenter une cinétique plus lente (au moins 48 heures de réaction) et peut poser des problèmes de solubilité dans certains cas (nécessité de purifier le colorant formé par chromatographie sur colonne de silice). Dans certains cas, le flavylium, à pH acide, étant peu soluble dans les solvants organiques, peut précipiter et être isolé facilement par simple filtration.

La sensibilité de l'ion flavylium aux conditions basiques/nucléophiles et sa faible solubilité dans les solvants organiques rendent la post-fonctionnalisation de ce composé plus difficile. C'est pourquoi, sauf exception, nous avons privilégié les modifications structurales sur les deux substrats de départ avant leur condensation en milieu acide. De plus, un large choix de substrats est disponible commercialement. Une stratégie basée sur un processus de screening en plaque 96 puits a donc été mise en place pour sélectionner efficacement les composés ayant les meilleures propriétés photophysiques. Seul le flavylium formé absorbe et émet dans le visible-PIR. Une simple mesure des spectres d'absorption et d'émission au moyen d'un lecteur de plaque hybride absorption/émission d'un mélange non purifié α-tétralone/salicylaldéhyde/H_2SO_4 dans l'éthanol permet ainsi cette sélection. Ainsi, une

bibliothèque de données spectroscopiques de plus d'une centaine d'ions flavyliums a pu être obtenue.

Différentes stratégies de synthèse ont été mises en place pour obtenir les substrats non commerciaux désirés (Figure 17). Des amines primaires ou secondaires peuvent être obtenues par simple substitution nucléophile à partir de la α-tétralone amine. Néanmoins, l'α-tétralone étant un mauvais nucléophile, de faibles réactivités peuvent être observées (Figure 17). Toujours à partir de la α-tétralone amine, la formation d'un sel de diazonium grâce au nitrite de sodium permet alors l'introduction d'un large choix de nucléophiles (Figure 17). Ensuite, à partir d'une α-tétralone substituée par un groupement partant (Br, Cl, OTf…), différents couplages organométalliques sont possibles comme le couplage C-N de Buchwald-Hartwig[99] ou le couplage d'Ullmann[100], permettant l'introduction d'amines secondaires ou tertiaires cycliques ou non (Figure 17). Enfin, certains salicylaldéhydes non commerciaux peuvent être formés à partir de dérivés phénoliques par formylation grâce à la réaction de Vilsmeier-Haack[101] (Figure 17).

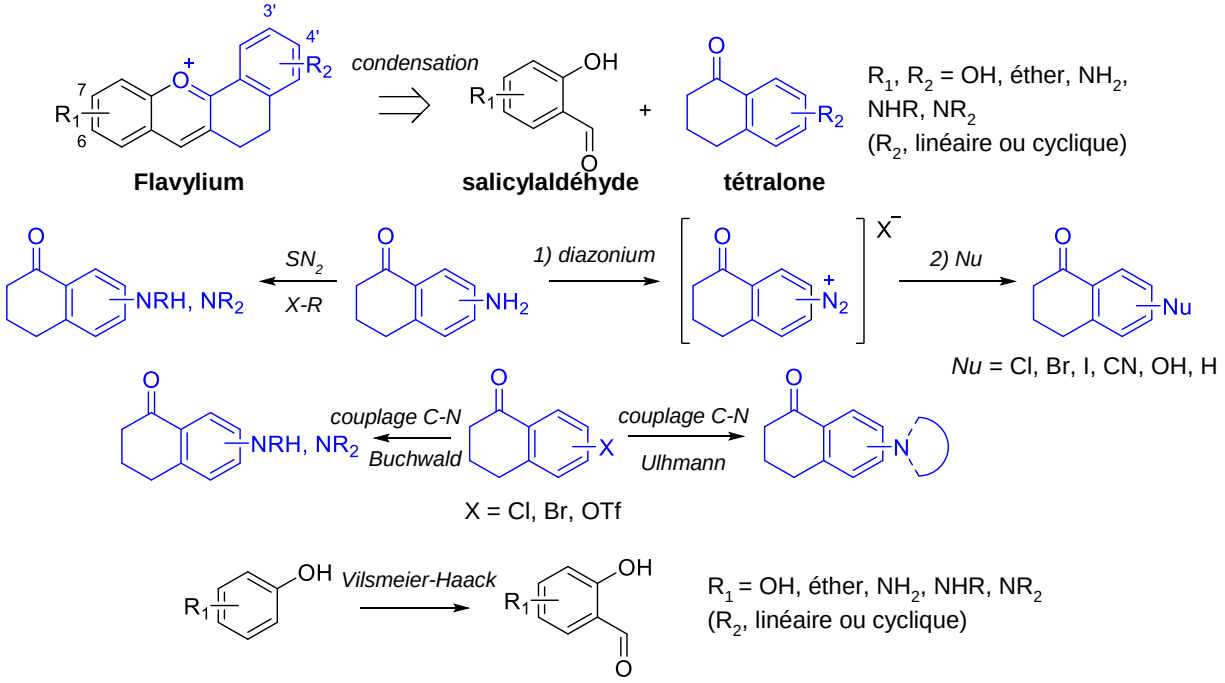

Figure 17: Accessibilité du fluorophore **flavylium** et diversité de synthèse de la **α-tétralone** et du **salicylaldéhyde**. Condensation: HCl conc., acide formique, 60°C ou AcCl, EtOH, EtOAc, 0°C à 25°C. 1) Diazotation: $NaNO_2$, H_2O. 2) Nu: CuX ou KX. Couplage C-N Buchwald-Hartwig: NRH ou NR_2, $Pd(OAc)_2$, BINAP, Cs_2CO_3, toluene, 100°C, 3h. Couplage Ullmann: HNR_2, CuI, base, ligand. Vilsmeier-Haack : $POCl_3$, DMF.

<u>Les relations structures-propriétés (RSP) des flavyliums rigides :</u>

Grâce à notre bibliothèque de fluorophores flavyliums, nous avons pu évaluer leurs RSP. L'atout principal de cette famille de fluorophores est leur solubilité aqueuse. Par conséquent, les mesures photophysiques ont été effectués dans un tampon aqueux contenant un électrolyte support (NaCl 0,1 M, pH 7,41) se rapprochant de la concentration ionique d'un

plasma sanguin. Les composés présentant les meilleures propriétés optiques sont ceux fonctionnalisés en positions 7 et 4' du squelette flavylium. Les groupements éther (OMe, OR) sont moins tolérés en raison de leur faible effet électrodonneur (effet inductif attracteur et effet mésomère donneur), tandis que les groupes hydroxyles apportent des propriétés intéressantes. Comme pour les anthocyanes, plusieurs espèces colorées peuvent être observées selon le pH du milieu, donnant lieu à des systèmes fluorogéniques ou ratiométriques pH-sensibles tout à fait intéressantes.

Les fonctions amines, grâce à leur caractère électrodonneur par effet inductif et mésomère, offrent les meilleurs résultats photophysiques avec des rendements quantiques (Φ) allant de 14% à 37% dans l'eau à pH neutre en présence de 0,1 M de NaCl et induisent un déplacement bathochrome, offrant une émission dans le rouge-PIR (maximum d'émission à ≈ 620–650 nm). Ces propriétés sont particulièrement recherchées pour répondre à nos objectifs d'imagerie par fluorescence. Nous allons donc les examiner plus en détail ci-dessous (Figure 18) :

- **Modification de la position 4'** (Figure 18) : une amine primaire **(1)** est moins efficace qu'une amine secondaire **(2)** ou tertiaire **(3)**. L'amine tertiaire NEt_2 **(4)** conduit par contre à un faible effet ICT (de l'amine vers le noyau pyrilium) et a un fort effet TICT, inhibant ainsi sa fluorescence. En effet, il a été montré qu'une amine acyclique pouvait, à l'état excité (suivant son encombrement stérique, sa structure et ses propriétés électroniques), entrainer la rotation de la liaison C-N, conduisant à une désexcitation non-radiative par TICT[102]. La substitution par une amine cyclique (à 3, 4, 5 ou 6 chainons) ou l'introduction d'un substituant suffisant encombrant permet de réduire ou d'annuler cet effet TICT, améliorant ainsi les propriétés d'émission du composé[103] **(5-6)**.
- **Modification de la position 7** (Figure 18) : l'introduction d'un diméthylamine à un effet positif sur le rendement quantique (composé **(7)** versus composé **(3)**). Cependant, l'introduction d'une morpholine en combinaison avec la pyrrolidine n'a pas eu l'effet escompté (**(8)** *versus* **(6)**). Malgré cela, la morpholine avec un diméthyle amine permet d'améliorer les propriétés d'émission (**(9)** *versus* **(3)**).

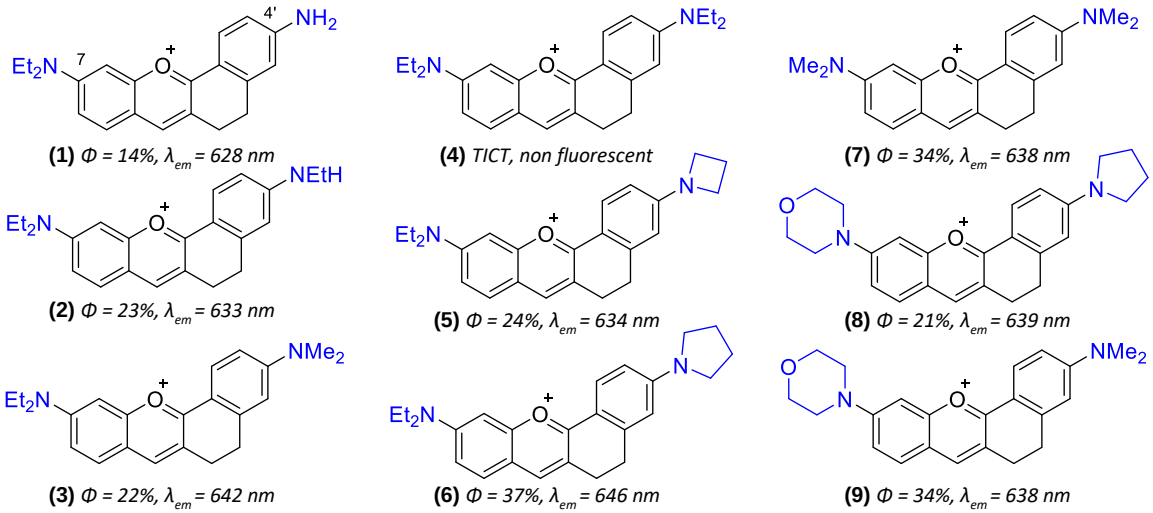

Figure 18: Flavylium rigides aminés et leurs propriétés photophysiques dans un tampon aqueux (NaCl 0,1 M, pH 7,41). Déplacement de Stockes ≈ 30–40 nm. Contre ion Cl^-.

Pour conclure, nous avons donc réussi, sur une petite série de composés synthétisés, à obtenir des fluorophores et applicables avec des propriétés photophysiques convaincantes (brillants, stables entre pH 1 et 9, photostables et émettant dans le rouge-PIR), comparables à celles de fluorophores commerciaux, validant ainsi leur potentiel pour de futures applications.

Applications des flavyliums rigides au sein du laboratoire :

- Nous avons développé une série de flavyliums rigides ratiométriques pH-sensibles[94], permettant la mesure du pH intracellulaire par spectro-imagerie de fluorescence SImaging (preuve de concept sur des cellules BY-2 en collaboration avec les Drs. Hubert Schaller et Andréa Hemmerlin de l'IBMP, Strasbourg). Grâce à leurs groupements hydroxyles ionisables, plusieurs formes réversibles protonées peuvent être observées et caractérisées pour leurs propriétés d'émission *in cellulo*, offrant une réponse ratiométrique à 2 ou 3 canaux d'émission (Figure 19 **(A)**).
- Nous avons également utilisé des flavyliums rigides pour marquer des globules rouges parasités par *P. falciparum* (Figure 19 **(B)**). Ces composés pénètrent facilement ces globules rouges parasités qui sont marqués sélectivement à 5 µM au niveau de leur cytosol. Les globules rouges sains ne sont pas marqués et aucun effet négatif sur la viabilité des parasites n'a été observé. Nos composés marquent avec la même efficacité des globules rouges parasités par des souches 3D7 (souche sensible à la chloroquine), par *P. berghei* ainsi que des gamétocytes (collaboration avec le Dr Markus Ganter, Université d'Heidelberg, Allemagne).
- Une récente collaboration avec le Prof. Valérie Schini-Kerth (INSERM UMR1260, Strasbourg) a permis de valoriser notre série de composés de type flavylium rigide. Au moyen de la microscopie de fluorescence, nous avons montré que plusieurs de nos

composés sont accumulés et augmentent significativement la formation endothéliale de NO (effet vasodilatateur) par un mécanisme encore non résolu dans les cellules endothéliales (cellules recouvrant les vaisseaux sanguins) (Figure 19 **(C)**).

- Pour détecter le NO *in cellulo* (cellules endothéliales) par fluorescence, deux sondes flavyliums rigides possédant une diamine vicinale sur le cycle B ont été synthétisées. Ces systèmes sont connus pour former un cycle triazole en présence de NO conduisant à une espèce fluorescente[104] (Figure 19 **(D)**). Ces composés en cours d'analyse devraient agir comme sondes théranostiques (senseur de NO et promoteur de formation de NO) et permettront de progresser dans ce projet.
- Enfin, une sonde fluorogénique *N*-oxyde a été préparée pour détecter la présence de Fe(II) dans des cellules saines ou cancéreuse[105]. En présence de peroxyde d'hydrogène, les différentes espèces de Fe(II) libre dans une cellule conduisent généralement à la génération de stress oxydant (réaction de Fenton), provoquant la peroxydation des lipides et la mort cellulaire (par ferroptose). Le chromophore *N*-oxyde formé est non fluorescent (transfert d'électron photoinduit, PeT) et peut être désoxygéné sélectivement par le Fe(II) formant ainsi un dérivé aminé fluorescent (réponse fluorogénique (Figure 19 **(E)**).

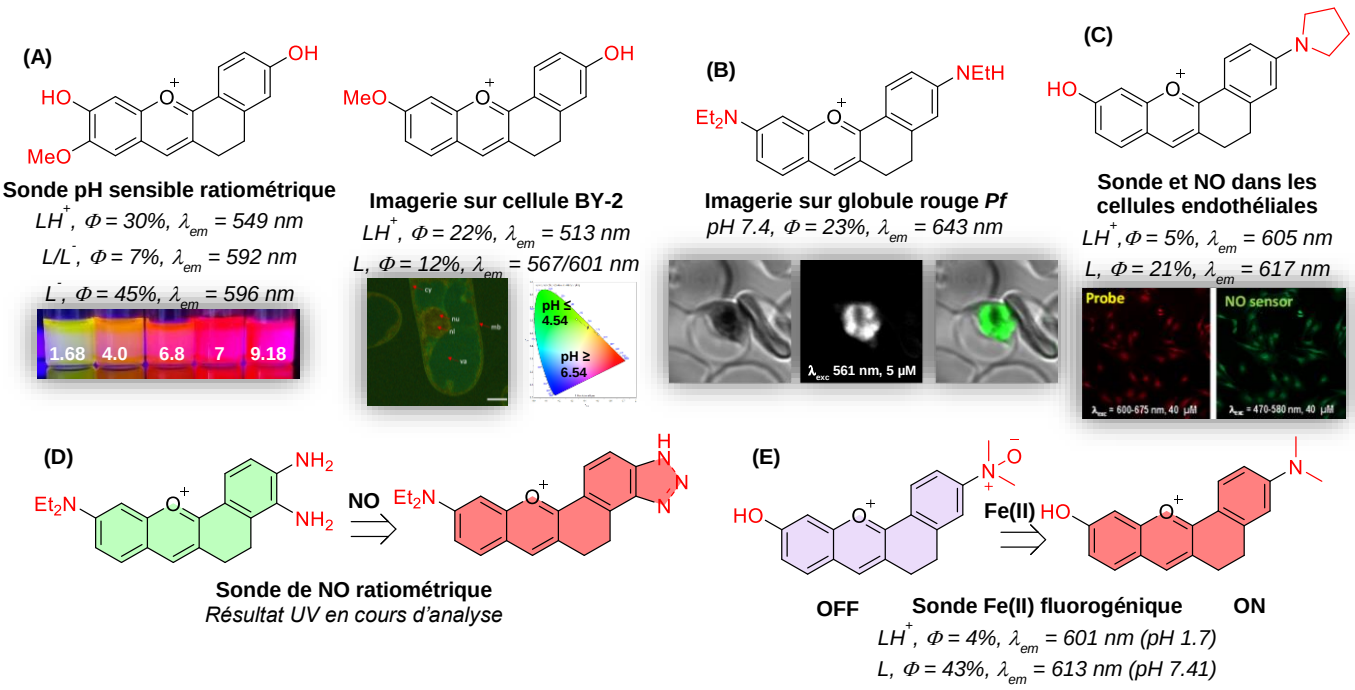

Figure 19: Différentes applications de flavyliums rigides mise en place au sein de l'équipe CBM. Projets (D) et (E) toujours en cours de développement. Hors sonde pH sensible, résultats optiques obtenus dans l'eau (NaCl 0,1 M, pH 7,41).

Toutes ces applications et preuves de concept en imagerie et en spectroscopie de fluorescence ont validé l'efficacité, la biocompatibilité, la perméabilité et la robustesse dans divers milieux biologiques (différentes cellules considérées) de cette famille de fluorophores. Nous pouvons donc poursuivre leur développement pour tenter d'atteindre nos objectifs.

1.3.3 Utilisation de la chimie clique en fluorescence

Depuis l'introduction des réactions chimiques dites « cliques » il y a environ 25 ans, ces dernières sont devenues omniprésentes et ont révolutionné les possibilités d'applications. Cette découverte a été récompensée en 2022 par le prix Nobel de chimie (Dr. C. R. Bertozzi[106], Dr. M. P. Meldal[107] et Dr. K. B. Sharpless[108]), entraînant une abondance de publications, brevets et applications sur ce sujet. Le succès de la chimie clique réside dans sa capacité à lier de façon covalente et orthogonale deux fonctions chimiques sans générer de produits secondaires toxiques dans un environnement biologique (ou non) avec une efficacité, une simplicité, une sélectivité et une rapidité extrêmes.

La première réaction de ce type qui a conduit à l'utilisation du terme « chimie clique » est la CuAAC (Copper(I)-Catalyzed Alkyne-Azide Cycloaddition). Introduite initialement par Huisgen en 1963[109], elle permet de former un triazole par cycloaddition [3+2] à partir d'un alcyne terminal et d'un azoture. Cependant, cette réaction n'est par régiosélective car elle conduit à la formation de deux isomères (1,4 et 1,5) et nécessite une température ainsi qu'un temps de réaction élevés. En 2001, Meldal puis Sharpless ont utilisé le cuivre(I) pour catalyser la réaction, permettant une réaction rapide, orthogonale, à température ambiante et régiosélective (1,4)[110] (Figure 20).

La seconde réaction clique introduite ici est la SPAAC (Strain-Promoted Azide-Alkyne Cycloaddition), publiée pour la première fois en 2004 par Bertozzi[111]. Cette réaction utilise un azoture et un alcyne contraint (cyclooctyne), permettant la formation d'un 1,2,3-triazole (Figure 20). À la différence de la CuAAC, cette réaction a l'avantage de ne pas nécessiter de catalyseur, ce qui la rend parfaitement biocompatible. Cependant, sa cinétique est généralement faible, et les cyclooctynes sont relativement hydrophobes et volumineux, augmentant le poids moléculaire final et conduisant à la formation de deux isomères si la cyclooctyne utilisée n'est pas symétrique.

Ces deux réactions ont rapidement évolué au fil des années[112]. De nombreuses améliorations concernant la cinétique, les conditions réactionnelles, la structure des substrats utilisés et les combinaisons possibles ont vu le jour. Aujourd'hui, la chimie clique s'est diversifiée, et de nouvelles réactions dites cliques ont été développées[113,114].

- **IEDDA** (Inverse Electron Demand Diels–Alder) : Cette réaction implique une tétrazine (diène) et un alcène contraint (diénophile), formant une pyridazine par cyclisation [4+2] (Figure 20).
- **Ligation de Staudinger-Bertozzi** : Elle permet de créer un amide à partir d'un azoture et d'une phosphine portant un ester. Elle est majoritairement appliquée dans le milieu vivant, bien que sa cinétique soit lente (Figure 20).

- **Formation d'oxime ou d'hydrazone** : Utilisée comme réaction clique, elle implique une alkoxylamine ou une hydrazine dans une condensation avec un carbonyle (Figure 20).
- **Réactions clique photo-induites** : Elles sont possibles entre un alcène et un tétrazole (Figure 20), ou entre un thiol et un alcène pour former un thiolène. Une photo-réaction peut également permettre de libérer une fonction cliquable de manière sélective.
- **Variantes de la SPAAC** : D'autres dipôles que l'azoture ont été utilisés donnant lieu à des variantes comme la SPANC[115], la SPSAC ou la SPICC[116], permettant de libérer un composé bioactif par exemple (Figure 20).
- **CuSAC** : Plus récemment, d'autres réactions cliques comme la CuSAC[117] ont été développées. Elles utilisent d'autres dipôles 1,3 stables appelés mésoioniques se substituant à l'azoture dans la réaction CuAAC, offrant ainsi de nouvelles possibilités (Figure 20).

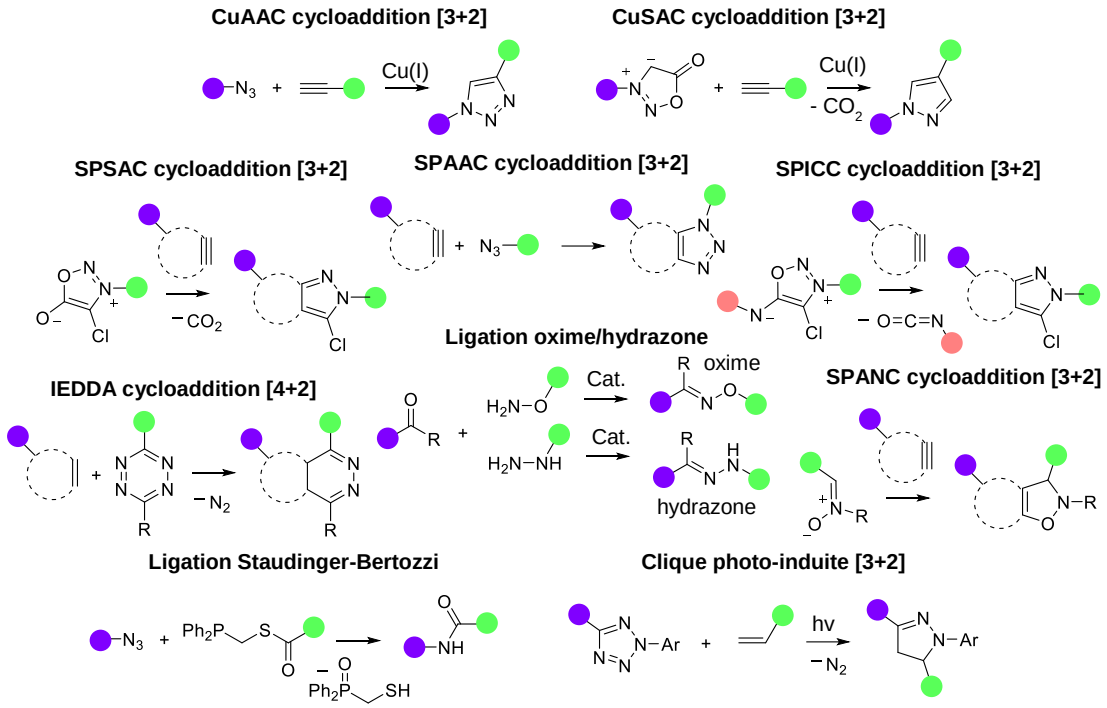

Figure 20: Différentes réactions cliques orthogonale. **CuAAC** (Copper catalyzed Azide to Alkyne Cycloaddition), **CuSAC** (Copper Catalyzed Sydnone Alkyne Cycloaddition), **SPSAC** (Strain Promoted Sydnone Alkyne Cycloaddition), **SPAAC** (Strain Promoted Azide to Alkyne Cycloaddition), **SPICC** (Strain Promoted Iminosydnone–Cycloalkyne Cycloaddition), **IEDDA** (Inverse Electron Demand Diels-Alder), **SPANC** (Strain Promoted Alkyne Nitrone Cycloaddition).

La chimie clique bioorthogonale a révolutionné l'imagerie et la spectroscopie par fluorescence. Elle permet de suivre une sonde dans son environnement biologique, d'élucider le mode d'action d'une molécule bioactive grâce à la stratégie de profilage de protéines par activité ABPP (ou AfBPP), ou d'identifier la cible biologique d'un composé. Le développement de sondes fluorescentes fonctionnalisées par un groupement cliquable est largement utilisé d'un point de vue commercial, scientifique et applicatif.

La majorité de ces sondes portent une fonction azoture ou alcyne car ces deux groupements peuvent être introduits facilement et offrent de nombreuses possibilités réactionnelles (CuAAC, SPAAC, ligation de Staudinger-Bertozzi). Néanmoins, elles souffrent des mêmes problématiques physicochimiques évoquées précédemment (prix, photo-stabilité, solubilité, faible résolution et faible contraste). En imagerie, pour éviter toute émission non spécifique du milieu biologique et améliorer le contraste de l'image, des sondes fluorescentes offrant une réponse fluorogénique ou ratiométrique suite à une réaction clique peuvent être utilisées. Cette réponse permet une résolution grandement améliorée, évite les lavages successifs de l'échantillon et permet une imagerie en temps réel après une réaction clique bioorthogonale. Sur ces principes, de nombreux pro-fluorophores azoturés ou alcynes ont été développés au cours des dernières années.

Exemple de fluorophores cliquables fluorogéniques :

- En 2004, Z. Zhou *et al.*[118] ont mis au point l'un des premiers systèmes fluorogéniques. Ils ont synthétisé une coumarine alcyne éteinte qui, après réaction clique CuAAC, devient fluorescente (Φ = 1,4% *versus* Φ = 25%). Les deux plus bas états excités (n,π*) non-émissif et (π,π*) émissif régissent le caractère fluorescent du chromophore. La formation du triazole modifie le transfert de charge, stabilisant l'orbitale (π,π*), ce qui induit une désactivation radiative uniquement à partir de celle-ci (Figure 21 **(A)**).
- La même année, K. Sivakumar *et al.*[119] ont mis au point une coumarine azoturée non fluorescente (par ICT) qui devient fluorescente après une réaction clique avec un alcyne terminal. Ils ont utilisé une méthode combinatoire (screening sur plaque de 96 puits) à partir de 9 coumarines azoturées et de 24 différents alcynes, afin d'évaluer rapidement les propriétés optiques de tous leurs systèmes (λ_{em} = 388-521 nm) (Figure 21 **(B)**).
- C. T. Jonathan *et al.*[120] ont démontré l'utilisation d'un système BODIPY-tétrazine fluorogénique (émission multipliée par 1600 dans l'eau) après une réaction IEDDA. Un mécanisme FRET (Fluorescence Resonance Energy Transfer) et TBET (Through Bond Energy Transfer) serait à l'origine de l'inhibition de la fluorescence entre les deux chromophores (Figure 21 **(C)**).
- Enfin, le groupe de C. Bertozzi[121] a décrit une série de fluorophores azoturés fluorogéniques, les CalFluor, non fluorescents à cause d'un phénomène de PeT entre l'azoture et le fluorophore, et devenant fluorescent (émission multipliée par 200 dans l'eau) après CuAAC. Une étude électrochimique (voltampérométrie cyclique) de ces composés montre bien que leurs systèmes azotures sont plus facilement oxydables (donneurs d'électrons) que les systèmes triazoles (Figure 21 **(D)**).

Ces avancées montrent l'importance et le potentiel de la chimie clique bioorthogonale pour développer des sondes fluorescentes innovantes et efficaces, ouvrant la voie à de nombreuses applications en biologie et en médecine.

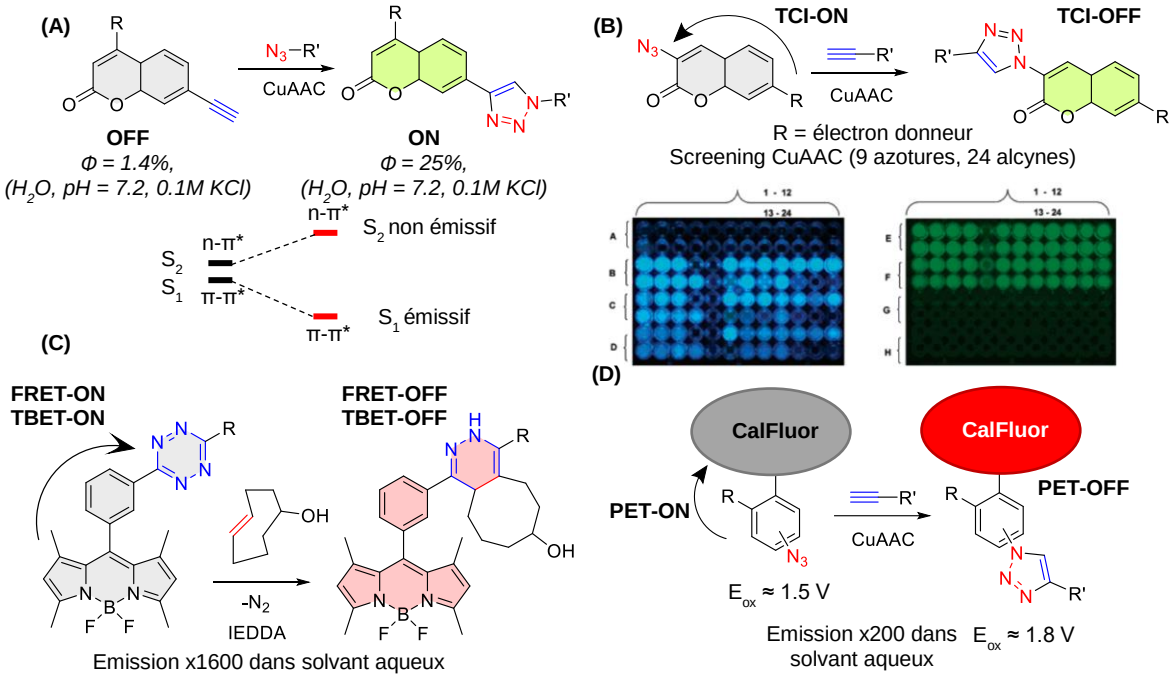

Figure 21: Exemple de fluorophores cliquables fluorogéniques en réponse à une réaction clique.

Les exemples de réactions cliques offrant une réponse ratiométrique sont largement moins documentés, et les fluorophores disposant d'une longueur d'onde d'émission différente avant et après clique sont extrêmement rares.

<u>Exemple de fluorophores cliquables ratiométriques :</u>

- En 2015, H. Fu *et al.*[122] ont utilisé le crézyl violet comme fluorophore azoture (λ_{em} = 566 nm) pour marquer des cellules cancéreuses MCF-7. La réaction clique SPAAC ou CuAAC produit un effet bathochrome du maximum d'émission (λ_{em} = 620 nm) grâce à un effet électrodonneur plus important du triazole formé (Figure 22 **(A)**).
- Y. Wen *et al.*[123] ont développé une naphthalimide azoture ne produisant pas directement une réponse ratiométrique après réaction clique, mais indirectement une fois le boro-ester clivé par oxydation. En cliquant leur sonde sur un peptide ciblant le noyau d'une cellule, ils ont pu détecter la présence de H_2O_2 après oxydation du boro-ester en acide boronique (λ_{em} = 403 nm *versus* 555 nm) (Figure 22 **(B)**).

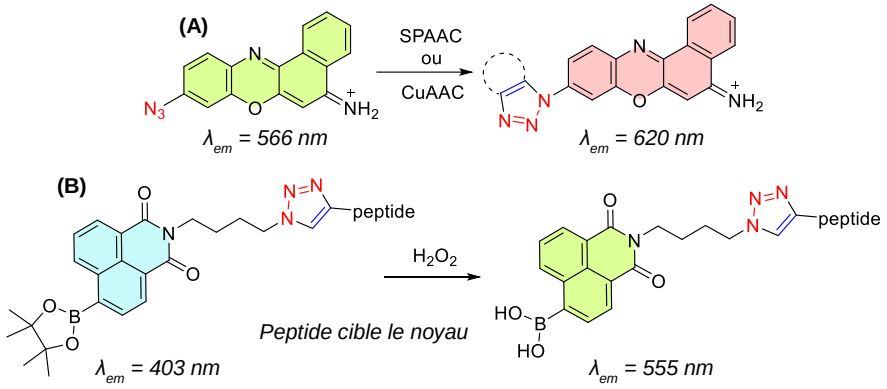

Figure 22: Exemple de fluorophores cliquables ratiométriques en réponse à une réaction clique ou de manière indirecte.

Cependant, l'utilisation de pro-fluorophores est généralement faite sur mesure en fonction du résultat souhaité. Par ailleurs très peu de ces sondes émettent dans le rouge-PIR, et le prix des sondes commerciales (les CalFluor sont commercialisés depuis peu à des prix dépassant 300€/mg) constitue un facteur limitant pour de nombreuses applications.

C'est pour cette raison que nous avons décidé de combiner ces deux domaines : chimie bioorthogonale et fluorophore flavylium rigide, en introduisant une fonction cliquable afin de répondre aux objectifs de cette thèse. Plusieurs possibilités ont été envisagées : la construction de flavyliums cliquables « toujours fluorescents ou always-ON » permettrait de valoriser rapidement cette famille de composés tout en localisant la cible biologique de nos bMDs (plus de détails sont disponibles dans le chapitre 3 de cette thèse). Nous nous sommes également intéressés au développement de pro-fluorophores offrant une réponse fluorogénique après réaction clique en combinaison avec nos bMDs (plus de détails sont disponibles dans le chapitre 3 de cette thèse).

1.4 Objectifs de recherche

Les deux objectifs principaux de cette thèse sont donc les suivants : valider les cibles biologiques des bMDs dans le parasite *P. falciparum* et poursuivre le développement des bMDs afin d'améliorer leurs activités et leurs biodisponibilités. Pour atteindre le premier objectif, nous nous sommes également intéressés au développement de fluorophores cliquables utilisables en imagerie par fluorescence.

A la suite de cette introduction, ce manuscrit de thèse est donc structuré en trois grands chapitres :

I. Développement de sondes bMDs cliquables :
- Utilisation des sondes dans une stratégie (pro-)AfBPP pour étudier leurs cibles protéiques dans le parasite *P. falciparum*.

- Imagerie par fluorescence pour visualiser leur lieu d'action dans les parasites *P. falciparum* et *T. gondii*.
- Synthèse d'analogues hétéroaromatiques de la plasmodione pour évaluer leurs cibles et leurs potentiels antiparasitaires.

II. Développement et exploitation de la famille de fluorophores flavyliums cliquables :

- Preuve de concept utilisant la chimie bioorthogonale en imagerie par fluorescence *in vitro*.
- Etude des systèmes fluorogéniques flavylium-bMDs.

III. Évaluation du potentiel antiparasitaire de pseudo-PDs et du groupement triazole :

- Remplacement du cycle benzylique par un groupement triazole-méthyle.
- Développement de pro-drogues pseudo-PDs portant un méthyle angulaire métabolisable sur le motif quinone.

Ces chapitres détaillent ainsi les avancées et les applications potentielles de nos recherches, visant à améliorer la compréhension et le traitement des infections parasitaires.

Chapitre II : Etude des cibles biologiques des 3-benzylménadiones chez les parasites *P. falciparum* et *T. gondii*

1.1 Utilisation de la stratégie (pro-)AfBPP et conception de sondes bMDs cliquables

1.1.1 Introduction et travaux préliminaires

Quelques temps avant mon arrivée, en 2021[124], l'équipe CBM a publié dans le journal *JACS*^{Au} la mise en place et l'optimisation d'une stratégie (pro-)AfBPP, utilisant une bMD-alcyne cliquable et des protéines purifiées comme modèle biologique (*h*GR et *Pf*GR). Cette stratégie a permis de valider trois sites de fixation au sein de ces deux protéines, validant l'utilisation des sondes bMDs photoactivables et cliquables comme outils de photoaffinité des protéines. L'élaboration de cette méthodologie a servi de base à l'article 1 de cette thèse afin d'étudier le photomarquage spécifique de protéines en mélanges complexes (protéomes entiers) et de déterminer les cibles protéiques des bMDs.

Cette stratégie est extrêmement utile et généralement choisie lorsque l'on souhaite connaitre la(les) cible(s) et le mode d'action d'une molécule active[125]. La méthodologie est complexe et difficile à mettre en place, mais au final, son résultat est crucial dans le développement de nouveaux médicaments. Elle nécessite la conception d'une sonde, basée sur la structure de la molécule active, composée de :

i. La molécule active, pour assurer la reconnaissance avec sa cible biologique
ii. Un groupement rapporteur pour extraire l'adduit médicament-protéine et analyser l'échantillon (fonction cliquable, fluorophore, biotine…)
iii. Un groupement photo-réactif pour créer un lien covalent avec sa cible (diazirine, benzophénone, azoture-aryle) sous photo-irradiation.

De cette façon, une fois l'adduit médicament-protéine formé, une fonction alcyne permet d'utiliser la chimie bioorthogonale en combinaison avec une biotine-azoture pour réaliser un enrichissement de l'échantillon par « pull-down » ou un fluorophore-azoture pour effectuer une séparation des adduits par électrophorèse sur gels d'acrylamide (SDS-PAGE) puis analyse de la fluorescence. De plus, ces techniques permettent d'analyser l'adduit formé par spectroscopie de masse. Dans notre cas, le choix de cette stratégie n'est pas anodin, car la PD une fois oxydée en PDO, puis réduite dans le parasite possède déjà le motif photo-activable benzophénone, ce qui justifie l'utilisation du terme « pro- » AfBPP. Ainsi, la première sonde analogue à la PDO, avec un alcyne en position para du groupement benzylique, a été synthétisée (**1** dans l'article *ChemBioChem*). J'ai d'ailleurs optimisé la voie de synthèse afin de la rendre plus accessible (76% contre 31% rendement totale en 4 étapes). Cette sonde a permis d'optimiser les différentes étapes de la stratégie AfBPP (CuAAC, condition, photo-

marquage, extraction…), avant d'utiliser le dérivé benzylménadione responsable de l'activité chez le parasite (**4** dans l'article *ChemBioChem*).

Ce sont principalement le Dr. Ilaria Iacucci (Post-Doc) et Victoria Monaco (PhD) qui ont optimisé les étapes de cette stratégie et réalisé l'étude protéomique, en utilisant d'abord leGSH comme protéine modèle, puis le protéome extrait de la levure *S. cerevisiae* comme organisme vivant modèle, et enfin le protéome extrait du parasite *P. falciparum*, préalablement incubé avec la sonde parente benzylmenadione cliquable (**4** dans l'article *ChemBioChem*). Cependant, de très faibles rendements étaient obtenus lors du photo-marquage (≈ 5%), réduisant considérablement le rendement global de toute la stratégie et compromettant la sensibilité et la pertinence du résultat final. C'est pourquoi nous avons décidé de synthétiser une nouvelle sonde cliquable alcyne portant un fluor en position 6 de la ménadione (**3** dans l'article *ChemBioChem*) (Figure 23). Nous avons vu dans l'introduction de cette thèse que l'introduction d'un atome de fluor en C-6 de la ménadione était parfaitement tolérée et conférait une résistance métabolique accrue. Le rôle premier de cet atome de fluor était cependant de rendre la NQ et le carbonyle de la benzophénone plus rapidement réductible (grâce à son effet inductif attracteur). Ainsi, comme le carbonyle va être photo-réduit, cette modification devrait améliorer le rendement du photo-marquage. L'effet désiré a été obtenu et prouvé en comparant les potentiels rédox des différentes sondes en électrochimie. Le rendement de photo-marquage est ainsi passé de 5% à 13%, puis à 21% selon les conditions, rendant la stratégie plus reproductible. La sonde benzyle a aussi été synthétisée (**5** dans l'article *ChemBioChem*) afin qu'elle puisse être étudiée dans le parasite *P. falciparum* (Figure 23). La synthèse des deux nouvelles sondes 6-fluoro-bMD-alcynes (**3** et **5**) n'est pas différente de celle des sondes **1** et **4**. La 6-fluoro-ménadione (synthétisée grâce à la stratégie naphtol[55] par le Dr. Nathan Trometer) est utilisée comme substrat à la place de la ménadione. Dans cet article, j'ai pu synthétiser les sondes **3** et **5**, mais aussi optimiser la synthèse des sondes **1** et **4**, ainsi que réaliser l'étude des propriétés rédox de tous ces composés par électrochimie.

Ces nouvelles sondes nous ont permis d'obtenir de nouveaux résultats présentés dans l'article 1, mais surtout d'identifier de nouvelles cibles protéiques chez le parasite *P. falciparum* et la levure, étape indispensable à la compréhension du mode d'action de nos molécules bioactives bMDs.

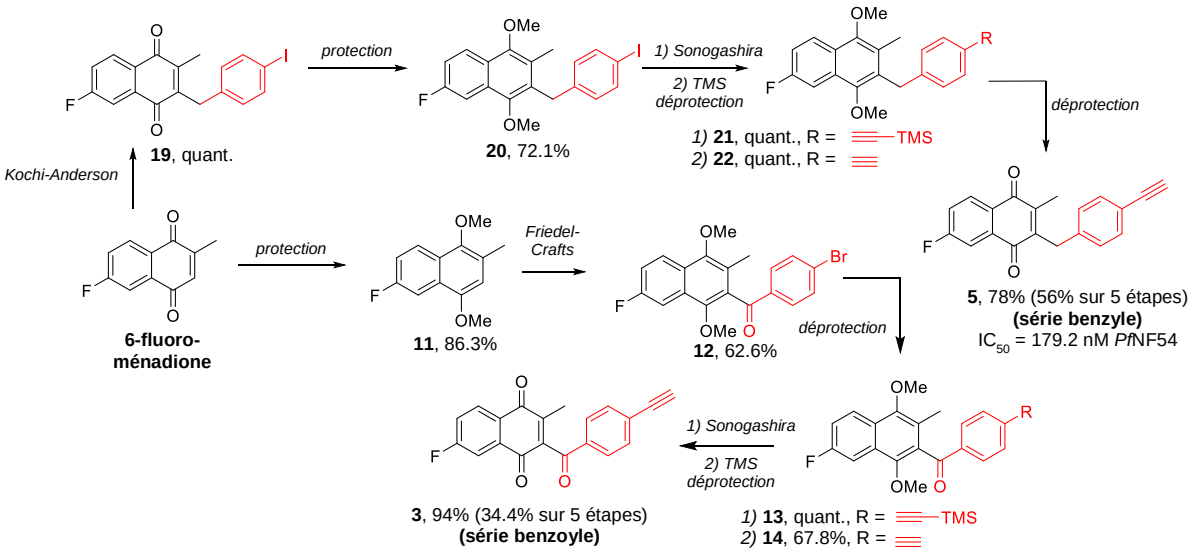

Figure 23: Synthèse des sondes 6-fluoro-bMD-alcynes **3** et **5** utilisées dans la stratégie (pro-)AfBPP. Kochi-Anderson: 4-iodophenylacetic acid, $AgNO_3$, $(NH_4)_2S_2O_8$, CH_3CN:H_2O, reflux, 4h. Protection: 1. $SnCl_2$, HCl, EtOH, 2h, 2. Me_2SO_4, acetone, KOH, MeOH, 60°C, 4h. Sonogashira: ethynyltrimethylsilane, CuI, $Pd(PPh_3)_2Cl_2$, NEt_3, 70°C, 20h. Friedel-Crafts: 4-bromobenzoic acid, TFAA, TfOH, DCM, 16h. TMS déprotection: TBAF, THF, 1.5h. Déprotection: CAN, CH_3CN:H_2O, 1h.

1.1.1 Article 1

Proteomic Profiling of Antimalarial Plasmodione Using 3-Benz(o)ylmenadione Affinity-Based Probes

Dr. Ilaria Iacobucci, Vittoria Monaco, Dr. Agnès Hovasse, Baptiste Dupouy, Dr. Rodrigue Keumoe, Dr. Bogdan Cichocki, Dr. Mourad Elhabiri, Dr. Brigitte Meunier, Dr. Jean-Marc Strub, Prof. Maria Monti, Dr. Sarah Cianférani, Dr. Stéphanie A. Blandin, Dr. Christine Schaeffer-Reiss, Dr. Elisabeth Davioud-Charvet

***ChemBioChem* accepted article**, publié en ligne le 19 Avril 2024

doi: 10.1002/cbic.202400187

Proteomic Profiling of Antimalarial Plasmodione Using 3-Benz(o)ylmenadione Affinity-Based Probes

Ilaria Iacobucci,[a],[b],[c],# Vittoria Monaco,[a],[b],[c],# Agnès Hovasse,[b] Baptiste Dupouy,[a] Rodrigue Keumoe,[d] Bogdan Cichocki,[a] Mourad Elhabiri,[a] Brigitte Meunier,[e] Jean-Marc Strub,[b] Maria Monti,[c] Sarah Cianférani,[b] Stéphanie A. Blandin,[d] Christine Schaeffer-Reiss,[b] Elisabeth Davioud-Charvet*[a]

[a] *Dr. I. Iacobucci, V. Monaco, B. Dupouy, Dr. B. Cichocki, Dr. M. Elhabiri, Dr. E. Davioud-Charvet*
Laboratoire d'Innovation Moléculaire et Applications (LIMA), Team Bio(IN)organic & Medicinal Chemistry,
UMR7042 CNRS-Université de Strasbourg-Université Haute-Alsace
European School of Chemistry, Polymers and Materials (ECPM), 25, rue Becquerel, 25, rue Becquerel, F-67087 Strasbourg (France)
E-mail: elisabeth.davioud@unistra.fr

[b] *Dr. I. Iacobucci, V. Monaco, Dr. A. Hovasse, Dr J.-M. Strub, Dr. S. Cianférani, Dr. C. Schaeffer-Reiss*
Laboratoire de Spectrométrie de Masse BioOrganique
IPHC UMR 7178 CNRS, Université de Strasbourg, 67087 Strasbourg (France)
Infrastructure Nationale de Protéomique ProFI - FR2048, 67087 Strasbourg, France

[c] *Dr. I. Iacobucci, V. Monaco, Prof. M. Monti*
Department of Chemical Sciences
University of Naples Federico II
Complesso Universitario di Monte Sant' Angelo, Via Cintia 26, I-80126 Napoli (Italy)

[d] *Dr. R. Keumoe, Dr.S. A. Blandin*
Institut de Biologie Moléculaire et Cellulaire,
INSERM U1257 - CNRS UPR9022 - Université de Strasbourg,
2, Allée Konrad Roentgen - 67084, Strasbourg (France)

[e] *Dr. Brigitte Meunier,*
Institute for Integrative Biology of the Cell (I2BC),
CEA, CNRS, Univ. Paris ‐ Sud, Université Paris ‐ Saclay,
91198 Gif ‐ sur ‐ Yvette cedex, France.

 # authors contributed equally as first co-authors

Supporting information for this article is available on the WWW under https://doi.org/.

Abstract: Understanding the mechanisms of drug action in malarial parasites is crucial for the development of new drugs to combat infection and to counteract drug resistance. Proteomics is a widely used approach to study host-pathogen systems and to identify drug protein targets. Plasmodione is an antiplasmodial early-lead drug exerting potent activities against young asexual and sexual blood stages in vitro with low toxicity to host cells. To elucidate its molecular mechanisms, an affinity-based protein profiling (AfBPP) approach was applied to yeast and *P. falciparum* proteomes. New (pro-)AfBPP probes based on the 3-benz(o)yl-6-fluoro-menadione scaffold were synthesized. With optimized conditions of both photoaffinity labeling and click reaction steps, the AfBPP protocol was then applied to a yeast proteome, yielding 11 putative drug-protein targets. Among these, we found four proteins associated with oxidoreductase activities, the hypothesized type of targets for plasmodione and its metabolites, and other proteins associated with the mitochondria. In *Plasmodium* parasites, the MS analysis revealed 44 potential plasmodione targets that need to be validated in further studies. Finally, the localization of a 3-benzyl-6-fluoromenadione AfBPP probe was studied in the subcellular structures of the parasite at the trophozoite stage.

Introduction

Functional proteomics is devoted to the elucidation of molecular mechanisms in living cells through the investigation of biomolecule interactions. Several approaches have been developed over the years depending on the nature of the interactions and the biomolecules involved,[1,2] leading to the establishment of specific branches of chemistry, such as chemical biology. In particular, chemical proteomics has emerged as a powerful tool to study the interactions between small molecules and proteins.[3,4] In this context, one of the approaches used to identify molecular or drug targets is affinity-based protein profiling (ABPP), a method pioneered by Cravatt and others.[5-8]

This approach, increasingly employed for target identification in malarial parasites, consists in using 'clickable' covalent inhibitor-based probes (ABPP probes)[9,10] or affinity-based photoactivatable and 'clickable' probes (AfBPP probes)[11] to facilitate chemical pulldowns of the probe-protein adducts. AfBPP probes contain both a photo-affinity group and a reporter group for bioorthogonal chemistry (typically an alkyne), which are attached to a compound of interest at a tolerant position. Live cells or extracted proteins from cell lysates are incubated with AfBPP probes and irradiated with UV light. UV exposure triggers the

photolabeling reactive moiety to form a covalent adduct with the protein target. Then, the 'clickable' reporter tag (alkyne) ensures the labeling of the protein-probe adduct(s) by copper(I)-catalyzed alkyne-azide cycloaddition (CuAAC) "click" reaction with an azide partner (e.g. biotin azide) used for enrichment (e.g. on avidin beads). The labeling step through the biotinylation reaction is required to purify the adducts by affinity-based strategies.[12]

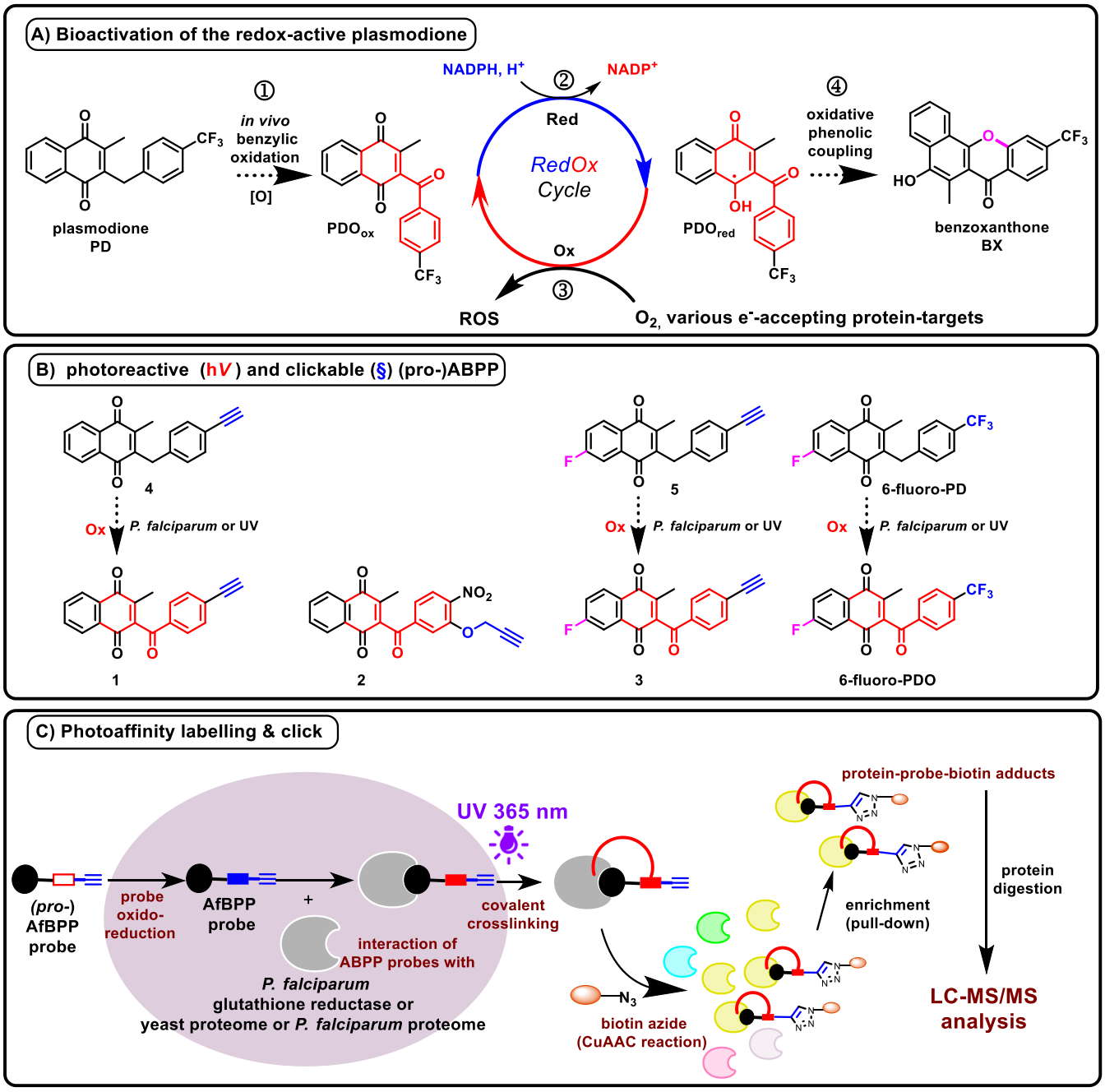

Figure 1. (A) Bioactivation of Plasmodione (**PD**): upon internalization in the parasite, plasmodione **PD** is proposed to generate **PDO$_{ox}$**, a drug metabolite, by benzylic oxidation (step ①), the 3-benzoylmenadione (benzoylMD), which, under its oxidized form, possesses a photoreactive benzophenone-like moiety (indicated in red). This metabolite is further reduced (step ②), and **PDO$_{red}$** takes part in oxidoreductase-mediated redox-cycling (step ③) leading to ROS-induced parasite death. (B) Plasmodione-affinity based probes (PD-AfBPP): The common scaffold of the PD-AfBPP probes **1**-**3** and **6-fluoro-PDO** is a photoreactive benzoylMD, functionalized by different electron-withdrawing groups in *para* position of the benzylic chain (-CF_3 or -alkyne), and a H or F at C-6 of the menadione core, affecting their photoreactivity. Introduction of the fluorine atom at C-6 of the menadione core was designed to improve the efficiency of the AfBPP probe. The parent benzylMDs, the (*pro*-)AfBPP probes **5**-**6** or the **6-fluoro-PD**, are not photoreactive *per se*, whereas the benzoylMD probes **1**-**3** are. (C) AfBPP strategy: this approach aims at identifying proteins that interact with the PD-AfBPP drug metabolite in living parasites incubated with a parent precursor designed as *(pro-)*PD-AfBPP. The PD-AfBPP probe is released from the (*pro*-)PD-AfBPP probe through benzylic oxidation upon bioactivation in the living cell or following UV irradiation. Upon UV irradiation, covalent crosslinking of PD-AfBPP to its potential targets in yeast and *P. falciparum* proteomes occurs and enrichment of the probe-protein-biotin adducts

is achieved by a CuAAC reaction between the probe-derived alkyne and the biotin azide. After streptavidin pulldown, enriched proteins are digested on-beads, and tryptic peptides identified by label-free quantitative mass spectrometry (LFQ) using LC-MS/MS.

Malaria is the most devastating tropical parasitic disease causing 619,000 deaths/year. It is both a cause and a consequence of poverty, mostly in Sub-Saharan Africa, by impacting social and economic lives. The limited arsenal of effective and nontoxic drugs to cure this devastating infectious disease and their inefficacy to kill resistant parasites, represent major public health challenges. The launching of new generation of antimalarial drugs active against artemisinin-resistant parasites and blocking transmission of the parasites to the mosquitoes would represent a big hope towards malaria control and elimination. The widespread development of drug-resistant parasite strains against the commonly used drug series of endoperoxides, illustrated by the lead drug artemisinin, creates a necessity to identify new drug targets and to develop original chemotypes with new modes of action (MoA). Open access to the full *Plasmodium* genome and proteome has brought new opportunities to identify novel drug targets. So far, very few oxidoreductases have been identified as antimalarial drug targets.[13,14]

In the last decade, we have discovered an early lead redox-active compound, called plasmodione (**PD**), belonging to the 3-benzylmenadione (benzylMD) family, with a unique mechanism of action[15] that has been partly deciphered (Figure 1, panel A). **PD** acts as a prodrug entering in a cascade of redox reactions, with highest activity in young early stages and gametocytes.[16] Its specific bioactivation generates a key 3-benzoylmenadione (benzoylMD) called plasmodione oxide (**PDO**) with increased oxidant properties.[17] The active metabolite $\mathbf{PDO_{ox}}$ was shown to act as a subversive substrate of various flavoenzymes, producing reduced **PDO** ($\mathbf{PDO_{red}}$) and initiating a redox-cycling process in the presence of oxygen or methemoglobin. This redox cycling produces damaging compounds such as the benzoxanthone (**BX**),[18] reactive oxygen species (ROS) and oxidative stress, and finally leads to parasite death. Through its key metabolite $\mathbf{PDO_{ox}}$, **PD** likely interacts with several oxidoreductases, associated with multiple vital processes of *P. falciparum*-parasitized red blood cells (pRBCs).

Recently, we designed innovative *(pro-)*AfBPP probes, based on the benzylMD skeleton, as prodrugs entering a cascade of photoredox-reactions to generate related AfBPP probes with a benzophenone-like structure, as found in $\mathbf{PDO_{red}}$.[19] The benzylMD core was photoreduced and then oxidized at the benzylic chain under UV irradiation.[20] The generated reduced benzoylMD covalently reacted with target proteins under UV irradiation. The probe-protein adducts were then clicked with biotin-PEG3-azide (BA) using the CuAAC reaction, pulled-down, digested and analyzed by LC-MS/MS. The AfBPP strategy has been successfully applied to recombinant glutathione reductases from the pRBC unit. Noteworthy, we used 3-benzylMD as (*pro*-)AfBPP probes for the following reasons: i) the released benzophenone-like unit is stable and can be generated in a cascade of redox-reactions catalyzed by oxidoreductases, as **PDO** is generated from **PD**[20]; ii) under high-energy excitation wavelength (350 nm), benzyl MDs can also be activated in benzoylMDs[20]; iii) the UV-light generated excited diradicaloid triplet species (benzophenone-like moiety) reacts preferentially with C–H bonds in the presence of water or other nucleophiles[21] and iv) if no C–H bond is available, the short-lived diradical species can then relax back to the ground state and reinstate the oxidized benzoylMD, rendering the excitation of the probe reversible in favor of specific labeling.[22]

The AfBPP probes used in the present work are shown in Figure 1, panel B. In particular, the former probes **1** and **2**[19] were used here to optimize the click reaction by employing tetrakis(acetonitrile)copper(I) instead of copper(II) sulfate. Regarding the photoaffinity labelling reaction, as we started from a low yield (5%), we designed and synthesized the new probe **3**, with a fluorine atom at C-6 (Figure 1B), with the aim of enhancing the photoreduction kinetics and increasing the yield of the photoalkylation reaction at the carbonyl group. Since yeast is sensitive to **PD** activity, we used it as a model system to test the whole optimized pipeline both in term of UV irradiation and click reaction conditions. In *S. cerevisiae* cell lysates where bioactivation may not occur, we used the new benzoylMD probe **3** in the AfBPP experiments. In addition, we incubated live *P. falciparum*-pRBCs with the novel *(pro-)*AfBPP probe **5** (Figure 1B), and applied the AfBPP workflow (UV irradiation + click reaction, Figure 1C) on cell lysates. The AfBPP strategy in yeast and *Plasmodium falciparum* revealed potential PD targets that need to be validated in further studies.

Results and Discussion

Following our seminal work with pure recombinant proteins,[19] we improved the (*pro*-)AfBPP methodology by optimizing both the yields of the photoirradiation and the click reaction (CuAAC) using previously reported and new probes and different readouts. We explored the possibility to do so in SDS-PAGE gels using a fluorophore coupled with an azide. However, we demonstrated that a CuAAC-independent fluorescence signal associated to **PDO**-protein adducts was produced by an Excited State Intramolecular Photoinduced Transfer (ESIPT) mechanism,[23] which precluded its use for this specific purpose (See supporting information, section B2.1 including Figures S1-S4).

Optimization of the Click Conditions in Aqueous Solutions

The optimization of the click reaction in quasi-physiological aqueous milieu and the setting up of the best conditions compatible with the proteomics pipeline are critical parameters to improve the whole AfBPP workflow yield. Starting from our reported conditions (i.e. 55% yield with a rhodamine-based fluorophore azide),[19] we first optimized the CuAAC yield using probe **1** and BA (See supporting information, Table S1, Figures S5-S8). To the best of our knowledge, the use of tetrakis(acetonitrile)copper(I) with bathocuproinedisulfonic acid

(BCDA) ligand has never been used before in ABPP/AfBPP experiments to catalyze the CuAAC reaction under aqueous conditions. It gave excellent results in our hands and the highest yield (85%) was reached using the following conditions: 24 µM probe (0.5% ACN in PBS), 300 µM Cu(I):BCDA, 50 µM biotin-PEG3-azide, 0.3% SDS at 56°C for 90 minutes under anaerobic conditions.

Design and Synthesis of Optimized Photoreactive 'Clickable' 3-benz(o)ylmenadiones

The workflow AfBPP methodology was effective on large amounts of purified recombinant protein, and we expected the same to be true when the probe is incubated with a complex protein mixture. However, this was not the case, likely due to the low yield of the UV crosslinking step (~5%)[19] Hence, we decided to first improve the photoreactivity of probe **1** by introducing a fluorine atom in C-6, leading to the 6-fluoro-benzoylMD-alkyne (probe **3**), to increase the benzoylMD photoreduction efficacy.

Using the synthetic route to prepare the benzoylMD probe **1**, originally described in ref.[19], we synthesized the new 3-benzyl- and 3-benzoylMD alkyne probes **5** and **3** bearing a fluorine atom at the position 6 of the naphthoquinone (See supporting information, section A including Scheme S1). The only modification to the synthesis pathway comes from the use of the 6-fluoro-menadione, as starting material, that was prepared in 6 steps in a high-yielding sequence recently described,[24] as starting material instead of the commercial menadione. Of note, in this work, the **6-fluoro-PDO** could also be obtained from the **6-fluoro-PD** using a photoredox reaction under UV light and in the presence of dioxygen to oxidize the benzylic position of the benzylMD leading to **6-fluoro-PDO** with 37% overall yield (2 steps).

Electrochemistry Characterization

Herein, we briefly describe the electrochemistry data acquired on the different probes synthesized in this work (See supporting information, Table S2 and Figures S9-S16). We compared the redox properties of the 6-H and 6-fluorinated benzylMDs. The typical electrochemical profiles of benz(o)ylMD[17,25] and menadione analogues[26] (2-methyl-1,4-naphthoquinone, NQ) have been already described and discussed in detail in previous studies. They rely on two consecutive one-electron reversible waves, which correspond to the sequential NQ core reduction leading to the semi-NQ and dihydro-NQ, respectively. For benzoylMDs (probes **1-3**, **PDO**, **6-fluoro-PDO**) a third weak and broad wave is observed at much more negative values and is attributed to redox process centered on the benzoyl carbonyl unit (See supporting information, Figures S11-S16). In the absence of the carbonyl group, the new benzylMD derivatives with an alkyne group in *para*, e.g. probe **4**, are significantly less oxidant compared to their benzoylMD congeners, as observed for **PD** vs **PDO**[17] and **4** vs **1**, making the reduction of semi-NQ to dihydro-NQ more difficult (See supporting information, Table S2). In the case of the benzoylMD, the substitution with an alkyne moiety has a significant effect on the redox process centered on the carbonyl function, without profoundly altering the redox properties centered on the NQ moiety. A difference of about 50 mV between the alkyne and trifluoromethyl group substituted in C-4' of the benzoylMDs (**1** vs **PDO**) is indeed detected, suggesting that the alkyne unit favors the carbonyl reduction. In probe **3**, both combined substitutions – a fluorine atom at C-6 of the menadione core and a *para*-alkyne function on its benzyl moiety – favor the reduction of the semi-NQ and the carbonyl function, an effect which was expected to improve the photo-crosslinking properties in an AfBPP application.

Optimization of the Photoaffinity Labeling of GSH with Probe 3

The photolabeling properties of probe **3** were tested in comparison to former probes **1-2**, and confirmed to provide better yield of reaction (13% in the best condition vs. 5%[19], See supporting information, Figure S17). The photolabeling was then investigated in the AfBPP conditions procedure, with 10% ACN, but gave poor yield results. Therefore, we introduced propan-2-ol as co-solvent. This solvent was already used in the benzophenone-like UV-irradiation reaction to favor radical triplet excited state formation.[27,28] The generated biradicaloid triplet excited state lifetime of the benzophenone is shorter in the presence of propan-2-ol than in other organic solvents. This can be very useful to avoid nonspecific labeling, especially when the probe interacts weakly with its target.[21] In the newly optimized conditions, the photolabeling reaction was carried out in a final percentage of 10% propan-2-ol and 10 µM probe **3** for 15 minutes of irradiation, yielding to 21% adduct (See supporting information, Figure S18).

Proteome Analysis of *S. cerevisiae*

We previously demonstrated that **PD** inhibits yeast respiratory growth and that the mitochondrial respiratory chain flavoprotein NADH-dehydrogenases play a key role in **PD** activity.[29] The deletion of the *NDE1* gene encoding the main NADH-dehydrogenase in yeast resulted in a decreased sensitivity to **PD**.[29] Before performing an AfBPP analysis on this model organism, we first performed a label-free quantitative proteomic study to evaluate the depth of our proteomic set up (1556 proteins representing 26% of the yeast open reading frames) as well as the effects of *NDE1* gene deletion (See supporting information, Figure S19).

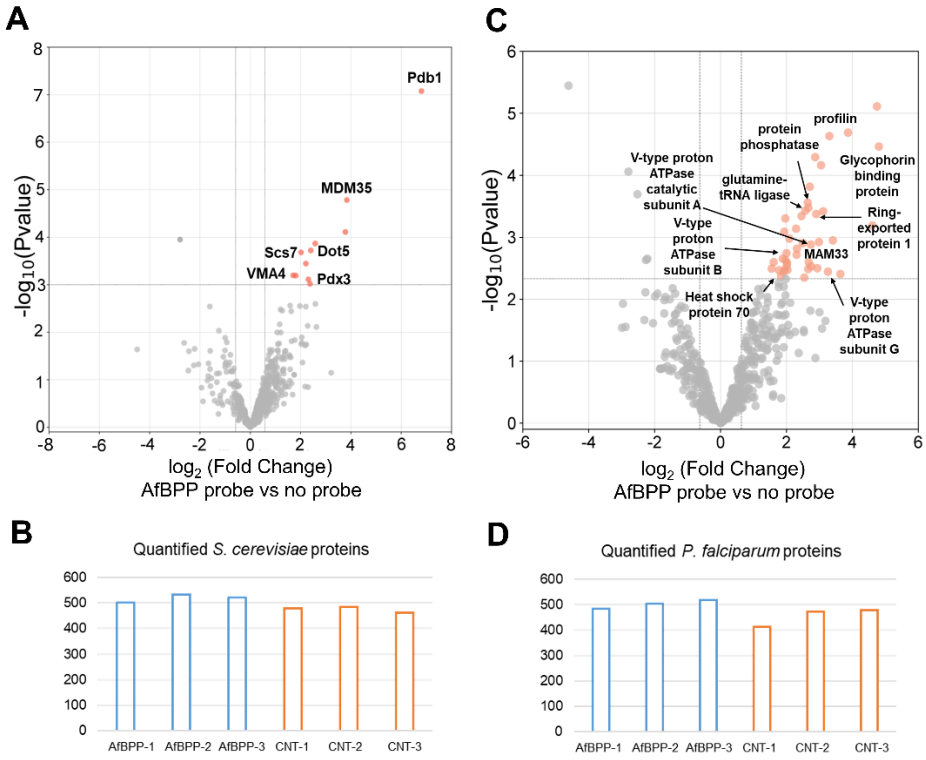

Figure 2. Volcano plots A and C represent *S. cerevisiae* proteins quantified in the AfBPP (AfBPP-1 to -3) *versus* control (CNT-1 to 3) experiments with probe **3,** and *P. falciparum* proteins quantified in the AfBPP (AfBPP-1 to -3) versus control (CNT-1 to -3) experiments with probe **5**, respectively. The red dots correspond to significantly enriched proteins in AfBPP samples. Panels B and D show the number of quantified proteins by replicate after stringent filtering for *S. cerevisiae* and *P. falciparum* respectively.

Affinity-Based Protein Profiling on *S. cerevisiae* Protein Extracts

We performed AfBPP on yeast using the optimized conditions. WT yeast cells were lysed and the protein extract quantified. For each condition, 400 µg were incubated with 10 µM probe **3**, or ACN (used as control), in the presence of 10% propan-2-ol, with irradiation at 350 nm over 15 minutes to cross link the probe to target proteins. The protein extracts were then subjected to the click reaction to biotinylate the clickable drug bound to the protein targets. After the click reaction, the sample was incubated with streptavidin beads, and the bound proteins were directly digested on beads. The peptide mixture was analyzed by nanoLC-MS/MS. Of the 875 proteins identified (Supplementary Table S2), roughly 500 proteins per replicate were quantified after stringent filtering (Figure 2, Panels A-B). Among these, 11 were found to be statistically more abundant in the AfBPP experiments than in the controls, given an FDR of less than 5% (Supplementary Table S3). Of these 11 proteins, 3 are involved in oxidoreductase activities (Pdb1, Dot5, Scs7) and one belongs to the yeast flavoproteome (Pdx3).[30] Interestingly Pdx3 is localized in the mitochondria and we previously showed that mitochondrial flavoenzymes played a key role in the activity of PD.[31] Pdb1 is the E1 beta subunit of the pyruvate dehydrogenase complex (PDH) also localized in the mitochondria. In addition to E1, PDH is formed of E2 (dihydrolipoamide acetyltransferase) and E3 (dihydrolipoamide dehydrogenase) components, with the structural protein Pdx1. We previously found that E3 (or Lpd1) and Lip2, acting in the attachment of lipoic acid groups to E2 were involved in PD activity.[31] The role of Pdb1 will be worth investigating. Dot5 and Scs7 are localized to the nucleus and the endoplasmic reticulum, respectively, but they might also be interesting to analyze.

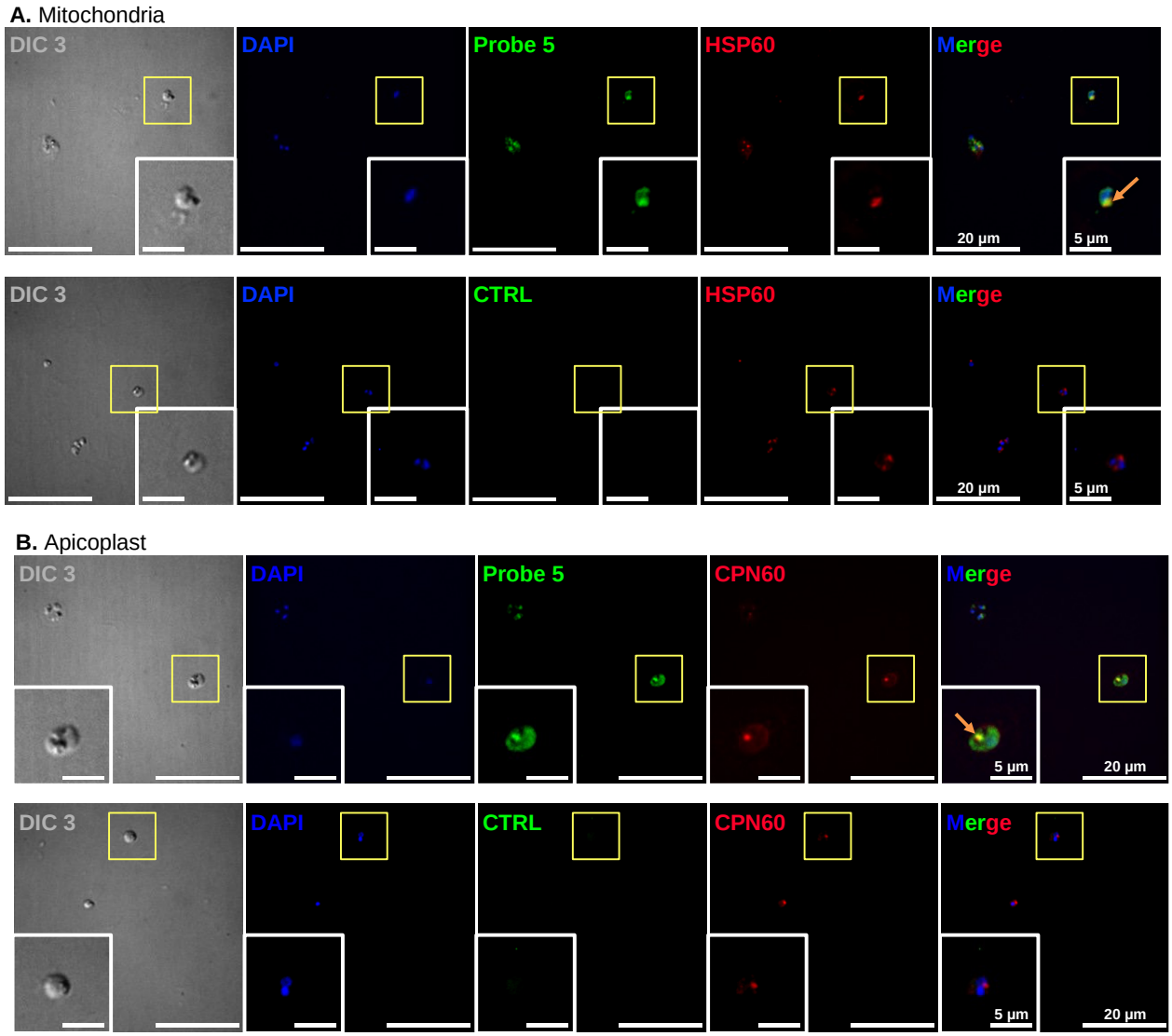

Figure 3. Cellular localization of probe **5** in asexual blood stages of *P. falciparum* (trophozoite stage) after 2h of incubation. The probe was detected using CuAAC reaction with Alexa Fluor 488-azide (green). Nucleic acids were DAPI-stained (blue), and antibodies specific to *P. falciparum* HSP60 and CPN60 were used to localize the mitochondria (panel A, red) and the apicoplast (panel B, red), respectively. Controls were incubated without drugs. Data from 3 replicates.

Antimalarial Properties and Localization of (pro-) AfBPP Probes

Before performing AfBPP on *P. falciparum*, we first validated that the (*pro*-)AfBPP probes were active on parasites. **PD**, its 6-fluoro analogue **6-fluoro-PD**,[32] and probe **1**[19] are equally active against the CQ-resistant Dd2 strain with similar IC_{50} values. Probe **5** is also effective against *P. falciparum*, although less than **PD**, with IC_{50} values of 179.2 ± 27.2 nM and 46.6 ± 21.2 nM, respectively, on the drug sensitive strain NF54. As previously observed in both parasites[15,33] and yeast,[29,33] and despite being the key metabolites of benzylMDs,[20] benzoylMDs like probe **3** (the putative metabolite of probe **5**), do not display a high antimalarial activity, with IC_{50} of *ca.* 10-50 fold higher than those of the corresponding benzylMD. This can be explained by the poor internalization of benzoylMD metabolites in pRBCs or yeast when given to live cells. We further demonstrated that probe **5** was efficiently internalized into parasites. For this, parasites at the young trophozoite stage were incubated with probe **5**, or no probe as control, for 2 and 4h before fixation. Probe **5** was labeled with a fluorescent probe carrying an azide function (Alexa Fluor 488) through a click reaction (Figure 3). After 2 h or 4 h of incubation, probe **5** presented a general but heterogeneous distribution inside parasites, suggesting that it may be specifically concentrated in or around certain organelles. We therefore performed co-staining with antibodies against proteins that are specific to mitochondria and apicoplast (Figure 3). We observed an association of probe **5** and apicoplast or mitochondria signals in 32% and 48% of the parasites, respectively. This association did not appear to depend on the age of the parasite. The presence of probe **5** inside parasites, and its antimalarial activity indicated that we could use it as a (*pro*-)AfBPP probe to identify putative benzylMD targets in *P. falciparum*.

Affinity-Based Protein Profiling on *P. falciparum* Parasites

To perform the AfBPP in *P. falciparum*, and because of very limited material available at early stages, we incubated pRBCs (NF54 strain) at 24 h post invasion (young trophozoite stage) with 5 µM of *(pro-)*AfBPP probe **5**, or with 0.08% DMSO as control. pRBCs were lysed after 5 h of treatment, and the parasites washed to remove the excess of hemoglobin. Parasite pellets were then irradiated for 15 min and lysed, and protein extracts were subjected to click chemistry and pulldown according to our optimized protocol. The peptide mixture was analyzed by nanoLC-MS/MS. Proteins were identified using the *P. falciparum* NF54 proteome from the PlasmoDB database. Of the 960 proteins identified (Supplementary Table S4), roughly 500 proteins per replicate were quantified after stringent filtering (Figure 2, Panels C-D). Among these, 44 were found to be statistically more abundant in the AfBPP experiments than in the controls without probe, given an FDR of less than 5% (Supplementary Table S5).

We analyzed the localization and putative function of the 44 proteins (Supplementary Table S6). The list did not appear to be enriched in proteins from a specific subcellular organelle, which is in accordance with the general albeit heterogeneous localization of probe **5** (Figure 3). Of note, and although benzylMDs are expected to be activated by and to redox cycle with flavoenzymes, there was none in the list of enriched proteins in probe **5** samples. Still, we noted the presence of 3 subunits of the parasitic V-type proton ATPase, a complex that was also identified in the AfBPP experiment performed in yeast (VMA4). In *P. falciparum* trophozoites, the V-type proton ATPase controls the pH of the parasite cytosol and food vacuole.[34] Exposure of malarial parasites to oxidative stress triggers a drop in the intracellular ATP level and inhibits V-type H(+)-ATPase, causing a loss of pH control in both the parasite cytosol and the internal digestive vacuole.[35] Furthermore, the antimalarial ROS-inducer plakortin was reported to generate protein modifications at ring and trophozoite stages, by triggering lipid peroxidation and formation of 4-HNE-protein conjugates in pRBC with the V-type proton ATPase catalytic subunit A and heat shock protein Hsp70-1,[36] that was also pulled down with the AfBPP probe. The most enriched proteins in probe **5** samples are all essential for the parasite life cycle: a glycophorin binding protein (surface protein), 2 mitochondrial chaperonins, and profilin (cytoplasmic). It will be interesting to evaluate the contribution of some of these candidate genes in the MoA of benzylMDs, and to further identify putative **PD** target proteins, varying exposure time and exploring other parasite stages, notably rings that are especially sensitive to benzylMDs, and gametocytes.

Conclusions

The yeast and *P. falciparum* protein profiling data generated in the presence of **PD** affinity-based probes built on the 3-benz(o)ylmenadione motif are presented here in this first special issue "Chemical Biology *Tour de France*". After a first proof-of-concept with a pure recombinant protein,[19] yeast or plasmodial lysates were photoirradiated with new AfBPP or (pro-)AfBPP probes, and the proteins were pulled-down after a CuAAC reaction with BA, allowing us to evaluate the reactivity of the new probes in a MS-based target analysis. We demonstrated that (pro-)AfBPP probes are indeed suitable for the search and exploration of **PD** target proteins.

Altogether, these experiments not only represent a "*Tour de force*" in the field of chemical biology and probe design for antimalarial drugs, but also showcase how to approach such challenging tasks as target identification – which extends very generally to medicinal chemistry. Further optimization of the AfBPP probes and photoaffinity reaction conditions will be key in the future to investigate other *P. falciparum* stages with more limited material, notably rings and gametocytes, and various parasite strains expressing distinct degrees of susceptibilities to artemisinin.

Experimental Section

Chemistry. General

All the reagents and solvents were purchased from commercial sources and used as received, unless otherwise stated. The ^{1}H and ^{13}C NMR spectra were obtained in $CDCl_3$ as solvents using a 400 MHz or a 500 MHz spectrometer. Chemical shifts were reported in parts per million (δ). ^{1}H NMR data were reported as follows: chemical shift (δ ppm) (multiplicity, coupling constant (Hz), and integration). Multiplicities are reported as follows: s = singlet, d = doublet, t = triplet, q = quartet, m = multiplet, or combinations thereof. High-resolution mass spectroscopy (HRMS) spectra were recorded using the electron spray ionization (ESI) technique.

Chemistry. Synthesis of Precursors

Reactants and building blocks were purchased from commercial sources, such as Fluorochem, Sigma-Aldrich, BLDpharmtech or Alfa Aesar. 1,4-dimethoxy-2-methyl-naphthalene **7** was synthesized according to the previously published method.[37] **Synthesis of probes 1-5**, **6-fluoro-PDO.** Synthetic processes and chemical analyses were detailed in the supporting information (Scheme S1 and section B1).

Peptide Photolabeling under UV Irradiation

Photolabeling of the GSH peptide with the probe **3** was performed under UV-irradiation with a 350 nm light generated by eight RPR-3500A lamps of 200 W with a Rayonet photochemical reactor for different times at 16°C. Stock solutions of GSH (Sigma) were prepared in PBS 1x, instead, stock solutions of probe **3** were prepared in ACN. In all the reactions GSH and probe **3** stock solutions were deoxygenated separately and then mixed to start the photoreaction. Samples were deoxygenated by five alternative cycles of vacuum and argon flux in anaerobic vials, longer argon than vacuum cycles were used to avoid ACN evaporation. The different concentration of the probe and the GSH peptide used for the experiment were incubated and then irradiated for the specific time. After irradiation 1 nmol of each sample was analyzed by LC-MS with a Q-TOF mass spectrometer (maXis II, Bruker) coupled with an Agilent 1100 series LC. Samples were separated on an XBridge Peptide BEH (Waters) C18 column (300 Å, 3.5 µm, 2.1 mm × 250mm) column working at a 250 µL/min flow rate, using a non-linear 5-95% gradient of eluent B (0.08% TFA, in ACN LC-MS Grade) over 40 min.

Click Reaction Optimization in Aqueous Conditions

The CuAAC was optimized by tuning several conditions in terms of probe solvent, reaction temperature, copper complex catalyst (see Table 1). The reactions under anaerobic conditions were carried out as previously reported.[19] The Cu(I) complex catalyst (See supporting information, Table S1) was prepared by mixing bathocuproin sulfonate disodium salt hydrate (BCDA, ThermoFisher) and tetrakis(acetonitrile)copper(I) (BLD Pharmatech Gmb, Germany) under anaerobic conditions. Each reaction was carried out in the presence of 0.3% sodium dodecyl sulfate (SDS) final concentrations. The reactions were monitored over time and the products analyzed by LC-UV-MS with a Q-ToF (maXis II, Bruker) mass spectrometer coupled to an HPLC and DAD detector (Agilent). Samples were fractionated with an XBridge Peptide BEH C18 column (300 Å, 3.5 µm, 2.1 mm × 250 mm) column working at a 250 µL/min flow rate, using a non-linear 20-95% gradient of eluent B (0.08% TFA, in ACN LC-MS Grade) over 40 min. To calculate the yield of the reactions at each time, the peak areas of the extracted ion chromatogram (EIC) were used.

S. cerevisiae Cultures

The *S. cerevisiae* strains used were AD-9, referred as wild-type (WT) and its derived mutant *ΔNDE1* in which the gene encoding for the protein Nde1 was deleted.[29] The cells were grown at 28°C in a galactose medium (YPGal, yeast extract 1%, peptone 2%, galactose 2%, glucose 0.1%) and the culture was stopped at OD_{600} ≈2.5.

Proteomic Analysis of *S. cerevisiae* Cells

The yeast pellets were lysed by adding 1 mL of RIPA buffer to ≈ 200 mg of pellet. The resuspended pellets were subjected to 10 cycles of sonication (1 cycle = 30 sec sonication on and 30 sec off) at 4°C. The protein extracts were recovered by centrifugation at 16,000 g for 2 minutes at 25 °C. Triplicates of 50 µg of each lysate were subjected to enzymatic digestion with trypsin/LysC by using the single-pot, solid-phase-enhanced sample-preparation (SP3) technology. The peptide mixtures obtained were analyzed by nanoLC-MS/MS, the method is described below in the LC-MS/MS analysis part. The raw data obtained from the three wild-type and mutant samples were processed by MaxQuant for protein identification and quantification. Protein identification and quantification were performed with the software MaxQuant by using the UniProt database for *S. cerevisiae.* MaxQuant parameters for protein identification were set to 3 peptides at least, with 1% false discovery rate (FDR) confidence. We used Perseus software to perform the statistical analysis of the differentially expressed proteins. In particular, contaminants and reverse proteins were removed, proteins with 50% of valid values in at least WT or mutant group were retained for the following analysis. To obtain the differentially expressed proteins, a Student's t-test was performed fixing a 5% FDR (Benjamini-Hochberg adjusted p-value).

AfBPP Strategy on Recombinant *Pf*GR and Western Blot Analysis

PfGR (200 µg) was incubated with 10µM probe **2** and then photoirradiated at 350 nm for 10 minutes at 16°C. As control *PfGR* was incubated also with 0.5% ACN, in the absence of the probe. The click reaction was performed as described in the section 'Click reaction optimization in aqueous conditions', but adding an excess of 10x BA (Lumiprobe). The reaction mixture was precipitated by a classical methanol/chloroform procedure to remove the excess of unreacted species. The samples were resuspended in 200µl of 150 mM NaCl, 0.1% NP-40 in PBS and incubated over-night at 4°C with Pierce Streptavidin magnetic beads (10 µl), previously washed 5 times with the same buffer. The beads were washed one time with 300mM NaCl in PBS, two times with 0.1% SDS in PBS, and, finally, with PBS. The biotinylated protein was eluted by adding Laemli buffer and incubating 10 minutes at 95°C. The samples were loaded onto a 10% SDS-PAGE gel and then transferred onto a nitrocellulose membrane by means of Trans-Blot Turbo Transfer System (Bio-Rad). The membrane was blocked with 5% BSA in TBS, and then incubated over-night with 1:10,000 anti-biotin polyclonal antibody (ThermoFisher, cat. code #31852). Anti-Goat HRP antibody (ThermoFisher) incubation followed in 1:10,000 ratio for 45 minutes. The chemiluminescence signal was acquired after reaction with ECL substrate with ChemiDoc Touch Imaging System.

Affinity-Based Protein Profiling Procedure on *S. cerevisiae*

Yeast cells (AD1-9, WT) were lysed by overnight pellet incubation of the with lysis buffer (1% NP40, 150 NaCl, 1x PBS and protease inhibitors) and then by sonicating them 10 cycles (one cycles: 5 seconds sonication at 10% amplitude and 15 seconds on ice), then centrifuged for 10 minutes at 13,000 rpm at 4°C. Protein extract was recovered and quantified (Pierce Assay 660nm kit, Thermo Fisher) before to the deoxygenation protocol. Afterwards, protein extract was incubated for 15 minutes in triplicate with deoxygenated solution of the AfBPP probe **3** at 10 µM and 10% propan-2-ol (or CAN) used as control. The samples were then irradiated with an UV lamp at 350 nm for 15 minutes at 16°C. All the solutions were subjected to click reaction, by adding a molar excess of 25 times of BA in 300 µM Cu:BCDA solution under deoxygenated conditions over 90 minutes at 56°C. Reactions were stopped by adding EDTA in a final concentration of 5mM and by buffer exchange protocol by using Zeba spin cartridges (Thermo Fisher) by using 0.2% NP40, 150 mM NaCl, 1x PBS. The samples were then incubated overnight at 4°C with Streptavidin beads pre-washed with the same buffer used for the exchange protocol. The next day, the beads were washed 4 times (0.2% NP40, 300mM NaCl, 1x PBS (1x); 0.1% SDS (2x); 1x PBS (1x)) and then incubated with a solution of DDT 5 mM in ammonium bicarbonate 50 mM for 30 minutes at 37°C. A final concentration of 20 mM IAM in 50 mM ammonium bicarbonate was then added and the samples incubated for 30 minutes at 25°C in the dark. The beads were washed once with 50 mM ammonium bicarbonate and then incubated with 1:10 w/w trypsin/lys-C (Promega) solution in 50 mM ammonium bicarbonate at 37°C overnight. Peptides were eluted by washing the beads with ammonium bicarbonate, then dried and the peptide concentration was determined (Pierce™ Quantitative Peptide Assays & Standards, Product cat. code: #23275). The peptide mixtures were then subjected to a solid phase extraction (SPE) protocol using Oasis HBL 30 mg cartridges (Waters) and injected into an Orbitrap-Q Exactive Plus instrument, as reported in the "LC-MS/MS analysis" section, and data interpretation is reported in data analysis part.

In Vitro Anti-*Plasmodium* Activity Assays

The inhibition of intraerythrocytic parasite development by benzylMD derivatives and control agents (IC_{50} **PD** = 46.6 ± 21.2 nM) was determined in microtiter tests according to standard protocols. The *in vitro* antimalarial activity is expressed as 50 % inhibitory concentration (IC_{50}). For this, *P. falciparum* wild-type strain NF54 was cultured at 37 °C in RPMI medium containing 5 % human serum + 0.5% albumax and type A erythrocytes at a hematocrit of 3 % under a low-oxygen atmosphere (5 % CO_2, 5

% O_2, 90% N_2) and 95 % humidity following standard protocols.[38] These culture conditions were used for all *P. falciparum* experiments. Synchronous ring stage parasites (0-3 hpi) were obtained by centrifugation on a 75% percoll density centrifugation followed by 5% sorbitol treatment.[39] Inhibitors were dissolved at 6 mM in 100% DMSO, diluted in culture medium and added at decreasing concentrations (1/3 serial dilutions in duplicates) to synchronized ring stage parasite cultures in microtiter plates (0.5 % parasitemia, 1.5 % hematocrit) and incubated for 72 h. The final inhibitor concentrations in each assay ranged from 1.4 nM to 3 µM. Growth inhibition was determined in a SYBR green assay as described previously.[40,41] Experiments were performed at least three times independently.

Bioimaging of (pro-) AfBPP Probe 5 in *P. falciparum* Trophozoites

Trophozoite stages of *Plasmodium falciparum* NF54 strain (5% parasitemia, 1.5% hematocrit) were incubated with probe **5** at 10 µM for 2 or 4 hours. Dual Click chemistry and immuno-staining were performed on fixed blood smear according to the described protocol[42] with some modifications. In brief, thin blood smears were fixed with 4% (w/v) paraformaldehyde in PBS and permeabilized for 10 min with 0.1% Triton X-100 in PBS. The click reaction was then performed for 30 minutes at room temperature with 5 µM of Alexa Fluor 488 Azide (Thermo Fisher, ref A10266) in the presence of $CuSO_4$ in the "Click-it" Cell Reaction Buffer Kit (Thermo Fisher, ref C10269) according to manufacturer's conditions. The samples were then processed for co-staining with the mitochondria and apicoplast specific antibodies as follows. The slides were blocked with 3% (w/v) BSA in PBS for 15 minutes and incubated either with (1) mouse polyclonal antibodies raised against the mitochondrial protein *Pf*HSP60 (1:500 dilution in 3% BSA) (kind gift of Philippe Grellier, Muséum National d'Histoire Naturelle, Paris) followed by goat anti-mouse IgG conjugated with Alexa Fluor 647 (1:1000 dilution in 3% BSA) (Thermo Fisher, ref A21235), or with (2) rabbit polyclonal antibodies raised against *Toxoplasma gondii* CPN60 (1:500 dilution in 3% BSA, cross-reacting with *Pf*CPN60)[43] followed by goat anti-rabbit IgG conjugated with Alexa Fluor 647 (1:1000 dilution in 3% BSA) (Thermo Fisher, ref A21244). Parasite nuclei were stained with DAPI (1:1000 dilution in PBS) (Thermo Fisher, ref 62248). The slides were mounted in Immu-Mount (Epredia, ref 9990402) and image acquisition (z-series) was realized on a Zeiss axio observer Z1 inverse microscope equipped with a CSU-X1 Yokogawa spinning disk and an EMCCD camera Roper Evolve, and using a Plan apochromat 100x/1.40 oil objective. Images were processed with Fiji software (ImageJ2, version 2.14.0/1.54f) and final figures were compiled using the Quickfigures plugin. The images presented correspond to the sum of intensity projection of the z-series.

Affinity-Based Protein Profiling Procedure on *P. falciparum*

The *in-situ* AfBPP procedure closely follows the methodology outlined by Nardella and coworkers.[44] with some modifications. Tightly synchronized trophozoites stage parasite culture was obtained by subjecting late-stage schizont parasites to a 75% Percoll density centrifugation, followed by the collection of 0-3 hpi young newly formed rings with 5% sorbitol treatment. Parasites were then further cultured for 24h. Highly synchronized trophozoites of *P. falciparum NF54* cultures (5% parasitemia and 3% hematocrit, 25mL culture each) were treated with 5 µM of the *(pro-)*AfBPP probe **5** or 0.08% DMSO for a duration of 5h. All treatments were carried out in triplicate. Subsequently, parasites were harvested by saponin lysis (using 0.15% saponin in ice-cold 1X PBS) and thoroughly washed in ice-cold 1X PBS to eliminate hemoglobin contaminants. Parasite pellets were resuspended in 1mL of 1X PBS and transferred to glass tube compatible with photo-irradiation. They were exposed to a 15-minute irradiation at 350 nm on ice using a UV lamp. Parasite were then centrifuged and incubated for 5 minutes in 100µL lysis buffer (PBS 1x, 1% SDS, 1 mM dithiothreitol (DTT) protease inhibitors cocktail), subjected to three cycle of freeze (-80°C, 5min)/thaw (42°C, 2min), sonicated 10 times for 5 seconds at 10% amplitude and centrifuged for 10 minutes at 13000 rpm at 4°C. The protein extracts were quantified and for each condition, 300 µg were subjected to the click reaction by adding BA in a final concentration of 1 mM in 300 µM Cu:BCDA solution in deoxygenated conditions for 90 minutes at 56°C. Reactions were stopped by adding EDTA to a final concentration of 5 mM and processed as for the yeast AfBPP protocol previously described.

LC-MS/MS analysis

NanoLC-MS/MS analyses were performed with a nanoAcquity UPLC device (WatersCorporation, Milford, MA, USA) coupled to a Q-Exactive Plus mass spectrometer (ThermoFisher Scientific, Waltham, MA, USA). Peptide separation was performed on an Acquity UPLC BEH130 C18 column (250 mm × 75 µm with 1.7-µm-diameter particles) and a Symmetry C18 precolumn (20 mm × 180 µm with 5-µm-diameter particles, Waters). The solvent system consisted of 0.1% formic acid (FA) in water and 0.1% FA in ACN starting from 1% to 35% of eluent B over 79 minutes. The system was operated in data dependent acquisition mode with automatic switching between MS and MS/MS modes. The ten most abundant ions were selected on each MS spectrum for further isolation on a scan ranging from 300 to 1800 m/z. HCD fragmentation method was used with a collision energy (NCE) set to 27. The dynamic exclusion time was set to 60 sec.

Data Analysis

Raw data files were uploaded in MS Angel software and peptide quantification performed with MASCOT interface by using the following parameters: "trypsin" as enzyme with at least one missed cleavage, "carbamidomethyl" as a fixed modification, "oxidation of Met" as variable modifications, 0.05 Da as MS/MS tolerance, and 5 ppm as peptide tolerance. Specific databases were used for the protein identification, the Uniprot database for *S. cerevisiae* and PlasmoDB database for the *P. falciparum* NF54 strain (sequence protein fasta file release number 66). Results were then imported into Proline software (http://proline.profiproteomics.fr/)[45] to validate (1% FDR at PSM and protein level) and quantify the protein identified. Prostar software was used for the statistical analysis.[46]

To be considered, proteins must be identified in all 3 replicates in at least one condition. Protein abundances were normalized using 0.15% quantile centering overall. Imputation of missing values was done using the approximation of the lower limit of quantification by the 2.5% lower quantile of each replicate intensity distribution ("det quantile"). A Limma moderated t-test was applied on the dataset to perform differential analysis. p-Values calibration was corrected using adapted Benjamini-Hochsberg method[47,48] and False Discovery Rate was optimized for each pairwise comparison.

Supporting Information

Pages S2-S3: A. Synthetic Procedures (including Scheme S1); Pages S3-S7: B1. Characterization of Compounds & Materials; Pages S7-S12: B2.1. Characterization of the photo-crosslinked and probe-reacted protein adducts (including Figures S1-S4); Page S13-S15: B2.2. Optimization of the click reaction with probes **1 – 3** (including Table S1 and Figures S5-S7); Page S16: B2.3. Detection of the photo-crosslinked PfGR and the protein-probe 2-adducts by Western-blot and Immunofluorescence

(including Figure S8); Pages S17-S21: B2.4. Electrochemistry (including Table S2 and Figures S9-S16); Pages S22-S23: B2.5. Optimization of the peptide GSH photolabeling in the presence of new probe **3** (including Figures S17-S18); Page S24: B2.6. Proteome analysis of *S. cerevisiae* strains by MS analysis (including Figure S19); Page S24: C. Data Deposition; Pages S25-S42: ^{1}H, ^{19}F, and ^{13}C {^{1}H} NMR spectra of all new compounds.

Supplementary Tables: S1-S6. Data are available via ProteomeXchange with identifier PXD050982.

Acknowledgements

E.D.-C. and S.A.B. wish to thank the Laboratoire d'Excellence (LabEx) ParaFrap [ANR-11-LABX-0024], for funding, providing B.D.'s PhD salary, and for initiating and fostering this scientific research and collaboration. This work was also supported by the European Campus EUCOR, via the seed-money program ("ROSkillers" project), Région Grand'Est program "Compétences Recherche Jeunes Chercheurs – Attractivité Année 2022" with the project "plasmo.Fish&Click" and for the postdoc salary to I. I.. This work was further funded by grants from CNRS Mission pour les initiatives transverses et interdisciplinaires (MITI "Vie & Lumière" program, grant to E.D.-C., S.A.B. and C.S.), from the ANR-FNS (ANR-22-CE93-0005-01, "ROS Action" project to E.D-C., B.M. and S.A.B.). V.M.'s 6 month-training in Strasbourg was supported by the University of Naples (PhD salary) and a STSM grant from the COST Action CA21111 "OneHealth.Drugs". E.D.-C. and B.D. thank Matthieu Roignant for the complete chemical analysis of compound 6-fluoro-1,4-dimethoxy-2-methylnaphthalene **11**. The French Proteomic Infrastructure (ProFI; ANR-10-INBS-08-03, FR2048) is acknowledged for its support to the MS-based proteomics analysis. R.K. is grateful to the IBMC Insectary platform and to Jean Daniel Fauny and Romain Vauchelle from the IBMC Microscopy Platform for their training and guidance in fluorescence microscopy. The laboratories also receive support from CNRS (E.D.-C., S.A.B., C.S. and B.M.), Inserm (S.A.B.) and from the University of Strasbourg (E.D.-C., S.A.B. and C.S.).

Conflict of Interests

The authors declare no conflict of interest.

Abbreviations

ACN, acetonitrile; AfBPP, affinity-based protein profiling; BA, biotin azide; BCDA, Bathocuproinedisulfonic acid; benzoylMD, 3-benzoylmenadione; benzylMD, 3-benzylmenadione; β-met, β-mercaptoethanol; CHX, cyclohexane; CuAAC, copper(I)-catalyzed alkyne-azide cycloaddition; DCM, dichloromethane; EIC, extracted ion chromatogram; FA, formic acid; FDR, false discovery rate; GSH, glutathione; ESIPT, excited state intramolecular photoinduced transfer; LFQ, label-free differential quantitative; MoA, mode of action; PD, plasmodione; PDO, plasmodione oxide; pRBC, parasitized red blood cells; TCEP, Tris(2-carboxyethyl)phosphine; T, toluene.

Keywords: Activity-Based Protein Profiling • Antiprotozoal agents • Biological Chemistry and Chemical Biology • Photoaffinity Labeling • Proteomics

[1] I. Iacobucci, V. Monaco, F. Cozzolino, M. Monti, *J Proteomics.* **2021**, *230*, 103990.
[2] F. Cozzolino, I. Iacobucci, V. Monaco, M. Monti, *J Proteome Res.* **2021**, *20*, 3018.
[3] K. Lu, C. Mansfield, M. Fitzgerald, E. Derbyshire, *ChemBiochem*. **2021**, *22*, 2591.
[4] Y. Gao, M. Ma, W. Li, X. Lei, *Adv Sci*. **2023**, e2305608.
[5] M. Evans, B. Cravatt, *Chem. Rev.* **2006**, *106*, 3279.
[6] B. Cravatt, A. Wright, J. Kozarich, *Annu. Rev. Biochem*. **2008**, *77*, 383.
[7] A. Berger, P. Vitorino, M. Bogyo, *Am J Pharmacogenomics,* **2004**, *4*, 371.
[8] M. Nodwell, S. Sieber, *Top Curr Chem.* **2012**, *324*, 1.
[9] L. Carvalho, G. Bernardes, *ChemMedChem*. **2022**, 17, e202200174.
[10] M. Bogyo, *Trends Parasitol*. **2023**, *39*, 83.
[11] H. Fang, B. Peng, S. Y. Ong, Q. Wu, L. Li, S. Q. Yao. *Chem Sci.* **2021**, *12*, 8288.
[12] L. Wankyu, Z. Huang, C. W Am Ende, U. Seneviratne, *STAR Protoc.* **2021**, *2*, 100593.
[13] R. Fuerst, R. Breinbauer, *ChemBiochem.* **2021**, *22*, 630.
[14] L. Krammer, R. Breinbauer. *Isr. J. Chem.* **2023**, *63*, e202200086.
[15] T. Müller, L. Johann, B. Jannack, M. Brückner, D. Lanfranchi, H. Bauer, C. Sanchez, V. Yardley, C. Deregnaucourt, J Schrével, M. Lanzer, R. Schirmer, E. Davioud-Charvet, *J. Am. Chem. Soc.* **2011**, *133*, 11557.
[16] K. Ehrhardt, C. Deregnaucourt, A. Goetz, T. Tzanova, B. Pradines, S. Adjalley, S. Blandin, D. Bagrel, M. Lanzer, E. Davioud-Charvet, *Antimicrob. Agents Chemother.* **2016**, *60*, 5146.
[17] P. Sidorov, I. Desta, M. Chessé, D. Horvath, G. Marcou, A. Varnek, E. Davioud-Charvet, M. Elhabiri, *ChemMedChem.* **2016***, 11*, 1339.
[18] M. Bielitza, D. Belorgey, K. Ehrhardt, L. Johann, D. Lanfranchi, V. Gallo, E. Schwarzer, F. Mohring, E. Jortzik, D. Williams, K. Becker, P. Arese, M. Elhabiri, E. Davioud-Charvet, *Antioxid. Redox. Signal.* **2015**, *22*, 1337.
[19] B. Cichocki, V. Khobragade, M. Donzel, L. Cotos, S. Blandin, C. Schaeffer-Reiss, S. Cianférani, J. Strub, M. Elhabiri, E. Davioud-Charvet, *JACS^{Au},* **2021**, *1*, 669.
[20] B. Cichocki, M. Donzel, K. Heimsch, M. Lesanavičius, L. Feng, E. Montagut, K. Becker, A. Aliverti, M. Elhabiri, N. Cenas, E. Davioud-Charvet, *ACS Infect. Dis.* **2021**, *7*, 1996.
[21] G. Dormán, H. Nakamura, A. Pulsipher, G. Prestwich, *Chem Rev*. **2016**, *116*, 15284.
[22] E. Karaj, S. Sindi, L. Viranga Tillekeratne, *Bioorg Med Chem.* **2022**, *62*, 116721.
[23] N. Trometer, B. Cichocki, Q. Chevalier, J. Pécourneau, J. Strub, A. Hemmerlin, A. Specht, E. Davioud-Charvet, M. Elhabiri, *J. Org. Chem.* **2023**, *89*, 2104.
[24] N. Trometer, M. Roignant, E. Davioud-Charvet, *Org. Process Res. Dev.* **2022**, *26*, 1152.
[25] L. Cotos, M. Donzel, M. Elhabiri, E. Davioud-Charvet, *Chem*. *Eur. J.* **2020**, *26*, 3314.
[26] M. Elhabiri, P. Sidorov, E. Cesar-Rodo, G. Marcou, D. Lanfranchi, E. Davioud-Charvet, D. Horvath, A. Varnek, *Chemistry,* **2015**, *21*, 3415.
[27] H. Görner, *J. Photochem. Photobiol.* **2011**, *224*, 135.
[28] K. Grzyb, R. Frański, T. Pedzinski, *J Photochem Photobiol B.* **2022**, *234*, 112536.
[29] P. Mounkoro, T. Michel, S. Blandin, M. Golinelli-Cohen, E. Davioud-Charvet, B. Meunier, *Free Radic Biol Med.* **2019**, *141*, 269.
[30] V. Gudipati, K. Koch, W. Lienhart, P. Macheroux, *Biochim Biophys Acta.* **2014**, *1844*, 535.
[31] P. Mounkoro, T. Michel, M. Golinelli-Cohen, S. Blandin, E. Davioud-Charvet, B. Meunier, *Free Radic Biol Med.* **2021**, *162*, 533.
[32] E. Rodo, L. Feng, M. Jida, K. Ehrhardt, M. Bielitza, J. Boilevin, M. Lanzer, D. Williams, D. Lanfranchi, E. Davioud-Charvet, *Eur. J. Org. Chem.* **2016**, *11*, 1982.
[33] L. Feng, D. Lanfranchi, L. Cotos-Munoz, E. Cesar Rodo, K. Ehrhardt, A. Goetz, H. Zimmerman, F. Fenaille, S. Blandin, E. Davioud-Charvet, *Org. Biomol. Chem.* **2018**, *16*, 2647.
[34] M. Forgac, *Nat Rev Mol Cell Biol.* **2007**, *8*, 917.
[35] D. Schalkwyk, K. Saliba, G. Biagini, P. Bray, K. Kirk, *PLoS One*. **2013**, *8*, e58933.
[36] O. Skorokhod, D. Davalos-Schafler, V. Gallo, E. Valente, D. Ulliers, A. Notarpietro, G. Mandili, F. Novelli, M. Persico, O. Taglialatela-Scafati, P. Arese, E. Schwarzer, *Free Radic Biol Med.* **2015**, *89*, 624.
[37] W. Friebolin, B. Jannack, N. Wenzel, J. Furrer, T. Oeser, C. Sanchez, M. Lanzer, V. Yardley, K. Becker, E. Davioud-Charvet, *J. Med. Chem.* **2008**, *51*, 1260.
[38] W. Trager, J. Jensen, *Science,* **1976**, *193*, 673.
[39] C. Lambros, J. Vanderberg, *J. Parasitol.* **1979**, *65*, 418.
[40] M. Smilkstein, N. Sriwilaijaroen, J. Kelly, P. Wilairat, M. Riscoe, *Antimicrob. Agents Chemother.* **2004**, *48*, 180.

[41] D. Beez, C. Sanchez, W. Stein, M. Lanzer, *Antimicrob. Agents Chemother.* **2011**, *55*, 50.
[42] C. J. Tonkin, G. G. Van Dooren, T. P. Spurck, N. S. Struck, R. T. Good, E. Handman, A. F. Cowman, G. I. McFadden, *Mol. Biomol. Parasitol.* **2004**, *137*, 13.
[43] S. Agrawal, G. G. Van Dooren, W. L. Beatty, B. Striepen, *J Biol. Chem.* **2009**, *284*, 33683.
[44] F. Nardella, I. Dobrescu, H. Hassan, F. Rodrigues, S. Thiberge, L. Mancio-Silva, A. Tafit, C. Jallet, V. Cadet-Daniel, S. Goussin, A. Lorthiois, Y. Menon, N. Molinier, D. Pechalrieu, C. Long, F. Sautel, M. Matondo, M. Duchateau, G. Médard, B. Witkowski, A. Scherf, L. Halby, P. Arimondo, *iScience.* **2023**, *26*, 105940.
[45] D. Bouyssié, A. Hesse, E. Mouton-Barbosa, M. Rompais, C. Macron, C. Carapito, A. Gonzalez de Peredo, Y. Couté, V. Dupierris, A. Burel, J. Menetrey, A. Kalaitzakis, J. Poisat, A. Romdhani, O. Burlet-Schiltz, S. Cianférani, J. Garin, C. Bruley, *Bioinformatics.* **2020**, *36*, 3148.
[46] S. Wieczorek, F. Combes, C. Lazar, Q. Giai Gianetto, L. Gatto, A. Dorffer, A. Hesse, Y. Couté, M. Ferro, C. Bruley, T. Burger, *Bioinformatics,* **2017**, *33*, 135.
[47] Y. Benjamini, Y. Hochberg, *J. Royal Stat. Soc. Ser.* **1995**, *57*, 289.
[48] Y. Benjamini, Y. Hochberg, *J. Educ. Behav. Stat.* **2000**, *25*, 60.
[49] J. Cox, M. Mann, *Nat Biotechnol.* **2008**, *26*, 1367.
[50] S. Tyanova, T. Temu, P. Sinitcyn, A. Carlson, M. Hein, T. Geiger, M. Mann, J. Cox, *Nat Methods,* **2016**, *13*, 731.
[51] E. W. Deutsch, N. Bandeira, Y. Perez-Riverol, V. Sharma, J. Carver, L. Mendoza, D. J. Kundu, S. Wang, C. Bandla, S. Kamatchinathan, S. Hewapathirana, B. Pullman, J. Wertz, Z. Sun, S. Kawano, S. Okuda, Y. Watanabe, B. MacLean, M. MacCoss, Y. Zhu, Y. Ishihama, J. A. Vizcaíno. The ProteomeXchange Consortium at 10 years: 2023 update. Nucleic Acids Res. **2023**, *51*(D1): D1539–D1548.

1.1.2 Les points importants de l'article 1

- **Synthèse de deux nouvelles sondes cliquables 6-fluorées** (sonde **3** et **5**) et optimisation de la voie de synthèse des sondes cliquables déjà existantes (sonde **4** et **1**).
- **Étude électrochimique des sondes** montrant que les sondes **3** et **5** sont réduites plus rapidement, offrant un meilleur rendement lors de l'étape de photo-marquage.
- **Optimisation des étapes clés de la stratégie** (par augmentation des rendements des réactions : clique, photo-marquage, pull-down, enrichissement et analyse protéomique), rendant la méthodologie plus accessible et reproductible.
- **Localisation de la sonde 5 dans *P. falciparum*** (via CuAAC), révélant une accumulation dans la mitochondrie (48%) et l'apicoplaste (32%) chez les jeunes trophozoïtes, confirmant ces organelles comme des lieux primaires impliqués dans le mode d'action des bMDs.
- **Applications de la stratégie AfBPP dans la levure *S. cerevisiae* avec la sonde 3**, révélant 11 protéines-cibles majeures, dont plusieurs présentant des activités oxydoréductases et localisées dans les mitochondries. Ces résultats suggèrent que le plasmodione perturbe les processus mitochondriaux essentiels.
- **Utilisation de la stratégie (pro-)AfBPP avec la sonde 5 dans les trophozoïtes de *P. falciparum***, permettant d'identifier 44 protéines cibles potentielles. La plupart sont impliquées dans des processus essentiels comme la régulation du pH cytosolique et les fonctions mitochondriales. L'absence de flavoenzymes parmi les cibles identifiées a été notée, bien qu'elles aient été proposées dans l'hypothèse du mode d'action des bMDs.

1.2 Utilisation de la stratégie d'imagerie bioorthogonale dans les parasites *P. falciparum*, *T. gondii* et développement de bMD-hétéroaromatiques

1.1.3 Introduction et synthèse de β-pyridine- et β-pyrimidine-bMDs

Les sondes bMD-alcynes précédemment introduites possèdent de bonnes activités antiparasitaires et nous ont permis d'investiguer les cibles biologiques de nos bMDs (article 1). Afin de mieux connaitre les cibles biologiques des bMDs dans deux parasites protozoaires de l'ordre des Apicomplexa, possédant un apicoplaste comme organelle essentiel pour la survie chez l'hôte humain, nous avons entrepris la synthèse d'une nouvelle sonde portant un groupement pyrimidine connu pour augmenter les propriétés PC/PK de la molécule finale. Ainsi, j'ai débuté ma thèse par la synthèse de la sonde bMD-pyrimidine-alcyne en 7 étapes avec un rendement global de 30% (**3v** dans l'article 2) (Figure 24). Malheureusement, l'introduction de la pyrimidine n'est pas tolérée par le parasite *P. falciparum* (IC_{50} = 1.648 µM *Pf*NF54 contre 49 nM *Pf*Dd2 avec un phényl remplaçant la pyrimidine), mais présente une bonne activité chez son parasite voisin *T. gondii* (IC_{50} = 5.25 µM *T. gondii* contre 9 µM avec un phényl remplaçant la pyrimidine).

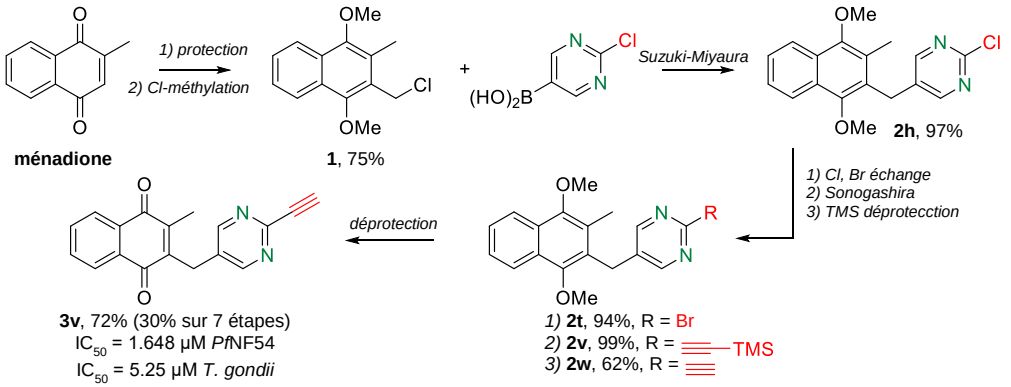

Figure 24: Synthèse de la sonde bMD-pyrimidine-alcyne **3v** utilisée en imagerie bioorthogonale. *Protection*: 1. $SnCl_2$, HCl, EtOH, rt, 2h, 2. Me_2SO_4, acétone, KOH, MeOH, 60°C, 4h. *Cl-méthylation*: CH_2O, HCl, 80°C, 2h. *Suzuki-Miyaura*: $Pd(PPh_3)_4$, Na_2CO_3, DME:H_2O, 100°C, 1h. *Cl, Br échange*: TMSBr, propionitrile, 100°C, 5h. *Sonogashira*: éthynyltriméthylsilane, CuI, $Pd(PPh_3)_2Cl_2$, NEt_3, 70°C, 20h. *TMS déprotection*: TBAF, THF, 1.5h. *Déprotection*: CAN, CH_3CN:H_2O, 1h.

Comme évoqué dans l'introduction, plusieurs de nos dérivés bMDs sont également actifs dans le bas µM chez le parasite apicomplexe *T. gondii*. L'intérêt d'utiliser ce parasite réside dans la diversité des outils cellulaires et moléculaires mis en place dans les nombreux laboratoires étudiant ce parasite, comme les outils d'immunofluorescence. Notre objectif est de développer une méthodologie d'imagerie bioorthogonale en utilisant la réaction de CuAAC avec un fluorophore azoture et nos sondes bMD-alcynes. Cette approche nous permettrait, de localiser nos molécules au sein des parasites *P. falciparum* et *T. gondii*, afin d'identifier et de valider leurs cibles biologiques. Grâce à nos collaborateurs biologistes (Dr. Sébastien Besteiro, Montpellier et Dr. Stéphanie A. Blandin, Strasbourg), cette étude d'imagerie a pu être

réalisée. Nous avons également étudié l'impact de ces molécules sur la morphologie du parasite *T. gondii* et sur la biosynthèse des acides gras (Dr. Cyrille Y. Botté, Grenoble).

Pendant cette thèse, j'ai aussi synthétisé les deux premières sondes bMDs azotures. Ces sondes sont très actives dans le parasite *P. falciparum* (**13**, IC_{50} = 32 nM *Pf*NF54 ; **16**, IC_{50} = 151 nM *Pf*NF54, dans l'article 2) et permettent une méthodologie basée sur les réactions SPAAC et CuAAC. Elles devraient nous permettre d'obtenir des résultats d'imagerie différents en fonction de leurs activités et du type de réaction clique utilisée. Malheureusement, les essais de localisation dans le parasite *T. gondii* utilisant la stratégie CuAAC n'ont pas été concluants (plus d'information dans l'article 2 de cette thèse).

Cet article s'inscrit également dans un projet de chimie médicinale et d'étude SAR de dérivés bMDs hétéroaromatiques (principalement azotés) afin d'améliorer les propriétés PC et PK de la plasmodione. Cependant, l'introduction de ces groupements n'est pas possible avec la réaction de Kochi-Anderson[59] ou avec l'alkylation C-H[64] développée au sein de l'équipe (Figure 25). C'est pourquoi, avant mon arrivée, le Dr. Maxime Donzel (PhD) et le Dr. Matthieu Roignant (Post-doc) avaient développé une stratégie de synthèse basée sur un couplage C-C de Suzuki-Miyaura pour introduire un noyau hétéroaromatique. Une vingtaine de composés avaient ainsi été obtenus.

Parmi eux, les dérivés α-pyridine (**3b**) et α-pyrimidine (**3i**), analogues de la PD, se sont avérés particulièrement actifs sur *P. falciparum*. Nous nous sommes donc intéressés à la synthèse de leurs régioisomères β. Cependant, la stratégie basée sur la réaction de Suzuki-Miyaura n'est pas compatible avec ce type de substrat, car la formation d'un zwitterion *N*-H adjacent au bore va conduire à une rapide protodéborylation[126] pendant la fragmentation C-B (Figure 25). Ainsi, un projet parallèle a été mis en place pour trouver une nouvelle méthodologie de synthèse menant à ces dérivés β-*N*-hétéroaromatiques.

Mon objectif était de mettre en place une synthèse toujours basée sur le couplage de Suzuki-Miyaura, mais en inversant les groupements réactifs (Figure 25). De cette manière, les dérivés borés sur la partie ménadione devraient être plus stables pendant la réaction de couplage, permettant l'introduction des β-*N*-hétéroaromatiques. Deux stratégies différentes sont possibles, l'une basée sur la synthèse d'un dérivé boré aromatique **(1)** et l'autre basée sur un dérivé boré aliphatique **(2)**.

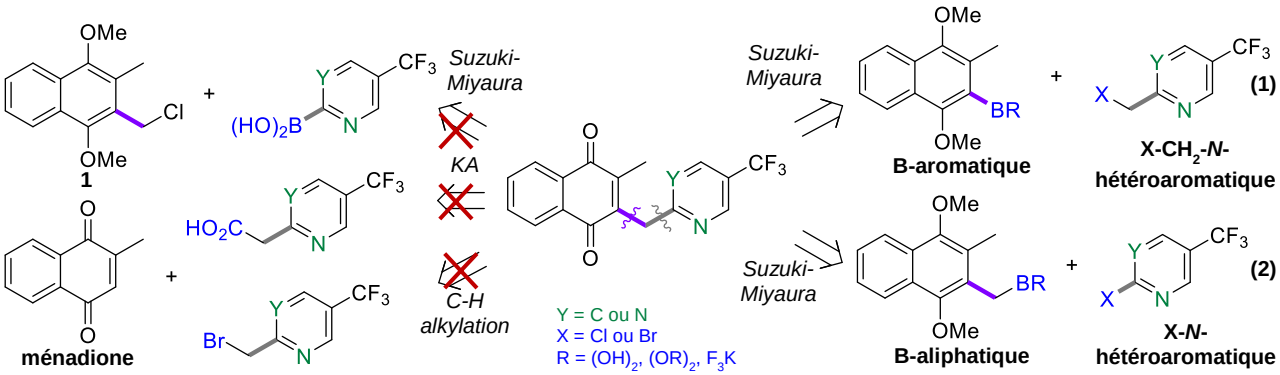

Figure 25: Stratégie de synthèse afin d'obtenir les β-*N*-hétéroaromatique-bMDs. KA = Kochi-Anderson.

Concernant la stratégie **(1)**, plusieurs dérivés borés[127] ont été préparés pour évaluer leur réactivité et leur stabilité pendant le couplage C-C :

i. Un acide boronique **4a** obtenu à partir du dérivé bromé **4**, par échange halogène-métal.
ii. Un trifluoroborate **4b** obtenu de la même façon après traitement avec du difluorure de potassium.
iii. Un ester boronique (Pin) **4c** obtenu par couplage de Miyaura avec $B_2(Pin)_2$ comme source de bore.
iv. Un ester boronique (Epin) boré (inspiré de Oka N. *et al.*[128,129]), mais lors couplage de Miyaura avec $B_2(Epin)_2$, uniquement le produit H-substitué a été observé (Figure 26). Cette instabilité est probablement due à un encombrement stérique de l'ester boré conduisant à une protodéborylation.

Cette stratégie nécessite un substrat X-CH_2-*N*-hétéroaromatique, cependant, aucun n'est accessible commercialement. Plusieurs tentatives de synthèse ont été étudiées à partir de dérivés *N*-hétéroaromatiques, mais elles n'ont pas conduit à des résultats positifs. Néanmoins, une réaction modèle a été réalisée à partir d'un dérivé commercial non hétéroaromatique (chlorométhyl-4-CF_3-benzène) avec le sel de trifluroborate **4b**. Le produit désiré a été obtenu quantitativement, confirmant le potentiel de cette voie de synthèse. Aucun couplage n'a été réalisé avec les dérivés borés B(Pin) et $B(OH)_2$, mais ils devraient conduire à des résultats similaires (Figure 26).

Stratégie (1)

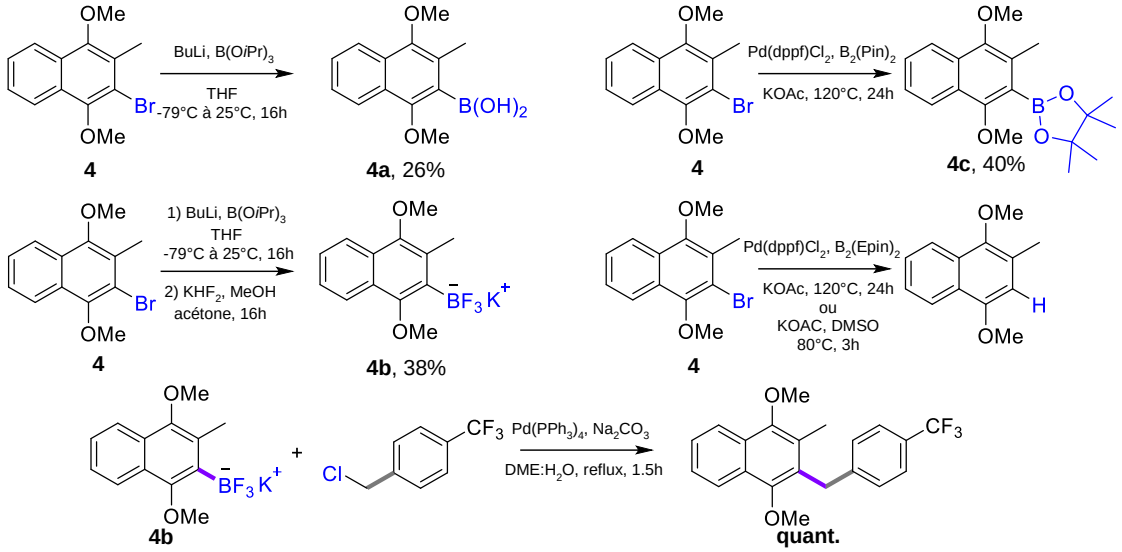

Figure 26: Stratégie **(1)** basée sur les dérivés borés aromatiques. Les conditions de synthèse des différents intermédiaires et produits sont disponibles dans la partie expérimentale de ce manuscrit.

Pour la stratégie **(2)**, trois sources différentes de dérivés borés ont été obtenues :

i. Un trifluoroborate **1a** obtenu par couplage de Miyaura avec **1** et $B_2(Pin)_2$ après traitement avec du difluorure de potassium

ii. Un ester boronique (Pin) **1b** obtenu par couplage de Miyaura avec $B_2(Pin)_2$ comme source de bore

iii. Un ester boronique (Epin) boré **1c** obtenu de la même façon avec $B_2(Epin)_2$ (Figure 27).

Stratégie (2)

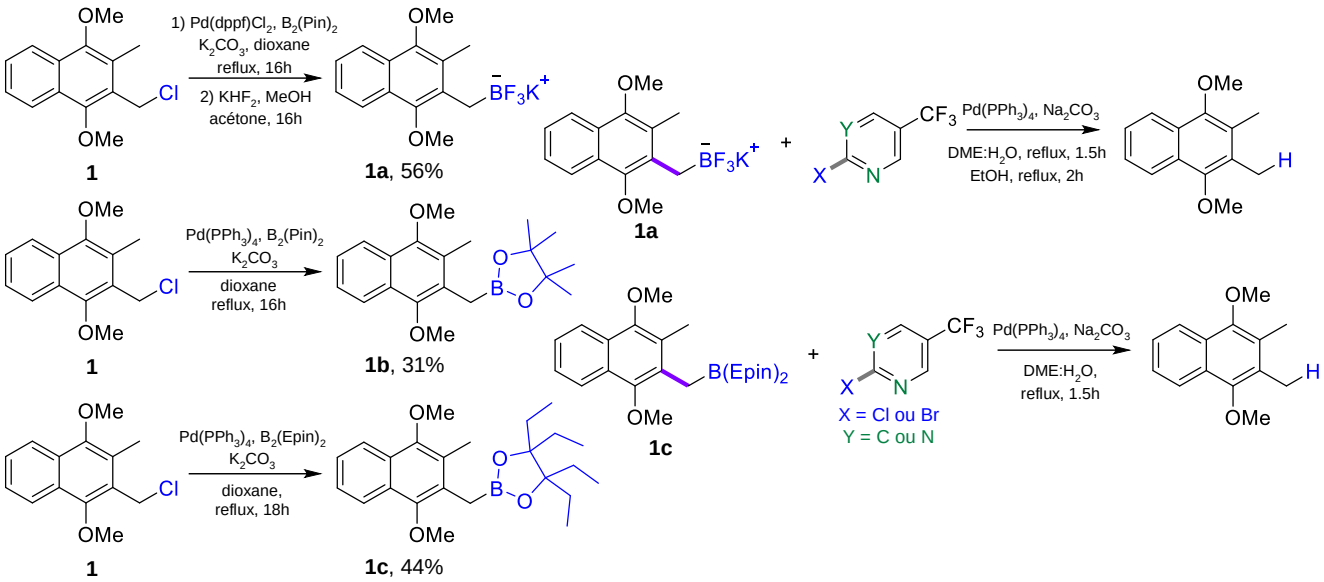

Figure 27: Stratégie **(2)** basée sur les dérivés borés aliphatiques. Les conditions de synthèse des différents intermédiaires et produits sont disponibles dans la partie expérimentale de ce manuscrit.

Le couplage de Suzuki-Miyaura avec un substrat X-*N*-hétéroaromatique commercial s'est avéré limitant. Plusieurs solvants, bases et catalyseurs ont été évaluées à partir des dérivés borés **1a** et **1c** mais ont rapidement conduit à la formation du produit protodéborylé. Nous supposons que ces dérivés borés aliphatiques ne sont pas stables dans les conditions aqueuses alcalines du couplage de Suzuki-Miyaura (Figure 27). Ce couplage nécessiterait une étude plus approfondie afin de comprendre l'origine de cette instabilité et de sélectionner des conditions catalytiques (ligand/métal) spécifiques.

En conclusion, nous avons pu explorer de nouvelles possibilités, améliorant l'accessibilité des dérivés borés ménadiones pour le futur. La stratégie **(1)** aurait pu être applicable si les substrats *N*-hétéroaromatiques étaient plus accessibles, tandis que la stratégie **(2)** prouve l'instabilité des dérivés borés aliphatiques[130,131]. Finalement, nous avons obtenu ces composés grâce à une voie de synthèse publiée dans un brevet par PTC therapeutics[132], utilisant un couplage de Negishi à partir de **1** et des dérivés X-*N*-hétéroaromatiques. Une transmétalation zinc/palladium est réalisable *in situ*, évitant les conditions limitantes de transmétalation bore/palladium. Après déprotection oxydante au CAN, les produits désirés β-pyridine et β-pyrimidine ont été formés (**3l** et **3m** respectivement dans l'article 2) (**3l**, IC_{50} = 69 nM *Pf*NF54 et 5.7 µM *T. gondii* ; **3m**, IC_{50} = 414 nM *Pf*NF54 et 2.1 µM *T. gondii*).

1.2.1 Article 2

3-benzylmenadiones and their heteroaromatic analogues target the apicoplast of Apicomplexa parasites: Synthesis and bioimaging studies

Baptiste Dupouy, Maxime Donzel, Matthieu Roignant, Sarah Charital, Rodrigue Keumoe, Yoshiki Yamaryo-Botté, Alexander Feckler, Mirco Bundschuh, Yann Bordat, Matthias Rottmann, Pascal Mäser, Cyrille Y. Botté, Stéphanie A. Blandin, Sébastien Besteiro, Elisabeth Davioud-Charvet

***ACS Infectious Diseases* accepted article,** publié en ligne le 26 Septembre 2024

doi: 10.1021/acsinfecdis.4c00304

3-benzylmenadiones and their heteroaromatic analogues target the apicoplast of Apicomplexa parasites: Synthesis and bioimaging studies

Baptiste Dupouy,[1,#] Maxime Donzel,[1,#] Matthieu Roignant,[1,#] Sarah Charital,[2] Rodrigue Keumoe,[3] Yoshiki Yamaryo-Botté,[2] Alexander Feckler,[4] Mirco Bundschuh,[4] Yann Bordat,[5] Matthias Rottmann,[6] Pascal Mäser,[6,7] Cyrille Y. Botté,[2] Stéphanie A. Blandin,[3] Sébastien Besteiro,[5] Elisabeth Davioud-Charvet*[,1]

# authors contributed equally as first co-authors

* Correspondence E-mail Address: elisabeth.davioud@unistra.fr

[1] UMR7042 CNRS-Unistra-UHA, Laboratoire d'Innovation Moléculaire et Applications (LIMA), Bio(in)organic & Medicinal Chemistry Team, European school of Chemistry, Polymers and Materials (ECPM), 25, rue Becquerel, F-67087 Strasbourg, France.

[2] Apicolipid Team, Institut pour l'Avancée des Biosciences, CNRS UMR5309,INSERM U1209, Université Grenoble Alpes, Bat. Jean Roget, Domaine de la Merci, F-38700 La Tronche, France.

[3] INSERM, CNRS, Université de Strasbourg, U1257 / UPR9022, Mosquito Immune Responses IBMC, 2 Allée Konrad Roentgen, F-67000 Strasbourg, France.

[4] Functional Aquatic Ecotoxicology, Institute for Environmental Sciences (iES), RPTU Kaiserslautern-Landau, Fortstrasse 7, D-76829 Landau, Germany

[5] UMR5294 CNRS-Université de Montpellier, Laboratory of Pathogens and Host Immunity (LPHI), Place Eugène Bataillon, Bâtiment 24, CC 107, F-34095 Montpellier cedex 5, France.

[6] Swiss Tropical and Public Health Institute, Kreuzstrasse 2, CH-4123 Allschwil, Switzerland.

[7] University of Basel, Petersgraben 1, CH-4001 Basel, Switzerland.

ABSTRACT:

The apicoplast is an essential organelle for the viability of apicomplexan parasites *Plasmodium falciparum* or *Toxoplasma gondii*, which has been proposed as a suitable drug target for the development of new antiplasmodial drug-candidates. Plasmodione, an antimalarial redox-active lead drug is active at low nM concentrations on several blood stages of *Plasmodium* such as early rings and gametocytes. Nevertheless, its precise biological targets remain unknown. Here, we described the synthesis and the evaluation of new heteroaromatic analogues of plasmodione, active on asexual blood *P. falciparum* stages and *T. gondii* tachyzoites. Using a bioimaging-based analysis, we followed the morphological alterations of *T. gondii* tachyzoites and revealed a specific loss of the apicoplast upon drug treatment. Lipidomic and fluxomic analyses determined that drug treatment severely impacts apicoplast-hosted FASII activity in *T. gondii* tachyzoites, further supporting that the apicoplast is a primary target of plasmodione analogues. To follow the drug localization, 'clickable' analogues of plasmodione were designed as tools for fluorescence imaging through a Cu(I)-catalyzed Azide-Alkyne Cycloaddition reaction. Short-time incubation of two probes with *P. falciparum* trophozoites and *T. gondii* tachyzoites showed that the clicked products localize within, or in the vicinity of, the apicoplast of both Apicomplexa parasites. In *P. falciparum* the fluorescence signal was also associated with the mitochondrion, suggesting that bioactivation and activity of plasmodione and related analogues are potentially associated to these two organelles in malaria parasites.

KEYWORDS: apicoplast, CuAAC-based imaging, lipidomics, plasmodione, *Plasmodium falciparum*, *Toxoplasma gondii*

Collectively, parasites of the phylum Apicomplexa are responsible for widespread life-threatening diseases of human and cattle with major human and economic consequences. The most devastating of these is Malaria, a major tropical parasitic disease that was responsible for 249 million human cases and 608,000 deaths worldwide in 2022, mostly affecting young children below the age of 8 in Sub-Saharan Africa (1). *Plasmodium* is the causative agent of malaria, the most lethal species being *P. falciparum*, which is responsible for malaria complications such as cerebral malaria or severe anemia. Resistance to artemisinin (ART-R), alone or in combination therapies also known as ACTs, has emerged in southeast Asia, and in the last decade multidrug-resistance of *Plasmodium* toward broadly-used antimalarial drugs has spread all over the world. About 95% of cases and deaths are located in Africa, with young children and pregnant women particularly at risk. At the molecular level, ART-R is principally linked to a subset of about 20 mutations in the propeller domain of *P. falciparum* kelch13 (*Pf*K13) protein. However, in the past few years, multiple independent emergences of *Pf*K13 mutations have been associated with multidrug resistance, and in some area, decreased ACT efficacy was found independent of *Pf*K13 mutations in Africa. The emergence of ART-R in Africa has thus generated a high concern regarding the loss of efficacy of ACT partner drugs in Africa (2). Therefore, new drugs exhibiting distinct mechanism(s) of action that would allow counteracting parasite resistance to drugs in use are urgently needed to sustain and develop treatments against malaria.

In the last decade, we discovered and developed a new potent class of antiplasmodial compounds, the 3-benzylmenadiones (3) with high efficacy against the human erythrocytic stages of *P. falciparum*, in particular against young rings and gametocytes (4). They display no sign of toxicity in host cells or in mice, and have low risk for of glucose-6-phosphate dehydrogenase (G6PD)-deficient populations or populations with hemoglobinopathies (5). The mechanism of action of these redox-cyclers (parent drug or their metabolites) likely involves their bioactivation through a cascade of redox reactions followed by redox-cycling (Scheme 1).

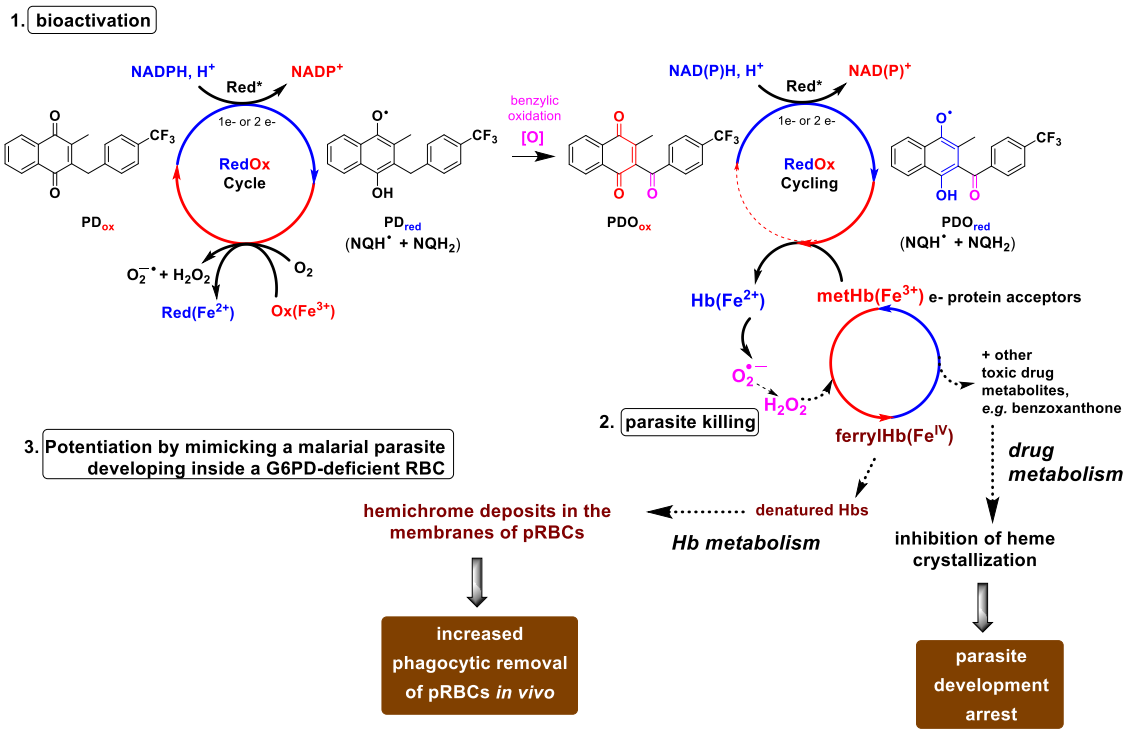

Scheme 1. Proposed mechanisms of action of the antimalarial early-lead plasmodione prodrug (**PD**) generating toxic metabolites in *P. falciparum*-parasitized red blood cells (pRBC). A first electron (e^-) transfer leading to the semiquinone $NQH^•$ (or a two-e^- transfer leading to the dihydro-quinone NQH_2), followed by oxygen insertion at the benzylic position, is proposed to be involved in the drug bioactivation (step 1: bioactivation). This can be catalyzed in enzymatic assays *in vitro* by several relevant pRBC flavoenzymes, including *h*GR: human glutathione reductase, *Pf*GR: *P. falciparum* glutathione reductase, or *Pf*FNR: *P. falciparum* ferredoxin-$NADP^+$ reductase. For the sake of clarity, only the one-e^--reduced $NQH^•$ species was drawn in the developed structures. We previously demonstrated that the second one-electron transfer leading to the dihydronaphthoquinone dianion NQ^{2-} is highly sensitive to the nature of the benzoyl substitution (*p*-CF_3 in **PDO** *vs.* diverse substituted 3-benzoylmenadiones, see (6)). By generating toxic metabolites, step 2 could lead to parasite killing. In pRBCs, **PD** mimics the effects of mutations in glucose-6-phosphate dehydrogenase (G6PD) gene encoding the main producer of NADPH in RBCs (Step 3). Carriers of the most frequent low-activity G6PD variants are hematologically normal but present a higher turnover of their RBCs due to oxidative stress and membrane-bound hemichrome in RBCs. It results in phagocytic removal by macrophages and short half-life of RBCs, limiting malaria development.

To understand the mechanism of action of 3-benzylmenadiones, in particular of the most potent antiplasmodial lead plasmodione (**PD**), at the cellular level, we conducted different approaches, including fused-Grx-roGFP-based imaging studies (5,7), physicochemical studies (8-10), genetic screening in yeast (11,12), synthesis of metabolites (5,6,13), chemical tools for proteomics (14), and metabolomics (7). While **PD** affects the redox equilibrium of *P. falciparum*-infected RBCs, its mechanism of action is likely pleiotropic. Each step in the cascade of redox reactions can be catalyzed by different proteins in the different parasitic stages that are sensitive to the compound, supporting the potentially complex behavior of redox-cyclers. In addition, metabolites generated from redox-cyclers are produced in trace amounts, requiring sensitive analytic methods to characterize their mode of action. For instance, using a heavy $^{13}C_{18}$-isotopically-enriched **PD**, we have recently shown that the apicoplast *P. falciparum* ferredoxin-$NADP^+$ reductase (*Pf*FNR) was able to generate key drug metabolites (**PD-bzol** and **PDO**) through a 2 h-long redox cycling of **PD** (7). Furthermore, by using the genetically-encoded hGrx1-roGFP2 fluorescent glutathione redox sensor, we could visualize the oxidative stress generated by **PD** in the apicoplast of blood-stage malaria parasites (7). This suggests that a fast pulse of reactive oxygen species (ROS) is released in the apicoplast, possibly mediated by **PD** redox cycling catalyzed by *Pf*FNR

and/or other apicoplast flavoenzymes. However, many other electron protein acceptors could account for the killing effects of **PD** in the various stages of *P. falciparum*.

The basic six-membered heterocycles, pyridine and pyrimidine, are widely represented in numerous natural products and used in medicinal science (15, 16). The replacement of benzyl rings by *N*-heteroaromatics on small organic molecule can have a huge impact on both drug biological activities and physicochemical properties. These last parameters can include the hydrophilicity due to their low basicity especially in acid conditions, the ability to form hydrogen bonds with surrounding molecules due to nitrogen lone pair and the bioisosteric replacement of amine, amide, or benzene rings by the heterocycles (17). A few of aza-analogues of 3-benzylmenadiones have been previously synthesized to examine the effect of nitrogen in the menadione core on redox potentials and inhibitory capabilities (18). **PD** is highly lipophilic, so with this in mind and in order to improve the pharmacokinetic properties of the series, here we report the synthesis and evaluation of the antiplasmodial activity of heteroaromatic analogues of **PD** and various 3-benzylmenadione derivatives (Figure 1).

Moreover, a considerable uncertainty remains about the cellular target(s) of **PD**, that have, so far, been essentially investigated through phylogenetically-distant model organisms like yeast, or by hypothesis-driven targeted experiments in *P. falciparum*. *P. falciparum* can be cultured *in vitro* and manipulated genetically. Still the ring stage is one of the smallest eukaryotic cells known (~1–2 µm), which is a considerable hurdle for microscopic studies and phenotypic characterization. On the other hand, closely-related apicomplexan parasite *Toxoplasma gondii* is more amenable to cell biology studies because of its larger size and the availability of many cell markers and the relative ease with which the parasite can be studied with various microscopic techniques. *T. gondii* and *P. falciparum* share much of their underlying biology, thus *T. gondii* is also an attractive model to decipher key features related to the Apicomplexa phylum (19). *T. gondii* is responsible for human toxoplasmosis which, although less lethal than malaria, is a major chronic public health problem worldwide: about one third of the human population is infected with this parasite than can cause severe symptoms in immunocompromised individuals (in the context of HIV, leukemia, cancer therapies, or organ transplant) (20). Thus, in parallel, we conducted an initial structure-activity relationship (SAR) study with a reduced number of compounds in *T. gondii* tachyzoites (the stage responsible for the acute phase of the disease) and tracked several **PD**-based probes that allowed us to confirm that **PD** is likely primarily targeting the apicoplast and apicoplast-related functions in Apicomplexa.

Finally, we performed the first ecotoxicity study of our compounds in two model organisms, an algae and a planktonic crustacean. Results of such studies will be key to further inform the MedChem pipeline and improve the safety of novel antiparasitic 3-benzylmenadiones.

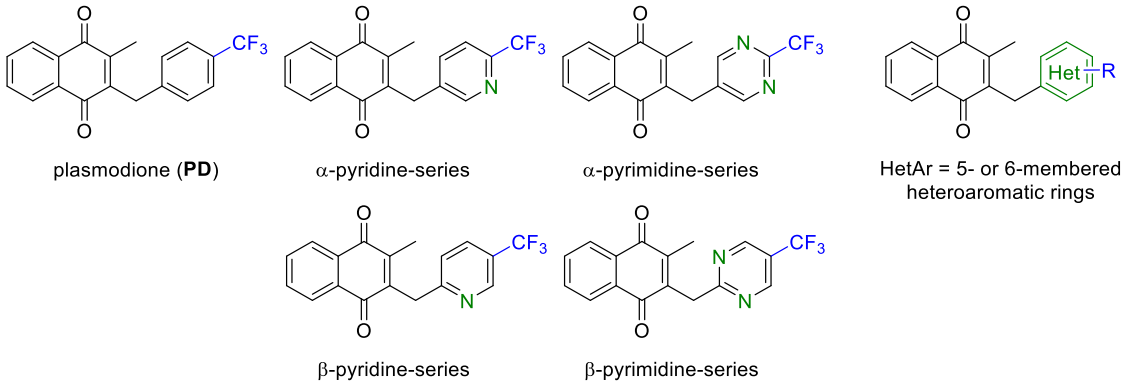

Figure 1. Heteroaromatic analogues of plasmodione and related 3-benzylmenadiones.

■ RESULTS AND DISCUSSION

Synthesis of Heteroaromatic Plasmodione Analogues.

The general synthetic route for most of the 3-heterobenzyl-menadione derivatives is presented in Scheme 2. It involved the sequential reduction then protection from the commercially-available menadione and chloromethylation of 1,4-dimethoxy-2-methylnaphthalene (3). The resulting chloromethyl derivative **1** was engaged in a Suzuki cross-coupling reaction, using the corresponding boronic acid heteroaryl building blocks. This reaction successfully promoted the formation of the desired product with moderate to excellent yields from 57% for **2q** to 99% for **2n**. Nevertheless, due to incompatibility of the Suzuki cross-coupling reaction with starting α-boron-pyridine and -pyrimidine (even in excess), a Negishi cross-coupling was performed from the corresponding α-halide-pyridine and -pyrimidine, yielding the desired products **3m** and **3l** with moderate yield (21). This incompatibility could be explained by a fast protodeboronation in the Suzuki conditions especially with an *N*-H, or polarized *N*C-H group adjacent to the boronate that can stabilize it during C-B fragmentation or an adjacent antibonding orbital (C−*N*σ*) that can overlap with the carbanion formally generated during C-B fragmentation (22). Subsequently, the 1,4-quinone moiety was recovered by oxidative demethylation. Only **3s** was obtained in a different way from menadione by applying a Kochi-Anderson reaction leading to the desired product in one step.

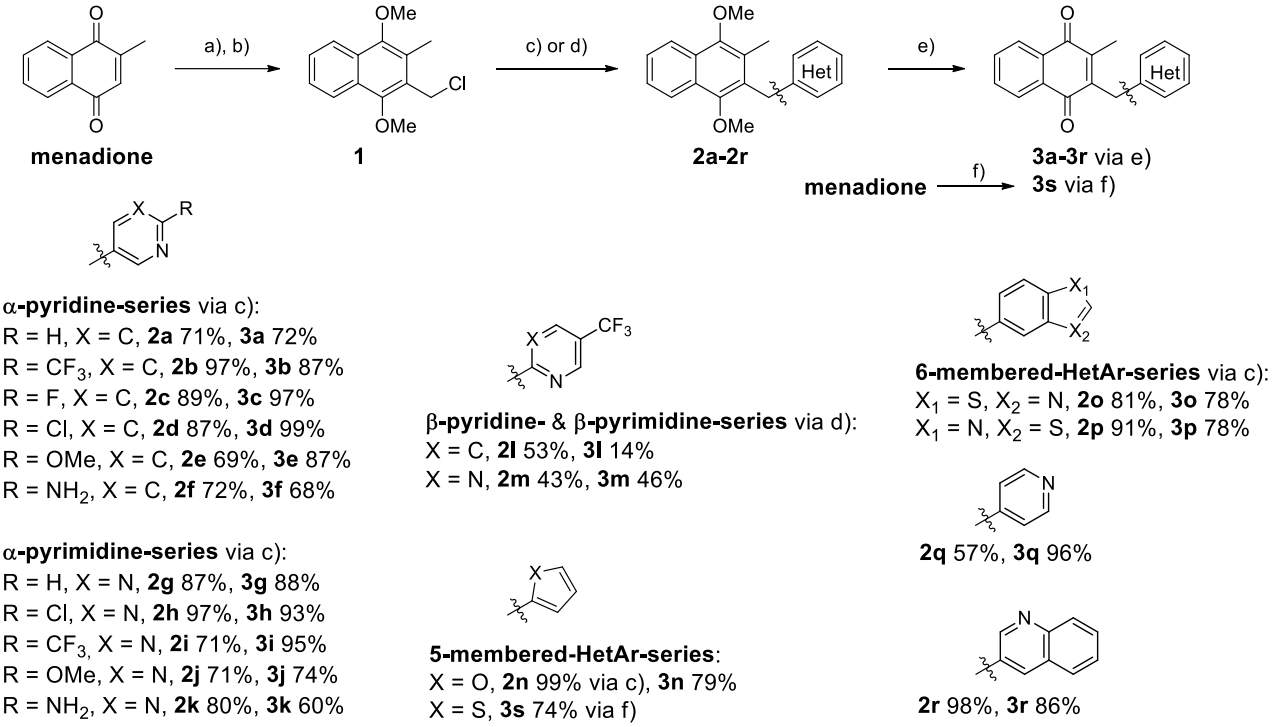

Scheme 2. Synthesis of heteroaromatic analogues of plasmodione. Reaction conditions: a) 1. $SnCl_2$, HCl, EtOH, rt, 2 h, 2. Me_2SO_4, acetone, KOH, MeOH, 60°C, 4 h, 93%; b) CH_2O, HCl, 80°C, 2 h, 81%; c) $Pd(PPh_3)_4$, Na_2CO_3, DME:H_2O, 100°C, 1 h and corresponding boronic acid; d) 1. Mg, LiCl, $ZnCl_2$, THF, rt, 2 h, 2. $Pd(PPh_3)_4$, THF, 80°C, 24 h, and corresponding halide; e) CAN, CH_3CN:H_2O, rt, 1 h; f) 2-thiopheneacetic acid, $AgNO_3$, $(NH_4)_2S_2O_8$, CH_3CN:H_2O, reflux, 4h.

Post-modification of α-chloro-pyrimidine **2h** was performed to obtain either the bromo α-pyrimidine after a halogen substitution using TMSBr, or the cyano α-pyrimidine after a nucleophilic aromatic substitution using NaCN. The desired α-pyrimidine **3t** and **3u** were subsequently obtained with good yield after an oxidative demethylation (Scheme 3).

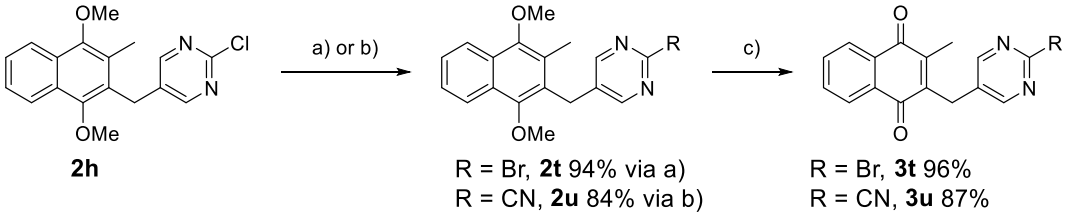

Scheme 3. Synthetic post-modification to prepare the bromo α-pyrimidine **3t** or the cyano α-pyrimidine **3u**. Reaction conditions: a) TMSBr, propionitrile, 100°C, 5 h; b) NaCN, DABCO, DMSO:H_2O, 50°C, 20 h; c) CAN, CH_3CN:H_2O, rt, 1 h.

Synthesis of clickable plasmodione analogues. The clickable alkyne **8** was synthesized using the reported synthetic route (14) under the compound code **11** with the following slight modifications. The first four steps were launched from crude mixtures without any purification step to isolate the intermediates, enabling a significant gain of time and yield. The single purification was performed after the oxidative demethylation allowing production of the desired product with a 46% overall yield (Scheme 4). Another clickable alkyne **3v**, this time bearing a α-pyrimidine, was obtained with the goal of increasing the aqueous solubility to enhanced the activity. The synthetic route involves a three-steps protocol

starting from α-pyrimidine **2t** described above by a Sonogashira cross-coupling reaction with a TMS protected ethynyl, then its deprotection using TBAF followed by the oxidative demethylation (Scheme 4).

Two azido analogues of **PD** were also synthesized to validate its biological target with additional bioimaging results based on a Cu(I)-catalyzed Azide-Alkyne Cycloaddition reaction (CuAAC). Compound **16** was obtained in three steps from menadione by sequential Kochi-Anderson reaction, then a hydrogenation using Pd/C to reduce the nitro group into the amine, followed by a diazotransfer reaction using a water/ionic liquid mixture (1-methyl-2-oxopyrrolidin-1-ium hydrogen sulfate) in a mortar producing the desired azido derivative (23) (Scheme 4). Another azido analogue was synthesized with the azide in β position of the para trifluoromethyl group to give the clickable **PD** analogue **13**. The synthetic route starts by a Suzuki cross-coupling from chloromethyl derivative **1** and the Bpin boronic ester **9** obtained by Miyaura borylation. After an oxidative demethylation and finally the same two steps as for **16**, the desired product was obtained with a 12% overall yield (Scheme 4).

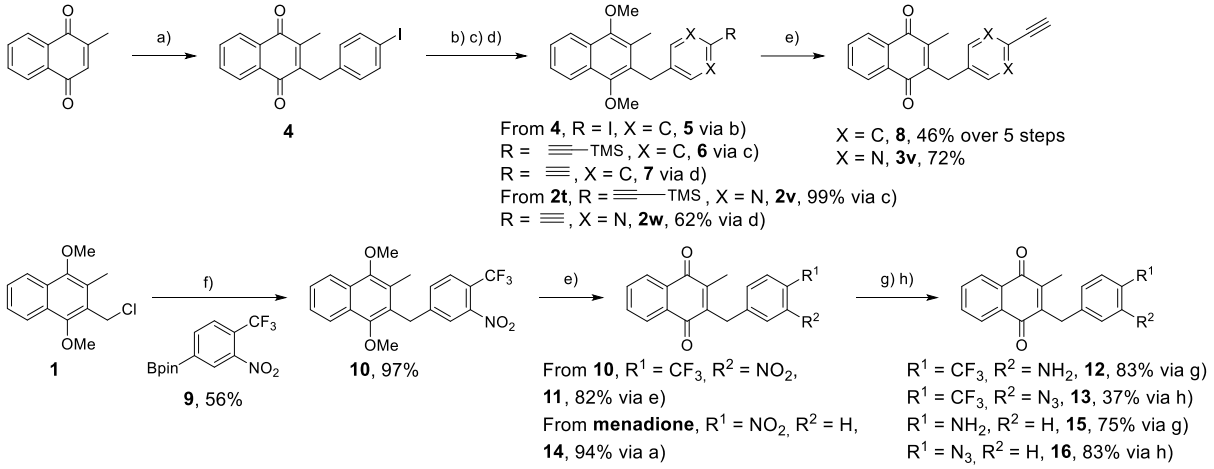

Scheme 4. Synthesis of the clickable 3-benzylmenadione alkynes **8**, **3v** and 3-benzylmenadione azides **13**, **16**. Reaction conditions: a) 4-iodophenylacetic acid or 4-nitrophenylacetic acid, $AgNO_3$, $(NH_4)_2S_2O_8$, CH_3CN:H_2O, reflux, 4 h; b) 1. $SnCl_2$, HCl, EtOH, rt, 2 h, 2. Me_2SO_4 acetone, KOH, MeOH, 60°C, 4 h; c) ethynyltrimethylsilane, CuI, $Pd(PPh_3)_2Cl_2$, NEt_3, 70°C, 20 h; d) TBAF, THF, rt, 1.5 h; e) CAN, CH_3CN:H_2O, rt, 1 h; f) 9, $Pd(PPh_3)_4$, Na_2CO_3, DME:H_2O, 100°C, 1 h; g) 1. Pd/C, EtOH, EtOAc, rt, 16 h, 2. Acetone, rt, 72 h; h) $NaNO_2$, NaN_3, H_2O:ionic liq., rt, 30 min.

Antimalarial activity of heteroaromatic analogues of plasmodione and related 3-benzylmenadiones.

The antimalarial activity of the synthesised **PD** analogues and their related 3-benzylmenadiones was measured against *P. falciparum* strain NF54 using a [^{3}H]-hypoxanthine incorporation assay (24) (Table 1). All compounds displayed submicromolar IC_{50} activity values with the exception of the low micromolar activity observed with compounds **3g**, **3r**, and **3v**. The most active compounds **3b**, **3l**, **3t**, **8** (clickable compound) and **13** had IC_{50} values below 100 nM and thus were comparable to **PD**.

Table 1. Initial SAR study: *In vitro* antiplasmodial and cytotoxicity data expressed as IC_{50} and CC_{50} values, respectively, and calculated physicochemical properties.

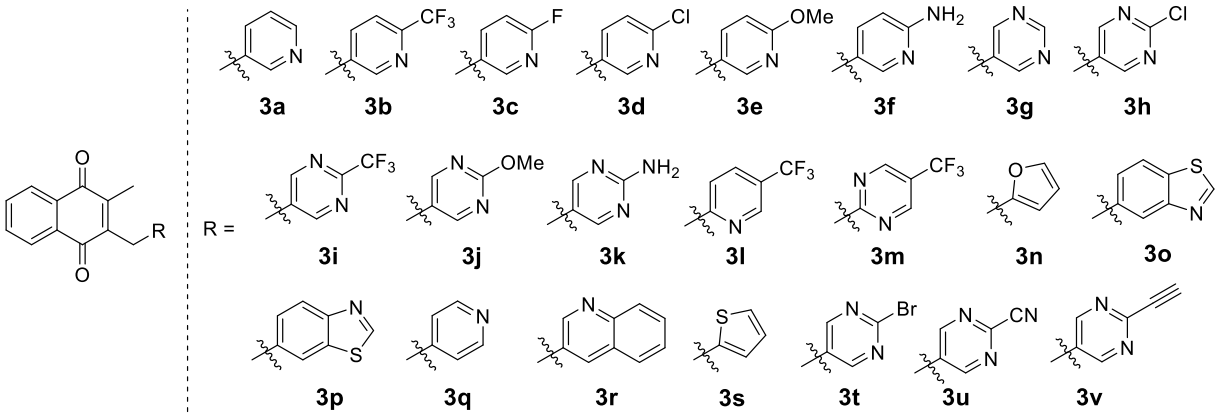

Product	Synthetic Process	NF54 IC_{50} (μM)[a]	L6 CC_{50} (μM)	cLogP	tPSA
3a	Suzuki	0.596	33.5	3.04	46.5
3b	Suzuki	0.065	48.3	4.07	46.5
	Negishi	0.078 ± 0.024	50.9		
3c	Suzuki	0.368	55.1	3.26	46.5
3d	Suzuki	0.496	56.1	3.83	46.5
3e	Suzuki	0.295	53.4	3.86	55.73
3f	Suzuki	0.309	nd	2.71	72.52
3g	Suzuki	1.586	24.8	2.08	58.86
3h	Suzuki	0.251	58.4	2.83	58.86
3i	Suzuki or Negishi	0.194 ± 0.125	179.2	3.03	58.86
3j	Suzuki + post	0.809	86.9	3.03	68.09
3k	Suzuki + post	0.738	Not determined yet	2.07	84.88
3l	Negishi	0.069 ± 0.024	8.82	4.07	46.5
3m	Negishi	0.414 ± 0.293	17.56	3.03	58.86
3n	Suzuki	0.501	4.2	3.71	43.37
3o	Suzuki	0.235	50.29	4.47	46.5
3p	Suzuki	0.37	49.81	4.47	46.5
3q	Suzuki	0. 109[b]	3.12[c]	3.04	46.5
3r	Suzuki	1.538	136.3	4.42	46.5
3s	Kochi-Anderson	0.427	19.4	4.18	34.14
3t	Suzuki + post	0.041	39.9	2.98	58.86
3u	Suzuki + post	0.816	13.9	1.80	82.65
3v	Suzuki + post	1.648	4.67	2.35	58.86
PD	Kochi-Anderson	0.043 ± 0.002	141.7	5.42	34.14

CQ	-	4.0 ± 0.37 ng/ml			
artesunate	-	2.2 ± 0.66 ng/ml			
Podophyllotoxin	-		0.018-0.010		

[a]: Values are the mean IC_{50} value of (2) independent determinations. [b]: IC_{50} (µM) with the ^{3}H-hypoxanthine incorporation-based assay using the *P. falciparum* Dd2 strain, which is sensitive to **PD**, and resistant to chloroquine (IC_{50} CQ = 0.148 µM), as reported in (18). [c]: CC_{50} (µM) using the human MRC-5 cell line, as reported in (18). "post" means post-functionalization.

The β-pyrimidine 3-benzylmenadione analogue 3m is a potent inhibitor of *T. gondii* tachyzoites growth *in vitro*.

A set of selected α- and β-pyridines and pyrimidines analogues of PD and other 3-benzylmenadiones were tested for their impact on the growth of *T. gondii* tachyzoites by plaque assay (Supporting Information, Figure S1). This assay allows the visualization of the successive lytic cycles of the tachyzoites that generate plaques in the host cell monolayer if parasite fitness is not affected. Atovaquone, a 2-hydroxy-naphthoquinone inhibiting the mitochondrial respiratory chain, and well-known inhibitor of *T. gondii* tachyzoite growth (25), was also included in the analysis. All compounds displayed an effect on parasite growth, with an IC_{50} in the low micromolar range (Table 2, Supporting Information, Figure S2). Although these IC_{50} values were at least 20-fold higher than the one of atovaquone, PD and its derivatives remain potent inhibitors of *Toxoplasma* tachyzoites growth *in vitro*.

Table 2. IC_{50} values of plasmodione-derived compounds on *T. gondii* tachyzoites, *P. falciparum*-infected red blood cells, and CC_{50} values to express the cytotoxicity against the rat L6 cell line.

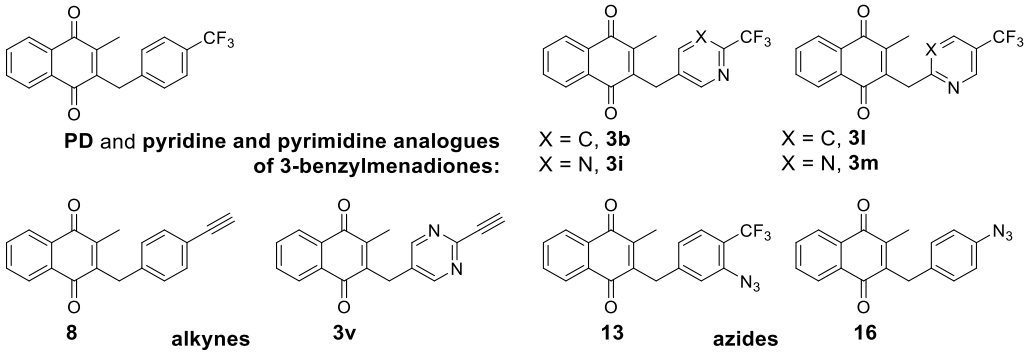

Product	Series	alkyne or azide	*P. falciparum* NF54 IC_{50} (µM) as mean ± SD	*T. gondii* IC_{50} (µM)[b]	L6 CC_{50} (µM)
3b	α-pyridine	-	0.078 ± 0.024	5.2 ± 0.74	50.9
3i	α-pyrimidine	-	0.194 ± 0.125	8.0 ± 3.01	179.2
3l	β-pyridine	-	0.069 ± 0.024	5.7 ± 0.55	8.82
3m	β-pyrimidine	-	0.414 ± 0.293	2.1 ± 0.30	17.56
3v	α-pyrimidine	alkyne	1.648	5.25 ± 0.43	4.67
8		alkyne	0.049 ± 0.015[a]	9 ± 1.51	52.30

13	3-benzyl-menadione	azide	0.0325	nd	63.6
16		azide	0.151	nd	39.65
PD	3-benzyl-menadione lead	-	0.043 ± 0.002	4.0 ± 1.36	141.7
Artesunate	control	-	0.0057 ± 0.0017	-	-
Atovaquone	control	-	-	0.102 ± 0.01	-

[a]: IC_{50} (µM) with the SYBR green assay using the *P. falciparum* Dd2 strain, which is sensitive to PD (20 ± 5), DHA (IC_{50} DHA = 0.7 ± 0.2), to methylene blue (IC_{50} MB = 7 ± 0.3), and resistant to chloroquine (IC_{50} CQ = 189 ± 12), (14). [b]: IC_{50} values for each compound were calculated based on three independent plaque assays conducted with *T. gondii* tachyzoites as illustrated (Supporting information, Figure S1).

The apicoplast is the primary target of plasmodione and related heteroaromatic 3-benzylmenadiones derivatives in *T. gondii*.

As the mode of action of **PD** has been recently linked with enzymatic activities hosted by the mitochondrion in yeast (11,12) and the apicoplast in *Plasmodium* (7), we investigated the impact of the three selected 1,4-naphthoquinones on the morphology of these organelles in *Toxoplasma* by immunofluorescence. To this end, we used the E2 subunit of pyruvate dehydrogenase (PDH-E2) (26) and the F1 beta ATPase (27) as protein markers of the apicoplast and mitochondrion, respectively. We selected **PD** (with an IC_{50} value of 4 µM), as well as both α-pyrimidine **3i** and β-pyrimidine **3m** (the 1,4-naphthoquinones with the least and the most impact on *T. gondii* growth, with IC_{50} values of about 8 and 2 µM, respectively) to further study their effect on tachyzoite morphology during the intracellular development of the parasites. For this, intracellular parasites were incubated for three days in the presence of 10 µM of each compound. Immunofluorescence labelling with a marker of the inner membrane complex (a structure made of flattened vesicles underlying the plasma membrane), allowed visualization of developing daughter cells during cell division, which is usually synchronized within each parasitophorous vacuole (Figure 2A). Upon drug treatment, parasite division appeared largely asynchronous within the vacuoles, suggesting that parasite division was affected (Figure 2A). The overall aspect of the mitochondrion, a single organelle with different morphological forms in the parasites (28), was slightly but significantly affected by treatment with the three compounds (Figures 2B and 2C). It will be interesting to investigate whether they also affect mitochondrial metabolism. On the other hand, all three compounds showed a marked impact on the apicoplast, with up to 30% of individual parasites and up to 60% of the parasite-harbouring parasitophorous vacuoles displaying a potential loss of the organelle, as assessed by the loss of the PDH-E2 signal (Figures 2A and 2C).

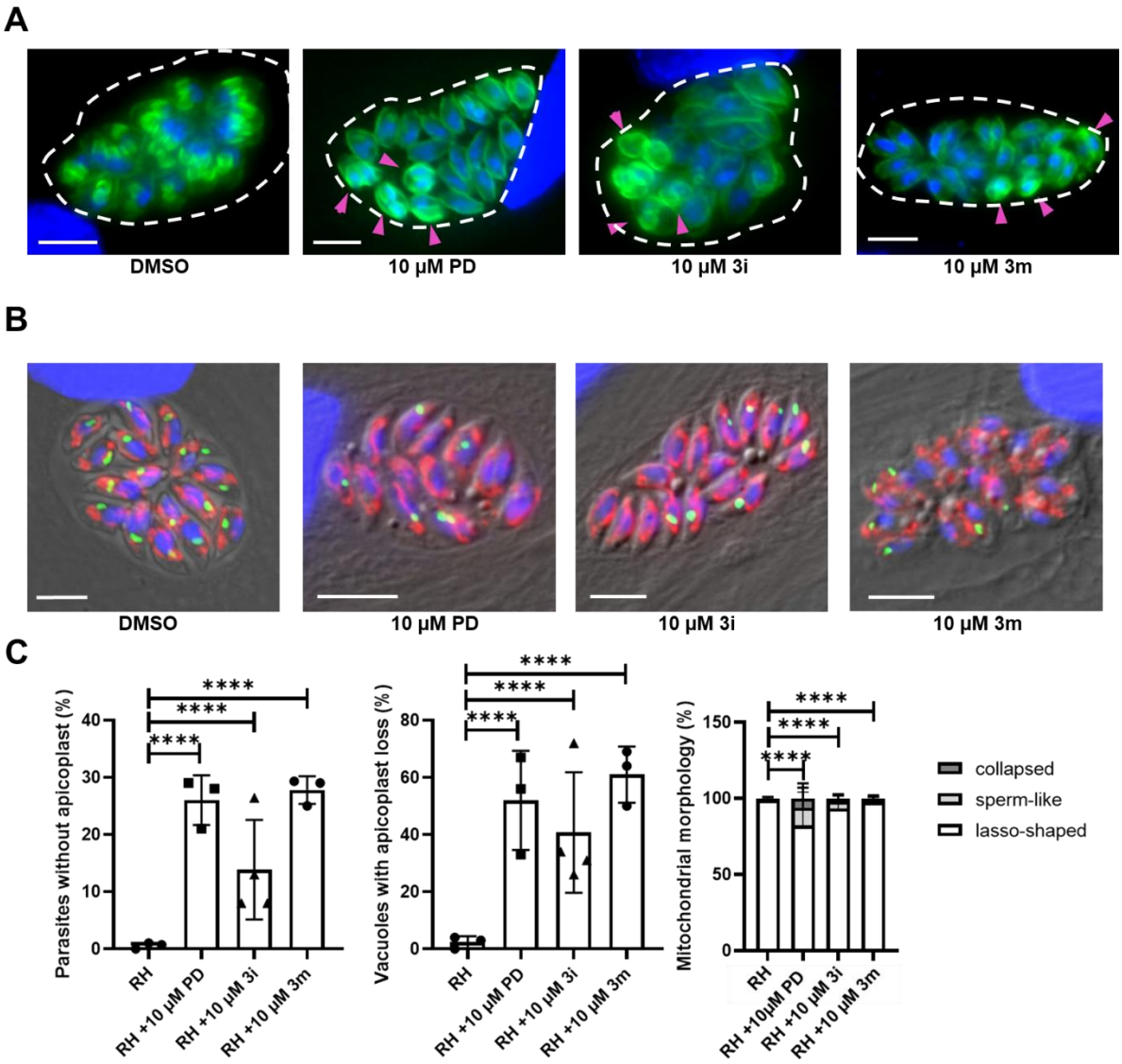

Figure 2. Effect of plasmodione-derived compounds on *T. gondii* parasite division and organelle morphology. **A**) Treatment with PD-derived compounds impacts parasite division. While parasite division is usually synchronized within the same vacuole (outlined with dashed lines), treatment with PD, or compounds **3i** and **3m** for 3 days at 10 µM led to heterogenous vacuoles containing several dividing parasites (arrowheads) together with non-dividing ones as determined by staining with the inner membrane complex marker IMC3 (green). DNA was stained with DAPI (blue). Scale bar represents 10 µm. **B**) PD-derived compounds impact the homeostasis of the apicoplast. Parasites were treated for three days with each compound and the apicoplast (green) and mitochondrion (red) were stained with specific antibodies. DNA was stained with DAPI (blue). RH is a laboratory-adapted type I *T. gondii* strain. Merged images between fluorescent signals and differential interference contrast are shown. Scale bar=5 µM. **C**) Quantification of apicoplast loss *per* vacuole or *per* parasite and of mitochondrial morphology in treated parasites. Percentages for each experiment, and mean ± SD of at least *n*=3 independent biological replicates are plotted. Differences between treated and untreated parasites were analysed using Fisher's exact test based on the total number of parasites that were counted (parasite counts *per* condition and *per* experiment are summarized in the supporting Information, Tables S1-S3).**** $p \leq 0.0001$.

Lipidomic profile of neosynthesized fatty acids in the apicoplast of *T. gondii* tachyzoites under drug treatment.

The apicoplast has a central metabolic contribution to the fitness of *T. gondii* tachyzoites. Indeed, the organelle is known to be a major metabolic hub for the parasite (29) notably being the centre for *de novo* synthesis of fatty acids (FA) via its type II prokaryotic Fatty Acid Synthesis pathway (FASII), and of lysophosphatidic acid, a central phospholipid precursor. Both pathways are essential for bulk phospholipid synthesis, membrane biogenesis and thus intracellular parasite survival (30,31). To further determine the impact of the compounds on the apicoplast, and hence its metabolic activity, we investigated whether the FASII pathway was still active upon treatment with the most active β-pyrimidine **3m**. To do so, we used our state-of-the-art approach based on stable isotope labelling combined to mass spectrometry-based lipidomic analysis (32-34). The apicoplast FASII is the only pathway that can use ^{13}C converted from U-^{13}C-glucose by the parasite glycolysis to PEP that is imported into the apicoplast to generate FA (31,32). Hence, monitoring the ^{13}C incorporation into parasite FA/lipids by GCMS-based lipidomics analyses provides direct evidence on the activity of apicoplast FASII. Briefly parasites treated or not with compound **3m** were grown in human host cells in the presence of U-^{13}C-glucose (uniformly-^{13}C labeled glucose). Short times of drug incubation in *T. gondii* tachyzoites were chosen for subsequent ^{13}C incorporation analyses to identify the effects of **3m** on FASII upon using ^{13}C-glucose labelling coupled to GCMS analyses.

In the absence of the drug, the distribution of FA species from C14:0 to C24:0 was found as previously reported (31) upon ^{13}C integration from ^{13}C glucose catabolism. Tachyzoites treated with **3m** for short times, i.e. 4h to retain a fair proportion of organelles, showed significant effects on their global FA synthesis profiles from C14:0 to C24:0 (Figure 3A). Upon drug treatment, the analysis and quantification of FA species according to parasite cell numbers (nanomoles of lipids/parasite/sample), showed an overall decrease in the amount of most major FASII-synthesized FAs (Figure 3A). This reduction in major C14:0, C16:0, C16:1 species would be consistent with a reduced FASII activity, subsequent to the inhibition of an apicoplast protein target resulting in apicoplast loss. To confirm this reduction in apicoplast FASII activity, we carefully analysed ^{13}C incorporation in the isotopomers of C14:0 made by the apicoplast FASII. We confirmed that the *de novo* synthesis of C14:0 FA species in the apicoplast is drastically inhibited upon **3m** treatment of *T. gondii* tachyzoïtes. This effect is clearly seen from M10 to M14 isotopologues as there is almost no ^{13}C incorporation in the full chain length upon drug treatment. The apparent greater ^{13}C incorporation from M0 to M9 isotopologues may be explained by the fact that *T. gondii* tachyzoites grow in host cell types that can potentially provide them with more FA resources. Of note, the nutrient-rich *in vitro* culture systems also mask some important contributions to scavenge exogenous metabolites as precursors of FA, as previously documented (31,35). The distribution of ^{13}C incorporation in the isotopomers of C16:0 and C16:1 follows the same pattern upon drug treatment (see Supporting information, Figures S3 to S10). Concerning the elongated species synthesized in the endoplasmic reticulum from C18:0, C18:1 to C20:0, C22:0, C24:0, there is almost no ^{13}C incorporation in the full chain length in the presence of β-pyrimidine **3m**.

Taken together, these lipidomics analyses thus confirm that the apicoplast FASII activity is compromised by the treatment, likely due to an early disruption of the global homeostasis of the apicoplast.

A

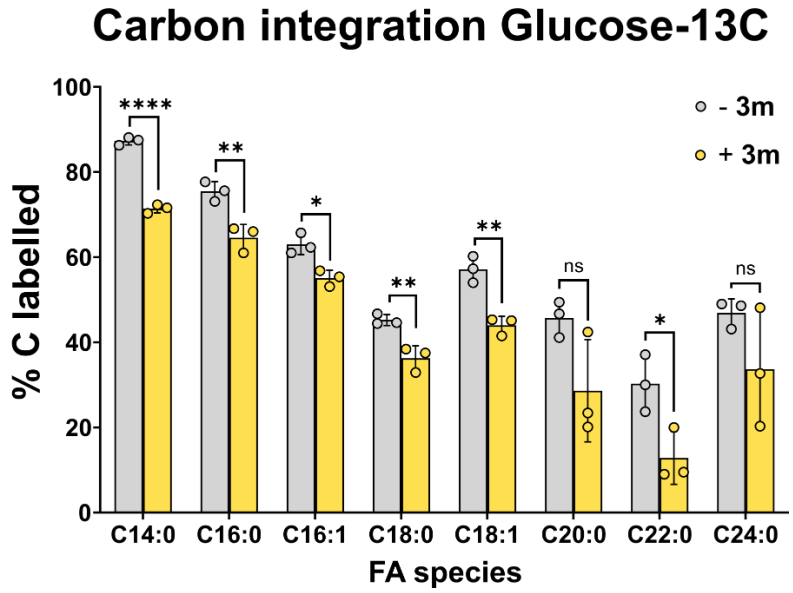

B

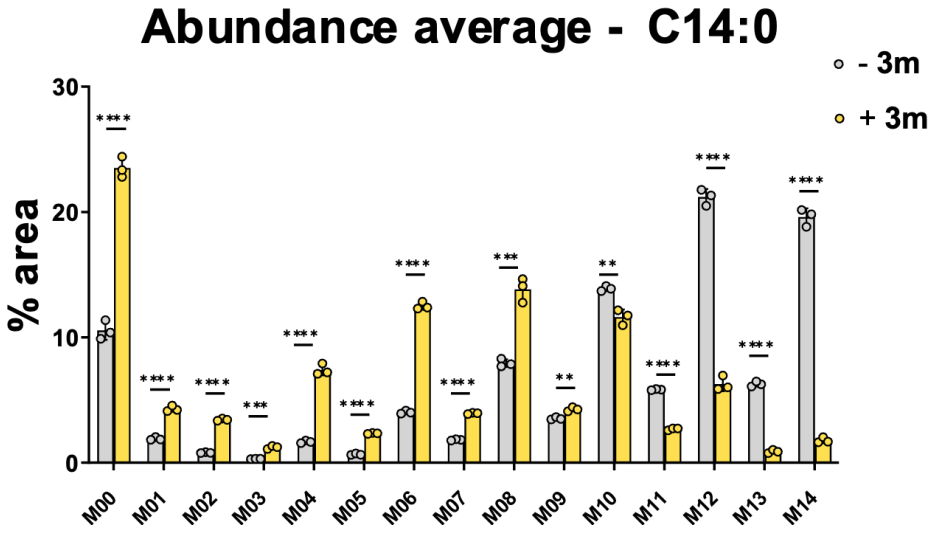

Figure 3. A) Effect of the PD-derived compound 3m on the de novo synthesis of fatty acids via the apicoplast FASII based on U-^{13}C-glucose labelling coupled to GCMS analyses in *T. gondii* tachyzoites. Incorporation of ^{13}C from the apicoplast FASII is significantly reduced in all parasite FA species. **B**) ^{13}C incorporation analysis in the isotopomers of C14:0 made by the apicoplast FASII. *De novo* synthesis of C14:0 fatty acids in the apicoplast is drastically inhibited upon compound **3m** treatment of *T. gondii* tachyzoites, as there is almost no ^{13}C incorporation in the full chain length.
Values, mean ± SEM of 3 independent replicates were plotted. Differences between treated (yellow) and untreated (gray) parasites were analysed by a t-test for each lipidomic analysis (GraphPad Prism 10): ns, non-significant; *, p<0.05; **, p<0.01; ***, p<0.001; ****, p<0.0001.

Drug localization studies in *T. gondii* tachyzoites.

To gain further insights into a specific impact of the compounds on the apicoplast in *T. gondii*, we used the clickable compounds **3v** and **8** to perform localisation experiments. These alkyne derivatives were found to have similar IC_{50} on the growth of *T. gondii* tachyzoites as the 3-benzylmenadione they derived from (Table 2). Microscopy analysis of fluorescent dye-conjugated compounds and co-staining with an

apicoplast-resident protein showed an accumulation of compounds **3v** and **8** in the organelle after 6 hours of incubation (Figure 4A). This was in sharp contrast to the control condition in which the click reaction was performed with the fluorescent azide without prior incubation with the compounds, and for which fluorescent labelling was distributed homogenously in the cytosol (Figure 4A). The enrichment of the compounds at the apicoplast was further confirmed by analysing the distribution of the fluorescence signal in the parasites (Figure 4B). Apicoplast labelling was consistently observed in the majority of *Toxoplasma* tachyzoites: 85 ± 8% with compound **3v** and 75 ± 3% with compound **8** (*n*=3 independent experiments, an average of 50 parasites were counted for each condition). Altogether, these data strongly suggest that 3-benzylmenadiones act on *T. gondii* by targeting primarily the apicoplast and have a marked effect on the organelle that is likely contributing to their impact on parasite growth.

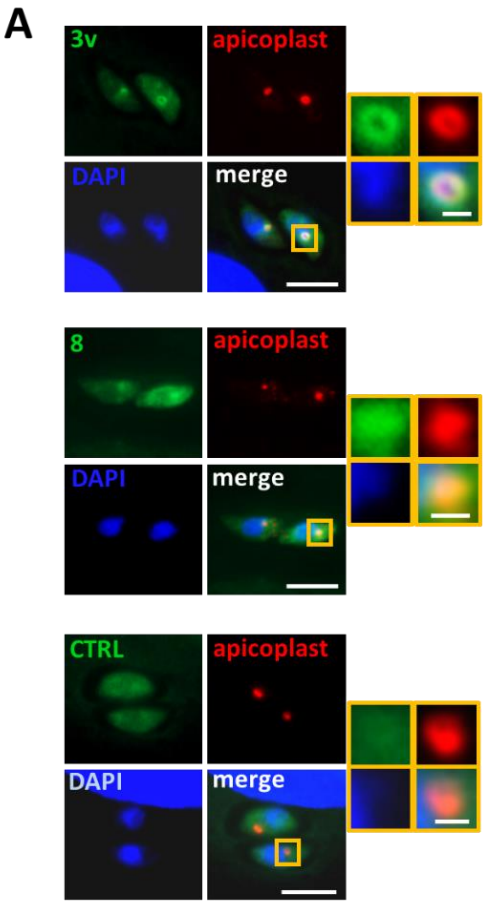

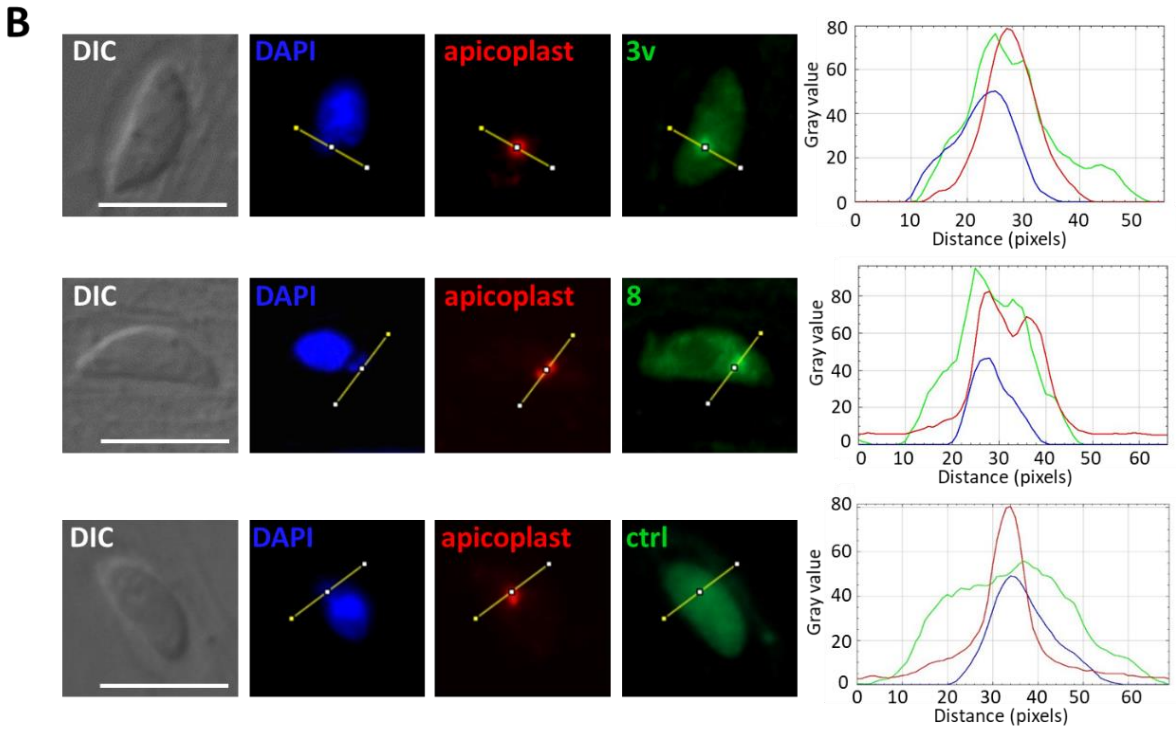

Figure 4. A) **3v** and **8** were incubated for 6 hours with intracellular tachyzoites and were labelled with a fluorescent azide by click chemistry (green) before co-staining with the anti-PDH-E2 antibody to label the apicoplast (red). DNA was stained with DAPI (blue). Magnified insets show the vicinity of the apicoplast to highlight colocalization. In the control (bottom), the click reaction with the fluorescent azide was performed without pre-incubation with a PD-derived compound. Scale bar represents 5 µm (large field) or 0.5 µm (inset).
B) Fluorescence intensity profiles show the distribution of fluorescence across the orange line (x-axis). The fluorescence intensities are plotted along the y-axis and highlight the close proximity of the peaks for apicoplast-localized DNA (in blue, the apicoplast has its own genome), apicoplast-resident protein PDH-E2 (in red) and PD-derived compound (in green). Scale bar represents 5 µm.

A localization experiment was also performed on azido **PD** analogues **13** and **16**. However, no fluorescence signal could be observed after 6 h of incubation and the click reaction using the commercial Alexa Fluor 488 alkyne. This may be explained by the fact that aryl azides are known to be unstable under the click reaction conditions (i.e. the presence of biological reductant or UV irradiation), although in our case we validated their stability *in vitro* (Supporting information, Figures S11-S13, NMR spectra of the azido derivative **16** incubated for 24 h under excess of sodium ascorbate, GSH, or cysteine).

Drug localization in *P. falciparum* trophozoites.

We further used two clickable probes, namely probes **3v** and **8**, on trophozoites of *P. falciparum* NF54 strain. Young trophozoite parasites were treated with the probes for 2 and 4 h to assess their distribution and potential colocalization with specific organelles such as the mitochondria or apicoplast. The results revealed distinct patterns for the two probes. Probe **3v** exhibited a homogeneous distribution within the parasite, with no noticeable accumulation (see Supporting information, Figure S14). In contrast, probe **8** distribution was heterogenous and usually accumulated close to, or colocalized with, the mitochondrion or apicoplast (Figure 5 and Supporting information, Figure S15). We observed an association of probe **8** with the mitochondria or apicoplast signals in 27-30% and 19-24% of the

parasites, respectively (n=2 independent experiments, an average of 140 parasites were counted for each condition, Supporting information, Table S4). Of note, the fact that probe **8** signal appeared punctuated even when not associating with the labelled organelle (Figure S15) suggests that it accumulated in other organelles, including possibly mitochondria when the apicoplast was labelled, and reciprocally. It will be interesting to investigate whether this colocalization varies with exposure time, parasite stage or drug concentration. Of note, probe **3v** demonstrated lower antiplasmodial activity compared to probe **8**, which raises the possibility of a correlation between the probe activity and its specific accumulation in organelles within the parasite.

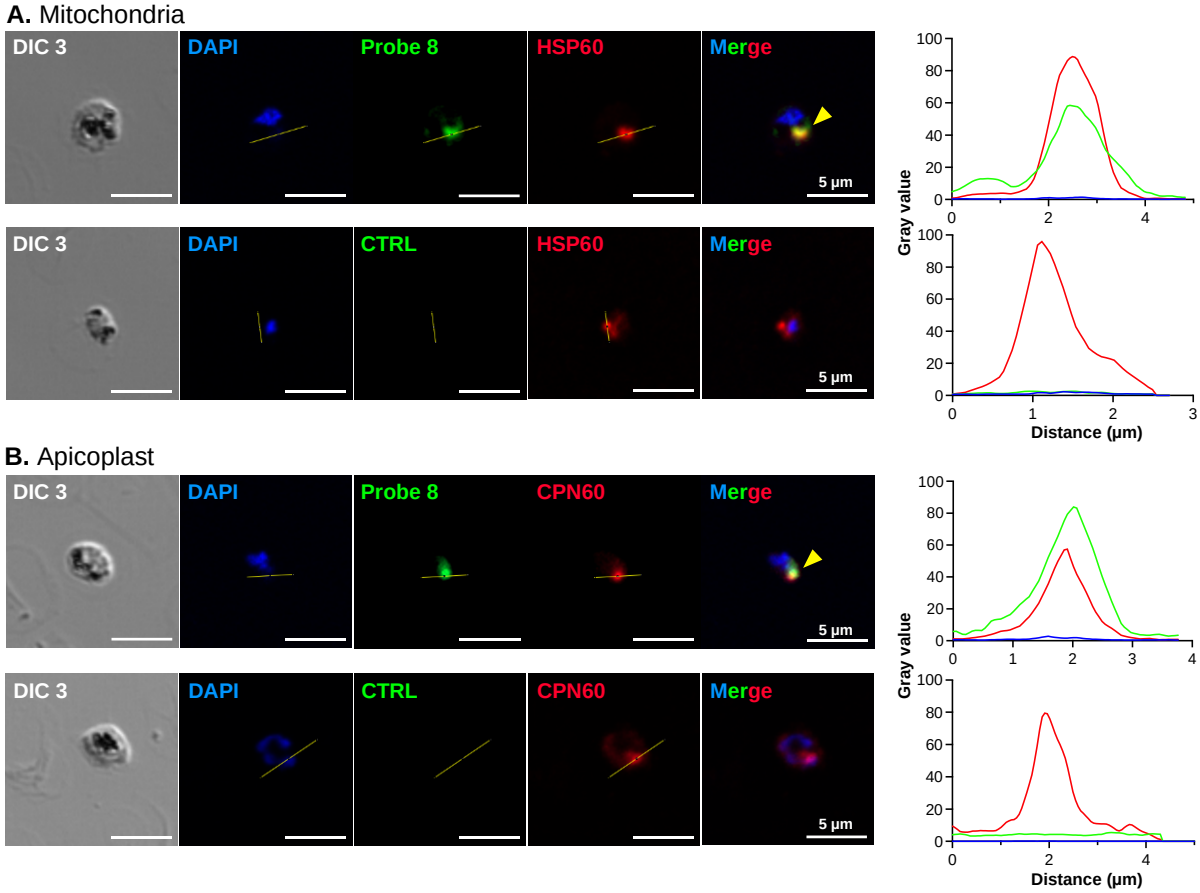

Figure 5. Subcellular localization of probe **8** in asexual blood stages of *P. falciparum* (trophozoite stage) after 2h of incubation. The probe was detected using CuAAC reaction with Alexa Fluor 488-azide (green). Nucleic acids were DAPI-stained (blue), and antibodies specific to *P. falciparum* HSP60 and CPN60 were used to localize the mitochondria (panel **A**, red) and apicoplast (panel **B**, red), respectively. Colocalization is of probe **8** and the organelle is indicated by yellow arrowheads. Fluorescence intensity profiles were plotted as graphs along the yellow line (x-axis). In control experiments, the click reaction with the fluorescent azide was performed without pre-incubation of parasites with probe 8. Representative images from 2 biological replicates.

As in *T. gondii*, exposure of *P. falciparum* parasites to **PD** or probe **8**, in this case at 50 nM, i.e., at their IC_{50} and for 14 h and 48 h, led to a strong reduction or complete disappearance of the mitochondria and/or apicoplast signal in 3-12% of all parasites, indicating that these organelles are lost (Figure 5). Of note, the percentage of parasites devoid of apicoplast increased at cycle n+1 (48 h) as compared to 14 h, which is usually observed when the apicoplast is targeted. The fact that probe **8** is enriched in mitochondria and apicoplast, and that these two organelles are lost in some parasites upon treatment, suggest that parasite killing upon 3-benzylmenadione treatment may be mediated by an effect of the

drug on the apicoplast and/or mitochondria, although we cannot exclude that the loss of apicoplast and/or mitochondria could be a consequence, rather than the cause, of parasite death.

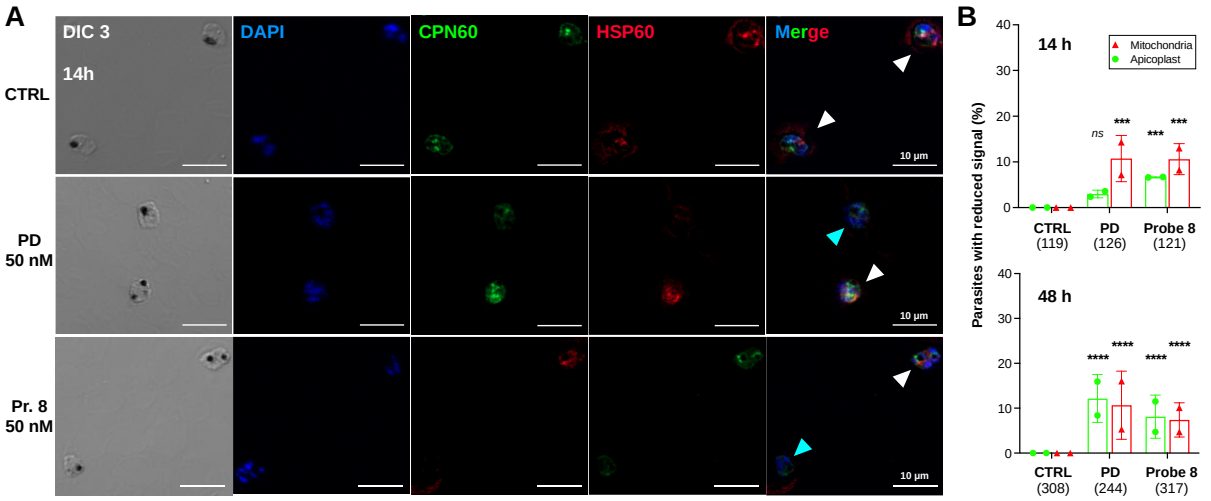

Figure 6. Morphological analysis of *P. falciparum* parasites after exposure to PD or probe **8** at 50 nM. **A**) Subcellular localization of apicoplast (CPN60, green), mitochondria (HSP60, red) and nucleic acids (DAPI, blue) in asexual blood stages of *P. falciparum* (trophozoite stage) after 14 h of treatment and in untreated parasites (CTRL). Parasites presenting normal apicoplast and mitochondria signal are indicated with white arrowheads, those presenting reduced/no signal for both markers are indicated with cyan arrowheads. Representative images from 2 independent experiments. **B**) Quantification of apicoplast and mitochondrial loss in parasites after 14 h and 48 h of exposure to PD or probe **8** at 50 nM. Data from the same experiments as **A**. Percentages for each experiment and mean ± SD are plotted. Differences between treated and untreated parasites were analyzed using Fisher's exact test based on the total number of parasites that were counted (indicated in brackets below each condition; parasite counts *per* condition and *per* experiment are summarized in the Supporting Information, Table S4). *ns*, non-significant; ***, p<0.005; ****, p<0.0001.

Discussion on the structure-activity relationships.

The main conclusions on the structure/activity relationships tested in this study are summarised in Table 3, including anti-Apicomplexa activities based on IC_{50} values, imaging of morphological alterations, drug localization by the CuAAC reaction and lipidomics analyses.

Our results demonstrate that the apicoplast is a major target of 3-benzylmenadiones in *T. gondii*. Indeed, treatment of *T. gondii* tachyzoites with three compounds, **3m, 3i** and **PD**, led to alterations in the apicoplast (i.e. a reduction of the number of parasites carrying an apicoplast). These alterations were more severe upon treatment with **3m** and **PD** that are more potent on *T. gondii* tachyzoites, than with **3i** presenting a higher IC_{50} value. Lipidomics analyses confirmed that the FASII pathway, located in the apicoplast was strongly affected by **3m** treatment. Finally, using two clickable probes with different potencies, **3v** and **8**, we also demonstrate that the 3-benzylmenadiones localise in the apicoplast, with a correlation between potency and concentration of the probe.

In *P. falciparum*, the 'clickable' benzylmenadione-alkyne probe **8** exhibited similar IC_{50} values as the lead **PD** (IC_{50} ca. 45 nM) whereas probe **3v** was less potent (IC_{50} > 2 µM). Both compounds were found to accumulate in the parasites by CuAAC-based imaging. Still, their distribution was different: probe **3v** was homogenously distributed in the parasite while probe **8** showed subcellular accumulations that

colocalised with the apicoplast and mitochondria in 20-30% of the cases. The differences in probe distribution and colocalization patterns may reflect variations in their potency, mechanism of action or affinity for specific targets.

Table 3. Structure-activity relationships.

Structure-Activity relationships	***T. gondii*** tachyzoites	***P. falciparum*** trophozoites
Activity (based on IC_{50}): + → -	**3m** > **PD** > **3b** = **3v** > **3l** > **3i** = **8**	**PD** = **8** > **3l** > **3b** > **3i** > **3m** > **3v**
Morphological alterations	**3m** > **PD** > **3i** (apicoplast disrupted)	**nd**
Drug localization by click	**3v** > **8** (in apicoplast)	**8** > **3v** (in apicoplast & mitochondria)
Lipidomics	**3m** (apicoplast FASII lipids affected)	nd

Discussion on the possible mode of action of 3-benzylmenadiones.

The loss of the apicoplast is often associated with the delayed death of the parasite, which is usually the case for most housekeeping pathways and processes held in the apicoplast, such as organellar genome replication/transcription/translation. Hence, most apicoplast inhibitors that are directed against prokaryotic-like pathways of the apicoplast, such as clindamycin, doxycycline or azithromycin, induce a delayed death of the parasite (36-38). It is also the case for some inhibitors affecting non-housekeeping processes, such as single metabolic pathways of the apicoplast (i.e., fatty acid synthesis, isoprenoid synthesis, heme and iron-sulfur cluster, see ref. 29, 39). This phenomenon was partially explained by the loss of the apicoplast causing the slow arrest of protein prenylation in subsequent parasite generation (37). Indeed, the abrogation of several apicoplast pathways at the same time, and/or disruption of the import of major metabolic precursors in the apicoplast can lead to immediate death instead (40). Therefore, it is actually difficult to characterize apicoplast disruption only based on the detection of delayed death. Taken together, our IFAs, and lipidomics/fluxomics data suggest that at least one of the relevant **PD** targets is in the apicoplast. Of note, in *P. falciparum*, the partial association of the 'clickable' 3-benzylmenadione **8** (this study) and of a 'clickable' 6-fluoro-3-benzylmenadione probe (41), both potent antimalarial compounds, with the apicoplast and mitochondria, is coherent with previous data we obtained in both yeast (mitochondria only) and *P. falciparum,* as detailed below.

First, we previously demonstrated that **PD** inhibits yeast respiratory growth and that the mitochondrial respiratory chain flavoprotein NADH-dehydrogenases play a key role in **PD** activity, and **PDO** redox-cycling (11). Indeed, the deletion of the NDE1 gene encoding the main NADH dehydrogenase in yeast resulted in a decreased sensitivity to **PD** (11). It will be worth investigating whether the homologous parasite protein *Pf*NDH2 is also involved in **PD** mode of action in *P. falciparum.*

Second, and regarding the role of the apicoplast in the mode of action of **PD**, our observations are also in agreement with recent data published by Cichocki *et al.* (7). Using the genetically-encoded redox sensor hGrx1-roGFP2 expressed in different subcellular compartments of transgenic *P. falciparum* parasites, an oxidative burst was detected in the apicoplast 5 min after **PD** treatment (7), while oxidative

stress only peaked 4 h after drug exposure in the cytosol (5). The fact that **PD** influences the apicoplast redox potential more rapidly than the cytosolic one suggests that **PD** bioactivation may occur in the apicoplast. This could be mediated by **PD** redox cycling catalyzed by an apicoplast flavoenzyme such as *P. falciparum* ferredoxin-$NADP^+$ reductase (*Pf*FNR). Indeed, this enzyme can catalyze single-electron reduction of quinones (42) accompanied by high redox cycling and $O_2^{-\bullet}$ formation, which would be coherent with the early oxidative burst observed in the apicoplast. We also previously demonstrated that the efficient *Pf*FNR-catalyzed **PD** bioactivation produced both **PD** key metabolites, **PD-bzol** and **PDO** (7). Finally, we have recently identified several potential **PD** targets in yeast and *P. falciparum* using an affinity-based proteome profiling strategy with a photoreactive and 'clickable' 6-fluoro benzylmenadione probe (41). For instance, of the 11 proteins identified in yeast, 3 are involved in oxidoreductase activities (Pdb1, Dot5, Scs7) and one belongs to the yeast flavoproteome (Pdx3). Interestingly, Pdb1 is the E1 beta subunit of the pyruvate dehydrogenase complex (PDH), localized in the mitochondria in yeast, but its orthologous surrogate is found in the apicoplast of *Plasmodium* parasites. In addition to E1, PDH is formed of E2 (dihydrolipoamide acetyltransferase) and E3 (dihydrolipoamide dehydrogenase) components, with the structural protein Pdx1. We previously found that E3 (or Lpd1) and Lip2, acting in the attachment of lipoic acid groups to E2 are involved in **PD** activity (12). Hence, the role of *Pf*PDH in **PD** bioactivation will be worth investigating.

In conclusion, the data produced here and in our previous reports provide several lines of evidence pointing towards a mode of action of **PD** and analogues targeting both the parasite apicoplast and mitochondria, with the bioactivation of **PD** into potent metabolites possibly occurring in the apicoplast. Further genetic and functional validations are required to confirm this model.

Ecotoxicity.

The second objective of this work aimed at investigating the overall environmental impact of our compounds.

In a first preliminary study based on a selection of three 3-benzylmenadione representatives and heteroaromatic analogues, **PD**, **3b** and **3i** (see structures in Table 2) exhibited heterogenous toxicities towards algae and invertebrates, as indicated by the calculated EC_{10}-, EC_{20}-, and EC_{50}-values. After being exposed for 96 h to increasing concentrations of the drugs, the algae *Desmodesmus subspicatus* was affected strongly by **PD**, followed by α-pyridine **3b** and α-pyrimidine **3i**, and all values were in the sub-micromolar range. Of note, *Desmodesmus* is a plastid-bearing green algae, and given the potential link between the mode of action of **PD**-derivatives and the apicomplexan plastid, it might be interesting to further investigate whether these compounds may have a more general impact on plastid-bearing organisms. Planktonic crustacean *Daphnia magna*, was generally less affected, and the compounds with the strongest effect were **3b**, followed by **3i** and **PD** (Table 4). While the number of tested species is quite limited, these data suggest that primary producers are significantly more sensitive than primary consumers. These results call for an extended ecotoxicity analysis with more test species and a particular attention directed to primary producers potentially driving the environmental risk of these

compounds. While environmental concentrations have not been estimated during this study, the ecotoxicological data point to **PD** having the highest environmental risks followed by **3b** and **3i**. This information can, under the umbrella of the One Health Concept, guide the drug development by actively selecting for the most efficient but still environmentally least risky molecules.

These data will enter a database to build a sharable guideline-like document useful for drug designer and managers of environmental risks. Drug ecotoxicity is an emerging environmental problem, raising increasing attention in the field in pharmaceutical use/manufacturing. Therefore, optimization of 3-benzylmenadiones, headed by **PD**, will progress in a more sustainable approach following the principles of an optimal activity and safety profile in humans, animals and other organisms found in the environment.

Table 4. EC-values (± 95% confidence interval) derived from the toxicity tests. Concentrations are given in µM. n.d. = not determined, as response did not reach the effect level.

Test item	Test organism	EC_{10}	EC_{20}	EC_{50}
PD	*D. subspicatus*	0.015 ± 0.013	0.214 ± 0.062	0.556 ± 0.081
	D. magna	169.45 ± 63.57	222.71 ± 59.02	336.52 ± 44.55
3b	*D. subspicatus*	0.28 ± 0.12	0.70 ± 0.15	n.d.
	D. magna	1.77 ± 0.32	2.28 ± 0.26	3.34 ± 0.16
3i	*D. subspicatus*	n.d.	n.d.	n.d.
	D. magna	1.89 ± 2.39	6.09 ± 4.03	n.d.

Conclusion.

Our study takes advantage of the synthesis of chemical derivatives of **PD** and the use of two related parasite models to investigate the mode of action of this lead compound. Our results highlighted some differences. First, **PD** derivatives were less active in *T. gondii* (low micromolar range) as in *P. falciparum* blood stages (nanomolar range). This could be explained by the presence of new permeability pathways in *Plasmodium*-infected erythrocytes. Indeed, this parasite modifies extensively the host cell membrane that becomes highly permeable to various types of solutes, facilitating the uptake of small compounds, including drugs (43). To reach *T. gondii*, on the other hand, drugs have to cross a series of non-permeable membranes (i. e., the host plasma membrane, the parasitophorous vacuole membrane, the parasite plasma membrane). Thus, **PD**-derived compounds may have to be optimized for their ability to cross membranes if they need to be used in the context of toxoplasmosis.

Another noticeable difference is that, while **PD**-derivatives accumulated in *T. gondii* apicoplast, and treatment with **PD** and analogues clearly affected the morphology and function of the organelle, clickable probe **8** did show a heterogenous localization in *P. falciparum*, but less clearly associated with the apicoplast. Indeed, it showed association with the mitochondrion or the apicoplast in 20-30% of parasites only. Of note, this association with apicoplast and mitochondrion is coherent with studies on the mechanism of action of **PD** in *P. falciparum* (7), and in yeast (11), that proposed both apicoplast- and

mitochondrion-based oxidoreductases as potential activators of the pro-drug and redox-cyclers. The differences between the two apicomplexan models do not rule out a conservation of end targets between them, and the converging evidence pointing to a conserved involvement of the apicoplast remains to be investigated further.

■ METHODS

Chemistry. General. All the reagents and solvents were purchased from commercial sources and used as received, unless otherwise stated. The ^{1}H, ^{19}F and, and ^{13}C $\{^{1}H\}$ NMR spectra were obtained in $CDCl_3$ or DMSO-d_6 as solvents using a 400 MHz or a 500 MHz spectrometer. Chemical shifts were reported in parts *per* million (δ). ^{1}H NMR data were reported as follows: chemical shift (δ ppm) (multiplicity, coupling constant (Hz), and integration). Multiplicities are reported as follows: s = singlet, d = doublet, t = triplet, q = quartet, m = multiplet, or combinations thereof. High-resolution mass spectroscopy (HRMS) spectra were recorded using the electron spray ionization (ESI) technique.

General procedure for the Suzuki coupling between 2-(chloromethyl)-1,4-dimethoxy-3-methylnaphthalene and aryl or heteroarylboronic species.

General conditions are a modification of a previously published procedure (44). In a sealable tube, 2-(chloromethyl)-1,4-dimethoxy-3-methylnaphthalene **1** (1 equiv.), the desired heteroarylboronic acid (1.2 equiv.) and sodium carbonate (2.1 equiv.) were dissolved in a 2:1 mixture of dimethoxyethane:water (0.15 M). The mixture was bubbled 30min with argon, and then tetrakis(triphenylphosphine)palladium (2-5 mol%) was added at once. The tube was sealed and the mixture was heated 1 h at 100 °C under stirring. The mixture was then, allowed to cool down to room temperature, diluted with water and extracted three times with ethyl acetate. Reunited organic layers were washed with brine, dried over magnesium sulfate, filtered and the solvent was removed under reduced pressure to afford a crude which was purified on silica gel chromatography using the adequate eluant system to afford the desired coupling product.

3-((1,4-dimethoxy-3-methylnaphthalen-2-yl)methyl)pyridine (2a). 5 mol% $Pd(PPh_3)_4$, Eluant (CHX/EtOAc, 5/5, v/v, UV), yellowish solid, 71% yield. m.p. 105-106 °C. ^{1}H NMR (500 MHz, $CDCl_3$) δ 8.50 (dd, *J* = 2.3, 1.0 Hz, 1H), 8.41 (dd, *J* = 4.8, 1.6 Hz, 1H), 8.12 – 8.04 (m, 2H), 7.63 – 7.42 (m, 2H), 7.39 – 7.32 (m, 1H), 7.13 (ddd, *J* = 7.8, 4.8, 0.9 Hz, 1H), 4.25 (s, 2H), 3.86 (s, 3H), 3.85 (s, 3H), 2.26 (s, 3H). ^{13}C $\{^{1}H\}$ NMR (126 MHz, $CDCl_3$) δ 150.75, 150.73, 149.9, 147.5, 136.1, 135.7, 128.3, 128.0, 127.3, 126.6, 126.1, 125.8, 123.5, 122.6, 122.4, 62.4, 61.6, 30.3, 12.8. HRMS (ESI) calcd. for $C_{19}H_{20}NO_2$: 294.1489. Found: 294.1490 ($M+H^+$).

5-((1,4-dimethoxy-3-methylnaphthalen-2-yl)methyl)-2-(trifluoromethyl)pyridine (2b). 5 mol% $Pd(PPh_3)_4$, Eluant (CHX/EtOAc, 9/1, v/v, UV), translucid oil, 97% yield. ^{1}H NMR (500 MHz, $CDCl_3$) δ 8.64 (d, *J* = 1.4 Hz, 1H), 8.16 – 8.04 (m, 2H), 7.61 – 7.46 (m, 4H), 4.31 (s, 2H), 3.87 (s, 3H), 3.86 (s, 3H), 2.26 (s, 3H). ^{19}F $\{^{1}H\}$ NMR (471 MHz, $CDCl_3$) δ -67.68. ^{13}C $\{^{1}H\}$ NMR (101 MHz, $CDCl_3$) δ 150.82, 150.81, 150.1, 145.9 (q, *J* = 34.6 Hz), 139.7, 136.8, 128.4, 127.2, 127.0, 126.3, 126.2, 125.9, 122.5, 121.8 (q, *J* = 273.7 Hz), 120.3 (q, *J* = 2.7 Hz), 62.3, 61.5, 30.1, 12.8. HRMS (ESI) calcd. for $C_{20}H_{19}F_3NO_2$: 362.1362. Found: 362.1368 ($M+H^+$).

5-((1,4-dimethoxy-3-methylnaphthalen-2-yl)methyl)-2-fluoropyridine (2c). 2 mol% $Pd(PPh_3)_4$, Eluant (CHX/EtOAc, 9/1, v/v, UV), white solid, 89% yield. m.p. 120-121 °C. ^{1}H NMR (400 MHz, $CDCl_3$) δ 7.94 – 7.70 (m, 3H), 7.40 – 7.19 (m, 3H), 6.54 (ddd, *J* = 8.4, 3.1, 0.6 Hz, 1H), 3.98 (s, 1H), 3.63 (s, 3H), 3.61 (s, 3H), 2.03 (s, 3H). ^{19}F $\{^{1}H\}$ NMR (377 MHz, $CDCl_3$) δ -72.09 (d, *J* = 8.0 Hz). ^{13}C $\{^{1}H\}$ NMR (101 MHz, $CDCl_3$) δ 162.4 (d, *J* = 237.2 Hz), 150.8, 150.6, 146.9 (d, *J* = 14.4 Hz), 141.0 (d, *J* = 7.6 Hz), 133.6 (d, *J* = 4.5 Hz), 128.3, 127.9, 127.3, 126.4, 126.2, 125.8, 122.6, 122.5, 109.3 (d, *J* = 37.4 Hz), 62.4, 61.6, 29.4 (d, *J* = 1.5 Hz), 12.8. HRMS (ESI) calcd. for $C_{19}H_{19}FNO_2$: 312.1394. Found: 312.1403 ($M+H^+$).

2-chloro-5-((1,4-dimethoxy-3-methylnaphthalen-2-yl)methyl)pyridine (2d). 5 mol% $Pd(PPh_3)_4$, Eluant (CHX/EtOAc, 9/1, v/v, UV), white solid, 87% yield. m.p. 123-124 °C. ^{1}H NMR (400 MHz, $CDCl_3$)

δ 8.19 (dd, *J* = 2.6, 0.8 Hz, 1H), 8.07 – 7.91 (m, 2H), 7.51 – 7.38 (m, 2H), 7.26 (dd, *J* = 8.2, 2.5 Hz, 1H), 7.08 (dd, *J* = 8.2, 0.7 Hz, 1H), 4.13 (s, 2H), 3.78 (s, 3H), 3.77 (s, 3H), 2.18 (s, 3H). ^{13}C {^{1}H} NMR (101 MHz, $CDCl_3$) δ 150.8, 150.7, 149.5, 149.2, 138.7, 135.1, 128.4, 127.6, 127.3, 126.37, 126.33, 125.9, 124.2, 122.6, 122.5, 62.5, 61.6, 29.6, 12.8. HRMS (ESI) calcd. for $C_{19}H_{19}ClNO_2$: 328.1099. Found: 328.1102 ($M+H^+$).

5-((1,4-dimethoxy-3-methylnaphthalen-2-yl)methyl)-2-methoxypyridine (2e). 2 mol% $Pd(PPh_3)_4$, Eluant (CHX/EtOAc, 95/05, v/v, UV), translucid oil, 69% yield. ^{1}H NMR (400 MHz, $CDCl_3$) δ 8.14 – 8.04 (m, 2H), 8.02 – 7.94 (m, 1H), 7.58 – 7.44 (m, 2H), 7.32 (dd, *J* = 8.5, 2.6 Hz, 1H), 6.61 (dd, *J* = 8.6, 0.7 Hz, 1H), 4.16 (s, 2H), 3.89 (s, 3H), 3.85 (s, 3H), 3.85 (s, 3H), 2.28 (s, 3H). ^{13}C {^{1}H} NMR (101 MHz, $CDCl_3$) δ 162.8, 150.68, 150.65, 146.0, 138.9, 128.7, 128.6, 128.2, 127.3, 126.7, 125.9, 125.7, 122.6, 122.4, 110.7, 62.4, 61.5, 53.4, 29.4, 12.7. HRMS (ESI) calcd. for $C_{20}H_{22}NO_3$: 324.1594. Found: 324.1617 ($M+H^+$).

5-((1,4-dimethoxy-3-methylnaphthalen-2-yl)methyl)pyridin-2-amine (2f). 7 mol% $Pd(PPh_3)$, Eluant (EtOAc, 10, v/v, UV), orange solid, 72% yield. m.p. = 95-97 °C. ^{1}H NMR (400 MHz, $CDCl_3$) δ 8.08 (tdd, *J* = 5.3, 4.0, 3.2 Hz, 2H), 7.91 (s, 1H), 7.74-7.61 (m, 2H), 7.15 (dd, *J* = 8.5, 2.3 Hz, 1H), 6.38 (d, *J* = 8.4 Hz, 1H), 4.36 (s, 2H), 4.10 (s, 2H), 3.85 (s, 3H), 3.84 (s, 3H), 2.28 (s, 3H). ^{13}C {^{1}H} NMR (101 MHz, $CDCl_3$) δ 156.7, 150.4, 147.1, 137.9, 128.6, 128.5, 125.8, 125.5, 122.4, 122.2, 108.8, 62.3, 61.4, 29.3, 12.6.

5-((1,4-dimethoxy-3-methylnaphthalen-2-yl)methyl)pyrimidine (2g). 5 mol% $Pd(PPh_3)_4$, Eluant (CHX/EtOAc, 5/5, v/v, UV), beige solid, 87% yield. m.p. 104-105 °C. ^{1}H NMR (500 MHz, $CDCl_3$) δ 9.04 (s, 1H), 8.54 (s, 2H), 8.13 – 7.98 (m, 2H), 7.61 – 7.41 (m, 2H), 4.22 (s, 2H), 3.88 (s, 3H), 3.86 (s, 3H), 2.29 (s, 3H). ^{13}C {^{1}H} NMR (126 MHz, $CDCl_3$) *δ* 156.9, 156.8, 150.9, 150.8, 133.9, 128.5, 127.3, 126.7, 126.4, 125.9, 122.6, 122.5, 62.5, 61.7, 28.1, 12.9. HRMS (ESI) calcd. for $C_{18}H_{19}N_2O_2$: 295.1441. Found: 295.1450 ($M+H^+$).

5-((1,4-dimethoxy-3-methylnaphthalen-2-yl)methyl)-2-(trifluoromethyl)pyrimidine (2i). 2 mol% $Pd(PPh_3)_4$, Eluant (CHX/EtOAc, 8/2, v/v, UV), white solid, 71% yield. ^{1}H NMR (400 MHz, $CDCl_3$) δ 8.70 (s, 2H), 8.23 – 7.97 (m, 2H), 7.68 – 7.33 (m, 2H), 4.28 (s, 2H), 3.90 (s, 3H), 3.86 (s, 3H), 2.30 (s, 3H). ^{19}F {^{1}H} NMR (377 MHz, $CDCl_3$) δ -70.15. ^{13}C {^{1}H} NMR (101 MHz, $CDCl_3$) δ 157.6, 154.9 (q, *J* = 36.8 Hz), 151.0, 150.8, 136.4, 128.6, 127.2, 126.6, 126.1, 125.8, 125.6, 122.6, 122.5, 119.8 (q, *J* = 275.1 Hz), 62.4, 61.6, 28.0, 12.9. HRMS (ESI) calcd. for $C_{19}H_{18}F_3N_2O_2$: 363.1315. Found: 363.1307 ($M+H^+$).

2-((2-methoxypyrimidin-5-yl)methyl)-3-methylnaphthalene-1,4-dione (2j). 2 mol% $Pd(PPh_3)_4$, Eluant (CHX/EtOAc, 6/4, v/v, UV), translucid oil, 71% yield. 2j was isolated with an unknown inseparable compound and was used in the next step without any further purification. ^{1}H NMR (400 MHz, $CDCl_3$) δ 8.31 (s, 2H), 8.18 – 7.95 (m, 2H), 7.60 – 7.44 (m, 2H), 4.13 (s, 2H), 3.95 (s, 3H), 3.88 (s, 3H), 3.85 (s, 3H), 2.30 (s, 3H). HRMS (ESI) calcd. for $C_{19}H_{20}N_2NaO_3$: 347.1366. Found: 347.1357 ($M+Na^+$).

5-((1,4-dimethoxy-3-methylnaphthalen-2-yl)methyl)pyrimidin-2-amine (2k). 2 mol% $Pd(PPh_3)$, Eluant (CHX/EtOAc, 8/2, v/v, UV), white solid, 80% yield. m.p. 198-200 °C.^{1}H NMR (400 MHz, $CDCl_3$) δ 8.04-8.00 (m, 2H), 7.99 (s, 2H), 7.57-7.51 (m, 2H), 6.45 (s, 2H), 3.97 (s, 2H), 3.83 (s, 3H), 3.78 (s, 3H), 2.26 (s, 3H). ^{13}C {^{1}H} NMR (101 MHz, $CDCl_3$) δ 162.7, 157.8 (2C), 150.34, 150.30, 129.1, 127.8, 127.1, 126.7, 126.5, 126.3, 122.7, 122.5, 121.5, 62.6, 61.6, 26.8, 12.9. HRMS (ESI) calcd. for $C_{18}H_{20}N_3O_2$: 310.1550. Found: 310.1539 ($M+H^+$).

2-((1,4-dimethoxy-3-methylnaphthalen-2-yl)methyl)furan (2n). 2 mol% $Pd(PPh_3)_4$, Eluant (CHX/EtOAc, 98/02, v/v, UV), translucid oil, 99% yield. ^{1}H NMR (400 MHz, $CDCl_3$) δ 8.19 – 8.03 (m, 2H), 7.62 – 7.46 (m, 2H), 7.34 (dd, *J* = 1.8, 0.9 Hz, 1H), 6.27 (dd, *J* = 3.2, 1.9 Hz, 1H), 5.85 (dq, *J* = 3.2, 1.1 Hz, 1H), 4.27 (s, 2H), 3.92 (s, 3H), 3.90 (s, 3H), 2.41 (s, 3H). ^{13}C {^{1}H} NMR (101 MHz, $CDCl_3$) δ 154.3, 150.7, 150.4, 141.1, 128.2, 127.3, 127.1, 126.9, 125.9, 125.5, 122.6, 122.3, 110.4, 105.9, 62.6, 61.5, 26.3, 12.4. HRMS (ESI) calcd. for $C_{18}H_{19}O_3$: 283.1329. Found: 283.1334 ($M+H^+$).

5-((1,4-dimethoxy-3-methylnaphthalen-2-yl)methyl)benzo[*d*]thiazole (2o). 2 mol% $Pd(PPh_3)$, Eluant (CHX/EtOAc, 7/3, v/v, UV), white solid, 81% yield. m.p. = 139-141 °C. ^{1}H NMR (400 MHz, $CDCl_3$) δ 8.94 (s, 1H), 8.22-8.04 (m, 2H), 7.89 (s, 1H), 7.82 (d, *J* = 8.3 Hz, 1H), 7.60-7.48 (m, 2H), 7.31 (d, *J* = 8.2 Hz, 1H), 4.46 (s, 2H), 3.88 (s, 3H), 3.87 (s, 3H), 2.31 (s, 3H). ^{13}C {^{1}H} NMR (101 MHz, $CDCl_3$) δ 154.3, 153.8, 150.7, 150.5, 139.2, 131.3, 128.8, 128.1, 127.3, 126.9, 126.3, 125.9, 125.5, 122.7, 122.5, 122.3, 121.6, 62.4, 61.5, 32.7, 12.8. HRMS (ESI) calcd. for $C_{21}H_{20}NO_2S$: 350.1209. Found: 350.1202 ($M+H^+$).

6-((1,4-dimethoxy-3-methylnaphthalen-2-yl)methyl)benzo[*d*]thiazole (2p). 2 mol% $Pd(PPh_3)$, Eluant (CHX/EtOAc, 8/2, v/v, UV), colorless oil, 91% yield. ^1H NMR (400 MHz, $CDCl_3$) δ 8.90 (s, 1H), 8.14-8.10 (m, 2H), 8.03 (d, *J* = 8.4 Hz, 1H), 7.59 (s, 1H), 7.55-7.51 (m, 2H), 7.41-7.37 (m, 1H), 4.43 (s, 2H), 3.87 (s, 3H), 3.86 (s, 3H), 2.28 (s, 3H). ^{13}C {^1H} NMR (101 MHz, $CDCl_3$) δ 153.5, 151.8, 150.8, 150.7, 138.6, 134.3, 128.9, 128.3, 127.4, 127.2, 127.0, 126.1, 125.7, 123.4, 122.7, 122.4, 120.8, 62.5, 61.6, 32.8, 12.9. HRMS (ESI) calcd. for $C_{21}H_{20}NO_2S$: 350.1209. Found: 350.1210 ($M+H^+$).

4-((1,4-dimethoxy-3-methylnaphthalen-2-yl)methyl)pyridine (2q). 5 mol% $Pd(PPh_3)_4$, Eluant (CHX/EtOAc, 5/5, v/v, UV), yellowish oil, 57% yield. ^1H NMR (400 MHz, $CDCl_3$) δ 8.52 – 8.40 (m, 2H), 8.23 – 7.97 (m, 2H), 7.68 – 7.40 (m, 2H), 7.14 – 6.99 (m, 2H), 4.26 (s, 2H), 3.86 (s, 3H), 3.83 (s, 3H), 2.23 (s, 3H).

3-((1,4-dimethoxy-3-methylnaphthalen-2-yl)methyl)quinoline (2r). 5 mol% $Pd(PPh_3)_4$, Eluant (CHX/EtOAc, 7/3, v/v, UV), yellowish solid, 97% yield. m.p. 91-92 °C. ^1H NMR (500 MHz, $CDCl_3$) δ 8.92 (d, *J* = 2.3 Hz, 1H), 8.17 – 8.10 (m, 2H), 8.07 (dd, *J* = 8.4, 1.0 Hz, 1H), 7.69 – 7.59 (m, 3H), 7.58 – 7.50 (m, 2H), 7.46 (ddd, *J* = 8.1, 6.7, 1.2 Hz, 1H), 4.44 (s, 2H), 3.87 (s, 6H), 2.29 (s, 3H). ^{13}C {^1H} NMR (126 MHz, $CDCl_3$) δ 151.9, 150.9, 150.8, 146.9, 133.9, 133.5, 129.2, 128.8, 128.4, 128.3, 127.9, 127.6, 127.4, 126.7, 126.2, 125.8, 122.7, 122.5, 62.6, 61.6, 30.5, 12.9. HRMS (ESI) calcd. for $C_{23}H_{22}NO_2$: 344.1645. Found: 344.1659 ($M+H^+$).

Post-functionalization of Suzuki coupling adducts.

5-((1,4-dimethoxy-3-methylnaphthalen-2-yl)methyl)pyrimidine-2-carbonitrile (2u). Conditions derived from a previously published procedure (46). To a solution of sodium cyanide (2 equiv., 44.7 mg, 0.91 mmol) and DABCO (0.2 equiv., 10.8 mg, 0.09 mmol), in a mixture of dimethyl sulfoxide (1.5 mL) and water (0.2 mL), **2h** (1 eq., 150 mg, 0.46 mmol) in dimethyl sulfoxide (1.5 mL) was added dropwise and the reaction mixture was stirred at 50 °C 20 h. After TLC analysis showed complete conversion, the mixture was allowed to cool down to room temperature and was extracted twice with diethyl ether. The reunited organic layers were washed with brine, dried over magnesium sulfate, filtered and the solvent was removed under reduced pressure. The product was purified by silica gel chromatography (CHX/EtOAc, 75/25, v/v, UV) to afford 5-((1,4-dimethoxy-3-methylnaphthalen-2-yl)methyl)pyrimidine-2-carbonitrile (122 mg, 84%) as white solid. m.p. 111-112 °C. ^1H NMR (400 MHz, $CDCl_3$) δ 8.64 (s, 2H), 8.16 – 7.97 (m, 2H), 7.63 – 7.43 (m, 2H), 4.27 (s, 2H), 3.90 (s, 3H), 3.86 (s, 3H), 2.29 (s, 3H). ^{13}C {^1H} NMR (101 MHz, $CDCl_3$) δ 157.8, 151.1, 150.8, 143.1, 137.2, 128.7, 127.2, 126.7, 126.2, 125.54, 125.52, 122.67, 122.68, 115.9, 62.4, 61.7, 28.3, 12.9. HRMS (ESI) calcd. for $C_{19}H_{18}N_3O_2$: 320.1394. Found: 320.1403 ($M+H^+$).

Synthesis of the Kochi-Anderson coupling products 3s.

2-methyl-3-(thiophen-2-ylmethyl)naphthalene-1,4-dione (3s). Menadione (1 equiv., 100 mg, 0.58 mmol) and 2-thiopheneacetic acid (2 equiv., 165.14 mg, 1.16 mmol) were dissolved in acetonitrile (9 mL) and water (3 mL). The mixture was heated to 85 °C and silver nitrate (0.35 equiv., 34.53 mg, 0.20 mmol) with ammonium persulfate (0.35 equiv., 172.29 mg, 0.76 mmol) were added. The reaction was stirred for 4 h at 85 °C in the dark. The solvent was removed in vacuum and then extracted three times with ethyl acetate. Reunited organic layers were washed with water, dried over magnesium sulfate, filtered and the solvent was removed under reduced pressure. The crude oil was purified by silica gel chromatography (T/CHX, 7/3, v/v, UV) to afford 2-methyl-3-(4-nitrobenzyl)naphthalene-1,4-dione (115 mg, 75%) as yellow solid). m.p. = 96-97 °C. ^1H NMR ($CDCl_3$, 400 MHz) δ 8.11-8.03 (m, 2H), 7.71-7.65 (m, 2H), 7.11 (dd, *J* = 4.5, 1.8 Hz, 1H), 6.89 (d, *J* = 4.5 Hz, 2H), 4.18 (s, 2H), 2.29 (s, 3H). ^{13}C {^1H} NMR ($CDCl_3$, 101 MHz) δ 185.3, 184.2, 144.4, 144.1, 139.9, 133.61, 133.59, 132.1, 132.0, 126.9, 126.5, 126.4, 125.8, 124.2, 27.0, 13.1. HRMS (ESI) calcd. for $C_{16}H_{12}NaO_2S$: 291.0450. Found: 291.0455 ($M+Na^+$).

General procedure for the oxidative deprotection.

1,4-dimethoxy-3-benzylmenadione derivates (1 equiv.) was dissolved in stirring acetonitrile (0.08 M). Then, at room temperature, CAN (2.1 equiv.) dissolved in water (0.25 M) was added drop by drop. The mixture was stirred at room temperature during 1 h. Then after TLC analysis showed complete conversion, the aqueous layer was extracted three times with dichloromethane. Combined organic layers were dried over magnesium sulfate, filtered and the solvent was removed under reduced pressure. Purification by silica gel chromatography was performed using the adequate eluent.

2-methyl-3-(pyridin-3-ylmethyl)naphthalene-1,4-dione (3a). Eluant (CHX/EtOAc, 5/5, v/v, UV), yellow solid, 74% yield. m.p. 100-101 °C. ^{1}H NMR (400 MHz, $CDCl_3$) δ 8.54 – 8.51 (m, 1H), 8.43 (dd, *J* = 4.8, 1.6 Hz, 1H), 8.16 – 7.97 (m, 2H), 7.70 (dd, *J* = 5.8, 3.3 Hz, 2H), 7.54 (ddd, *J* = 7.9, 2.4, 1.6 Hz, 1H), 7.18 (ddd, *J* = 7.8, 4.8, 0.9 Hz, 1H), 4.01 (s, 2H), 2.25 (s, 3H). ^{13}C {^{1}H} NMR (101 MHz, $CDCl_3$) δ 185.2, 184.6, 150.0, 148.0, 144.8, 144.4, 136.2, 133.9, 133.85, 133.83, 132.2, 131.9, 126.6, 126.5, 123.7, 30.0, 13.4. HRMS (ESI) calcd. for $C_{17}H_{14}NO_2$: 264.1019. Found: 264.1018 ($M+H^+$).

2-methyl-3-((6-(trifluoromethyl)pyridin-3-yl)methyl)naphthalene-1,4-dione (3b). Eluant (CHX/EtOAc, 8/2, v/v, UV), yellow solid, 87% yield. m.p. 108-109 °C. ^{1}H NMR (500 MHz, $CDCl_3$) δ 8.66 (d, *J* = 2.2 Hz, 1H), 8.20 – 7.97 (m, 2H), 7.89 – 7.68 (m, 3H), 7.58 (dd, *J* = 8.1, 0.8 Hz, 1H), 4.09 (s, 2H), 2.28 (s, 3H). ^{19}F {^{1}H} NMR (471 MHz, $CDCl_3$) δ -67.81. ^{13}C {^{1}H} NMR (126 MHz, $CDCl_3$) δ 184.9, 184.4, 150.3, 146.6 (q, *J* = 34.8 Hz), 145.2, 143.5, 137.5, 137.4, 133.94, 133.92, 132.1, 131.9, 126.7, 126.6, 121.6 (q, *J* = 279.6 Hz), 120.5 (q, *J* = 2.7 Hz), 30.0, 13.6. HRMS (ESI) calcd. for $C_{18}H_{13}F_3NO_2$: 332.0893. Found: 332.0915 ($M+H^+$).

2-((6-fluoropyridin-3-yl)methyl)-3-methylnaphthalene-1,4-dione (3c). Eluant (CHX/EtOAc, 8/2, v/v, UV), yellow solid, 97% yield. m.p. 103-104 °C. ^{1}H NMR (500 MHz, $CDCl_3$) δ 8.13 (d, *J* = 2.6 Hz, 1H), 8.08 (ddd, *J* = 7.4, 5.8, 3.3 Hz, 2H), 7.72 (dd, *J* = 5.8, 3.3 Hz, 2H), 7.67 (td, *J* = 8.1, 2.6 Hz, 1H), 6.84 (dd, *J* = 8.4, 3.0 Hz, 1H), 4.00 (s, 2H), 2.27 (s, 3H). ^{19}F {^{1}H} NMR (377 MHz, $CDCl_3$) δ -70.88 (d, *J* = 7.7 Hz). ^{13}C {^{1}H} NMR (126 MHz, $CDCl_3$) δ 185.1, 184.6, 162.6 (d, *J* = 238.4 Hz), 147.5 (d, *J* = 14.7 Hz), 144.8, 144.2, 141.5 (d, *J* = 7.8 Hz), 133.97, 133.92, 132.1, 131.9, 131.5 (d, *J* = 4.7 Hz), 126.65, 126.61, 109.6 (d, *J* = 37.5 Hz), 29.1, 13.4. HRMS (ESI) calcd. for $C_{17}H_{13}FNO_2$: 282.0925. Found: 282.0920 ($M+H^+$).

2-((6-chloropyridin-3-yl)methyl)-3-methylnaphthalene-1,4-dione (3d). Eluant (CHX/EtOAc, 8/2, v/v, UV), yellow solid, 99% yield. m.p. 120-121 °C. ^{1}H NMR (500 MHz, $CDCl_3$) δ 8.30 (d, *J* = 2.5 Hz, 1H), 8.11 – 7.96 (m, 2H), 7.75 – 7.63 (m, 2H), 7.51 (dd, *J* = 8.2, 2.6 Hz, 1H), 7.20 (d, *J* = 8.2 Hz, 1H), 3.97 (s, 2H), 2.25 (s, 3H). ^{13}C {^{1}H} NMR (126 MHz, $CDCl_3$) δ 184.9, 184.4, 149.8, 149.7, 144.9, 143.9, 139.1, 133.9, 133.8, 132.9, 132.1, 131.9, 126.6, 126.5, 124.3, 29.3, 13.4. HRMS (ESI) calcd. for $C_{17}H_{13}ClNO_2$: 298.0629. Found: 298.0648 ($M+H^+$).

2-((6-methoxypyridin-3-yl)methyl)-3-methylnaphthalene-1,4-dione (3e). Eluant (CHX/EtOAc, 9/1, v/v, UV), yellow solid, 87% yield. m.p. 120-121 °C. ^{1}H NMR (400 MHz, $CDCl_3$) δ 8.11 – 7.95 (m, 3H), 7.67 (dd, *J* = 5.8, 3.3 Hz, 2H), 7.50 (dd, *J* = 8.6, 2.5 Hz, 21), 6.67 (d, *J* = 8.6 Hz, 1H), 3.91 (s, 2H), 3.88 (s, 3H), 2.24 (s, 3H). ^{13}C {^{1}H} NMR (101 MHz, $CDCl_3$) δ 185.2, 184.6, 162.8, 145.9, 144.7, 144.4, 139.9, 133.77, 133.74, 132.1, 131.9, 126.7, 126.5, 126.4, 111.0, 53.8, 29.0, 13.3. HRMS (ESI) calcd. for $C_{18}H_{15}NO_3$: 294.1125. Found: 294.1125 ($M+H^+$).

2-((6-aminopyridin-3-yl)methyl)-3-methylnaphthalene-1,4-dione (3f). Eluant (EtOAc, 10, v/v, UV), orange solid, 68% yield. m.p. 122-124 °C. ^{1}H NMR (400 MHz, $CDCl_3$) δ 8.08 (dt, J = 5.9, 3.0 Hz, 2H), 7.95 (s, 1H), 7.76-7.60 (m, 2H), 7.35 (dd, J = 8.5, 2.3 Hz, 1H), 6.44 (d, J = 8.5 Hz, 1H), 4.59 (s, 2H), 3.86 (s, 2H), 2.26 (s, 3H). ^{13}C {^{1}H} NMR (101 MHz, $CDCl_3$) δ 185.4, 184.8, 156.9, 146.8, 145.0, 144.3, 139.0, 133.7, 132.2, 132.1, 126.6, 126.5, 109.3, 29.1, 13.3.

2-methyl-3-(pyrimidin-5-ylmethyl)naphthalene-1,4-dione (3g). Eluant (CHX/EtOAc, 5/5, v/v, UV), yellow solid, 88% yield. m.p. 110-111 °C. ^{1}H NMR (500 MHz, $CDCl_3$) δ 9.04 (s, 1H), 8.64 (s, 2H), 8.10 – 7.98 (m, 2H), 7.76 – 7.61 (m, 2H), 3.98 (s, 2H), 2.27 (s, 3H). ^{13}C {^{1}H} NMR (126 MHz, $CDCl_3$) δ 184.8, 184.3, 157.2, 157.0, 145.1, 143.2, 133.96, 133.92, 132.07, 132.04, 131.8, 126.6, 27.8, 13.5. HRMS (ESI) calcd. for $C_{16}H_{13}N_2O_2$: 265.0972. Found: 265.0982 ($M+H^+$).

2-((2-chloropyrimidin-5-yl)methyl)-3-methylnaphthalene-1,4-dione (3h). Eluant (CHX/EtOAc, 7/3, v/v, UV), yellow solid, 93% yield. m.p. 163-164 °C. ^{1}H NMR (400 MHz, $CDCl_3$) δ 8.54 (s, 2H), 8.20 – 7.92 (m, 2H), 7.85 – 7.57 (m, 2H), 3.96 (s, 2H), 2.29 (s, 3H). ^{13}C {^{1}H} NMR (101 MHz, $CDCl_3$) δ 184.6, 184.1, 159.7, 159.6, 145.1, 142.6, 133.96, 133.97, 131.9, 131.6, 130.6, 126.6, 126.5, 27.1, 13.5. HRMS (ESI) calcd. for $C_{16}H_{12}ClN_2O_2$: 299.0582. Found: 299.0596 ($M+H^+$).

2-methyl-3-((2-(trifluoromethyl)pyrimidin-5-yl)methyl)naphthalene-1,4-dione (3i). Eluant (CHX/EtOAc, 8/2, v/v, UV), yellow solid, 95% yield. m.p. 195-196 °C. ^{1}H NMR (400 MHz, $CDCl_3$) δ 8.82 (s, 2H), 8.25 – 8.01 (m, 2H), 7.84 – 7.65 (m, 2H), 4.08 (s, 2H), 2.32 (s, 3H). ^{19}F {^{1}H} NMR (377 MHz, $CDCl_3$) δ -70.23. ^{13}C {^{1}H} NMR (101 MHz, $CDCl_3$) δ 184.6, 184.2, 158.0, 155.3 (q, *J* = 37.1 Hz), 145.5, 142.4, 134.4, 134.2, 134.1, 132.1, 131.7, 126.8, 126.7, 119.7 (q, *J* = 275.1 Hz), 27.9, 13.7. HRMS (ESI) calcd. for $C_{17}H_{12}F_3N_2O_2$: 333.0845. Found: 333.0868 ($M+H^+$).

2-((2-methoxypyrimidin-5-yl)methyl)-3-methylnaphthalene-1,4-dione (3j). Eluant (CHX/EtOAc, 7/3, v/v, UV), yellow solid, 74% yield. m.p. 161-162 °C. ^{1}H NMR (400 MHz, $CDCl_3$) δ 8.40 (s, 2H), 8.10 – 7.96 (m, 2H), 7.67 (dd, *J* = 5.8, 3.3 Hz, 2H), 3.92 (s, 3H), 3.87 (s, 2H), 2.25 (s, 3H). ^{13}C {^{1}H} NMR (101 MHz, $CDCl_3$) δ 184.9, 184.3, 164.6, 159.2, 144.5, 143.8, 133.86, 133.82, 132.0, 131.8, 126.57, 126.54, 124.9, 54.9, 26.7, 13.4. HRMS (ESI) calcd. for $C_{17}H_{15}N_2O_3$: 295.1077. Found: 295.1087 ($M+H^+$).

2-((2-aminopyrimidin-5-yl)methyl)-3-methylnaphthalene-1,4-dione (3k). (DCM/MeOH, 9/1, v/v, UV), orange solid, 60% yield. m.p. = degradation after 200 °C. ^{1}H NMR (500 MHz, DMSO) δ 8.12 (s, 2H), 8.01 – 7.96 (m, 2H), 7.84 – 7.80 (m, 2H), 6.46 (s, 2H), 3.73 (s, 2H), 2.18 (s, 3H). ^{13}C {^{1}H} (126 MHz, DMSO) δ 184.6, 184.2, 162.4, 144.1, 143.8, 133.9, 133.8, 131.7, 131.5, 125.9, 125.8, 119.5, 13.0. HRMS (ESI) calcd. for $C_{16}H_{14}N_3O_2$: 290.1081. Found: 280.1081 ($M+H^+$).

2-(furan-2-ylmethyl)-3-methylnaphthalene-1,4-dione (3n). Eluant (CHX/EtOAc, 98/02, v/v, UV), orange solid, 74% yield. m.p. 83-84 °C. ^{1}H NMR (400 MHz, $CDCl_3$) δ 8.21 – 7.95 (m, 2H), 7.86 – 7.58 (m, 2H), 7.27 (dd, *J* = 1.9, 0.9 Hz, 1H), 6.26 (dd, *J* = 3.2, 1.9 Hz, 1H), 6.07 (dd, *J* = 3.2, 0.9 Hz, 1H), 4.03 (s, 2H), 2.28 (s, 3H). ^{13}C {^{1}H} NMR (101 MHz, $CDCl_3$) δ 185.3, 184.1, 151.3, 145.0, 142.4, 141.6, 133.6, 133.6, 132.2, 132.0, 126.6, 126.4, 110.5, 106.8, 25.6, 13.1.

2-(benzo[*d*]thiazol-5-ylmethyl)-3-methylnaphthalene-1,4-dione (3o). Eluant (CHX/EtOAc, 8/2, v/v, UV), yellow solid, 78% yield. m.p. = 148-149 °C. ^{1}H NMR ($CDCl_3$, 400 MHz) δ 8.97 (s, 1H), 8.06 (dt, *J* = 5.7, 3.1 Hz, 2H), 7.95 (s, 1H), 7.85 (d, *J* = 8.2 Hz, 1H), 7.83-7.57 (m, 1H), 7.36 (d, *J* = 8.1 Hz, 2H), 4.18 (s, 2H), 2.27 (s, 3H). ^{13}C {^{1}H} NMR ($CDCl_3$, 101 MHz) δ 185.3, 184.6, 154.8, 153.9, 145.0, 144.8, 136.6, 133.6 (2C), 132.1 (2C), 132.0, 126.7, 126.5, 126.4, 123.1, 122.0, 32.3, 13.4. HRMS (ESI) calcd. for $C_{19}H_{13}NNaO_2S$: 342.0559. Found: 342.0555 ($M+Na^+$).

2-(benzo[*d*]thiazol-6-ylmethyl)-3-methylnaphthalene-1,4-dione (3p). Eluant (CHX/EtOAc, 8/2, v/v, UV), yellow solid, 78% yield. m.p. = 146-147 °C. ^{1}H NMR ($CDCl_3$, 400 MHz) δ 8.95 (s, 1H), 8.15-8.06 (m, 2H), 8.04 (d, *J* = 8.3 Hz, 1H), 7.81 (s, 1H), 7.71 (dd, *J* = 5.7, 3.3 Hz, 2H), 7.42 (d, *J* = 7.8 Hz, 1H), 4.19 (s, 2H), 2.29 (s, 3H). ^{13}C {^{1}H} NMR ($CDCl_3$, 101 MHz) δ 185.3, 184.7, 154.3, 152.4, 144.9, 144.7, 135.9, 134.8, 133.65, 133.64, 132.1, 132.0, 127.3, 126.6, 126.4, 123.6, 121.5, 32.4, 13.5. HRMS (ESI) calcd. for $C_{19}H_{14}NO_2S$: 320.0740 Found: 320.0740 ($M+H^+$).

2-methyl-3-(pyridin-4-ylmethyl)naphthalene-1,4-dione (3q). Compound **3q** was not purified, yellow solid, 96% yield. ^{1}H NMR (400 MHz, $CDCl_3$) δ 8.64 (s, 2H), 8.27 – 7.96 (m, 2H), 7.87 – 7.71 (m, 2H), 7.64 (s, 2H), 4.21 (s, 2H), 2.29 (s, 3H). ^{13}C {^{1}H} NMR (101 MHz, $CDCl_3$) δ 184.5, 184.2, 156.2, 146.4, 143.4, 141.8, 134.3, 134.2, 132.1, 131.6, 126.86, 126.83, 126.3, 33.2, 13.9.(17)

2-methyl-3-(quinolin-3-ylmethyl)naphthalene-1,4-dione (3r). Eluant (CHX/EtOAc, 5/5, v/v, UV), yellow solid, 86% yield. m.p. 190-191 °C. ^{1}H NMR (400 MHz, $CDCl_3$) δ 8.87 (d, *J* = 2.2 Hz, 1H), 8.14 – 8.06 (m, 2H), 8.05 (dd, *J* = 8.5, 1.0 Hz, 1H), 7.92 (dd, *J* = 2.3, 1.0 Hz, 1H), 7.75 – 7.68 (m, 3H), 7.64 (ddd, *J* = 8.4, 6.9, 1.5 Hz, 1H), 7.49 (ddd, *J* = 8.1, 6.8, 1.2 Hz, 1H), 4.20 (s, 2H), 2.31 (s, 3H). ^{13}C {^{1}H} NMR (101 MHz, $CDCl_3$) δ 185.2, 184.6, 151.7, 147.1, 144.9, 144.4, 134.8, 133.8, 133.8, 132.2, 132.0, 131.1, 129.3, 129.2, 128.1, 127.6, 126.9, 126.6, 126.5, 30.2, 13.6. HRMS (ESI) calcd. for $C_{21}H_{16}NO_2$: 314.1176. Found: 314.1177 ($M+H^+$).

2-((2-bromopyrimidin-5-yl)methyl)-3-methylnaphthalene-1,4-dione (3t). Eluant (CHX/EtOAc, 75/25, v/v, UV), yellow solid, 96% yield. m.p. 165-166 °C. ^{1}H NMR (400 MHz, $CDCl_3$) δ 8.48 (s, 2H), 8.11 – 8.00 (m, 2H), 7.80 – 7.60 (m, 2H), 3.94 (s, 2H), 2.28 (s, 3H). ^{13}C {^{1}H} NMR (101 MHz, $CDCl_3$) δ 184.7, 184.2, 159.6, 151.3, 145.2, 142.7, 134.1, 134.0, 132.0, 131.7, 131.1, 126.78, 126.74, 27.2, 13.6. HRMS (ESI) calcd. for $C_{16}H_{12}BrN_2O_2$: 343.0077. Found: 343.0099 ($M+H^+$).

5-((3-methyl-1,4-dioxo-1,4-dihydronaphthalen-2-yl)methyl)pyrimidine-2-carbonitrile (3u). Eluant (CHX/EtOAc, 7/3, v/v, UV), yellow solid, 87% yield. m.p. 179-180 °C. ^{1}H NMR (400 MHz, $CDCl_3$) δ 8.76 (s, 2H), 8.10 – 7.99 (m, 2H), 7.81 – 7.61 (m, 2H), 4.06 (s, 2H), 2.31 (s, 3H). ^{13}C {^{1}H} NMR (101 MHz, $CDCl_3$) δ 184.5, 184.2, 158.1, 145.7, 143.4, 142.0, 135.2, 134.2, 134.1, 132.0, 131.6, 126.8, 126.7, 115.7, 28.2, 13.7. HRMS (ESI) calcd. for $C_{17}H_{12}N_3O_2$: 290.0924. Found: 290.0918 ($M+H^+$).

Plasmodium falciparum assays and bioimaging.

Parasite culture and antiplasmodial assays. The *P. falciparum* growth inhibition assay was used to determine the 50% inhibitory concentration (IC_{50}) of a given compound. Compounds were dissolved in DMSO at 10 mM. The stocks were kept at 4°C for usually ≥2 weeks. For the assay, 4-fold concentrated solutions of all compounds were prepared freshly in screening medium. The *P. falciparum* growth

inhibition assay method described here was based on the published protocol (24). The readout method is based on incorporation of radiolabelled hypoxanthine into the parasites DNA, which serves as indicator of parasite growth (24,47). In brief, naïve parasites of strain NF54 were exposed to a serial dilution of compounds for 72 hours. After 48 h, a [^{3}H]-hypoxanthine (0.25 µCi) solution is added to each well, and the plates are incubated for another 24 h. Plates are harvested with a Betaplate cell harvester (Perkin, Elmer, Waltham, US), which transfers the lysed red blood cells onto a glass fiber filter (Microbeta FilterMate). The dried filters are inserted into plastic foil with 10 mL of scintillation fluid and counted in a Betaplate liquid scintillation counter (Perkin Elmer, Waltham, US). The results are recorded as counts *per* minute *per* well at each compound concentration. Data are transferred into a graphics program (e.g., Excel) and expressed as percentage of the values for untreated controls (24,47). Chloroquine Diphosphate (Sigma C6628) and Artesunate (Mepha) were included as reference compound(s) in every experiment.

Parasite culture for bioimaging. Parasites were maintained in fresh A+ human red blood cells at a 3% hematocrit in complete medium: RPMI 1640 (Gibcom, ref 72400-021) supplemented with 25 mM HEPES, 0.25 % Albumax II (Thermo Fisher, ref 11021029), 5 % inactivated human serum, 2X hypoxanthine (C.C.pro, ref z-41-M), and 10 µg/mL gentamicin (Gibco, ref 15710-064). Cultures were incubated at 37 °C in a humidified atmosphere with 5% O_2, 5% CO_2, and 90% N_2.

3-Benzylmenadione probe localisation. *P. falciparum* NF54 trophozoites (5% parasitemia, 1.5% hematocrit) were subjected to incubation with probes **3v** and **8** at a concentration of 10 µM for 2 h. Subsequently, dual Click chemistry and immuno-staining procedures were conducted on fixed blood smears following the described protocol (48), albeit with some modifications. In brief, thin blood smears were fixed using 4% (w/v) paraformaldehyde in PBS for 10 min at RT, and then permeabilized for 10 min using 0.1% Triton X-100 in PBS. The Click reaction was carried out for 30 minutes at room temperature using 5 µM of Alexa Fluor 488 Azide (Thermo Fisher Scientific, ref A10266) in the presence of $CuSO_4$ and the "Click-it" Cell Reaction Buffer Kit (Thermo Fisher Scientific, ref C10269) following the manufacturer's instructions. The samples then underwent co-staining with antibodies specific to mitochondria and apicoplast. The smears were first blocked with 3% (w/v) BSA in PBS for 15 minutes and then incubated with either (i) mouse polyclonal antibodies against the mitochondrial protein PfHSP60 (1:500 in 3% BSA) (kindly provided by Philippe Grellier, Muséum National d'Histoire Naturelle, Paris) followed by goat anti-mouse IgG conjugated with Alexa Fluor 647 (Thermo Fisher Scientific, ref A21235, 1:1000 in 3% BSA), or (ii) rabbit polyclonal antibodies against Toxoplasma gondii CPN60 (1:500 in 3% BSA, cross-reacting with PfCPN60) (49) followed by goat anti-rabbit IgG conjugated with Alexa Fluor 647 (Thermo Fisher Scientific, ref A21244, 1:1000 in 3% BSA). Parasite nuclei were stained with DAPI (Thermo Scientific, ref 62248, 1:1000 in PBS) for 5 min at RT. Finally, the slides were mounted in Immu-Mount (Epredia, ref 9990402).

Morphological modifications after treatment with 3-benzylmenadiones. *P. falciparum* NF54 trophozoites (1.5% parasitemia, 1.5% hematocrit) were subjected to incubation with **PD** and probe 8 at their IC_{50} concentration (50 nM) for 14 and 48 h. Thin blood smears were fixed using 4% (w/v) paraformaldehyde in PBS for 10 min at RT, permeabilized for 10 min using 0.1% Triton X-100 in PBS, and blocked with 3% (w/v) BSA in PBS for 15 min. The samples were then co-stained with a mix of antibodies specific to mitochondria and apicoplast (same as above) followed by incubation with cocktail of goat anti-mouse IgG conjugated with Alexa Fluor 647 (Thermo Fisher Scientific, ref A21235, 1:1000 in 3% BSA), and goat anti-rabbit IgG conjugated with Alexa Fluor 488 (Thermo Fisher Scientific, ref A11008 1:1000 in 3% BSA). Parasite nuclei were stained with DAPI (Thermo Scientific, ref 62248, 1:1000 in PBS) for 5 min at RT, and the slides were mounted in Immu-Mount (Epredia, ref 9990402).

Image acquisition and analysis. Imaging was performed using a Zeiss LSM 980 Airyscan 2 laser-scanning microscope built around an Axio Observer 7 body and equipped with an Airyscan 2 super-resolution detector, and controlled by Zen Blue 3.8 software. Image processing was conducted using Fiji software (ImageJ2, version 2.14.0/1.54f), and the final figures were compiled using the Quickfigures plugin. Probe association with a specific organelle, and fluorescence intensity of the two organelles for the analysis of morphological modifications were evaluated by eye by two evaluators. The differences in terms of morphology (signal vs. reduction/absence of signal for a given organelle) between treated and untreated parasites were analysed for statistical significance based on the total number of parasites that were observed for each category using Fisher's exact test in Prism 10 (GraphPad).

Cytotoxicity assays with the rat L6 cell line. Cytotoxicity was determined in vitro against rat L6 myoblasts as described earlier (50). Cell proliferation was assessed with resazurin, and the generally cytotoxic agent podophyllotoxin served as the positive control.

Toxoplasma gondii assays and bioimaging.

Parasite culture. Type I *T. gondii* tachyzoites (RH strain, ref. 51) were maintained by serial passage in human foreskin fibroblast (HFF, American Type Culture Collection, CRL 1634) cell monolayer grown in Dulbecco's modified Eagle medium (supplemented with 5% decomplemented fetal bovine serum, 2-mM l-glutamine and a cocktail of penicillin-streptomycin (Gibco) at 100 µg/ml.

Plaque assays and IC_{50} calculations. Confluent monolayers of HFFs were infected with freshly egressed parasites, which were left to grow for 7 days in the presence of compound (added to various final concentrations), or with the vehicle only (DMSO, whose added volume corresponded to the highest concentration of compound). Cells were then fixed with 4% v/v PFA and plaques were revealed by staining with a 0.1% crystal violet solution (V5265, Sigma-Aldrich). Images were acquired with an Olympus MVX10 macro zoom microscope equipped with an Olympus XC50 camera. Plaque area measurements were done using ZEN software (Zeiss). Plaque areas from three independent biological replicates were plotted relative to compound concentrations and IC_{50} values using a nonlinear regression model software (*Graphpad* Prism 8).

Immunofluorescence assays. Immunofluorescence assays (IFA) were performed as described previously (52). Briefly, intracellular tachyzoites grown on coverslips containing HFF monolayers, were fixed for 20 min with 4% (w/v) paraformaldehyde in PBS and permeabilized for 10 min with 0.3% Triton X-100 in PBS. Coverslips were subsequently blocked with 0.1% (w/v) BSA in PBS and primary antibodies used (at 1/1,000) to detect subcellular structures were rabbit anti-IMC3 (53) to outline the parasite shape, rabbit anti-pyruvate dehydrogenase-E2 (35) to detect the apicoplast, and mouse anti-F1-ATPase beta subunit (kind gift of P. Bradley, UCLA) to detect the mitochondrial network. The differences between treated and untreated parasites were analysed for statistical significance based on the total number of parasites that were observed for each category using Fisher's exact test in Prism 10 (GraphPad).

Lipidomic profile of neosynthesized fatty acids in the apicoplast of *T. gondii* tachyzoites under drug treatment.

Total lipid analysis: Total lipids were extracted in chloroform/methanol/water (1:3:1, v/v/v) containing FFA (free fatty acids C13:0, 10 nmol) and PC (21:0/21:0, 10 nmol) as internal standards for extraction. Next, the polar and apolar metabolites were separated by phase partitioning by adding chloroform and water to give the ratio of chloroform/methanol/water as 2:1:0.8 (v/v/v). For lipid analysis, 50 µL of the extract was directly dried and dissolved in 2:1 choloform:methanol and trimethylsulfonium hydroxide (TMSH, Macherey Nagel) for total fatty acid content. Resultant FAMEs were then analyzed by GC-MS as previously described (33,34,54). All FAMEs were identified by comparison of retention time and mass spectra from GC-MS with authentic chemical standards. The concentration of FAMEs was quantified after initial normalization to different internal standards.

Tracking FASII origin fatty acids (monitoring de novo FA synthesis by the parasite apicoplast FASII). Treated or untreated parasites were infected to a confluent monolayer of HFF in glucose-free-DMEM (1% FBS) supplemented with U-^{13}C-glucose or U-^{12}C-glucose at a final concentration of 800 µM, with or without ATc (0.5 µgml−1). The parasites were harvested up to 48 h post treatement and metabolically quenched in a dry ice and ethanol slurry in a tube until the sample reached 4 °C. Lipids were extracted, derivatized using TMSH (Macherey-Nagel) and analyzed by GC-MS as described above. ^{13}C incorporation to each fatty acid was calculated as the percent of the metabolite pool containing one or more ^{13}C atoms after correction for natural abundance and the amount of ^{13}C-carbon source in the culture medium. Isotopomers (isotopic isomers) are molecular species from the same metabolite that are compositionally identical but are constitutionally and/or stereochemically isomeric because of isotopic substitution (55) (i.e. the presence of ^{13}C stable isotope(s) instead of naturally occurring ^{12}C isotope in the FA molecule in our case). The degree of the incorporation of ^{13}C into fatty acids (% carbon incorporation) was determined by the mass isotopomer distribution (MID) of each FAMEs. MID was obtained from the shift in isotopic mass dependent on the amount of ^{12}C carbons compared to the integration of ^{13}C carbon atoms. The total abundance of ^{13}C-labeled fatty acids was obtained by calculating the concentration of all isotopomers of ^{13}C-labeled FAMEs and finally normalizing to authentic internal standards and parasite number. Differences between treated and untreated parasites were analysed using a t-test for each lipidomic analysis (GraphPad Prism 10).

Fluorescence imaging of the compounds using click-chemistry. Intracellular parasites were incubated with the alkyne derivatives of 3-benzyl-menadiones at 10 µM for 6 h. They were then fixed

with 4% (w/v) paraformaldehyde in PBS and permeabilized for 10 min with 0.3% Triton X-100 in PBS, before performing the click reaction with Alexa Fluor 488 Azide (ThermoFisher ref. A10266) and the "Click-it" Cell Reaction Buffer Kit (ThermoFisher ref. A10269) according to the conditions suggested by the manufacturer. Briefly, the click reaction was performed for 30 min at room temperature with 5 µM of Alexa Fluor 488 Azide in the presence of $CuSO_4$, and for co-staining with the apicoplast marker, the samples were then processed for IFA as described above. Colocalized signals were scored by eye, based on image superimposition and the analysis of dual color fluorescence images for colocalized pixels.

Ecotoxicity Assays

Desmodesmus subspicatus assays

***Desmodesmus* culture.** The algae *D. subspicatus* (SAG 86.81; Culture Collection of Algae, Göttingen University, Germany) were maintained in a climate-controlled cabinet (SANZO; EWALD Innovationstechnik GmbH, Germany) at a temperature of 21 ± 1°C with a light:dark photoperiod of 16:8 hours (5000-5500 lux; cool-white illumination). The culture was grown in a nutrient medium (56) and subjected to continuous stirring at a rate of 250 rpm while receiving constant aeration.

For the inoculum culture of *D. subspicatus* used in the subsequent toxicity tests, a preparation was made three days prior to the start of each test, carried out in the same nutrient medium (56). To achieve this, 5 mL of the algae solution were transferred into 5 L of Kuhl-medium and placed in a climate-controlled cabinet at 21 ± 1°C, with constant illumination and stirring.

***Desmodesmus* growth inhibition testing.** During a series of acute toxicity tests, *Desmodesmus* algae were exposed to three test substances, namely **PD**, **3b**, and **3i**. In short, the test medium used was Kuhl-medium, and each acute toxicity test followed the OECD guideline 201 (57) for a duration of up to 96 h (for specific test concentrations see Table 5). In each microcosm (n=3), the initial biomass of algae did not exceed 0.5 mg dry weight *per* liter, and the initial cell concentration ranged from 2.0 to 5.0 x 10^3 cells/mL. The microcosms were sealed with cotton caps to prevent the entry of dust while allowing for gas exchange. These microcosms were maintained in a climate-controlled cabinet under the conditions mentioned earlier. Every 24 hours, the number of algal cells in the microcosms was quantified using relative fluorescence units, measured with a multiplate reader (Tecan Infinite® M200, Tecan Group Ltd., Switzerland) using excitation and emission wavelengths at 420 nm and 670 nm, respectively. Relative fluorescence units were converted to cell numbers *per* mL using pre-established calibration curves.

Daphnia magna assays

***Daphnia* culture.** *Daphnia magna* (Clone V; Eurofins-GAB, Niefern-Oeschelbronn, Germany) were maintained as a permanent culture in a climate-controlled room at a temperature of 20 ± 1°C with a 16:8 h light:dark photoperiod (800-1000 lux; OSRAM L 58W/21-840 ECO, Germany). Reconstituted hard water was used as medium, prepared following the guidelines for conducting acute toxicity tests outlined in ASTM (58). The medium was supplemented with vitamins (biotin, thiamine, cyanocobalamin; as *per* OECD (2004), selenium, and 20 µL/L of Seaweed (equivalent to 8 mg total organic carbon/L; Marinure®, Glenside, Scotland). Until the start of the toxicity tests, the medium was replaced three times *per* week and organisms were fed daily with the alga *D. subspicatus* in a size-dependent manner at an equivalent of 66-100 µg C/animal.

***Daphnia* immobility testing.** During a series of acute toxicity tests, *Daphnia* were exposed to three test substances, namely **PD**, **3b**, and **3i**. In short, the test medium used was ASTM reconstituted hard water; however, food or seaweed supplements were not added. Each acute toxicity test followed the OECD guideline 202 (OECD, 2004) but the study duration was extended to 96 hours. In each replicate (n=4), five juvenile *Daphnia* (less than 24 h-old) were subjected to increasing concentrations of the test substances, and their immobility was assessed as an indicator of toxicity every 24 hours (for specific test concentrations see Table 5). All tests were conducted under the same temperature and light conditions as previously described.

Table 5. Concentrations of the test items used in toxicity tests with *D. subspicatus* and *D. magna.*

Test item	Test organism	Concentrations tested (µM)
PD	*D. subspicatus*	0, 0.0625, 0.125, 0.25, 0.5, 1
	D. magna	0, 31.25, 62.5, 125, 250, 500, 1000

3b	*D. subspicatus*	0, 0.0625, 0.125, 0.25, 0.5, 1
	D. magna	0, 0.21875, 0.4375, 0.875, 1.75, 3.5, 7
3i	*D. subspicatus*	0, 0.0625, 0.125, 0.25, 0.5, 1
	D. magna	0, 0.625, 1.25, 2.5, 5, 10, 20

Data evaluation. For acute toxicity tests with *Desmodesmus* and *Daphnia*, effective concentrations of the test item causing 10%, 20%, and 50% in the test organisms (i.e., EC10, EC20, and EC50, respectively) were determined after 96 h of exposure using the statistical software R (59). Several dose-response models (always with lower limit at 0) were used to fit the data using the R package "drm" (60) and the models fitting the data best were selected based on visual judgement and Akaike's information criterion.

■ ASSOCIATED CONTENT

The Supporting Information is available free of charge at https://pubs.acs.org/doi/

Supporting Information (ESI) content: Procedures and additional data: pages S2-S3 – anti-*T. gondii* activity of the selected compounds in plaque assays for evaluating the lytic cycle of *Toxoplasma gondii* (Figure S1) and IC_{50} curves based on plaque area (Figure S2); pages S4-S7 – lipidomics data (Figures S3-S10); pages S8-S9 – Stability of azido derivative **16** (Figures S11-S13); page S10 – Subcellular localization of probe **3v** in asexual blood stages of *P. falciparum* (trophozoite stage) after 2 h of incubation (Figure S14) ; page S11 – Subcellular localization of probe **8** in asexual blood stages of *P. falciparum* (trophozoite stage) after 2 h of incubation (Figure S15) ; pages S12-S13 – Parasite and vacuole counts for apicoplast loss and parasite counts for mitochondrial morphology in *T. gondii* (Table S1-S3); page S14 – Morphological analysis of *P. falciparum* parasites for the presence of mitochondria and apicoplast upon treatment with PD or probe **8** (50 nM) and in untreated control parasites (Table S1) ; pages S15-S68 – ^{1}H, ^{19}F and ^{13}C $\{^{1}H\}$ NMR spectra of compounds **1−16**. (PDF)

■ AUTHOR INFORMATION

Corresponding Author

Elisabeth Davioud-Charvet – UMR7042 CNRS-Unistra-UHA, Laboratoire d'Innovation Moléculaire et Applications (LIMA), Bio(in)organic & Medicinal Chemistry Team, European school of Chemistry, Polymers and Materials (ECPM), 25, rue Becquerel, F-67087 Strasbourg, France; orcid.org/0000-0001-7026-4034; Phone: +33 (0)3.20.68.85.26.20.; Email: elisabeth.davioud@unistra.fr

Authors

Baptiste Dupouy, Maxime Donzel, Matthieu Roignant − CNRS-Université de Strasbourg-Université Haute-Alsace UMR7042, Laboratoire d'Innovation Moléculaire et Applications (LIMA), Team Bio(IN)organic & Medicinal Chemistry, European School of Chemistry, Polymers and Materials (ECPM), 25, rue Becquerel, F-67087 Strasbourg, France;

Yann Bordat, Sébastien Besteiro − UMR5294 CNRS-Université de Montpellier, Laboratory of Pathogens and Host Immunity (LPHI), Place Eugène Bataillon, Bâtiment 24, CC 107, 34095 Montpellier cedex 5, France

Sarah Charital, Yoshiki Yamaryo-Botté, Cyrille Y. Botté − UMR5309 CNRS INSERM UGA, ApicoLipid Group, IAB Institut Jean Roget, Domaine de la Merci, 38700 La Tronche, France

Rodrigue Keumoe, Stéphanie A. Blandin − INSERM, CNRS, Université de Strasbourg, U1257 / UPR9022, Mosquito Immune Responses, IBMC, 2 Allée Konrad Roentgen, F-67000 Strasbourg, France ; orcid.org/0000-0003-4566-1200

Matthias Rottmann, Pascal Mäser − Swiss Tropical and Public Health Institute, Department of Medical Parasitology and Infection Biology, CH-4123 Allschwil, Switzerland; University of Basel, CH-4003 Basel, Switzerland

Pascal Mäser – University of Basel, CH-4003 Basel, Switzerland; orcid.org/0000-0003-3122-1941.

Alexander Feckler, Mirco Bundschuh − Functional Aquatic Ecotoxicology, Institute for Environmental Sciences (iES), RPTU Kaiserslautern-Landau, Fortstrasse 7, 76829 Landau, Germany; orcid.org/0000-0003-4876-220X

Author Contributions

B.D., M.D., M.R. synthesized the compounds described in this present work; Y. B., C. S., Y. Y.-B., R. K., R. M. and P.R., M.B. and A.F. generated and analyzed data. E.D.C., S.A.B., S.B., C.B. analyzed the data and wrote the paper.

Notes

The authors declare no competing financial interest.

■ ACKNOWLEDGMENTS

E.D.-C., S.A.B., C.Y.B., and S.B. wish to thank the Laboratoire d'Excellence (LabEx) ParaFrap [ANR-11-LABX-0024], for funding, providing B.D.'s PhD salary, and for initiating and fostering this scientific research and collaboration. This work was furthermore supported by the European Campus EUCOR, via the seed-money program ("ROSkillers" project, E.D.-C., S.A.B., M.R., P.M.) between Strasbourg and Basel Universities, and the Agence Nationale de la Recherche, France (Program ANR-PRCI with FNS, Project "ROSaction", grant ANR-22-CE93-0005-01 to E.D-C., S.A.B., M.R., P.M.; Program ANR-PRC, project "PlasmoPrim", grant ANR-17-CE15-0013-01 to E.D-C., S.A.B., including Ph.D. student salary to M.D.), the CNRS innovation (Program maturation, project "ROS-palu" to E.D-C., S.A.B., including postdoc salary to M.R.). C.Y.B., Y.Y.B., and S.C. were supported by Agence Nationale de la Recherche, France (Project ApicoLipidAdapt grant ANR-21-CE44-0010, Project Apicolipidtraffic grant ANR-23-CE15-0009-01), the Fondation pour la Recherche Médicale (FRM EQU202103012700), LIA-IRP CNRS Program (Apicolipid project), the Université Grenoble Alpes (IDEX ISP-IRGA Apicolipid), Région Auvergne Rhone-Alpes for the lipidomics analyses platform (Grant IRICE Project GEMELI), the CEFIPRA via a Collaborative Research Program Grant (Project 6003-1). We are grateful to the IBMC Insectary platform which is part of and supported by several networks (CORTECS, IBiSA and Emerg'In), and to Jean Daniel Fauny and Romain Vauchelle from the IBMC Microscopy Platform for their training and guidance in fluorescence microscopy**. We acknowledge the IBMP Cell Imaging Facility, member of the national infrastructure France-BioImaging supported by the French National Research Agency (ANR-10-INBS-04) for image acquisitions.** The laboratories also receive support from CNRS (E.D.-C., and S.A.B.), Inserm (S.A.B.) and from the University of Strasbourg (E.D.-C., S.A.B.).

ABBREVIATIONS

BCl_3 = boron trichloride; CuAAC = Copper(I) catalyzed Azide-Alkyne Cycloaddition; DCM = dichloromethane; FAs = fatty acids; MeOH = methanol; m.p. = melting point; NEt_3 or TEA = triethylamine; rt = room temperature; TBAI = tetra-n-butylammonium iodide; CHX = cyclohexane; T = toluene; EtOAc = ethyl acetate; AcOH = acetic acid.

■ REFERENCES

(1) WHO malaria report 2023 for the year 2022.
(2) Rosenthal, P. J.; Asua, V.; Bailey, J. A.; Conrad, M. D.; Ishengoma, D. S.; Kamya, M. R.; Rasmussen, C.; Tadesse, F. G.; Uwimana, A.; Fidock, D. A. The emergence of artemisinin partial resistance in Africa: how do we respond? ***Lancet Infect Dis.*** **2024**, S1473-3099(24)00141-5.
(3) Müller, T.; Johann, L.; Jannack, B.; Brückner, M.; Lanfranchi, D. A.; Bauer, H.; Sanchez, C.; Yardley, V.; Deregnaucourt, C.; Schrével, J.; Lanzer, M.; Schirmer, R. H.; Davioud-Charvet, E. Glutathione reductase-catalyzed cascade of redox reactions to bioactivate potent antimalarial 1,4-naphthoquinones – A new strategy to combat malarial parasites. ***J. Am. Chem. Soc.*** **2011**, *133*, 11557-11571.
(4) Ehrhardt, K.; Deregnaucourt, C.; Goetz, A.-A.; Tzanova, T.; Pradines, B.; Adjalley, S. H.; Blandin, S.; Bagrel, D.; Lanzer, M.; Davioud-Charvet, E. The redox-cycler plasmodione is a fast acting antimalarial lead compound with pronounced activity against sexual and early asexual blood-stage parasites. ***Antimicrob. Agents Chemother.*** **2016**, *60*, 5146-5158.
(5) Bielitza, M.; Belorgey, D.; Ehrhardt, K.; Johann, L.; Lanfranchi, D. A.; Gallo, V.; Schwarzer, E.; Mohring, F.; Jortzik, E.; Williams, D. L.; Becker, K.; Arese, P.; Elhabiri, M.; Davioud-Charvet E. Antimalarial NADPH-consuming redox-cyclers as superior G6PD deficiency copycats. ***Antioxid. Redox Signal.*** **2015**, *22*, 1337-1351.
(6) Cotos, L.; Donzel, M.; Elhabiri, M.; Davioud-Charvet, E. A mild and versatile Friedel-Crafts methodology for the diversity-oriented synthesis of redox-active 3-benzoylmenadiones with tuneable redox potentials. ***Chemistry*** **2020**, *26*, 3314-3325.
(7) Cichocki, B.; Donzel, M.; Heimsch, K. C.; Lesanavičius, M.; Feng, L.; Montagut, E. J.; Becker, K.; Aliverti, A.; Elhabiri, M.; Cenas, N.; Davioud-Charvet, E. *Plasmodium falciparum* ferredoxin-$NADP^+$ reductase-catalyzed redox cycling of plasmodione generates both predicted key drug metabolites: Implication for antimalarial drug development. ***ACS Infect. Dis.*** **2021**, *7*, 1996-2012.
(8) Johann, L.; Lanfranchi, D. A.; Davioud-Charvet, E.; Elhabiri, M. A physico-biochemical study on potential redox-cyclers as antimalarial and anti-schistosomal drugs. ***Curr. Pharm. Des.*** **2012**, *18*, 3539-3566.
(9) Elhabiri, M.; Sidorov, P.; Cesar-Rodo, E.; Marcou, G.; Lanfranchi, D. A.; Davioud-Charvet, E.; Horvath, D.; Varnek, A. Electrochemical properties of substituted 2-methyl-1,4-naphthoquinones: redox behavior predictions. ***Chemistry*** **2015**, *21*, 3415-3424.
(10) Sidorov, P.; Desta, I.; Chessé, M.; Horvath, D.; Marcou, G.; Varnek, A.; Davioud-Charvet, E.; Elhabiri, M. Redox polypharmacology is an emerging strategy to combat malarial parasites. ***ChemMedChem*** **2016**, *11*, 1339–1351.
(11) Mounkoro, P.; Michel, T.; Blandin, S.; Golinelli-Cohen, M.-P.; Davioud-Charvet, E.; Meunier, B. Investigating the mode of action of the redox-active antimalarial drug plasmodione using the yeast model. ***Free Radic. Biol. Med.*** **2019**, *141*, 269–278.
(12) Mounkoro, P.; Michel, T.; Golinelli-Cohen, M.-P.; Blandin S.; Davioud-Charvet, E.; Meunier, B. A role for the succinate dehydrogenase in the mode of action of the redox-active antimalarial drug, plasmodione. ***Free Radic. Biol. Med.*** **2021**, *162*, 533-541.
(13) Feng, L.; Lanfranchi, D. A.; Cotos-Munoz, L.; Cesar Rodo, E.; Ehrhardt, K.; Goetz, A.-A.; Zimmerman, H.; Fenaille, F.; Blandin, S.; Davioud-Charvet, E. Synthesis of plasmodione metabolites and ^{13}C-enriched plasmodione as chemical tools for drug metabolism investigation. ***Org. Biomol. Chem.*** **2018**, *16*, 2647-2665.
(14) Cichocki, B.; Khobragade, V.; Donzel, M.; Cotos, L.; Blandin, S.; Schaeffer-Reiss, C.; Cianférani, S.; Strub, J.-M.; Elhabiri, M.; Davioud-Charvet, E. A new class of valuable (pro-)activity-based protein profiling probes: application to the redox-active antimalarial drug, plasmodione. ***JACS^{Au}*** **2021**, *1*, 669-689.
(15) Fienberg, S.; Eyermann, C. J.; Arendse, L. B.; Basarab, G. S.; McPhail, J. A.; Burke, J. E.; Chibale, K. Structural Basis for Inhibitor Potency and Selectivity of Plasmodium falciparum Phosphatidylinositol 4-Kinase Inhibitors. ***ACS Infect. Dis.*** **2020**, *6*, 3048-3063.
(16) Mehta, N., Ferrins, L., Leed, S. E., Sciotti, R. J., Pollastri, M. P. Optimization of Physicochemical Properties for 4-Anilinoquinoline Inhibitors of Plasmodium falciparum Proliferation. ***ACS Infect. Dis.*** **2018**, *4*, 577-591.
(17) Meanwell, N. A. Chapter Five - A Synopsis of the Properties and Applications of Heteroaromatic Rings in Medicinal Chemistry. ***Adv. Heterocycl. Chem.*** **2017**, *123*, 245-361.
(18) Lanfranchi, D. A.; Cesar-Rodo, E.; Bertrand, B.; Huang, H.-H.; Day, L.; Johann, L.; Elhabiri, M.; Becker, K.; Williams, D. L.; Davioud-Charvet, E. Synthesis and biological evaluation of 1,4-naphthoquinones and quinoline-5,8-diones as antimalarial and schistosomicidal agents. ***Org. Biomol. Chem.*** **2012**, *10*, 6375-6387.
(19) Kim, K.; Weiss, L. M. Toxoplasma gondii: the model apicomplexan. ***Int. J. Parasitol.*** **2004**, *34*, 423-432.
(20) Sanchez, S. G., Besteiro, S. The pathogenicity and virulence of Toxoplasma gondii. ***Virulence*** **2021**, *12*, 3095-3114.
(21) Uteuliyev, M. M.; Shu, L.; Richards, S. J.; Warkentin, A. A.; Davis, D. Naphthoquinone derivatives for treatment of oxidative stress disorders and their preparation. PTC Therapeutics, Inc. World Intellectual Property Organization, WO2020252414 A1, 2020-12-17
(22) Cox, P. A.; Leach, A. G.; Campbell, A. D.; Lloyd-Jones, G. C. Protodeboronation of Heteroaromatic, Vinyl, and Cyclopropyl Boronic Acids: pH-Rate Profiles, Autocatalysis, and Disproportionation. ***J Am Chem Soc.*** **2016**, *138*, 9145-9157.
(23) Hajipour, A. R.; Mohammadsaleh, F. Preparation of Aryl Azides from Aromatic Amines in N-Methyl-2-Pyrrolidonium Bisulfate. ***Org. Prep. Proced. Int.*** **2011**, *43*, 451-455.

(24) Snyder, C.; Chollet, J.; Santo-Tomas, J.; Scheurer, C.; Wittlin S. In vitro and in vivo interaction of synthetic peroxide RBx11160 (OZ277) with piperaquine in *Plasmodium* models. ***Exp. Parasitol.*** **2007**, *115*, 296-300.
(25) Araujo, F. G.; Huskinson, J.; Remington, J. S. Remarkable in Vitro and in Vivo Activities of the Hydroxynaphthoquinone 566C80 against Tachyzoites and Tissue Cysts of Toxoplasma Gondii. ***Antimicrob. Agents Chemother.*** **1991**, *35*, 293–299.
(26) Fleige, T.; Fischer, K.; Ferguson, D. J.; Gross, U.; Bohne, W. Carbohydrate metabolism in the Toxoplasma gondii apicoplast: localization of three glycolytic isoenzymes, the single pyruvate dehydrogenase complex, and a plastid phosphate translocator. ***Eukaryot. Cell.*** **2007**, *6*, 984-996.
(27) Huet, D., Rajendran, E., van Dooren, G. G., Lourido, S. Identification of cryptic subunits from an apicomplexan ATP synthase. ***Elife*** **2018**, 7:e38097.
(28) Ovciarikova, J.; Lemgruber, L.; Stilger, K. L.; Sullivan, W. J.; Sheiner, L. Mitochondrial Behaviour throughout the Lytic Cycle of *Toxoplasma gondii*. ***Sci. Rep.*** **2017**, *7*, 42746.
(29) Botté C. Y., Dubar F., McFadden G.I., Maréchal E., Biot C. *Plasmodium falciparum* apicoplast drugs: targets or off-targets? ***Chem Rev.*** **2012**, 112, 1269-1283.
(30) Waller, R. F.; Ralph, S. A.; Reed, M. B.; Su, V.; Douglas, J. D.; Minnikin, D. E.; Cowman, A. F.; Besra, G. S.; McFadden, G. I. A type II pathway for fatty acid biosynthesis presents drug targets in Plasmodium falciparum. ***Antimicrob. Agents Chemother.*** **2003**, *47*, 297-301.
(31) Ramakrishnan, S.; Docampo, M. D.; Macrae, J. I.; Pujol, F. M.; Brooks, C. F.; van Dooren, G. G.; Hiltunen, J. K.; Kastaniotis, A. J.; McConville, M. J.; Striepen, B. Apicoplast and endoplasmic reticulum cooperate in fatty acid biosynthesis in apicomplexan parasite Toxoplasma gondii. ***J. Biol. Chem.*** **2012**, *287*, 4957-4971.
(32) Amiar, S.; MacRae, J. I.; Callahan, D. L.; Dubois, D.; van Dooren, G. G.; Shears, M. J.; Cesbron-Delauw, M. F.; Maréchal, E.; McConville, M. J.; McFadden, G. I.; Yamaryo-Botté, Y.; Botté, C. Y. Apicoplast-Localized Lysophosphatidic Acid Precursor Assembly Is Required for Bulk Phospholipid Synthesis in Toxoplasma gondii and Relies on an Algal/Plant-Like Glycerol 3-Phosphate Acyltransferase. ***PLoS Pathog.*** **2016**, *12*, e1005765.
(33) Amiar, S.; Katris, N. J.; Berry, L.; Dass, S.; Duley, S.; Arnold, C. S.; Shears, M. J.; Brunet, C.; Touquet, B.; McFadden, G.I.; Yamaryo-Botté, Y.; Botté, C. Y. Division and Adaptation to Host Environment of Apicomplexan Parasites Depend on Apicoplast Lipid Metabolic Plasticity and Host Organelle Remodeling. ***Cell Rep.*** **2020**, 30, 3778-3792.e9.
(34) Dass, S.; Shunmugam, S.; Berry, L.; Arnold, C. S.; Katris, N. J.; Duley, S.; Pierrel, F.; Cesbron-Delauw, M. F.; Yamaryo-Botté, Y.; Botté, C. Y. Toxoplasma LIPIN is essential in channeling host lipid fluxes through membrane biogenesis and lipid storage. ***Nat. Commun.*** **2021**, *12*, 2813.
(35) Renaud, E. A.; Pamukcu, S.; Cerutti, A.; Berry, L.; Lemaire-Vieille, C.; Yamaryo-Botté, Y.; Botté, C. Y.; Besteiro, S. disrupting the plastidic iron-sulfur cluster biogenesis pathway in *Toxoplasma gondii* has pleiotropic effects irreversibly impacting parasite viability. ***J. Biol. Chem.*** **2022**, *298*, 102243.
(36) Kennedy, K.; Crisafulli, E. M.; Ralph, S. A. Delayed Death by Plastid Inhibition in Apicomplexan Parasites. ***Trends Parasitol.*** **2019**, *35*, 747-759.
(37) Kennedy, K.; Cobbold, S. A.; Hanssen, E.; Birnbaum, J.; Spillman, N. J.; McHugh, E.; Brown, H.; Tilley, L.; Spielmann, T.; McConville, M. J.; Ralph, S. A. Delayed death in the malaria parasite Plasmodium falciparum is caused by disruption of prenylation-dependent intracellular trafficking. ***PLoS Biol.*** **2019**, *17*, e3000376.
(38) Amrane, D.; Primas, N.; Arnold, C. S.; Hutter, S.; Louis, B.; Sanz-Serrano, J.; Azqueta, A.; Amanzougaghene, N.; Tajeri, S.; Mazier, D.; Verhaeghe, P.; Azas, N.; Botté, C.; Vanelle, P. Antiplasmodial 2-thiophenoxy-3-trichloromethyl quinoxalines target the apicoplast of Plasmodium falciparum. ***Eur J Med Chem.*** **2021**, *224*, 113722.
(39) Charital, S.; Lourdel, A.; Quansah, N.; Botté, C. Y.; Yamaryo-Botté, Y. Monitoring of Lipid Fluxes Between Host and Plastid-Bearing Apicomplexan Parasites. Methods Mol. Biol. 2024, 2776, 197-204.
(40) Brooks, C. F.; Johnsen, H.; van Dooren, G. G.; Muthalagi, M.; Lin, S. S.; Bohne, W.; Fischer, K.; Striepen, B. The toxoplasma apicoplast phosphate translocator links cytosolic and apicoplast metabolism and is essential for parasite survival. ***Cell Host Microbe*** **2010**, *7*, 62-73.
(41) Iacobucci, I.; Monaco, V.; Dupouy, B.; Hovasse, A.; Keumoe, R.; Cichocki, B.; Elhabiri, M.; Blandin, S. A.; Meunier, B.; Strub, J.-M.; Monti, M.; Cianférani, S.; Schaeffer-Reiss, C.; Davioud-Charvet, E. Proteomic profiling of antimalarial plasmodione using 3-benz(o)ylmenadione affinity-based probes. ***ChemBioChem*** **2024**, **2024**, 25(15):e202400187.
(42) Lesanavičius, M.; Aliverti, A.; Šarlauskas, J.; Čėnas, N. Reactions of Plasmodium falciparum Ferredoxin:NADP+ Oxidoreductase with Redox Cycling Xenobiotics: A Mechanistic Study. ***Int. J. Mol. Sci.*** **2020**, *21*, 3234.
(43) Staines, H. M.; Ellory, J. C.; Chibale, K. The new permeability pathways: targets and selective routes for the development of new antimalarial agents. ***Comb. Chem. High Throughput Screen***. **2005**, *8*, 81-88.
(44) Henry, N.; Enguehard-Gueiffier, C.; Thery, I.; Gueiffier, A. One-Pot Dual Substitutions of Bromobenzyl Chloride, 2-Chloromethyl-6-halogenoimidazo[1,2-*a*]pyridine and -[1,2-*b*]pyridazine by Suzuki–Miyaura Cross-Coupling Reactions. ***Eur. J. Org. Chem*****.** **2008**, *2008*, 4824-4827.
(45) Schlosser, M., Cottet, F. Silyl-Mediated Halogen/Halogen Displacement in Pyridines and Other Heterocycles. ***Eur. J. Org. Chem*****.** **2002**, 2002, 4181-4184.
(46) Šturala, J.; Boháčová, S.; Chudoba, J.; Metelková, R.; Cibulka, R. Electron-Deficient Heteroarenium Salts: An Organocatalytic Tool for Activation of Hydrogen Peroxide in Oxidations. ***J. Org. Chem*****.** **2015**, *80*, 2676−2699.
(47) Desjardins, R. E.; Canfield, C. J.; Haynes, J. D.; Chulay, J. D. Quantitative assessment of antimalarial activity in vitro by a semiautomated microdilution technique. ***Antimicrob. Agents Chemother.*** **1979**, *16*, 710-718.
(48) Tonkin, C. J.; Van Dooren, G. G.; Spurck, T. P.; Struck, N. S.; Good, R. T.; Handman, E.; Cowman, A. F.; McFadden, G. I. Localization of Organellar Proteins in Plasmodium Falciparum Using a Novel Set of Transfection Vectors and a New Immunofluorescence Fixation Method. ***Mol. Biochem. Parasitol.*** **2004**, *137*, 13–21.

(49) Agrawal, S.; Van Dooren, G. G.; Beatty, W. L.; Striepen, B. Genetic Evidence That an Endosymbiont-Derived Endoplasmic Reticulum-Associated Protein Degradation (ERAD) System Functions in Import of Apicoplast Proteins. ***J. Biol. Chem.*** **2009**, *284*, 33683–33691.
(50) Bernal, F. A.; Kaiser, M.; Wünsch, B.; Schmidt, T. J. Structure-Activity Relationships of Cinnamate Ester Analogues as Potent Antiprotozoal Agents. ***ChemMedChem.*** **2020**, 15, 68-78.
(51) Sabin, A. B. Toxoplasmic Encephalitis in Children. ***JAMA*** **1941**, *116*, 801.
(52) Semenovskaya, K.; Lévêque, M. F.; Berry, L.; Bordat, Y.; Dubremetz, J.; Lebrun, M.; Besteiro, S. TgZFP2 Is a Novel Zinc Finger Protein Involved in Coordinating Mitosis and Budding in Toxoplasma. ***Cell. Microbiol.*** **2020**, *22*, e13120.
(53) Anderson-White, B. R.; Ivey, F. D.; Cheng, K.; Szatanek, T.; Lorestani, A.; Beckers, C. J.; Ferguson, D. J. P.; Sahoo, N.; Gubbels, M.-J. A Family of Intermediate Filament-like Proteins Is Sequentially Assembled into the Cytoskeleton of Toxoplasma gondii. ***Cell. Microbiol.*** **2011**, *13*, 18–31.
(54) Dubois, D.; Fernandes, S.; Amiar, S.; Dass, S.; Katris, N. J.; Botté, C. Y.; Yamaryo-Botté, Y. Toxoplasma gondii acetyl-CoA synthetase is involved in fatty acid elongation (of long fatty acid chains) during tachyzoite life stages. ***J. Lipid Res.*** **2018**, *59*, 994-1004.
(55) Stoll S. Isotopomers and Isotopologues: The History behind the Confusion. *Chem. Educator* **2007**, 12, 1–3.
(56) Kuhl, A.; Lorenzen, H. Handling and culturing of Chlorella. ***Methods in cell physiology*** **1964**, 1, 159-187, Prescott, DM, ed.
(57) OECD. OECD Guidelines for the testing of chemicals. Test Guideline 201: freshwater alga and cyanobacterial, growth inhibition test. Organisation for Economic Co-operation and Development, Paris; **2011**.
(58) ASTM Standard E729. Standard guide for conducting acute toxicity tests on test materials with fishes, macroinvertebrates, and amphibian; **2007**.
(59) R Core Team. R: a language and environment for statistical computing, version 4.3.1. R Foundation for Statistical Computing. Vienna, Austria; **2023**. https:// www.R-project.org/
(60) Ritz, C.; Baty, F.; Streibig, J. C.; Gerhard, D. Dose-response analysis using R. ***PLoS One*** **2015**, *10*, e0146021.

1.2.2 Les points importants de l'article 2

- **Synthèse de sondes cliquables :** portant un motif pyrimidine alcyne (sonde **3v**) et portant un azoture (sondes **13** et **16**).
- **Création d'une nouvelle série de dérivés bMD-hétéroaromatiques** (≈ 20 molécules), afin d'améliorer les propriétés PK/PC et l'activité des bMDs, montrant des résultats d'activité encourageants.
- **Etude de l'impact des composés 3m, 3i et PD sur la morphologie du parasite *T. gondii***, induisent une forte perturbation de l'apicoplaste et des mitochondries, entraînant une réduction signification de la viabilité des parasites.
- **Analyse lipidomique avec le composé 3m**, évaluation de son effet sur la voie FASII dans l'apicoplaste, affectant le métabolisme lipidique de *T. gondii*. Cela fournit un aperçu mécanistique du mode d'action de ces composés au niveau moléculaire.
- **Localisation des sondes 3v et 8 sur *T. gondii*** (via CuAAC), révélation d'une forte accumulation dans l'apicoplaste des trophozoïtes, confirmant cette organelle comme cible principale des bMDs.
- **Localisation des sondes 3v et 8 sur *P. falciparum*** (via CuAAC), la sonde **8** montre une accumulation dans la mitochondrie (27-30%) et l'apicoplaste (19-24%), soutenant le mode d'action des bMDs.

Chapitre III : Développement de fluorophores flavyliums cliquables et leur valorisation en imagerie par fluorescence

1.1 Synthèse de sondes flavyliums azoturés utilisables en imagerie par fluorescence

1.1.1 Travaux préliminaires

Avant mon arrivée dans l'équipe CBM, le développement de flavyliums azoturés avait déjà été initié, avec pour objectif principal d'obtenir une réponse ratiométrique ou fluorogénique après une réaction clique à partir d'un flavylium portant un azoture directement substitué au squelette. Grâce aux travaux antérieurs ainsi qu'aux projets réalisés par deux étudiants de Master que j'ai supervisé durant ma thèse (Quentin Riehl M1 et Manon Aniel M1), nous avons obtenu plusieurs résultats préliminaires qui ont conduit à l'élaboration de diverses sondes fluorescentes, comme décrite dans les articles 3 et 4 de cette thèse.

Pour synthétiser ces flavyliums azotures, nous avons utilisé la méthodologie de synthèse présentée dans l'introduction, reposant sur une condensation acide entre une α-tétralone et un salicylaldéhyde. L'introduction d'une fonction azoture en position 7 ou 4' a donc tout d'abord été envisagée, car elle devait offrir les meilleurs résultats photophysiques, comme le suggèrent les RSP décrits dans l'introduction.

Plusieurs méthodes permettent de former des azotures aryles[133], les plus couramment utilisées étant :

i. L'azidation à partir d'une source d'azoture (NaN_3, $TMSN_3$) d'un sel de diazonium formé par diazotation d'un dérivé aminé.
ii. La substitution nucléophile aromatique (SN_{ar}) à l'aide d'un dérivé chloro- ou fluoro-aryle ou par substitution nucléophile classique (SN_2).
iii. L'échange halogène-métal (Li, Mg) pour générer un carbone aromatique nucléophile capable d'attaquer un azoture électrophile tel que le tosyl-azoture (TsN_3).
iv. L'obtention d'azotures à partir d'une hydrazine aryle en présence d'un réactif nitro ($NaNO_2$, HNO_2, N_2O_4).
v. La réaction de diazo-transfert entre une arylamine et un dérivé sulfonyl-azoture.

Étant donné la disponibilité de la 6-amino-α-tétralone (60€/25g) et du 3-aminophénol (33€/25g), ainsi que l'usage de la réaction de diazotation dans notre équipe pour introduire divers nucléophiles, nous avons choisi de conserver cette méthodologie pour obtenir nos dérivés azoturés. Nous avons ainsi généré notre sel de diazonium en utilisant une méthode originale dans un mortier, combinant un liquide ionique (1-méthyl-2-oxopyrrolidin-1-ium hydrogen sulfate)[134] pouvant être recyclé en fin de réaction si nécessaire) mélangé à de l'eau, $NaNO_2$ et une arylamine. L'ajout de NaN_3 permet alors la formation *in situ* de l'azoture (Figure 28). Cette méthode permet d'obtenir très rapidement (en 30 min) l'azoture aryle souhaité avec

un bon, voire excellent, rendement. Par ailleurs, l'utilisation du liquide ionique permet de stabiliser le sel de diazonium formé comme intermédiaire. Enfin, une condensation acide permet de produire les flavyliums azotures désirés **23**, **24** et **25** (Figure 28). Il est à noter que la réaction de diazotation suivie d'une azidation peut également être réalisée directement sur le flavylium amine en dernière étape démontrant la possibilité de post-fonctionnalisation de nos ondes. Trois premières sondes cliquables flavyliums ont ainsi été synthétisées par les étudiant(e)s de Master.

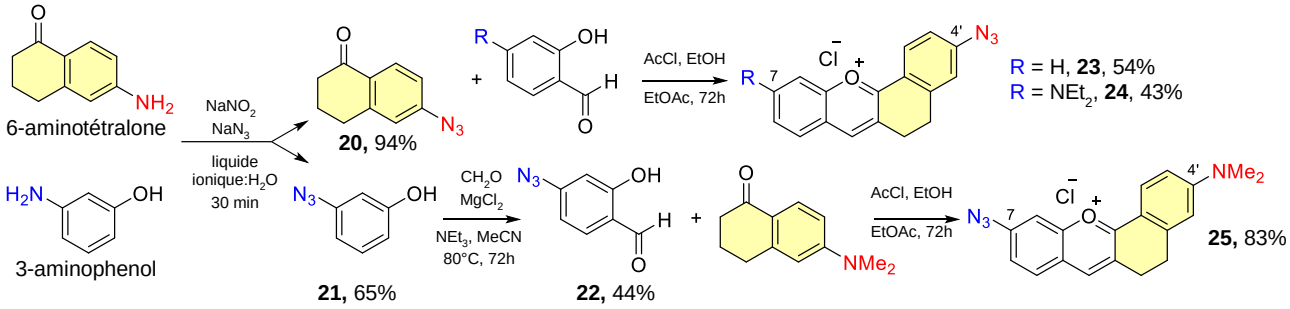

Figure 28: Synthèse des flavyliums azotures **23**, **24** et **25** fonctionnalisés en position 7 ou 4'. Les conditions de synthèse des différents intermédiaires et produits sont disponibles dans la partie expérimentale de ce manuscrit.

Ces sondes se sont révélées majoritairement non fluorescentes, probablement en raison d'une inhibition par PeT ou ICT entre l'azoture et le fluorophore. Seule la sonde **23** émet (λ_{em} = 512 nm à pH 7,41 et λ_{em} = 520 nm dans l'éthanol), probablement parce qu'elle n'est pas substituée en position 7 par un groupement électrodonneur. Egalement, plusieurs tentavives de réaction de CuAAC avec une sonde bMD-alcyne (sonde **1**) ont été conduites et ont montrées une faible réactivité ainsi qu'une photosensiblité importante. Les adduits flavylium-bMD obtenus après CuAAC (avec les sondes **23** et **25** conduisant respectivement aux adduits **23-1** et **25-1**) ne présentent pas de fluorescence, probablement en raison d'un effet PeT avec le bMD oxydé (accepteur d'électron). Par manque de recul et d'expérience sur ce projet, nous n'avons pas approfondi davantage ces systèmes, qui auraient pu offrir une réponse fluorogénique une fois le bMD réduit (voir article 4). Nous avons également observé des problèmes de photostabilité (photoréduction de l'azoture) et des problèmes de stabilité chimique au cours de la réaction (réduction de l'azoture). Au cours de ce projet, nous avions également synthétisé leurs analogues aminés pour servir de référence face à ces problèmes de réduction. Il est intéressant de noter qu'un effet bathochrome est observé pour le dérivé amino de la sonde **23** (**23_{red}**) (λ_{em} = 556 nm, Φ = 9,5% à pH 7,41 et λ_{em} = 564 nm, Φ = 12,4% dans l'éthanol), offrant ainsi une réponse ratiométrique en cas de réduction éventuelle (possibilité de suivre par exemple H_2S grâce à une réponse ratiométrique originale sur un

système extrêmement simplifié, cf. introduction) (Figure 29). Ce projet sera néanmoins poursuivi dans le futur par mon équipe d'accueil.

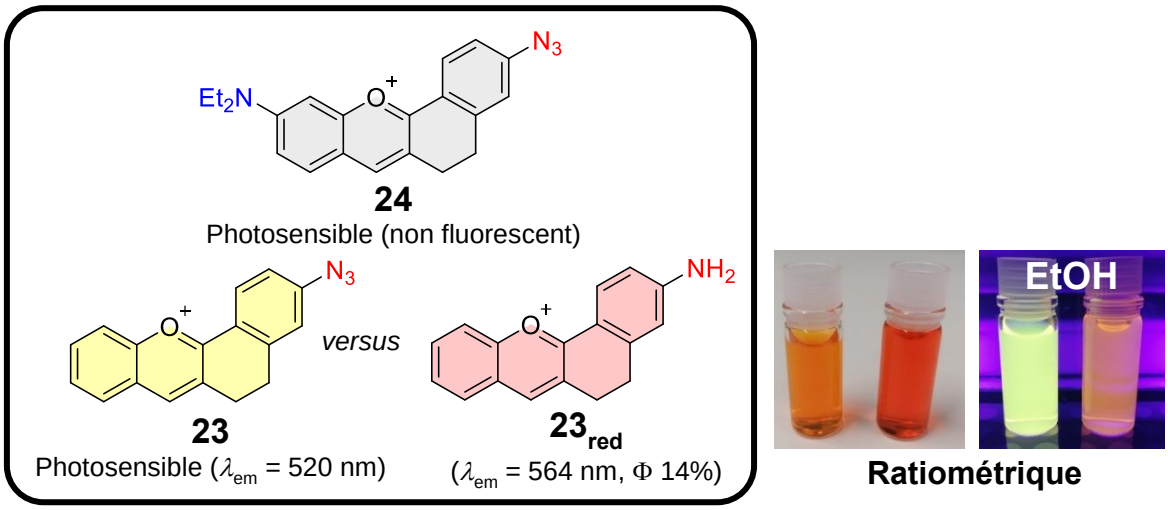

Figure 29: Propriétés photophysiques et photographies des couples de fluorophores azoturés **24** et **23/23red**. Données mesurées et images prises dans l'éthanol. Contre ion Cl^-.

Face à ces résultats insatisfaisants et à une connaissance limitée au moment de cette étude des effets électroniques entre le flavylium et bMD, nous avions décidé de mettre entre parenthèses le développement de ces sondes pour lesquelles la fonction azoture est directement substituée sur le chromophore. Pour surmonter ce problème, nous avons alors envisagée l'introduction d'un espaceur entre le chromophore et l'azoture. Cette approche, couramment utilisée pour les fluorophores cliquables commerciaux (article 3 de cette thèse), permet de maintenir l'intégrité des deux espèces au sein d'un environnement biologique. Elle est particulièrement intéressante lorsque le système comporte deux sondes actives (électrophore bMD et chromophore flavylium dans notre cas).

À partir de ces résultats préliminaires, un projet d'imagerie par fluorescence a été initié grâce aux différentes sondes cliquables flavylium-PEG-N_3 obtenues. Leur synthèse, leurs propriétés optiques et physicochimiques, ainsi que leurs valorisations dans une approche de chimie bioorthogonale avec des phytostérols alcynes sont détaillées dans l'article 3 de cette thèse.

1.1.2 Article 3

Bringing phytosterols to light with bioinspired fluorophore azides using bioorthogonal chemistry

Baptiste Dupouy, Andréa Hemmerlin, Quentin Chevalier, Valérie Mazan, Elisabeth Davioud-Charvet, Hubert Schaller, and Mourad Elhabiri

Article still under progress

Bringing phytosterols to light with bioinspired fluorophore azides using bioorthogonal chemistry

Baptiste Dupouy,[a] Andréa Hemmerlin,[b] Quentin Chevalier,[b] Valérie Mazan,[a] Elisabeth Davioud-Charvet,[a*] Hubert Schaller,[b*] and Mourad Elhabiri[a*]

[a] Université de Strasbourg, Université de Haute-Alsace, CNRS, LIMA, UMR 7042, Equipe Chimie Bioorganique et Médicinale, ECPM, 25 Rue Becquerel, 67000 Strasbourg, France

[b] Institut de Biologie Moléculaire des Plantes/Unité Propre de Recherche 2357, Centre National de la Recherche Scientifique-Université de Strasbourg, Strasbourg, France, F-67084

Email: Elisabeth Davioud-Charvet (Elisabeth.davioud@unistra.fr) Hubert Schaller (hubert.schaller@ibmp-cnrs.unistra.fr), Mourad Elhabiri (elhabiri@unistra.fr)

Abstract

Fluorescence imaging based on functionalized small-molecule dyes plays an important role in chemical biology due to its non-invasive nature, sensitivity and specificity. Conventional azido dyes used in bioorthogonal chemistry, for example, suffer from drawbacks such as tedious preparation, high costs, altered physico-chemical properties, poor penetration into cells or limited emission ranges. In an attempt to overcome these problems, we have developed a new series of azido fluorophore probes. These are based on rigidified flavylium ions functionalized with polyethylene glycol (PEG) chains of varying lengths to introduce a terminal azide group without compromising the fluorescent properties of the dye. The azide function acts as a bioorthogonal handle, allowing the probes to participate in click reactions while maintaining high fluorescence efficiency and (photo)stability. Chemical screening with absorption/emission plate reading has identified optimal substitution patterns on the flavylium ring, producing dyes with improved photophysical characteristics in the red-NIR spectral region. A multi-step synthesis of these dyes led to the preparation of three key derivatives with PEG-1, PEG-2 and PEG-3 chains. The best candidates exhibit strong intramolecular charge transfer properties, resulting in high fluorescence brightness, photostability, aqueous solubility and tunable emission spectra, making them suitable for advanced imaging applications. As a proof of concept, these azido fluorophores were investigated with BY-2 tobacco cells, demonstrating efficient uptake, staining and stability with these living cells.

Keywords: Fluorescent imaging, bioorthogonal chemistry, fluorophore azides, flavylium, click chemistry, red-NIR emission, phytosterols

Introduction

Fluorescence imaging based on small-molecule dyes is undoubtedly one of the most important approaches with renewed interest [1,2] that can help tackling challenges in biology thanks to its non-invasiveness, sensitivity, specificity and rapid response time. With deep imaging in the near infrared (NIR) [3,4] or with 2-photon absorption (TPA) chromophores, it is possible to track a biological event, while minimizing photo-damage to the cells and/or avoiding cell auto-fluorescence. [5] Equipped with functional units, these fluorophores can act as valuable molecular tools for investigating biological processes. [6] Tagging a (bio)molecule of interest with bulky, hydrophobic and/or charged amphiphilic fluorescent probes can, however, alter its physicochemical properties and negatively impacts its cell entry, localization, or affinity to receptors or enzymes. To overcome these drawbacks, these fluorophores can alternatively be applied to any (bio)molecule using the so-called bioorthogonal chemistry (i.e. group of chemical reactions occurring in a biological medium without interfering with biomolecules or biochemical processes). [7,8a] Bioorthogonal chemistry constitutes one of the most outstanding achievements in this domain [8b] and has deeply transformed chemical biology over the two last decades. [9-11] The vast majority of current bioorthogonal chemistry applications are covered by cycloaddition reactions, [12-14] among which the most popular Cu(I)-catalyzed (CuAAC) and the strain-promoted (SPAAC) azide-alkyne cycloaddition reactions. [15-17]

Involved in both CuAAC and SPAAC bioorthogonal reactions, the azide function constitutes a valuable reporter, as it: *i*) is absent in most living organisms, *ii*) is kinetically stable, and *iii*) does not induce cross-linking reactions with biomolecules. With a fluorescent unit, it can contribute to the visualization of a site or mechanism of action (MoA), a biological target, a metabolic process, or the transport of a (bio)molecule of interest. Most of the organic fluorophores emitting in the red-NIR domain are based on xanthene (including fluorescein, rhodamines and silicon rhodamines), [18] cyanine, [19] oxazine, or BODIPY [20] cores. Their valuable fluorescence properties have greatly stimulated their development into advanced fluorescent azide probes (high brightness and absorptivity, large Stokes shifts, modulated emission, red-NIR emission, structural diversity, etc.). [21-24] For example, CuAAC strategies have been described in which the fluorescent azide and the Cu(I) catalyst are combined in the same ensemble. [25,26] Also worth mentioning is the recent development of photoactivatable fluorogenic azide-alkyne click (PFAAC) reactions, which allow the sequential generation of the fluorescent backbone after click chemistry by photoirradiation (e.g. photoclick reactions of tetrazole-ene derivatives [27]). Photoconvertible systems (e.g. intramolecular photocyclization of diazaxanthilidene [28]) can also be used to modulate the fluorescence properties of the clicked probe after photoirradiation. The properties, preparation, advantages or drawbacks of the fluorescent scaffolds in the frame of bioimaging have been reviewed in excellent reports, [29-30] and selected examples of “Always-ON” fluorescent azides (mostly commercial) from these families are shown in Figure 1 and in the supporting information (Figures S1-S4 and Tables S1-S4 in the ESI). To a lesser extent, other fluorescent azide labels have been developed in the form of oligothiophene, [31] coumarin, [32] benzoxadiazole [33] and (benzo)thiazole, [34] to name but a few.

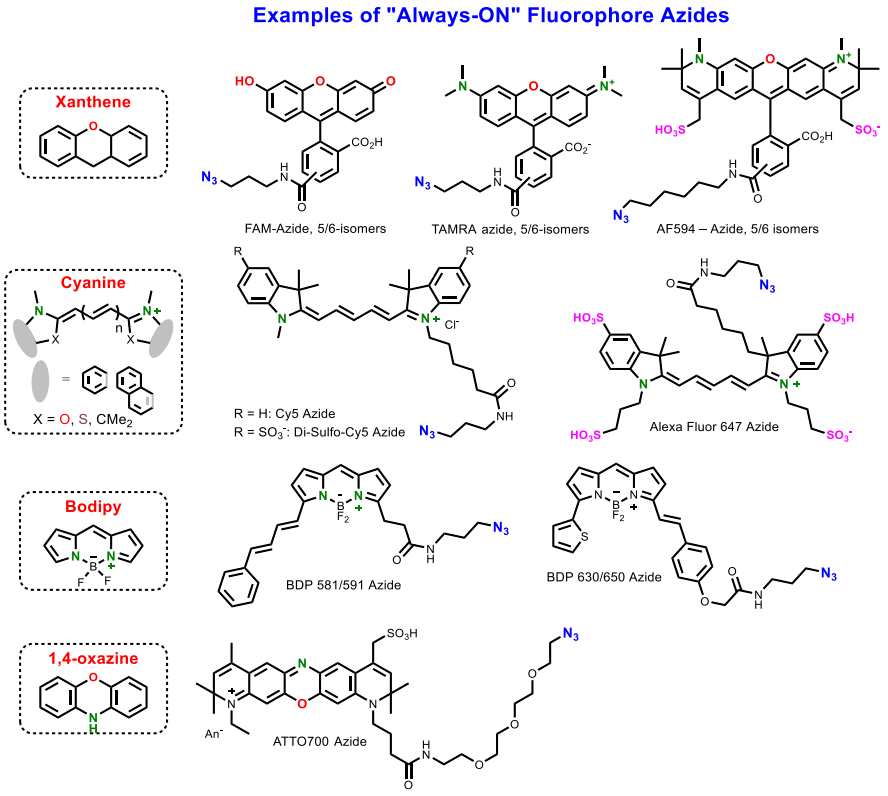

Figure 1. Chemical structures of the selected fluorophore azides behaving as "always-on" from commercial sources or literature data.

A survey of the physicochemical and photophysical data for the "Always-ON" azide fluorophores selected in Tables S1-S4 (See ESI) shows that compounds emitting at $\lambda > 590$ nm have MW between 590 and 1200 g mol^{-1} and low to very low aqueous solubilities, as indicated by calculated log S values between -5 and -11.4. Furthermore, their synthesis is often tedious and the possibilities for structural diversification are limited. Besides, the azide functions are introduced via long alkyl or PEG chains far from the fluorescent core.

As a potential alternative, we have thus focused in this work on a series of flavylium cations (i.e. 2-aryl-substituted benzopyrylium, Figure 2) as potential candidates to generate new fluorophore azides for bioorthogonal chemistry. [35-37] These latter are versatile molecules of biological importance that encompass the ubiquitous pigments called anthocyanin(din)s responsible of the diversity of colors displayed by numerous plants. [35-38] Fine-tuning of the natural anthocyanidin scaffold results in a diverse spectrum of absorbance colors. However, rare examples of naturally occurring fluorescent anthocyanins have been reported [39] mainly due to their instability in weakly acidic aqueous media (i.e. nucleophilic water reaction on the 2 or 4-position of ring B, Figure 2) [40] and poor quantum yield. Free rotation through the single bond between B and C rings (TICT state) indeed dissipates away the excitation energy (Figure 2). [41] Stiffening by means of an ethyl bridge inhibits this free rotation and induces bathochromic and hyperchromic shifts in longest wavelength absorption (i.e. marked effects for compounds substituted with a 7-donor group) and significantly increased fluorescence quantum yields. To date, limited rigid flavylium based dyes have been in use for cell imaging and these are described in the excellent review published by Sun, Y. *et al*. [36] Only a few of the systems described are

functionalized with an azide function. [42-44] These “pro-fluorophores” have exclusively been used for the selective detection of H_2S by reducing the azide function, thereby reinstating the fluorescent properties of the chromophore (strong ICT effect of azide group). Herein, we have prepared and extensively studied a new series of rigid flavylium compounds in which an azide group has been introduced via a variable length PEG chain (1 to 3) on an ethylamine substituent (Figure 2). The latter strategy greatly simplifies the design of the fluorophore and minimizes the impact on its emission properties. The best candidates have been selected by means of a plate reader approach on the basis of absorption and emission measurements. These systems offer many advantages over existing “Always-ON” azide fluorophores, including good solubility and aqueous stability, much lower MW, good photostability, ease of synthesis, large scale preparation and easy tunability of emission range.

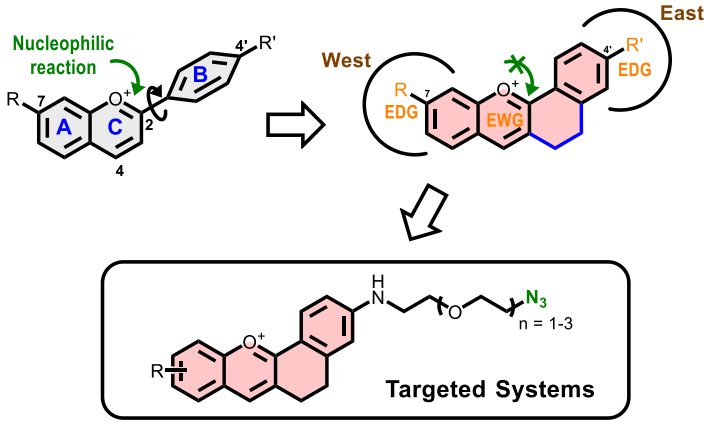

Figure 2. Chemical structures of the targeted azido-dyes. EDG = electron-donating group. EWG = electron-withdrawing group.

As a proof of concept, these pegylated fluorophore azides were considered in click reactions with an alkyne-phytosterol. This work in progress is being carried out in a cell model consisting of BY-2 tobacco cells and monitored by fluorescence imaging.

Results and Discussion

Screening approach. Prior to the synthesis of the various dyes with the PEG chains separating the chromophore from the azide function, we carried out a screening study using a hybrid absorption/emission plate reader to select the best substitution pattern on the western part of the dye (Figure 2). This approach was carried out only on derivatives with a PEG-2 chain. Various salicylaldehyde derivatives (15 examples) were combined to the α-tetralone derivative **1** in ethanol in the presence of an excess of sulfuric acid. The intermediate **1** and the various salicylaldehyde derivatives did not absorb in the visible range or absorb at markedly different wavelengths or with a much weaker absorptivity, so that the formation of the dye could be easily visualized by either naked eyes, absorption or emission spectrophotometry (Figures S12-S20 in the ESI). The emission spectra were normalized to the absorbance at the excitation wavelength to allow direct comparison of all dyes generated in the wells (Scheme 1). For most salicylaldehyde derivatives, a reaction was clearly observed after 15 days of reaction at room temperature, demonstrating the reactivity of these compounds, whatever their substitution. Comparison of the spectroscopic data (Table 1) provided

interesting information, with two series of dyes easily identified. Substitution of the western part (Figure 2) by a cyclic (morpholine) or acyclic amine (diethylamine or dimethylamine) or, to a lesser extent, by a catecholate group, protected or not by methyl functions, produces the brightest dyes emitting in the red-NIR spectral region.

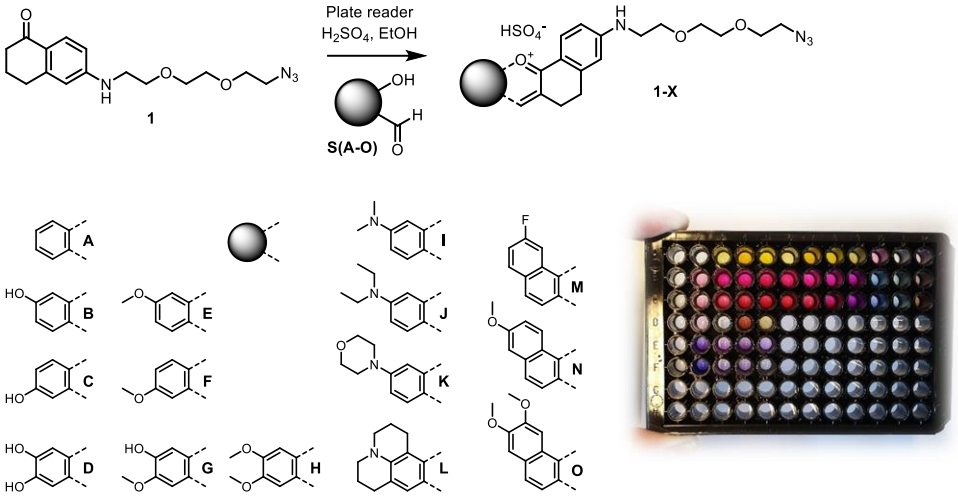

Scheme 1. Screening (by absorption and emission) of PEG-2-azido dyes by varying the western substitution of the dye using 15 salicylaldehyde derivatives.

Table 1. Photophysical data recorded for the flavylium dyes generated in the wells by reaction of **1** with salicylaldehydes **S(A-O)** in ethanol with excess of sulfuric acid.

Cmpd	λ_{abs}	λ_{em}	Stokes shift (cm^{-1})	Fluo intensity ($x10^2$ ua)
1-A	519	588/636	2 260	2.44
1-B	555	595/sh638	1 210	10.94
1-C	531/sh557	598/646	1 230	6.53
1-D	560	604/sh649	1 300	26.14
1-E	534/555	595/640	1 200	13.86
1-F	530/sh559	597/646	1 140	7.82
1-G	560	603/sh647	1 270	28.35
1-H	Sh541/561	605/sh649	1 300	20.64
1-I	583	636	1 430	27.81
1-J	605	638	860	51.70
1-K	587	635	1 290	34.76
1-L	615	654	970	8.99
1-M	543	614/669	2 130	2.6
1-N	Sh554/580	620/670	1 110	5.55
1-O	553/575	618/668	1 210	5.51

The errors on the quantum yields the λ_{abs} and λ_{em} are estimated to be ± 2 nm.

With regard to the compound **1-A**, the PEG-2-amino substitution at the 4'-position induces strong mesomeric and inductive electron-donating effects, allowing strong conjugation with the pyrilium C ring that behaves as a powerful EWG. [46] The flavylium ion is therefore strongly stabilized by intramolecular charge transfer (ICT) leading to a high degree of co-planarity between the benzo-pyrilium moiety and

the phenyl group in position 2. This has been emphasized by the X-ray data of 7-(*N*,*N*-diethylamino)-4′-hydroxyflavylium [45] or 4'-(*N*,*N*-dimethylamino)-flavylium [46] that showed a strong double bond character of the C(4')-N bond and an almost planar structure as well as by theoretical investigations. [47] Stiffening by means of an ethyl bridge contributes further to the stabilization of the flavylium ion and the planarity of the chromophore. In light of these data, an extended conjugation is thus anticipated to take place between the donor (PEG-2 amino substitution) and the acceptor (pyrilium C unit) within these rigid dyes due to strong ICT character (Scheme 2). [47] As a consequence, protonation of the amino group (e.g. pK_a = -0.67 for 7-(*N,N*-diethylamino)-4′-hydroxyflavylium [45]; pK_a = -0.4 for 7-(*N,N*-dimethylamino)-flavylium [46]) and hydration of the flavylium cation (i.e. aqueous stability of these compounds up to pH > 9) are more difficult to achieve. Compound **1** and related derivatives can therefore be regarded as streptocyanine polymethine dyes [48] (Scheme 2) with electronic resonance between the tertiary nitrogen atom and the trivalent positively charged oxygen of the pyrilium unit separated by 2 methine units.

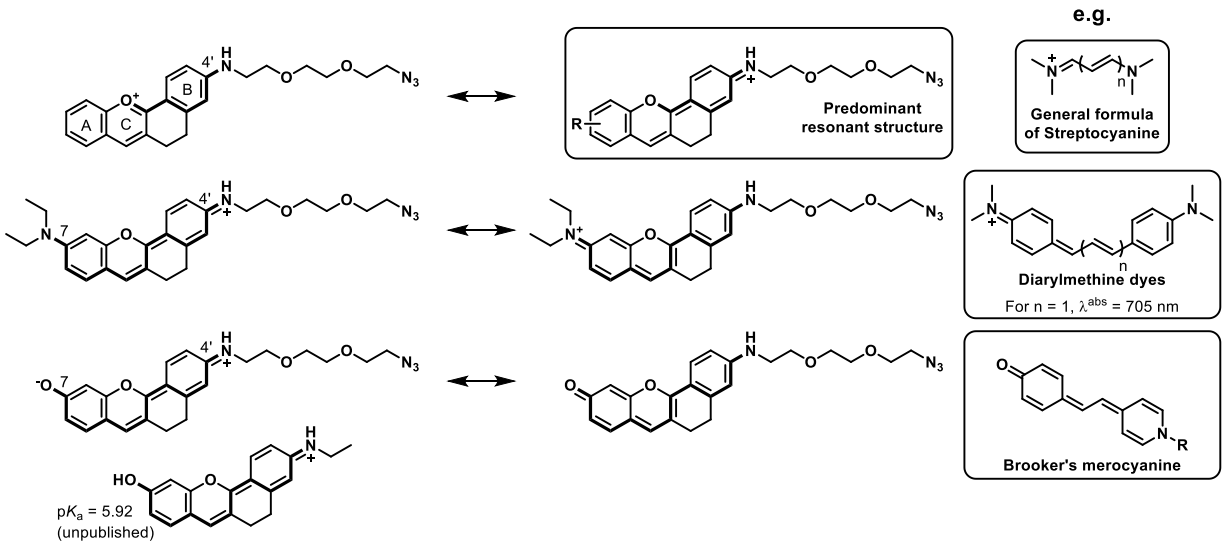

Scheme 2. Resonance effects within amino-substituted flavylium ions.

Substituted with an alkylamine or hydroxyl group in position 7, these dyes behave like diarylmethine [49-50] or merocyanine dyes [51-53] (Scheme 2). This property causes the absorption maximum of the S_0-S_1 transition to be shifted by almost 100 nm when comparing, for example, **1-A** to compounds **1-I** or **1-J**. For polymethine dyes (Scheme 2), elongation of the polymethine chain in the symmetric dyes by one *trans*-vinylene group has been reported to result in a bathochromic shift of the absorption maximum by about 100 nm. [49,54] Comparison of **1-I** (λ_{abs} = 583 nm) with a related diarylmethine dye (n = 1, λ_{abs} = 705 nm, Scheme 2), however, demonstrates different scaffolds due to the nature of the substitution and the dissymmetry. [55] These preliminary data thus indicate that the compounds obtained from our screening approach are characterized by a strong CT character with the electronic nature of the substituent(s) on the western part modulating the optical and photophysical properties of the dye. Compound **1-J** therefore displays the best photophysical characteristics (λ_{abs}, λ_{em}, brightness) and the choice was therefore made to substitute a diethylamine group on the western part of the chromophore to synthesize the corresponding pegylated azide derivatives.

Synthesis. A set of azido dyes were generated by introducing a polyethylene glycol (PEG) spacer of varying length between the chromophore responsible for the fluorescence emission (flavylium ion) and the reactive function (azide) for the CuAAC cycloaddition (Figure 2). Before developing this chemistry, we first synthesized a flavylium ion model; parent to the desired ones, with a diethylamino donor group in position 7 and an ethylamino group (**2**) in position 4'. The photophysical study of this compound allowed us to assess the influence of the PEG-azide chain on the fluorescence properties of the target systems. **2** was obtained directly after acid condensation between 4-diethylamino-salicylaldehyde and 6-ethylamino-α-tetralone **3** obtained by monoethylation of 6-amino-α-tetralone (Scheme 3).

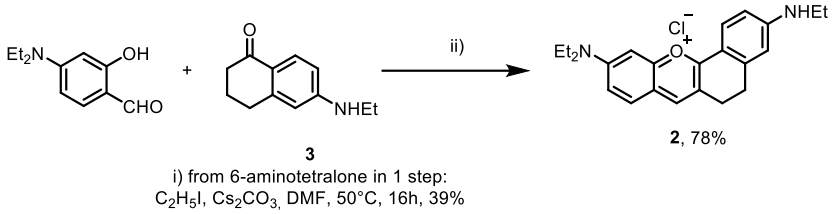

Scheme 3. Synthetic route for the preparation of the dye model **2**. ii) HCl, HCOOH, 60°C, 48h.

On the basis of the photophysical data obtained for **2** (*vide infra*), three flavylium ions substituted by an azido-PEG chain of variable length were then prepared. These compounds represent a homogeneous series of dyes in which the PEG(n) chain (-[O-CH_2-CH_2]n-) increases sequentially (n = 1-3), allowing its effect on the photophysical properties of the fluorescent probe to be assessed. Each of these compounds required a desymmetrization of the PEG unit, which can be carried out before or after substitution of the 6-amino-α-tetralone. The fluorescent probe **F-1**, which has a PEG-1 chain, was synthesized in six steps (Scheme 4). The asymmetric linker with amine and terminal azide functions (i.e. 2-(2-azidoethoxy)ethanamine) was prepared using the method originally described by Schwabacher *et al*. [56] The modified procedure starts with the synthesis of the chain from diethylene glycol by tosylation of the two hydroxyl groups giving compound **4**, followed by nucleophilic substitution to introduce two azide functions. A Staudinger reaction from **5** reduces only one azide unit to the corresponding amine function, allowing desymmetrization of the PEG-1 unit and resulting in the key precursor **6**. [57] The latter was then subjected to a Buchwald-Hartwig C-*N* coupling with **7** obtained by tosylation of 6-hydroxy-α-tetralone. Finally, an acid condensation with the salicylaldehyde derivative of interest (4-diethylamino-2-hydroxyl-benzaldehyde) led to the formation of the targeted dye **F1** in 18.6% global yield for the six steps (Scheme 4). For the latter conditions, a new protocol was developed to generate and control HCl gas *in situ* (reacting acetyl chloride with ethanol to form ethyl acetate, the solvent of the reaction).

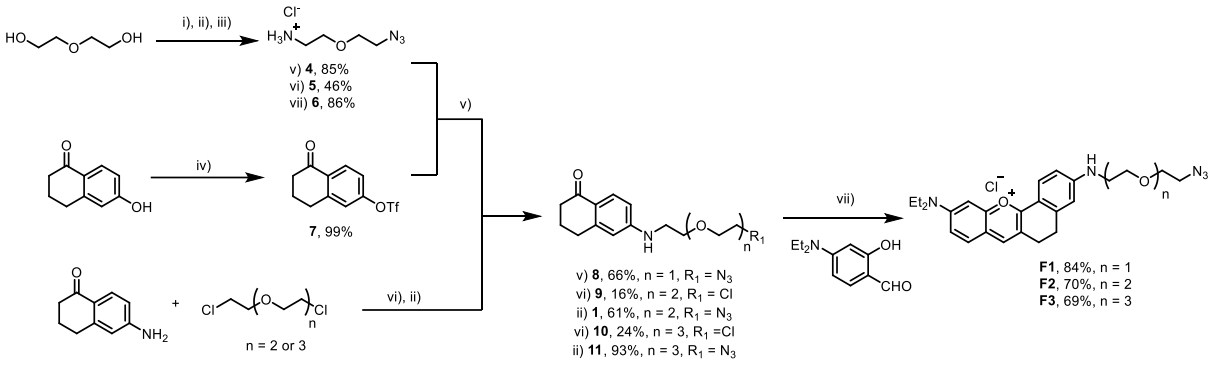

Scheme 4. Synthetic route for the preparation of pegylated (n = 1, 2 and 3) azido-dyes **F1**, **F2** and **F3**. ; i) TsCl, KOH, DCM, 0°C to rt, 16h; ii) NaN_3, DMF, 60°C, 24h; iii) HCl, PPh_3, EtOAc, 16h; iv) Tf_2O, pyr, DMC, 0°C to rt, 2h; v) $Pd(OAc)_2$, BINAP, Cs_2CO_3, toluene, 100°C, 3h; vi) DIPEA, NaI, MeCN, reflux, 48h; vii) AcCl, EtOH, EtOAc, 0°C to rt, 72h.

Two other dyes with an intermediate length PEG-2 (**F2**) or a long PEG-3 chain (**F3**) were prepared in a three steps synthetic approach (Scheme 4). This starts with two sequential nucleophilic substitutions including an initial nucleophilic substitution with low yields of 1,2-*bis*(2-chloroethoxy)ethane or *bis*(2-(2-chloroethoxy)ethyl)ether with 6-amino-α-tetralone. The second chlorine atom was then substituted with NaN_3 in excellent yields, giving access to the precursors of interest (**1** and **11**). Acid condensation with 4-diethylamino-2-hydroxyl-benzaldehyde led to the formation of the targeted dyes **F2** and **F3** with global yield of 7% and 15.4%, respectively.

Photophysical properties. The photophysical data measured for the azide dyes and their corresponding amino analogue are listed in Table 2 (Figures S8-S11 in the ESI). Due to the cationic nature of the flavylium chromophore and the presence of a chloride counter-anion, all the fluorescent dyes prepared in this work display good aqueous solubility, allowing their use as fluorescent tags in biological media (Figure S5 in the ESI). In order to mimic physiological conditions as closely as possible, the photophysical data were measured in a buffered aqueous solution at neutral pH (pH 7.41) containing 0.1 M NaCl. Parallel measurements were also carried out in ethanol acidified with TFA. For all compounds (Figures S8-S11 in the ESI), the absorption spectrum is dominated by a single long-wavelength absorption band corresponding to a single S_0-S_1 long-wavelength transition with significant CT character. S_0-S_2 transitions are possible, but with much lower intensity and little to no CT character. [47] The optical data obtained for **1-J** during the screening assay were confirmed for the synthesized compound **F2** (Table 2). In ethanol, **F2** is characterized by λ_{abs} and λ_{em} values of 606 nm and 633 nm, respectively, in agreement with the data extracted from the screening assay (Table 1). In addition, **F2** proved to be a bright fluorescent compound both in ethanol (Φ = 63.9 % and brightness B = 16 870 M^{-1} cm^{-1}) and in aqueous solution at pH 7.41 (Φ = 30.4 % and B = 5 740 M^{-1} cm^{-1}). Comparison of the **2** prototype with the pegylated derivatives **F1** (PEG-1), **F2** (PEG-2) and **F3** (PEG-3) clearly shows that the length of the PEG chain and the presence of a terminal azide moiety have no influence on the photophysical properties of the fluorescent scaffold. To go further, detailed investigations of **2** have demonstrated aqueous stability over a wide pH range (from 1 to 9, Figure S6 in the ESI). The stiffening by means of an ethyl bridge and the strong CT character thus result in robust dyes and limit the hydration reactions well known for these 2-phenyl-1-benzopyrilium derivatives. [46] The ability of **2** to lead to dimer

or oligomer formation in aqueous solution was also assessed by absorption spectrophotometry. Increasing the dye concentration resulted in the clear formation of a new absorption band at shorter wavelengths (Figure S7 in the ESI). This feature is a clear signature of dimer formation, as has already been observed for Rhodamine 6G (R6G) [58,59] or Methylene Blue (MB). [60] The dimer formation was associated to an equilibrium constant K_{Dim} of 2870 ± 900 M^{-1} that agrees those reported for R6G (6200 ± 300 M^{-1}) [58,59] and MB (6800 M^{-1}) [60]. The electronic spectra of **2** dimers evidenced two absorptions lying at lower and higher energies with respect to the monomer. As with R6G, this indicates the presence of dimers H and J leading to an oblique arrangement of molecular transition moments, which results into absorption band splitting. For **2** (Figure S7 in the ESI), the formation of the dimer is characterized by an absorption splitting at about 560 nm ($\varepsilon^{560} \sim 8.2 \times 10^4$ M^{-1} cm^{-1}) and 630 nm ($\varepsilon^{630} \sim 1.8 \times 10^4$ M^{-1} cm^{-1}) thus leading to a $\varepsilon^{630}/\varepsilon^{560}$ ratio of ~ 0.22. According to the exciton theory, [61] such a value likely reflects the predominance of a twisted sandwich geometry (i.e. sandwich type geometry with some deviation from exact parallel plane arrangement, Figure S7 in the ESI). A value of ~ 50.3° was calculated for the angle between directions of transition dipole moments in the dimer. This value is comparable to that measured for R6G in water (61.9°). [59] Considering the low K_{Dim} value measured for **2**, we can rule out the formation of dimeric species during spectroscopic measurements or imaging experiments (*vide infra*).

Table 2. Photophysical data recorded for the flavylium dyes in buffered aqueous solutions containing 0.1 M NaCl and in acidified ethanol.

Cmpd	λ_{abs} (nm)	λ_{em} (nm)	ε (x 10^4 M^{-1} cm^{-1})	Φ^{abs} (%)	Stokes shift (cm^{-1})	Brightness (M^{-1} cm^{-1})	Solvent
2	594	633	3.49	23	1 040	8 030	pH 7.41[a]
	606	633	6.99	68	700	47 530	EtOH
F1	593	633	4.55	23.6	1 070	10 920	pH 7.41[a]
	605	633	6.96	54.9	730	38 210	EtOH
F2	598	638	1.89	30.4	1 110	5 740	pH 6.86[b]
	606	633	2.64	63.9	700	16 870	EtOH
F3	594	634	7.49	26.5	1 110	19 850	pH 7.41[a]
	606	635	9.85	55.6	750	54 770	EtOH

[a] Aqueous buffer at pH 7.41 + 0.1 M NaCl. [b] Aqueous buffer at pH 6.86 + 0.1 M NaCl. PS = photosensitive. The errors on the quantum yields Φ, the λ_{abs} and λ_{em} are estimated to be ± 10% and ± 1 nm, respectively.

As a result of these investigations, the pegylated compounds **F1**, **F2** and **F3** have been identified as interesting click chemistry partners. These compounds are fully competitive with most commercial compounds in terms of photophysical properties. In addition, they are characterized by lower MW, a simplified design, good aqueous solubilities and stabilities over a wide pH range. The convergent synthesis of the PEG-2 and PEG-3 derivatives can be achieved in a straightforward manner (3 steps, Scheme 4), with the possibility of scale-up, a very attractive cost price and the introduction of structural diversity on ring A (Figure 2) in the final step.

Preliminary fluorescence imaging

Preliminary fluorescence imaging experiments were carried out with the prototype compound **2** and the PEG-3 azido derivative **F3** on tobacco BY-2 cells. This approach was first used to assess whether these

dyes can be internalized prior to any click chemistry experiments and to measure their emission spectrum in different organelles of these cells using confocal Spectral imaging (SImaging). SImaging indeed allows the simultaneous detection of fluorescence emitted in several independent channels with a resolution of < 10 nm/channel, enabling the spectrum of the emitting species to be reconstructed *in cellula*. [62] Figure 3 first show BY-2 tobacco treated with **2** at 5 µM for 5 minutes with two different settings for the excitation and detection of emission fluorescence using SImaging: λ_{exc} = 405 nm with emission range from 415 to 664 nm, and λ_{exc} = 488 nm with emission range from 504 to 664 nm. As seen on the fluorescence images, a bright red fluorescent signal is clearly visible along the cell periphery, which is cytoplasma surrounding the unlabeled plant cell vacuole. The emission spectrum of **2** measured in aqueous solution buffered at pH 7.41 obtained from our spectrofluorimetric analysis was compared with those measured by SImaging at λ_{exc} = 405 nm and λ_{exc} = 488 nm in the living BY-2 cells and showed an excellent agreement demonstrating that neither the cells, nor the dye are altered during the fluorescence imaging experiments. In addition, no emission of the fluorophore was observed outside the cell indicating its absence in the culture medium. The **2** compound is photostable without any degradation or fading when excited.

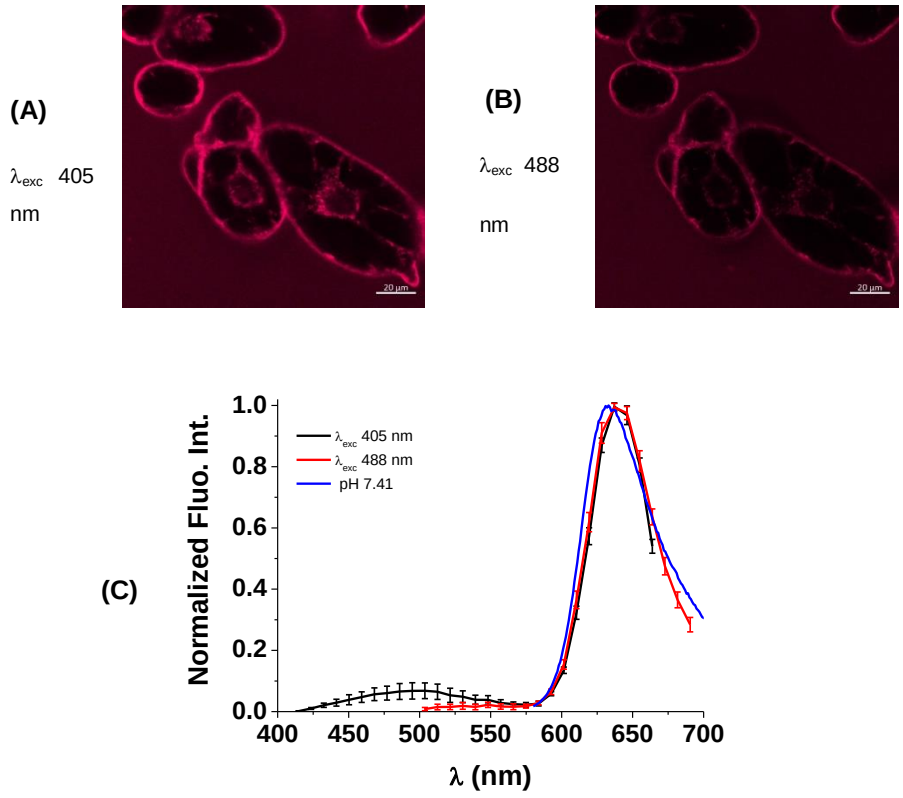

Figure 3. Fluorescence observed by SImaging in the cytoplasma of tobacco BY-2 cells in the presence of **2** (5 µM). Lambda stack scan mode image (the bar corresponds to 20 µm) for **2** (5 µM) recorded at λ_{exc} = 405 nm **(A)** and λ_{exc} = 488 nm **(B)**. **(C)** Average of normalized fluorescence spectra (> 20 spectra) measured *in cellulo* by SImaging at λ_{exc} = 405 nm and λ_{exc} = 488 nm on BY-2 cells compared with the emission spectrum measured *in tubo* in an aqueous solution buffered to pH 7.41. These data capture the uptake of **2** within 5 min by BY-2 cells, resulting in a specific red fluorescence. The laser power was set to 5%.

To go further, a second series of experiments was carried out with the **2** prototype using excitation at 561 nm (Figure 4). While the **2** dye was sensitized at λ_{exc} of 405 and 488 nm, the excitation at 561 nm is much closer to the absorption maximum of **2**, which is centered at 594 nm in aqueous solution buffered

at pH 7.41 (Table 2). The data from these new experiments show that, in addition to the cytoplasma and organelles it contains, **2** the nucleus (nu) in particular the nucleolus (nl) is also labelled. SImaging confirms that **2** is not altered within these different organelles. To ensure that **2** effectively labels mitochondria, a co-localization experiment with the commercially available MitoTracker Orange (MTO), was carried out (Figure 4). Similarly to **2**, MTO is a cationic fluorophore that is taken up and electrophoretically accumulates in mitochondria in response to the very negative potential of the mitochondrial membrane. [63] However, unlike commercially available fluorophores (e.g. tetramethylrhodamine methylester, Rhodamine 123), MTO has a reactive chloromethyl group that can form covalent bonds with thiols on proteins or peptides, resulting in a trapping of the fluorophores inside the mitochondria. [64] Thus, SImaging confirms that **2** is able to effectively label the mitochondria of living BY-2 cells.

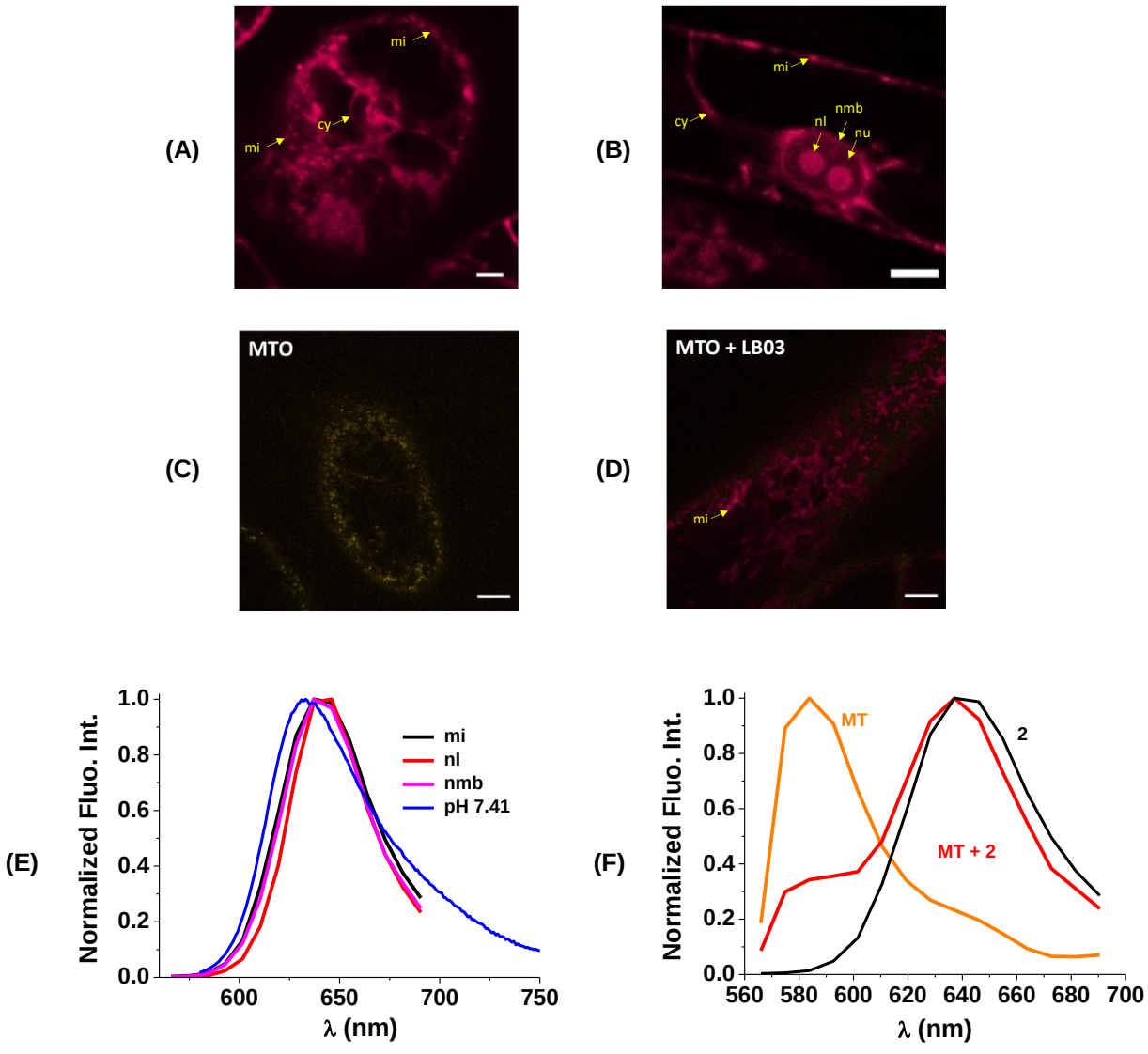

Figure 4. Fluorescence observed by SImaging in the cytoplasm (cy), nucleus (nu), nucleoli (nl), nuclear membrane (nmb) and mitochondria (mi) of living BY-2 cells in the presence of **2**. Images of λ-view (the bar corresponds to 5 µm) recorded at λ_{exc} = 561 nm of living BY-2 cells treated for 5 min with 5 µM of (**A** and **B**) **2** alone, (**C**) MTO alone and (**D**) a mixture of MTO and **2**. (**E**) Average normalized fluorescence spectra (> 20 spectra) measured *in cellulo* by SImaging at λ_{exc} = 561 nm on BY-2 cells compared with the emission spectrum measured *in tubo* in an aqueous solution buffered to pH 7.41. These data capture the uptake of **2** within 5 min by BY-2 cells, resulting in a specific

red fluorescence. (**F**) Normalized fluorescence spectra measured *in cellulo* by SImaging at λ_{exc} = 561 nm on BY-2 cells treated with MTO and a mixture of MTO and **2** demonstrating a colocalization of MTO and **2** in mitochondria and an effective staining of the latter organelle. The laser power was set to 5%.

We then focused on the compound **F3** with a PEG-3 chain. SImaging measurements performed by treating BY-2 cells with 10 µM **F3** showed efficient uptake of these dyes (Figure 5), with comparable labelling of the same organelles as observed with **2**. The SImaging emission spectra also showed the integrity of the dye not only after 10 minutes but also after 4 hours of treatment of BY-2 cells, indicating the high (photo)stability of **F3**. After 3-4 hours of treatment, **F3** also appeared to partially diffuse into the vacuoles of BY-2 cells (Figure 5). **F3** does not diffuse outside the cell as indicated by its absence in the culture medium.

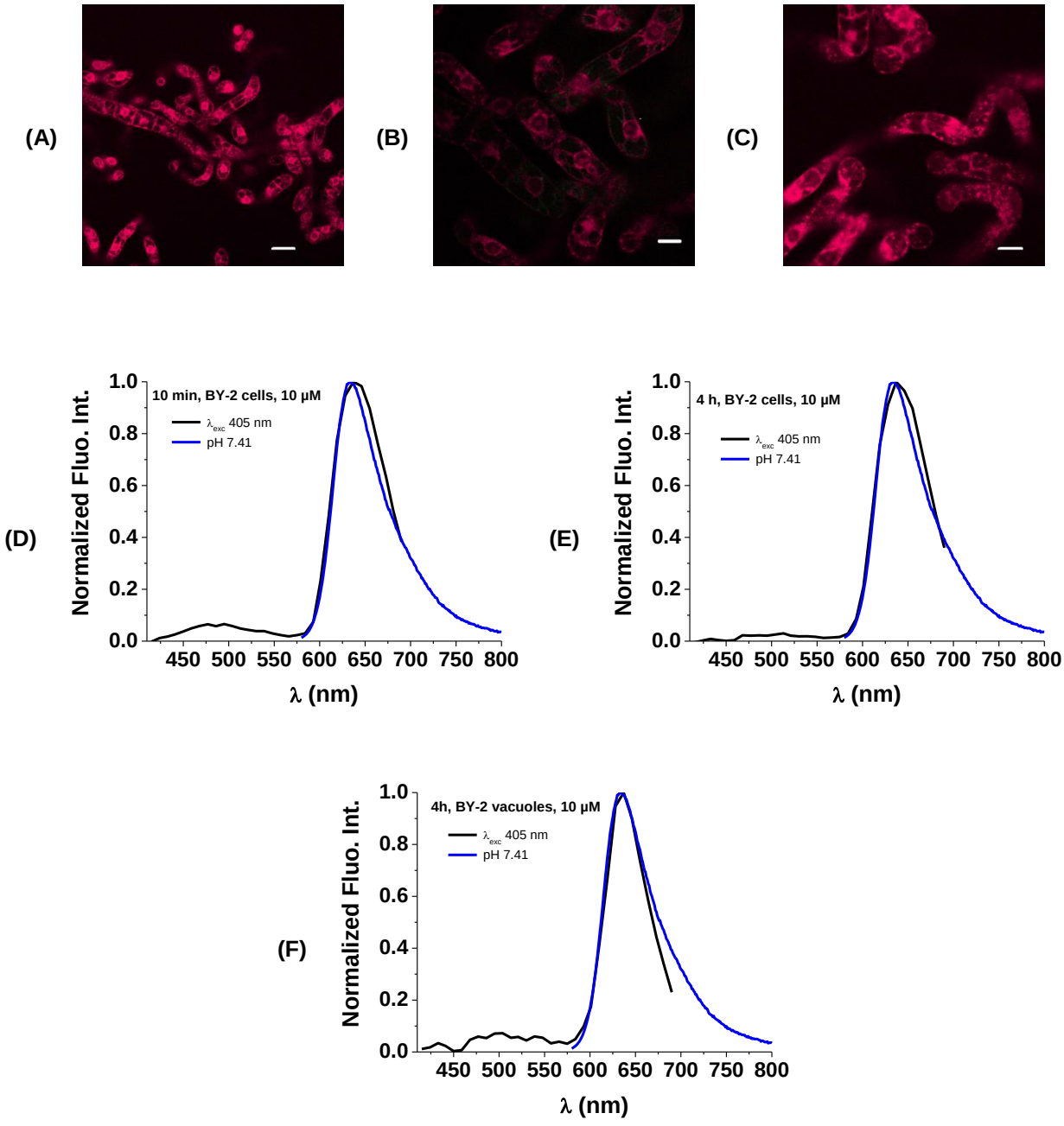

Figure 5. Fluorescence observed by SImaging of living BY-2 cells in the presence of **F3**. Lambda stack scan mode images (the bar corresponds to 50 µm for **A** and 20 µm for **B** and **C**) recorded at λ_{exc} = 405 nm of living BY-2 cells treated for (**A**) 5 minutes, (**B**) 60 minutes and (**C**) 3h with 10 µM of **F3**. (**E**) Average normalized fluorescence spectra

(> 10 spectra) measured *in cellulo* by SImaging at λ_{exc} = 405 nm on BY-2 cells compared with the emission spectrum measured *in tubo* in an aqueous solution buffered to pH 7.41 and measured after (**C**) 10 minutes and (**D**) 4h of treatment. These spectrophotometric data capture the uptake of **F3** within 10 min and 4 hours by BY-2 cells, resulting in a specific red fluorescence. The laser power was set to 5%.

Conclusion

This study describes the development of a new class of bio-inspired azide fluorophore probes for natural dyes, anthocyanins and, more specifically, flavylium (2-aryl-benzopyrylium) ions. These have been developed for applications in the field of bioorthogonal chemistry, with a particular interest in the study of the metabolism and the molecular function of phytosterols in plant cells. By the introduction of polyethylene glycol (PEG) chains of different lengths, a terminal azide functionality has been effectively incorporated without affecting the intrinsic fluorescence properties of the flavylium-based dyes. The flavylium ion was rigidified by an ethylene bridge for improvement of (photo)chemical stability and photophysical properties. The synthesis of several derivatives with superior photophysical properties, especially in the red-NIR spectral region desirable for cell imaging, was achieved by screening/selection of the appropriate substitution unit using a hybrid absorption/emission plate reader. The synthesized dyes have strong ICT properties contributing to high (photo)stability, good aqueous solubility and tunable emission colors. The photophysical properties of the corresponding dyes are not affected by the length of the PEG chain (PEG-1 to PEG-3). All these properties make them interesting for advanced bio-imaging techniques. The efficiency of the rapid incorporation of these azido fluorophores has been demonstrated on tobacco BY-2 cells, revealing a marked red labelling of several organelles of interest (nuclear system, mitochondria). The integrity of these fluorophores does not appear to be compromised even after being combined 4 hours with BY-2 cells, as shown by the data obtained using SImaging techniques. In addition to their ease of synthesis, structural diversity and robust fluorescence properties (high brightness, photostable), these new tools have potential as versatile tools for a variety of biological applications. An ongoing study is investigating bioorthogonal chemistry approaches with phytosterol alkynes both at the cellular level (BY-2 cells) and at the level of tomato (*Solanum lycopersicum*) plant organs of young plantlets.

Competing Interest Statement

The authors declare no conflict interest.

Acknowledgements

This work has been published under the framework of the idex Unistra and benefits from a funding (2017/W17RPD29) from the state managed by the French National Research Agency as part of the investments for the future program. The authors wish to thank the Laboratoire d'Excellence (LabEx) ParaFrap consortium for funding [ANR-11-LABX-0024], and creating a proper framework for this scientific research. The authors would like to thank Gilles Ulrich (ICPEES UMR7515 CNRS-Unistra) for making his Fluoromax 4 instrument available for the quantum yield measurements. The authors also warmly thank Manon Aniel, Lucas Furst and Quentin Riehl for partially contributing to this work.

References

[1] Galas, L.; Gallavardin, T.; Bénard, M.; Lehner, A.; Schapman, D.; Lebon, A.; Komuro, H.; Lerouge, P.; Leleu, S.; Franck, X. “Probe, Sample, and Instrument (PSI)”: The Hat-Trick for Fluorescence Live Cell Imaging. *Chemosensors* **2018**, *6* (3), 40. https://doi.org/10.3390/chemosensors6030040.

[2] Lavis, L. D. Chemistry Is Dead. Long Live Chemistry! *Biochemistry* **2017**, *56* (39), 5165–5170. https://doi.org/10.1021/acs.biochem.7b00529.

[3] Ding, F.; Zhan, Y.; Lu, X.; Sun, Y. Recent Advances in Near-Infrared II Fluorophores for Multifunctional Biomedical Imaging. *Chem. Sci.* **2018**, *9* (19), 4370–4380. https://doi.org/10.1039/C8SC01153B.

[4] Ding, C.; Ren, T. Near Infrared Fluorescent Probes for Detecting and Imaging Active Small Molecules. *Coord. Chem. Rev.* **2023**, *482*, 215080. https://doi.org/10.1016/j.ccr.2023.215080.

[5] Donaldson, L. *Molecules* **2020**, *25* (10), 2393. doi: 10.3390/molecules25102393.

[6] de Moliner, F.; Kielland, N.; Lavilla, R.; Vendrell, M. Modern Synthetic Avenues for the Preparation of Functional Fluorophores. *Angew. Chem. Int. Ed.* **2017**, *56* (14), 3758–3769. https://doi.org/10.1002/anie.201609394.

[7] Hang, H. C.; Yu, C.; Kato, D. L.; Bertozzi, C. R. A Metabolic Labeling Approach toward Proteomic Analysis of Mucin-Type O-Linked Glycosylation. *Proc. Natl. Acad. Sci. U.S.A.* **2003**, *100* (25), 14846–14851. https://doi.org/10.1073/pnas.2335201100.

[8] Nguyen, S. S.; Prescher, J. A. Developing Bioorthogonal Probes to Span a Spectrum of Reactivities. *Nat. Rev. Chem.* **2020**, *4* (9), 476–489. https://doi.org/10.1038/s41570-020-0205-0.

[9] Devaraj, N. K. The Future of Bioorthogonal Chemistry. *ACS Cent. Sci.* **2018**, *4* (8), 952–959. https://doi.org/10.1021/acscentsci.8b00251.

[10] Porte, K.; Riberaud, M.; Châtre, R.; Audisio, D.; Papot, S.; Taran, F. Bioorthogonal Reactions in Animals. *ChemBioChem* **2021**, *22* (1), 100–113. https://doi.org/10.1002/cbic.202000525..

[11] Simon, C.; Lion, C.; Spriet, C.; Baldacci-Cresp, F.; Hawkins, S.; Biot, C. One, Two, Three: A Bioorthogonal Triple Labelling Strategy for Studying the Dynamics of Plant Cell Wall Formation In Vivo. *Angew. Chem. Int. Ed.* **2018**, *57* (51), 16665–16671. https://doi.org/10.1002/anie.201808493.

[12] Rigolot, V.; Biot, C.; Lion, C. To View Your Biomolecule, Click inside the Cell. *Angew. Chem. Int. Ed.* **2021**, anie.202101502. https://doi.org/10.1002/anie.202101502.

[13] Handula, M.; Chen, K.-T.; Seimbille, Y. IEDDA: An Attractive Bioorthogonal Reaction for Biomedical Applications. *Molecules* **2021**, *26* (15), 4640. https://doi.org/10.3390/molecules26154640.

[14] Zhao, H.; He, Y.; Lo, Y.; Song, H.; Lu, J. Fluorescent Probes Based on Bioorthogonal Reactions: Construction Strategies and Applications. *Trends Anal. Chem.* **2023**, *169*, 117388. https://doi.org/10.1016/j.trac.2023.117388.

[15] Decuypère, E.; Plougastel, L.; Audisio, D.; Taran, F. Sydnone–Alkyne Cycloaddition: Applications in Synthesis and Bioconjugation. *Chem. Commun.* **2017**, *53* (84), 11515–11527. https://doi.org/10.1039/C7CC06405E.

[16] Porte, K.; Riomet, M.; Figliola, C.; Audisio, D.; Taran, F. Click and Bio-Orthogonal Reactions with Mesoionic Compounds. *Chem. Rev.* **2021**, *121* (12), 6718–6743. https://doi.org/10.1021/acs.chemrev.0c00806.

[17] Liu, H.; Audisio, D.; Plougastel, L.; Decuypere, E.; Buisson, D.-A.; Koniev, O.; Kolodych, S.; Wagner, A.; Elhabiri, M.; Krzyczmonik, A.; Forsback, S.; Solin, O.; Gouverneur, V.; Taran, F. Ultrafast Click Chemistry with Fluorosydnones. *Angew. Chem. Int. Ed.* **2016**, *55* (39), 12073–12077. https://doi.org/10.1002/anie.201606495.

[18] Li, J.; Hu, M.; Yao, S. Q. Rapid Synthesis, Screening, and Identification of Xanthone- and Xanthene-Based Fluorophores Using Click Chemistry. *Org. Lett.* **2009**, *11* (14), 3008–3011. https://doi.org/10.1021/ol9010344.

[19] Benson, R. C.; Kues, H. A. Absorption and Fluorescence Properties of Cyanine Dyes. *J. Chem. Eng. Data* **1977**, *22* (4), 379–383. https://doi.org/10.1021/je60075a020.

[20] Samanta, S.; Lai, K.; Wu, F.; Liu, Y.; Cai, S.; Yang, X.; Qu, J.; Yang, Z. Xanthene, Cyanine, Oxazine and BODIPY: The Four Pillars of the Fluorophore Empire for Super-Resolution Bioimaging. *Chem. Soc. Rev.* **2023**, *52* (20), 7197–7261. https://doi.org/10.1039/D2CS00905F.

[21] Meng, G.; Guo, T.; Ma, T.; Zhang, J.; Shen, Y.; Sharpless, K. B.; Dong, J. Modular Click Chemistry Libraries for Functional Screens Using a Diazotizing Reagent. *Nature* **2019**, *574* (7776), 86–89. https://doi.org/10.1038/s41586-019-1589-1.

[22] Bag, S. S.; Kundu, R. Installation/Modulation of the Emission Response via Click Reaction. *J. Org. Chem.* **2011**, *76* (9), 3348–3356. https://doi.org/10.1021/jo200231k.

[23] Nagy, K.; Orbán, E.; Bősze, S.; Kele, P. Clickable Long-Wave “Mega-Stokes” Fluorophores for Orthogonal Chemoselective Labeling of Cells. *Chem. Asian J.* **2010**, *5* (4), 773–777. https://doi.org/10.1002/asia.200900477.

[24] Kele, P.; Li, X.; Link, M.; Nagy, K.; Herner, A.; Lőrincz, K.; Béni, S.; Wolfbeis, O. S. Clickable Fluorophores for Biological Labeling—with or without Copper. *Org. Biomol. Chem.* **2009**, *7* (17), 3486. https://doi.org/10.1039/b907741c.

[25] Flon, V.; Bénard, M.; Schapman, D.; Galas, L.; Renard, P.-Y.; Sabot, C. Fluorophore-Assisted Click Chemistry through Copper(I) Complexation. *Biomolecules* **2020**, *10* (4), 619. https://doi.org/10.3390/biom10040619.

[26] Bevilacqua, V.; King, M.; Chaumontet, M.; Nothisen, M.; Gabillet, S.; Buisson, D.; Puente, C.; Wagner, A.; Taran, F. Copper-Chelating Azides for Efficient Click Conjugation Reactions in Complex Media. *Angew. Chem. Int. Ed.* **2014**, *53* (23), 5872–5876. https://doi.org/10.1002/anie.201310671.

[27] Xiao, M.; Zhang, Y.; Li, R.; Li, S.; Wang, D.; An, P. Photoactivatable Fluorogenic Azide-Alkyne Click Reaction: A Dual-Activation Fluorescent Probe. *Chem. Asian J.* **2022**, *17* (17), e202200634. https://doi.org/10.1002/asia.202200634.

[28] Jun, J. V.; Haney, C. M.; Karpowicz, R. J.; Giannakoulias, S.; Lee, V. M.-Y.; Petersson, E. J.; Chenoweth, D. M. A “Clickable” Photoconvertible Small Fluorescent Molecule as a Minimalist Probe for Tracking Individual Biomolecule Complexes. *J. Am. Chem. Soc.* **2019**, *141* (5), 1893–1897. https://doi.org/10.1021/jacs.8b13094.

[29] Ding, C.; Ren, T. Near Infrared Fluorescent Probes for Detecting and Imaging Active Small Molecules. *Coord. Chem. Rev.* **2023**, *482*, 215080. https://doi.org/10.1016/j.ccr.2023.215080.

[30] Li, Y.; Liu, T.; Sun, J. Recent Advances in N-Heterocyclic Small Molecules for Synthesis and Application in Direct Fluorescence Cell Imaging. *Molecules* **2023**, *28* (2), 733. https://doi.org/10.3390/molecules28020733.

[31] Capobianco, M. L.; Barbarella, G.; Manetto, A. Oligothiophenes as Fluorescent Markers for Biological Applications. *Molecules* **2012**, *17* (1), 910–933. https://doi.org/10.3390/molecules17010910.

[32] Sivakumar, K.; Xie, F.; Cash, B. M.; Long, S.; Barnhill, H. N.; Wang, Q. A Fluorogenic 1,3-Dipolar Cycloaddition Reaction of 3-Azidocoumarins and Acetylenes. *Org. Lett.* **2004**, *6* (24), 4603–4606. https://doi.org/10.1021/ol047955x.

[33] Key, J. A.; Cairo, C. W. Identification of Fluorogenic and Quenched Benzoxadiazole Reactive Chromophores. *Dyes Pigm.* **2011**, *88* (1), 95–102. https://doi.org/10.1016/j.dyepig.2010.05.007.

[34] Herner, A.; Nikić, I.; Kállay, M.; Lemke, E. A.; Kele, P. A New Family of Bioorthogonally Applicable Fluorogenic Labels. *Org. Biomol. Chem.* **2013**, *11* (20), 3297. https://doi.org/10.1039/c3ob40296g.

[35] Pina, F.; Melo, M. J.; Laia, C. A. T.; Parola, A. J.; Lima, J. C. Chemistry and Applications of Flavylium Compounds: A Handful of Colours. *Chem. Soc. Rev.* **2012**, *41* (2), 869–908. https://doi.org/10.1039/C1CS15126F.

[36] Sun, Y.; Sun, P.; Li, Z.; Qu, L.; Guo, W. Natural Flavylium-Inspired Far-Red to NIR-II Dyes and Their Applications as Fluorescent Probes for Biomedical Sensing. *Chem. Soc. Rev.* **2022**, *51* (16), 7170–7205. https://doi.org/10.1039/D2CS00179A.

[37] Cruz, L.; Basílio, N.; Mateus, N.; de Freitas, V.; Pina, F. Natural and Synthetic Flavylium-Based Dyes: The Chemistry Behind the Color. *Chem. Rev.* **2022**, *122* (1), 1416–1481. https://doi.org/10.1021/acs.chemrev.1c00399.

[38] Khoo, H. E.; Azlan, A.; Tang, S. T.; Lim, S. M. Anthocyanidins and Anthocyanins: Colored Pigments as Food, Pharmaceutical Ingredients, and the Potential Health Benefits. *Food Nutr. Res.* **2017**, *61* (1), 1361779. https://doi.org/10.1080/16546628.2017.1361779.

[39] Duval, R.; Duplais, C. Fluorescent Natural Products as Probes and Tracers in Biology. *Nat. Prod. Rep.* **2017**, *34* (2), 161–193. https://doi.org/10.1039/C6NP00111D.

[40] Figueiredo, P.; Elhabiri, M.; Saito, N.; Brouillard, R. Anthocyanin Intramolecular Interactions. A New Mathematical Approach To Account for the Remarkable Colorant Properties of the Pigments Extracted from *Matthiola Incana*. *J. Am. Chem. Soc.* **1996**, *118* (20), 4788–4793. https://doi.org/10.1021/ja9535064.

[41] Haucke, G.; Czerney, P.; Igney, C.; Hartmann, H. Absorption Spectra and Fluorescence Behaviour of Benzopyrylium Compounds. *Ber. Bunsenges. Phys. Chem.* **1989**, *93* (7), 805–815. https://doi.org/10.1002/bbpc.19890930712.

[42] Lin, X.; Chen, Y.; Wang, S.; Liu, K.; Kong, F. Construction of a Novel Cell-Trappable Fluorescent Probe for Hydrogen Sulfide (H_2S) and Its Bio-Imaging Application. *Anal Bioanal Chem* **2019**, *411* (27), 7127–7136. https://doi.org/10.1007/s00216-019-02090-9.

[43] Liu, X.; Lei, H.; Hu, Y.; Fan, X.; Zhang, Y.; Xie, L.; Huang, J.; Cai, Q. A Turn-on Fluorescent Nanosensor for H_2S Detection and Imaging in Inflammatory Cells and Mice. *Spectrochim. Acta A Mol. Biomol. Spectrosc.* **2023**, *297*, 122739. https://doi.org/10.1016/j.saa.2023.122739.

[44] Li, Z.; Gao, J.; Guo, Z.; Zhao, H.; Liu, L.; Wang, M.; Zhang, P.; Chen, G.; Li, X.; Wei, C. Monitoring the Fluctuation of H2S in Insulin-Resistant HepG2 Cells and Diabetic Mice with a Dual-Locked NIR Fluorescent Probe. *Sens. Actuators B Chem.* **2022**, *353*, 131141. https://doi.org/10.1016/j.snb.2021.131141.

[45] Moncada, M. C.; Fernández, D.; Lima, J. C.; Parola, A. J.; Lodeiro, C.; Folgosa, F.; Melo, M. J.; Pina, F. Multistate Properties of 7-(N,N-Diethylamino)-4′-Hydroxyflavylium. An Example of an Unidirectional Reaction Cycle Driven by PH. *Org. Biomol. Chem.* **2004**, *2* (19), 2802–2808. https://doi.org/10.1039/B409260K.

[46] Roque, A.; Lodeiro, C.; Pina, F.; Maestri, M.; Dumas, S.; Passaniti, P.; Balzani, V. Multistate/Multifunctional Systems. A Thermodynamic, Kinetic, and Photochemical Investigation of the 4'-Dimethylaminoflavylium Compound. *J. Am. Chem. Soc.* **2003**, *125* (4), 987–994. https://doi.org/10.1021/ja0287276.

[47] Sun, L.; Silva, G. T. M.; Quina, F. H.; Lischka, H.; Aquino, A. J. A. Ab Initio Investigation of Substituent Effects on the Excited Electronic States of Flavylium Cation Analogues of Anthocyanin Pigments. *Comput. Theor. Chem.* **2022**, *1216*, 113851. https://doi.org/10.1016/j.comptc.2022.113851.

[48] Mustroph, H. Streptocyanine Dyes. *Phys. Sci. Rev.* **2021**, *6* (6), 137–147. https://doi.org/10.1515/psr-2020-0198.

[49] Kachkovski, A. D.; Kovalenko, N. M. Electronic Properties of Polymethine Systems. Part 4. Vinylene Shift. *Dyes Pigm.* **1997**, *35* (2), 131–148. https://doi.org/10.1016/S0143-7208(96)00094-0.

[50] Mustroph, H.; Horobin, R. W. Classification and Naming of Polymethine Dyes Used as Staining Agents for Microscopy. A Short Guide for Biomedical Investigators. *Biotech. Histochem.* **2023**, *98* (8), 545–553. https://doi.org/10.1080/10520295.2023.2263837.

[51] Mustroph, H. Merocyanine Dyes. *Phys. Sci. Rev.* **2022**, *7* (3), 143–158. https://doi.org/10.1515/psr-2020-0145.

[52] Shirinian, V. Z.; Shimkin, A. A. Merocyanines: Synthesis and Application. In *Heterocyclic Polymethine Dyes*; Strekowski, L., Ed.; Topics in Heterocyclic Chemistry; Springer Berlin Heidelberg: Berlin, Heidelberg, 2008; Vol. 14, pp 75–105. https://doi.org/10.1007/7081_2007_110.

[53] Morley, J. O.; Morley, R. M.; Fitton, A. L. Spectroscopic Studies on Brooker's Merocyanine. *J. Am. Chem. Soc.* **1998**, *120* (44), 11479–11488. https://doi.org/10.1021/ja982302v.

[54] Guarin, C. A.; Villabona-Monsalve, Juan. P.; López-Arteaga, R.; Peon, J. Dynamics of the Higher Lying Excited States of Cyanine Dyes. An Ultrafast Fluorescence Study. *J. Phys. Chem. B* **2013**, *117* (24), 7352–7362. https://doi.org/10.1021/jp400278t.

[55] Pronkin, P.; Tatikolov, A. Isomerization and Properties of Isomers of Carbocyanine Dyes. *Sci* **2019**, *1*(1), 19; https://doi.org/10.3390/sci1010019

[56] Schwabacher, A. W.; Lane, J. W.; Schiesher, M. W.; Leigh, K. M.; Johnson, C. W. Desymmetrization Reactions: Efficient Preparation of Unsymmetrically Substituted Linker Molecules. *J. Org. Chem.* **1998**, *63* (5), 1727–1729. https://doi.org/10.1021/jo971802o.

[57] a) Niskanen, J.; Karesoja, M.; Aseyev, V.; Qiu, X.; Winnik, F. M.; Tenhu, H. Thermal Response of a PVCL–HA Conjugate. *J. Polym. Sci., Part A: Polym. Chem.* **2016**, *54* (3), 425–436. https://doi.org/10.1002/pola.27794. b) El Khoury, A.; Seidler, P. M.; Eisenberg, D. S.; Harran, P. G. Catalytic Synthesis of PEGylated EGCG Conjugates That Disaggregate Alzheimer's Tau. *Synthesis* **2021**, *53* (22), 4263–4271. https://doi.org/10.1055/a-1509-5904.

[58] a) Arbeloa, F. L.; Ojeda, P. R.; Arbeloa, I. L. Dimerization and Trimerization of Rhodamine 6G in Aqueous Solution. Effect on the Fluorescence Quantum Yield. *J. Chem. Soc., Faraday Trans. 2* **1988**, *84* (12), 1903. https://doi.org/10.1039/f29888401903. B)

[59] Terdale, S.; Tantray, A. Spectroscopic Study of the Dimerization of Rhodamine 6G in Water and Different Organic Solvents. *J. Mol. Liq*. **2017**, *225*, 662–671. https://doi.org/10.1016/j.molliq.2016.10.090.

[60] Blank, O.; Davioud-Charvet, E.; Elhabiri, M. Interactions of the Antimalarial Drug Methylene Blue with Methemoglobin and Heme Targets in *Plasmodium Falciparum* : A Physico-Biochemical Study. *Antioxid. Redox Signal.* **2012**, *17* (4), 544–554. https://doi.org/10.1089/ars.2011.4239

[61] Kasha, M.; Rawls, H. R.; Ashraf El-Bayoumi, M. The Exciton Model in Molecular Spectroscopy. *Pure Appl. Chem.* **1965**, *11* (3–4), 371–392. https://doi.org/10.1351/pac196511030371.

[62] Chevalier, Q.; Gallé, J.-B.; Wasser, N.; Mazan, V.; Villette, C.; Mutterer, J.; Elustondo, M. M.; Girard, N.; Elhabiri, M.; Schaller, H.; Hemmerlin, A.; Vonthron-Sénécheau, C. Unravelling the Puzzle of Anthranoid Metabolism in Living Plant Cells Using Spectral Imaging Coupled to Mass Spectrometry. *Metabolites* **2021**, *11* (9), 571. https://doi.org/10.3390/metabo11090571.

[63] Neikirk, K.; Marshall, A. G.; Kula, B.; Smith, N.; LeBlanc, S.; Hinton, A. MitoTracker: A Useful Tool in Need of Better Alternatives. *European Journal of Cell Biology* **2023**, *102* (4), 151371. https://doi.org/10.1016/j.ejcb.2023.151371.

[64] Kholmukhamedov, A.; Schwartz, J.M.; Lemasters, J.J. MitoTracker Probes and Mitochondrial Membrane Potential. Shock, 2013, 39 (6) 543. https://doi.org/10.1097/SHK.0b013e318292300d

1.1.3 Les points importants de l'article 3

- **Développement de sondes fluorescentes cliquables :** Une nouvelle série de fluorophores azoturés, basés sur des ions flavylium rigidifiés, a été développée via une méthodologie de criblage par lecteur de plaque absorption/émission afin de sélectionner les meilleurs candidats. Ces sondes disposent de chaînes PEG de longueur différente, leur permettant ainsi de participer à des réactions bioorthogonales clique sans altérer leurs propriétés de fluorescence.
- **Propriétés photophysiques :** Ces sondes possèdent d'excellentes propriétés photophysiques, dues à un transfert de charge intramoléculaire important entre le groupement amino électrodonneur et le pyrilium central électroattracteur. Cela se traduit par de fortes brillances, une bonne photostabilité, une solubilité aqueuse élevée et une émission dans le proche rouge-PIR.
- **Influence de la longueur de la chaîne PEG :** La longueur de la chaîne PEG (PEG-1, PEG-2 ou PEG-3) n'affecte pas les propriétés du fluorophore azoturé, offrant ainsi de nombreuses possibilités d'application sans compromettre les performances du fluorophore.
- **Caractéristiques des sondes produites à pH 7,41 (0.1 M NaCl) :** Flavylium-PEG-1 (**F1**) (λ_{em} = 633 nm, Φ = 23,6%); Flavylium-PEG-2 (**F2**) (λ_{em} = 638 nm, Φ = 30,4%); Flavylium-PEG-3 (**F3**) (λ_{em} = 634 nm, Φ = 26,5%).
- **Compatibilité bioorthogonale :** Ces sondes ont été conçues pour être compatibles avec la chimie bioorthogonale, démontrant des réactions efficaces avec les phytostérols alcynes. Elles sont ainsi parfaitement adaptées à des applications avancées en bioimagerie, notamment pour suivre des processus biologiques complexes. Des mesures d'imagerie de fluorescence par fluorescence SImaging avec des cellules de tabac BY-2 montrent leur efficacité de pénétration, de marquage et de stabilité.

1.2 Développement de système flavylium-bMDs et étude de leurs propriétés physicochimiques

1.2.1 Introduction

En continuité avec l'étude précédente, nous avons appliqué la stratégie bioorthogonale sur nos composés bioactifs bMDs pour explorer leurs cibles biologiques dans les globules rouges parasités par *P. falciparum*. L'objectif initial était d'utiliser directement les flavylium-PEG cliquables avec la sonde bMD-alcyne (sonde **4**, IC_{50} = 49 nM, *Pf*NF54), décrites dans le chapitre 2 de cette thèse, dans le cadre d'une stratégie d'imagerie par fluorescence de la réaction CuAAC.

Nous avons donc envoyé la sonde **F2** (chaine PEG-2) à nos collaborateurs biologistes, les Drs. Sébastien Besteiro (UMR5294 CNRS-Université de Montpellier) et Stéphanie A. Blandin (U1257/UPR9022, INSERM-CNRS-Université de Strasbourg), pour l'incorporer dans leurs études des cibles biologiques des bMDs chez, respectivement, les parasites *T. gondii* et *P. falciparum* (voir chapitre 2, article 2). Cependant, malgré quelques essais de réaction clique CuAAC sur cellules fixées parasitées (*T. gondii*), le marquage ne semblait pas spécifique et aucune fluorescence n'a pu être obtenue. En conséquence, par faute de temps pour optimiser les conditions, le marquage bioorthogonale a été réalisé dans cet article en utilisant des kits commerciaux (Alexa Fluor 488 Azide) utilisés en routine par l'équipe du Dr Besteiro pour obtenir des résultats interprétables chez *T. gondii*. Par faute de temps, nous n'avons donc pas pu approfondir l'étude de la réponse du système flavylium-bMD.

Dans l'introduction de cette thèse et dans l'article 3, nous avions démontré que les flavyliums azoturés ou non pouvaient être efficacement internalisés, respectivement, dans les globules rouges infectés par le parasite *P. falciparum* et les cellules de tabac BY-2, ce qui élimine les potentiels problèmes de perméabilité ou de solubilité. De plus, toutes nos sondes flavyliums azoturés sont actives sur *P. falciparum* (voir article 4), ce qui les rend potentiellement applicables dans cette stratégie. La difficulté rencontrée avec la réaction CuAAC pourrait donc être attribuée à une inhibition par transfert d'électron photoinduit PeT entre le flavylium (donneur d'électrons) et le bMD (accepteur d'électrons). La forme oxydée du bMD prédominante au sein du globule rouge parasité, pourrait entrainer un effet PeT conduisant à une inhibition de la fluorescence de l'ion flavylium (fluorescence-OFF), expliquant ainsi les difficultés rencontrées. Une étude en conditions réductrices ou avec différentes longueurs de chaines (PEG-1 et PEG-3) aurait pu permettre une meilleure compréhension de ces phénomènes. Cet aspect sera considéré dans le futur par mon équipe d'accueil.

Néanmoins, nous avons valorisé nos fluorophores flavyliums en les combinant avec les sondes bMDs développées. Plusieurs systèmes flavylium-bMD ont été obtenus et analysés

par des approches photophysiques, électrochimiques et théoriques (collaboration avec le Dr. Denis Jacquemin, Université de Nantes). Ainsi, dans l'article 4, les processus photophysiques et physicochimiques entre le flavylium (chromophore) et le bMD (électrophore), combinés grâce à des outils de la chimie clique, seront discutés en détail.

Un sous-projet a été également développé pour atteindre les mêmes objectifs visés dans ce chapitre, à savoir sonder les bMDs dans le parasite et valoriser nos fluorophores flavyliums. Ce projet repose sur la réaction SPAAC impliquant les sondes bMDs azotures décrites dans le chapitre 2 et une sonde flavylium rigide portant un alcyne contraint. Ce choix a été motivé par plusieurs raisons : un alcyne contraint fonctionnalisable (DBCO-acide) était disponible en quantité appréciable (collaboration passée) ; la SPAAC, ne nécessitant pas de catalyse au cuivre(I), offre une meilleure biocompatibilité, ce qui pourrait améliorer la résolution et la précision des résultats en imagerie par fluorescence ; des sondes bMDs azotures actives sur *P. falciparum* (sonde **13**, IC_{50} = 32 nM et sonde **16**, IC_{50} = 151 nM, *Pf*NF54) ont été développées ; enfin, la réponse fluorescente devrait différer de celle observée avec la stratégie CuAAC du fait d'un éloignement accrue de la sonde fluorescente flavylium de son partenaire bMD diminuant les processus PeT pouvant s'opérer.

Nous avons donc synthétisé une sonde flavylium portant en position terminale un alcyne contraint DBCO. Le modèle flavylium fonctionnalisé avec une diéthylamine en position 7 et un espaceur PEG-2 en position 4' ont été conservés afin d'avoir les meilleurs propriétés photophysiques. La synthèse a débuté par la formation de l'α-tétralone-PEG-2-amine **29** en 3 étapes, suivie d'une condensation acide pour obtenir le flavylium amine **30**. Enfin, une amidification avec le DBCO-acide a conduit à la formation de la sonde **F2-DBCO** avec un rendement global de 25% sur cinq étapes (Figure 30).

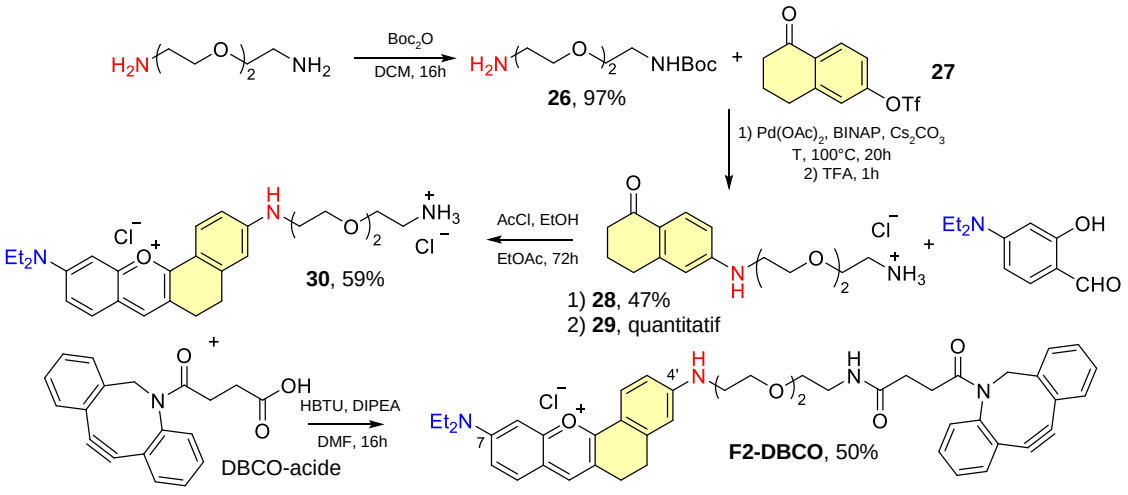

Figure 30: Synthèse de la sonde flavylium-PEG-2-DBCO **F2-DBCO** cliquable par SPAAC. Les conditions de synthèse des différents intermédiaires et produits sont disponibles dans la partie expérimentale de ce manuscrit.

D'un point de vue des propriétés photophysiques, cette sonde est similaire aux flavyliums azoturés présentés dans l'article 3 (λ_{em} = 633 nm, Φ = 26%, pH 6,9). De plus, la sonde **30** aminée pourrait être valorisée et fonctionnalisée avec d'autres systèmes (sondes duales…), car ses propriétés optiques sont également intéressantes (λ_{em} = 633 nm, Φ = 22%, pH 7,41). Ces résultats indiquent que l'ajout du DBCO-acide ne modifie pas les propriétés photophysiques du chromophore, bien qui sa solubilité soit affectée par l'ajout du DBCO-acide à caractère hydrophobe. Étant donné que la distance entre le chromophore et l'électrophore (espaceur + DBCO) est plus importante, la fluorescence après réaction clique avec une sonde bMD-azoture ne devrait pas être inhibée significativement par effet PeT. En outre, cette sonde est active sur le parasite *P. falciparum* (IC_{50} = 506 nM *Pf*NF54) et devrait pouvoir être internalisée dans le parasite. En conclusion, la sonde **F2-DBCO** pourrait être valorisée à l'avenir en combinaison avec les bMD-azotures ou d'autres azotures, pour développer une application en imagerie cellulaire. Celle-ci sera par exemple prochainement utilisée avec nos collègues spécialisés en biologie moléculaire des plantes avec des phytostérols azotures.

1.2.2 Article 4

Click coupling of flavylium dyes with plasmodione analogues: Towards new redox-sensitive pro-fluorophores

Baptiste Dupouy, Leandro Cotos-Munoz, Annika Binder, Lucie Borkova, Matthias Rottmann, Pascal Mäser, Denis Jacquemin, Markus Ganter, Elisabeth Davioud-Charvet, and Mourad Elhabiri

Chemistry-A European Journal **submitted article,** soumis le 4 Octobre 2024

Click coupling of flavylium dyes with plasmodione analogues: Towards new redox-sensitive pro-fluorophores

Baptiste Dupouy,[a] Leandro Cotos-Munoz,[a] Annika Binder,[b] Lucie Borkova,[a] Matthias Rottmann,[c] Pascal Mäser,[c,d] Denis Jacquemin,[e,f] Markus Ganter,[b] Elisabeth Davioud-Charvet,[a] and Mourad Elhabiri[a]*

[a] Université de Strasbourg, Université de Haute-Alsace, CNRS, , UMR 7042, Laboratoire d'Innovation Moléculaire et Applications (LIMA), Equipe Chimie Bio(IN)organique et Médicinale, ECPM, 25 Rue Becquerel, 67000 Strasbourg, France

[b] Heidelberg University, Medical Faculty, Centre for Infectious Diseases, Im Neuenheimer Feld 324/344, 69120 Heidelberg, Germany

[c] Swiss Tropical and Public Health Institute, Kreuzstrasse 2, CH-4123 Allschwil, Switzerland.

[d] University of Basel, Petersgraben 1, CH-4001 Basel, Switzerland.

[e] Nantes Université, CNRS, CEISAM, F- 44000 Nantes, France

[f] Institut Universitaire de France (IUF), F-75005 Paris, France

Email: Mourad Elhabiri (elhabiri@unistra.fr)

Abstract

The development of redox-sensitive molecular fluorescent probes for the detection of redox changes in *Plasmodium falciparum*-parasitized red blood cells remains of interest due to the limitations of current genetically encoded probes. This study describes the design, screening and synthesis of new pro-fluorophores based on flavylium azido dyes coupled by CuAAC click chemistry to alkynyl analogues of plasmodione oxide, the key metabolite of the potent redox-active antimalarial plasmodione. The photophysical and electrochemical properties of these probes were evaluated, focusing on their fluorogenic responses. The influence of both the redox status of the quinone and the length of the PEG chain (PEG1-3) separating the fluorophore from the electrophore on the photophysical properties was also investigated. The fluorescence quenching by photoinduced electron transfer is reversible and of high amplitude for probes in oxidized quinone forms and fluorescence is reinstated for reduced hydroquinone forms. Our results also demonstrate that shortening the PEG chain has the effect of enhancing the fluorogenic response, most likely due to non-covalent interactions between the two chromophores. All these systems were evaluated for their antiparasitic activities and a preliminary fluorescence imaging approach allowed demonstrating the efficacy of the fluorescent flavylium dyes in *P. falciparum* parasitized red blood cells, paving the way for future parasite imaging studies to monitor cellular redox processes.

Introduction

Despite the critical influence of redox environment on key parasitic events (e.g. hemoglobin digestion, heme crystallization, drug partitioning, resistance, and oxidative stress), redox mapping of *Plasmodium falciparum* -parasitized red blood cells (*p*RBCs) still remains difficult, [1,2] and small-molecule redox probes extremely limited. [3] Progress has been made with genetically-encoded redox probes derived from green fluorescent protein (GFP), such as, redox-sensitive yellow FP - rxYFP, redox-sensitive GFPs roGFPs, and HyPer. [4-6] These have been successfully employed for measurement of the glutathione redox potential in the parasite cytosol [7-9] but are, however, not suited for redox measurements under acidic conditions. [10] Such genetically-encoded probes for redox mapping of *P. falciparum* parasites are furthermore difficult to handle due to the time and resources needed for their construction, and display limitations, e.g. blue/green/yellow fluorescence; red FPs mainly based on sea organisms; [11] no two photons absorption (TPA) properties excepted for proteins with λ^{em} > 600 nm; no post-functionalization possible... The search for novel small-molecule probes for *in situ* real-time monitoring thus remains of paramount importance to get further insight into the mechanism of action (MoA) of current and ongoing antimalarial drugs and for producing reliable data with regard to candidate parameters contributing to drug resistance. The low and transient physiological concentrations of most RONS (reactive oxygen and nitrogen species) [12,13] indeed require selective, rapid, and reversible detection strategies, with the development of bright fluorophores allowing detection across a broad spectrum of wavelengths (visible-red-NIR). Such fluorophores should also benefit from substantial Stokes shifts and possess tunable electrochemical properties to span the whole range of biologically relevant redox potentials. In addition to these constraints, good solubility in water, biological compatibility (i.e., membrane permeability, subcellular localization, no cytotoxicity, no alteration of the cellular redox homeostasis, low protein interference), specificity for the target organelle are several essential parameters to be considered. [14]

Many fluorescent systems have been described for the detection of redox processes, [12,15-18] but they are very often based on irreversible or reaction-based interactions between RONS and the probe, thus precluding accurate assessments of redox changes and intracellular fluctuations (e.g. chronic high or transient levels of RONS). [19-21] Reversible probes [22] overcome this limitation and allow the monitoring of temporal changes in the redox state of living cells. Several reviews [23-25] provide a complete overview of the reversible [26] redox probes available to date. The strategy commonly used to obtain such fluorescent redox probes consists of using electrophores (e.g. molecular scaffolds or metal complexes, Scheme 1), [27] whose response to an (electro)chemical stimulus is reversible (e.g. nitroxyl radicals, [16] quinone/hydroquinone, [28] chalcogen-based derivatives with sulphur, selenium or tellurium, [16,29] flavins, tetrathiafulvalenes…) and whose redox state can alter the fluorescence of a covalently linked fluorescent unit, typically through Photoinduced electron Transfer (PeT).

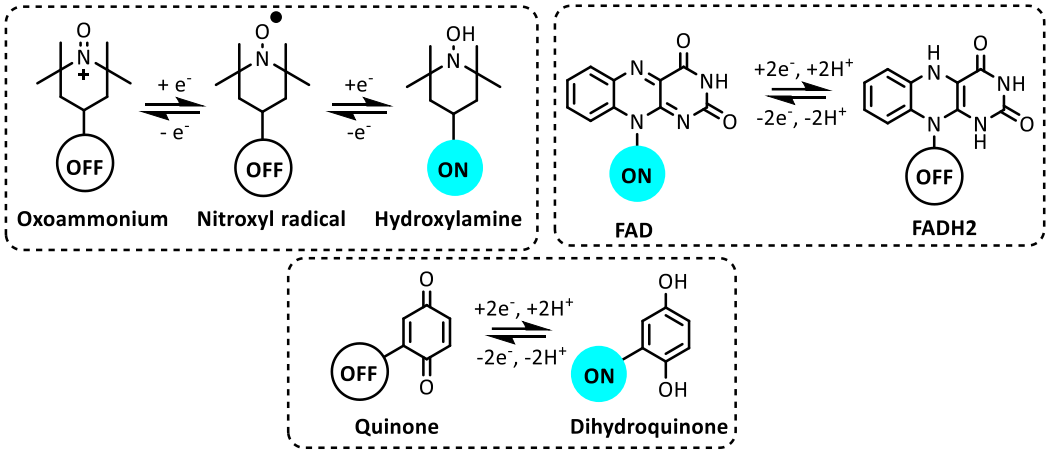

Scheme 1. Reversible redox-sensitive units commonly reported and used to construct redox-responsive fluorescent probes for biological applications.

Other redox-responsive systems with intrinsic adjustable fluorescence properties (ON-OFF or ratiometric systems) depending on their oxidation state and allowing a reversible reaction can also be mentioned; blue-emitting resazurin/pink-emitting resorufin/non fluorescent dihydroresorufin, [30] blue-emitting dihydroethidine/red-emitting ethidium, [31] red-NIR-emitting methylene blue/non fluorescent leucomethylene, [32] …

With particular reference to fluorescent redox probes based on hydroquinone/quinone pair, Scheme 2 provides an overview of the photophysical properties, photoinduced mechanism and efficiency of different systems described so far. Most of the systems described are based on quinones conjugated or fused to fluorescent dyes such as Ru(bipy), BODIPY, rhodamine, triazine or cyanine complexes. Quinones coupled to fluorophores via a spacer are less common examples and no approach has been described to evaluate the effect of the length of the spacer (e.g. PEG-type). For example, the red luminescent compounds $[Ru(bipy)_2(bipy\text{-}Q)]^2$ [33] and $[Ru(bpy)^2(PAIDH)]^{2+}$ [34], based on a Ru(II) center, yield a 4-fold (luminescence spectra of the isolated compounds) and 600-fold (luminescence spectra obtained by exhaustive electrolysis) increase, respectively, after reduction of the quinone moiety. However, these systems are characterized by low quantum yields in degassed solution and have not been applied to biological systems. Redox-responsive fluorescent probes were also designed using a BODIPY reporting scaffold as exemplified by BD-PHQ [35] (110-fold increase upon reduction with 1.1 M sodium ascorbate in 5% v/v Triton–X/H_2O) or H2B-QH2 [36] (200-fold increase upon reduction with $NaBH_4$). To the very best of our knowledge, none of these two models was applied in a biological system. Of interest is a related aza-BODIPY [37] coupled to an *ortho*-quinone whose redox-response was achieved by pH variation (oxidation under basic conditions and reversible reduction at acidic pH). Hydroquinones are indeed known to undergo autoxidation under basic conditions. [41] This aza-BODIPY was successfully used to monitor extracellular pH difference between normal tissue and tumor both *in vitro* U87 glioma and *in vivo* breast cancer in mice. Also worth mentioning is the reversible photoacoustic probe, BDP-DOH, based on a BODIPY reporter and a quinone sensor, which has been used to image the local redox state *in vivo* by monitoring dynamic changes in the redox couple, superoxide anion ($O_2^{\bullet-}$) and glutathione (GSH). [38] Also, in the BODIPY field, the engineered compound FerriBRIGHT [39] is one of rare compounds (with TCAO and PY-CAO, *vide infra*) in which the oxidized

quinone form is fluorescent while the reduced hydroquinone state undergoes a PeT quenching. When combined with a cyanine fluorophore, the dopamine-based DA-Cy [40] compound undergoes a 20-fold decrease in fluorescence during oxidation, a process that is irreversibly reversed by the addition of thiols. This system was implemented in living HL-7702 cells and fresh rat hippocampus tissues to image H_2O_2 oxidation and thiols reduction processes. Similarly, a related water-soluble cyanine dye [41] has been described as able to reversibly respond to oxidation ($NaIO_4$) or reduction (GSH, 16-fold increase) reactions. In particular, for bioreductants such as GSH, cysteine or ascorbate, the emission centered at 660 nm was restored in short times (~ 30 s). This system has been applied to image living cells (A549 and J774.1). As additional examples, the 1,4-benzoquinone/rhodamine-based probe (Rh-Q) [42] and its related analogues also act as fluorogenic probes and were shown to undergo a 6-fold fluorescence quenching upon oxidation with excess of $[Cu(phen)_2]^{2+}$, which can be rapidly reversed by the addition of cysteine. This probe was readily internalized by HeLa living cells and predominates in the form of hydroquinone due to the reducing milieu. However, these probes were difficult to be oxidized *in vitro* either by $[Cu(phen)_2]^{2+}$ or after permeabilization with saponine followed by addition of H_2O_2 and horseradish peroxidase. Of interest is also the quinone-triazine (TCA) probe that can respond to one (1P) or two-photon (2P) excitation. Oxidation by $O_2^{\bullet-}$ generates TCAO that displays 1000- and 3-fold greater fluorescence emission upon 1P and 2P excitation, respectively. TCAO was reversibly reduced to TCA by GSH [43] and this dye was successfully used in dual-mode fluorescence imaging for tracking $O_2^{\bullet-}$ fluctuations in hepatocytes, zebrafish and mice during mimicked ischemia-reperfusion injury. Similar to TCAO, the 1P and 2P PY-CA [44] fluorogenic probe is also oxidatively turned on with $O_2^{\bullet-}$ (1000-fold greater fluorescence emission upon 1P excitation) and quenched by GSH. The oxidized PY-CAO has been used for imaging of $O_2^{\bullet-}$ levels in 4T1 cells, in a mouse tumor tissue and in wild-type *Caenorhabditis elegans* worms. Finally, to complete this non-exhaustive survey, naphtho[2,3-c]pyran-5,10-dione was used for developing fluorescent redox probes. [45] While the oxidized form is not fluorescent, reduction with $NaBH_4$ afforded a red fluorescent (Φ = 0.07) hydroquinone when substituted with *N,N*-dimethylaminophenyl. A highly reversible ON/OFF push-pull system was developed by combining a fluorescent dansyl moiety with a phenyl-carbazoloquinone redox sensor via an NH bridge. [46] Neither of these last two examples has been used in a biological investigation.

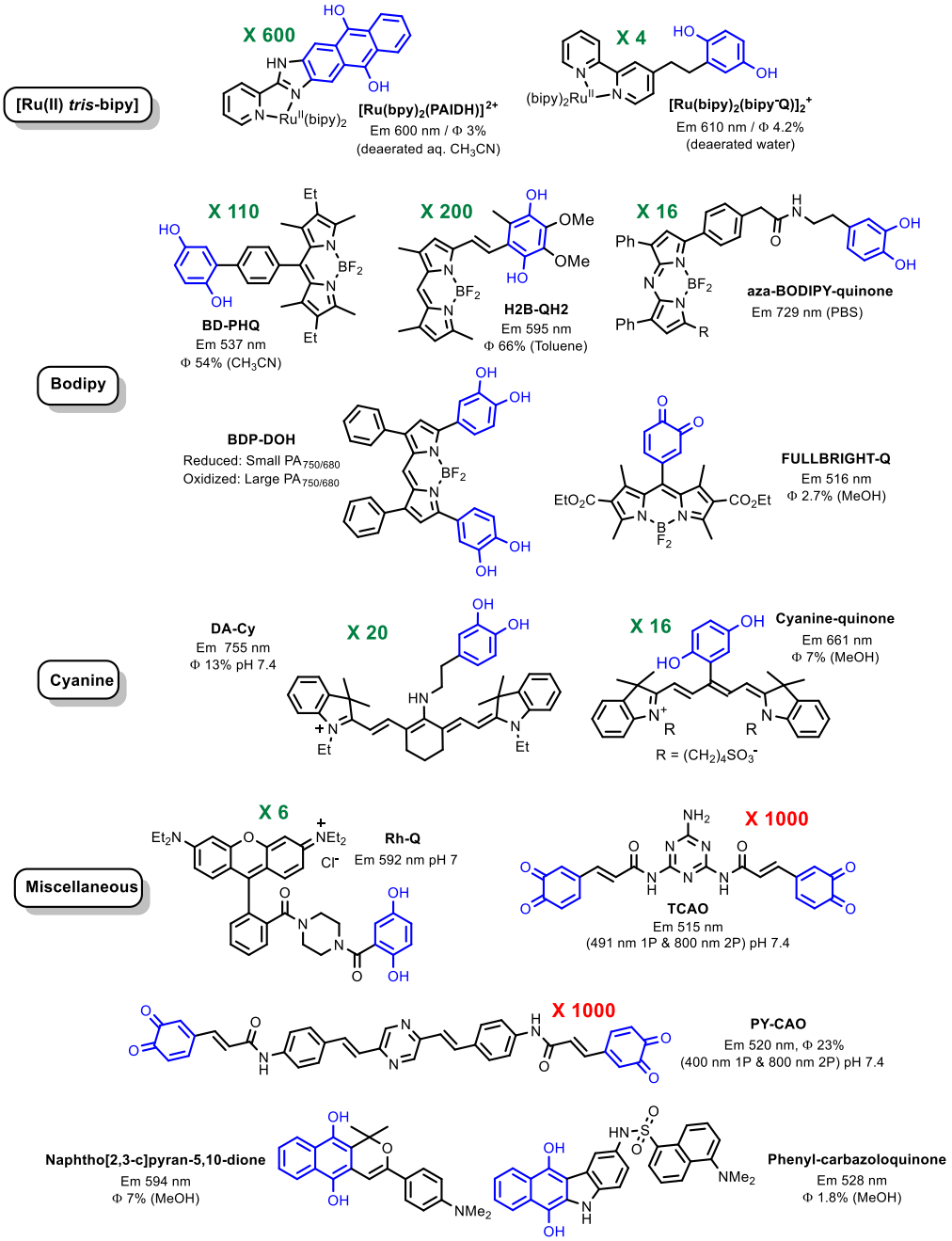

Scheme 2. Chemical structures and photophysical properties of fluorescent redox probes based on hydroquinone/quinone pair (red: increased fluorescence upon oxidation; green: increased fluorescence upon reduction).

Our team has recently developed lab-made fluorescent tools derived from flavylium ions whose properties and chemical structure can be tailored to the desired applications. [47] Using straightforward synthetic routes, bright, water-soluble and photostable azide dyes were accessible at the 100 mg scale thus allowing the preparation, characterization and investigation of the click adducts with alkynyl-3-benzoylmenadiones (benzoyl-MD alkyne), a series of redox-active derivatives recently developed as photoaffinity labeling agents – upon (photo)reduction – for activity-based protein profiling ABPP. [48,49] Of note, the parent 3-benzylmenadiones, represented by the most potent antiplasmodial agent called plasmodione (**PD**), display potent antimalarial activities.

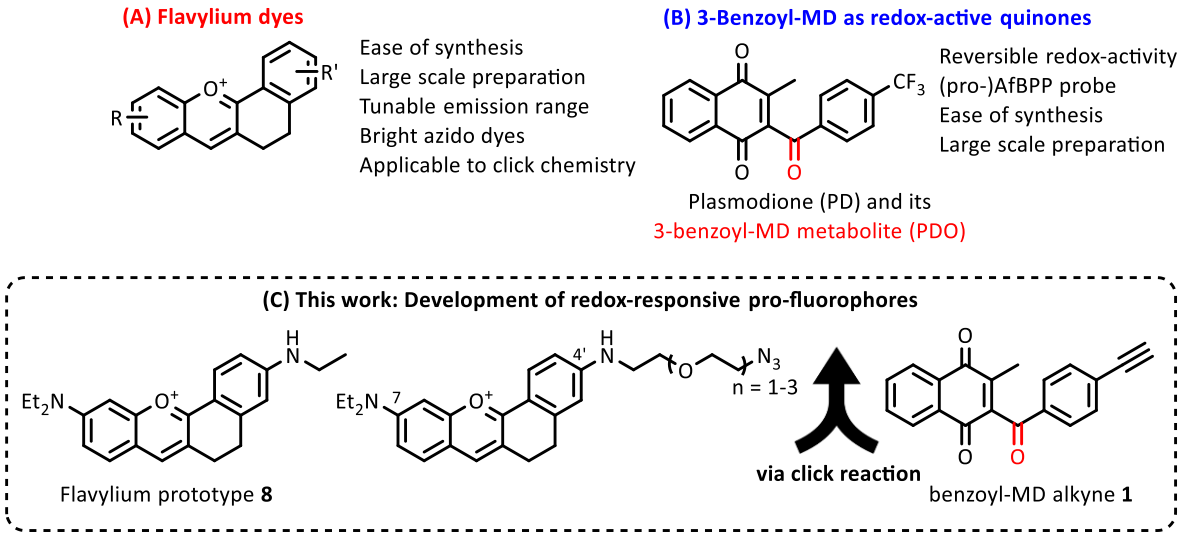

Scheme 3. Chemical structures of the tools investigated in this work and main objectives.

Following a preliminary study, we observed that the adducts clicked with the benzoyl-MD alkynes were almost fully quenched compared to the flavylium PEG-azide fluorophore (Scheme 3) likely due to a PeT process, while under their protected state (i.e. 1,4-dimethoxy-naphthalene core), no fluorescence quenching was observed. Following this observation, we thus postulated that the reduced species might display the same redox properties as the protected benzoyl-MD, allowing an OFF-ON fluorogenic property in response to an enzymatic reduction. In this work, we report on the design and selection of fluorescent probes and click adducts, their synthesis and detailed photophysical and electrochemical characterization. The influence of the length of the PEG chain on the fluorogenic response was also investigated. Finally, fluorescence of flavylium dyes was visualized in living *p*RBCs to demonstrate their effective penetration, paving the way for future imaging approaches to measure redox processes within *p*RBCs.

Results and Discussion

Screening approach. In our previous study, [47] we developed azide fluorophores based on rigid flavylium dyes connected to a terminal azide function separated by a variable-length PEG chain. We were able to reach bright compounds emitting in the red-NIR domain and demonstrated that the length of the PEG chain (1 to 3 monomers) had no influence on the photophysical properties of the dye. Interestingly, the CuAAC cycloaddition of a benzoyl-MD with one of those containing a PEG-2 chain showed a strong quenching of the fluorescence emission of the dye (*vide infra*) suggesting that photoinduced processes occurred within the hybrid molecule. To deepen our understanding, we carried out a simple screening by absorption/emission plate reading with the PEG-2 analogue so as to pinpoint the best substitution pattern for achieving both the highest brightness and the largest response amplitudes upon click reaction with the benzoyl-MD alkyne **1** ([49], under the same compound code). Since the fluorophore can be generated in a final step by condensation in an acidic medium ($EtOH/H_2SO_4$), the previously described tetralone-PEG-2-azide (**2**) [47] intermediate was first subjected to a CuAAC-type cycloaddition reaction with benzoyl-MD alkyne (**1**) and its reduced analogue protected as a 1,4-dimethoxy-naphthalene (**10**) ([49], under the same compound code) (Scheme 4). A first

screening carried out with 15 different salicylaldehydes allowed comparing the flavylium-PEG-2-azide dyes with their derivative clicked to **1**, and thus assessing the impact of the incorporation of a benzoyl-MD alkyne by CuAAC on the fluorescence emission properties of the dye (Figures S1-S17 in the ESI). Optical measurements and comparisons between the different systems can be indeed made without the need for purification, as the visible absorption and fluorescence signal is generated by the newly formed flavylium moiety. The emission spectra were normalized to the absorbance at the excitation wavelength to allow direct comparison of all dyes generated in the wells (Scheme 4).

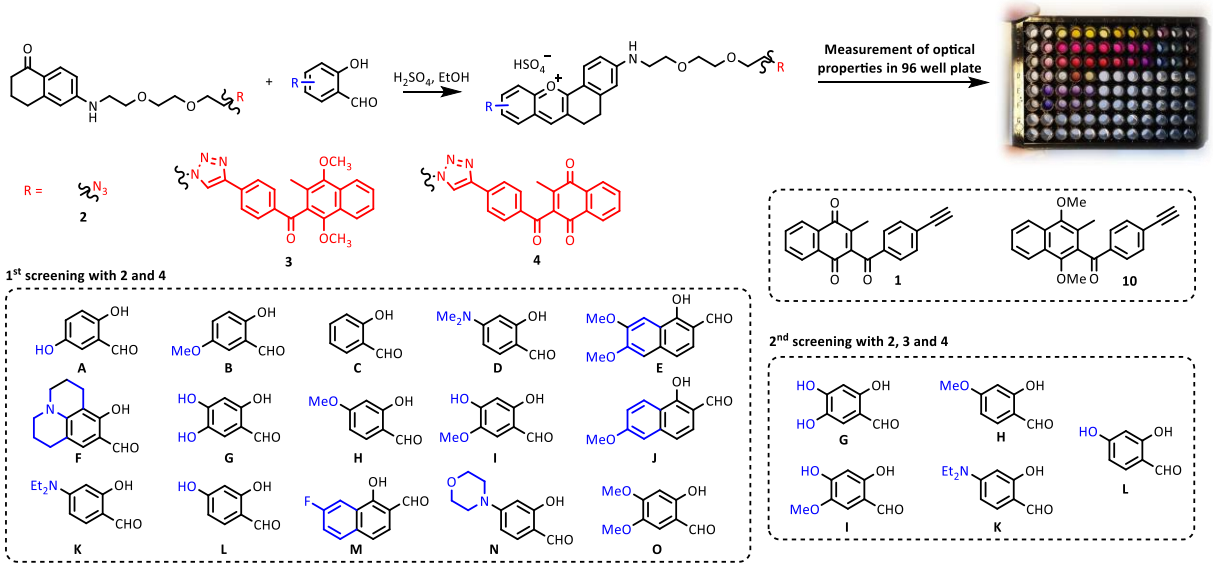

Scheme 4. Screening (by absorption and emission) of PEG-2 dyes by varying the substitution of the dye using 15 salicylaldehyde derivatives and the substitution of the PEG using **2**, **3** and **4**.

Comparison of the spectroscopic data (Table 3) provided interesting information. The incorporation of a benzoyl-MD unit by click chemistry always leads to a quenching of the fluorescence emission (at least half the emission of flavylium PEG azide). Flavylium dyes with alkylamino (**D**, **K** and **N**) or dimethoxy (**O**) substitutions, which act as electron donor groups (EDG), showed the strongest quenching effects. The same dyes, among some others (**D**, **G**, **I**, **K**, **N** and **O**, Table 3), are also the brightest compounds in their free azido form. The incorporation of a benzoyl-MD moiety by click chemistry therefore results in a significant extinction of the emission intensity of the dye but does not alter markedly its position or shape, suggesting the absence of direct interactions in the excited state between the two chromophores (i.e. the flavylium and benzoyl-MD core). Similarly, no significant change in the absorption spectra was observed hinting that there is no precipitation or π-π stacking. Last, extending the π-electron delocalization with an additional phenyl ring (salicylaldehydes **E**, **J** and **M**) does not specifically modify the emission wavelength of the flavylium ion and results in dyes of lowest brightness (Table 3).

Table 3. Photophysical data recorded for the flavylium adducts generated in the wells by reaction of **2**, **3** and **4** with salicylaldehydes **A-O** in ethanol with excess of sulfuric acid.

	Adducts (with 2)			**Adducts (with 4)**	**Adducts (with 3)**
Aldehyde	**λ_{abs}** (nm)	**λ_{em}** (nm)	**Fluo intensity** (x10^2 ua)	**Fluo. Int. *vs* adducts**	**Fluo. Int. *vs* adducts**

				(2)	(2)
A	531/557sh	598/646	6.6	x 0.48	
B	530/557sh	596/646	7.8	x 0.45	
C	518	587/633/689	5.3	x 0.48	
D	583	635	**28.1**	x 0.13	
E	555/578sh	615/669	5.6	x 0.43	
F	579/615sh	654	10.3	x 0.31	
G	561	604/649	**26.1**	x 0.36	x 1.22
H	535sh/554	594/636	14.2	x 0.5	x 1.79
I	560	603/647	**23.2**	x 0.34	x 1.01
J	580/554sh	619/670	5.6	x 0.45	
K	605	638	**71.7**	**x 0.20**	**x 1.04**
L	535sh/556	595/636	11.1	x 0.37	x 1.53
M	543	613/663	2.6	x 0.56	
N	587	635	**35.0**	**x 0.20**	
O	560	605/649	**20.6**	**x 0.25**	

Errors on quantum yields, λ^{abs} and λ^{em} are estimated to be $\pm$ 2 nm.

A second screening experiment using absorption/emission plate reading was performed using only five selected salicylaldehydes (**G**, **H**, **I**, **K** and **L**) and the tetralones **2** and **3** (Scheme 4 and Figures S17-S21 in the ESI). Compound **3** was obtained by CuAAC reaction between **2** and **10**, which is the reduced form of **1** protected by methyl group to prevent the spontaneous oxidation of the dihydroquinone into the quinone moiety. This chemical modification results in benzoyl-MDs that are much less oxidizing (*vide infra*) and more electron-rich. Interestingly, no fluorescence quenching was observed when **3** was used demonstrating that the electronic poorness (oxidized benzoyl-MD, **1**) or richness (reduced benzoyl-MD, **10**) of the naphthoquinone is critical for quenching the emission of the combined fluorophore. These results thus suggest that PeT can take place between the flavylium dye, acting as an electron donor, and the benzoyl-MD in its oxidized form, an electron acceptor. Upon reduction, the electron quinone acceptor becomes less oxidizing, as only the ketone of the benzoyl moiety can be reduced (*vide infra*). This renders the PeT process thermodynamically not favored and thus does not alter the emission of the fluorophore. Absorption and emission measurements confirmed that salicylaldehyde **K** was the best compromise, with high brightness and quenching amplitude in the presence of the oxidized benzoyl-MD.

Synthesis. We synthesized the hybrid molecules using salicylaldehyde **K** and the alkynes derived from oxidized benzoyl-MD **1** and the reduced/protected benzoyl-MD **10**. Furthermore, we investigated how the length of the PEG spacer linking the flavylium to the redox-active moiety (the benzoyl-MD) affects the optical properties of the click adducts. Three PEG spacer lengths were selected: short (n = 1), intermediate (n = 2) and long (n = 3). Following the screening approach (*vide supra*), we were able to assess the best decoration for the optimized optical properties of the flavylium fluorophore using salicylaldehyde **K**. Flavylium azide dyes containing a short (**F1**, n = 1) or intermediate (**F2**, n = 2) PEG chain have already been described in another work. [47] The preparation of compounds **1** and **10** has also been described previously. [49]

First, **F1** was clicked with **10** and **1** in acetonitrile in the presence of $Cu(CH_3CN)_4(BF_4)$ and bathocuproin to afford compounds **F1-10** and **F1-1**, respectively, in good yields (Scheme 5). Following this approach, **F2-1** containing a PEG-2 chain was prepared from **F2** and **1** using the same experimental conditions. Alternatively, we have also demonstrated that **F2-1** can be synthesized by first a CuAAC reaction of the α-tetralone functionalized in position 6 by a PEG-2-azide moiety (**2**) with the benzoyl-MD alkyne **1** to give the click α-tetralone **3** in excellent yields. Acid condensation (HCl gas generated *in situ* by reaction of acetyl chloride with ethanol in ethyl acetate) of **3** with salicylaldehyde **K** then afforded **F2-1** in a global 69% yield for the two steps. The same strategy was used to obtain the homologous dye **F2-10** in a two-step process with a total ~ 50 % yield. These two approaches demonstrate the versatility of our synthetic strategy, as the CuAAC reaction can be carried out as either the first or the second step in the proposed synthetic routes. The dyes with the longest PEG chain (n = 3) were obtained from the α-tetralone PEG-3-azide **5** by CuAAC click reaction with the alkynes **10** and **1** followed by acid condensation. These two steps were carried out without purification of the intermediates **6** and **7** to afford the final compounds **F3-10** and **F3-1** in moderate overall yields of 30-40%.

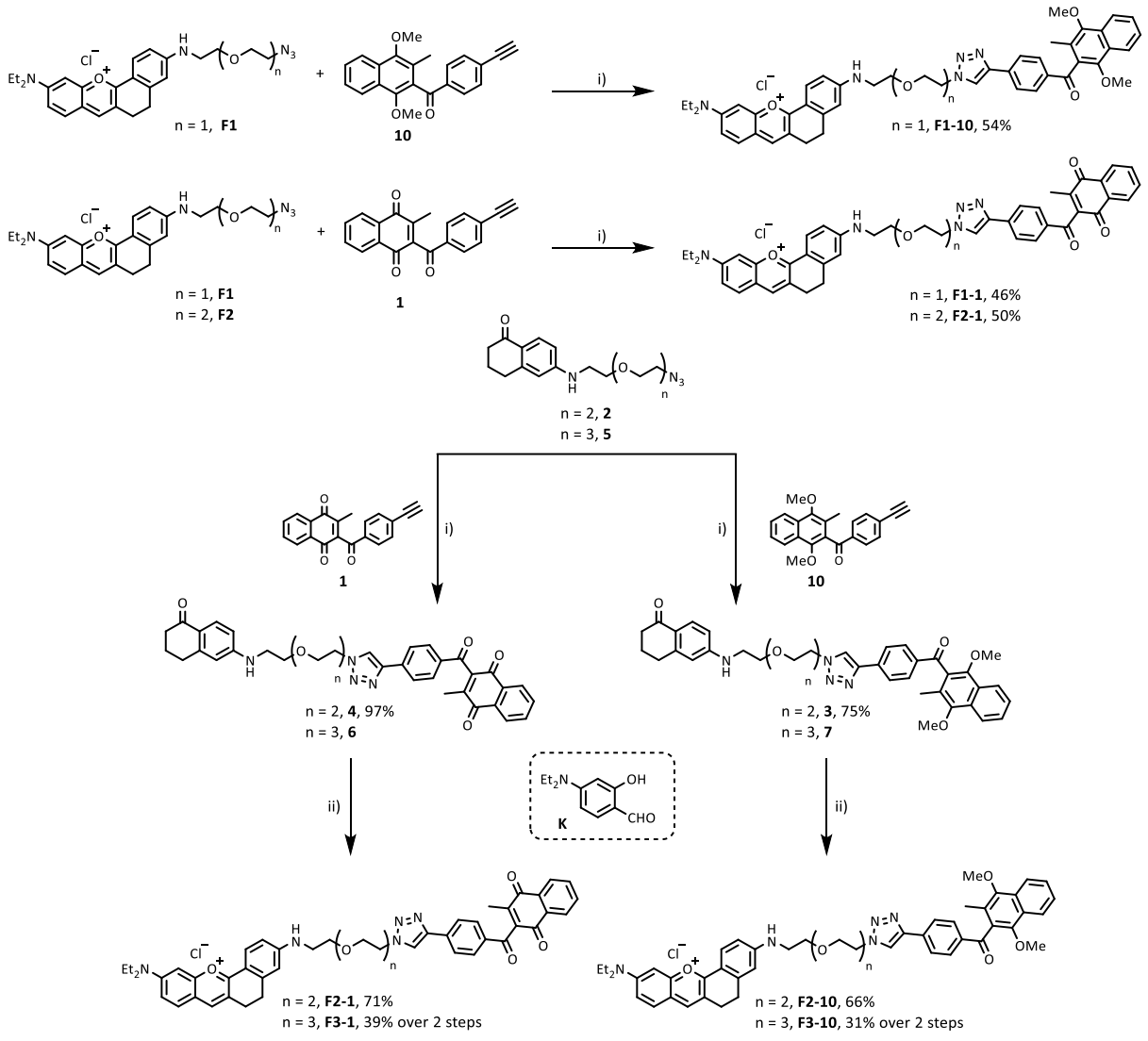

Scheme 5. Synthetic route for the formation of the click adducts with PEG (n = 1, 2 and 3) chains with **10** or **1**. i) bathocuproin, $Cu(MeCN)_4(BF_4)$, MeCN; ii) AcCl, EtOH, EtOAc, 0°C to rt, 72h.

Photophysical properties. A simple screening strategy based on a simple chemical reaction (condensation of a α-tetralone and a salicylaldehyde under acidic conditions) was implemented to generate a library of spectroscopic data (absorption and emission) for almost 40 different combinations. This approach has provided essential information and allowed synthesis efforts to be focused on the most promising derivatives (Scheme 5). A photophysical characterization of the flavylium-PEG-azides has already been carried out in a previous work [47] and has shown high brightness (quantum yields in the range of 25-30%) for the red-NIR emitting systems, without any significant influence of the length of the spacer. One of the advantages of using these clickable flavylium-PEG-azides is their solubility in water due to the cationic nature of the dye and the presence of PEG moieties. However, the synthesized click adducts with the hydrophobic benzoyl-MD **10** or **1** (Scheme 5) showed a significant loss of aqueous solubility (Figure S22 in the ESI). To assess the effect of the presence of the benzoyl-MD (oxidized or reduced/protected states) on the photophysical properties under the best possible conditions, we showed that 15% by volume of DMSO was at least required to reach an appropriate solubility of the click adducts in aqueous buffer (pH 7.41 + 0.1 M NaCl) (Figure S23 in the ESI for **F1-10**). The photophysical data recorded in such conditions as well as in ethanol are given in Table 4 and the corresponding absorption, emission and excitation spectra are available in Figures S24-S32 in the ESI.

Table 4. Photophysical data obtained for the flavylium-PEG-azides and their click adducts with **10** and **1** in buffered aqueous solutions at pH 7.41 containing 0.1 M NaCl and 15% volume of DMSO.

	Compd.	**λ_{abs}** (nm)	**λ_{em}** (nm)	**ε** (x 10^4 $M^{-1}.cm^{-1}$)	**Φ_{abs}** (%)	**Stokes shift** (cm^{-1})	**Brightness** (M^{-1} cm^{-1})	**Cond.**
Ref.	**8**	594	633	3.49	23.0	1040	8000	a[47]
	8	599	638	5.26	28.3	1020	14800	b
PEG-1	**F1**	593	633	4.55	23.6	1070	10400	a[47]
	F1	598	638	5.62	26.3	1050	14800	b
	F1-1	601	633	2.28	1.3	840	300	b
	F1-10	608	639	3.71	23.1	800	8600	b
PEG-2	**F2**	594	636	1.76	22.4	1110	3900	a[47]
	F2	598	638	1.89	30.4	1050	5700	b
	F2-1	605	640	4.37	2.2	900	1000	b
	F2-10	603	639	4.32	30.1	935	13000	b
PEG-3	**F3**	594	634	7.49	26.5	1110	19900	a[47]
	F3	598	637	8.62	27.4	1020	23600	b
	F3-1	604	637	3.63	6.7	860	2400	b

	F3-10	602	639	4.64	29.4	960	13600	b

Experimental Conditions: [a] Aqueous buffer at pH 7.41 (0.1 M NaCl); [b] Aqueous buffer at pH 7.41 (0.1 M NaCl) containing 15% of DMSO by volume. The errors on the quantum yields Φ, the λ_{abs} and λ_{em} are estimated to be ± 10% and ± 1 nm, respectively. Ref. = reference dye **8** lacking PEG and azide unit (Scheme 3).

As already demonstrated, [47] the photophysical data recorded for flavylium-PEG-azides in a water/DMSO (85/15 *v/v*) mixture buffered to pH 7.41 first show that the length of the PEG chain or the addition of DMSO has no significant effect on the emission properties of the fluorophore. These compounds are all characterized by a very bright emission in the red-NIR spectral window. Addition by CuAAC of a benzoyl-MD unit in its oxidized form significantly quenches the emission centered on the flavylium dye, confirming the observations deduced from the screening approach. Reduction of the benzoyl-MD electrophore (in its protected form) did not alter the dye emission, demonstrating that its high electron richness prevented the PeT process. A comparison of the quantum yields of adducts with benzoyl-MD in oxidized and reduced forms shows that the shorter the spacer length, the greater the quenching efficiency. For the system based on the shorter PEG chain (n = 1, **F1-1** *vs.* **F1-10**) a quenching efficiency of almost 95% was measured, whereas for the analogue with a longer PEG chain (n = 3, **F3-1** *vs.* **F3-10**) it was only 75% (Figure 1 and Figure S33 in the ESI). Since this process is intramolecular in our case, this significant quenching is most likely explained by the close distance between the electron donor and electron acceptor, which favors the PeT process and results in an efficient fluorogenic system. Other intramolecular non-covalent interactions can be also proposed (*vide infra*).

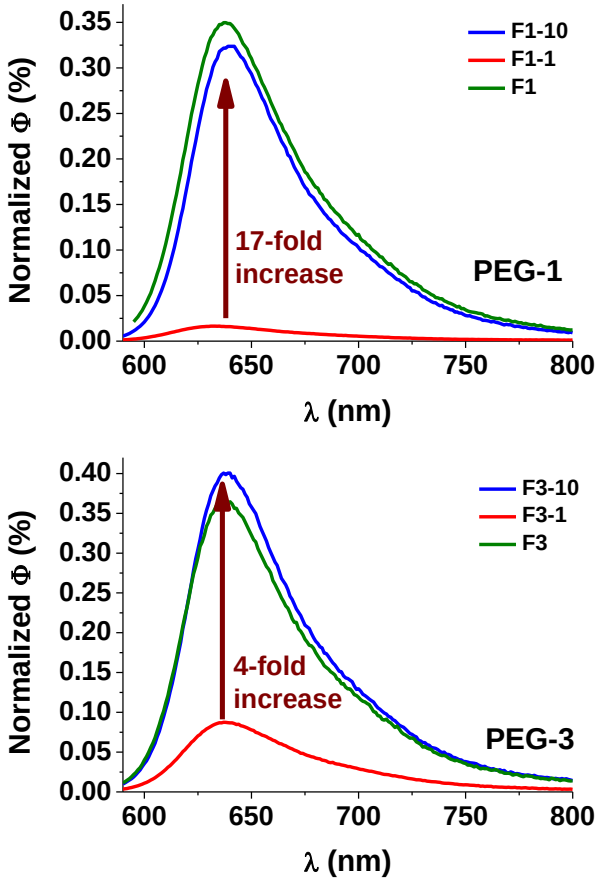

(A) **(B)**

Figure 1. Emission spectra of (**A**) the flavylium-PEG-1 azide **F1** compared to its click analogues with oxidized (**F1-1**) and reduced/protected (**F1-10**) benzoyl-MDs and (**B**) the flavylium-PEG-3 azide **F3** compared to its click analogues with oxidized (**F3-1**) and reduced/protected (**F3-10**) benzoyl-MDs recorded in buffered aqueous solution at pH 7.41 (0.1 M NaCl; 15% volume of DMSO). The emission spectra have been normalized with respect to their quantum yield (area under the curve).

DFT calculations. To ascertain the possibility of PeT with the oxidized benzoyl-MD electrophore, [20] we have performed DFT calculations (see the ESI for details), and the main results are displayed in Figure 2. We have considered the fluorophore and the donor naphthoquinone in both its reduced and oxidized forms. As can be seen, the HOMO of the fluorophore is unsurprisingly the highest, so that after photoexcitation the donor cannot transfer an electron from its HOMO, a statement holding for both the oxidized and reduced forms. However, the LUMO of the dye is significantly above the one of the quinoidal form, allowing PeT (and hence emission quenching) as shown in Figure 2. In the dihydronaphthoquinone structure, such PeT becomes impossible since the LUMO of the donor becomes too high. These results are consistent with experimental observations. Note that we have also considered the di-OMe-donor and the alignment of the molecular orbitals is mostly unchanged as compared to the di-OH structure.

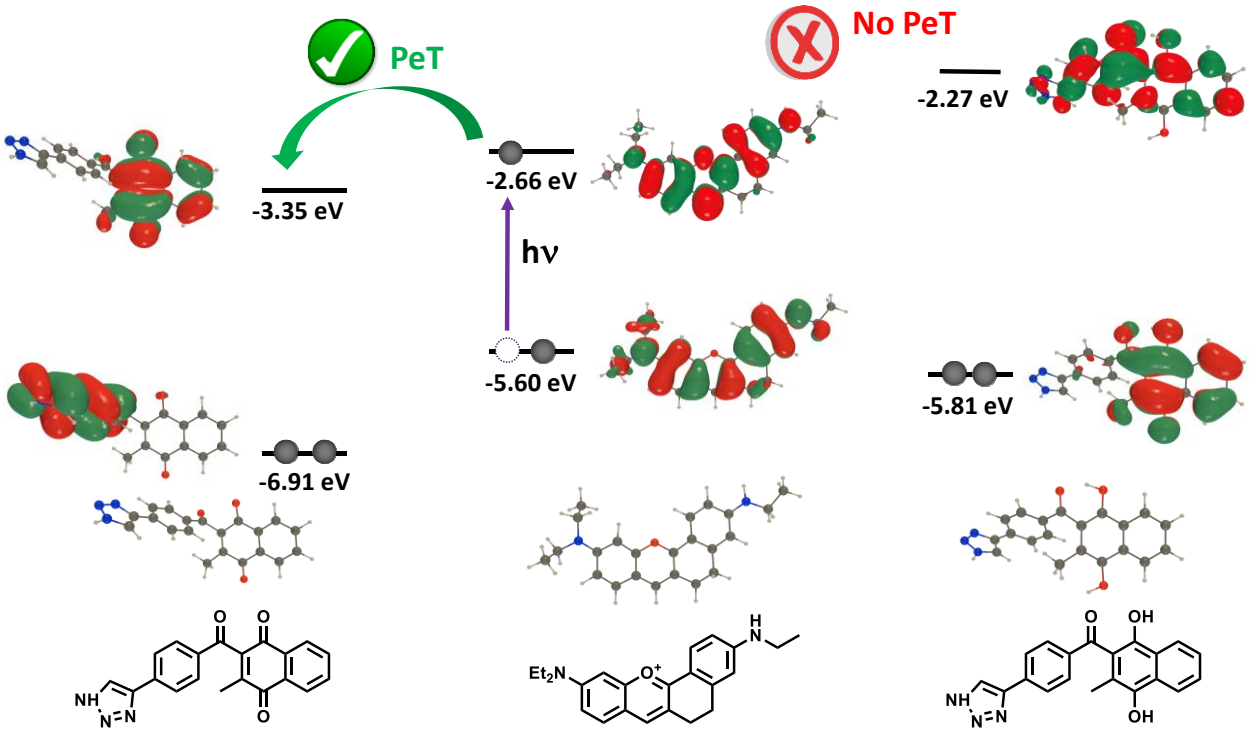

Figure 2. Representation of the frontier MO (energy and topology) of the dye and the oxidized and reduced forms as determined by DFT. See the ESI for technical details.

Redox-sensitive fluorescence properties. Upon reduction and protection as a 1,4-dimethoxy-naphthalene core, the electron richness of the naphthoquinone increases making it unresponsive to reduction (*vide supra*). In that case, PeT is prevented, leading to fluorophores as bright as the parent flavylium-PEG azides. As mentioned above, **PDO**$_{ox}$ can be reduced to **PDO**$_{red}$ in a continuous redox cycle in *p*RBCs. Following this concept, we thus postulate that the hybrid molecules, similarly to **PDO**$_{ox/red}$, can display the same redox behavior, allowing an OFF-ON fluorogenic property in response

to enzymatic reduction (*vide infra*). To provide an experimental proof of concept, **F2-1** was reduced by photoirradiation at 365 nm. UV-photoreduction of (benzo)quinones in propan-2-ol (*i*PrOH) is known to generate semiquinone radicals and dihydroquinone. [50-52] Upon UV-excitation, the photo-excited 1,4-naphthoquinone core generates an triplet state that can be trapped by an hydrogen atom donor such as *i*PrOH. [53,54] Photoirradiation at 365 nm [52] in *i*PrOH for 90 minutes of **F2-1** resulted in a strong enhancement (4-fold increase) of the fluorescence emission (Figure 3) compared to a non-illuminated batch. This clearly substantiates that the reduction of the benzoyl-MD moiety prevents the PeT quenching and reinstates partly the fluorescence emission of the flavylium dye. It should also be noted that the absorption spectra of the irradiated and non-irradiated solutions were only slightly affected (decrease of less than 12% in the main absorption), demonstrating the high photostability of the flavylium fluorophore when subjected to a strong and continuous UV photoexcitation for a very long period (90 minutes).

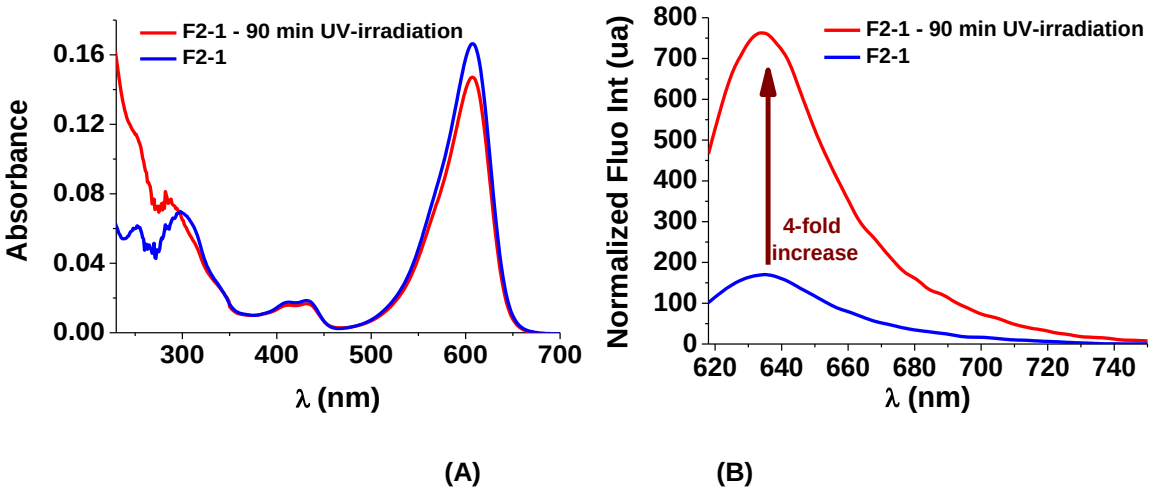

Figure 3. (**A**) UV-visible absorption spectra and (**B**) normalized (with respect to the absorbance value at the λ_{exc} of **F2-1** (2.5 µM) at t = 0 and after 90 minutes of UV-photoirradiation at 365 nm (Rayonet photochemical reactor equipped with 16 UV lamps of 14 W and maintained at 16°C) in *i*PrOH. λ_{exc} = 618 nm; 1% attenuator; excitation and emission bandwidth = 12.5 nm. The absorption and emission spectra were measured directly after irradiation. The comparison is made by integrating the area under the emission curves. The quantum yield measured for **F2-1** (not irradiated) is 10.6% in *i*PrOH (Figure S28 in the ESI).

We also tested the reduction of **F2-1** by reaction with 1 mM solution of bio-reductants such as glutathione (GSH) and cysteine (Cys) for 24 hours. An increase in fluorescence was also observed, but less than under photoirradiation (2.4-fold for GSH and 2.7-fold for Cys). In addition, a significant decrease in the main absorption band was observed, demonstrating a loss of fluorophore stability under these experimental conditions (1 mM of GSH or Cys) after 24 hours of reaction (Figures S34 and S35 in the ESI). Although the increase in fluorescence emission does not reach the expected value, the results show that the reduction of **F2-1** is possible in biological media and can be monitored by emission fluorescence.

Redox properties. Several model compounds were first investigated, including **1** (benzoyl-MD alkyne), [49] **10** (reduced benzoyl-MD alkyne protected by methyl groups) and the flavylium **8** fluorophore prototype (Scheme 3). The analogues with PEG-azide chains were not considered in this study due to the likely electrochemical reduction of the azide function. In DMSO, **1** is characterized by the presence

of two waves (1-electron transfer each) separated by about 700 mV (Figure S36 in the ESI). These correspond to the first step to the reduction of 1,4-naphthoquinone to 1,4-naphtho-semiquinone ($E^1_{1/2}$ = -0.44 V *vs.* Ag/AgCl/3MKCl) and to the second step to the reduction of the latter to dihydro-1,4-naphthoquinone ($E^2_{1/2}$ = -1.15 V *vs.* Ag/AgCl/3MKCl). Each of the redox waves is quasi-reversible, as indicated by the potential difference of about 90 mV between the maxima of the anodic and cathodic peaks. At much more negative potentials, a third 1-electron redox wave ($E^3_{1/2}$ = -1.56 V *vs.* Ag/AgCl/3MKCl) of quasi-reversible nature, attributed to the carbonyl of the benzoyl unit, can be observed. [55,56] As anticipated, the redox waves centered on the 1,4-naphthoquinone core are absent for the reduced/protected **10,** and the CV and SWV spectra show the presence of only 2 quasi-reversible redox waves ($E^1_{1/2}$ = -1.44 V and $E^1_{1/2}$ = -1.76 V *vs.* Ag/AgCl/3MKCl, Figure S37 in the ESI) attributed to the benzoyl carbonyl function. These electrochemical data are consistent with those measured for benzophenone derivatives. [57]

There is scarce electrochemical data available for compounds analogous to the rigid flavylium **8**. [58-61] In DMSO, only an irreversible oxidation peak at 0.32 V (*vs.* Ag/AgCl/3MKCl) and an irreversible reduction peak at -0.67 V (*vs.* Ag/AgCl/3MKCl) were observed. [60] For these rigid flavylium dyes bearing an amino unit on 4'-position (Scheme 6), [47] a significant intramolecular charge transfer (ICT) is anticipated to take place between the donor (ethylamino substitution) and the acceptor (pyrilium C unit) (Scheme 6-**II**). The irreversible 1-electron reduction might therefore correspond to the reduction of ethanaminium unit to a α-amino radical (Scheme 6-**III**). [62] The latter radical most likely equilibrates with the pyranyl radical (Scheme 6-**IV**). It has been also shown that pyrilium derivatives can undergo an irreversible 1-electron reduction reaction to generate a pyranyl radical, which can rapidly undergo dimerization (Scheme 6-**V**). Such a dimer was shown to undergo a 2-electron oxidation to reinstate the starting pyrilium (Scheme 6). [63,64] The same mechanism was also proposed for some cyanine derivatives. [65] As observed for anilines, the pyrilium stabilized form (Scheme 6-**I**) with an ethylamino substitution can undergo a 1-electron anodic oxidation to lead to an aniline radical cation (Scheme 6-**VI**). The latter can be deprotonated to afford a neutral radical (Scheme 6-**VIII**) or can equilibrate with its resonant structure **VII** (Scheme 6). [66] For **8** whose structure **II** is predominant in solution, we therefore hypothesized an ECE (Electron transfer – Chemical reaction – Electron transfer) mechanism involving structures **I**, **II**, **III**, **IV, VI** and **VII** and explaining the large gap between the reduction and the oxidation peaks. Dimerization observed between two pyranyl radicals or two oxidized aniline radicals (tail-to-tail, head-to-tail or head-to-head coupling) is unlikely to occur due to strong steric interactions that could take place.

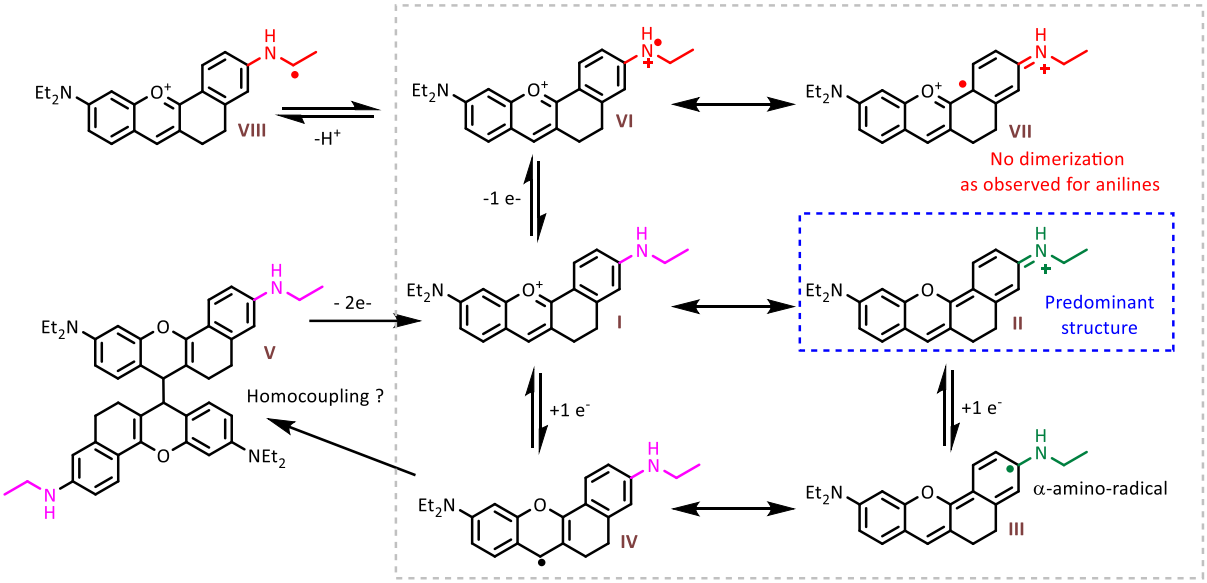

Scheme 6. Putative electrochemical processes occurring with the rigid flavylium prototype dye **8**.

To assess the possibility of PeT process between the models **8** and **1**, the oxidation and reduction potentials of the fluorophore **8** in its lowest excited state were roughly evaluated using the Rhem-Weller model (Figures S36-S38 in the ESI) based on the ground state potentials and the UV-Vis absorption spectra recorded in DMSO. [67,68] In the initial stage of the PeT process, a photon is indeed absorbed by **8**, resulting in a photoexcited state with significantly altered redox properties (E^*_{ox} = -1.58 V and E^*_{red} = 1.16 V *vs.* SCE). An electron transfer step thus follows in which the photoexcited state acts as a reductant in the presence of **1** that behaves as an electron acceptor (E^2_{red} = -1.15 V and E^1_{red} = -0.44 V *vs.* SCE). Reduction and protection by methyl groups significantly alters the electrochemical behavior of the 1,4-naphthoquinone moiety (E^2_{red} = -1.76 V and E^1_{red} = -1.44 V *vs.* SCE), whose electron-donating nature prevents deactivation by PeT.

In the case of the oxidized benzoyl-MDs, CuAAC chemistry with the rigid flavylium dye leads to hybrid assemblies **F1-1** (PEG-1), **F2-1** (PEG-2) and **F3-1** (PEG-3) whose redox properties are significantly modified. Although the two redox processes centered on the 1,4-naphthoquinone moiety can be clearly observed, increasing the length of the PEG chain has the effect of shifting the redox potentials of the first redox wave towards cathodic potentials (Table 5 and Figures S36, S40, S42 and S44 in the ESI). The latter is buried under the fluorophore redox peaks, making them difficult to observe. The largest effect is observed for the second redox process centered on the 1,4-naphthoquinone moiety. The shorter the PEG chain, the smaller the potential gap between the two quinone-centered redox waves, increasing gradually from 220 mV for **F1-1** to 650 mV for **F3-1** (Figure 4). This suggests that during the 1-electron reduction of the naphthoquinone moiety and of the flavylium ion, the radical species formed are able to associate via radical-radical interactions. These intramolecular interactions thus facilitate the second reduction of the quinone moiety. The longer the PEG chain, the less this type of interaction is favored, resulting in electrochemical properties centered on the 1,4-quinone unit comparable to those of model **1**.

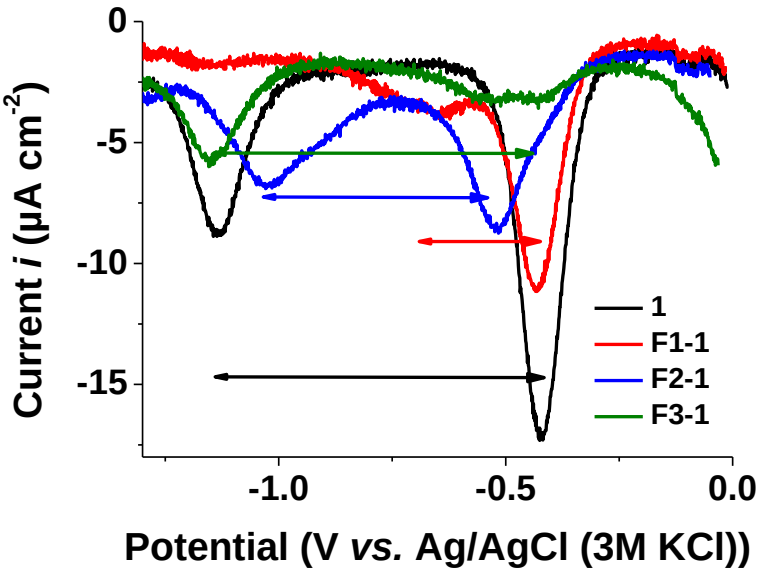

Figure 4. Comparison of the SWV voltamperograms recorded for **1**, **F1-1** (PEG-1), **F2-1** (PEG-2) and **F3-1** (PEG-3). Solvent: DMSO, I = 0.1 M n-Bu_4NPF_6, T = 25°C, v = 200 mV s^{-1}. Reference electrode = Ag/AgCl/KCl(3M), working electrode = glassy carbon disk of 0.07 cm^2 area; auxiliary electrode = Pt wire.

We then turned to the hybrid molecules **F1-10** (PEG-1), **F2-10** (PEG-2) and **F3-10** (PEG-3) in which the benzoyl-MD unit is reduced and protected by methyl groups (Figures S37, S41, S43, S45 and S46 in the ESI). Irrespective of the PEG chain length, the electrochemical behavior is comparable, demonstrating the absence of redox interactions between the two electrophores. The electrochemical profile of these systems can be defined by the presence of two irreversible redox waves shifted by almost 200 mV (electronic effect of the triazole function) towards cathodic potentials compared to **10** (in some cases the second wave is not observed). For all these systems, a quasi-reversible weak redox wave centered on the flavylium dye can be also observed at potentials comparable to those of the **8**-free system (Table 5).

Table 5. Redox properties of the hybrid molecules studied by cyclic (CV) and square wave (SVW) voltammetries.

		Benzoyl-MD core									Flavylium core		
		1st redox NQ			2nd redox NQ			3rd redox CO					
	Cmpd.	E_{pc}	E_{pa}	$E_{1/2}$ CV SWV	E_{pc}	E_{pa}	$E_{1/2}$ CV SWV	E_{pc}	E_{pa}	$E_{1/2}$ CV SWV	E_{pc}	E_{pa}	$E_{1/2}$ CV SWV
	1	-0.49	-0.40	-0.44 -0.42	-1.21	-1.10	-1.15 -1.14	-1.62	-1.50	-1.56 -1.54			
	10[a]							-1.49	-1.39	-1.44 -1.41			
								-1.89	-1.64	-1.76 -1.72			
	8										-0.67	-0.32	-0.62
PEG-1	**F1-1**	-0.50	-0.42	-0.46 -0.43	-0.73	-0.62	-0.68 -0.65	-1.24	nd	nd -1.18	nd[b]	nd[b]	nd[b]
PEG-1	**F1-10**[a]							-1.70	-1.55	-1.63 -1.59	-0.71	-0.59	-0.65 -0.66
PEG-1								nd	nd	-1.97			
PEG-2	**F2-1**	-0.55	-0.41	-0.48 -0.52	-1.05	-0.89	-0.97 -1.03	-1.40	nd	nd -1.29	nd[b]	nd[b]	nd[b]
PEG-2								-1.64	-1.53	-1.59	-0.78	-0.58	-0.68

	F2-10[a]							-2.07	nd	-1.56 nd -1.95			-0.65
PEG-3	**F3-1**	-0.57	-0.47	-0.52 -0.52	-1.21	-1.12	-1.17 -1.15	-1.66	nd	nd -1.68	nd[b]	nd[b]	nd[b]
	F3-10[a]							-1.67	1.56	-1.62 -1.59	nd[b]	-0.30	nd[b]

E_{pc} (potential of the cathodic peak - reduction), E_{pa} (potential of the anodic peak - oxidation), $E_{1/2}$ (half-wave redox potential). E_{pa}, E_{pc} and $E_{1/2}$ are given in V. Solvent: DMSO, I = 0.1 M n-Bu_4NPF_6, T = 25°C, v = 200 mV s^{-1}. Reference electrode = Ag/AgCl/KCl(3M), working electrode = glassy carbon disk of 0.07 cm^2 area; auxiliary electrode = Pt wire. [a] redox processes centered on carbonyl groups. [b] hidden by the 1st benzoyl-MD redox wave. nd = not determined. na = not applicable.

Imaging of model 8 with *P. falciparum* parasitized RBC. Preliminary imaging experiments with *p*RBCs were then performed with the prototype fluorophore **8**. For this, a culture with parasites of different age was incubated for approximately 10 minutes with 500 µM, 50 µM, and 5 µM **8** prior to imaging (Figure 5). At the highest concentration, we detected staining of the parasite in the DIC image, while the fluorescent signal appeared to be predominantly in the parasite's nuclei (Figure 5A, left). At 50 µM and 5 µM, **8** stained the parasite evenly, with a substantially reduced fluorescent signal in the food vacuole at the lowed concentration (Figure 5A, middle, right). In addition, at all tested concentrations of **8**, we did neither detect a fluorescent signal of the parasitized RBCs nor uninfected RBCs. We also detected a similar staining pattern in gametocytes when incubated 5 µM **8** (Figure 5B). As short-term exposure to **8** for imaging did not show any adverse effects on the viability of 3D7 (chloroquine-sensitive strain) parasites, we next determined the IC_{50} of **8** over two developmental cycles (Figure 5D). For this, we cultured the parasites for two developmental cycles in the presence of different concentrations of the fluorophore (two biological replicates in technical triplicates, compared to the untreated as control = 100 %) and we found an IC_{50} of **8** at 60 nM. Together, these data suggest that **8** efficiently enters and stains only the parasite with no detectable adverse effects over short periods of time.

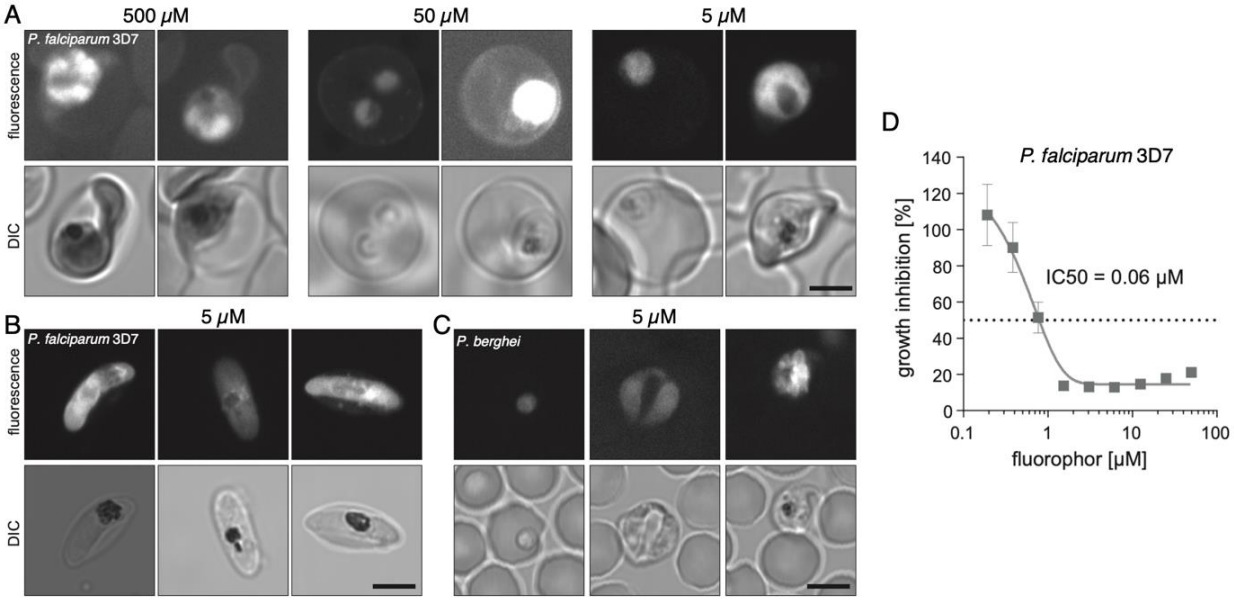

Figure 5. Dye 8 selectively stains *Plasmodium* parasites. **A**) *P. falciparum* infected red blood cells of a mixed culture of asexual stages were incubated with **8** at three different concentrations (500 µM, 50 µM, 5 µM) for approximately 10 min. **B**) gametocytes were incubated with **8** (5 µM) for approximately 10 min. **C**) *P. berghei* infected red blood cells were incubated with **8** (5 µM) for approximately 10 min. Excitation and emission range were as following: Ex: 561 nm, Em.: 570-780 nm, scale bars: 5 µm. **D**) Cytotoxicity assay of synchronized ring stages

incubated for two cell cycles in the presence of different concentrations of **8**. Each concentration was setup in technical triplicates. Parasitemia was examined via SYBR intensity. IC_{50} was determined in comparison to untreated control (= 100 %). Shown are mean values of biological duplicates. IC_{50} value was determined by GraphPad Prism with sigmoidal curve fitting (non-linear regression, dose-response inhibition with three parameters), error bars represent SEM.

In vitro antimalarial activity. All compounds were then tested for their ability to inhibit the growth of the chloroquine-sensitive *P. falciparum* strain NF54 in culture by determining the concentration of inhibition required to block the growth of the parasite by 50% (IC_{50} values, Table 6). As previously described, 3-benzoyl-MDs, the major metabolites resulting from benzyl oxidation in vivo, do not exhibit high antimalarial activity, with IC_{50} values 10-50 times higher than those of the corresponding parent 3-benzyl-MD (e.g. IC_{50} > 1000 nM for **PDO** vs. IC_{50} = 43 $\pm$ 2 nM for **PD**, Table 6) when given externally. [48,71,69] This may be explained by the greater planarity and polarity of 3-benzoyl-MD metabolites compared to their non-oxidised congeners, resulting in very poor internalisation into *p*RBCs. While this has been very clearly described for **PD** and **PDO**, it remains true after substitution by an alkyne function leading to benzyl-MD alkyne (Scheme 4) and **1** (IC_{50} 907 nM for **1** vs. IC_{50} = 49 $\pm$ 15 nM for benzyl-MD alkyne, Table 6). The parasite imaging study carried out on **8** showed excellent internalisation of this dye into *p*RBCs with no apparent adverse effects to these cells over short periods of time. Furthermore, **8** has high activity in *P. falciparum* (3D7 chloroquine-sensitive strain, Table 6). Compounds substituted by a PEG-azide chain of increasing length (**F1**, **F2** and **F3**, Table 6) were not active in a *P. falciparum* NF54 strain, as shown by IC_{50} values in the µM range in contrast to the first observations with **8** on *P. falciparum* 3D7 strain (IC_{50} about 60 nM). This clearly demonstrates the detrimental effect of introducing a PEG-azido chain on antimalarial activity. Interestingly, adducts clicked with an analogue of **PDO** in its oxidised (**F1-1**, **F2-1** and **F3-1**) or reduced/protected (**F1-10**, **F2-10** and **F3-10**) form had IC_{50} values 4 to 5 times lower than those not clicked with the azide dye. This demonstrates that combination with a rigid flavylium cation ensures easier internalisation of the **benzoyl-MD** derivatives that would be difficult or impossible in the absence of the fluorescent partner. While the click adducts have interesting activities against *P. falciparum*-NF54 strain, the measured IC_{50} values suggest that these hybrid compounds may have potential as fluorogenic redox probes under suitable conditions without altering significantly the *p*RBCs.

Table 6. Averaged IC_{50} values (nM) for 3-benzylMD-flavylium adducts and derivatives against *P. falciparum* NF54 strain.[a]

	Cmpd.	IC_{50} (nM) *P. falciparum* NF54
Benz(o)ylMD	PD	43 ± 2 (2)[c,[70]]
	BenzylMD alkyne	49 ± 15 (3)[b,[70]]
	PDO	> 1000 [71]
	1	907 (3)[a]
flavylium	8	600[c,d]
PEG-1	F1	1343 $\pm$ 407 (2)
	F1-1	396 $\pm$ 74 (2)
	F1-10	241 $\pm$ 42 (2)
PEG-2	F2	348 $\pm$ 107 (2)

	F2-1	314 (1)
	F2-10	331 ± 94 (2)
PEG-3	**F3**	1042 ± 316 (2)
	F3-1	296 ± 80 (2)
	F3-10	318 ± 113 (2)
Controls	**Chloroquine**	3.9 ± 0.5 (2) ng/ml
	Artesunate	2.1 ± 0.3 (2) ng/ml

[a] Activity against cultured parasites of *P. falciparum* NF54 strain (sensitive to chloroquine) is presented as mean IC_{50} values (the value in parentheses indicates the number of repeats). [b] IC_{50} value with the SYBR green assay using the *P. falciparum* Dd2 strain assay (resistant strain to chloroquine, sensitive to **PD**, DHA and methylene blue). [c] Activity against cultured parasites of 3D7 strain (sensitive to chloroquine). Chloroquine and artesunate were used as standard drugs. [d] see Scheme 4 for chemical structures.

Conclusion

This work describes, for the first time, the synthesis of rigid flavylium azides and their successful combination, by tethering with variable-length PEG spacers, with drug metabolites (i.e., plasmodione metabolites or benzoylMD derivatives) acting as valuable and promising redox cyclers. This preliminary approach allowed us to develop, by screening and selection, a new series of readily accessible azide fluorescent probes based on flavylium-type dyes, with the ultimate aim of detecting redox changes in pRBCs. By incorporating them by means of CuAAC-type click chemistry to plasmodione analogues in an alkyne form and by optimizing the length of the PEG chain, flavylium/benzoyl-MD hybrid probes with appropriate photophysical, electrochemical and biological properties were thus prepared and investigated in depth. These probes allow a significant reversible quenching of the fluorescence by the PeT process. The length of the PEG spacer is critical, and the use of a short PEG-1 chain is very likely to induce radical-radical interactions between the reduced species, thereby contributing to the enhancement of the fluorogenic response. With a PEG-3 chain, however, these latter non-covalent interactions are minimized, highlighting only the effects of the PeT process. Taken together, our results emphasize the great potential of these hybrid probes for real-time redox monitoring in parasitized erythrocytes, particularly in conditions where traditional genetically encoded redox probes may fail. Ultimately, these preliminary results pave the way for the study of redox processes in *p*RBCs, potentially offering a promising toolbox for a better understanding of the mechanisms underlying the action of antimalarial drugs inducing gradients of reactive oxygen species.

Competing Interest Statement. The authors declare no conflict interest.

Keywords: Click chemistry, fluorophore azide, redox probe, flavylium, PeT process

Acknowledgements. This work has been published under the framework of the idex Unistra and benefits from a funding (2017/W17RPD29) from the state managed by the French National Research Agency as part of the investments for the future program. The Jean-Marie Lehn Foundation in Strasbourg, France is also acknowledged for funding this work (Post-doc salary to L.C., project Fluoplasmo). The authors also wish to thank the Laboratoire d'Excellence (LabEx) ParaFrap consortium for funding (ANR-11-LABX-0024, E.D.-C.) and creating a proper framework for this scientific research (PhD salary to B.D.) as well as the Agence Nationale de la Recherche, France (Program ANR-PRCI

with FNS, Project “ROSaction”, grant ANR-22-CE93-0005-01 to E.D-C., M.R., P.M). The authors would like to thank Gilles Ulrich (ICPEES UMR7515 CNRS-Unistra) for making his Fluoromax 4 instrument available for the quantum yield measurements. The authors also warmly thank Manon Aniel, Quentin Riehl, Marc Castelló Escuriet and David García Gallego for partially contributing to this work. D.J. is indebted to the CCIPL/GlidID computational center installed in Nantes for computational resources. M.G. is supported by the Health + Life Science Alliance Heidelberg Mannheim and receives state funding approved by the State Parliament of Baden-Württemberg. This work was further supported by the German Research Foundation – project number 240245660 – SFB 1129 to MG. The authors are grateful to the Infectious Diseases Imaging Platform (IDIP) at the Center for Infectious Diseases, Heidelberg, Germany, for the microscopy support.

References

[1] Martinovich, G. G.; Cherenkevich, S. N.; Sauer, H. Intracellular Redox State: Towards Quantitative Description. *European Biophysics Journal* **2005**, *34* (7), 937–942. https://doi.org/10.1007/s00249-005-0470-3.

[2] Sun, Y.; Sun, P.; Guo, W. Fluorescent Probes for Iron, Heme, and Related Enzymes. *Coordination Chemistry Reviews* **2021**, *429*, 213645. https://doi.org/10.1016/j.ccr.2020.213645.

[3] Jiang, X.; Wang, L.; Carroll, S. L.; Chen, J.; Wang, M. C.; Wang, J. Challenges and Opportunities for Small-Molecule Fluorescent Probes in Redox Biology Applications. *Antioxidants & Redox Signaling* **2018**, *29* (6), 518–540. https://doi.org/10.1089/ars.2017.7491.

[4] Mohring, F.; Jortzik, E.; Becker, K. Comparison of Methods Probing the Intracellular Redox Milieu in Plasmodium Falciparum. *Molecular and Biochemical Parasitology* **2016**, *206* (1–2), 75–83. https://doi.org/10.1016/j.molbiopara.2015.11.002.

[5] Mohring, F.; Rahbari, M.; Zechmann, B.; Rahlfs, S.; Przyborski, J. M.; Meyer, A. J.; Becker, K. Determination of Glutathione Redox Potential and pH Value in Subcellular Compartments of Malaria Parasites. *Free Radical Biology and Medicine* **2017**, *104*, 104–117. https://doi.org/10.1016/j.freeradbiomed.2017.01.001.

[6] Kostyuk, A. I.; Panova, A. S.; Bilan, D. S.; Belousov, V. V. Redox Biosensors in a Context of Multiparameter Imaging. *Free Radical Biology and Medicine* **2018**, *128*, 23–39. https://doi.org/10.1016/j.freeradbiomed.2018.04.004.

[7] Kasozi, D.; Mohring, F.; Rahlfs, S.; Meyer, A. J.; Becker, K. Real-Time Imaging of the Intracellular Glutathione Redox Potential in the Malaria Parasite Plasmodium Falciparum. *PLoS Pathogens* **2013**, *9* (12), e1003782. https://doi.org/10.1371/journal.ppat.1003782

[8] Mohring, F.; Rahbari, M.; Zechmann, B.; Rahlfs, S.; Przyborski, J. M.; Meyer, A. J.; Becker, K. Determination of Glutathione Redox Potential and PH Value in Subcellular Compartments of Malaria Parasites. *Free Radical Biology and Medicine* **2017**, *104*, 104–117. https://doi.org/10.1016/j.freeradbiomed.2017.01.001

[9] Heimsch, K. C.; Gertzen, C. G. W.; Schuh, A. K.; Nietzel, T.; Rahlfs, S.; Przyborski, J. M.; Gohlke, H.; Schwarzländer, M.; Becker, K.; Fritz-Wolf, K. Structure and Function of Redox-Sensitive Superfolder Green Fluorescent Protein Variant. *Antioxidants & Redox Signaling* **2022**, *37* (1–3), 1–18. https://doi.org/10.1089/ars.2021.0234.

[10] Meyer, A. J.; Dick, T. P., Fluorescent Protein-Based Redox Probes. Antioxidants & Redox Signaling **2010**, *13*, 621-650. https://doi.org/10.1089/ars.2009.2948

[11] Andreu, N.; Zelmer, A.; Wiles, S. Noninvasive Biophotonic Imaging for Studies of Infectious Disease. *FEMS Microbiology Reviews* **2011**, *35* (2), 360–394. https://doi.org/10.1111/j.1574-6976.2010.00252.x

[12] Bai, X.; Ng, K. K.-H.; Hu, J. J.; Ye, S.; Yang, D. Small-Molecule-Based Fluorescent Sensors for Selective Detection of Reactive Oxygen Species in Biological Systems. *Annu. Rev. Biochem.* **2019**, *88* (1), 605–633. https://doi.org/10.1146/annurev-biochem-013118-111754.

[13] Weidinger, A.; Kozlov, A. Biological Activities of Reactive Oxygen and Nitrogen Species: Oxidative Stress versus Signal Transduction. *Biomolecules* **2015**, *5* (2), 472–484. https://doi.org/10.3390/biom5020472.

[14] Jiang, X.; Wang, L.; Carroll, S. L.; Chen, J.; Wang, M. C.; Wang, J. Challenges and Opportunities for Small-Molecule Fluorescent Probes in Redox Biology Applications. *Antioxidants & Redox Signaling* **2018**, *29* (6), 518–540. https://doi.org/10.1089/ars.2017.7491.

[15] Zhang, L.; Zhang, L.; Zhang, X.; Zhao, Y.; Fang, S.; You, J.; Chen, L. Responsive Fluorescent Probes for Cellular Microenvironment and Redox Small Biomolecules. *TrAC Trends in Analytical Chemistry* **2023**, *169*, 117377. https://doi.org/10.1016/j.trac.2023.117377.

[16] Kaur, A.; New, E. J. Bioinspired Small-Molecule Tools for the Imaging of Redox Biology. *Acc. Chem. Res.* **2019**, *52* (3), 623–632. https://doi.org/10.1021/acs.accounts.8b00368.

[17] Park, S. Y.; Yoon, S. A.; Cha, Y.; Lee, M. H. Recent Advances in Fluorescent Probes for Cellular Antioxidants: Detection of NADH, hNQO1, H2S, and Other Redox Biomolecules. *Coordination Chemistry Reviews* **2021**, *428*, 213613. https://doi.org/10.1016/j.ccr.2020.213613.

[18] Jiao, X.; Li, Y.; Niu, J.; Xie, X.; Wang, X.; Tang, B. Small-Molecule Fluorescent Probes for Imaging and Detection of Reactive Oxygen, Nitrogen, and Sulfur Species in Biological Systems. *Anal. Chem.* **2018**, *90* (1), 533–555. https://doi.org/10.1021/acs.analchem.7b04234.

[19] Chen, X.; Tian, X.; Shin, I.; Yoon, J. Fluorescent and Luminescent Probes for Detection of Reactive Oxygen and Nitrogen Species. *Chem. Soc. Rev.* **2011**, *40* (9), 4783. https://doi.org/10.1039/c1cs15037e.

[20] Wu, Z.; Guo, Y.; Jiang, W.; Yang, Y.; Wei, P.; Yi, T. Recent Process in Organic Small Molecular Fluorescent Probes for Tracking Markers of Tumor Redox Balance. *TrAC Trends in Analytical Chemistry* **2024**, *170*, 117461. https://doi.org/10.1016/j.trac.2023.117461.

[21] Wu, L.; Sedgwick, A. C.; Sun, X.; Bull, S. D.; He, X.-P.; James, T. D. Reaction-Based Fluorescent Probes for the Detection and Imaging of Reactive Oxygen, Nitrogen, and Sulfur Species. *Acc. Chem. Res.* **2019**, *52* (9), 2582–2597. https://doi.org/10.1021/acs.accounts.9b00302.

[22] Huang, Y.; Cao, X.; Deng, Y.; Ji, X.; Sun, W.; Xia, S.; Wan, S.; Zhang, H.; Xing, R.; Ding, J.; Ren, C. An Overview on Recent Advances of Reversible Fluorescent Probes and Their Biological Applications. *Talanta* **2024**, *268*, 125275. https://doi.org/10.1016/j.talanta.2023.125275

[23] Kaur, A.; Kolanowski, J. L.; New, E. J. Reversible Fluorescent Probes for Biological Redox States. *Angewandte Chemie International Edition* **2016**, *55* (5), 1602–1613. https://doi.org/10.1002/anie.201506353.

[24] Li, B.; He, Z.; Zhou, H.; Zhang, H.; Cheng, T. Reversible Fluorescent Probes for Chemical and Biological Redox Process. *Chinese Chemical Letters* **2017**, *28* (10), 1929–1934. https://doi.org/10.1016/j.cclet.2017.08.055.

[25] Lou, Z.; Li, P.; Han, K. Redox-Responsive Fluorescent Probes with Different Design Strategies. *Acc. Chem. Res.* **2015**, *48* (5), 1358–1368. https://doi.org/10.1021/acs.accounts.5b00009.

[26] Zhan, J.; Song, W.; Ge, E.; Dai, L.; Lin, W. Reversible Fluorescent Probes for Biological Dynamic Imaging: Current Advances and Future Prospects. *Coordination Chemistry Reviews* **2023**, *493*, 215321. https://doi.org/10.1016/j.ccr.2023.215321.

[27] Kwon, N.; Kim, D.; Swamy, K. M. K.; Yoon, J. Metal-Coordinated Fluorescent and Luminescent Probes for Reactive Oxygen Species (ROS) and Reactive Nitrogen Species (RNS). *Coordination Chemistry Reviews* **2021**, *427*, 213581. https://doi.org/10.1016/j.ccr.2020.213581.

[28] Dias, G. G.; King, A.; De Moliner, F.; Vendrell, M.; Da Silva Júnior, E. N. Quinone-Based Fluorophores for Imaging Biological Processes. *Chem. Soc. Rev.* **2018**, *47* (1), 12–27. https://doi.org/10.1039/C7CS00553A.

[29] Manjare, S. T.; Kim, Y.; Churchill, D. G. Selenium- and Tellurium-Containing Fluorescent Molecular Probes for the Detection of Biologically Important Analytes. *Acc. Chem. Res.* **2014**, *47* (10), 2985–2998. https://doi.org/10.1021/ar500187v.

[30] Tian, L.; Feng, H.; Dai, Z.; Zhang, R. Resorufin-Based Responsive Probes for Fluorescence and Colorimetric Analysis. *J. Mater. Chem. B* **2021**, *9* (1), 53–79. https://doi.org/10.1039/D0TB01628D.

[31] Kalyanaraman, B.; Hardy, M.; Podsiadly, R.; Cheng, G.; Zielonka, J. Recent Developments in Detection of Superoxide Radical Anion and Hydrogen Peroxide: Opportunities, Challenges, and Implications in Redox Signaling. *Archives of Biochemistry and Biophysics* **2017**, *617*, 38–47. https://doi.org/10.1016/j.abb.2016.08.021.

[32] Jeuken, L.; Orrit, M.; Canters, G. Single-Molecule Fluorescence in Redox Chemistry. *Current Opinion in Electrochemistry* **2023**, *37*, 101196. https://doi.org/10.1016/j.coelec.2022.101196.

[33] Goulle, V.; Harriman, A.; Lehn, J.-M. An Electro-Photoswitch: Redox Switching of the Luminescence of a Bipyridine Metal Complex. *J. Chem. Soc., Chem. Commun.* **1993**, No. 12, 1034. https://doi.org/10.1039/c39930001034.

[34] Yuan, Y.-X.; Chen, Y.; Wang, Y.-C.; Su, C.-Y.; Liang, S.-M.; Chao, H.; Ji, L.-N. Redox Responsive Luminescent Switch Based on a Ruthenium(II) Complex [Ru(Bpy)2(PAIDH)]2+. *Inorganic Chemistry Communications* **2008**, *11* (9), 1048–1050. https://doi.org/10.1016/j.inoche.2008.05.026.

[35] Benniston, A. C.; Copley, G.; Elliott, K. J.; Harrington, R. W.; Clegg, W. Redox-Controlled Fluorescence Modulation in a BODIPY-Quinone Dyad. *Eur J Org Chem* **2008**, *2008* (16), 2705–2713. https://doi.org/10.1002/ejoc.200800191.

[36] Greene, L. E.; Godin, R.; Cosa, G. Fluorogenic Ubiquinone Analogue for Monitoring Chemical and Biological Redox Processes. *J. Am. Chem. Soc.* **2016**, *138* (35), 11327–11334. https://doi.org/10.1021/jacs.6b06899.

[37] Han, L.; Liu, M.; Ye, D.; Zhang, N.; Lim, E.; Lu, J.; Jiang, C. Tumor Cell Membrane-Targeting pH-Dependent Electron Donor-Acceptor Fluorescence Systems with Low Background Signals. *Biomaterials* **2014**, *35* (9), 2952–2960. https://doi.org/10.1016/j.biomaterials.2013.12.020.

[38] Zheng, J.; Zeng, Q.; Zhang, R.; Xing, D.; Zhang, T. Dynamic-Reversible Photoacoustic Probe for Continuous Ratiometric Sensing and Imaging of Redox Status in Vivo. *J. Am. Chem. Soc.* **2019**, *141* (49), 19226–19230. https://doi.org/10.1021/jacs.9b10353.

[39] Kennedy, D. P.; Kormos, C. M.; Burdette, S. C. FerriBRIGHT: A Rationally Designed Fluorescent Probe for Redox Active Metals. *J. Am. Chem. Soc.* **2009**, *131* (24), 8578–8586. https://doi.org/10.1021/ja901653u.

[40] Yu, F.; Li, P.; Song, P.; Wang, B.; Zhao, J.; Han, K. Facilitative Functionalization of Cyanine Dye by an on–off–on Fluorescent Switch for Imaging of H2O2 Oxidative Stress and Thiols Reducing Repair in Cells and Tissues. *Chem. Commun.* **2012**, *48* (41), 4980. https://doi.org/10.1039/c2cc30985h.

[41] Heing-Becker, I.; Achazi, K.; Haag, R.; Licha, K. Hydroquinone-Functionalized Cyanine Dye as Reduction-Sensitive Probe for Imaging of Biological Reducing Species. *Dyes and Pigments* **2022**, *201*, 110198. https://doi.org/10.1016/j.dyepig.2022.110198.

[42] Kierat, R. M.; Thaler, B. M. B.; Krämer, R. A Fluorescent Redox Sensor with Tuneable Oxidation Potential. *Bioorganic & Medicinal Chemistry Letters* **2010**, *20* (4), 1457–1459. https://doi.org/10.1016/j.bmcl.2009.03.171.

[43] Zhang, W.; Li, P.; Yang, F.; Hu, X.; Sun, C.; Zhang, W.; Chen, D.; Tang, B. Dynamic and Reversible Fluorescence Imaging of Superoxide Anion Fluctuations in Live Cells and in Vivo. *J. Am. Chem. Soc.* **2013**, *135* (40), 14956–14959. https://doi.org/10.1021/ja408524j.

[44] Zhang, W.; Wang, X.; Li, P.; Huang, F.; Wang, H.; Zhang, W.; Tang, B. Elucidating the Relationship between Superoxide Anion Levels and Lifespan Using an Enhanced Two-Photon Fluorescence Imaging Probe. *Chem. Commun.* **2015**, *51* (47), 9710–9713. https://doi.org/10.1039/C5CC01670C.

[45] Shie, T.-L.; Lin, C.-H.; Lin, S.-L.; Yang, D.-Y. Synthesis of 1,1,3-Trisubstituted Naphtho[2,3-c]pyran-5,10-dione Derivatives as Potential Redox Switches. *Eur. J. Org. Chem.* **2007**, 4831–4836. https://doi.org/10.1002/ejoc.200700426

[46] Illos, R. A.; Shamir, D.; Shimon, L. J. W.; Zilbermann, I.; Bittner, S. N-Dansyl-Carbazoloquinone; a Chemical and Electrochemical Fluorescent Switch. *Tetrahedron Letters* **2006**, *47* (31), 5543–5546. https://doi.org/10.1016/j.tetlet.2006.05.139.

[47] Dupouy, B.; Hemmerlin, A.; Mazan, V.; Schaller, H.; Davioud-Charvet, E.; Elhabiri, M. Bringing phytosterols to light with bioinspired fluorophore azides using bioorthogonal chemistry. Submitted 2024.

[48] Cichocki, B. A.; Khobragade, V.; Donzel, M.; Cotos, L.; Blandin, S.; Schaeffer-Reiss, C.; Cianférani, S.; Strub, J.-M.; Elhabiri, M.; Davioud-Charvet, E. A Class of Valuable (Pro-)Activity-Based Protein Profiling Probes: Application to the Redox-Active Antiplasmodial Agent, Plasmodione. *JACS Au* **2021**, *1* (5), 669–689. https://doi.org/10.1021/jacsau.1c00025.

[48] Iacobucci, I.; Monaco, V.; Hovasse, A.; Dupouy, B.; Keumoe, R.; Cichocki, B.; Elhabiri, M.; Meunier, B.; Strub, J.M.; Monti, M.; Cianférani, S.; Blandin, S.A.; Schaeffer-Reiss, C.; Davioud-Charvet, E. Proteomic Profiling of Antimalarial Plasmodione Using 3-Benz(o)ylmenadione Affinity-Based Probes. *ChemBioChem* **2024**, *25*, e202400187. https://doi.org/e202400187. doi.org/10.1002/cbic.202400187

[49] Görner, H. Photoreactions of 2-Methyl-5-Isopropyl-1,4-Benzoquinone. *Journal of Photochemistry and Photobiology A: Chemistry* **2004**, *165* (1–3), 215–222. https://doi.org/10.1016/j.jphotochem.2004.03.020.

[50] Poulsen, J. R.; Birks, J. W. Photoreduction Fluorescence Detection of Quinones in High-Performance Liquid Chromatography. *Anal. Chem.* **1989**, *61* (20), 2267–2276. https://doi.org/10.1021/ac00195a012.

[51] Trometer, N.; Cichocki, B.; Chevalier, Q.; Pécourneau, J.; Strub, J.-M.; Hemmerlin, A.; Specht, A.; Davioud-Charvet, E.; Elhabiri, M. Synthesis and Photochemical Properties of Fluorescent Metabolites Generated from Fluorinated Benzoylmenadiones in Living Cells. *J. Org. Chem.* **2024**, *89* (4), 2104–2126. https://doi.org/10.1021/acs.joc.3c00620.

[52] Donzel, M.; Elhabiri, M.; Davioud-Charvet, E. Bioinspired Photoredox Benzylation of Quinones. *J. Org. Chem.* **2021**, *86* (15), 10055–10066. https://doi.org/10.1021/acs.joc.1c00814.

[53] Görner, H. Photoprocesses of P-Naphthoquinones and Vitamin K1: Effects of Alcohols and Amines on the Reactivity in Solution. *Photochem Photobiol Sci* **2004**, *3* (1), 71–78. https://doi.org/10.1039/b306670n.

[54] Sidorov, P.; Desta, I.; Chessé, M.; Horvath, D.; Marcou, G.; Varnek, A.; Davioud-Charvet, E.; Elhabiri, M. Redox Polypharmacology as an Emerging Strategy to Combat Malarial Parasites. *ChemMedChem* **2016**, *11* (12), 1339–1351. https://doi.org/10.1002/cmdc.201600009.

[55] Cotos, L.; Donzel, M.; Elhabiri, M.; Davioud-Charvet, E. A Mild and Versatile Friedel–Crafts Methodology for the Diversity-Oriented Synthesis of Redox-Active 3-Benzoylmenadiones with Tunable Redox Potentials. *Chem. Eur. J.* **2020**, *26* (15), 3314–3325. https://doi.org/10.1002/chem.201904220.

[56] Michielli, R. F.; Elving, P. J. Electrochemical Reduction of Benzophenone in Aprotic Medium. Effect of Proton Availability. *J. Am. Chem. Soc.* **1968**, *90* (8), 1989–1995. https://doi.org/10.1021/ja01010a011.

[57] Prima, E. C.; Nuruddin, A.; Yuliarto, B.; Kawamura, G.; Matsuda, A. Combined Spectroscopic and TDDFT Study of Single-Double Anthocyanins for Application in Dye-Sensitized Solar Cells. *New J. Chem.* **2018**, *42* (14), 11616–11628. https://doi.org/10.1039/C8NJ01202D.

[58] Avó, J.; Petrov, V.; Basílio, N.; Jorge Parola, A.; Pina, F. Evidence against the Twisted Intramolecular Charge Transfer (TICT) Model in 7-Aminoflavylium Derivatives. *Dyes and Pigments* **2016**, *135*, 86–93. https://doi.org/10.1016/j.dyepig.2016.06.007.

[59] Ferreira Da Silva, P.; Lima, J. C.; Quina, F. H.; Maçanita, A. L. Excited-State Electron Transfer in Anthocyanins and Related Flavylium Salts. *J. Phys. Chem. A* **2004**, *108* (46), 10133–10140. https://doi.org/10.1021/jp047300d.

[60] Pinto, A. L.; Máximo, P.; Pina, J.; Calogero, G.; Laia, César. A. T.; Parola, A. J.; Lima, J. C. Exploring the Impact of Structural Rigidification of Amino-Substituted Bio-Inspired Flavylium Dyes in DSSCs. *Dyes and Pigments* **2023**, *218*, 111495. https://doi.org/10.1016/j.dyepig.2023.111495.

[61] Leitch, J. A.; Rossolini, T.; Rogova, T.; Maitland, J. A. P.; Dixon, D. J. α-Amino Radicals via Photocatalytic Single-Electron Reduction of Imine Derivatives. *ACS Catal.* **2020**, *10* (3), 2009–2025. https://doi.org/10.1021/acscatal.9b05011.

[62] Berberova, N. T.; Dorofeenko, G. N.; Okhlobystin, O. Yu. Electrochemical Reduction of Pyrylium Salts in an Aprotic Medium. *Chem. Heterocycl. Compd.* **1977**, *13* (3), 250–253. https://doi.org/10.1007/BF00470304.

[63] Guel, B.; Tountian, D.; Bonzy-Coulibaly, Y.; Traore, H.; Sié Sib, F. Étude voltamétrique des sels de styryl-2 et styryl-4 pyrylium. *C. R. Chimie* **2007**, *10*, 535-545.

[64] Lenhard, J. R.; Cameron, A. D. Electrochemistry and Electronic Spectra of Cyanine Dye Radicals in Acetonitrile. *J. Phys. Chem.* **1993**, *97* (19), 4916–4925. https://doi.org/10.1021/j100121a009.

[65] Jaworski, J. S.; Kalinowski, M. K. Electrochemistry of Anilines. In *PATAI'S Chemistry of Functional Groups*; Rappoport, Z., Ed.; Wiley, 2007; pp 871–929. https://doi.org/10.1002/9780470871737.ch16.

[66] Buzzetti, L.; Crisenza, G. E. M.; Melchiorre, P. Mechanistic Studies in Photocatalysis. *Angew. Chem. Int. Ed.* **2019**, *58* (12), 3730–3747. https://doi.org/10.1002/anie.201809984.

[67] Suppan, P.; Vauthey, E. The Energy Balance of Photoinduced Electron Transfer Reactions. *Journal of Photochemistry and Photobiology A: Chemistry* **1989**, *49* (1–2), 239–248. https://doi.org/10.1016/1010-6030(89)87121-7.

[68] Feng, L.; Lanfranchi, D. A.; Cotos, L.; Cesar-Rodo, E.; Ehrhardt, K.; Goetz, A.-A.; Zimmermann, H.; Fenaille, F.; Blandin, S. A.; Davioud-Charvet, E. Synthesis of Plasmodione Metabolites and ^{13}C-Enriched Plasmodione as Chemical Tools for Drug Metabolism Investigation. *Org. Biomol. Chem.* **2018**, *16* (15), 2647–2665. https://doi.org/10.1039/C8OB00227D.

[69] Dupouy, B.; Donzel, M.; Roignant, M.; Charital, S.; Keumoe, R.;Yamaryo-Botté, Y.; Feckler, A.; Bundschuh, M.; Bordat, Y.; Rottmann, M.; Mäser, P.; Botté, C. Y.; Blandin, S. A.; Besteiro, S.; Davioud-Charvet, E. 3-benzylmenadiones and their heteroaromatic analogues target the apicoplast of Apicomplexa parasites: Synthesis and bioimaging studies, *ACS Inf. Dis.* **2024**, in press,

[70] Müller, T.; Johann, L.; Jannack, B.; Brückner, M.; Lanfranchi, D. A.; Bauer, H.; Sanchez, C.; Yardley, V.; Deregnaucourt, C.; Schrével, J.; Lanzer, M.; Schirmer, R. H.; Davioud-Charvet, E. Glutathione Reductase-Catalyzed Cascade of Redox Reactions To Bioactivate Potent Antimalarial 1,4-Naphthoquinones – A New Strategy to Combat Malarial Parasites. *J. Am. Chem. Soc.* **2011**, *133* (30), 11557–11571. https://doi.org/10.1021/ja201729z.

1.2.3 Les points importants de l'article 4

- **Développement de sondes fluorescentes sensibles au rédox :** En utilisant la même méthodologie combinatoire de screening par lecture de plaque absorption/émission que dans l'article 3, cette étude a permis de sélectionner les meilleurs candidats tout en approfondissant la compréhension des interactions entre le flavylium et le bMD sous sa forme oxydée ou réduite, $bMD_{ox/red}$.
- **Synthèse de systèmes flavyliums-$bMD_{ox/red}$ optimisés :** Par utilisation de longueur d'espaceur variable (PEG-1, PEG-2 et PEG-3) (6 systèmes au total), l'étude a permis d'évaluer l'influence de la longueur des chaînes PEG sur les propriétés photophysiques des sondes, ce qui a notre connaissance n'avait jamais été réalisé ou décrit dans ce domaine de recherche (fluorophore azoturé).
- **Extinction réversible de la fluorescence :** Du fait de processus PeT, lorsque l'unité bMD est sous forme oxydée (quinone) la fluorescence est inhibée, tandis qu'elle est restaurée sous sa forme réduite (hydroquinone). Les chaînes PEG les plus courtes conduisent aux réponses fluorogéniques les plus fortes et inversement pour les plus longues.
- **Propriétés photophysiques et électrochimiques et approche théorique :** Les sondes synthétisées ont démontré une émission dans le spectre rouge-PIR, ainsi qu'un comportement électrochimique particulier. Au-delà du processus PeT, le raccourcissement des chaines (PEG-1 en particulier) autorise une interaction radical-radical entre la bMD réduite à 1 électron et le flavylium réduit, renforçant l'extinction de fluorescence. Par ailleurs, une étude théorique, basée sur les différences d'énergie des orbitales moléculaires et menée sur des modèles pertinents, a confirmé le mécanisme d'extinction PeT.
- **Imagerie par fluorescence chez *P. falciparum* et activité antipaludique :** L'imagerie par fluorescence sur un modèle flavylium rigide a démontré que les flavyliums marquent efficacement les érythrocytes parasités sans affecter les cellules non infectées (la sonde est localisée dans le cytosol à 5 µM). Par ailleurs, les adduits flavylium-bMDs ont démontré une activité antipaludique modérée *in vitro*, confirmant leur perméabilité cellulaire et leur potentiel pour l'imagerie des processus rédox dans les cellules vivantes. L'unité flavylium sert de cheval de Troie pour faciliter l'internalisation dans des globules rouges infectés des bMD oxydées en position benzylique (benzoylMD) qui ne sont peu ou pas internalisées en absence du fluorophore.
- **Potentiel en tant que sondes rédox :** Ces sondes offrent un fort potentiel pour l'étude des mécanismes rédox de médicaments antipaludiques de type *redox-cyclers* ainsi que d'autres processus biologiques, en particulier dans des conditions où les sondes

génétiquement codées ne fonctionnent pas efficacement (conditions acides des vacuoles digestives).

-

Chapitre IV : Synthèse d’une série de composés triazole-méthyle-ménadiones et poursuite du développement de pseudo-PDs

1.3 Synthèse de α- et β-triazole-méthyle-ménadiones et évaluation de leurs activités antiparasitaires

1.1.1 Introduction

Comme mentionné dans l'introduction, notre molécule de référence, la plasmodione, présente des propriétés PC et PK peu satisfaisantes pour une administration par voie orale, telles que sa solubilité, sa lipophilicité et sa surface polaire. Ces caractéristiques entrainent une biodisponibilité *in vivo* insuffisante et une élimination rapide du composé actif. L'article 2 a montré que des modifications structurales de la partie est du squelette bMD pouvaient améliorer certaines propriétés. Par exemple, l'introduction de groupements *N*-hétéroaromatiques permet de réduire la lipophilicité (clog P) et d'augmenter la surface polaire (tPSA), tout en préservant une activité antiparasitaire significative et sans altérer les propriétés rédox du composé. Cependant, cette fonctionnalisation entraine généralement une augmentation de la cytotoxicité du composé. De plus, aucun dérivé *N*-hétéroaromatique n'a montré une efficacité supérieure à celle de notre molécule de référence, le composé le plus actif **3l** (IC_{50} = 69 nM *Pf*NF54, β-pyridine).

À la suite du développement des composés *N*-hétéroaromatiques décrits dans l'article 2, nous avons décidé d'explorer des bMDs comportant un groupement 1,2,3-triazole-méthyle en remplacement du cycle benzylique. Ce choix est motivé par plusieurs avantages du groupement triazole :

i. Il améliore la surface polaire, la lipophilicité et la solubilité par rapport à d'autres dérivés *N*-hétéroaromatiques comme la pyridine et la pyrimidine.
ii. Il constitue un bioisostère des fonctions amide, ester et des cycles aromatiques.
iii. Il favorise les interactions avec les biomolécules, telles que les liaisons hydrogènes, les interactions dipôle-dipôle ou les empilement π-π.
iv. C'est l'un des groupements « azole » les plus fréquemment rencontré dans la littérature en chimie médicinale.
v. Sa synthèse, via la réaction clique CuAAC, est en parfaite adéquation avec les thématiques abordées durant cette thèse et offre beaucoup de possibilité en matière de diversité structurale.

Cette étude vise à investiguer l'activité antiparasitaire (*P. falciparum* et *S. mansoni*) d'un certain nombre de dérivés triazole-méthyle-ménadiones obtenus grâce à la chimie clique. Nous allons donc pouvoir évaluer les relations structure-activité de cette série de composés, ainsi que leurs propriétés physicochimiques et électrochimiques. Nous avons ainsi obtenu une

trentaine de triazole-méthyle-ménadiones, dont l'étude est décrite dans l'article 5 de cette thèse.

Le groupement 1,2,3-triazole est largement très présent dans la littérature, en particulier en chimie médicinale, en raison des propriétés bénéfiques évoquées précédemment. Il a été exploité dans le développement de composés anti-VIH[135], anticancéreux[136–138], antibactériens[139,140] et antiparasitaires. Voici un aperçu des travaux les plus pertinents disponibles dans la littérature :

A. Une équipe brésilienne[141] a développé un nouveau composé 1,2,3-triazole plus actif que le benznidazole contre le parasite *Trypanosma cruzi* (*T. cruzi*), responsable de la maladie de Chagas (IC_{50} = 7.3 µM contre 21.5 µM benznidazole sur épimastigotes de *T. cruzi*). Des tests *in vitro* et *in vivo* ont montré une faible toxicité et une réduction de la parasitémie de 99.4% après traitement chez la souris (100 mg/kg) (Figure 31 (A)).
B. Nayera W. Hassan *et al.*[142] ont synthétisé une série de coumarines 1,2,3-triazole à des fins antileishmania (*L. major*). Certains de ces composés se sont révélés plus actifs et moins toxiques que la miltefosine, offrant des perspectives prometteuses pour le développement futur (Figure 31 (B)).
C. A. Singh *et al.*[143] ont développé des molécules hydrides 4-amino-quinoline/chalcone/ferrocényl. Les dérivés conjugués par une chaine carbonée aliphatique flexible sont plus actifs sur *P. falciparum* que ceux conjugués par un cycle aromatique (IC_{50} = 370 nM *Pf*W2) (Figure 31 (C)).
D. La stratégie d'hybridation combinant deux pharmacophores a déjà conduit au développement de la ferroquine (FQ) et des hybrides chloroquine-artémisinine (CQ-ART). Sur un principe similaire, une équipe indienne a synthétisé des dérivés d'ART alcyne et azoture (GB-1 et GB-2) (Figure 31 (D)), mais les dimères se sont révélés inactifs[144].
E. En 2020, M. W. Pertino *et al.*[145] ont synthétisé une librairie de triazoles-lapachols pour améliorer l'activité et la biodisponibilité du lapachol, un composé antitrypanosome. L'introduction du groupement triazole a conduit à une amélioration de l'activité des composés sur les parasites *T. cruzi* et Leishmania (Figure 31 (E)).
F. La même année, une équipe a développé des naphtoquinones-triazoles antileishmania[146], menant à la découverte d'une molécule de référence. Le mode d'action et les cibles biologiques de cette molécule sont encore en cours d'identfication (Figure 31 (F)).
G. Récemment, C. A. C. Menozzi *et al.*[147] ont évalué le groupement nitrotriazole pour remplacer les groupements 1,3,4-triazole ou nitro-imidazole présents sur le posaconazole et le benznidazole (composé anti-*T. cruzi*). L'introduction d'un nitrotriazole a significativement amélioré l'activité du composé par rapport au benznidazole (IC_{50} = 0.39 µM contre 1.5 µM benznidazole *T. cruzi*) (Figure 31 (G)).

H. Dans une autre étude[148], les propriétés bioisostériques du groupement triazole ont été exploitées, permettant de remplacer la fonction amide du benznidazole et offrant des perspectives intéressantes (Figure 31 (H)).

(A)

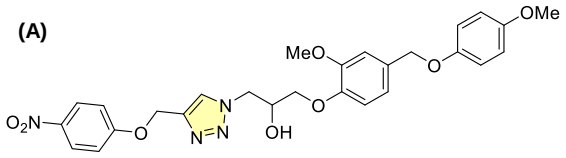

IC_{50} = **7.3 µM** *T. cruzi* (Epimastigote) - **99.4%** réduction parasitémie (100 mg/kg)
CC_{50} = **598.1 µM** H9c2
(benznidazole: IC_{50} = 21.5 µM, CC_{50} = 1694.5 µM)

(B)

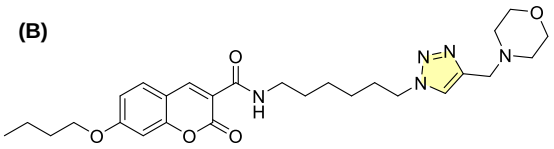

IC_{50} = **0.4 µM** *L. major* (Antipromastigote) et **0.68 µM** *L. major* (Antimastigote)
CC_{50} = **244.3 µM** VERRO cell
(Miltefosine: IC_{50} = 7.89 µM *L. major* (Antipromastigote) et 8.06 µM *L. major* (Antimastigote), CC_{50} = 99.7 µM VERRO cell)

(C)

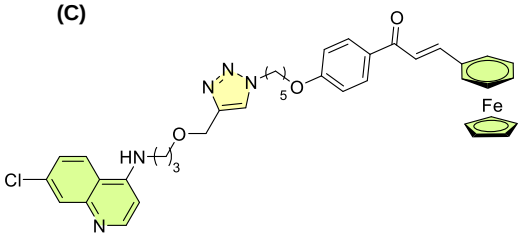

IC_{50} = **0.37 nM** *Pf*W2, CC_{50} = **18.2 µM** HeLa cell
(CQ: IC_{50} = 0.06 µM, FQ: IC_{50} = 0.0081 µM)

(D)

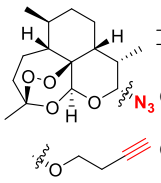

engagé dans la formation de dimère par CuAAC

GB-2: **59%** réduction parasitémie (50mg/kg)

GB-1: **64.4%** réduction parasitémie (50mg/kg)

(ART: 65.5% réduction parasitémie (50mg/kg))

(E)

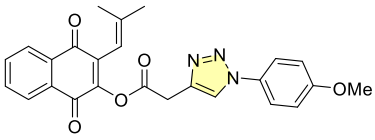

IC_{50} = **18.5 µM** *T. cruzi* (Epimastigote) - IC_{50} = **18 µM** *L. brazilensis*
CC_{50} = **180 µM** NCTC929

(F)

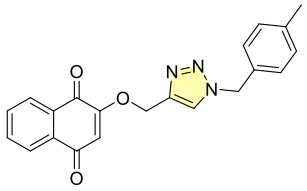

IC_{50} = **0.81 µM** *L. donovani* - IC_{50} = **1.48 µM** *L. major*
CC_{50} = **65 µM** HEK-293

(G)

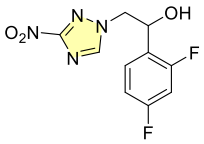

IC_{50} = **0.39 µM** *T. cruzi* - CC_{50} = **1200 µM** L929 – SI = **3077**
(benznidazole: IC_{50} = 1.5 µM - CC_{50} = 2113 µM – SI = 1409)

(H)

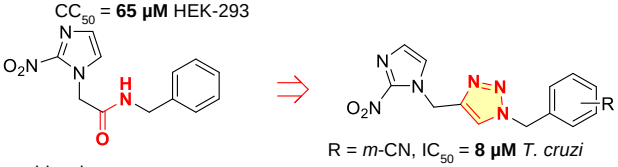

benznidazole:
IC_{50} = **4 µM** *T. cruzi* (Amastigote)
IC_{50} = **13 µM** *T. cruzi* (Trypomastigote)

R = *m*-CN, IC_{50} = **8 µM** *T. cruzi* (Amastigote)
IC_{50} = **3 µM** *T. cruzi* (Trypomastigote)
R = 2-CH_3-5-NO_2, IC_{50} = **4.4 µM** *T. cruzi* (Amastigote)
IC_{50} = **22 µM** *T. cruzi* (Trypomastigote)

Figure 31: Exemples de composés antiparasitaires possédant un groupement triazole. Chaque comparaison avec une molécule de référence (benznidazole, ART, CQ, FQ, miltefosine) est étudiée sur le même parasite, la même souche et le même stade parasitaire que la molécule ci-jointe.

1.1.2 Article 5

Synthesis of 1,2,3-Triazole-Methyl-Menadione Derivatives: Evaluation of Electrochemical and Antiparasitic Properties against two Blood-Dwelling Parasites

Dupouy Baptiste, Karpstein Tanja, Häberli Cécile, Keiser Jennifer, Cal Monica, Rottmann Matthias, Mäser Pascal, Elhabiri Mourad, Davioud-Charvet Elisabeth

***ChemMedChem* submitted article,** soumis le 15 Septembre 2024

Synthesis of 1,2,3-Triazole-Methyl-Menadione Derivatives: Evaluation of Electrochemical and Antiparasitic Properties against two Blood-Dwelling Parasites

Dupouy Baptiste,[1] Karpstein Tanja,[2] Häberli Cécile,[2] Cal Monica,[2] Rottmann Matthias,[2] Mäser Pascal,[2,3] Keiser Jennifer,[2,3] Elhabiri Mourad,[1] Davioud-Charvet Elisabeth[1,*]

* Correspondence E-mail Address: elisabeth.davioud@unistra.fr

[1] UMR7042 CNRS-Unistra-UHA, Laboratoire d'Innovation Moléculaire et Applications (LIMA), Bio(in)organic & Medicinal Chemistry Team, European school of Chemistry, Polymers and Materials (ECPM), 25, rue Becquerel, F-67087 Strasbourg, France.

[2] Swiss Tropical and Public Health Institute, Kreuzstrasse 2, CH-4123 Allschwil, Switzerland.

[3] University of Basel, Petersgraben 1, CH-4001 Basel, Switzerland.

Abstract:

This study explores the synthesis and evaluation of novel 1,2,3-triazole-methyl-1,4-naphthoquinone hybrids, focusing on their electrochemical properties and antiparasitic efficacies against two human blood-dwelling parasites *Plasmodium falciparum* and *Schistosoma mansoni*. Using copper-catalyzed azide-alkyne cycloaddition (CuAAC), a well-established tool in click chemistry, two synthetic routes were assessed to develop α- and β-[triazole-methyl]-menadione derivatives. By optimizing the CuAAC reaction conditions, yields were significantly improved, reaching up to 94% for key intermediates and resulting in the formation of a library of approximately 30 compounds. Biological evaluation of the compounds in antiparasitic drug assays demonstrated notable antischistosomal potencies, while no significant activity was observed for the same series against *P. falciparum* parasites. Electrochemical and 'benzylic' oxidation studies confirmed that the active 'benzoyl' metabolite responsible for the antiplasmodial activity of plasmodione cannot be generated. These findings highlight the potential of triazole-linked menadione hybrids as promising early candidates for antischistosomal drug development, and provides insights into structure-activity relationships crucial for future therapeutic strategies.

Keywords:

CuAAC, Click chemistry, plasmodione, 1,2,3-triazole, *Plasmodium falciparum*, *Schistosoma mansoni*

Introduction

Malaria is an infectious disease caused by the protozoan parasite *Plasmodium*, which is transmitted by the bite of an infected *Anopheles* mosquito. It is most prevalent in the Sub-Saharan Africa and in tropical and sub-tropical regions. In 2022, there was 249 million cases of malaria – well above the estimated number of cases before the COVID-19 pandemic, and an increase of five million over 2021, killing an estimated 608,000 people in 2022, mainly children under the age of five years in sub-Saharan Africa. [1] Five major species of the *Plasmodium* parasite – *P. falciparum, P. malariae, P. vivax, P. ovale, P. knowlesi* – can infect humans; the most severe forms of the disease, leading to cerebral malaria, severe anaemia and ultimately death are largely caused by *P. falciparum*. However, most of the drugs among them chloroquine, atovaquone, or artemisinin available to treat these diseases are subject to resistance, which limit their effectiveness. [2] Besides, schistosomiasis is an acute and chronic neglected tropical disease caused by *Schistosoma* trematode worms. There are two major forms of schistosomiasis – intestinal and urogenital – caused by five main species of blood flukes that infect humans: *S. mansoni*, *S. japonicum*, *S. haematobium*, *S. intercalatum* and *S. mekongi*. The intermediate host of the parasite, various species of freshwater snails, transfer human infection through skin contact with infective cercariae. [3] According to the World Health Organization report published in 2023, 251.4 million people are infected, more than 700 million people are at risk of infection and currently estimated – but likely underestimated – 11,792 deaths globally per year. [4] The disease is often co-endemic with malaria and

is found in most of Africa, Brazil, China, and the Philippines. In addition, urogenital *schistosomiasis* and genital *schistosomiasis* caused by *S. haematobium* increases the risk of HIV co-infection and cervical precancer lesions in women with a nearly four-fold higher susceptibility. [5]

Over the last decade, our team have invested much effort in a potent antiparasitic series of compounds known as 3-benzylmenadione (bMD) that target the redox homeostasis of two blood-feeding parasites, such as *P. falciparum* parasitizing human red blood cells (*p*RBC) [6,7] or the *S. mansoni* flatworms. [8] Most of the research was focused on medicinal chemistry of the antiplasmodial early lead plasmodione (**PD**)[9] (Figure 1), in particular on the understanding of its mode of action (MoA) [10-12] and the optimization of its biological activity and pharmacokinetic (PK) properties. [13,14] Although its MoA has been partially deciphered in yeast, [15] we demonstrated that the 3-benzoylmenadione (**PDO**) (Figure 1) is a key metabolite generated from **PD** through a bioactivation process. [12,16] **PDO** is generated via a two steps sequence: reduction of the 1,4-naphthoquinone electrophore to semi-naphthoquinone [17] by flavoenzymes that thus enables oxidation of the benzylic position by insertion of O_2. [12] The resulting **PDO** then acts as a subversive substrate in a redox cycle involving an endogenous reductant, oxygen and/or methemoglobin. [6,10,15] This redox cycle not only slows down the process of methemoglobin catabolism (digestion through proteolysis and hemozoin formation), but also produces other harmful drug metabolites and reactive oxygen species (ROS) that ultimately leads to the death of the parasite. [10]

One of the main advantages that medicinal chemistry can bring to enhance the potency of a lead molecule is to bring subtle modifications of its physiochemical properties through introduction of chemical diversity in order to improve its PK properties. In particular the enhancement of the aqueous solubility and the decrease of the lipophilicity of derivatives based on a bMD scaffold is one of the target strategies in this work. We have therefore investigated the effect of introducing nitrogen-containing aromatics into the backbone of the lead molecule. A first step towards this goal has been achieved through the development of a series of aza-benzylmenadiones [8] (Figure 1), while improving the solubility properties, also increased the cytotoxicity towards human cells through their effects on electrochemical properties of the aza-menadione core. The chemical modifications on the west side of the molecule were therefore abandoned and efforts focused on the east side of the molecule.

Recently, we have shown that the introduction of various substituted pyridine (py) and pyrimidine (pyr) moieties on the eastern part (Figure 1) led to promising antimalarial activities without generating undesirable side effects (e.g. increased cytotoxicity). [18] Following this concept, 1,2,3-triazole (TRZ) motifs were thus considered to improve the properties of the pharmacophore. TRZ rings, which are bioisosters of amide and ester functions, have indeed a high stability, dipole moment and hydrogen bonding ability that enhances their pharmacological properties, in particular their influence on target-drug interactions, metabolism and PK properties. [19] Over the last decade, advances in click chemistry (e.g. Cu-catalyzed azide-alkyne cycloaddition or CuAAC) [20] have not failed to stimulate interest in antiparasitic TRZs in medicinal chemistry of naphthoquinone moieties. [21-25] A recent review also describes the many developments in life sciences based on 1,4,5-trisubstituted halo-1,2,3-triazole scaffolds. [19] Therefore, we hypothesized that the introduction of α- or β-TRZ (Figure 1) could contribute

to improve the antischistosomal and antimalarial activities of our substituted menadione series. In this work, we thus evaluated in depth the effect of the introduction of TRZ moieties on the antiparasitic activity against two different parasites and the consequences on the physico-chemical properties.

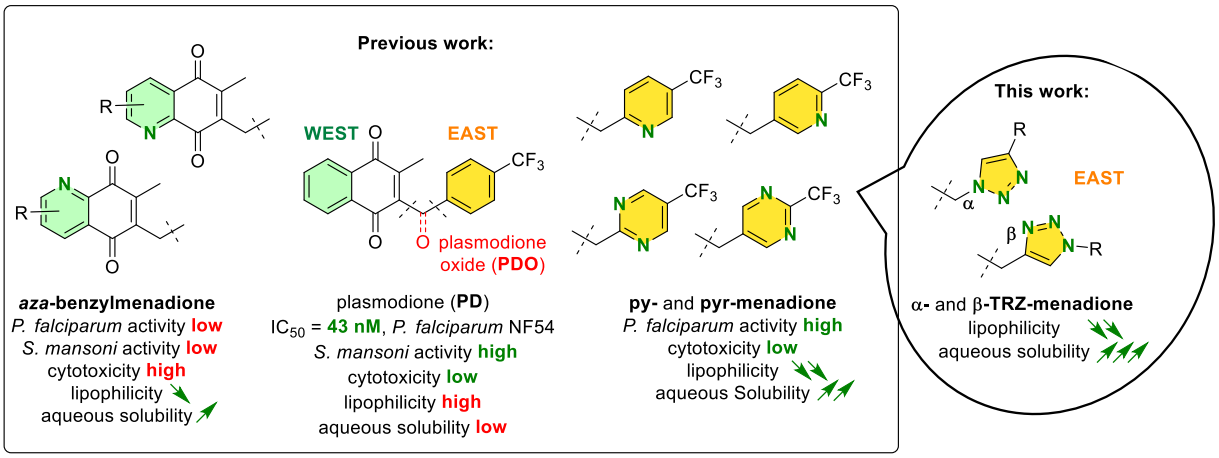

Figure 1. Work progress following introduction of *N*-heteroaromatics in the aromatic rings of 3-benzylmenadiones, from the eastern to the western part.

Results and discussion

Synthesis of 1,2,3-[TRZ-methyl]-menadiones.

Two different synthetic routes were initially considered to obtain the α- or β-[TRZ-methyl]-menadione derivatives (Figure 2). Route **(1)** involves the use of a protected menadione as starting material, i.e. 1,4-dimethoxy-2-methylnaphthalene, functionalized with azide or alkyne groups to be engaged in a CuAAC reaction. Since the carbonyls are protected, straightforward post-functionalization can be initiated, followed by deprotection to generate the α- or β-[TRZ-methyl]-menadione in three steps. Route **(2)** directly involves the unprotected menadione, generating [TRZ-methyl]-menadiones in only one step, but greatly reduces the possibilities of post-functionalization and limits the accessibility to the desired product.

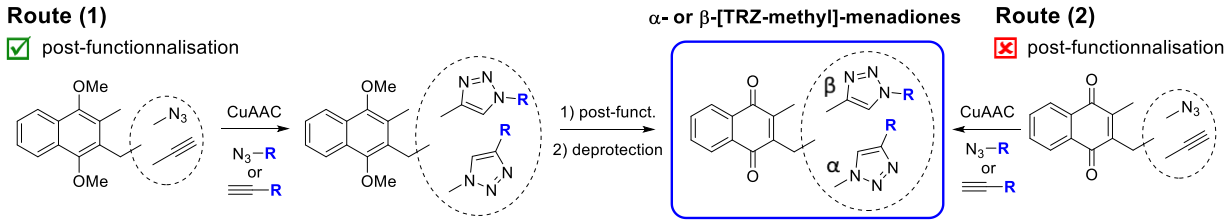

Figure 2. Accessibility of α- or β-[TRZ-methyl]-menadione through two different routes with their pros and cons.

Our initial goal was to avoid limiting steps while introducing structural diversity into the TRZ in order to better understand the structure-activity relationships (SAR). Therefore, we first investigated the synthetic route **(1)**. This route involved the synthesis of two menadione derivatives converted to 2-methyl-1,4-dimethoxynaphthalene homologues, the azide **1** and the alkyne **2**. The azido derivative was obtained

from menadione through sequential reduction and protection (intermediate 1,4-dimethoxy-2-methylnaphthalene), followed by chloromethylation (intermediate 2-(chloromethyl)-1,4-dimethoxy-3-methylnaphthalene), and finally nucleophilic substitution with sodium azide producing **1** in three steps with a 74% overall yield. For the alkyne, the synthesis started with intermediate 1,4-dimethoxy-2-methylnaphthalene, followed by a formylation reaction to give the compound **3**. The corresponding aldehyde was then alkynylated with acetylene-TMS (trimethylsilylacetylene) to afford the secondary alcohol **4**, which was reduced to **5**. The TMS protecting group was finally removed in the final step to produce the targeted terminal alkyne **2** in a five steps sequence in 53% overall yield.

The CuAAC click reaction [26-28] was then investigated using the azide **1** and a TMS-acetylene model to select the optimal experimental conditions applicable to different alkynes (Table 1). As the CuAAC reaction has been very popular since its discovery, a large number of experimental conditions are thus available in the literature. Inspired by the original review by Meldal and Tornøe, [29] we initially used copper iodide CuI as the catalyst. However, only 5% of the targeted **α6** click product was obtained (Table 1, entry 1). Increasing the amount of catalyst and using DMSO as the solvent and triethylamine TEA as the amine base led to a significant improvement (Table 1, entry 2). In the proposed mechanism, the generation of Cu-acetylide from Cu(I) requires an amine base and/or a high temperature. However, in our case, increasing the temperature and reaction time led to degradation of the starting product (Table 1, entry 3). The use of other more classical conditions, such as a copper sulphate ($CuSO_4$) catalyst and sodium ascorbate as reductant, resulted in only 4% of the target product (Table 1, entry 4). Finally, we turned to the use of $Cu(MeCN)_4BF_4$ as the catalyst, as the latter has the advantage of being a source of Cu(I) soluble in organic solvents. These new conditions considerably improved the yield of the CuAAC reaction, giving **α6** in 94% yield (Table 1, entry 5). Following the click reaction, the TMS group of **α6** was deprotected with TBAF to give the compound **α7** in 66% yield. Finally, an oxidative demethylation reaction with BCl_3/TBAI afforded the first α-[TRZ-methyl]-menadione (**α8**) in moderate yield of 40%. The total yield for these three steps to afford **α8** is about 25%. Noteworthy is to mention that **α8** could only be obtained by route (**1**), and not by route (**2**), as it will be discussed below.

The experimental conditions for the CuAAC reaction were then optimized (Table 1, entry 5) and subsequently applied to the alkyne **2** in combination with a model azide, the benzyl azide. However, no reaction occurred, even when a chelator of Cu(I) (i.e. bathocuproine [30]) was used to stabilize copper in its +I oxidation state, to improve its reactivity and prevent its oxidation (Table 1, entry 6 and 7). In addition, the optimized condition from entry 5 (Table 1) was tested with three different alkynes. Starting with azido **1** (Table S1 in the ESI), the reaction with propargyl bromide only led to the starting material, accompanied with an undetermined by-product, which could correspond to a stable intermediate of the CuAAC catalytic cycle. Finally, when propargyl alcohol or 3-methylbutynol was used, the reaction quantitatively reduced the azide function of compound **1** (Table S1 in the ESI). Taken together, these results suggest that the CuAAC reaction is highly dependent on the nature of the substrate when using the protected menadiones **1** and **2**.

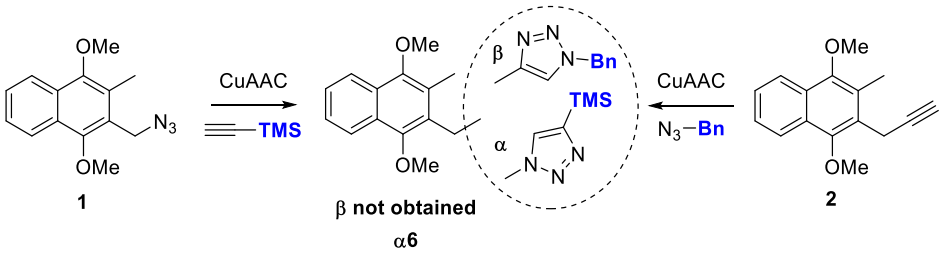

Table 1. Evaluation of the reactivity of **1** and **2** under different CuAAC reaction conditions.

Entry	Cpmd	Catalyst/reductant or ligand	Solvent	Conditions[a]	Yield[b] [%]
1	**1**	CuI (0.3 eq.)	MeCN (0.6 M)	r.t., 48 h	5[c]
2	**1**	CuI (0.75 eq.), TEA	DMSO (0.2 M)	r.t., 48 h	39[c]
3	**1**	CuI (0.5 eq.), TEA	DMSO (0.2 M)	50 °C, 72 h	degradation[c]
4	**1**	$CuSO_4$ (0.15 eq.)/Na ascorbate (0.8 eq.)	DMF/H_2O (9/1) (0.6 M)	r.t., 48 h	4[c]
5	**1**	$Cu(MeCN)_4BF_4$ (0.5 eq.)	MeCN (0.1 M)	50 °C, 72 h	98[c]
6	**2**	$Cu(MeCN)_4BF_4$ (0.5 eq.)	MeCN (0.1 M)	50 °C, 72 h	0[d]
7	**2**	$Cu(MeCN)_4BF_4$ (0.5 eq.)/bathocuproine (0.5 eq.)	DCM (0.1 M)	r.t., 72 h	0[d]

[a] Under argon atmosphere. [b] Isolated yield. [c] 3 equiv. of alkyne used. [d] 2 equiv. of azide used.

Following these first results, we then investigated the synthetic route **(2)**. The corresponding alkyne- (**10**) and azido-functionalized (**9**) menadione derivatives were obtained from **1** and **2** by oxidative demethylation, achieving high yields (i.e. 95% and 94%, respectively). We selected the conditions from Table 1 and tested them to investigate the accessibility to [TRZ-methyl]-menadiones. To introduce substituents compatible with desired physico-chemical properties, we synthesized several non-commercial alkynes and azides. Alkynes were readily obtained by a one-step nucleophilic substitution from propargyl bromide (Figure S13 in the ESI). As far as azide derivatives are concerned, a three steps sequence starting from ethanolamine allowed their access, first, with a diazo transfer reaction leading to compound **11**, then a tosylation of the alcohol function allowing access to compound **12** and finally a nucleophilic substitution reaction carried out to introduce the desired group (Figures S11 and S12 in the ESI). The results indicated that the various functional groups were well tolerated under the CuAAC conditions, allowing access to the targeted α- and β-[TRZ-methyl]-menadiones in low to good yields (Figure 3). Selected side-chains tethered on the alkyne or azide groups were inspired by the structures of antischistosomal drugs, e.g. nitro-, amino-, and methanol groups are found in oxamniquine, the piperidine ring is inspired by the quinolyl cycle of oxamniquine, oxopiperidinyl and piperazine cycles as similar to those found in praziquantel, and finally fluorine atoms and cyano groups have been observed in various antischistosomal derivatives described in literature. [31]

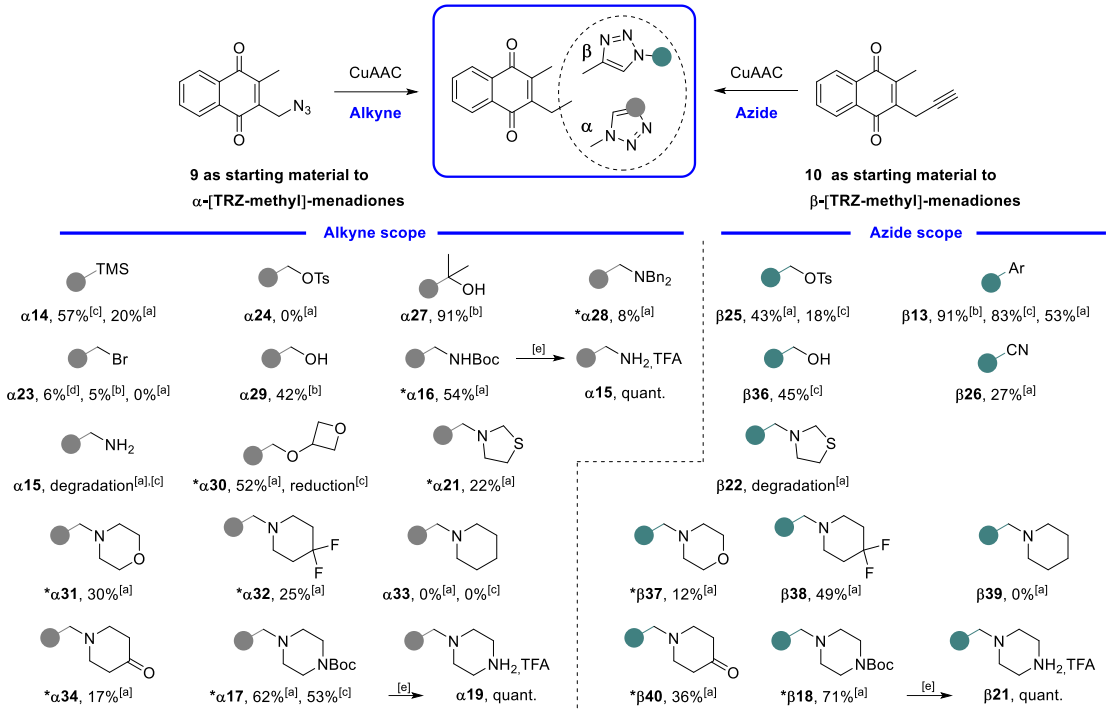

Figure 3. Access to [TRZ-methyl]-menadiones from **9** or **10** by CuAAC reaction. *****Products obtained from corresponding alkyne or azide crude mixture (two-steps yield). All yields are isolated yields. [a] 1.2 equiv. of azide or alkyne, $CuSO_4$ (0.2 equiv.)/Na ascorbate (0.4 eq.), THF/H_2O (7/3, 0.02 M), r.t., 16 h. [b] 1.5 equiv. of azide or alkyne, $Cu(MeCN)_4BF_4$ (0.1 equiv.), DCM (0.1 M), 40 °C, 16 h, under argon. [c] 1.5 equiv. of azide or 2 equiv. of alkyne, $Cu(MeCN)_4BF_4$ (0.4 equiv.)/bathocuproine (0.4 equiv.), DCM (0.1 M), 40 °C, 72 h, under argon. [d] 2 equiv. of alkyne, $Cu(MeCN)_4BF_4$ (0.1 eq.)/bathocuproine (0.1 equiv.), MeCN (0.01 M), 80 °C, 72 h, under argon. [e] 32 equiv. of TFA, DCM (0.06 M), r.t., 1 h.

Despite successful synthesis of many [TRZ-methyl]-menadiones, challenges remained with the deprotection of the TRZ-substituted side-chain. We were unable to debenzylate **β13** either by palladium-catalyzed hydrogenation or under the conditions (*tert*-butoxide/DMSO/O_2) described by Deaton-Rewolinski *et al*. [32] Similarly, deprotection of **α14** only led to degradation, using either fluoride or methanolate conditions. This unusual low reactivity could be explained by the fact that the menadione core is an efficient electron acceptor, which, in reduced form, is very sensitive to nucleophiles and/or bases (Michael acceptor). Attempts were thus made to protect the [TRZ-methyl]-menadione under conditions used for 1,4-dimethoxy-2-methylnaphthalene (Figure 3). However, this only led to the degradation of the starting material, highlighting the limitation of post-modifications in synthetic route (**2**) to access [TRZ-methyl]-menadione derivatives. As direct introduction of the amine was not tolerated by the CuAAC conditions (potential interaction with Cu(I)), the free amino-α-TRZ **α15** was therefore obtained by TFA deprotection of the *N*-Boc protected amine **α16**. In contrast, the use of hydroxyl or *O*-oxetane groups were well tolerated, affording the targeted products in moderate to excellent yields (Figure 3). In addition, several six-membered aliphatic heterocycles diversely substituted were introduced without much difficulty, except for unsubstituted piperidine, which was not tolerated to access either α- or β-isomers, likely because of methyl deprotonation of the menadione core. By TFA deprotection of **α17** and **α18**, piperazine derivatives **α19** and **α20** were quantitatively obtained, respectively (Figure 3). For five-membered heterocycles, only thiazolidine was tested, producing **α21** in 22% yield, while **β22** was formed in a small amount but degraded after a few hours (yield not quantified).

Other functional groups of interest were also considered, e.g. Br or OTs (**α23**, **α24**). The bromo-α-TRZ **α23** was obtained in very low yield. As observed for **1** (Table S1 in the ESI) different by-products were generated (not isolated), which could be linked to the competition between the generation of Cu-acetylide, Glaser coupling [33] and oxidative coupling. The tosyl-β-TRZ **β25** was obtained in moderate yield, but post-functionalization by nucleophilic substitution with morpholine in mild conditions led to the degradation of the starting material. In contrast, its isomer **α24** was not obtained. For the electron-withdrawing substitution, only the cyano group was tested, giving the desired derivative **β26**. Although successful for a large number of substituents, these results highlight the drawbacks of direct CuAAC click chemistry with unprotected reactive menadiones or for their post-functionalization. Nevertheless, through this proposed methodological approach, we could demonstrate that the synthetic route (**2**) (Figure 3) allowed the preparation of a series of [TRZ-methyl]-menadiones in one single step (i.e. without protection/deprotection of the menadione core).

Synthesis of 1,2,4-triazole-, 3-nitro-1,2,4-triazole- and 2-nitroimidazole-menadiones.

To introduce more compatible structural diversity within the α- and β-[TRZ-methyl]-menadiones, other five-membered *N*-heteroaromatic groups of varying diversity (Figure 4) were considered. For example, the 1,2,4-TRZ derivative (**41**) was obtained in moderate yield and NMR data was studied in detail. The latter is prepared from intermediate 2-(chloromethyl)-1,4-dimethoxy-3-methylnaphthalene by nucleophilic substitution with the commercially available secondary amine *N*-heteroaromatic followed by an oxidative demethylation of **42**. The importance of a nitro group was also evaluated and the compounds 3-nitro-1,2,4-TRZ (**43**) and 2-nitroimidazole (**44**) were prepared in moderate yields using the same methodology as for other triazoles.

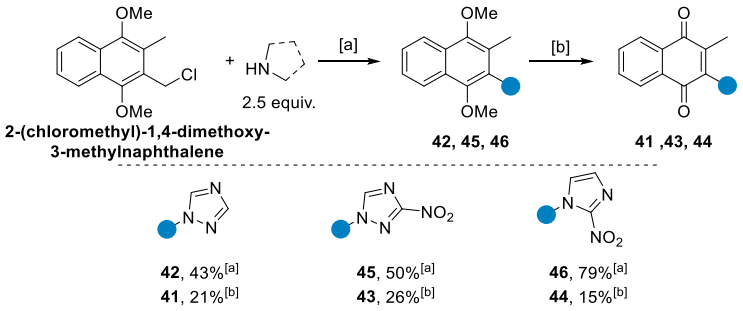

Figure 4. Synthesis of menadione derivatives containing a five-membered *N*-heteroaromatic ring. Conditions: [a] 2.5 equiv. of the corresponding secondary amine, 3 equiv. TEA, MeCN (0.05 M), 80 °C, 16 h. [b] 2 equiv. TBAI, 6 equiv. BCl_3, DCM (0.01 M), -78 °C, 16 h.

Antiparasitic activities and toxicity against human cells of [TRZ-methyl]-menadiones.

All [TRZ-methyl]-menadiones were tested for antimalarial and antischistosomal activities using standard 72 h assays and for cytotoxicity on L6 cells derived from rat skeletal myoblasts (ATCC CRL-1458) (Table 2). Growth inhibition of *P. falciparum* (NF54 strain) using the [^{3}H]-hypoxanthine incorporation assay [34]

or *in vitro* drug efficacy testing on two different *S. mansoni* life stages (newly transformed schistosomula (NTS) [35] and adult worms). IC_{50} values of the compounds were determined accordingly by measuring the concentration of the inhibitor required to reduce the growth (*P. falciparum*) or the viability (*S. mansoni*) of the parasites by 50%. In addition, the drug effect on the viability of *S. mansoni* NTS was evaluated after a 72 h exposure time, at a concentration of 10 µM for all our compounds. If the compound showed significant activity (>70% drug effect), the same test was performed with a lower concentration of 1 µM (Table 2). Regarding activity against *P. falciparum*, the α-[TRZ-methyl]-menadione series (including the other 5-membered-*N*-heteroaromatic isomers, (Figure 3) clearly show no efficacy with IC_{50} values far above 1 µM. Interestingly, half of the β-[TRZ-methyl]-menadione series showed promising antischistosomal activity in the NTS assay with IC_{50} values in the sub-micromole range. In particular, compounds **β38** and **β18** exhibited low IC_{50} values of 0.332 and 0.465 µM, respectively. Notably, the deprotected form of **β18**, compound **β20**, is inactive, indicating the negative effect of the presence of an ionisable free amine on the antiparasitic activity of the molecule. Comparison of the β-[TRZ-methyl]-menadione series with the pyridine- and pyrimidine-substituted menadiones recently published by our team [18] clearly showed that the 6-membered-*N*-heteroaromatics are generally more potent than their 5-membered congeners, with IC_{50} values below 1 µM for most of them (Table 2). The data obtained allowed us to demonstrate the absence of antimalarial activity for the α-TRZ and a moderate activity for the β-isomers. These results could be explained by alterations of the redox properties of the naphthoquinone electrophore depending on the type of heteroaromatic introduced and its nature (isomer). It should be noted that 3-benzylmenadiones or their heteroaromatic analogues were proposed to act as prodrugs and are prone to benzylic oxidation within pRBCs, which can significantly alter the reactivity and the electrochemical properties of the generated metabolites, as well as the influence of these substitutions on the menadione moiety (see below). [17,36,37]

Screening against NTS at 10 µM for 72 h revealed that approximately 80% of the 28 triazoles tested inhibited NTS viability by at least 70%, with IC_{50} values between 1.89 and 0.81 µM (Table 3). The most potent triazoles were then retested at a tenfold lower concentration. The results showed that **α15**, which bears a free amine, was the most active of the series, with a mortality of almost 54% and an IC_{50} value of 0.81 µM. It is interesting to note that although the series of 5-membered heteroaromatics showed no or only moderate antimalarial activity, almost all these triazoles showed potent antischistosomal activity, with NTS mortality in the order of 35-54% at 1 µM. To investigate this further, additional studies were carried out on *S. mansoni* adult worms at a concentration of 10 µM to 25 µM after 72 h exposure (Table 3). At a concentration of 25 µM, 85% of [TRZ-methyl]-menadiones showed a mortality of over 50% and were therefore retested at a 2.5 times lower concentration. Most have antischistosomal activity in the 40-50% mortality range. Two compounds in particular, **β13** and **β36**, stand out with much higher mortality rate of 56.9% and 64.7% respectively at 10 µM. By comparison, with 54.1% activity at 10 µM, **PD** (Table 3), one of our leading antimalarials, was already shown to be very potent against adult worms. [38] With the exception of **43** (Table 3), a compound that is very active on the NTS is not necessarily very active on the adult worms (48.1% at 10 µM), and *vice versa*, as has been demonstrated with our series of compounds here. No clear correlation between α- or β-substituted triazoles and *S. mansoni*

antischistosomal activity could be observed. This suggests that [TRZ-methyl]- or 3-benzyl-menadiones have different penetration properties in *S. mansoni* compared to *P. falciparum*, and consequently, possible distinct targets/drug transports mechanisms in these two hemoglobin-feeding parasites. 1,2,3-TRZ are known to allow simultaneous metal coordination and hydrogen bond donation (through dipole–ion interaction), making a synergistic increase of both CH-acidity and *N*-donor strength. [39] Here, in our study and from others [40], 1,2,3-TRZ exert - via their ambivalent character – excellent antischistosomal activities through better PK and penetration properties. Similarly to 1,2,3-triazoles, our previous study on 1,2,3,4-tetrazoles clearly highlighted the bioisosteric character of this heterocycle to mimic the negative charge of carboxylic acids. [41] Several works also reported the potent antischistosomal activities of carboxylic acids. [31,42]

Table 2. Antimalarial activity against *P. falciparum* NF54 strain, antischistosomal activity against *S. mansoni* NTS[a] and cytotoxicity on L6 cells.

Compound	Menadione-substituent	NF54 IC_{50} µM	L6 CC_{50} µM	SI[c]	NTS activity[b] % (±), 72 h		NTS IC_{50} µM, 72 h	SI[d]
					10 µM	1 µM		
α-1,2,3-triazole								
α8	α-TRZ	>10	6.24		100 (0)	34 (2)	1.05	5.9
α14	α-TRZ (TMS)	7.20	18.24	2.5	91.72 (2.1)	38 (2)	1.57	11.6
α15	α-TRZ (NH_2)	>10	-		100 (0)	54.17 (0)	-	
α16	α-TRZ (NHBoc)	>10	-		40.26 (5.6)	-	-	
α17	α-TRZ (piperidine-Boc)	1.46	-		75.26 (0.3)	50 (0)	1.50	
α19	α-TRZ (piperidine)	>10	-		100 (0)	43.75 (2.1)	0.93	
α21	α-TRZ (thiazolidine)	>10	-		42.35 (7.7)	-	-	
α23	α-TRZ (Br)	5.55	18.23	3.3	89.58 (2.1)	36 (4)	1.02	17.9
α27	α-TRZ (tBuOH)	>10	7.27		100 (0)	34(4)	1.05	6.9
α28	α-TRZ (NBn_2)	1.91	-		44.35 (1.5)	-	-	
α29	α-TRZ (OH)	>10	6.69		100 (0)	34 (6)	1.05	6.4
α30	α-TRZ (O-Oxetane)	>10	7.10		100 (0)	32 (0)	1.08	6.6
α31	α-TRZ (morpholine)	>10	-		100 (0)	39.58 (2.1)	0.98	
α32	α-TRZ (difluoropiperidine)	2.84	-		87.5 (12.5)	45.83 (4.2)	1.48	
α34	α-TRZ (4-piperidone)	>10	-		100 (0)	41.67 (4.2)	0.95	
β-1,2,3-triazole								
β13	β-TRZ (Bn)	0.89	49.16	55.2	58.33 (4.2)	-	-	
β18	β-TRZ (piperidine-Boc)	0.465	-		71.17 (3.8)	33.33 (0)	1.89	
β20	β-TRZ (piperidine)	6.51	-		91.84 (8.2)	33.33 (4.2)	1.67	
β25	β-TRZ (OTs)	0.77	44.41	57.7	41.47 (4.2)	-	-	
β26	β-TRZ (CN)	1.89	-		85.46 (10.5)	43.75 (6.3)	1.54	
β36	β-TRZ (OH)	1.847	17.55	9.5	97.92 (2.1)	36 (4)	1.44	12.2
β37	β-TRZ (morpholine)	5.95	-		50.51	-	-	
β38	β-TRZ (difluoropiperidine)	0.332	-		83.42 (8.4)	41.67 (0)	1.60	
β40	β-TRZ (4-piperidone)	2.07	-		100 (0)	35.42 (2.1)	-	
5-membered-*N*-heteroaromatic								
41	α-1,3,4-TRZ	7.48	-		100 (0)	45.83 (4.2)	0.90	
43	α-3-nitro-1,2,4-TRZ	>10	-		100 (0)	50 (0)	0.86	
44	α-2-nitroimidazole	>10	-		100 (0)	35.42 (2.1)	1.03	
6-membered-*N*-heteroaromatic (pyridine, pyrimidine) and reference drugs								
47[e]	γ-py-CF_3	0.078 ± 0.024[e]	50.9	652.6			-	
48[e]	β-py-CF_3	0.069 ± 0.024[e]	8.82	127.8			-	
49[e]	γ-pyr-CF_3	0.194 ± 0.125[e]	179.20	923.7			-	
50[e]	β-pyr-CF_3	0.414 ± 0.293[e]	17.56	42.4			-	
PD[f]	benzyl-CF_3	0.043 ± 0.002[e]	141.70	3295.3	46.43 (0)		11.3	12.5
CQ		0.004 ± 0.00037 µg/ml[e]						

[a] Praziquantel displayed CC_{50} and IC_{50} values of 96 µM and 2.2 µM against *S. mansoni* NTS, respectively (data from ref. [43]). [b] Effect in percentage in NTS assays after 72 h. [c] Selectivity index for the anti-*P. falciparum* NF54 activity: CC_{50} (L6)/IC_{50} (NF54). [d] Selectivity index for the anti-*S. mansoni* NTS activity: CC_{50} (L6)/IC_{50} (NTS). [e]

from reference [18]. [f] PD displayed an IC_{50} value of 11.3 µM in the NTS assay (data from ref. [38]). "-" means not tested.

Table 3. Antischistosomal activity against *S. mansoni* adult worms.[a]

Compound	Adult worms[b] % (±), 25 µM			Adult worms[b] % (±), 10 µM		
	24h	48h	72h	24h	48h	72h
α8	46 (1)	50 (0)	54.9 (2)	41.3 (1)	42.8 (0)	43.8 (5.1)
α14	50.9 (4)	51.05 (9.4)	70.55 (2)	39.37 (1)	39.75 (5.1)	43.8 (5.1)
α15	50.4 (2.5)	50 (0)	52.75 (4.6)	37 (3.7)	44.4 (0)	45.35 (0.9)
α16	54.25 (10.5)	54.55 (0.4)	55.55 (7.4)	-	-	-
α17	43.75 (4.2)	45.45 (0.4)	50.95 (0.9)	41.65 (2.8)	45.35 (0.9)	46.25 (1.9)
α19	43.8 (0)	48.45 (0.6)	62.5 (4.2)	43.55 (8.3)	46.25 (1.9)	46.25 (1.9)
α21	43.5 (2.3)	46.4 (2.6)	51.85 (3.7)	-	-	-
α23	39.95 (1.2)	50 (0)	50 (1)	38.4 (0)	44.85 (2)	44.85 (2)
α27	43.85 (5.1)	44.8 (1)	45.1 (2)	39.37 (1.9)	40.8 (0)	40.8 (0)
α28	45.2 (7.7)	46.45 (0.6)	48.1 (0)	-	-	-
α29	43.95 (1.1)	56.25 (4.2)	57.85 (1)	39.37 (1.9)	39.75 (1)	43.8 (5.1)
α30	47 (0.1)	51.05 (5.2)	52.9 (0)	46.9 (4.1)	47.9 (1)	48.05 (2.9)
α31	45.45 (0.4)	46.45 (0.6)	54.65 (0.9)	29.6 (3.7)	44.4 (0)	47.2 (2.8)
α32	43.15 (2)	44.65 (0.9)	51.85 (1.9)	40.7 (7.4)	40.7 (3.7)	43.5 (2.8)
α34	36.45 (1)	42.75 (1)	50 (0)	35.15 (1.9)	42.55 (1.9)	47.2 (2.8)
β13	53.95 (0.9)	56.3 (0)	58.8 (0)	49.95 (1)	55.1 (0)	56.9 (0)
β18	33.33 (0)	46.9 (3.1)	49.9 (0.9)	29.6 (3.7)	41.65 (2.8)	44.4 (0)
β20	48.35 (4.6)	48.45 (0.6)	50 (5.6)	34.25 (0.9)	50 (5.6)	50 (5.6)
β25	34.05 (4.7)	42.7 (3.1)	48.05 (1)	33.6 (1)	35.65 (1)	43.1 (0)
β26	38.55 (1)	44.8 (1)	46.95 (1.2)	37.95 (4.6)	43.5 (4.6)	45.35 (4.6)
β36	48.05 (2.9)	55.25 (1)	66.7 (0)	44.85 (6.1)	51 (0)	64.7 (0)
β37	40.3 (2.8)	43.5 (2.3)	49.05 (4.6)	-	-	-
β38	41.3 (3.8)	41.45 (0.2)	53.75 (1.9)	37 (3.7)	41.65 (2.8)	44.4 (0)
β40	46.45 (0.6)	47.4 (1.6)	55.55 (1.9)	45.4 (6.5)	47.2 (2.8)	49.05 (0.9)
41	41.7 (0)	45.8 (0)	54.65 (4.6)	40.75 (1.9)	44.4 (0)	50 (0)
43	41.7 (2.1)	45.85 (2.1)	51.85 (1.9)	37.95 (4.6)	40.7 (3.7)	48.15 (1.9)
44	48.55 (1.5)	56.85 (3.9)	71.3 (6.5)	42.55 (1.9)	43.5 (0.9)	44.4 (0)
PD[c]	73.95 (0.5)	75 (0)	76.5 (0)	50 (1)	50 (0)	54.15 (4.2)

[a] Praziquantel displayed an IC_{50} value of 0.1 µM against adult worms (data from ref. [43]). [b] Effect in percentage on adult worms after 24 h, 48 h, and 72 h. [c] PD displayed an IC_{50} value of 8.6 µM in the adult worm assay (data from ref. [38]). "-" means not tested.

Physico-chemical properties of the most potent [TRZ-methyl]-menadiones.

While it is essential to optimize the efficacy of our compounds against the target parasites, it is also important to characterize the pharmacological profile of these compounds. By introducing *N*-heteroaromatic groups, in particular triazoles, we aimed to improve the oral bioavailability and the physico-chemical properties of the 3-benzylmenadione series. Therefore, an *in silico* prediction of

several key PK parameters was performed using the SwissADME [44] web tool for compounds **β38**, **β18**, **β13**, **β36** and **47**, **48**, **49**, **50**, **PD** and **CQ** (used as reference) based on their antimalarial and antischistosomal activities. The Lipinski's and Veber's rules, [45,46] which are the most widely used drug-likeness filters, were used in this work. The physico-chemical properties of the selected compounds, including their molecular weight (MW), number of hydrogen bonds acceptors/donors (HBA/HBD) and total polar surface area (tPSA) were calculated and are presented in Table 4. In addition, Table 4 presented their predicted *n*-octanol/water partition coefficient (clog P), their solubility, their number of rotatable bonds and the number of violations of Lipinski's rules. All compounds studied fulfilled Lipinski's five rules and showed interesting predicted bioavailability properties. They also have acceptable tPSA [47] values below 140 $Å^2$, suggesting acceptable solubility values above 0.0001 mg/L. The lead antimalarial molecule, plasmodione **PD**, has a low aqueous solubility and a relatively high lipophilicity. By introducing *N*-heteroatomic moieties, we have attempted to improve these properties. Clear trends in lipophilicity were observed for the *N*-heteroaromatic series. Each addition of aromatic nitrogen tends to reduce the log P by about one unit, from benzyl to pyridine to pyrimidine and triazole. Compared to benzyl (**PD**) or pyridine (**47**, **48**) or pyrimidine (**49**, **50**) substitution, the introduction of a triazole significantly improved the aqueous solubility of the molecule. Despite improvements in these physico-chemical properties, there is no correlation with their ability to kill the *P. falciparum* parasite. Compounds with poor aqueous solubility and high lipophilic are most likely the most potent against *P. falciparum* (i.e. **PD** and neutral **CQ**). Whereas, for their antischistosomal potencies we can conclude that lipophilicity and aqueous solubility are not necessarily determinant in our case, as shown by the diverse physico-chemical profiles of **PD** (clog P: 4.4), **β13** (clog P: 3.1), and **β36** (clog P: 1.3), all of which demonstrate strong efficacy against *S. mansoni* adult worms (54.1%, 56.9% and 64.7%, respectively). While González *et al.* [48] suggested an optimal lipophilicity (clog P ≤ 2.5) for better aqueous solubility and parasite penetration to enhance antischistosomal potency, our compounds deviate from this trend, with **PD** and **β13** exhibiting higher clog P values. Despite this, they remain highly effective, similar to praziquantel (clog P: 2.4), suggesting that in this case, the relationship between physico-chemical properties and antischistosomal activity may involve other factors rather than just lipophilicity and aqueous solubility. The introduction of α- or β-TRZ into our pharmacophores has enabled us to make progress towards our goal of identifying more potent compounds with improved PK properties against various parasites of interest.

Table 4. Predicted physico-chemical parameters of the most potent compounds. [a] Molecular weight (g/mol). [b] Number of hydrogen bond acceptors/number of hydrogen bond donors. [c] Total polar surface area (Å^2). [d] Average of five predicted logarithm of compound's partition coefficient between *n*-octanol and water. [e] Solubility (mg/L). [f] Number of violations of Lipinski's rules.

Compound	MW[a]	HBA/HBD[b]	Number of rotatable bonds	tPSA[c]	clog P[d]	Solubility[e]	Lipinski violations[f]
Ref values	≤500	≤10/≤5	≤10	≤140	≤5	>0.0001	≤1
β13	343.38	4/0	4	64.85	3.09	23.0	0
β18	465.54	7/0	8	97.63	2.48	70.9	0
β36	297.31	5/1	4	85.08	1.35	1490	0
β38	400.42	7/0	5	68.09	2.69	43.1	0
47	331.29	6/0	3	47.03	3.79	15.4	0
48	331.29	6/0	3	47.03	3.77	15.4	0
49	332.28	7/0	3	59.92	3.28	39	0
50	332.28	7/0	3	59.92	3.26	39	0
PD	330.30	5/0	3	34.14	4.43	6.89	0
CQ	319.87	2/1	8	28.16	4.15	9.05	0
praziquantel	312.41	2/0	2	40.62	2.4	94.3	0

Redox properties of [TRZ-methyl]-menadiones.

To provide a possible explanation for the lack of activity of this series against *P. falciparum* and the contrast that exists between the activities against *S. mansoni* worms and *P. falciparum* parasite, we investigated the redox properties of the menadione electrophore for α- or β-[TRZ-methyl]-menadiones (Figure 5). For the sake of comparison, β-[TRZ-methyl]-menadione **β36** and α-[TRZ-methyl]-menadione **α29** bearing a hydroxymethyl substituent on the TRZ moiety were studied and compared to **PD** used as reference (Figure S1 to S10 in the ESI). The typical electrochemical profile of menadione derivatives, including **PD** and **PDO**, has been already described in detail in previous studies. [17,36,37] It relies on two consecutive one-electron reversible waves, which correspond to the sequential reduction of the 1,4-naphthoquinone core leading to the semi-naphthoquinone and dihydro-naphthoquinone, respectively. In this work, we have not considered anode potentials greater than 0.1 V. The comparison of the redox properties of **β36** (β-TRZ, (Figure S2 in the ESI) with the benzylmenadione **PD** (Figure S1 in the ESI) firstly shows a comparable electrochemical profile (Table 5), except for a third irreversible wave observed at a much more negative value of -1.88 V (*vs.* Ag/AgCl/3M KCl), which could be attributed to the reduction of the triazole unit (Figure S3 in the ESI). [49,50] While the methylene bridge is expected to act as an effective electronic insulator, the weak differences observed for the two redox waves can be explained by possible non-covalent interactions (e.g. hydrogen bond [51] between the triazole and the negatively charged semiquinone [52,53] , CH-π or dipole-dipole [36]).

The study of the electrochemical properties of the α-[TRZ-methyl]-menadione **α29** is much more complex. Although it is characterized by two main redox waves separated by more than 600 mV comparable to **β36** and **PD**, each of the main waves is composed of two reversible waves separated by

about 170 mV for the first redox process and about 100 mV for the second one (Figure S4 in the ESI). Similarly to **β36**, a third irreversible redox wave can be observed at more negative potentials (-1.63 V *vs.* Ag/AgCl/3M KCl) that can be assigned to the TRZ unit. It is interesting to note that when the scanning potential is shifted to more negative values (down to -2.5 V, Figure S5 in the ESI), a change in the intensity of each of the 2 waves corresponding to each 1-electron transfer process is observed, but without changing the global shape (i.e. position of each redox peaks) of the voltammogram. Regardless of the complexity of the **α29** voltammogram, its CV and SWV profiles remain comparable to that of **β36**, with the first redox waves at the same potentials as **PD** and **β36** and a second redox wave that is more oxidizing than that measured for **PD** and comparable to that of **β36** (Table 5, Figure S6 in the ESI). Note that the electronic UV-visible absorption spectra recorded for these three compounds (i.e. **PD**, **β36** and **α29**) are comparable indicating an unaffected 1,4-naphthoquinone core (π–π* transitions centered at about 330 nm, Figure S7 in the ESI) by the benzyl or TRZ-methyl substitution. The main structural differences between **β36** and **α29** are: *i*) the position of the α- or β-TRZ-methyl relative to the menadione core and *ii*) the position of the substituent on the triazole. To first investigate the possible effect of the hydroxymethyl substituent, we performed the same electrochemical experiment on the unsubstituted α-[TRZ-methyl]-menadione **α8** (Figures S8 and S9 in the ESI). **α8** displays exactly the same profile as **α29** (when reduced to -2.0 V or to -2.5V), implying that only the triazole position (α-TRZ *vs*. β-TRZ) relative to menadione alters the electrochemical profile without any influence of the hydroxymethyl substituent (Figure S10 in the ESI). We therefore hypothesized that for α-[TRZ-methyl]-menadiones a new electroactive product is generated during the electrochemical process, [54] a product also characterized by two reversible redox waves shifted towards anodic currents of more than 100 mV. This new unidentified species most likely involves the α-[TRZ-methyl] unit, the intensity ratio of each of the redox waves being modified according to the potential window considered.

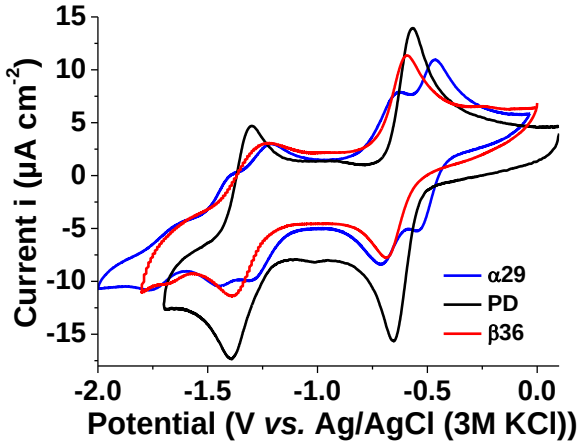

Figure 5. Comparison of the CV spectra recorded for **α29** (1.07 mM, blue curve) **PD** (1.13 mM, black curve) and **β36** (0.93 mM, red curve). Solvent: DMSO; *I* = 0.1 M *n*-Bu_4NPF_6; v = 200 mV s^{-1}. Reference electrode = KCl(3 M)/Ag/AgCl; working electrode = glassy carbon disk of 0.07 cm^2 area; auxiliary electrode = Pt wire.

Table 5: Electrochemical data measured using cyclic voltammetry (CV)[a] and Square Wave Voltammetry (SWV)[b]. Solvent: DMSO; *I* = 0.1 M *n*-Bu_4NPF_6, v = 200 mV s^{-1}. NA: not applicable. [c] blended signals.

Compound	$E^1_{1/2}(\Delta E)^{[a]}/E^1_{1/2}{}^{[b]}$ [V(mV)][a]/[V][b]	$E^{1*}_{1/2}(\Delta E)^{[a]}/E^{1*}_{1/2}{}^{[b]}$ [V(mV)][a]/[V][b]	$E^2_{1/2}(\Delta E)^{[a]}/E^2_{1/2}{}^{[b]}$ [V(mV)][a]/[V][b]	$E^{2*}_{1/2}(\Delta E)^{[a]}/E^{2*}_{1/2}{}^{[b]}$ [V(mV)][a]/[V][b]	$E^3_{1/2}(\Delta E)^{[a]}/E^3_{1/2}{}^{[b]}$ [V(mV)][a]/[V][b]
PD[12,36]	-0.63 (84) / -0.59	NA	-1.35 (88)/-1.32	NA	NA
β36	-0.64 (90) / -0.61	NA	-1.31 (164) / -1.28	NA	-1.88
α29	-0.67 (86) / -0.65	-0.50 (84) / -0.49	-1.41 (76) / -1.34	-1.26 (102) / -1.23	-1.63
α8	-0.68 (88) / -0.65	- 0.52 (64) / -0.48	-1.39 / -1.24[c]		-1.62

'Benzylic' oxidation of [TRZ-methyl]-menadiones.

Based on our previous work with **PD** and its analogues [6,12] (i.e. benzyl oxidation to produce a highly active metabolite), the biological activity of [TRZ-methyl]-menadiones in *P. falciparum* could be based on their ability to undergo oxidation at the same carbon position *in vivo* to produce an active metabolite. In the case of [TRZ-methyl]-menadiones, the phenyl group has been indeed replaced by a heteroaromatic fragment and the nitrogen atom substituted to the methylene bridge (oxidation position) could therefore have a significant effect on oxygen insertion and therefore menadione activity. Note that for triazoles in the α-position, oxidation of the methylene group would lead to an amide bond after oxidation, which could significantly alter the redox properties of the naphthoquinone electrophore. [TRZ-methyl]-menadiones have little or no activity against *P. falciparum* (Table 2) and this lack of activity may be related to the inability of these compounds to generate the oxidized metabolite.

To investigate this property further, we used the photoredox conditions established by our team, [11,12] which allow the oxidation of 3-benzylmenadione (in the presence of O_2) under reducing conditions (photoirradiation with a hydrogen donor). These conditions perfectly mimic the enzymatic catalytic conditions. Menadione is known to be reduced to dihydro-menadione via a semi-quinone by photoreduction in isopropanol, and [55] we have demonstrated that benzylic oxidation is possible by insertion of O_2 from the corresponding reduced species. [12] We therefore subjected two [TRZ-methyl]-menadiones bearing inert substituents to photo-oxidation conditions (UV irradiation for 72 h in an oxygen atmosphere), namely compounds **α14** and **β13** (Figure 6). These experiments were performed in a dichloromethane/isopropanol (1/1) mixture to avoid solubility issues. As expected, only **β51**, the oxidized form of **β13**, was obtained in 27% yield, while **α14** either remained intact or underwent degradation due to the high-energy excitation conditions. These data are in excellent agreement with the antiplasmodial activities (Table 2), which show that the α-[TRZ-methyl]-menadiones have little or no activity against this pathogen, while the β-analogues are moderately active compared to **PD**. This also suggests different action or drug transport mechanisms in *S. mansoni*, as we were able to clearly demonstrate that both α- and β-[TRZ-methyl]-menadiones were active on NTS and adult worms.

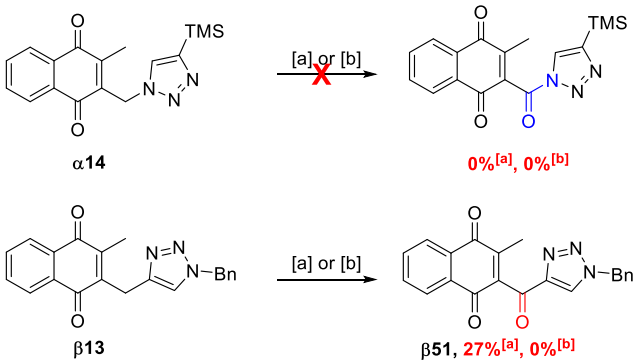

Figure 6. Oxidation of α- or β-[TRZ-methyl]-menadiones via UV-irradiation or chemical conditions. Condition [a]: DCM/*i*PrOH (1/1, 0.01 M), under O_2 atmosphere and UV-irradiation 350 nm (i.e. a Rayonet photochemical reactor equipped with 16 UV lamps of 14 W), 15 °C, 72 h. Condition [b] from Baltas *et al.* (reference [56]): 4 equiv. TBHP, 0.1 eq. CuI, MeCN (0.1 M), r.t., 20 h.

To go even further, 3-benzylmenadiones can be chemically oxidized to benzoyl derivatives under harsher conditions. Indeed, Baltas *et al.* have described [56] a method for the preparation of α-keto-1,2,3-triazoles from benzyl-triazoles in the presence of *tert*-butyl hydroperoxide (TBHP) and catalytic amounts of copper iodide (Figure 6). However, neither α- nor β-[TRZ-methyl]-menadiones were found to be reactive under these experimental conditions. This may be explained by the fact 1,4-naphthoquinone is a very electron-deficient group, already highly oxidized and acting as a strong EWG presumably requiring much harsher conditions. Among the numerous systems considered by Baltas *et al.*, only nitrobenzyl was tested (NO_2 is a potent EWG that can be reduced). In the same report, no oxidation of the *N*-substituted benzyl moiety of the triazole ring was described as possible, confirming our hypothesis that α-[TRZ-methyl]-menadiones cannot be oxidized. We thus confirm that oxidation of β-[TRZ-methyl]-menadiones is possible *in tubo* (27% for **β51**) and that this is comparable to the conversion observed for **PD** (37%) under comparable experimental conditions. [57] In the case of α-[TRZ-methyl]-menadiones or the various 5-membered-*N*-heteroaromatic menadiones, the presence of a nitrogen atom in the α-position significantly reduces this possibility, leading to compounds with little or no activity against *P. falciparum*.

Conclusion

Our goal was to revisit and improve the antiparasitic bMD series with the introduction of a triazole as "MedChem friendly" moiety. In this study, we were able to synthesize a library of about 30 compounds distributed in two series of α- and β-[TRZ-methyl]-menadiones, through one single step using CuAAC click chemistry. This modification led to a clear increase of aqueous solubility while decreasing the lipophilicity of our compounds, which significantly improved their bioavailability. However, their antimalarial evaluation revealed that, 1,2,3-triazoles were not internalized/active in general. By contrast, β-[TRZ-methyl]-menadiones **β13** and **β36** were highly potent against *in vitro* adult *S. mansoni* worms. Therefore, this highlights that the introduction of α- or β-TRZ-methyl resulted in differential antimalarial *versus* antischistosomal activities of compounds. To explain this contrast, we evaluated their

electrochemical properties and their ability to undergo benzylic oxidation via a photo-reduction process. We demonstrated that the 1,2,3-triazole moiety does not necessarily affect the redox properties of the menadione core, while the insertion of oxygen in the benzylic position was totally altered, making the generation of the active metabolite in *P. falciparum* impossible for an α-TRZ and not favored for a β-TRZ. This study clearly raises the question that 3-benzylmenadiones or [TRZ-methyl]-menadiones share different MoA/penetration processes in *S. mansoni* worms compared to those in *P. falciparum* parasite. Future studies will aim to continue the development of [TRZ-methyl]-menadione series for a better SAR comprehension as antischistosomal compounds while investigate their MoA and evaluate possible distinct biological targets or drug transport mechanisms.

Supporting Information

Table of contents: Supporting Information (ESI) content: pages S2-S8 (Figure S1-S10) – electrochemistry CV, SWV curves and UV-visible absorption curve; page S9 (Table S1) – CuAAC reaction with **1** using different conditions; pages S10-S12 – By-product and reduction after CuAAC from **1**; pages S13-S15 (Figure S11-S12) – synthesis of azido-substrates engaged in the CuAAC reaction to form β-[TRZ-methyl]-menadione; pages S16-S17 (Figure S13) – synthesis of alcyne-substrates engaged in the CuAAC reaction to form α-[TRZ-methyl]-menadione; pages S18-S65 – ^{1}H, ^{19}F {^{1}H} and ^{13}C {^{1}H} NMR spectra of compounds **1−β51**.

Acknowlegements

E.D.-C. wish to thank the Laboratoire d'Excellence (LabEx) ParaFrap [ANR-11-LABX-0024], for funding, providing B.D.'s PhD salary, and for initiating and fostering this scientific research and collaboration. This work was furthermore supported by the Agence Nationale de la Recherche, France (Program ANR-PRCI with FNS, Project "ROSaction", grant ANR-22-CE93-0005-01 to E.D-C., M.R., P.M. The laboratory (E.D.-C.) also received support from CNRS and from the University of Strasbourg.

Conflict of Interests

The authors declare no conflict of interest.

Abbreviations: CuAAC: copper catalysed azide to alkyne cycloaddition, TRZ: triazole, PD: plasmodione, PDO: plasmodione-oxyde, bMD: 3-benzyl-menadione, MoA: mode of action, PC: physico-chemical, PK: pharmaco-kinetic, SAR: structure activity relationship, TEA: triethylamine, DMSO: dimethylsulphoxide, DCM: dichloromethane, DMF: dimethylformamide, THF: tetrahydrofurane, TFA: trifluoroacetic acid, TBAI: tetra-butylammonium iodide, NTS: newly transformed schistosomula, TBHP: tert-butyl hydroperoxide, EWG: electron withdrawing group, CHX: cyclohexane, CV: cyclic voltammetry, SWV: scare wave voltammetry.

References

[1] WHO, World malaria report 2023.

[2] P. J. Rosenthal, V. Asua, J. A. Bailey, M. D. Conrad, D. S. Ishengoma, M. R. Kamya, C. Rasmussen, F. G. Tadesse, A. Uwimana, D. A. Fidock. The emergence of artemisinin partial resistance in Africa: how do we respond? *Lancet Infect Dis.* **2024**, *24*(9):e591-e600.

[3] A. G. P. Ross, A. C. Sleigh, G. R. Olds, G. M. Williams, D. P. Mcmanus. Schistosomiasis. *N. Engl. J. Med.* **2002**, *346*, 1212-1220.

[4] WHO, fact sheet Schistosomiasis (Bilharzia), 2023.

[5] A. S. Sturt, E. L. Webb, S. C. Francis, R. J. Hayes, A. L. Bustinduy. Beyond the barrier: Female Genital Schistosomiasis as a potential risk factor for HIV-1 acquisition. *Acta Trop.* **2020**, *209*, 105524.

[6] T. Müller, L. Johann, B. Jannack, M. Brückner, D. A. Lanfranchi, H. Bauer, C. Sanchez, V. Yardley, C. Deregnaucourt, J. Schrével, M. Lanzer, R. H. Schirmer, Davioud-Charvet, E. Glutathione reductase-catalyzed cascade of redox reactions to bioactivate potent antimalarial 1,4-naphthoquinones – A new strategy to combat malarial parasites. *J. Am. Chem. Soc.* **2011**, *133*, 11557-71.

[7] K. Ehrhardt, E. Davioud-Charvet, H. Ke, A. Vaidya, M. Lanzer, Deponte M. The mitochondrial electron transport chain is dispensable for the antimalarial activities of methylene blue and the lead 1,4-naphthoquinone 2-[4-(trifluoromethyl)benzyl]-menadione. *Antimicrob. Agents Chemother.* **2013**, *57*, 2114-2120.

[8] D. A. Lanfranchi, E. Cesar-Rodo, B. Bertrand, H.-H. Huang, L. Day, L. Johann, M. Elhabiri, K. Becker, D. L. Williams, E. Davioud-Charvet. Synthesis and Biological Evaluation of 1,4-Naphthoquinones and Quinoline-5,8-Diones as Antimalarial and Schistosomicidal Agents. *Org. Biomol. Chem.* **2012**, *10*, 6375.

[9] K. Ehrhardt, C., Deregnaucourt A.-A. Goetz, T. Tzanova, B. Pradines, S. H. Adjalley, S. Blandin, D. Bagrel, M. Lanzer, E. Davioud-Charvet. The redox-cycler plasmodione is a fast acting antimalarial lead compound with pronounced activity against sexual and early asexual blood-stage parasites. *Antimicrob. Agents Chemother.* **2016**, *60*, 5146-58.

[10] M. Bielitza, D. Belorgey, K. Ehrhardt, L. Johann, D. A. Lanfranchi, V. Gallo, E. Schwarzer, F. Mohring, E. Jortzik, D. L. Williams, K. Becker, P. Arese, M. Elhabiri, E. Davioud-Charvet. Antimalarial NADPH-Consuming Redox-Cyclers As Superior Glucose-6-Phosphate Dehydrogenase Deficiency Copycats. *Antioxid. Redox Signal.* **2015**, *22*, 1337–1351.

[11] B. A. Cichocki, V. Khobragade, M. Donzel, L. Cotos, S. Blandin, C. Schaeffer-Reiss, S. Cianférani, J.-M. Strub, M. Elhabiri, E. Davioud-Charvet. A Class of Valuable (Pro-)Activity-Based Protein Profiling Probes: Application to the Redox-Active Antiplasmodial Agent, Plasmodione. *JACS*^{Au} **2021**, *1*, 669–689.

[12] B. A. Cichocki, M. Donzel, K. C. Heimsch, M. Lesanavičius, L. Feng, E. J. Montagut, K. Becker, A. Aliverti, M. Elhabiri, N. Čėnas, E. Davioud-Charvet. *Plasmodium Falciparum* Ferredoxin-NADP $^{+}$ Reductase-Catalyzed Redox Cycling of Plasmodione Generates Both Predicted Key Drug Metabolites: Implication for Antimalarial Drug Development. *ACS Infect. Dis.* **2021**, *7*, 1996–2012.

[13] E. C. Rodo, L. Feng, M. Jida, K. Ehrhardt, M. Bielitza, J. Boilevin, M. Lanzer, D. L. Williams, D. A. Lanfranchi, E. Davioud-Charvet. A platform of regioselective methodologies to access to polysubstituted 2-methyl-1,4-naphthoquinones derivatives: scope and limitations. *Eur. J. Org. Chem.* **2016**, *11*, 1982–1993.

[14] K. Urgin, M. Jida, K. Ehrhardt, T. Müller, M. Lanzer, L. Maes, E. Davioud-Charvet. Pharmacomodulation of the antimalarial plasmodione: synthesis of biaryl- and *N*-arylalkylamine analogues, antimalarial activities and physicochemical properties. *Molecules* **2017**, 22, *161*, 1-32.

[15] P. Mounkoro, T. Michel, S. Blandin, M. P. Golinelli-Cohen, E. Davioud-Charvet, B. Meunier. Investigating the mode of action of the redox-active antimalarial drug plasmodione using the yeast model. *Free Radic Biol Med.* **2019**, *141*, 269-278.

[16] L. Feng, D. A. Lanfranchi, L. Cotos-Munoz, E. Cesar Rodo, K. Ehrhardt, , A.-A. Goetz, H. Zimmerman, F. Fenaille, S. Blandin, E. Davioud-Charvet. Synthesis of plasmodione metabolites and ^{13}C-enriched plasmodione as chemical tools for drug metabolism investigation. *Org. Biomol. Chem.* **2018**, *16*, 2647-2665.

[17] P. Sidorov, I. Desta, M. Chessé, D. Horvath, G. Marcou, A. Varnek, E. Davioud-Charvet, M. Elhabiri. Redox Polypharmacology as an Emerging Strategy to Combat Malarial Parasites. *ChemMedChem* **2016**, *11*, 1339–1351.

[18] B. Dupouy, M. Donzel, M. Roignant, S. Charital, R. Keumoe, Y. Yamaryo-Botté, A. Feckler, M. Bundschuh, Y. Bordat, M. Rottmann, P. Mäser, C. Y. Botté, S. A. Blandin, S. Besteiro, E. Davioud-Charvet. 3-benzylmenadiones and their heteroaromatic analogues target the apicoplast of Apicomplexa parasites: Synthesis and bioimaging studies. *ACS Inf. Dis.* **2024**, id-2024-00304k.R2 - Manuscript Accepted 13-Sep-2024.

[19] D. Coelho, Y. Colas, M. Ethève-Quelquejeu, E. Braud, L. Iannazzo. Halo-1,2,3-triazoles: Valuable Compounds to Access Biologically Relevant Molecules. *ChemBioChem* **2024**, *25* (10), e202400150.

[20] H. C. Kolb, M. G. Finn, K. B. Sharpless. Click Chemistry: Diverse Chemical Function from a Few Good Reactions. *Angew. Chem. Int. Ed.* **2001**, *40* (11), 2004–2021.

[21] E. N. Da Silva, I. M. M. De Melo, E. B. T. Diogo, V. A. Costa, J. D. De Souza Filho, W. O. Valença, C. A. Camara, R. N. De Oliveira, A. S. De Araujo, F. S. Emery, M. R. Dos Santos, C. A. De Simone, R. F. S. Menna-Barreto, S. L. De Castro. On the Search for Potential Anti-Trypanosoma Cruzi Drugs: Synthesis and Biological Evaluation of 2-Hydroxy-3-Methylamino and 1,2,3-Triazolic Naphthoquinoidal Compounds Obtained by Click Chemistry Reactions. *Eur. J. Med. Chem.* **2012**, *52*, 304–312.

[22] S. Oramas-Royo, P. López-Rojas, Á. Amesty, D. Gutiérrez, N. Flores, P. Martín-Rodríguez, L. Fernández-Pérez, A. Estévez-Braun. Synthesis and Antiplasmodial Activity of 1,2,3-Triazole-Naphthoquinone Conjugates. *Molecules* **2019**, *24*(21), 3917.

[23] M. W. Pertino, A. F. De La Torre, G. Schmeda-Hirschmann, C. Vega, M. Rolón, C. Coronel, A. Rojas De Arias, K. Leal López, P. Carranza-Rosales, E. Viveros Valdez. Synthesis, Trypanocidal and Anti-Leishmania Activity of New Triazole-Lapachol and nor-Lapachol Hybrids. *Bioorg. Chem.* **2020**, *103*, 104122.

[24] E. N. da Silva Júnior, G. A. M. Jardim, C. Jacob, U. Dhawa, L. Ackermann, S. L. de Castro. Synthesis of quinones with highlighted biological applications: A critical update on the strategies towards bioactive compounds with emphasis on lapachones. *Eur. J. Med. Chem.* **2019**, *179*, 863-915.

[25] R. M. Costa Souza, L. M. L. Montenegro Pimentel, L. K. M. Ferreira, V. R. A. Pereira, A. C. D. S. Santos, W. M. Dantas, C. J. O. Silva, R. M. De Medeiros Brito, J. L. Andrade, V. F. De Andrade-Neto, R. T. Fujiwara, L. L. Bueno, V. A. Silva Junior, L. Pena, C. A. Camara, B. Rathi, R. N. De Oliveira. Biological Activity of 1,2,3-Triazole-2-Amino-1,4-Naphthoquinone Derivatives and Their Evaluation as Therapeutic Strategy for Malaria Control. *Eur. J. Med. Chem.* **2023**, *255*, 115400.

[26] E. Haldón, M. C. Nicasio, P. J. Pérez. Copper-Catalysed Azide–Alkyne Cycloadditions (CuAAC): An Update. *Org. Biomol. Chem.* **2015**, *13* (37), 9528–9550.

[27] S. Neumann, M. Biewend, S. Rana, W. H. Binder. The CuAAC: Principles, Homogeneous and Heterogeneous Catalysts, and Novel Developments and Applications. *Macromol. Rapid Commun.* **2020**, *41* (1), 1900359.

[28] M. Meldal, F. Diness. Recent Fascinating Aspects of the CuAAC Click Reaction. *Trends in Chemistry* **2020**, *2* (6), 569–584.

[29] M. Meldal, C. W. Tornøe. Cu-Catalyzed Azide−Alkyne Cycloaddition. *Chem. Rev.* **2008**, *108* (8), 2952–3015.

[30] V. O. Rodionov, S. I. Presolski, D. Díaz Díaz, V. V. Fokin, M. G. Finn. Ligand-Accelerated Cu-Catalyzed Azide−Alkyne Cycloaddition: A Mechanistic Report. *J. Am. Chem. Soc.* **2007**, *129* (42), 12705–12712.

[31] L. Johann, D. Belorgey, K. Becker, H.-H. Huang, L. Day, D.L. Williams, E. Davioud-Charvet. Synthesis and evaluation of 1,4-naphthoquinone ether derivatives as SmTGR inhibitors and new antischistosomal drugs. *FEBS J.* **2015**, 282, 3199-3217.

[32] A. A. Haddach, A. Kelleman, M. V. Deaton-Rewolinski. An Efficient Method for the N-Debenzylation of Aromatic Heterocycles. *Tetrahedron Lett.* **2002**, *43* (3), 399-402.

[33] J. E. Hein, V. V. Fokin. Copper-catalyzed azide-alkyne cycloaddition (CuAAC) and beyond: new reactivity of copper(I) acetylides. *Chem. Soc. Rev.* **2010**, *39*, 1302-15.

[34] C. Snyder, J. Chollet, J. Santo-Tomas, C. Scheurer, S. Wittlin. In Vitro and in Vivo Interaction of Synthetic Peroxide RBx11160 (OZ277) with Piperaquine in Plasmodium Models. *Exp. Parasitol.* **2007**, *115*, 296–300.

[35] F. C. Lombardo, V. Pasche, G. Panic, Y. Endriss, J. Keiser. Life cycle maintenance and drug-sensitivity assays for early drug discovery in *Schistosoma mansoni*. *Nat Protoc.* **2019**,*14*, 461-481.

[36] M. Elhabiri, P. Sidorov, E. Cesar-Rodo, G. Marcou, D. A. Lanfranchi, E. Davioud-Charvet, D. Horvath, A. Varnek. Electrochemical properties of substituted 2-methyl-1,4-naphthoquinones: redox behavior predictions. *Chem.-Eur. J*. **2015**, *21*, 3415-3424.

[37] L. Cotos, M. Donzel, M. Elhabiri, E. Davioud-Charvet. A Mild and Versatile Friedel–Crafts Methodology for the Diversity-Oriented Synthesis of Redox-Active 3-Benzoylmenadiones with Tunable Redox Potentials. *Chem. Eur. J.* **2020**, *26* (15), 3314–3325.

[38] E. Cesar-Rodo, B. Dupouy, C**.** Häberli, D. L. Williams, J**.**-M**.** Strub, P. Mäser, M. Rottmann, J. Keiser, D. A. Lanfranchi, E. Davioud-Charvet. Regioselective synthesis of potential non-quinonoid prodrugs of plasmodione: drug metabolism studies and antiparasitic properties against two hemoglobin-feeding parasites. Submitted on 01-09-2024, **2024**, Nr-3212870.

[39] R. Tepper, B. Schulze, P. Bellstedt, J. Heidler, H. Görls, M. Jäger, U. S. Schubert. Halogen-Bond-Based Cooperative Ion-Pair Recognition by a Crown-Ether-Embedded 5-Iodo-1,2,3-Triazole. *Chem. Commun.* **2017**, *53* (14), 2260–2263.

[40] S. Singh, N. El-Sakkary, D. E. Skinner, P. P. Sharma, S. Ottilie, Y. Antonova-Koch, P. Kumar, E. Winzeler, Poonam, C. R. Caffrey, B. Rathi. Synthesis and Bioactivity of Phthalimide Analogs as Potential Drugs to Treat Schistosomiasis, a Neglected Disease of Poverty. Pharmaceuticals (Basel) **2020**,*13*(2):25.

[41] C. Biot, H. Bauer, R.H., Schirmer E. Davioud-Charvet. 5-Substituted tetrazoles as bioisosters of carboxylic acids. Bioisosterism and mechanistic studies on glutathione reductase inhibitors as antimalarials. *J. Med. Chem.* **2004**, *47*, 5972-5983.

[42] S. Biendl, C. Häberli, G. Chen, W. Wang, L. Zhong, J. Saunders, T. Pham, X. Wang, J. Wu, S. A. Charman, J. L. Vennerstrom, J. Keiser. In Vitro and In Vivo Antischistosomal Activity Profiling and Pharmacokinetics of Ozonide Carboxylic Acids. *ACS Infect Dis.* **2023**, *9*(3), 643-652.

[43] K. Ingram, I. A. Yaremenko, I. B. Krylov, L. Hofer, A. O. Terent'ev, J. Keiser. Identification of antischistosomal leads by evaluating bridged 1,2,4,5-tetraoxanes, alphaperoxides, and tricyclic monoperoxides. *J. Med. Chem.* **2012**, *55*, 8700-8711.

[44] A. Daina, O. Michielin, V. Zoete. SwissADME: A Free Web Tool to Evaluate Pharmacokinetics, Drug-Likeness and Medicinal Chemistry Friendliness of Small Molecules. *Sci Rep* **2017**, *7*, 42717.

[45] C. A. Lipinski, F. Lombardo, B. W. Dominy, P. J. Feeney. Experimental and Computational Approaches to Estimate Solubility and Permeability in Drug Discovery and Development Settings. *Adv. Drug Del. Rev.* **2001**, *43*, 3–26.

[46] D. F. Veber, S. R. Johnson, H.-Y. Cheng, B. R. Smith, K. W. Ward, K. D. Kopple. Molecular Properties That Influence the Oral Bioavailability of Drug Candidates. *J. Med. Chem.* **2002**, *45*, 2615–2623.

[47] J. Kelder, P. D. J. Grootenhuis, D. M. Bayada, L. P. C. Delbressine, J.-P. Ploemen. Polar Molecular Surface as a Dominating Determinant for Oral Absorption and Brain Penetration of Drugs. *Pharm. Res.* **1999**, *16*, 1514–1519.

[48] D. González Cabrera, J. Keiser, T. Spangenberg. Analysis of the Physicochemical Properties of Anti-Schistosomal Compounds to Identify Next-Generation Leads. *ACS Med Chem Lett.* **2024**, 15, 626-630.

[49] S. V. Lokesh, A. K. Satpati, B. S. Sherigara. Electrochemical Behavior of 1,2,4-Triazole and Benzotriazole at Glassy Carbon Electrode in Acidic Media. *TOELEC J.* **2010**, *2*, 15–21.

[50] D. P. Day, T. Dann, D. L. Hughes, V. S. Oganesyan, D. Steverding, G. G. Wildgoose. Cymantrene–Triazole "Click" Products: Structural Characterization and Electrochemical Properties. *Organometallics* **2014**, *33*, 4687–4696.

[51] B. Schulze, U. S. Schubert. Beyond Click Chemistry – Supramolecular Interactions of 1,2,3-Triazoles. *Chem. Soc. Rev.* **2014**, *43*, 2522.

[52] Willson R. L. Semiquinone Free Radicals: Determination of Acid Dissociation Constants by Pulse Radiolysis. *J. Chem. Soc. D* **1971**, 1249-1250.

[53] P. D. Astudillo-Sánchez, D. Morales-Martínez, A. Sánchez, G. Rocha-Ortiz, M. Salas-Reyes. Electrochemical Study of the Interactions between Anionic Species of Menadione and Alkylated Nucleobases in Dimethylsulfoxide. *J. Electroanal. Chem*. **2017**, *801*, 104–113.

[54] A. D. R. Pontinha, C. M. Lombardo, S. Neidle, A. M. Oliveira-Brett. Triazole-Linked Phenyl Derivatives: Redox Mechanisms and in Situ Electrochemical Evaluation of Interaction with dsDNA. *Bioelectrochemistry* **2015**, *101*, 97–105.

[55] H. Görner. Photoreduction of Nitro-1,4-Naphthoquinones in Solution. *J. Photochem. Photobiol. A Chem.* **2011**, *224*, 135–140.

[56] S. Nawratil, M. Grypioti, C. Menendez, S. Mallet-Ladeira, C. Lherbet, M. Baltas. Synthesis of α-Keto-1,2,3-triazoles Through Copper Iodide Catalyzed Oxygenation. *Eur. J. Org. Chem.* **2014**, *2014*, 654–659.

[57] I. Iacobucci, V. Monaco, A. Hovasse, B. Dupouy, R. Keumoe, B. Cichocki, M. Elhabiri, B. Meunier, J. Strub, M. Monti, S. Cianférani, S. A. Blandin, C. Schaeffer-Reiss, E. Davioud-Charvet. Proteomic Profiling of Antimalarial Plasmodione Using 3-Benz(o)Ylmenadione Affinity-Based Probes. *ChemBioChem* **2024**, e202400187.

1.1.3 Les points importants de l'article 5

- **Synthèse des α- et β-[TRZ-méthyle]-ménadiones :** Deux voies de synthèse ont été explorées. La voie (2), utilisant des ménadiones non protégés, a permis l'introduction d'une grande diversité de substrats, aboutissant à une bibliothèque de près de 30 composés distincts, offrant ainsi une importante diversité structurale.
- **Efficacité antipaludique :** Les α-[TRZ-méthyle]-ménadiones se sont révélées inefficaces contre *P. falciparum*, tandis que les dérivés β ont montré une activité modérée, indiquant que les modifications structurales influencent leur efficacité contre ce parasite.
- **Propriétés rédox et oxydation benzylique :** L'analyse électrochimique a révélé que les dérivés β et α présentaient un profil électrochimique similaire à celui de la plasmodione. Cependant, les dérivés α sont incapables de générer le métabolite oxydé actif, expliquant leur inefficacité contre *P. falciparum*. Les dérivés β, quant à eux, peuvent générer ce métabolite, mais de manière bien moins efficace que la plasmodione. Globalement, l'introduction du groupement [TRZ-méthyle] modifie la capacité à produire les métabolites actifs contre ce parasite, entraînant une forte diminution de l'activité antipaludique.
- **Activité antischistosomale :** Les [TRZ-méthyle]-ménadiones ont montré une activité significative contre les NTS et les vers adultes de *S. mansoni*, avec une efficacité parfois supérieure à celle de la plasmodione. Notamment la réduction de la lipophilicité et l'augmentation de la solubilité aqueuse, favorise probablement une meilleure pénétration dans les vers parasites et une biodisponibilité accrue, justifiant ainsi l'amélioration de l'activité antischistosomale.
- **Relation structure-activité (SAR) :** L'étude a mis en évidence les différents mécanismes d'action des dérivés bMDs vis-à-vis de deux parasites hématophages (*P. falciparum* et *S. mansoni)*, démontrant que les triazoles substitués en α et en β se comportent différemment en termes de pénétration parasitaire, de métabolisation et d'activité.

1.2 Poursuite du développement de pseudo-PD comme molécules pro-drogue de la Plasmodione

1.2.1 Travaux préliminaires

Ce travail s'inscrit dans la continuité de l'amélioration de notre molécule de référence, en introduisant un nouveau mécanisme pro-drogue sur la plasmodione. Il y a une dizaine d'années, dans l'équipe CBM, le Dr. Don Antoine Lanfranchi (post-doctorant) et le Dr. Eléna Rodo (doctorante) avaient déjà initié ce projet. Leur travail sur l'élaboration de nouvelles méthodologies de synthèse visant à diversifier la structure du motif ménadione a permis la mise en place de ce projet de recherche. Grâce à la stratégie Diels-Alder[44,50–52] (décrite dans l'introduction), ils ont pu introduire un méthyle angulaire de manière régiosélective, en C-4a. Le but de l'équipe était d'étudier le possible effet pro-drogue, générant la pseudo-plasmodione ou ψ-PD, catalysé par une activité de type aromatase, porté par l'hémoglobine dans un environnement très oxydant. L'étude est présentée dans cet article (Figure 32).

La PD est déjà un composé pro-drogue, car elle est métabolisée en PDO (bioactif) par la *Pf*FNR[45,69] une fois internalisée dans le parasite *P. falciparum*. Cependant, selon un dogme bien établi dans la littérature, les propriétés rédox, la faible solubilité et la toxicité des quinones peuvent effrayer les industriels pour développer des médicaments de type *redox-cyclers*. C'est pourquoi nous envisageons aujourd'hui de poursuivre le développement de pro-drogues de la PD, tout en améliorant les propriétés PC/PK du composé. Le méthyle angulaire en alpha d'un carbonyle de la NQ perturbe l'aromaticité de la quinone entrainant deux effets principaux, i) l'amélioration des propriétés PC et PK de la molécule, ii) l'hydroxylation *in situ* et l'élimination via un mécanisme enzymatique, générant ainsi la PD dans le parasite (Figure 32).

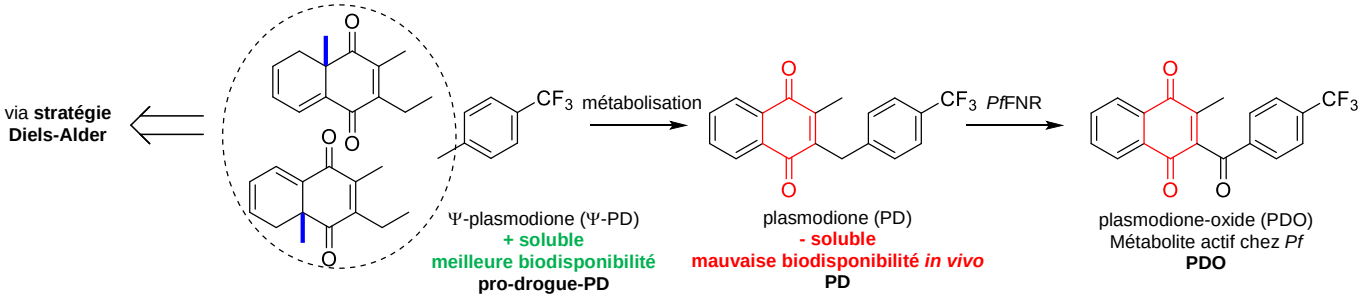

Figure 32: Stratégie de recherche à partir de composé Ψ-PD, pro-drogue de la PD métabolisable afin de libérer la PD dans un parasite hématophage.

La synthèse de ces composés présente un défi en termes de régiosélectivité. Heureusement, ces structures ont déjà pu être étudiées dans la littérature[149,150] grâce à l'introduction de groupements directeurs sulfinyle chiraux ou boroniques, permettant de contrôler leur réactivité et leur arrangement spatial. Des stratégies de synthèse multi-étapes, stéréosélectives et/ou régiosélectives, ont été mises en place dans l'article 6, conduisant à l'obtention d'une première 4a-ψ-PD. Pour ma part, j'ai synthétisé son régioisomère 8a-ψ-PD,

nouveau, et re-synthétisé le régioisomère 4a-ψ-PD à titre de comparaison, afin d'évaluer la différence de réactivité métabolique, d'activité antipaludique et antischistosome en fonction de la position du méthyl angulaire. J'ai également exploré d'autres voies de synthèse plus accessibles et étudié l'aptitude du méthyle angulaire à être métabolisé en condition biomimétique. Ces résultats sont disponibles dans l'article 6 de cette thèse.

1.2.2 Article 6

Regioselective synthesis of potential non-quinonoid prodrugs of plasmodione: antiparasitic properties against two hemoglobin-feeding parasites and drug metabolism studies

Elena Cesar Rodo, Baptiste Dupouy, Cécile Häberli, Jean-Marc Strub, David L. Williams, Pascal Mäser, Matthias Rottmann, Jennifer Keiser Don Antoine Lanfranchi, Elisabeth Davioud-Charvet

***Molecules* accepted article**, publié en ligne le 7 Novembre 2024

doi: 10.3390/molecules29225268

Regioselective synthesis of potential non-quinonoid prodrugs of plasmodione: antiparasitic properties against two hemoglobin-feeding parasites and drug metabolism studies

Elena Cesar Rodo,[1] Baptiste Dupouy,[1] Cécile Häberli,[2] Jean-Marc Strub,[3] David L. Williams,[4] Pascal Mäser,[2,5] Matthias Rottmann,[2] Jennifer Keiser,[2,5] Don Antoine Lanfranchi,[1,*] Elisabeth Davioud-Charvet[1,*]

1 Laboratoire d'Innovation Moléculaire et Applications (LIMA), Team Bio(IN)organic & Medicinal Chemistry, UMR7042 CNRS-Université de Strasbourg-Université Haute-Alsace, European School of Chemistry, Polymers and Materials (ECPM), 25, rue Becquerel, F-67087 Strasbourg (France).

2 Swiss Tropical and Public Health Institute, Kreuzstrasse 2, CH-4123 Allschwil (Switzerland).

3 Laboratoire de Spectrométrie de Masse BioOrganique (LSMBO), IPHC UMR 7178 CNRS, Université de Strasbourg, 67087 Strasbourg (France)

4 Department of Microbial Pathogens and Immunity, Rush University Medical Center, 1735 West Harrison Street, Chicago, IL 60612 (USA).

5 University of Basel, Petersgraben 1, CH-4001 Basel (Switzerland).

* Correspondence E-mail Address: elisabeth.davioud@unistra.fr; orcid.org/0000-0001-7026-4034

Abstract

ψ-1,4-naphthoquinones (ψ-NQ) are non-quinoid compounds in which aromaticity – found in 1,4-naphthoquinones – is broken by the introduction of an angular methyl at C-4a or -8a. This series was designed to act as prodrugs of 1,4-naphthoquinones in an oxidative environment. Furthermore, from a medicinal chemistry point of view, the loss of planarity of the scaffold might lead to an improved solubility and circumvent the bad reputation of quinones in the pharmaceutical industry. In this work, we illustrated the concept by the synthesis of ψ-plasmodione regioisomers as prodrugs of the antimalarial plasmodione. The presence of a chiral centre introduces a new degree of freedom to be controlled by enantioselectivity and regioselectivity of the cycloaddition in the Diels-Alder reaction. The first strategy that was followed was based on the use of a chiral enantiopure sulphoxide to govern the stereoselective formation of (+)ψ-NQ or (-)ψ-NQ, depending on the chirality of the sulphoxide (*R* or *S*). New sulfinylquinones were synthesized but were found to be ineffective in undergoing cycloaddition with different dienes under a wide range of conditions (thermal, Lewis acid). The second strategy was based on the use of boronic acid-substituted benzoquinones as auxiliaries to control the regioselectivity. In this methodology to prepare the (±)ψ-NQ racemates, promising results (very fast cycloaddition time: ~2 h) were obtained with boronic acid-based quinones **25** and **27** in the presence of 1-methoxy-1,3-butadiene, to generate the 4a- and the 8a-ψ-plasmodione regioisomers **1** and **2** (synthesised in 6 steps with a total yield of 10.5% and 4.1%, respectively. As the expected prodrug effect can only be revealed if the molecule undergoes an oxidation of the angular methyl, e.g. in blood-feeding parasites that digest haemoglobin from the host, the antimalarial and the antischistosomal properties of both (±)ψ-NQ regioisomers were determined in drug assays with *Plasmodium falciparum* and *Schistosoma mansoni*. Metabolic studies under quasi-physiological conditions and LC-MS analyses were undertaken to reveal the generation of plasmodione from both the 4a- and the 8a-Ψ-plasmodione regioisomers.

Keywords: angular methyl, antiplasmodial, antischistosomal, Diels-Alder cycloaddition, hemoglobin, plasmodione.

1. Introduction

Malaria is a human parasitic disease caused by the protozoan *Plasmodium* spp. parasites, which are transmitted through the bites of infected mosquitoes. It is mostly found in the Sub-Saharan Africa, tropical and sub-tropical areas and there are an estimated 249 million cases of malaria occurred in 85 malaria-endemic countries in 2022. An estimated 608 000 deaths occurred globally due to malaria in 2022, a mortality rate that mainly affects infants under five years of age in Sub-Saharan Africa. Five major species of the *Plasmodium* parasite can infect humans; the most serious forms of the disease – cerebral malaria, severe anemia and death – are largely caused by *P. falciparum*. Most of the drugs available to treat malaria are subject to resistance, which limits their effectiveness. In the last decade, our team has invested considerable effort in a series of potent compounds known as 3-benzylmenadiones targeting the redox equilibrium in *P. falciparum*-infecting red blood cells. Most of our research has focused on the lead molecule plasmodione (PD) [1,2] (Scheme 1) by developing chemical methodologies [3,4] to optimize new pharmacophores [5-7] and by understanding its mode(s) of action [8,9]. Another neglected disease, schistosomiasis (also called bilharziasis), is responsible for 251.4 million people million people infected in many tropical areas, resulting in 11,792 deaths globally *per* year [10]. However, these figures are likely underestimates of the current status of the disease and need to be reassessed. Schistosomiasis is due to 5 main species of flatworms (platyhelminth parasites), causing intestinal and urogenital infections in humans: *Schistosoma mansoni*, *S. japonicum*, *S. haematobium*, *S. intercalatum* and *S. mekongi*. The intermediate hosts of this hemoglobin-feeding parasite are of various species of freshwater snails, which transfer human infection through skin contact with infective cercariae [11]. Praziquantel has been used to treat schistosomiasis since the 1980s, but this drug is not effective against immature worms and is currently the only available medication, jeopardising the treatment if parasite drug resistance increases worldwide.

Plasmodione (PD) is a redox-active prodrug (Scheme 1) [12]. Its bioactivation in parasitized red blood cells involves a cascade of redox reactions generating a 3-benzoylmenadione (or plasmodione oxide, PDO) that interacts with hemoglobin digestion. Both pathways, i. e., drug bioactivation and hemoglobin catabolism, were demonstrated to produce a large amount of reactive oxygen species (ROS) in the parasites [13]. The drug-induced oxidative stress was visualized in the cytosol and the apicoplast of the parasites by using GFP-based biosensors [9,13]. Nevertheless, the high specificity of PD is based on the quasi-absence of methemoglobin in non-parasitized red blood cells, in accordance with its very low toxicity in glucose-6-phosphate dehydrogenase-sufficient or -deficient red blood cells.

Plasmodione contains both a quinone moiety, working as an electron reservoir for redox cycling, and an aromatic planar structure, which contributes to poor aqueous solubility and high lipophilicity. The electrophilic and oxidant properties of unsubstituted quinones [14] are well documented: they contribute to instability and high reactivity in cells due to prior enzyme-catalyzed reduction of the quinone, causing multiple issues and a directed toxicity [15]. Their ability to undergo multiple cycles of reduction and oxidation can damage and induce oxidative stress around the molecule before reaching their envisaged biological targets. To balance this dilemma, many electrochemical studies have shown that the electron-acceptor properties of quinones, causing the formation of radical semiquinone anion or dihydroquinone

dianion species responsible for *in vivo* oxidative stress, can be modulated by electron-withdrawing or -donating substituents of the electroactive core [12]. As previously observed for most of the 3-benzylmenadiones, plasmodione is not highly oxidant, in accordance with the absence of initial liability of toxicity in mammal cells [1,2]. After bioactivation through reduction and benzylic oxidation, redox-cycling generates a 3-benzoylmenadione (plasmodione oxide, PDO) with higher oxidant character. The electrochemical data recorded for diverse 3-acylated menadiones attest to a marked impact of the 4'-benzoyl substitution on the second electron transfer, leading to the dihydronaphthoquinone dianion (to up to 500 mV) [16].

In this work, we introduce an angular methyl to break the aromatic core of the quinone moiety of menadione (pseudo-menadione or ψ-menadione). We illustrate our exploration with the synthesis of both non-quinonoid plasmodione regioisomers, called here pseudo-plasmodiones **1** and **2** (4a- or 8a-ψ-plasmodiones, respectively) (Scheme 1). The introduction of an angular methyl can be beneficial for physicochemical and pharmacokinetic properties (PK). Indeed, by breaking the aromaticity of a molecule, its planarity and its three-dimensional geometry are directly affected, which could lead to an increase of the aqueous solubility of the molecule [17]. Furthermore, the angular methyl can be seen as a shield for direct bioreduction or nucleophilic attack, providing a stable molecule until its bioactivation in an oxidative environment, such as that found in parasites. With the aim to build a pro-drug of plasmodione (PD), we postulated that the angular methyl can be hydroxylated *in situ* by an aromatase-like activity present in the parasite, possibly catalyzed by hemoglobin in large excess, and therefore generate the active plasmodione *in situ* in the parasite (Scheme 1). This known catalytic process, e.g., in the formation of estrogens after aromatization of androgens, is catalyzed by aromatase [18] belonging to the cytochrome P-450 family [19]. The catalytic introduction of a double bond through oxidation of a methyl group followed by a C-C cleavage was also observed in fungal ergosterol synthesis involving the sterol 14α-demethylases (CYP51) [20]. To make this hydroxylation possible, CYP450 contains an iron of the prosthetic group, i.e., the molecule of heme in the Fe^{III} form, then reductase (NADPH), dioxygen works in pair with iron in a redox chain reaction to form a ferryl Fe^{III}-OOH and then make the acyl-carbone cleavage possible.

In the present work, we describe the synthesis of two regioisomeric analogues of plasmodione, the 4a-ψ-plasmodione **1** and the 8a-ψ-plasmodione **2** (Scheme 1). Furthermore, both the 4a-ψ-plasmodione **1** and the 8a-ψ-plasmodione **2** were tested for antimalarial and antischistosomal activities against blood-feeding parasites, *P. falciparum* and *S. mansoni*, two parasites that digest hemoglobin from the host and produce large amounts of hemozoin. We postulated that the angular methyl of the ψ-plasmodiones could be metabolized by an aromatase-like protein present in the parasite producing the active plasmodione through a beneficial pro-drug effect, and thus, we carried out biomimetic oxidation reactions in the presence of the 4a- (or 8a-)ψ-plasmodione **1** (or **2**), hematin, the NADPH-dependent *P. falciparum* Ferredoxin-$NADP^+$ Reductase (*Pf*FNR)-catalyzed PDO system (Scheme 1) [9].

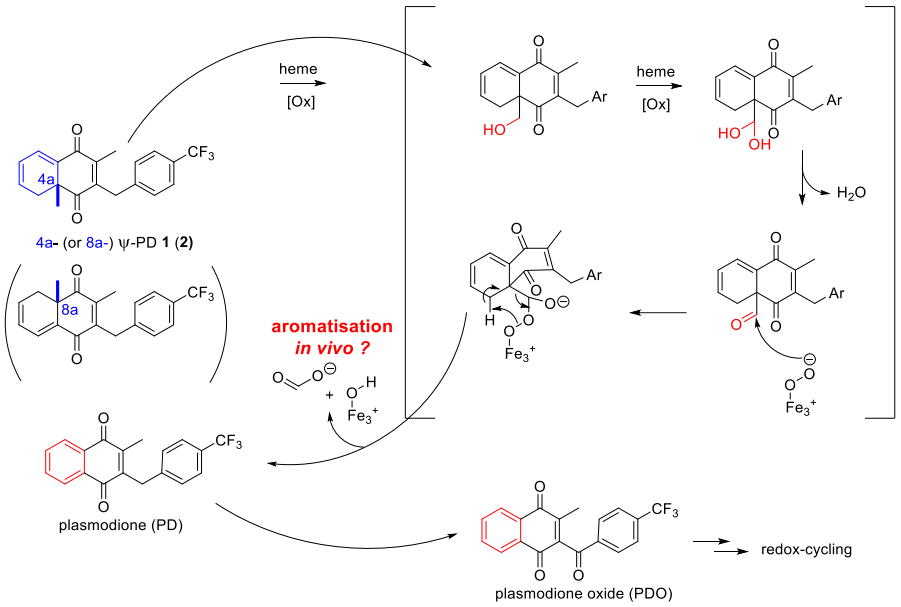

Scheme 1. Strategy based on the design of the potential pro-drug ψ-plasmodiones **1** and **2** regenerating the antiplasmodial plasmodione in situ through two successive hydroxylation steps by an aromatase-like activity using different cofactors (NADPH, O_2, H^+, Fe^{II}/Fe^{III}). Ar represents the 4'CF_3-aryl.

2. Results and discussion

From a chemical view, the real challenge is the introduction of a chiral center and, thereby, the control of the stereochemical and regiochemical course during the synthetic route. Well documented, the structure of 1,4-naphthoquinone is a recurrent building block in [4+2] Diels-Alder (DA) cycloadditions and controlling its regio/stereo selectivity is an essential task already described in the literature [21-24]. We drew on two different methodologies, both originally described by Carreño and co-workers [25,26]. The authors and some of us [27] were able to obtain an angular methyl-bearing enantiopure benzoquinone with a high enantiomeric excess from a Diels-Alder cycloaddition mediated by a sulfinylquinone (Scheme 2, Route A).

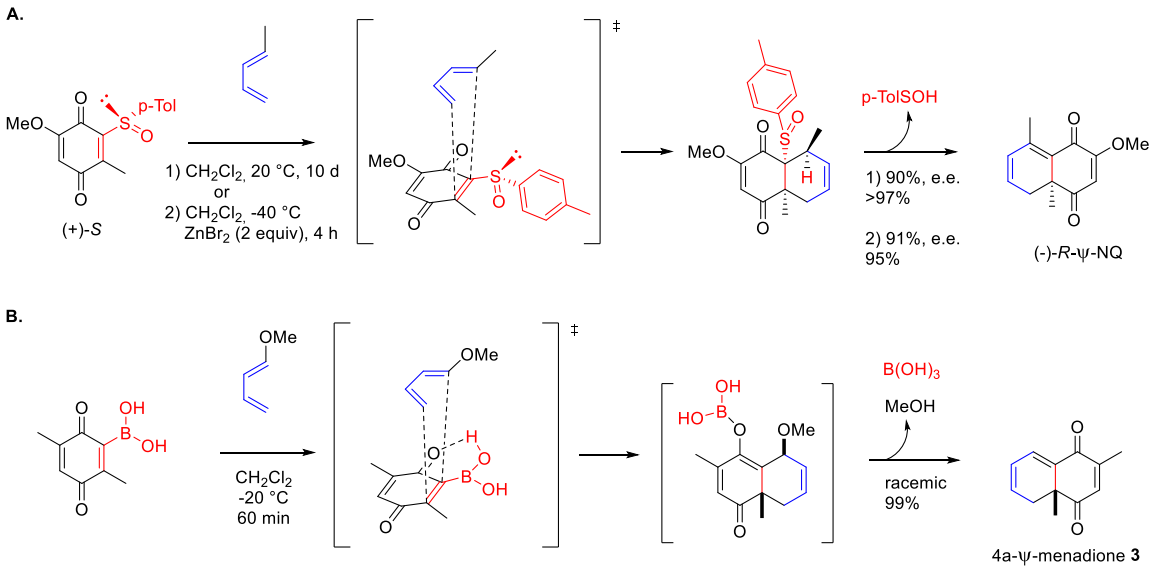

Scheme 2. Sulfoxides and boronic acid as auxiliaries in Diels-Alder reactions to prepare the chiral (-)-*R*-ψ-

naphthoquinone (ψ–NQ) and the 4a-ψ-menadione **3**. Route A. Regio- and stereo-selective cycloaddition in the presence of a chiral sulfinylquinone [27]. Route B. Regioselective cycloaddition in the presence of a boronic acid-substituted quinone [26].

This methodology, known as the introduction of chiral sulfinyl onto the dienophile, induces a regio/stereoselectivity of the reaction, which has been applied in various applications [28,29]. Carreño and co-workers also described the regioselective production of ψ-naphthoquinones (ψ–NQ) with an angular methyl group from boronic acids [24,26]. In this reaction, the boronic acid-substituted dienophile is more reactive than the sulfinylquinone to control the regioselectivity course of the reaction and self-elimination by protodeborylation, but the product **3** is obtained as a racemate (Scheme 2, Route B).

Therefore, we investigated these two methodologies (Scheme 3), depicted in Routes A & B, and established a successful pathway for the synthesis of the 4a- and 8a-ψ-plasmodione regioisomers **1** and **2** (Routes C & D).

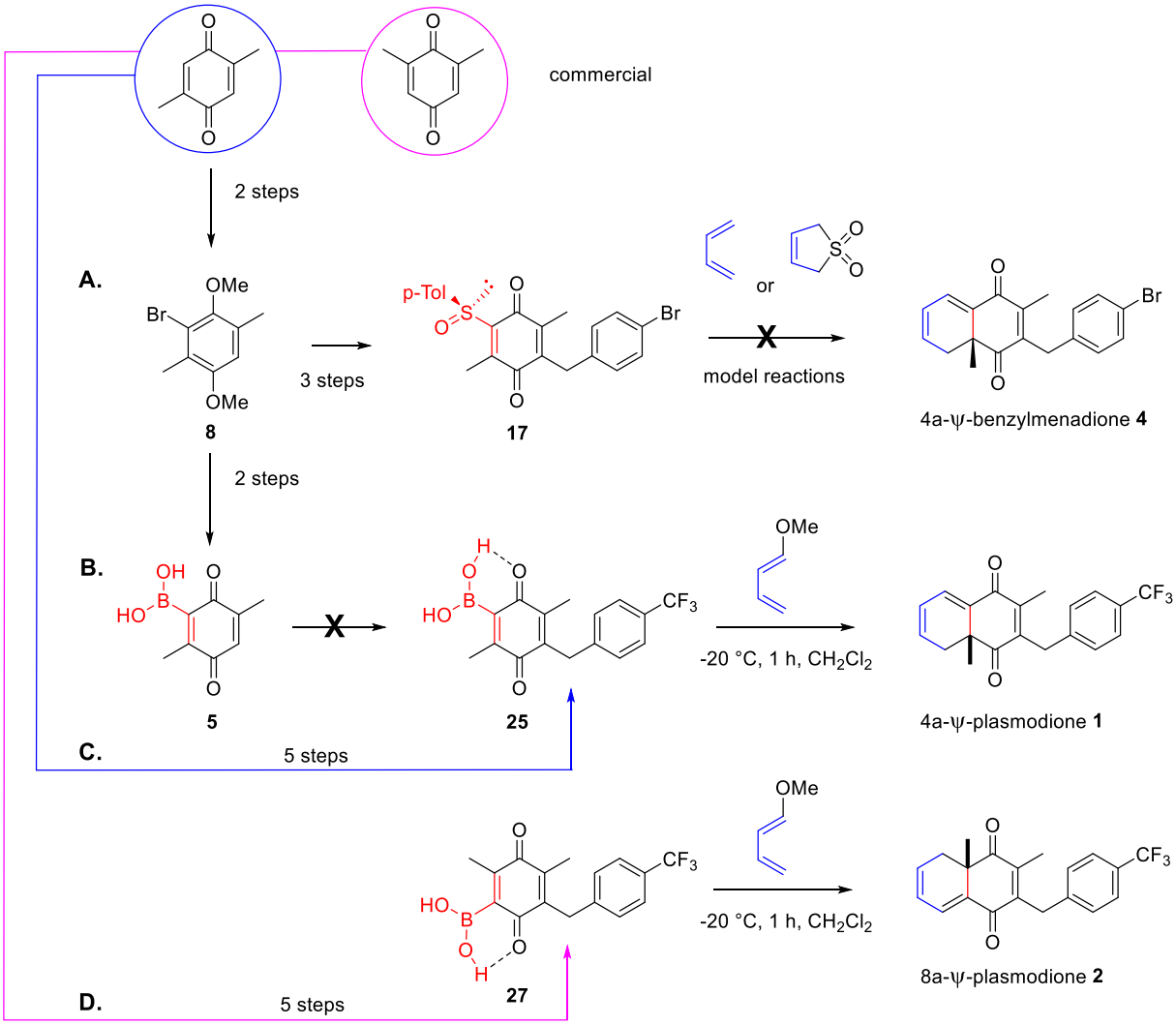

Scheme 3. Synthetic accessibility of 4a- or 8a-ψ-plasmodiones **1** and **2** through cycloadditions from commercially available precursors. Route A: The first process based on the regio-and stereo-selective cycloaddition in the presence of a chiral sulfinylquinone [27] was attempted in model reactions to produce a 4a-ψ-plasmodione analogue **4** with a 4'-Br instead of the 4'-CF_3 group. Routes B and C: the regioselective cycloaddition in the presence of a boronic acid-substituted quinone [26] was then attempted to prepare the 4a-ψ-plasmodione **1**, but required an

appropriate order of the steps to prepare the boronic acid-substituted quinone. Route D: The successful pathway to produce the 4a-ψ-plasmodione **1** was applied to produce the 8a-ψ-plasmodione **2**.

2.1. Preliminary investigations: Synthesis of the ψ-menadiones

First, we tried to obtain the ψ-menadiones using the methodology described by Carreño's group [24,26] from the corresponding benzoquinone-substituted boronic acids **5** and **6** (Scheme 4). Boronic acid **5** was synthesized from the corresponding commercially available benzoquinone precursor, i.e. the 2,5-dimethylbenzoquinone, by bromination with Br_2 leading to **7**. Then, after a two-step reduction/protection, the dimethoxy-bromobenzene **8** was engaged through a Br/Li exchange protocol in the reaction with $B(OiPr)_3$, followed by acidic hydrolysis of the boronated ester. Subsequent oxidative demethylation of **9** with cerium ammonium nitrate (CAN) gave the desired product **5**, which was isolated after four steps in a 30% overall yield (Scheme 4). Concerning the other regioisomer **6**, another synthetic route was performed [24,26], starting from the corresponding benzoquinone with a reduction of the quinone moiety followed by a bromination with *N*-bromosuccinimide (NBS) leading to **10**. Subsequent protection of the hydroxyl group gave **11** and finally the same two steps-pathway, as used for **5**, was applied to obtain **6** after four steps in 18% overall yield (Scheme 4).

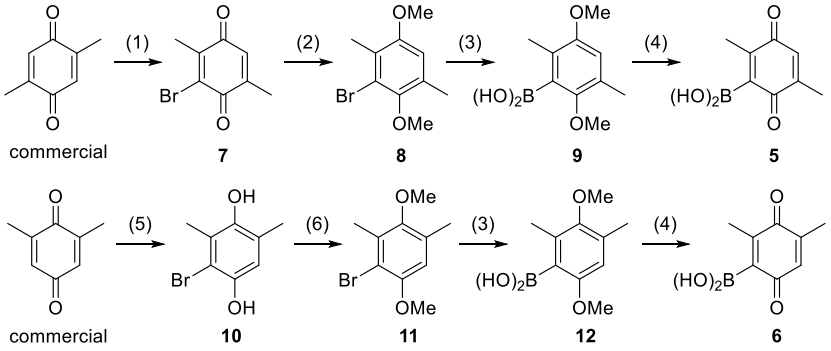

Scheme 4. Synthesis of 3,6-dimethyl-2-benzoquinone boronic acid **5**, and 3,5-dimethyl-2-benzoquinone boronic acid **6**. Conditions: (1) Br_2, DIPEA, CH_2Cl_2, 0 °C to r.t., 5 h, 72% for **7**; (2) 1. $SnCl_2$, HCl, EtOH, r.t., 2 h, 2. Me_2SO_4, acetone, KOH, MeOH, 60 °C, 4 h, 75%; (3) *n*-BuLi, $B(OiPr)_3$, THF, -78 °C to r.t., 16 h, HCl 1M, 55% for **9** and 54% over 2 steps for **12**; (4) CAN, ACN:H_2O (1:1), r.t., 1 h, 99% for **5** and 92% for **6**; (5) 1. $Na_2S_2O_4$, Et_2O:H_2O, r.t., 1 h, 2. NBS, ACN, r.t., 16 h, 36%; (6) K_2CO_3, Me_2SO_4, acetone, 60 °C, 4 h, engaged in the next step.

Both freshly prepared benzoquinone-substituted boronic acids were engaged in the Diels-Alder cycloaddition with 1-methoxy-1,3-butadiene and, after a short reaction time, led to compounds **3** and **13** in good to excellent yields (Scheme 5). Carreño's group described a domino process including the Diels-Alder cycloaddition reaction, a protodeboronation and an elimination of MeOH [24,26]. This exclusive reactivity under mild condition in short period of time without any Lewis-acid as catalyst is explained by the activation of the dienophile through a hydrogen bond between the boronic acid and quinoid carbonyle, which could not be established with a boron-free species [30]. Then, the regioselectivity of the reaction is fully controlled by the boron, with the *endo* attack of the diene from both faces (TS, Scheme 5). For example, the bottom attack could produce an undetected *ortho-cis* intermediate (A and B, Scheme 5) with the benzoquinone substituent facing upwards. From the reported study [24,26], the

reaction had been performed in an NMR tube in CD_2Cl_2, to demonstrate that the protodeboronated adduct was formed directly in the crude reaction before any workup. From different X-ray structures this protodeboronation took place in *trans* compared to the boron. Intermediate C (Scheme 5) *meta-trans* had then been proposed, with a subsequent *beta-cis* elimination of MeOH producing the desired product. Since the diene can attack from the top face of the dienophile, the two enantiomers were obtained, therefore **3** and **13** are racemates.

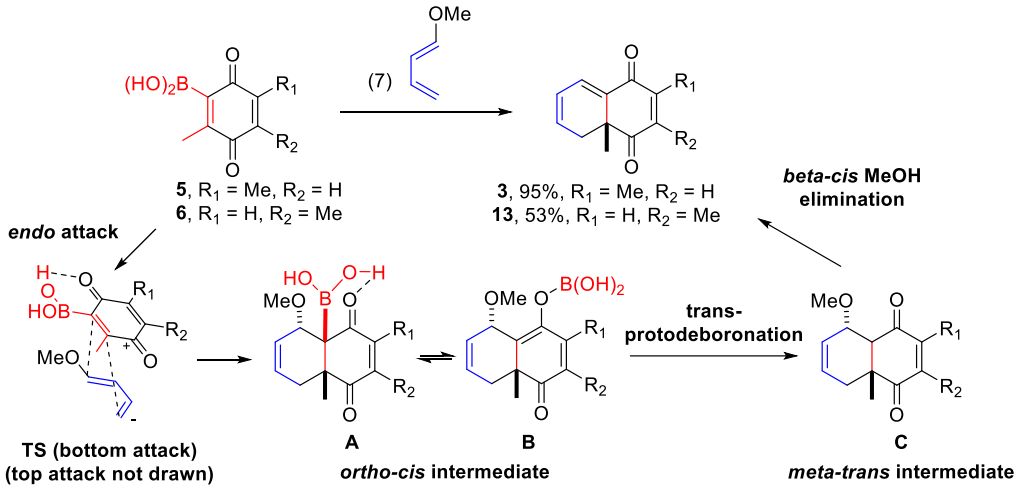

Scheme 5. Diels-Alder cycloadditions producing regioisomeric ψ-menadiones **3** and **13**, substituted by an angular methyl (only endo attack of the diene was drawn). Conditions: (7) CH_2Cl_2, -20 °C, 1 h.

2.2. Synthesis of ψ-Plasmodione regioisomers from sulfoxide-substituted 3-benzyl-benzoquinones

As drawn in Scheme 3 (route B), we first functionalized the starting dienophile by the Kochi-Anderson benzylation before the Diels-Alder cycloaddition (Scheme 6). Carreño's group [25] described the regio- and enantio-selective cycloaddition to access an enantiopure anthraquinone from chiral sulfinylquinone. Lanfranchi & Hanquet supported these selectivity results [27,31], which were due to the specific orientation of the chiral sulfinyl moiety, blocking one face and the other producing a single enantiomer. In the reported methodology, an *endo* attack was described producing an *ortho-cis* intermediate with an attack of the diene from the less hindered face, which is the top face, leading to the *R* absolute configuration with the angular methyl pointing downwards. Then, from this intermediate, the sulfinyl group can spontaneously be *beta-cis* eliminated producing sulfenic acid, which self-condensed to *p*-tosyl disulfide oxide and of the course producing the desired product [27].

Because this methodology gives access to enantiopure sulfinylquinones, we applied it to benzoquinone **8** (Scheme 6). First, compound **8** was engaged in a metalation and sulfinylation with the freshly prepared chiral (-)-*R*(*S*)-menthyl-*p*-toluenesulfinate **14** [32], leading to compound **15** with 47% yield. Then, direct oxidative demethylation using CAN afforded **16** in excellent yield. Finally, the Kochi-Anderson was performed using the 4-bromophenylacetic acid in a model reaction giving the sulfinylquinone **17** with 31% yield. We then tried to reproduce the Diels-Alder cycloaddition using the same diene and the reported condition [27]. However, our attempts were not successful using three different dienes: 1,3-

butadiene, trimethylsilyl-1,3-butadiene and sulfolene. The reaction only led to degradation or there was no reaction at all (Supplementary Materials, Table S1). The non-reactivity of the sulfinylquinone **17** can be explained by the fact that the benzyl chain is positioned on the opposite side to that occupied by the *p*-tosyl arm of the sulphoxide, creating steric hindrance on both sides of the dienophile to prevent the approach of the diene (see TS, Scheme 6).

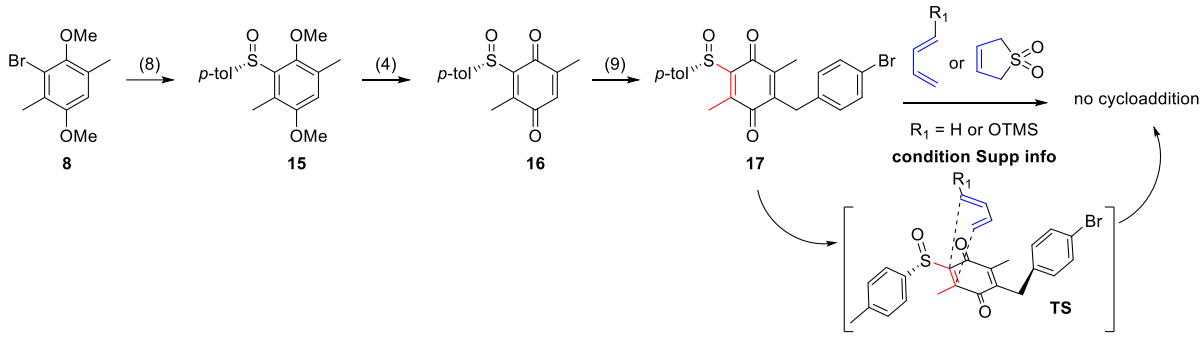

Scheme 6. Investigation on the regio- and stereo-selective Diels-Alder cycloaddition in the presence of a chiral sulfoxide. Conditions: (8) 1. $Mg_{(s)}$, THF, r.t., 2 h, 2. (-)-*R*(*S*)-menthyl-*p*-toluenesulfinate **14**, CH_2Br_2, 0 °C to r.t., 16 h, 47%; (4) CAN, ACN:H_2O (1:1), r.t., 1 h, 95%; (9) 4-bromopheneacetic acid or 4-trifluoromethylpheneacetic acid, $AgNO_3$, $(NH_4)_2S_2O_8$, ACN:H_2O (1:1), 90 °C, 4 h, 31% for **17**.

2.3. Preliminary investigations on the synthesis of ψ-plasmodiones from boronic acid-substituted 3-benzyl-benzoquinone

We then decided to perform the Kochi-Anderson reaction from compound **5** before the Diels-Alder reaction. However, the radical condition was not compatible with the boronic benzoquinone. In fact, Baran's team [33] described a C-H functionalization on a quinone under the Kochi-Anderson condition, with arylboronic acid via a nucleophilic radical addition, which could potentially create in our case a fast polymerization chain reaction or the homocoupling of **5** happening before the initial Kochi-Anderson (Scheme 7, Route A).

However, this limiting step opens possibilities to introduce the boronic acid after the benzylation of 3,6-dimethyl-2-benzoquinone **7** (Scheme 7, Route B) and 3,5-dimethyl-2-bromobenzoquinone **18** (Scheme 7, Route C) and potentially to obtain the desired ψ-plasmodione regioisomers after a final Diels-Alder reaction. We thus synthesized the new precursors **21** and **22**, respectively from compounds **19** and **20**, for the borylation, according to the reaction sequence shown in Scheme 7 (similarly to Scheme 4), with an overall yield of 42% and 24% from both commercial benzoquinones in three steps.

Oxidative demethylation of compound **23** with CAN at 0 °C gave a 2:1.5 mixture of boronic quinone **25** and the product of quinone dimerization **26**. These two products are easily separated by precipitation of the boronic quinone in CH_2Cl_2. Of note, Veguillas *et al.* also described the formation of a dimer (4,4'-dimethyl-1,1'-bicyclohexa-3,6-diene-2,2',5,5'-tetraone) in an almost quantitative yield during CAN oxidation of 4-methyl-2,5-dimethoxyphenyl boronic acid [24]. This is made via an oxidative radical coupling, likely due to the initial deboronation of starting boronic acid, followed by coupling of the intermediate radicals and evolution to the final product by oxidative demethylation [34].

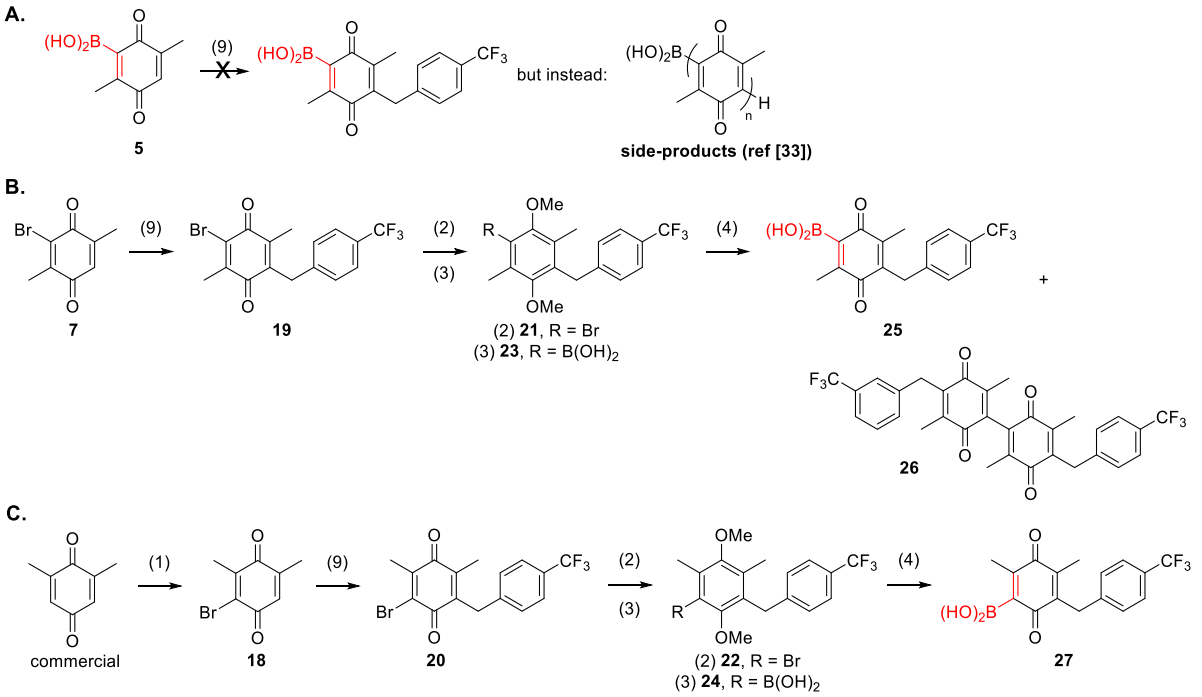

Scheme 7. Investigations on different synthetic routes to prepare boronic acid-substituted quinones. Route A. Attempt of benzylation of a boronic acid-substituted bromoquinone through the Kochi-Anderson conditions. Route B. Synthesis of the boronic acid-substituted bromoquinone **25** as starting reactant for the preparation of the 4a-ψ-plasmodione regioisomer **1**. Route C. Synthesis of the boronic acid-substituted bromoquinone **27** as starting reactant for the preparation of the 8a-ψ-plasmodione regioisomer **2**. Conditions: (9) 4-trifluoromethylpheneacetic acid, $AgNO_3$, $(NH_4)_2S_2O_8$, ACN:H_2O (1:1), 90 °C, 4 h, 77% for **19** and 66% for **20**; (2) 1. $SnCl_2$, HCl, EtOH, r.t., 2 h, 2. Me_2SO_4, acetone, KOH, MeOH, 60 °C, 4 h, 76% for **21** and 74% for **22**; (3) *n*-BuLi, B(O*i*Pr)$_3$, THF, -78 °C to r.t., 16 h, HCl 1M, 63% for **23** (NMR yield) and 46% for **24**; (4) CAN, ACN:H_2O (1:1), r.t., 1 h, 40% for **25** (and 60% for **26**, NMR yield**)** and 64% for **27**; (1) Br_2, DIPEA, CH_2Cl_2, 0 °C to r.t., 5 h, 49% for **18**.

2.4. Synthesis of ψ-plasmodiones from boronic acid-substituted 3-benzyl-benzoquinones

Finally, we introduced the boronic group after the Kochi-Anderson reaction and performed the Diels-Alder cycloaddition at the end. Beginning with the 4a-ψ-plasmodione regioisomer, compound **7** was engaged in a Kochi-Anderson reaction with 4-trifluoromethylpheneacetic acid producing compound **19** in good yield. Then, as for the synthesis of compound **5** (Scheme 4), the bromo-benzoquinone was protected giving compound **21** and a subsequent metalation followed by a borylation was performed, which led to the formation of the boronic acid **23** after hydrolysis. The corresponding boronic acid was directly engaged in the oxidative demethylation with CAN producing the boronic-benzoquinone **25** with 40% yield. Finally, the desired 4a-ψ-plasmodione **1** (10.5%, 6 steps) containing the angular methyl, was obtained through the Diels-Alder reaction (Scheme 8). The same Diels-Alder cycloaddition condition used in Carreño's group [24,26] was used to generate the 4a-ψ-plasmodione **1** in an excellent yield, producing the same regioisomer with the *endo* attack. By comparison with the sulfinyl methodology, we assumed that the Diels-Alder reaction was possible since the boronic acid is far less hindered. Therefore, the pendant benzyl of **25** did not block the attack of the diene or modified its approach. Furthermore, we applied the same methodology to generate the other regioisomer, the 8a-ψ-plasmodione **2** (4.1%, 6 steps) from **20** (Scheme 8).

In conclusion, we investigated different methodologies to produce non-quinonoid ψ-plasmodione regioisomers substituted with an angular methyl. The main limitation comes from the absence of reactivity of sulfinylquinones under Diels-Alder reaction condition due to steric hindrance. However, with boronic acids as auxiliary to govern the regioselectivity of the cycloaddition and by choosing the right order of chemical steps, we were able to overcome these limitations and produce the desired regioisomer products (Scheme 8).

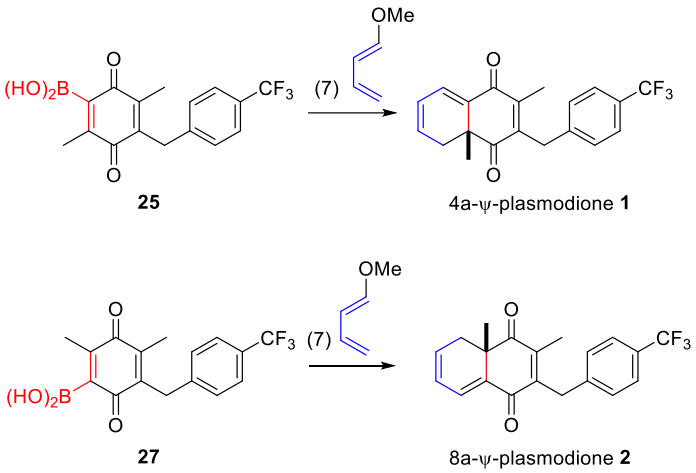

Scheme 8. Final synthetic route to obtain both 4a- and 8a- ψ-plasmodione regioisomers **1** and **2**. Conditions: (7) CH_2Cl_2, -20 °C, 1 h, 99% for **1** and 59% for **2**.

2.5. Antiparasitic activities and toxicity of ψ-plasmodione regioisomers

The antimalarial and the antischistosomal activities of both synthesised ψ-plasmodione regioisomers were measured against *P. falciparum* strain NF54 using the [^{3}H]-hypoxanthine incorporation assay [35], and against *S. mansoni* newly transformed schistosomula (NTS) [36] and against the *ex vivo* adult worms. Both quinone-free variants displayed low micromolar IC_{50} activity values around 2 µM against *P. falciparum*, values that are high in comparison with the potent antimalarial activity expressed by plasmodione (Table 1). The antischistosomal activities of both compounds was found relevant at 10 µM in the NTS, encouraging the determination of IC_{50} values both in the NTS and adult worm assays (Table 2). The antischistosomal potencies could suggest that a more effective prodrug effect took place in *S. mansoni*, both to release plasmodione and/or to express better properties by the non-aromatic ψ-PD analogues, e.g., a better penetration of ψ-plasmodiones across the tegument of the *S. mansoni* worms *versus* the membranes of the *Plasmodium falciparum*-parasitized red blood cells [37].

Table 1. *In vitro* antiplasmodial and cytotoxicity data expressed as IC_{50} and CC_{50} values, respectively, and calculated physicochemical properties of ψ-plasmodiones.

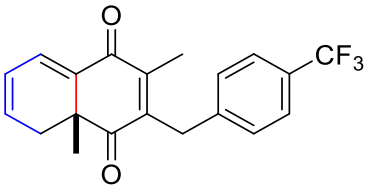

(±) 4a-ψ-plasmodione **1**

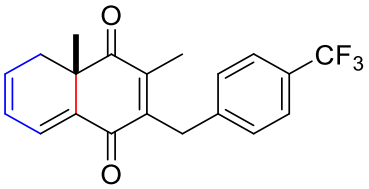

(±) 8a-ψ-plasmodione **2**

Product	NF54 IC_{50} (µM)[1]	L6 CC_{50} (µM)	cLogP	tPSA
1	1.850 ± 0.458	22.47	4.6	34.14
2	2.391 ± 0.825	25.56	4.6	34.14
PD	0.043 ± 0.002	141.7 / 43.48	5.4	34.14
CQ diphosphate	4.0 ng/ml	nd[2]	2.7	30.44
artesunate	1.52 ng/ml	nd[2]	2.9	100.52
Podophyllotoxin	nd[2]	0.010	1.3	92.68

[1]: IC_{50} (µM) values are the mean IC_{50} value of (2) independent determinations. They were determined in the ^{3}H-hypoxanthine incorporation-based assay using the *P. falciparum* NF54 strain. [2]: nd means "not determined".

Table 2. *In vitro* antischistosomal activities of ψ-plasmodiones.

Product	NTS	NTS	NTS	NTS
	Effect in % ± SD at 24h/48h/72h Test conc. 25 µM	**Effect in % ± SD at 24h/48h/72h Test conc. 10 µM**	**Effect in % ± SD at 24h/48h/72h Test conc. 1 µM**	**IC_{50} (µM) at 24h/48h/72h**
1	100 ± 0 100 ± 0 100 ± 0	34.59 ± 1.3 35.35 ± 0.7 71.70 ± 9.4	18.87 ± 1.9 26.42 ± 1.9 28.57 ± 2	2.7 2.4 2.0
2		34.52 ± 6.2 51.43 ± 8.6 86.79 ± 1.9	20.75 ± 0 32.08 ± 0 36.73 ± 2	17.4 8.5 1.7
PD	33.93 ± 1.8 51.67 ± 1.7 71.43 ± 0	30.36 ± 1.8 45 ± 1.7 46.43 ± 0		46.3 19.9 11.3
Product	**adult worms**	**adult worms**	**adult worms**	**adult worms**
	Effect in % ± SD at 24h/48h/72h Test conc. 25 µM	**Effect in % ± SD at 24h/48h/72h Test conc. 10 µM**	**Effect in % ± SD at 24h/48h/72h Test conc. 1 µM**	**IC_{50} (µM)[a] at 24h/48h/72h**
1	70.4 ±3.7 73.15 ± 2.8 88.9 ± 0	53.7 ±0.9 65.65 ± 3.1 66.7 ± 2.1	53.3 ± 0 58.3 ± 0 59.15 ± 0.8	0.8 0.2 0.6
2	44.4 ± 0 49.05 ± 0.9 51.9 ± 0	42.75 ± 1 48.05 ± 2.9 50 ± 0		22.7 17.3 15.2
PD	73.95 ± 0.5 75 ± 0 76.5 ± 0	50 ± 1 50 ± 0 54.15 ± 4.2		10.0 10.0 8.6

2.6. Metabolic studies

We have previously shown that the *P. falciparum* glutathione reductase-catalyzed redox-cycling assay in the presence of PDO and methemoglobin generates a ferrylhemoglobin in a 3 h-long cascade of redox reactions [13]. More recently, we also demonstrated that the *P. falciparum* ferredoxin-$NADP^+$

reductase (*Pf*FNR) efficiently catalyzes the benzylic oxidation of plasmodione in a 2 h-long lasting redox-cycling assay [9]. Here, we established a modified redox-cycling assay to study the oxidation of ψ-plasmodiones by heme under (per)ferryl state, which had been generated by the NADPH-dependent *Pf*FNR catalyzed redox cycling of PDO (Scheme 9). Of note, the reaction of heme (Fe^{3+}) with moderated excess of hydrogen peroxide has been recently demonstrated to affect the oxidation state of heme's iron with only a minimal degradation of the macrocyclic ring [38]. Changes in the oxidation state of the iron ion were suggested to be associated to the formation of ferryl heme species, i.e., the formation of Fe^{IV}=O or Fe^{IV}-OH ferryl species or a Fe^{V}=O perferryl species [18,39] that represent a hyperoxidized state of the iron ion. Hence, the cascade of redox reactions induced by *Pf*FNR-catalyzed PDO reduction in the presence of hematin in open air might form (per)ferryl heme species continuously as soon as NADPH is added in the superoxide anion radical-generating assay.

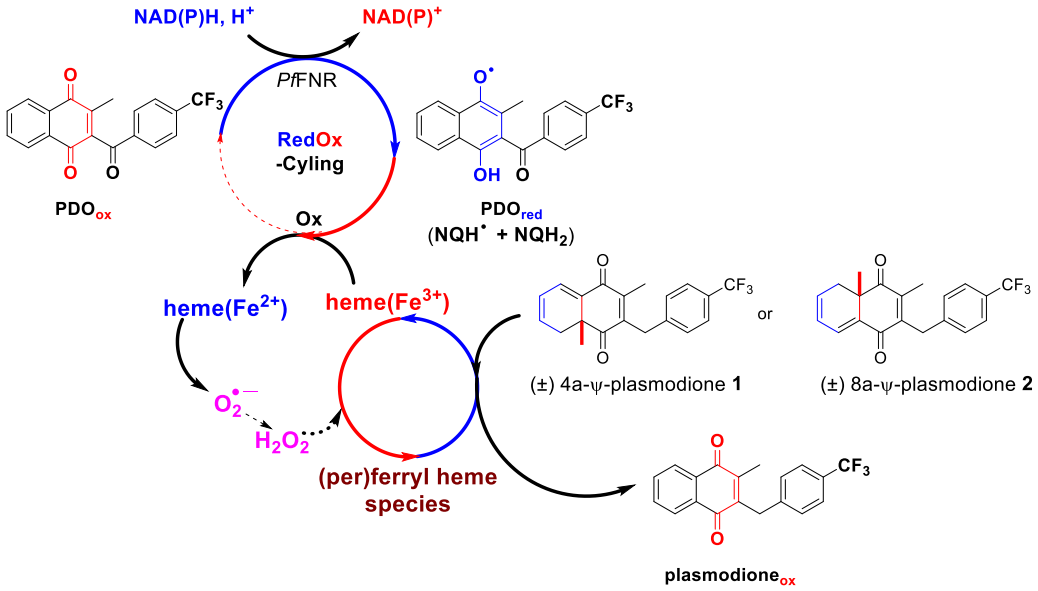

Scheme 9. Cascade of redox reactions catalysed by the NADPH-dependent *Pf*FNR generating (per)ferryl heme species in the presence of PDO and hematin(Fe^{3+}), and ψ-plasmodiones **1** or **2**.

During 3h-long lasting *Pf*FNR-catalyzed PDO redox cycling subjected to repetitive addition of NADPH, hematin(Fe^{3+}), NADPH and oxygen, we hypothesized that the angular methyl of the ψ-plasmodiones could be oxidized and then release plasmodione after cleavage of the C-C bond and aromatization. To validate whether plasmodione is generated in the redox reaction mixture under several conditions, we analyzed the content by LC-ESI-MS. As shown in Figure 1, we could clearly detect the formation of plasmodione at 25 °C and 37 °C. In the MS spectra of the chromatography peaks at RT = 48.7 min and 46.3 min were observed at *m/z* 331.0941, and 345.07, assigned to the species: PD ($[M+H]^+$ *m/z* = 331.09), and PDO_{ox} ($[M+H]^+$ *m/z* = 345.07). The exact mass of plasmodione was detected with an error of 0.1 ppm, attesting for the accurate assignment of the *m/z* peak to ss. In order to quantify the concentration of plasmodione generated in the 3 h course, we determined the area and intensity of *m/z* peaks after injection of plasmodione solutions at known concentrations: 1, 2, 5, 10 µM (Supplementary Materials, Figure S1). With the calibration plots, we determined the concentration of plasmodione generated in the reaction mixtures. All reaction mixtures involving 4a-ψ-plasmodione **1** or 8a-ψ-

plasmodione **2**, carried out at 25 °C or 37 °C, in the presence of hematin and the *Pf*FNR-catalyzed PDO redox-cycling system, exhibited the presence of plasmodione (RT = 48.7 min) at a concentration of 1.91 and 0.95 µM at 25 °C, respectively, or 4.04 and 2.65 µM at 37 °C, respectively (Supplementary Materials, Figure S2-S8).

Figure 1. Extracted ion chromatograms (EICs) corresponding to the mass of plasmodione (PD) (RT = 48.7 min) after LC-MS analysis of the reaction mixtures at 25 °C and 37 °C involving 4a-ψ-plasmodione **1** (Panel A) or 8a-ψ-plasmodione **2** (Panel B).

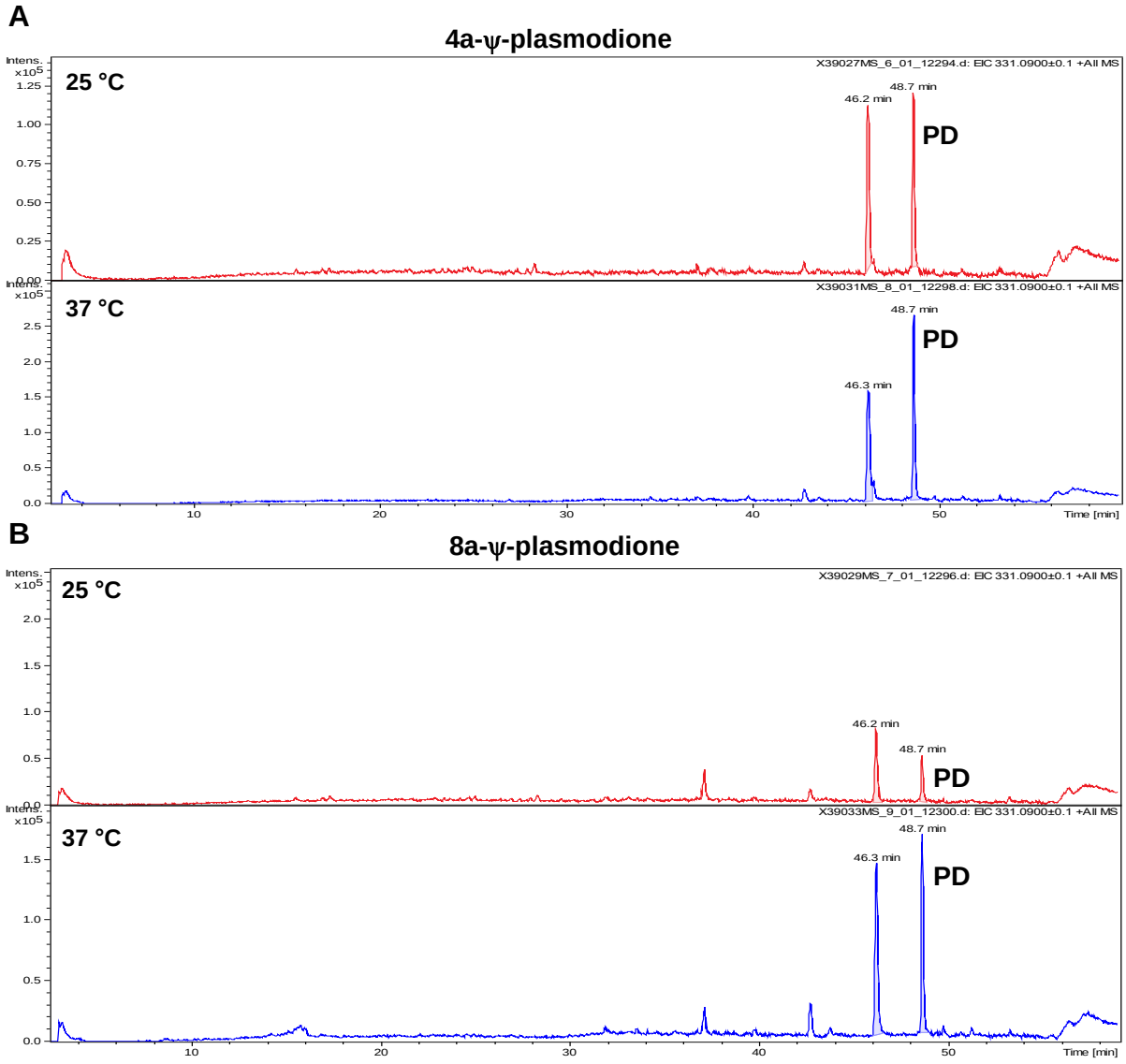

3. Materials and Methods

3.1. Chemistry: general

All the reagents and solvents were purchased from commercial sources and used as received, unless otherwise stated. The ^{1}H, ^{19}F $\{^{1}H\}$ and, and ^{13}C $\{^{1}H\}$ NMR spectra were obtained in $CDCl_3$, Acetone-d_6 as solvents using a 300 MHz or a 400 MHz or a 500 MHz spectrometer. Chemical shifts were reported in parts per million (δ). ^{1}H NMR data were reported as follows: chemical shift (δ ppm) (multiplicity,

coupling constant (Hz), and integration). Multiplicities are reported as follows: s = singlet, d = doublet, t = triplet, q = quartet, m = multiplet, or combinations thereof. High-resolution mass spectroscopy (HRMS) spectra were recorded using the electron spray ionization (ESI) technique. Reactants were purchased from commercial sources, such as Fluorochem, Sigma-Aldrich, BLDpharm and Alfa Aesar.

3.2. Synthesis of precursors

(-)-*R*(*S*)-menthyl-*p*-toluenesulfinate (14). Hydrated sodium *p*-tolylsulfinate (200 g) salt was previously dried by azeotropic distillation with toluene (500 ml) during 24 h. Dried sodium *p*-toluenesulfinate (50 g, 0.28 mmol, 1 equiv.) was added portionwise to a solution of thionyl chloride (50 mL, 0.69 mmol, 2.5 equiv.) in toluene (100 mL) at 0 °C. The mixture was stirred at room temperature for 1 h after the end of the addition. The reaction mixture was concentrated by distillation of the azeotrope $SOCl_2$/toluene under reduced pressure. The resulting oil was dissolved in anhydrous diethyl ether (130 mL) and the white slurry was cooled to 0 °C. At this temperature, a solution of (-)-menthol (43.8 g, 0.28 mmol, 1 equiv.) in pyridine (50 mL) was added dropwise. After the end of the addition, the mixture was stirred 2 h at 25 °C. The reaction was slowly quenched at 0 °C by distilled water (100 mL). The two phases were separated and the organic phase was washed with a 1M HCl solution, brine, dried over magnesium sulphate and solvent was removed under vacuum. The crude product was dissolved in acetone (100 mL) and a few drops of concentrated HCl solution were added. The resulting mixture was allowed to crystallize in the freezer. The resulting crystals were filtered and washed with cold hexane. The mother solution was concentrated and the same operation was repeated several times giving the desired product (75.2 g, 90%), as white crystal. M.p. = 110 °C. $[\alpha]^{25}D$ = -202. ^1H NMR (300 MHz, $CDCl_3$) δ 7.46 (m, J = 8.2 Hz, 4H), 4.12 (td, J = 11.0 Hz, J = 4.5 Hz, 1H), 2.40 (s, 3H), 2.28 (dtd, J = 12.1 Hz, J = 4.5 Hz, J = 1.9 Hz, 1H), 2.13 (sept d, J = 6.9 Hz, J = 2.6 Hz, 1H), 1.74 - 1.64 (m, 2H), 1.48 (m, 1H), 1.35 (ddd, J = 11.0, J = 3.2 Hz, J = 2.6 Hz, 1H,), 1.22 (td, J = 12.1 Hz, J = 11.0 Hz, 1H), 1.04 (dddd, J = 15.5 Hz, J = 11.0 Hz, J = 2.6 Hz, J = 1.1 Hz, 1H), 0.96 (d, J = 6.5 Hz, 3H), 0.92 - 0.82 (m, 1H), 0.86 (d, J = 6.9 Hz, 3H), 0.72 (d, J = 6.9 Hz, 3H). ^{13}C {^1H} NMR (75 MHz, $CDCl_3$) δ 143.2, 142.4, 129.6, 125.0, 80.1, 47.9, 42.9, 31.7, 25.2, 23.2, 22.0, 21.5, 20.8, 15.5. In accordance with a previously published method [32].

(*S*)-1,4-dimethoxy-2,5-dimethyl-3-(*p*-tolylsulfinyl)benzene (15). 2-Bromo-1,4-dimethoxy-3,5-dimethylbenzene **8** (2.5 g, 10.2 mmol, 1 equiv.) in 5 mL THF was added dropwise to solid magnesium (261.3 mg, 10.7 mmol, 1.05 equiv.) in 10 mL THF under argon. Dibromoethane (0.1 mL) was then added to initiate the reaction and the mixture was stirred for 2 h at 25 °C. It was then cooled at 0 °C and added dropwise to a solution of (-)-*R*(*S*)-menthyl-*p*-toluenesulfinate **14** (3.9 g, 13.3 mmol, 1.3 equiv.). The mixture was allowed to warm to 25 °C and stirred overnight. It was then cooled to 0 °C and saturated NH_4Cl was added. The crude product was extracted with diethyl ether, washed with brine, dried over magnesium sulphate and solvent was removed under vacuum. The crude product was finally purified by silica gel chromatography (CHX/EtOAc, 8/2, v/v, UV) to obtain the desired product (1.47 g, 47%) as a white solid. ^1H NMR (300 MHz, $CDCl_3$) δ 7.45 - 7.47 (d, J = 8.23 Hz, 2H), 7.23 - 7.25 (d, J = 8.06 Hz, 2H), 6.78 (s, 1H), 3.83 (s, 3H), 3.78 (s, 3H), 2.37 (s, 3H), 2.31 (s, 3H), 2.29 (s, 3H). $[\alpha]^{20}D$ = -180.46. In accordance with a previously published method [40].

3.3. General procedure of the bromination

To a solution of the corresponding substrate (1 equiv.) in CH_2Cl_2 (0.36 M), a solution of bromine (1.05 equiv.) in CH_2Cl_2 (1.26 M) was added dropwise at 0 °C. The mixture was stirred for 2h at 25 °C, when DIPEA (1(8) equiv.) was added. The mixture was stirred for 3 h at 25 °C and poured into water. Water was added and the crude product extracted three times with CH_2Cl_2, washed with water, dried over magnesium sulphate, and then, solvent was removed under vacuum. The crude product was finally purified by silica gel chromatography with the appropriate solvent.

3-bromo-2,5-dimethylcyclohexa-2,5-diene-1,4-dione (7). With 2,5-dimethylbenzoquinone, eluent (CHX/EtOAC, 9/1, v/v, UV), yellow solid, 77% yield. ^{1}H NMR (400 MHz, $CDCl_3$) δ 6.63 (q, J = 1.6 Hz, 1H), 2.19 (s, 3H), 2.10 (d, J = 1.6 Hz, 3H). ^{13}C {^{1}H} NMR (101 MHz, $CDCl_3$) δ 184.3, 179.9, 146.1, 145.7, 136.0, 133.2, 16.9, 16.6. In accordance with a previously published method [41].

3.4. General procedure of the reduction and protection of benzoquinone

The corresponding bromo-benzoquinone (1 equiv.) was solubilized in MeOH (0.26 M) then a solution of $SnCl_2$ (2.5 equiv.) in 37% HCl (4.12 equiv.) was added dropwise and the mixture was stirred 30 min at 25 °C until the solution came back yellowish. Most of the solvent was evaporated under vacuum, the white precipitate was rinsed with water. The powder was dissolved in acetone (0.26 M) and dry over magnesium sulfate. Under argon dimethyl sulfate (5 equiv.) was added to the previous mixture then a solution of KOH (5 equiv.) in MeOH (1 M) was added dropwise. When the addition was completed the mixture was stirred under reflux at 60 °C during 3 h. A 20% KOH aqueous solution (10 mL) was added to the mixture and organic solvent was removed under reduced pressure. The crude product was extracted three times with CH_2Cl_2, washed with water, dried over magnesium sulphate, and then, solvent was removed under vacuum. The crude product was finally purified by silica gel chromatography with the appropriate solvent.

2-bromo-1,4-dimethoxy-3,5-dimethylbenzene (8). With compound **7**, eluent (CHX/EtOAc, 8/2, v/v, UV), white solid, 80% yield. M.p. = 56-58 ºC. ^{1}H NMR (300 MHz, $CDCl_3$) δ 6.60 (s, 1H), 3.78 (s, 3H), 3.74 (s, 3H), 2.31 (s, 3H), 2.28 (s, 3H). ^{13}C {^{1}H} NMR (75 MHz, $CDCl_3$) δ 152.2, 151.1, 132.6, 130.1, 111.8, 111.4, 60.3, 56.5, 16.6, 16.4. HRMS (ESI) calcd. for $C_{10}H_{13}BrO_2$: 244.0099. Found: 244.0108 (M^+). In accordance with a previously published method [26].

1-bromo-2,5-dimethoxy-3,6-dimethyl-4-(4-(trifluoromethyl)benzyl)benzene (21). With compound **19**, eluent (T/CHX, 5/5, v/v, UV), colorless oil, 75% yield. ^{1}H NMR (400 MHz, $CDCl_3$) δ 7.49 (d, J = 8.1 Hz, 2H), 7.19 (d, J = 7.9 Hz, 2H), 4.10 (s, 2H), 3.75 (s, 3H), 3.57 (s, 3H), 2.39 (s, 3H), 2.14 (s, 3H). ^{19}F {^{1}H} NMR (377 MHz, $CDCl_3$) δ -62.34. ^{13}C {^{1}H} NMR (101 MHz, $CDCl_3$) δ 153.9, 152.3, 144.4 (q, J = 1.4 Hz), 131.3, 130.3, 130.0, 129.2, 128.4, 128.5 (q, J = 24.5 Hz),128.4, 125.5 (q, J = 3.1 Hz), 124.4 (q, J = 276 Hz), 119.7, 61.3, 60.4, 32.8, 17.1, 13.3. HRMS (ESI) calcd. for $C_{18}H_{19}BrO_2F_3$: 403.0515. Found: 403.0537 ($M+H^+$).

3.5. General procedure of the metalation and borylation of the protected bromo-benzoquinone

A solution of *n*-BuLi (1.2 equiv.) (1.6M in hexane) was added dropwise to a stirred solution of the corresponding protected bromo-benzoquinone (1 equiv.) in anhydrous THF (0.17 M) under argon at -78 °C. The mixture was stirred at -80 °C for 5 min and then triisopropyl borate (2.5 equiv.) was added dropwise at -78 °C. The mixture was stirred back to 25 °C for 16 h, quenched with HCl 1M, and the crude product extracted three times with EtOAc, washed with water, dried over magnesium sulphate, and then, solvent was removed under vacuum. The crude product was finally purified by silica gel chromatography with the appropriate solvent.

(2,5-dimethoxy-3,6-dimethylphenyl)boronic acid (9). With compound **8**, no purification, white solid, 55% NMR yield. ^{1}H NMR (300 MHz, Acetone-d_6) δ 6.68 (s, 1H), 3.76 (s, 3H), 3.68 (s, 3H), 2.20 (s, 3H), 2.13 (s, 3H). In accordance with a previously published method [26].

(2,5-dimethoxy-3,6-dimethyl-4-(4-(trifluoromethyl)benzyl)phenyl)boronic acid (23). With compound **21**, yellow oil, 63% NMR yield, not purified engaged in the next step.

3.6. General procedure of the oxidative demethylation of the protected benzoquinone

The corresponding protected benzoquinone (1 equiv.) was solubilized in acetonitrile (0.08 M) then a solution of CAN (2.2 equiv.) in water (0.24 M) was added. The mixture was stirred 1 h at 25 °C. Organic solvent was removed under reduced pressure and the crude product extracted three times with CH_2Cl_2, washed with water, dried over magnesium sulphate, and then, solvent was removed under vacuum. The crude product was finally purified by silica gel chromatography with the appropriate solvent.

(2,5-dimethyl-3,6-dioxocyclohexa-1,4-dien-1-yl)boronic acid (5). With compound **9**, no purification, yellow solid, 99% yield. ^{1}H NMR (300 MHz, $CDCl_3$) δ 6.64 (s, 2H), 6.58-6.59 (q, *J* = 1.52 Hz, 1H), 2.30 (s, 3H), 1.98 (d, *J* = 1.53 Hz, 3H). In accordance with a previously published method [26].

(*S*)-2,5-dimethyl-3-(*p*-tolylsulfinyl)cyclohexa-2,5-diene-1,4-dione (16). With compound **15**, no purification, red solid, 95% yield. ^{1}H NMR (300 MHz, $CDCl_3$) δ 7.64-7.67 (d, *J* = 8.24 Hz, 2H), 7.31 - 7.34 (d, *J* = 8.00 Hz, 2H), 6.65 (d, *J* = 1.54 Hz, 1H), 2.50 (s, 3H), 2.42 (s, 3H), 2.03 (d, *J* = 1.54 Hz, 3H). $[\alpha]^{20}$D = +602.5. In accordance with a previously published method [40].

(2,5-dimethyl-3,6-dioxo-4-(4-(trifluoromethyl)benzyl)cyclohexa-1,4-dien-1-yl)boronic acid (25). With compound **23**, no purification, yellow solid, 40% yield. ^{1}H NMR (300 MHz, $CDCl_3$) δ 7.41 (m,, *J* = 8.04, 4H), 6.76 (s, 2H), 3.94 (s, 2H), 2.40 (s, 3H), 2.11 (s, 3H). ^{19}F {^{1}H} NMR (376 MHz, $CDCl_3$) δ -62.51. ^{13}C {^{1}H} NMR (101 MHz, $CDCl_3$) δ 194.5, 187.5, 157.0, 155.3, 143.2, 143.1, 142.9, 142.6, 142.2, 128.9, 125.7, 125.6, 122.9, 32.2, 17.2, 15.5.

3.7. General procedure of the Kochi-Anderson reaction

The corresponding benzoquinone (1 equiv.) and the corresponding phenyl acetic acid (2 equiv.) were dissolved in a mixture of acetonitrile (0.06 M) and water (0.2 M). Then $AgNO_3$ (0.35 equiv.) and ammonium persulfate (1.3 equiv.) were added in the reaction mixture. The yellow mixture was protected from light and stirred under reflux for 3 h. Organic solvent was removed under reduced pressure and the crude product extracted three times with CH_2Cl_2, washed with water, dried over

magnesium sulphate, and then, solvent was removed under vacuum. The crude product was finally purified by silica gel by silica gel chromatography with the appropriate solvent.

2-bromo-3,6-dimethyl-5-((4-(trifluoromethyl)phenyl)methyl)cyclohexa-2,5-diene-1,4-dione (19). With compound **7** and 4-(trifluomethylphenyl)acetic acid, eluent (T/CHX, 7/3, v/v, UV), yellow oil, 77% yield. ^{1}H NMR (400 MHz, $CDCl_3$) δ 7.53 (d, J = 8.1 Hz, 2H), 7.29 (d, J = 8.3 Hz, 2H), 3.94 (s, 2H), 2.23 (s, 3H), 2.18 (s, 3H). ^{19}F {^{1}H} NMR (377 MHz, $CDCl_3$) δ -62.49. ^{13}C {^{1}H} NMR (101 MHz, $CDCl_3$) δ 183.9, 179.7, 145.9, 142.2, 142.1, 141.8 (q, J = 1.5 Hz), 135.9, 128.97 (q, J = 24.2 Hz), 128.94, 125.7 (q, J = 3.8 Hz), 124.2 (q, J = 279.6 Hz), 32.3, 17.3, 13.8. HRMS (ESI) calcd. for $C_{16}H_{13}BrO_2F_3$: 373.0046. Found: 373.0040 ($M+H^+$).

(*S*)-2-(4-bromobenzyl)-3,6-dimethyl-5-(*p*-tolylsulfinyl)cyclohexa-2,5-diene-1,4-dione (17). With compound **16** (S)-2,5-dimethyl-3-(*p*-tolylsulfinyl)cyclohexa-2,5-diene-1,4-dione (400 mg, 1.46 mmol, 1 equiv.) and 2-(4-bromophenyl)acetic acid (627.9 mg, 2.92 mmol, 2 equiv.), eluent (T/Et_2O, 95/5, v/v, UV), red solid, 31% yield. M.p. = 111-113 °C. ^{1}H NMR (300 MHz, $CDCl_3$) δ 7.66 (d, J = 8.22 Hz, 2H), 7.40 (d, J = 8.35 Hz, 2H), 7.32 (d, J = 8.19 Hz, 2H), 7.02 (d, J = 8.31 Hz, 2H), 3.79 (s, 2H), 2.50 (s, 3H), 2.41 (s, 3H), 2.08 (s, 3H). ^{13}C {^{1}H} NMR (75 MHz, $CDCl_3$) δ 185.7, 184.5, 146.7, 145.9, 143.2, 141.8, 141.6, 139.6, 136.3, 131.8, 130.3, 130.1, 124.9, 120.6, 31.9, 21.4, 12.5, 9.4. $[\alpha]^{20}D$ = 337.5.

3.8. General procedure of the Diels-Alder cycloaddition reaction

The corresponding boronic acid (1 equiv.) was solubilized in CH_2Cl_2 (0.07 M), then at -20 °C was added (3E/Z)-4-methoxybuta-1,3-diene (3 equiv.), the mixture was stirred 1 h at -20 °C. Water was added and the crude product was extracted three times with CH_2Cl_2, washed with water, dried over magnesium sulphate, and then, solvent was removed under vacuum. The crude product was finally purified by silica gel chromatography with the appropriate solvent.

(±)-2,4a-dimethyl-4a,5-dihydronaphthalene-1,4-dione (3). With compound **5**, no purification, yellow oil, 99% yield. ^{1}H NMR (300 MHz, $CDCl_3$) δ 7.05 (m, 1H), 6.56 (m, 1H), 6.20 (m, 2H), 2.57 (ddd, J = 19.1, 5.2, 1.4 Hz, 1H), 2.46 (m, 1H), 1.77 (t, J = 1.5 Hz, 3H), 1.17 (d, J = 1.4 Hz, 3H). In accordance with a previously published method [26].

(±)-2,4a-dimethyl-3-(4-(trifluoromethyl)benzyl)-4a,5-dihydronaphthalene-1,4-dione (1). With compound **25**, 2 fold-crystallized, yellow solid, 99% yield. M.p. = 59-61 °C (hexane). ^{1}H NMR (500 MHz, $CDCl_3$) δ 7.52 (d, J = 8.0 Hz, 2H), 7.28 (d, J = 8.0 Hz, 2H), 7.15 (dd, J = 5.4, 1.1 Hz, 1H), 6.32 – 6.22 (m, 2H), 4.08 (d, J = 14.2 Hz, 1H), 3.84 (d, J = 14.3 Hz, 1H), 2.60 (dd, J = 4.3, 1.7 Hz, 2H), 2.18 (s, 3H), 1.12 (s, 3H). ^{19}F {^{1}H} NMR (377 MHz, $CDCl_3$) δ -62.49. ^{13}C {^{1}H} NMR (126 MHz, $CDCl_3$) δ 200.3, 185.1, 148.1, 144.7, 142.1 (q, J = 1.6 Hz), 134.3, 133.5, 130.9, 128.9, 128.8 (q, J = 24 Hz), 125.8 (q, J = 3.7 Hz), 124.3 (q, J = 279.6 Hz), 123.6, 44.1, 33.1, 32.1, 24.9, 13.7. Elemental analysis calcd. for $C_{20}H_{17}F_3O_2$: C, 69.36; H, 4.95; found: C, 69.62; H, 5.08. HRMS (ESI) calcd. for $C_{20}H_{18}O_2F_3$: 347.1253. Found: 347.1244 ($M+H^+$).

3.9. Parasite culture and antiplasmodial drug assays

P. falciparum NF54 wild type parasites cultured in medium containing 0.5% Albumax II were used to test for compound activity on parasite multiplication using a [^{3}H]-hypoxanthine incorporation assay [35]. Compounds were dissolved in DMSO at 10 mM, serial dilutions prepared in hypoxanthine-free culture medium (7-step dilution series; 2-fold serial dilutions) and 100 µl aliquots dispensed in duplicates into 96-well cell culture plates. 100 µL asexual parasite culture suspension (prepared in hypoxanthine-free medium) were added to each well and mixed with the preloaded compounds to obtain a final hematocrit of 1.25% and a parasitemia of ~0.3%. Each plate included eight wells containing the DMSO vehicle alone (0.1% final concentration) and four wells containing uninfected RBCs (uRBC). After incubation for 48 h, 0.25 µCi of [^{3}H]-hypoxanthine was added per well and plates were incubated for an additional 24 h. Parasites were harvested onto glass-fiber filters using a Microbeta FilterMate cell harvester (Perkin Elmer, Waltham, USA) and radioactivity was counted using a MicroBeta2 liquid scintillation counter (Perkin Elmer, Waltham, USA). The results were recorded, processed by subtraction of the mean background signal obtained from the uRBC controls, and expressed as a percentage of the mean signal obtained from the untreated controls. [35,42]. Chloroquine diphosphate (Sigma C6628) and artesunate (Mepha) were included as reference compound(s) in every experiment.

3.10. Drug assay against *S. mansoni* NTS

Harvested *S. mansoni* cercariae (Liberian strain) obtained from infected *Biomphalaria glabrata* snails were mechanically transformed into newly transformed schistosomula (NTS) following standard procedures as described [36]. Artesunate and Praziquantel were previously tested in the drug assay against *S. mansoni* NTS [43]. 30-40 NTS were placed in each well of a 96-well plate with culture medium and the test compound (25 µM, 10 µM, 1 µM) for a final well volume of 250 µl. Culture medium was composed of M199 medium (Gibco, Waltham MA, USA) supplemented with 5% Horse Serum (Gibco, Waltham MA, USA), 1% penicillin/streptomycin mixture (Invitrogen, 100 U/ml) and 1% Mäser Mix [44]. Each compound was tested in triplicate. NTS incubated with no more than 1% DMSO served as control. NTS were kept in the incubator at 37°C and 5% CO_2 for up to 72 hours. After 24, 48 and 72 hours, the condition of the NTS was microscopically evaluated. Worms are scored as 0= dead; 0.25-1=reduced motility and significant tegument damage; 1.25-2= reduced motility or marked tegument damages 2.25-3= viable, nice tegument, good motility.

3.11. Drug assay against *ex vivo S. mansoni* adult worms

Female NMRI mice (age 3 weeks, weight ca. 14-20 g) were purchased from Charles River (Sulzfeld). The animals were allowed to adapt for 1 week under controlled conditions (21-24°C, 45-65% humidity, 12 hours light, and free access to water and rodent diet) before experimental handling. To obtain adult schistosomes, NMRI mice were infected subcutaneously with 80 to 100 cercariae. After 49 days, the mice were euthanized with CO_2 and the worms collected from the hepatic portal and mesenteric veins. Three pairs of adult worms were placed in each well of a 24-well plate with 2 mL culture medium and the test compound (25 µM, 10 µM). Culture medium was composed of RPMI 1640 (Invitrogen, Carlsbad, CA) supplemented with 5 % Horse Serum (Gibco, Waltham MA, USA) and 1% penicillin/streptomycin mixture (Invitrogen, 100 U/ml). Each compound was tested in duplicate. Artesunate and Praziquantel

were previously tested in the drug assay against *S. mansoni* adult worms [43]. Schistosomes incubation with no more than 1% DMSO served as control. Worms were kept in an incubator at 37°C and 5% CO_2 for up to 72 hours. After 24, 48 and 72 hours, the condition of the worms was microscopically evaluated and scored as described [36] above.

3.12. Cytotoxicity assays with the rat L6 cell line

Cell proliferation was assessed with resazurin, and the generally cytotoxic agent podophyllotoxin served as the positive control. L-6 cells, a primary cell line derived from rat skeletal myoblasts, were cultivated in RPMI 1640 medium supplemented with 1% L-glutamine (200 mM) and 10% fetal bovine serum. Cultures were maintained at 37 °C in an atmosphere of 5% CO_2. Assays were performed in 96-well plates, each well containing RPMI 1640 medium supplemented with 1% L-glutamine (200 mM), 10% fetal bovine serum, and 2000 L-6 cells. Plates were incubated at 37 °C under a 5% CO_2 atmosphere for 24 h. After that, compounds were dissolved in DMSO (10 mM or 10 mg/ml), serial drug dilutions of eleven 3-fold dilution steps covering a range from 100 to 0.002 µg/mL or 100 to 0.002 µM were prepared, and the plates incubated at 37 °C under 5% CO_2 for 70 h. After 70 h of incubation, 10 µL of resazurin solution (12.5 mg resazurin in 100 mL 1xPBS) was added per well and plates were incubated for an additional 2 h. After that the plates were read with a Spectramax Gemini EM microplate fluorometer (Molecular Devices) using an excitation wave length of 536 nm and an emission wave length of 588 nm. The results were expressed as percentage of the untreated controls [45,46]. Fifty percent inhibitory concentrations (IC_{50}) were estimated by linear interpolation [47].

3.13. *Pf*FNR-catalyzed PDO redox-cycling assay with ψ-Plasmodiones

The reaction mixtures in a total volume of 200 µL and final DMSO concentration of 10 % in 50 mM PBS buffer pH 7.0 contained 50 µM of ψ-PD, 13 µM hematin, and the *Pf*FNR-catalyzed PDO redox-cycling system consisting in 40 µM PDO, 100 µM NADPH and 0.5 µM *Pf*FNR. The reaction was started by addition of *Pf*FNR (4 µL) and sustained by subsequent addition of 100 µM of NADPH (in 2 µL) every 15 min for 3 h. Reactions were incubated at 25 °C or 37 °C for the time of redox cycling. For the controls 80 µM H_2O_2 was added instead of the *Pf*FNR-catalyzed PDO redox-cycling system. The reaction was started by addition of *Pf*FNR (0.5 µM) and collected after 3 h incubation at 25 °C or 37 °C. Collected samples were centrifuged and diluted with 30 µL DMSO before LC-MS analyses. LC-MS analyses of the reaction mixtures were performed using an Agilent 1100 series LC coupled to a maXis II Q-TOF mass spectrometer (Bruker, Germany). *Pf*FNR-catalyzed PDO redox-cycling reaction mixtures containing hematin and each ψ-plasmodione regioisomer was analyzed with the LC-MS system. The mass spectrometer operated with a capillary voltage of 4,500 V in positive mode. Acquisitions were performed on the mass range *m/z* 200-1850. Calibration was performed using the singly charged ions produced by a solution of Tune mix (G1969-85000, Agilent, U.S.A.). Compounds were separated on a XBridge Peptide BEH C18 column (300Å, 3.5 µm, 2.1 mm X 250 mm) column. The gradient was generated at a flow rate of 250 µL/min, at 60 °C by mixing two mobile phases. Phase A consisted of 0.1 % formic acid (FA) in water and phase B of 0.08 % FA in ACN. Phase B was increased from 5 to 85% in 45 min. Data analysis was performed by using Compass DataAnalysis 4.3 (Bruker Daltonics).

4. Conclusion

In this work, our aim was to introduce another chemical asset on our lead molecule plasmodione that can have a positive impact on the PK properties and can act as a shield for any detrimental effect coming from the complex host biological environment, in particular for long-term use of drug treatments. Thereby, from a Diels-Alder reaction we described the synthesis of racemic non-quinonoid ψ-plasmodione regioisomers, 4a-ψ-plasmodione **1** and 8a-ψ-plasmodione **2**. The real breakthrough to control the regiochemical course of the reaction was achieved by the introduction of a boronic acid on the quinone as the auxiliary group to allow the full control of the cycloaddition regioselectivity. The next challenge will be to decorate the ψ-plasmodiones with substituents that will influence the oxidation of angular methyl, but above all the cleavage of the C-C bond allowing aromatisation and release of plasmodione.

Supplementary Materials: The following are available online at www.mdpi.com/link. They include Pages S2-S3: Investigations on ψ-menadione post-functionalization (Scheme S1) and screening of Diels-Alder cycloaddition conditions in reactions using 3-benzylbenzoquinone 17 (Table S1); Pages S4-S7: Metabolic Studies by LC-MS analyses (Figures S1-S3); S8-S23: ^{1}H, ^{19}F and ^{13}C NMR spectra of key/new compounds.

Author Contributions: E.C.R. and B.D. synthetized the compounds; D.A.L. designed the synthetic methodologies; J.-M.S. supported the LC-MS analyses, C.H. performed the antischistosomal drug assays under J. K.'s supervision, D.L.W. initiated the NIH-funded project on redox-active antischistosomal 3-benzylmenadiones; E.D.-C. designed the pseudo-plasmodiones. P.M., M.R.; J.K., D.L.W., P.M. and E.D.-C. analyzed the data; E.C.R., B.D and E.D.-C. wrote the manuscript. All authors have read and agreed to the published version of the manuscript.

Funding: This research was funded by the Agence Nationale de la Recherche (ANR) and the (FNS) for funding our project in the frame of the ANR-FNS program [ANR-22-CE93-0005-01, "ROS Action" project to E.D-C., P.M. and M.R., J.K.]. The preliminary work was initially funded by the grant from National Institutes of Health (NIH), USA (project entitled "Redox balance and drug development in *Schistosoma mansoni*", grant 1R01AI065622-01A2 to D.L.W.) for allowing the set-up of the platform of synthetic methodologies (salary to D. A. L.). E.D.-C. and B.D. wish to thank the Laboratoire d'Excellence (LabEx) ParaFrap [ANR-11-LABX-0024], for funding, providing B.D.'s PhD salary, and for initiating and fostering the scientific research within the consortium. The laboratories also receive support from CNRS (E.D.-C.), and from the University of Strasbourg (E.D.-C., E.C.R.'s PhD salary).

Acknowlegements: E.D.-C. is grateful to Prof. A. Aliverti for the sample of *Pf*FNR.

Conflict of Interests

The authors declare no conflict of interest.

Abbreviations: The following abbreviations are used in this manuscript:

ACN, acetonitrile; benzoylMD, 3-benzoylmenadione; benzylMD, 3-benzylmenadione; CHX, cyclohexane; CAN, cerium ammonium nitrate; DIPEA, *N,N*- diisopropylethylamine; EIC, extracted ion chromatogram; FA, formic acid; MoA, mode of action; NBS, *N*-bromosuccinimide; NTS, newly transformed schistosomula; PD, plasmodione; PDO, plasmodione oxide; *Pf*FNR, *Plasmodium falciparum* Ferredoxin-NADP$^+$ Reductase; PK, pharmacokinetic properties; Ψ-, pseudo-; NQ, 1,4-naphthoquinones; ROS, reactive oxygen species; T, toluene.

References

1. Müller, T.; Johann, L.; Jannack, B.; Brückner, M.; Lanfranchi, D. A.; Bauer, H.; Sanchez, C.; Yardley, V.; Deregnaucourt, C.; Schrével, J.; Lanzer, M.; Schirmer, R. H.; Davioud-Charvet, E. Glutathione reductase-catalyzed cascade of redox reactions to bioactivate potent antimalarial 1;4-naphthoquinones – A new strategy to combat malarial parasites. *J. Am. Chem. Soc.* **2011**, *133*, 11557-11571. doi: 10.1021/ja201729z
2. Ehrhardt, K.; Deregnaucourt, C.; Goetz, A.-A.; Tzanova, T.; Pradines, B.; Adjalley, S. H.; Blandin, S.; Bagrel, D.; Lanzer, M.; Davioud-Charvet, E. The redox-cycler plasmodione is a fast acting antimalarial lead compound with pronounced activity against sexual and early asexual blood-stage parasites. *Antimicrob. Agents Chemother.* **2016**, *60*, 5146-5158. doi: 10.1128/AAC.02975-15
3. Rodo, E. C.; Feng, L.; Jida, M.; Ehrhardt, K.; Bielitza, M.; Boilevin, J.; Lanzer, M.; Williams, D. L.; Lanfranchi, D. A.; Davioud-Charvet, E. A platform of regioselective methodologies to access to polysubstituted 2-methyl-1;4-naphthoquinones derivatives: scope and limitations. *Eur. J. Org. Chem.* **2016**, *2016*, 1982–1993. doi: 10.1002/ejoc.201600144
4. Donzel, M.; Elhabiri, M.; Davioud-Charvet, E. A bioinspired photoredox benzylation of quinones. *J. Org. Chem.* **2021**, *86*, 10055-10066. doi: 10.1021/acs.joc.1c00814
5. Urgin, K.; Jida, M.; Ehrhardt, K.; Müller, T.; Lanzer, M.; Maes, L.; Davioud-Charvet, E. Pharmacomodulation of the antimalarial plasmodione: synthesis of biaryl- and *N*-arylalkylamine analogues; antimalarial activities and physicochemical properties. *Molecules* **2017**, *22*, 161, 1-32. doi: 10.3390/molecules22010161
6. Trometer, N.; Pecourneau, J.; Feng, L.; Navarro-Huerta, J. A.; Lazarin-Bidóia, D.; de Oliveira Silva Lautenschlager, S.; Maes, L.; Fortes Francisco, A.; Kelly, J. M.; Meunier, B.; Cal, M.; Mäser, P.; Kaiser, M.; Davioud-Charvet, E. Synthesis and Anti-Chagas Activity Profile of a Redox-Active Lead 3-Benzylmenadione Revealed by High-Content Imaging. *ACS Infect. Dis.* **2024**, *10*, 1808–1838. doi: 10.1021/acsinfecdis.4c00137
7. Dupouy, B.; Donzel, M.; Roignant, M.; Charital, S.; Yamaryo-Botté, Y.; Keumoe, R.; Bordat, Y.; Bundschuh, M.; Feckler, A.; Rottmann, M.; Mäser, P.; Blandin, S. A.; Botté, C. Y.; Besteiro, S.; Davioud-Charvet, E. 3-Benzylmenadiones and their heteroaromatic analogues target the apicoplast of Apicomplexa parasites: Synthesis and bioimaging studies. *ACS Infect. Dis.* **2024**, submitted.
8. Mounkoro, P.; Michel, T.; Blandin, S.; Golinelli-Cohen, M.-P.; Davioud-Charvet, E.; Meunier, B. Investigating the mode of action of the redox-active antimalarial drug plasmodione using the yeast model. *Free Radic Biol Med.* **2019**, *141*, 269–278. doi: 10.1016/j.freeradbiomed.2019.06.026
9. Cichocki, B. A.; Donzel, M.; Heimsch, K. C.; Lesanavičius, M.; Feng, L.; Montagut, E. J.; Becker, K.; Aliverti, A.; Elhabiri, M.; Čėnas, N.; Davioud-Charvet, E. Plasmodium Falciparum Ferredoxin-NADP$^+$ Reductase-Catalyzed Redox Cycling of Plasmodione Generates Both Predicted Key Drug Metabolites: Implication for Antimalarial Drug Development. *ACS Infect. Dis.* **2021**, *7*, 1996–2012. doi: 10.1021/acsinfecdis.1c00054
10. WHO, fact sheet Schistosomiasis (Bilharzia), **2023**.
11. Ross, A. G. P.; Sleigh, A. C.; Olds, G. R.; Williams, G. M.; Mcmanus, D. P. Schistosomiasis. *N. Engl. J. Med.* **2002**, *346*, 1212-1220. doi: 10.1056/NEJMra012396
12. Sidorov, P.; Desta, I.; Chessé, M.; Horvath, D.; Marcou, G.; Varnek, A.; Davioud-Charvet, E.; Elhabiri, M. Redox Polypharmacology as an Emerging Strategy to Combat Malarial Parasites. *ChemMedChem* **2016**, *11*, 1339–1351. doi: 10.1002/cmdc.201600009
13. Bielitza, M.; Belorgey, D.; Ehrhardt, K.; Johann, L.; Lanfranchi, D. A.; Gallo, V.; Schwarzer, E.; Mohring, F.; Jortzik, E.; Williams, D. L.; Becker, K.; Arese, P.; Elhabiri, M.; Davioud-Charvet E. Antimalarial NADPH-consuming redox-cyclers as superior G6PD deficiency copycats. *Antioxid. Redox Signal.* **2015**, *22*, 1337-1351. doi: 10.1089/ars.2014.6047
14. Elhabiri, M.; Sidorov, P.; Cesar-Rodo, E.; Marcou, G.; Lanfranchi, D. A.; Davioud-Charvet, E.; Horvath, D.; Varnek, A. Electrochemical properties of substituted 2-methyl-1;4-naphthoquinones: redox behavior predictions. *Chem.-Eur. J.* **2015**, *21*, 3415-3424. doi: 10.1002/chem.201403703
15. Monks, T.; Jones, D. The Metabolism and Toxicity of Quinones, Quinonimines, Quinone Methides, and Quinone-Thioethers. *Curr. Drug Metab.* **2002**, *3*, 425–438. doi: 10.2174/1389200023337388

16. Cotos, L.; Donzel, M.; Elhabiri, M.; Davioud-Charvet, E. A mild and versatile Friedel-Crafts methodology for the diversity-oriented synthesis of redox-active 3-benzoylmenadiones with tuneable redox potentials. *Chem. Eur. J.* **2020**, *26*, 3314-3325. doi: 10.1002/chem.201904220
17. Ishikawa, M.; Hashimoto, Y. Improvement in Aqueous Solubility in Small Molecule Drug Discovery Programs by Disruption of Molecular Planarity and Symmetry. *J. Med. Chem.* **2011**, *54*, 1539–1554. doi: 10.1021/jm101356p
18. Yoshimoto, F. K.; Guengerich, F. P. Mechanism of the third oxidative step in the conversion of androgens to estrogens by cytochrome P450 19A1 steroid aromatase. *J. Am. Chem. Soc.* **2014**, *136*, 15016-15025. doi: 10.1021/ja508185d
19. Denisov, I. G.; Makris, T. M.; Sligar, S. G.; Schlichting, I. Structure and chemistry of cytochrome P450. *Chem Rev.* **2005**, *105*, 2253-77. doi: 10.1021/cr0307143
20. Akhtar, M.; Wright, J. N.; Lee-Robichaud, P. A Review of Mechanistic Studies on Aromatase (CYP19) and 17α-Hydroxylase-17;20-Lyase (CYP17). *J. Steroid Biochem. Mol. Biol.* **2011**, *125*, 2–12. doi: 10.1016/j.jsbmb.2010.11.003
21. Nicolaou, K. C.; Snyder, S. A.; Montagnon, T.; Vassilikogiannakis, G. The Diels-Alder Reaction in Total Synthesis. *Angew. Chem. Int. Ed.* **2002**, *41*, 228–1698. doi: 10.1002/1521-3773(20020517)41:10<1668::AID-ANIE1668>3.0.CO;2-Z
22. Nawrat, C. C.; Moody, C. J. Quinones as Dienophiles in the Diels–Alder Reaction: History and Applications in Total Synthesis. *Angew. Chem. Int. Ed.* **2014**, *53*, 2056–2077. doi: 10.1002/anie.201305908
23. Corey, E. J. Catalytic Enantioselective Diels-Alder Reactions: Methods; Mechanistic Fundamentals; Pathways; and Applications. *Angew. Chem. Int. Ed.* **2002**, *41*, 1650–1667. doi: 10.1002/1521-3773(20020517)41:10<1650::AID-ANIE1650>3.0.CO;2-B
24. Veguillas, M.; Redondo, M. C.; García, I.; Ribagorda, M.; Carreño, C. M. Synthesis of Benzo- and Naphthoquinonyl Boronic Acids: Exploring the Diels–Alder Reactivity. *Chem. – Eur. J.* **2010**, *16*, 3707–3719. doi: 10.1002/chem.200902796
25. Carreño, M. C.; Urbano, A.; Fischer, J. Enantioselective Diels–Alder Approach to Angucyclinones from (S)-2-(*p*-Tolylsulfinyl)-1;4-Naphthoquinone and Substituted Racemic Vinylcyclohexenes. *Angew. Chem. Int. Ed. Engl.* **1997**, *36*, 1621–1623. doi: 10.1002/anie.199716211
26. Redondo, M. C.; Veguillas, M.; Ribagorda, M.; Carreño, M. C. Control of the Regio- and Stereoselectivity in Diels–Alder Reactions with Quinone Boronic Acids. *Angew. Chem. Int. Ed.* **2009**, *48*, 370–374. doi: 10.1002/anie.200803428
27. Lanfranchi, D. A.; Hanquet, G. Asymmetric Diels-Alder reactions of a new enantiomerically pure sulfinylquinone: a straightforward access to functionalized Wieland-Miescher ketone analogues with (R) absolute configuration. *J Org Chem.* **2006**, *71*, 4854-4861. doi: 10.1021/jo060486n
28. del Hoyo, A. M.; Urbano, A.; Carreño, M. C. Enantioselective Synthesis of Four Stereoisomers of Sulfinyl Ferrocenyl Quinones with Central; Planar; and Helical Chirality. *Org. Lett.* **2016**, *18*, 20–23. doi: 10.1021/acs.orglett.5b03029
29. Carreño, M. C.; Enríquez, Á.; García-Cerrada, S.; Sanz-Cuesta, M. J.; Urbano, A.; Maseras, F.; Nonell-Canals, A. Towards Configurationally Stable [4]Helicenes: Enantioselective Synthesis of 12-Substituted 7,8-Dihydro[4]Helicene Quinones. *Chem. – Eur. J.* **2008**, *14*, 603–620. doi: 10.1002/chem.200700762
30. Bhattacharya, A. K.; Miller, B. Formation and Rearrangements of Blocked Aromatic Molecules Substituted with O- Groups. *J. Org. Chem.* **1983**, *48*, 2412–2418. doi: 10.1021/jo00162a024
31. Jeanmart, L.; Mambourg, K.; Hanquet, G.; Lanners, S. The Diels-Alder Reaction of 1;4-Quinones in Hexafluoroisopropanol. *Arkivoc* **2024**, *5*, 202312140. doi: 10.24820/ark.5550190.p012.140
32. Solladié, G.; Hutt, J.; Girardin, A. Improved Preparation of Optically Active Methyl *p*-Tolyl Sulfoxide. *Synthesis* **1987**, *1987*, 173. doi: 10.1055/s-1987-27877
33. Fujiwara, Y.; Domingo, V.; Seiple, I. B.; Gianatassio, R., Del Bel, M., Baran, P. S. Practical C−H Functionalization of Quinones with Boronic Acids. *J. Am. Chem. Soc.* **2011**, *133*, 3292–3295. doi: 10.1021/ja111152z
34. Jacob III P., Callery P. S., Shulgin, A. T., Castagnoli Jr. N. A convenient synthesis of quinones from hydroquinone dimethyl ethers. Oxidative demethylation with ceric ammonium nitrate. *J. Org. Chem.* **1976**, *41*, 3627 –3629. doi: 10.1021/jo00884a035
35. Snyder, C., Chollet, J., Santo-Tomas, J., Scheurer, C., Wittlin S. In vitro and in vivo interaction of synthetic peroxide RBx11160 (OZ277) with piperaquine in *Plasmodium* models. *Exp. Parasitol.* **2007**, *115*, 296-300. doi: 10.1016/j.exppara.2006.09.016
36. Lombardo, F. C., Pasche, V., Panic, G., Endriss, Y., Keiser, J. Life cycle maintenance and drug-sensitivity assays for early drug discovery in Schistosoma mansoni. *Nat. Protoc.* **2019**, *14*, 461-481. doi: 10.1038/s41596-018-0101-y 10.1038/s41596-018-0101-y
37. González Cabrera, D.; Keiser, J.; Spangenberg, T. Analysis of the Physicochemical Properties of Anti-Schistosomal Compounds to Identify Next-Generation Leads. *ACS Med. Chem. Lett.* **2024**, *15*, 626-630. doi: 10.1021/acsmedchemlett.4c00026
38. Wiatr, M.; Hadzhieva, M.; Lecerf, M.; Noé, R.; Justesen, S.; Lacroix-Desmazes, S.; Dragon-Durey, M. A.; Dimitrov, J. D. Hyperoxidized Species of Heme Have a Potent Capacity to Induce Autoreactivity of Human IgG Antibodies. *Int. J. Mol. Sci.* **2023**, *24*, 3416. doi: 10.3390/ijms24043416
39. McCarty, K. D.; Tateishi, Y.; Hargrove, T. Y.; Lepesheva, G. I.; Guengerich, F. P. Oxygen-18 Labeling Reveals a Mixed Fe-O Mechanism in the Last Step of Cytochrome P450 51 Sterol 14α-Demethylation. *Angew. Chem. Int. Ed. Engl.* **2024**, *63*, e202317711. doi: 10.1002/anie.202317711

40. de Sousa A. L. F., Cardoso Filho J. E. P., Wladislaw B., Marzorati L., Di Vitta C. Studies on chemo- and diastereo-selectivity of the Diels-Alder reactions of sulfinyltoluquinones with cyclopentadiene. *Can. J. Chem.* **2009**, *87*, 1135-1143. doi: 10.1139/V09-070
41. Yu, D.; Ji, R.; Sun, Z.; Li, W.; Liu, Z.-Q. Electrochemical Chlorination and Bromination of Electron-Deficient CH Bonds in Quinones, Coumarins, Quinoxalines and 1,3-Diketones. *Tetrahedron Lett.* **2021**, *86*, 153514. doi: 10.1016/j.tetlet.2021.153514
42. Desjardins, R. E.; Canfield, C. J.; Haynes, J. D.; Chulay, J. D. Quantitative assessment of antimalarial activity in vitro by a semiautomated microdilution technique. *Antimicrob. Agents Chemother.* **1979**, *16*, 710-718. doi: 10.1128/AAC.16.6.710
43. Ingram, K.; Yaremenko, I. A.; Krylov, I. B.; Hofer, L.; Terent'ev, A. O.; Keiser, J. Identification of antischistosomal leads by evaluating bridged 1,2,4,5-tetraoxanes, alphaperoxides, and tricyclic monoperoxides. *J. Med. Chem.* 2012, *55*, 8700-8711. doi: 10.1021/jm3009184
44. Mäser, P.; Grether-Bühler, Y.; Kaminsky, R.; Brun, R. An anti-contamination cocktail for the in vitro isolation and cultivation of parasitic protozoa. *Parasitol. Res.* **2002**, *88*, 172-174. doi: 10.1007/s00436-001-0511-5
45. Page, B.; Page, M.; Noel, C. A new fluorometric assay for cytotoxicity measurements in-vitro. *Int. J. Oncol.* **1993**, *3*, 473-476. doi: 10.3892/ijo.3.3.473
46. Ahmed, S. A.; Gogal, R. M. Jr; Walsh, J. E. A new rapid and simple non-radioactive assay to monitor and determine the proliferation of lymphocytes: an alternative to [^{3}H]thymidine incorporation assay. *J. Immunol. Methods* **1994**, *170*, 211-224. doi: 10.1016/0022-1759(94)90396-4
47. Huber, W.; Koella, J. C. A comparison of three methods of estimating EC50 in studies of drug resistance of malaria parasites. *Acta Trop.* **1993**, *55*, 257–261. doi: 10.1016/0001-706x(93)90083-n
48. Anderson, J. M.; Kochi, J. K. Silver(II) Complexes in Oxidative Decarboxylation of Acids. *J. Org. Chem.* **1970**, *35*, 986–989. doi: 10.1021/jo00829a026

1.2.3 Les points importants de l'article 6

- **Synthèse des régioisomères ψ-Plasmodiones :** L'article décrit la synthèse de deux régioisomères analogue de la plasmodione **4a-ψ-plasmodione** et le **8a-ψ-plasmodione**, possédant un méthyle angulaire sur le motif quinone. Cette modification améliore la solubilité aqueuse et la lipophilicité, optimisant ainsi les propriétés PK de ces composés. La synthèse a été réalisée via une cycloaddition de Diels-Alder régiosélective, dirigée par un acide boronique.
- **Défis surmontés avec les acides boroniques :** Les sulfinylquinones chirales posaient des problèmes stériques dans la réaction de Diels-Alder. Leur remplacement par des acides boroniques a permis de surmonter ces obstacles et de synthétiser avec succès les deux ψ-plasmodiones.
- **Evaluation de la conversion métabolique :** Le méthyle angulaire des ψ-plasmodiones peut subir une oxydation via une cascade rédox « biomimétique » en présence d'hématine, de PDO, de *Pf*FNR et de NADPH, générant un flux continu d'anions superoxydes, libérant de la plasmodione *in tubo.* L'effet pro-drogue obtenu serait catalysé par les espèces (per)ferryl de l'hème généré dans les cycles redox.
- **Activités antiparasitaires :** Les ψ-plasmodiones ont montré une activité faible contre *P. falciparum*, mais une efficacité supérieure contre *S. mansoni* (NTS et vers adulte), particulièrement pour la **4a-ψ-plasmodione**, comparé à la plasmodione.
- **Hypothèse RSA :** Une conversion des ψ-plasmodiones en plasmodione limitée chez *P. falciparum* pourrait être causée par une mauvaise pénétration dans le parasite, affectant leur disponibilité/accumulation dans les organelles-cibles. En revanche, une meilleure conversion et une amélioration des propriétés PK/PC pourraient expliquer l'efficacité accrue chez le ver *S. mansoni*.

-

Conclusion générale et perspectives

Au cours de ces trois années au sein de l'équipe CBM, j'ai poursuivi deux principaux objectifs : i) contribuer à l'identification des cibles biologiques de la série de composés bMD chez le parasite *P. falciparum* par le développement d'outils chimiques, et ii) développer les bMDs pour améliorer leurs activités antiparasitaires par l'optimisation de leurs propriétés PC et PK et leur biodisponibilité.

Mon travail a d'abord été axé sur le développement de sondes 3-benzylménadiones cliquables : bMD-alcyne, bMD-pyrimidine-alcyne, 6-fluoro-bMD-alcyne et bMD-azoture. Ces sondes ont été valorisées au travers de divers projets interdisciplinaires afin d'atteindre nos objectifs. Nous avons ainsi pu mettre en évidence 44 cibles protéiques pertinentes chez le parasite *P. falciparum* en utilisant une stratégie (pro-)AfBPP basée sur la réaction clique CuAAC avec la 6-fluoro-bMD-alcyne. Par ailleurs, en collaboration avec nos collègues biologistes, nous avons mis en place une stratégie d'imagerie parasitaire combinant les sondes bMDs alcynes, la réaction clique CuAAC et un fluorophore azoturé commercial. Cette approche nous a permis de localiser nos composés bioactifs dans les parasites *P. falciparum* et *T. gondii*, révélant l'apicoplaste et la mitochondrie comme principales cibles des bMDs. Ces résultats ont été publiés en 2024 dans les journaux *ChemBioChem* et ACS *Infectious Diseases*.

En parallèle, j'ai poursuivi la synthèse de série bMD-*N*-hétéroaromatiques, initiée avec les Drs. Matthieu Roignant et Maxime Donzel, en particulier par l'introduction de groupements β-pyridine et β-pyrimidine. Une stratégie novatrice de couplage de Suzuki utilisant des dérivés ménadiones borés n'ayant pas abouti, un couplage de Negishi a cependant permis l'accès à ces composés ciblés, mettant en lumière de nouveaux résultats prometteurs contre le paludisme et la toxoplasmose. Ces travaux sont détaillés dans l'article publié dans *ACS Infectious Diseases* et consacré à la stratégie de bioimagerie avec la sonde bMD-pyrimidine-alcyne.

En réponse au premier objectif de thèse, nous avons également développé nos propres outils fluorescents basés sur une famille originale de fluorophores flavyliums cliquables et compatibles avec nos sondes bMDs. Une série de flavylium-azotures avec des propriétés photophysiques intéressantes (forte brillance en milieux aqueux, émission rouge-PIR, photostables, facilité d'accès…) a été synthétisée et utilisée en imagerie cellulaire montrant un potentiel d'application intéressant. Les systèmes cliqués flavylium-bMDs ont été synthétisés et ont démontré une comportement fluorogénique de type OFF-ON selon l'état rédox de la sous-unité bMD, exploitant ainsi le processus d'inhibition de fluorescence de type PeT et la distance entre les deux chromophores. Deux articles scientifiques ont été rédigés : l'un sur le développement des sondes fluorescentes cliquables et leur application en bioimagerie chez les plantes (chimie bioorthogonale de phytostérols alcynes (en cours de

réalisation), et le second basé sur l'étude des systèmes flavylium-bMDs et leur valorisation potentielle pour mesurer des gradients de stress oxydant dans des cellules vivantes (soumis à *Chemistry- A European Journal*).

Enfin, cette thèse a également permis de développer deux autres projets de chimie médicinale visant à optimiser notre molécule de référence pour répondre au second principal objectif. J'ai ainsi initié le développement d'une série de dérivés triazole-méthyle-ménadiones obtenus par réaction clique CuAAC. L'introduction de ce groupement a conduit à des composés très efficaces chez le parasite *S. mansoni*. Par ailleurs, nous avons poursuivi le développement de pro-drogues de la plasmodione en insérant un méthyle angulaire destiné à rompre l'aromaticité de la naphtoquinone, par une cycloaddition de Diels-Alder régiosélective. Ces modifications structurales ont amélioré les propriétés physicochimiques et pharmacocinétiques des composés. Ces résultats ont été soumis dans les journaux *Molecules* et *ChemMedChem*.

En conclusion, les résultats de cette thèse confirment que les bMDs possèdent plusieurs cibles biologiques distinctes chez *P. falciparum*, essentielles à la survie du parasite dans différentes organelles. Ils montrent également que l'amélioration des propriétés pharmacocinétiques de notre molécule de référence n'est pas toujours corrélée avec l'activité antiparasitaire, indiquant que les modifications structurales ont des effets multifactoriels sur nos composés.

Dans un avenir proche, nous prévoyons de mener des études supplémentaires sur les sondes bMD alcynes (AfBPP) ciblant deux stages parasitaires les plus sensibles aux bMDs chez *P. falciparum* : les anneaux et les gamétocytes. Par ailleurs, nous prévoyons de valoriser les sondes bMD azotures afin d'étudier leurs cibles chez *P. falciparum*, en combinaison avec notre sonde fluorescente flavylium-DBCO cliquable. Nous poursuivrons également notre projet sur la localisation des stérols alcynes dans les cellules de tabac à l'aide des sondes flavyliums cliquables, présentées dans l'article 3. Concernant le projet [TRZ-méthyle]-ménadione, les substrats de départ (ménadiones méthyle-alcyne et méthyle-azoture) seront prochainement utilisés pour réaliser des réactions clique *in situ* chez le vers adultes, en utilisant un partenaire fluorophore cliquable. Ces études d'imagerie permettront de visualiser la localisation des dérivés fluorescents [TRZ-méthyle]-ménadiones formés *in situ*, et de déterminer où les sondes sont générés dans les vers adultes. Enfin, d'autres analogues pseudo-« bMD » seront synthétisés au laboratoire afin d'évaluer cette nouvelle stratégie pro-drogue.

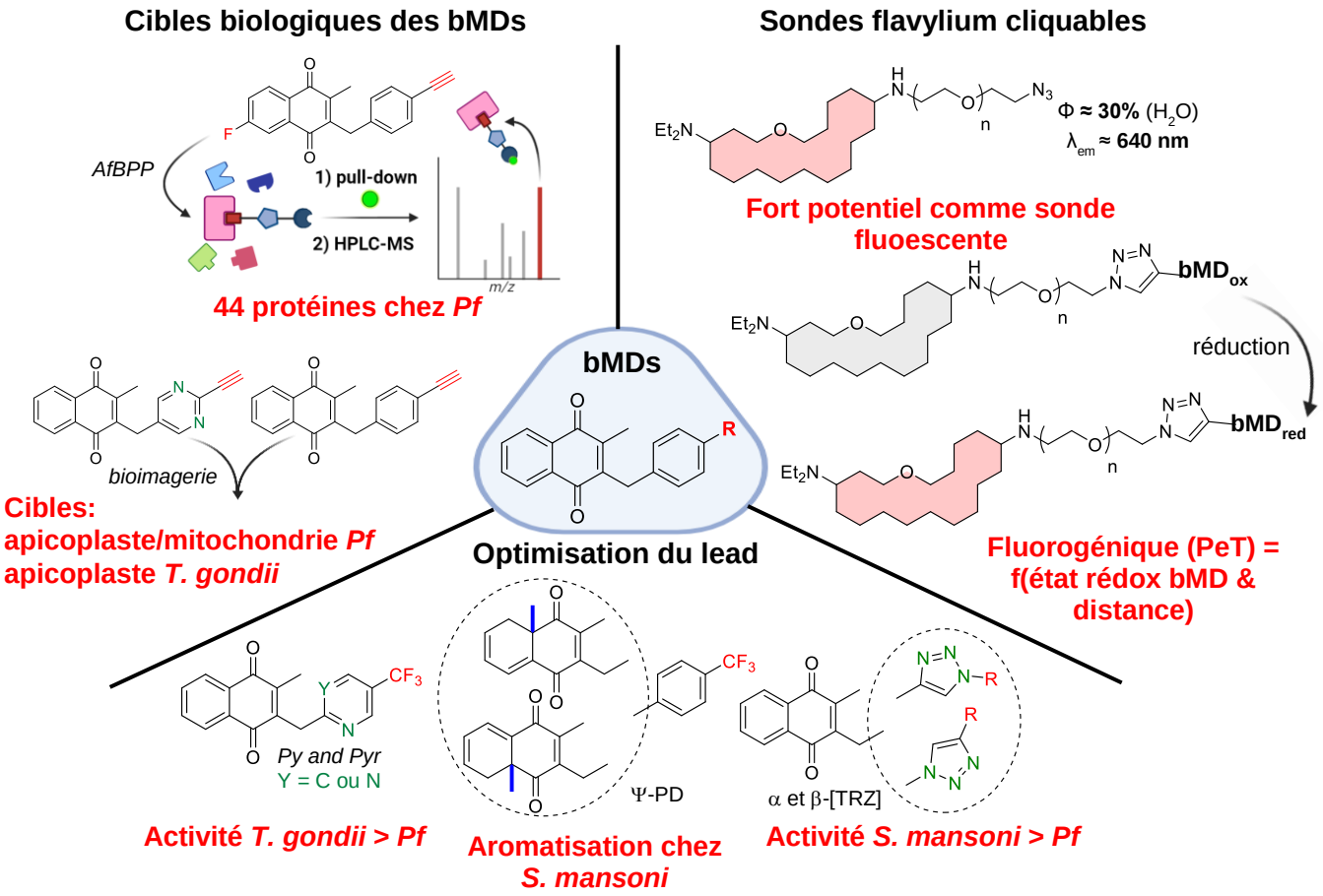
Cibles biologiques des bMDs
AfBPP
1) pull-down
2) HPLC-MS
m/z
44 protéines chez Pf
Sondes flavylium cliquables
Φ ≈ 30% (H2O)
λem ≈ 640 nm
Fort potentiel comme sonde fluoescente
bMDox
réduction
bMDred
Fluorogénique (PeT) = f(état rédox bMD & distance)
bioimagerie
Cibles:
apicoplaste/mitochondrie Pf
apicoplaste T. gondii
bMDs
Optimisation du lead
Py and Pyr
Y = C ou N
Activité T. gondii > Pf
Ψ-PD
Aromatisation chez S. mansoni
α et β-[TRZ]
Activité S. mansoni > Pf

Partie expérimentale

1.4 General information

La partie expérimentale est rédigée en anglais, car extraite des parties expérimentales de chaque article ou de résultats supplémentaires non publiés. Cette partie comprend toutes les molécules que j'ai pu synthétiser et présenter dans ce manuscrit, au sein d'articles et hors articles. La partie *Supporting Information* des articles publiés est disponible en ligne en *open access*. Concernant les articles non publiés, je vous joins un document séparé comprenant toutes les parties *Supporting Information* de ce mémoire de thèse.

Solvents and reagents: Starting materials and reagents were obtained from Sigma-Aldrich, ABCR GmbH & Co., Alfa Aesar, Fluorochem, BLDPharm and Apollo Scientific and used without further purification. Solvents were obtained from Carlo Erba, VWR and Fisher Scientific. All reactions were performed in standard glassware. Thin-layer chromatography (TLC) were performed using Merck silica gel plates (60 F-254, 0.25 mm) on aluminum sheets and revealed under UV lamp (325 and 254 nm). Crude mixtures were purified by flash column chromatography on silica gel 60 (230-400 mesh, 0.040-0.063 mm) purchased from VWR.

Nuclear Magnetic Resonance (NMR): NMR spectra were recorded on a Bruker Avance 400 apparatus (^{1}H NMR, 400 MHz - ^{13}C NMR, 101 MHz - ^{19}F NMR, 377 MHz) or Bruker Avance III HD 500 MHz apparatus (^{1}H NMR, 500 MHz - ^{13}C NMR, 126 MHz - ^{19}F NMR, 471 MHz – ^{11}B NMR, 160 MHz) at the ECPM. All chemical shifts (δ) are quoted in parts per million (ppm). The chemical shifts are referred to the used partial deuterated NMR solvent ($CDCl_3$: ^{1}H NMR, 7.26 ppm and ^{13}C NMR, 77.16 ppm – MeOD: ^{1}H NMR, 4.78 ppm and 3.31 ppm and ^{13}C NMR, 49.15 ppm – DMSO-d_6: ^{1}H NMR, 2.50 ppm and ^{13}C NMR, 39.51 ppm – Acetone-d_6: ^{1}H NMR, 2.05 ppm and ^{13}C NMR, 29.92 ppm and 206.68 ppm). The coupling constants (J) are given in Hertz (Hz). Resonance patterns are reported with the following notations: br (broad), s (singlet), d (doublet), t (triplet), q (quartet), m (multiplet) and their combinations.

Mass spectrometry: High-resolution mass spectrometry (HRMS) analyses were performed with a Bruker MicroTOF mass analyzer under ESI in the positive or negative ionization mode detection or APCI in the positive ionization mode detection (measurement accuracy ≤15 ppm) at the Service de Spectrométrie de Masse Fédération Chimie Le Bel in Strasbourg.

Melting point: Melting point are measured on Stuart SMP10 with temperature accuracy of ± 1.0°C at 20°C and ± 2.5°C at 300°C.

Infrared: FTIR spectra were recorded neat on a Perkin Elmer FTIR Spectrometer Spectrum Two. Spectra were analyzed using Spectrum software from PerkinElmer.

Photophysical properties: Stock solutions of the fluorescent dyes were prepared in EtOH and then diluted either in aqueous buffer solutions (NIST certified buffers at pH 1.68, 4.00, 6.86, 7.41 or 9.86) with 0.1 M NaCl or in EtOH to obtain solutions with an absorbance value of about 1. The absorbance spectra of the dyes in solution were then measured by UV-Vis absorption spectrophotometry from 220 to 800 nm with a Cary 5000 UV-Vis-NIR spectrophotometer (Agilent) prior to fluorescence measurements. The pH values of the buffer solutions were selected to ensure the predominant formation of a the flavylium species. Steady-state fluorescence (emission and excitation) spectra of solutions diluted 10-fold were then recorded with 3.5 mL Suprasil® quartz optical cells of 10 mm pathlength using a FluoroMax 4P (Horiba JobinYvon) spectrofluorimeter. For each compound, the instrumental parameters were adjusted with respect to the spectral response. The quantum yields of the fluorescent species (Φ_F) were measured on a FluoroMax 4P (Horiba JobinYvon) spectrofluorimeter and calculated by using the equation below with either rhodamine 6G (R6G, Φ = 0.88 in EtOH, λ_{em} = 488 nm) or cresyl

violet (Φ = 0.50 in EtOH, λ_{em} = 546 nm) used as references with respect to the emission properties of the investigated flavylium-based dyes.

$$\Phi_F = \Phi_R \frac{\int I_F A_R n_F^2}{\int I_R A_S n_R^2}$$

Φ_R corresponds to the quantum yield of reference. The indices F and R denote sample and reference, respectively. The integrals over I represent areas of the corrected emission spectra, A is the optical density at the excitation wavelength and n_R and n_F correspond to the refractive index of the reference and the sample solutions, respectively.

Parasite culture and antiplasmodial assays: The *P. falciparum* growth inhibition assay was used to determine the 50% inhibitory concentration (IC_{50}) of a given compound. Compounds were dissolved in DMSO at 10 mM. The stocks were kept at 4°C for usually ≥ 2 weeks. For the assay, 4-fold concentrated solutions of all compounds were prepared freshly in screening medium. The *P. falciparum* growth inhibition assay method described here was based on the published protocol[151]. The readout method is based on incorporation of radiolabelled hypoxanthine into the parasite's DNA, which serves as indicator of parasite growth[152]. In brief, naïve parasites of strain NF54 were exposed to a serial dilution of compounds for 72h. After 48h, a [3H]-hypoxanthine (0.25 µCi) solution is added to each well, and the plates are incubated for another 24h. Plates are harvested with a Betaplate cell harvester (Perkin, Elmer, Waltham, US), which transfers the lysed red blood cells onto a glass fiber filter (Microbeta FilterMate). The dried filters are inserted into plastic foil with 10 mL of scintillation fluid and counted in a Betaplate liquid scintillation counter (Perkin Elmer, Waltham, US). The results are recorded as counts per minute per well at each compound concentration. Data are transferred into a graphics program (e.g., Excel) and expressed as percentage of the values for untreated controls (Snyder et al., 2007, Desjardins et al, 1979). Chloroquine Diphosphate (Sigma C6628) and Artesunate (Mepha) were included as reference compound(s) in every experiment.

1.5 Chapitre II:

1.5.1 Article 1

Synthesis of precursors.

Reactants and building blocks were purchased from commercial sources, such as Fluorochem, Sigma-Aldrich and Alfa Aesar. 1,4-dimethoxy-2-methyl-naphthalene was synthesized according to the previously published method[153]. 6-fluoro-menadione was synthesized according to the previously published method[55].

Synthesis of Probe 1.

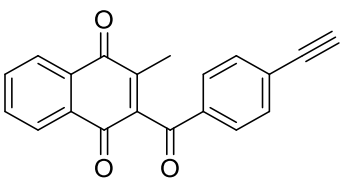

(4-bromophenyl)(1,4-dimethoxy-3-methylnaphthalen-2-yl)methanone (8). Synthesized according to the previously published method (for Cpd **2k**[124]) from 1,4-dimethoxy-2-methylnaphthalene (1 g, 4.9 mmol, 1 equiv.) and 4-bromobenzoic acid (1.5 g, 7.4 mmol, 1.5 equiv.). The reaction crude was not purified and was directly engaged in the next reaction.

(1,4-dimethoxy-3-methylnaphthalen-2-yl)(4-((trimethylsilyl)ethynyl)phenyl)methanone (9). Compound **8** (1.4 g, 3.7 mmol, 1 equiv.) was dissolved under argon in triethylamine (85 mL) in a dry double necked round bottom flask at 25°C. Then, $Pd(PPh_3)_2(Cl)_2$ (130 mg, 0.2 mmol, 0.05 equiv.), CuI (70 mg, 0.3 mmol, 0.1 equiv.) were added under argon and three cycles argon vacuum were performed, finally trimethylsilylacetylene (1.6 mL, 11.1 mmol, 3 equiv.) was added. The round bottom flask was stirred at 70°C for 24h. The reaction mixture was quenched with a 1/1 brine/water mixture and the aqueous phase was extracted three times with ethyl acetate, dried over magnesium sulfate and solvent was removed under vacuum. The crude was purified by silica gel chromatography (CHX/T, 2/8, v/v, UV) to afford the desired product **9** as a yellow oil (1.3 g, 87.3%). The product analysis was in accordance with that of Cpd **7c**[124].

(1,4-dimethoxy-3-methylnaphthalen-2-yl)(4-ethynylphenyl)methanone (10). Synthesized from compound **9** according to the previously published method. The product analysis was in accordance with that of Cpd **7d**[124].

2-(4-ethynylbenzoyl)-3-methylnaphthalene-1,4-dione (Probe 1). The desired product was synthesized from compound **10** according to the previously published method, purified with eluent (CHX/EtOAc, 9/1, v/v, UV, Rf = 0.4), and isolated as a yellow solid, 88%. The product analysis was in accordance with that of Cpd **7**[124]. ^{1}H NMR (400 MHz, $CDCl_3$) δ 8.23 – 8.13 (m, 1H), 8.09 – 8.04 (m, 1H), 7.90 – 7.83 (m, 2H), 7.83 – 7.75 (m, 2H), 7.65 – 7.54 (m, 2H), 3.29 (s, 1H), 2.06 (s, 3H).

Synthesis of Probe 4.

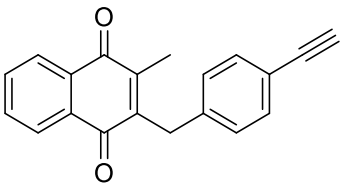

2-(4-iodobenzyl)-3-methylnaphthalene-1,4-dione (15) (Cpd **11a**[124]). Synthesized from menadione according to the previously published method, but without any purification, the crude mixture was directly engaged in the next step.

2-(4-iodobenzyl)-1,4-dimethoxy-3-methylnaphthalene (16). Synthesized from **15** according to the previously published method (Cpd **11b**[124]), but without any purification, the crude mixture was directly engaged in the next step.

((4-((1,4-dimethoxy-3-methylnaphthalen-2-yl)methyl)phenyl)ethynyl)trimethyl-silane (17) (Cpd **11c**[124]). Synthesized from **16** according to the previously published method but without any purification, the crude mixture was directly engaged in the next step.

2-(4-ethynylbenzyl)-1,4-dimethoxy-3-methylnaphthalene (18) (Cpd **11d**[124]). Synthesized from **17** according to the previously published method, but without any purification, the crude mixture was directly engaged in the next step.

2-(4-ethynylbenzyl)-3-methylnaphthalene-1,4-dione (Probe 4) (Cpd **11**[124]). The desired product was synthesized from compound **18** according to the previously published method, purified with eluant

(CHX/EtOAc, 8/2, v/v, UV, Rf = 0.3), and isolated as a yellow solid, 46% overall yield (over 5 steps). ^{1}H NMR (400 MHz, $CDCl_3$) δ 8.18 – 8.03 (m, 2H), 7.71 (dd, J = 5.8, 3.3 Hz, 2H), 7.44 – 7.30 (m, 2H), 7.22 – 7.14 (m, 2H), 4.03 (s, 2H), 3.03 (s, 1H), 2.23 (s, 3H).

Synthesis of Probe 3.

6-fluoro-1,4-dimethoxy-2-methylnaphthalene (11).

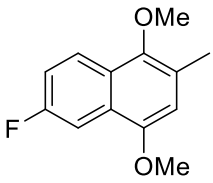

6-fluoro-menadione (1.5 g, 7.9 mmol, 1 equiv.), was solubilized in MeOH (30 mL) then a solution of tin chloride (3.7 g, 19.7 mmol, 2.5 equiv.) in 37% aqueous HCl (2.7 mL, 32.5 mmol, 4.1 equiv.) was added dropwise and the mixture was stirred 30 min at 25°C until the solution came back yellowish. Most of the solvent were evaporated under vacuum, the yellow precipitate was rinsed with water. The powder was dissolved in acetone (30 mL) and dried over magnesium sulfate. Under argon, dimethyl sulfate (3.7 mL, 39.4 mmol, 5 equiv.) was added to the previous mixture then a solution of KOH (2.2 g, 39.4 mmol, 5 equiv.) in MeOH (7.5 mL) was added drop by drop. When the addition was completed the mixture was stirred at reflux 60°C during 1h. A 20% aqueous solution of KOH (20 mL) was added to the mixture and organic solvent were removed under vacuum. The aqueous phase was extracted three times with dichloromethane, dried over magnesium sulfate and solvent was removed under vacuum (CHX/T, 5/5, v/v, UV, Rf = 0.6). The crude residue gives the desired product **11** (1.5 g, 86.3%) as a beige solid. M.p. = 52-53°C. ^{1}H NMR (400 MHz, $CDCl_3$) δ 8.07 (dd, J = 9.2, 5.6 Hz, 1H), 7.88 (dd, J = 10.6, 2.7 Hz, 1H), 7.32 (ddd, J = 9.2, 8.3, 2.7 Hz, 1H), 6.64 (s, 1H), 3.95 (s, 3H), 3.89 (s, 3H), 2.48 (s, 3H). ^{19}F NMR ($CDCl_3$, 377 MHz) δ -116.24 (ddd, J = 10.3, 8.4, 5.5 Hz). ^{13}C {^{1}H} NMR ($CDCl_3$, 101 MHz) δ 160.3 (d, J = 243.9 Hz), 150.9 (d, J = 5.1 Hz), 147.1 (d, J = 1.4 Hz), 126.1 (d, J = 8.8 Hz), 125.7 (d, J = 0.8 Hz), 124.8 (d, J = 2.5 Hz), 124.2 (d, J = 8.7 Hz), 116.3 (d, J = 25.2 Hz), 107.9, 106.3 (d, J = 22.5 Hz), 61.2, 55.5, 16.0. HRMS (ESI+) calcd. for $C_{13}H_{14}FO_2$: 221.0972. Found: 221.0971 ($M+H^+$).

(4-bromophenyl)(7-fluoro-1,4-dimethoxy-3-methylnaphthalen-2-yl)methanone (12).

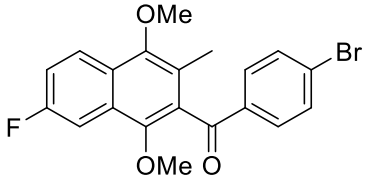

Compound **11** (1.5 g, 6.8 mmol, 1 equiv.) and 4-bromobenzoic acid (2 g, 10.2 mmol, 1.5 equiv.) were dissolved in dichloromethane (68 mL). At 0°C, TFAA (1.9 mL, 13.6 mmol, 2 equiv.) was added. After stirring for 10 min, TfOH (0.3 mL, 3.4 mmol, 0.5 equiv.) was cautiously added and the reaction mixture was allowed to warm up slowly to 25°C and stirred for 16h. Then, the reaction was quenched with an aqueous saturated $NaHCO_3$ solution. The aqueous phase was extracted three times with dichloromethane, dried with anhydrous magnesium sulfate and solvent was removed under vacuum. The crude was purified by silica gel chromatography (CHX/T, 2/8, v/v, UV, Rf = 0.5) to afford the desired product **12** (1.7 g, 62.6%) as an orange oil (still some CHX). ^{1}H NMR (400 MHz, $CDCl_3$) δ 8.19 – 8.08 (m, 1H), 7.74 – 7.69 (m, 2H), 7.65 (ddd, J = 10.0, 2.6, 0.6 Hz, 1H), 7.62 – 7.55 (m, 2H), 7.35 (ddd, J = 9.2, 8.2, 2.6 Hz, 1H), 3.90 (s, 3H), 3.78 (s, 3H), 2.20 (s, 3H). ^{19}F {^{1}H} NMR (377 MHz, $CDCl_3$) δ -113.55. ^{13}C {^{1}H} NMR (101 MHz, $CDCl_3$) δ 196.2, 161.3 (d, J = 247.1 Hz), 150.8 (d, J = 1.5 Hz), 148.7 (d, J = 5.4 Hz), 135.9, 132.3, 131.8, 131.1, 129.4, 128.3 (d, J = 8.7 Hz), 126.6, 125.5 (d, J = 8.8 Hz), 122.9 (d, J = 2.5 Hz), 117.6 (d, J = 25.4 Hz), 106.6 (d, J = 22.5 Hz), 63.6, 61.8, 12.8. HRMS (ESI+) calcd. for $C_{20}H_{17}BrFO_3$: 403.0340. Found: 403.0326 ($M+H^+$).

(7-fluoro-1,4-dimethoxy-3-methylnaphthalen-2-yl)(4-((trimethylsilyl)ethynyl)phenyl)methanone (13).

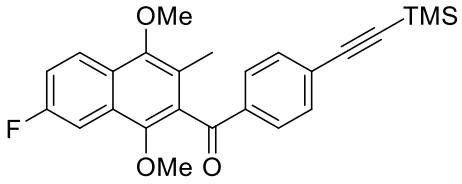

Compound **12** (682.1 mg, 1.7 mmol, 1 equiv.) was dissolved under argon in triethylamine (42.3 mL) in a dry double necked round bottom flask at 25°C. Then, $Pd(PPh_3)_2(Cl)_2$ (71.2 mg, 0.1 mmol, 0.06 equiv.), CuI (32.2 mg, 0.2 mmol, 0.1 equiv.) were added under argon and three cycles argon vacuum were performed, finally trimethylsilylacetylene (0.7 mL, 5.1 mmol, 3 equiv.) was added. The round bottom flask was stirred at 70°C for 20h. The reaction mixture was quenched with a 1/1 brine/water mixture and the aqueous phase was extracted three times with ethyl acetate, dried with anhydrous magnesium sulfate and solvent was removed under vacuum. The crude was purified by silica gel chromatography (CHX/EtOAc, 9/1, v/v, UV, Rf = 0.7) to afford the desired product **13** as a yellow oil quantitatively. ^{1}H NMR (400 MHz, $CDCl_3$) δ 8.13 (dd, J = 9.2, 5.5 Hz, 1H), 7.80 – 7.74 (m, 2H), 7.65 (dd, J = 10.0, 2.6 Hz, 1H), 7.53 – 7.50 (m, 2H), 7.34 (ddd, J = 9.3, 8.3, 2.6 Hz, 1H), 3.89 (s, 3H), 3.77 (s, 3H), 2.18 (s, 3H), 0.25 (s, 9H). ^{19}F {^{1}H} NMR (377 MHz, $CDCl_3$) δ -113.73. ^{13}C {^{1}H} NMR (101 MHz, $CDCl_3$) δ 196.5, 161.3 (d, J = 246.9 Hz), 150.8, 148.7 (d, J = 5.3 Hz), 136.5, 132.4, 132.1, 129.5, 128.9, 128.4 (d, J = 8.8 Hz), 126.6, 125.5 (d, J = 8.9 Hz), 122.9 (d, J = 2.5 Hz), 117.6 (d, J = 25.4 Hz), 106.6 (d, J = 22.5 Hz), 104.17, 98.9, 88.1, 86.1, 63.5, 61.8, 12.8, -0.06. HRMS (ESI+) calcd. for $C_{25}H_{26}FO_3Si$: 421.1630. Found: 421.1623 ($M+H^+$).

(4-ethynylphenyl)(7-fluoro-1,4-dimethoxy-3-methylnaphthalen-2-yl)methanone (14).

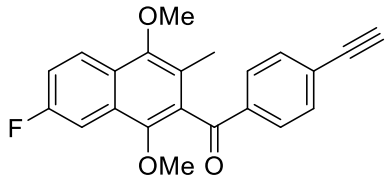

To a solution of compound **13** (930 mg, 2.2 mmol, 1 equiv.) in THF (43 mL) was added at 25°C another solution of TBAF (1 M in THF) (6.6 mL, 6.6 mmol, 3 equiv.). The crude mixture was stirred for 3h and then the reaction was hydrolyzed with saturated aqueous ammonium chloride. The aqueous phase was extracted three times with ethyl acetate, dried with anhydrous magnesium sulfate and solvent was removed under vacuum. The crude was purified by silica gel chromatography (CHX/EtOAc, 10/0 to 9/1, v/v, UV, Rf = 0.7) to afford the desired product **14** as a yellow solid (522.4 mg, 67.8%). M.p. 121-123°C. ^{1}H NMR (400 MHz, $CDCl_3$) δ 8.14 (dd, J = 9.2, 5.4 Hz, 1H), 7.82 – 7.76 (m, 2H), 7.65 (ddd, J = 10.0, 2.6, 0.5 Hz, 1H), 7.59 – 7.52 (m, 2H), 7.35 (ddd, J = 9.2, 8.3, 2.6 Hz, 1H), 3.90 (s, 3H), 3.78 (s, 3H), 3.26 (s, 1H), 2.19 (s, 3H). ^{19}F {^{1}H} NMR (377 MHz, $CDCl_3$) δ -113.65. ^{13}C {^{1}H} NMR (101 MHz, $CDCl_3$) δ 196.5, 161.3 (d, J = 246.9 Hz), 150.8 (d, J = 1.7 Hz), 148.7 (d, J = 5.2 Hz), 136.9, 132.6, 132.0, 129.5, 128.4 (d, J = 8.8 Hz), 127.8, 126.6, 125.5 (d, J = 8.9 Hz), 122.9 (d, J = 2.6 Hz), 117.6 (d, J = 25.4 Hz), 106.6 (d, J = 22.5 Hz), 82.9, 80.9, 63.6, 61.8, 27.2, 12.8. HRMS (ESI+) calcd. for $C_{22}H_{18}FO_3$: 349.1234. Found: 349.1225 ($M+H^+$).

3-(4-ethynylbenzoyl)-6-fluoro-2-methylnaphthalene-1,4-dione (Probe 3).

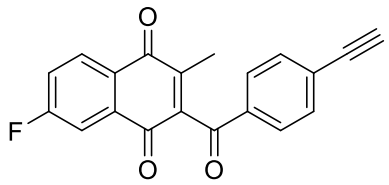

Compound **14** (135 mg, 0.4 mmol, 1 equiv.) was dissolved in acetonitrile (4.6 mL), then under stirring CAN (467.4 mg, 0.8 mmol, 2.2 equiv.) dissolved in water (1.6 mL) was added. The reaction mixture was stirred for 1h at 25°C. Once the reaction was complete, acetonitrile was removed under vacuum and the aqueous phase was extracted three times with dichloromethane, dried with anhydrous magnesium sulfate and solvent was removed under vacuum (CHX/EtOAc, 9/1, v/v, UV, Rf = 0.3). The desired product **3** was obtained as a yellow solid (116 mg, 94%). M.p. 142-144°C. ^{1}H NMR (400 MHz, $CDCl_3$) δ 8.22 (dd, J = 8.6, 5.2 Hz, 1H), 7.88 – 7.81 (m, 2H), 7.71 (dd, J = 8.3, 2.6 Hz, 1H), 7.63 – 7.57 (m, 2H), 7.51 – 7.41 (m, 1H), 3.30 (s, 1H), 2.07 (s, 3H). ^{19}F {^{1}H} NMR (377 MHz, $CDCl_3$) δ -100.79. ^{13}C NMR (101 MHz, $CDCl_3$) δ 192.6, 183.5, 182.3, 166.4 (d, J = 258.6 Hz), 144.8, 144.2, 135.3, 134.3 (d, J = 8.0 Hz), 132.9, 130.3 (d, J =

9.0 Hz), 129.1, 128.7, 128.7, 121.6 (d, *J* = 22.6 Hz), 113.3 (d, *J* = 23.5 Hz), 82.6, 81.6, 13.8. HRMS (ESI+) calcd. for $C_{20}H_{12}FO_3$: 319.0765. Found: 319.0758 ($M+H^+$).

Synthesis of Probe 5.

6-fluoro-3-(4-iodobenzyl)-2-methylnaphthalene-1,4-dione (19).

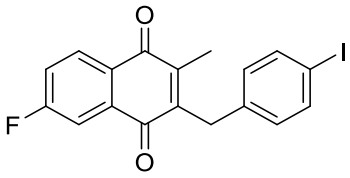

6-fluoro-menadione (250 mg, 1.3 mmol, 1 equiv.) and 2-(4-iodophenyl)acetic acid (689 mg, 2.6 mmol, 2 equiv.) were dissolved in a mixture of acetonitrile (20 mL) water (7 mL). Then $AgNO_3$ (78.2 mg, 0.5 mmol, 0.35 equiv.) and ammonium persulfate (390 mg, 1.7 mmol, 1.3 equiv.) was added in the reaction mixture. The reaction was stirred for 4h at 85°C in the dark. The solvent was removed in vacuum and then extracted three times with ethyl acetate. Reunited organic layers were washed with water, dried with anhydrous magnesium sulfate, filtered and the solvent was removed under reduced pressure. The crude was purified by silica gel chromatography (CHX/DCM, 5/5, v/v, UV, Rf = 0.7) to afford the desired product **19** quantitatively as a yellow solid. M.p. 91-93°C. ^{1}H NMR (400 MHz, $CDCl_3$) δ 8.13 (dd, *J* = 8.6, 5.3 Hz, 1H), 7.72 (dd, *J* = 8.6, 2.7 Hz, 1H), 7.61 – 7.57 (m, 2H), 7.36 (ddd, *J* = 8.6, 8.0, 2.7 Hz, 1H), 7.01 – 6.93 (m, 2H), 3.96 (s, 2H), 2.24 (s, 3H). ^{19}F {^{1}H} NMR (377 MHz, $CDCl_3$) δ -102.31. ^{13}C {^{1}H} NMR (126 MHz, $CDCl_3$) δ 183.9, 183.5, 166.1 (d, *J* = 257.0 Hz), 144.9, 138.5, 137.8, 137.6, 134.6, 132.7, 130.9, 129.7 (d, *J* = 8.7 Hz), 128.8 (d, *J* = 3.2 Hz), 120.9 (d, *J* = 22.5 Hz), 113.3 (d, *J* = 23.4 Hz), 32.2, 13.5. HRMS (ESI+) calcd. for $C_{18}H_{13}FIO_2$: 406.9939. Found: 406.9922 ($M+H^+$).

6-fluoro-3-(4-iodobenzyl)-1,4-dimethoxy-2-methylnaphthalene (20).

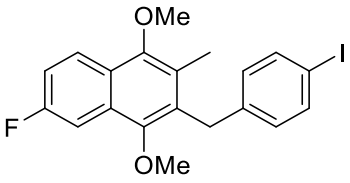

Compound **19** (550 mg, 1.3 mmol, 1 equiv.), was solubilized in MeOH (5.1 mL) then a solution of tin chloride (642 mg, 3.4 mmol, 2.5 equiv.) in 37% aqueous HCl (0.5 mL, 5.6 mmol, 4.12 equiv.) was added dropwise and the mixture was stirred 30 min at 25°C until the solution came back yellowish. Most of the solvent was evaporated under vacuum, the yellow precipitate was rinsed with water. The powder was dissolved in acetone (5.1 mL) and dried with anhydrous magnesium sulfate. Under argon, dimethyl sulfate (0.6 mL, 6.8 mmol, 5 equiv.) was added to the previous mixture then a solution of KOH (379.8 mg, 6.8 mmol, 5 equiv.) in MeOH (1.3 mL) was added drop by drop. When the addition was completed the mixture was stirred at reflux 60°C during 1h. A 20% aqueous solution of KOH (10 mL) was added to the mixture and organic solvent were removed under vacuum. The aqueous phase was extracted three times with dichloromethane, dried with anhydrous magnesium sulfate and solvent was removed under vacuum (CHX/T, 2/8, v/v, UV, Rf = 0.4). The crude residue gave the desired product **20** (426 mg, 72.1%) as an orange oil. ^{1}H NMR (400 MHz, $CDCl_3$) δ 7.99 (dd, *J* = 9.3, 5.6 Hz, 1H), 7.58 (ddd, *J* = 10.4, 2.6, 0.5 Hz, 1H), 7.47 – 7.40 (m, 2H), 7.17 (ddd, *J* = 9.1, 8.3, 2.7 Hz, 1H), 6.80 – 6.69 (m, 2H), 4.10 (s, 2H), 3.75 (s, 3H), 3.71 (s, 3H), 2.12 (s, 3H). ^{19}F {^{1}H} NMR (377 MHz, $CDCl_3$) δ -114.71. ^{13}C {^{1}H} NMR δ 161.0 (d, *J* = 245.3 Hz), 150.7, 150.2 (d, *J* = 5.3 Hz), 140.0, 137.8, 137.6, 130.3, 130.1, 128.3 (d, *J* = 8.5 Hz), 126.1 (d, *J* = 2.5 Hz), 125.2 (d, *J* = 8.5 Hz), 116.2 (d, *J* = 25.3 Hz), 106.3 (d, *J* = 22.3 Hz), 91.1, 62.3, 61.7, 32.5, 12.7. HRMS (ESI+) calcd. for $C_{20}H_{19}FIO_2$: 437.0408. Found: 437.0409 ($M+H^+$).

((4-((7-fluoro-1,4-dimethoxy-3-methylnaphthalen-2-yl)methyl)phenyl)ethynyl)trimethylsilane (21).

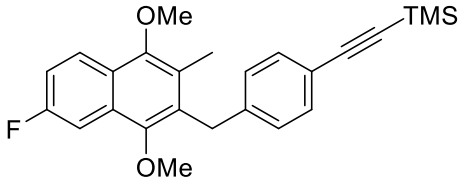

Compound **20** (426 mg, 1 mmol, 1 equiv.) was dissolved under argon in triethylamine (24.4 mL) in a dry double necked round bottom flask at 25°C. Then, $Pd(PPh_3)_2(Cl)_2$ (41 mg, 0.06 mmol, 0.06 equiv.), CuI (18.6 mg, 0.1 mmol, 0.1 equiv.) were added under argon and three cycles argon vacuum were performed, finally trimethylsilylacetylene (0.4 mL, 2.9 mmol, 3 equiv.) was added. The round bottom flask was stirred at 70°C for 24h. The reaction mixture was quenched with a 1/1 brine/water mixture and the aqueous phase was extracted three times with ethyl acetate, dried with anhydrous magnesium sulfate and solvent was removed under vacuum (CHX/T, 2/8, v/v, UV, Rf = 0.6). The crude residue gives the desired product **21** quantitatively as a brown oil. ^{1}H NMR (500 MHz, $CDCl_3$) δ 8.08 (dd, *J* = 9.2, 5.6 Hz, 1H), 7.69 – 7.64 (m, 1H), 7.36 – 7.32 (m, 2H), 7.29 – 7.23 (m, 2H), 7.03 (dt, *J* = 8.7, 0.8 Hz, 2H), 4.24 (s, 2H), 3.83 (s, 3H), 3.78 (s, 3H), 2.19 (s, 3H), 0.22 (s, 9H). ^{19}F {^{1}H} NMR (377 MHz, $CDCl_3$) δ -114.88. ^{13}C {^{1}H} NMR (126 MHz, $CDCl_3$) δ 161.1 (d, *J* = 245.2 Hz), 150.7, 150.2 (d, *J* = 5.3 Hz), 141.1, 131.7 (d, *J* = 8.0 Hz), 130.3, 129.6 (d, *J* = 7.4 Hz), 128.5, 128.3 (d, *J* = 8.6 Hz), 128.1, 127.3, 126.3 (d, *J* = 2.3 Hz), 125.2, 125.2, 120.8, 116.2 (d, *J* = 25.4 Hz), 106.4 (d, *J* = 22.3 Hz), 105.2, 93.8, 62.3, 61.7, 32.9, 12.7, 0.1. HRMS (ESI+) calcd. for $C_{25}H_{28}FO_2Si$: 407.1837. Found: 407.1808 ($M+H^+$).

3-(4-ethynylbenzyl)-6-fluoro-1,4-dimethoxy-2-methylnaphthalene (22).

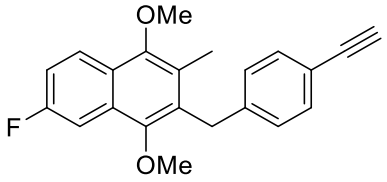

To a solution of compound **21** (470 mg, 1.2 mmol, 1 equiv.) in THF (22.5 mL) was added at 25°C another solution of TBAF trihydrate (1.1 g, 3.5 mmol, 3 equiv.) in THF (11.2 mL). The crude mixture was stirred for 3h at 25°C and then the reaction was hydrolyzed with saturated aqueous ammonium chloride. The aqueous phase was extracted three times with ethyl acetate, dried with anhydrous magnesium sulfate and solvent was removed under vacuum (CHX/T, 2/8, v/v, UV, Rf = 0.5). The crude residue gives the desired product **22** quantitatively as a brown oil. ^{1}H NMR (500 MHz, $CDCl_3$) δ 8.08 (dd, *J* = 9.2, 5.6 Hz, 1H), 7.67 (dd, *J* = 10.4, 2.6 Hz, 1H), 7.37 (d, *J* = 8.3 Hz, 2H), 7.29 – 7.23 (m, 1H), 7.06 (d, *J* = 7.7 Hz, 2H), 4.25 (s, 2H), 3.84 (s, 3H), 3.80 (s, 3H), 3.02 (s, 1H), 2.21 (s, 3H). ^{19}F {^{1}H} NMR (377 MHz, $CDCl_3$) δ -114.85. ^{13}C {^{1}H} NMR (126 MHz, $CDCl_3$) δ 161.1 (d, *J* = 245.3 Hz), 150.7, 150.2 (d, *J* = 5.3 Hz), 141.4, 132.4, 128.3 (d, *J* = 8.6 Hz), 128.2, 126.2 (d, *J* = 2.6 Hz), 125.3, 125.2, 119.8, 116.2 (d, *J* = 25.4 Hz), 106.4 (d, *J* = 22.3 Hz), 83.8, 62.3, 61.7, 32.9, 12.7. HRMS (ESI+) calcd. for $C_{22}H_{19}O_2F_{23}Na$: 357.1261. Found: 357.1258 ($M+Na^+$).

3-(4-ethynylbenzyl)-6-fluoro-2-methylnaphthalene-1,4-dione (Probe 5).

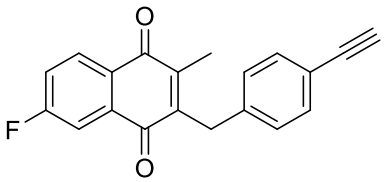

Compound **22** (404 mg, 1.2 mmol, 1 equiv.) was dissolved in acetonitrile (14.5 mL), then under stirring CAN (1.5 g, 2.7 mmol, 2.2 equiv.) dissolved in water (4.8 mL) was added. The reaction mixture was stirred for 1h at 25°C. Once the reaction was complete, acetonitrile was removed under vacuum and the aqueous phase was extracted three times with dichloromethane, dried with anhydrous magnesium sulfate and solvent was removed under vacuum (CHX/EtOAc, 9/1, v/v, UV, Rf = 0.3). The crude residue gives the desired product **5** quantitatively (287.6 mg, 78%) as an orange solid. M.p. 102-104°C. ^{1}H NMR (500 MHz, $CDCl_3$) δ 8.13 (dd, *J* = 8.6, 5.2 Hz, 1H), 7.73 (dd, *J* = 8.6, 2.6 Hz, 1H), 7.41 – 7.33 (m, 3H), 7.19 – 7.13 (m, 2H), 4.02 (s, 2H), 3.03 (s, 1H), 2.24 (s, 3H). ^{19}F {^{1}H} NMR (377 MHz, $CDCl_3$) δ -102.37. ^{13}C {^{1}H} NMR (126 MHz, $CDCl_3$) δ 184.1, 183.6, 166.1 (d, *J* = 257.0 Hz), 145.1 (d, *J* = 3.1 Hz), 138.9, 134.67 (d, *J* = 7.8

Hz), 132.6, 129.8 (d, *J* = 8.7 Hz), 128.8 (d, *J* = 3.3 Hz), 128.7, 120.9 (d, *J* = 22.4 Hz), 120.5, 113.2 (d, *J* = 23.5 Hz), 83.5, 77.3, 32.6, 13.5. HRMS (ESI+) calcd. for $C_{20}H_{13}O_2F_{23}Na$: 327.0792. Found: 327.0792 ($M+Na^+$).

Synthesis of 6-fluoro-PDO.

6-fluoro-2-methyl-3-(4-(trifluoromethyl)benzyl)naphthalene-1,4-dione (6-fluoro-PD) (Cpd **17e**[44])**.**

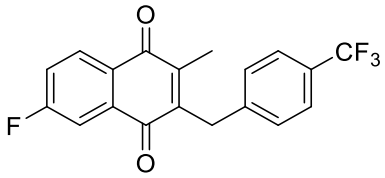

6-fluoro-menadione (500 mg, 2.6 mmol, 1 equiv.) and 4-(trifluoromethyl)phenylacetic acid (1 g, 5.3 mmol, 2 equiv.) were dissolved in acetonitrile (40 mL) and water (13.5 mL). The mixture was heated to 85°C and silver nitrate (156.3 mg, 0.9 mmol, 0.35 equiv.) with ammonium persulfate (780 mg, 3.4 mmol, 1.3 equiv.) were added. The reaction was stirred for 4h at 85°C in the dark. The solvent was removed in vacuum and then extracted three times with ethyl acetate. Reunited organic layers were washed with water, dried over magnesium sulfate, filtered and the solvent was removed under reduced pressure (CHX/EtOAc, 8/2, v/v, UV, Rf = 0.4). The crude, mainly containing **6-fluoro-PD** as an orange oil, was directly engaged in the next reaction without purification.

6-fluoro-2-methyl-3-(4-(trifluoromethyl)benzoyl)naphthalene-1,4-dione (6-fluoro-PDO).

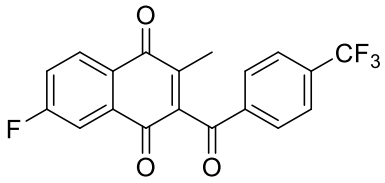

In a tube was dissolved in a mixture of propan-2-ol (1.3 mL) and DCM (1.7 mL), **6-fluoro-PD** (100 mg, 0.3 mmol, 1 equiv.), then the mixture was stirred 72h under dioxygen at 16°C under UV irradiation. Solvents were removed under reduced pressure and the crude was purified by silica gel chromatography (CHX/DCM, 5/5, v/v, UV, Rf = 0.3) to afford **6-fluoro-PDO** as a yellow solid (38.5 mg, 37%). M.p. 155-157°C. ^{1}H NMR (400 MHz, $CDCl_3$) δ 8.23 (dd, *J* = 8.6, 5.2 Hz, 1H), 8.01 (d, *J* = 7.8 Hz, 2H), 7.77 (d, *J* = 8.2 Hz, 2H), 7.70 (dd, *J* = 8.3, 2.6 Hz, 1H), 7.47 (td, *J* = 8.3, 2.7 Hz, 1H), 2.08 (s, 3H). ^{19}F {^{1}H} NMR (377 MHz, $CDCl_3$) δ -63.31, -100.54. ^{13}C {^{1}H} NMR (101 MHz, $CDCl_3$) δ 192.6, 183.3, 182.3 (d, *J* = 1.7 Hz), 166.5 (d, *J* = 258.8 Hz), 145.2, 143.8 (d, *J* = 1.9 Hz), 138.3, 135.8 (q, *J* = 32.8 Hz), 134.2 (d, *J* = 8.0 Hz), 130.4 (d, *J* = 9.0 Hz), 129.6, 126.4 (q, *J* = 3.8 Hz), 123.4 (q, *J* = 271.7 Hz), 121.8 (d, *J* = 22.5 Hz), 113.4 (d, *J* = 23.6 Hz), 27.0, 13.8. HRMS (ESI+) calcd. for $C_{19}H_{11}F_4O_3$: 363.0639. Found: 363.0635 ($M+H^+$).

1.5.2 Introduction et synthèse de β-pyridine- et β-pyrimidine-bMDs

Synthesis of aromatic and aliphatic boronic menadione.

2-(chloromethyl)-1,4-dimethoxy-3-methylnaphthalene (1).

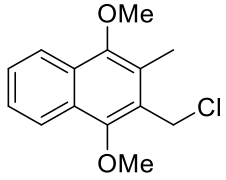

1,4-dimethoxy-2-methylnaphthalene (4 g, 19.8 mmol, 1 equiv.), paraformaldehyde (3.13 g, 98.9 mmol, 5 equiv.) and 37% aqueous hydrochloric acid (50 mL) were heated at 80°C during 2h. The mixture was cooled down, diluted with water and extracted three times with ethyl acetate. The reunited organic layers were washed with brine, dried over magnesium sulfate, filtered and the solvent was removed under reduced pressure. The crude oil was purified by silica gel chromatography (CHX/T, 8/2, v/v, UV)

to afford **1** (4.08 g, 81%) as a colorless oil which crystallized on standing, in accordance to the literature[132]. ^{1}H NMR (400 MHz, $CDCl_3$) δ 8.08 (dd, J = 7.6, 1.8 Hz, 2H), 7.58 – 7.41 (m, 2H), 4.92 (s, 2H), 4.04 (s, 3H), 3.89 (s, 3H), 2.53 (s, 3H).

2-bromo-1,4-dimethoxy-3-methylnaphthalene (4).

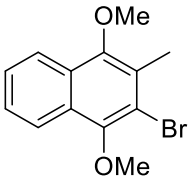

To a solution of 1,4-dimethoxy-2-methylnaphthalene (800 mg, 3 mmol, 1 equiv.) in chloroform (9.3 mL) was added NBS (792 mg, 4.4 mmol, 1.5 equiv.). The reaction mixture was stirred at reflux for 3h. After addition of H_2O, the organic layer was separated and the aqueous layer was extracted with dichloromethane. The combined organic layers were washed with saturated aqueous $NaHCO_3$ and brine, dried over $MgSO_4$ and concentrated under reduced pressure. The crude was purified by flash chromatography on silica gel (T, UV) to afford quantitatively a red solid **4**, in accordance to the literature[154]. ^{1}H NMR (400 MHz, $CDCl_3$) δ 8.17 – 8.09 (m, 3H), 7.58 – 7.50 (m, 3H), 4.03 (s, 3H), 3.91 (s, 3H), 2.61 (s, 3H).

(1,4-dimethoxy-3-methylnaphthalen-2-yl)boronic acid (4a).

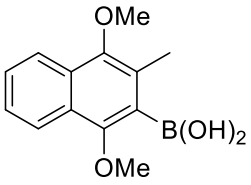

Compound **4** (1 g, 3.5 mmol, 1 equiv.) was solubilized in anhydrous THF (20.3 mL) under argon at -78°C then *n*-BuLi (2.7 mL, 4.3 mmol, 1.2 equiv.)(1.6 M in hexanes) was added dropwise, let it stir 10 min at -78°C under argon. Then triisopropyl borate (2 mL, 8.9 mmol, 2.5 equiv.) was added dropwise at -78°C under argon. After 10 min, the mixture was allowed to warm to 25°C and was stirred overnight. The mixture was quenched with 1 M HCl and then extracted with diethyl ether. The organic layer was dried over $MgSO_4$, filtered and concentrated under vacuum. The crude was purified on a small flash chromatography on silica gel (CHX/EtOAc, 75/25, v/v, UV) to afford a yellowish white solid **4a** (229.5 mg, 26.2%), in accordance to the literature[149]. ^{1}H NMR (500 MHz, $CDCl_3$) δ 8.05 – 7.95 (m, 2H), 7.53 – 7.41 (m, 2H), 6.43 – 6.36 (m, 2H), 3.94 (s, 3H), 3.82 (s, 3H), 2.50 (s, 3H). ^{11}B {^{1}H} NMR (160 MHz, $CDCl_3$) δ 30.55. ^{13}C {^{1}H} NMR (126 MHz, $CDCl_3$) δ 157.5, 150.2, 130.1, 129.8, 127.2, 126.7, 125.5, 125.4, 122.5, 122.3, 63.6, 61.2, 15.5.

Potassium (1,4-dimethoxy-3-methylnaphthalen-2-yl)trifluoroborate (4b).

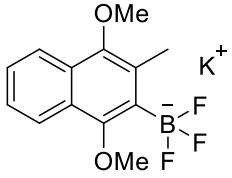

A solution of *n*-BuLi (2.4 mL, 3.9 mmol, 1.1 equiv.)(1.6 M in hexanes) was added dropwise to a stirred solution of compound **4** (1 g, 3.5 mmol, 1 equiv.) in anhydrous THF (14 mL) under argon at -78°C. The mixture was stirred at -78°C for 30 min and then triisopropyl borate (1.6 mL, 7.1 mmol, 2 equiv.) was added dropwise at -78°C. Let the mixture it stirs back to 25°C for 16h. Quench with HCl 1 M extract with ethyl acetate, dry over $MgSO_4$, filter and evaporated. The brown solid was dissolved in MeOH (8.6 mL) cooled down to 0°C and a solution of potassium hydrofluoride fluoride (1.1 g, 14.2 mmol, 4 equiv.) in water (1.7 mL) was added dropwise. The mixture was stirred at 25°C for 16h and then evaporated. Hot acetone was added, filter, rinse with hot acetone and evaporate. This procedure was repeat two times. Finally, the crude was recrystallized in cold diethyl ether and after filtration and drying it lead to the pure product **4b** (411.4 mg, 37.5%) as a white solid (still contain acetone). M.p. = 122-124°C. ^{1}H NMR (400 MHz, MeOD) δ 8.06 – 7.99 (m, 1H), 7.95 (dd, J = 7.6, 1.6 Hz, 1H), 7.36 (dqd, J = 8.2, 6.8, 1.5 Hz, 2H), 3.87 (s, 3H), 3.80 (s, 3H), 2.53 (q, J = 1.5 Hz, 3H). ^{19}F {^{1}H} NMR (377 MHz, MeOD) δ -134.79 (d, J = 84.6 Hz). ^{13}C {^{1}H} NMR (101 MHz, MeOD) δ 156.2, 150.3, 133.2, 129.3, 129.0, 125.9, 125.1, 123.5, 122.5, 63.1 (q, J = 2.4 Hz), 61.0, 15.3 (q, J = 2.9 Hz). HRMS (ESI+) calcd. for $C_{13}H_{13}BF_3O_2$: 269.0966. Found: 269.0982 (M^+).

2-(1,4-dimethoxy-3-methylnaphthalen-2-yl)-4,4,5,5-tetramethyl-1,3,2-dioxaborolane (4c).

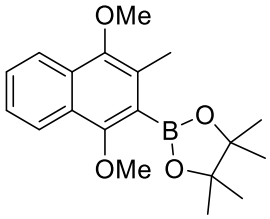

Under argon with a flame dried seal tube with a magnetic stir bar was charged with dichlorobis(triphenylphosphine)palladium (12.5 mg, 0.02 mmol, 0.02 equiv.), KOAc (104.7 mg, 1.07 mmol, 1.2 equiv.), bis(pinacolato)diboron (237.1 mg, 0.9 mmol, 1.05 equiv.) and compound **4** (250 mg, 0.9 mmol, 1 equiv.). The reaction vial was transferred to a preheated oil bath at 120°C. The reaction was stirred at 120°C for 24h leading to a black mixture at the end. The reaction mixture was extracted with EtOAc, filter and the solvent were removed under reduced pressure. The crude was purified on a small flash chromatography on silica gel (T, UV) to afford **4c** (10 mg, 3.4%) as a brown oil. ^{1}H NMR (500 MHz, $CDCl_3$) δ 8.05 (ddt, *J* = 9.1, 8.5, 1.0 Hz, 2H), 7.52 – 7.48 (m, 1H), 7.44 (ddd, *J* = 8.2, 6.8, 1.4 Hz, 1H), 3.98 (s, 3H), 3.85 (s, 3H), 2.47 (s, 3H), 1.45 (s, 12H). ^{11}B {^{1}H} NMR (160 MHz, $CDCl_3$) δ 32.07. ^{13}C NMR {^{1}H} (126 MHz, $CDCl_3$) δ 156.5, 149.8, 129.9, 128.5, 127.1, 126.6, 125.1, 122.6, 122.3, 84.2, 63.6, 61.3, 25.0, 15.5. HRMS (ESI+) calcd. for $C_{19}H_{25}KBO_4$: 367.1477. Found: 367.1496 ($M+K^+$).

Potassium ((1,4-dimethoxy-3-methylnaphthalen-2-yl)methyl)trifluoroborate (1a).

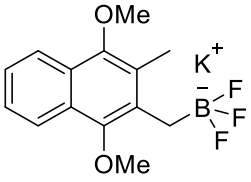

Under argon with a flame dried balloon with a magnetic stir bar was charged with tetrakis(triphenylphosphine)palladium (230 mg, 0.2 mmol, 0.05 equiv.), K_2CO_3 (1.6 g, 12 mmol, 3 equiv.), bis(pinacolato)diboron (1.2 g, 4.8 mmol, 1.2 equiv.) and compound **1** (1 g, 4 mmol, 1 equiv.) with anhydrous dioxane (26.6 mL). The reaction was stirred at 100°C for 16h under argon, leading to a black mixture at the end. The reaction mixture was filter on a silica pad and rinse with DCM. After evaporation the crude was solubilized in MeOH (4 mL) then potassium hydrofluoride fluoride (1.8 g, 23.9 mmol, 6 equiv.) in 6.55 ml of water was added dropwise at 0°C, let it stir 2h at 0°C then evaporate. Add hot acetone filter and evaporate repeat it 2 times. Finally, recrystallization in diethyl ether was performed let it stir for 16h. After filtration, the solid was dried leading to pure product **1a** (718 mg, 55.9%) as light brown powder. M.p. = 115-117°C. ^{1}H NMR (500 MHz, MeOD) δ 8.01 – 7.86 (m, 2H), 7.34 (dddd, *J* = 17.9, 8.1, 6.7, 1.4 Hz, 2H), 3.84 (s, 3H), 3.80 (s, 3H), 2.43 (s, 3H), 2.00 (q, *J* = 6.5 Hz, 2H). ^{19}F {^{1}H} NMR (471 MHz, MeOD) δ -138.69 (d, *J* = 63.3 Hz). ^{13}C {^{1}H} NMR (126 MHz, MeOD) δ 150.6, 149.1, 136.7, 129.3, 128.4, 127.1, 125.7, 124.9, 122.8, 122.6, 61.4, 61.4, 25.0, 13.4 (d, *J* = 2.8 Hz). HRMS (ESI+) calcd. for $C_{14}H_{15}BF_3O_2$: 283.1123. Found: 283.1129 (M^+).

2-((1,4-dimethoxy-3-methylnaphthalen-2-yl)methyl)-4,4,5,5-tetramethyl-1,3,2-dioxaborolane (1b).

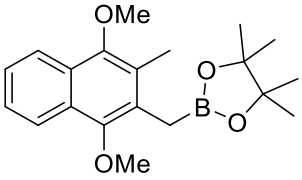

Under argon with a flame dried balloon with a magnetic stir bar was charged with tetrakis(triphenylphosphine)palladium (46.1 mg, 0.04 mmol, 0.05 equiv.), K_2CO_3 (330.7 mg, 2.4 mmol, 3 equiv.), bis(pinacolato)diboron (243.1 mg, 1 mmol, 1.2 equiv.) and compound **1** (200 mg, 0.8 mmol, 1 equiv.) with anhydrous dioxane (5.3 mL). The reaction was stirred at 100°C for 16h under argon. The reaction mixture turned black, it was filter on a silica pad rinse with DCM and evaporate under reduced pressure. The crude was purified on a small flash chromatography on silica gel (CHX/EtOAc, 95/5, v/v, UV) to afford a yellowish white powder (with small impurities) **1b** (83.4 mg, 30.5%)(contains a small impurity). M.p. = 75-77°C. ^{1}H NMR (500 MHz, $CDCl_3$) δ 8.07 – 8.01 (m, 2H), 7.45 – 7.41 (m, 2H), 3.88 (d, *J* = 4.6 Hz, 6H), 2.46 (s, 2H), 2.37 (s, 3H), 1.25 (s, 12H). ^{11}B {^{1}H} NMR (160 MHz, $CDCl_3$) δ 33.65. ^{13}C {^{1}H} NMR (126 MHz, $CDCl_3$) δ 149.9, 149.3, 129.1, 127.3, 127.1, 126.9, 125.2, 125.0, 122.2, 122.1, 83.5, 61.4, 61.3, 28.4, 24.9, 13.3.

3,4-diethylhexane-3,4-diol.

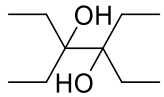

Magnesium (2.5 g, 94.6 mmol, 2 equiv.) was added in a two neck balloon under argon then add 60 ml of THF and cooled down to 0°C. Add titanium(IV) chloride (5.2 mL, 47.3 mmol, 1 equiv.) dropwise leave a neck open to release HCl (g), let it stir under argon at 0°C for 30 min with an additional 35 mL of THF (yellow to green heterogenous mixture). Add 3-pentanone (5 mL, 47.3 mmol, 1 equiv.) dropwise under argon at 0°C, then let it stir for 16h at 25°C under argon. The mixture was quenched with saturated Na_2CO_3 at 0°C, filter the precipitate on a silica pad, rinse with DCM. Extract with EtOAc, dry over $MgSO_4$, filter and evaporated. The crude was purified on a small flash chromatography on silica gel (CHX/EtOAc, 5/5 to 2/8, v/v, UV) to afford 3,4-diethylhexane-3,4-diol (654.3 mg, 7.9%) as a colorless oil, in accordance to the literature[129]. ^{1}H NMR (400 MHz, $CDCl_3$) δ 1.97 (s, 2H), 1.62 (qd, J = 7.5, 3.5 Hz, 8H), 0.94 (t, J = 7.5 Hz, 12H). ^{13}C {^{1}H} NMR (101 MHz, $CDCl_3$) δ 79.0, 27.5, 9.2.

4,4,5,5-tetraethyl-2-(4,4,5,5-tetraethyl-1,3,2-dioxaborolan-2-yl)-1,3,2-dioxaborolane (B_2Epin_2).

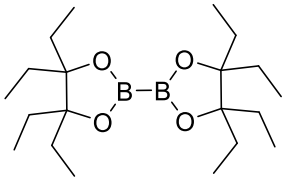

3,4-diethylhexane-3,4-diol (655 mg, 3.8 mmol, 2 equiv.) was solubilized in dry toluene (18.8 mL) with KOAc (516.4 mg, 5.2 mmol, 2.8 equiv.) then dimethyl(1,2,2-tris(dimethylamino)diboran-1-yl)amine (0.4 mL, 1.9 mmol, 1 equiv.) was added. Let it stir 5h at 90°C under reflux. Filter the precipitate rinse with toluene and evaporated. It led to the pure product quantitatively **B_2Epin_2** (730.8 mg) as yellow/white solid, in accordance to the literature[129]. ^{1}H NMR (400 MHz, $CDCl_3$) δ 1.76 – 1.56 (m, 16H), 0.90 (t, J = 7.5 Hz, 24H). ^{11}B {^{1}H} NMR (128 MHz, $CDCl_3$) δ 22.1. ^{13}C {^{1}H} NMR (101 MHz, $CDCl_3$) δ 88.5, 88.4, 26.5, 26.4, 9.1, 8.8.

2-((1,4-dimethoxy-3-methylnaphthalen-2-yl)methyl)-4,4,5,5-tetraethyl-1,3,2-dioxaborolane (1c).

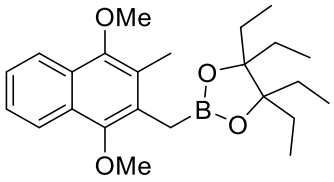

Under argon with a flame dried balloon with a magnetic stir bar was charged with tetrakis(triphenylphosphine)palladium (23 mg, 0.02 mmol, 0.05 equiv.), K_2CO_3 (165.4 mg, 1.2 mmol, 3 equiv.), **B_2Epin_2** (175.2 mg, 0.48 mmol, 1.2 equiv.) and compound **1** (100 mg, 0.4 mmol, 1 equiv.) with anhydrous dioxane (2.7 mL). The reaction was stirred at 100°C for 16h under argon. The reaction mixture turned black, it was filter on a silica pad rinse with DCM and evaporate under reduced pressure. The crude was analyzed by ^{1}H NMR and show the presence of the desired product with the protodeboronated side product (30% estimated NMR yield). The crude was directly engaged in the next reaction without purification to avoid any degradation.

1.5.3 Article 2

General procedure for the Suzuki coupling between compound 1 and aryl or heteroarylboronic species.

General conditions are a modification of a previously published procedure[61]. In a sealable tube, compound **1** (1 equiv.), the desired heteroarylboronic acid (1.2 equiv.) and sodium carbonate (2.1 equiv.) were dissolved in a 2:1 mixture of dimethoxyethane:water (0.15 M). The mixture was bubbled 30 min with argon, and then tetrakis(triphenylphosphine)palladium (2-5 mol%) was added at once. The tube was sealed and the mixture was heated 1h at 100°C under stirring. The mixture was then, allowed to

cool down to 25°C, diluted with water and extracted three times with ethyl acetate. Reunited organic layers were washed with brine, dried over magnesium sulfate, filtered and the solvent was removed under reduced pressure to afford a crude which was purified on silica gel chromatography using the adequate eluant system to afford the desired coupling product.

2-chloro-5-((1,4-dimethoxy-3-methylnaphthalen-2-yl)methyl)pyrimidine (2h).

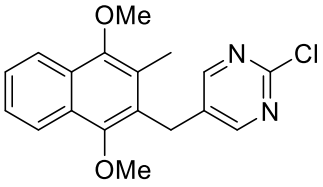

2 mol% $Pd(PPh_3)_4$, eluant (CHX/EtOAc, 9/1, v/v, UV), white solid, 97% yield. M.p. 88-89°C. ^{1}H NMR (400 MHz, $CDCl_3$) δ 8.43 (s, 2H), 8.13 – 8.00 (m, 2H), 7.61 – 7.43 (m, 2H), 4.18 (s, 2H), 3.88 (s, 3H), 3.85 (s, 3H), 2.29 (s, 3H). ^{13}C {^{1}H} NMR (101 MHz, $CDCl_3$) δ 159.4, 150.9, 150.7, 132.6, 128.5, 127.2, 126.5, 126.2, 126.0, 125.7, 122.6, 122.5, 62.4, 61.6, 27.3, 12.9. HRMS (ESI+) calcd. for $C_{18}H_{18}ClN_2O_2$: 329.1051. Found: 329.1054 ($M+H^+$).

1,4-dimethoxy-2-methyl-3-((3-nitro-4-(trifluoromethyl)phenyl)methyl)naphthalene (10).

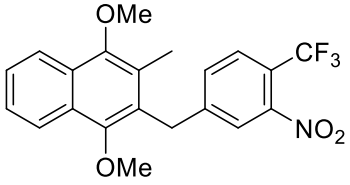

7 mol% $Pd(PPh_3)_4$, 1.2 equiv. of **9**, eluant (CHX/EtOAc, 9/1, v/v, UV), yellowish solid, 81% yield. M.p. 114-116°C. ^{1}H NMR (400 MHz, $CDCl_3$) δ 8.16 – 8.04 (m, 2H), 7.70 – 7.63 (m, 2H), 7.60 – 7.48 (m, 2H), 7.46 – 7.37 (m, 1H), 4.36 (s, 2H), 3.87 (d, J = 0.8 Hz, 6H), 2.26 (s, 3H). ^{19}F {^{1}H} NMR (377 MHz, $CDCl_3$) δ -59.77. ^{13}C {^{1}H} NMR (101 MHz, $CDCl_3$) δ 151.0, 150.9, 147.5, 132.0, 128.6, 128.1 (q, J = 5.1 Hz), 127.3, 126.6, 126.5, 126.1, 126.0, 124.7, 123.6, 122.7, 122.6, 121.4 (q, J = 34.0 Hz), 120.8, 62.5, 61.7, 32.6, 12.9. HRMS (ESI+) calcd. for $C_{21}H_{19}F_3NO_4$: 406.1261. Found: 406.1259 ($M+H^+$).

Post-functionalization.

2-bromo-5-((1,4-dimethoxy-3-methylnaphthalen-2-yl)methyl)pyrimidine (2t).

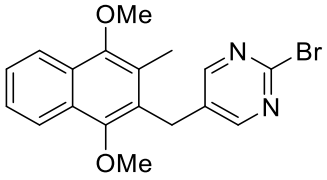

To a solution of **2h** (150 mg, 0.46 mmol, 1 equiv.) in propionitrile (1.5 mL) was added trimethylbromosilane (0.12 mL, 0.91 mmol, 2 equiv.). A white precipitate appeared. The mixture was heated at reflux 5h and allowed to cool down to 25°C. The mixture was treated with an aqueous saturated sodium bicarbonate solution. The aqueous layer was extracted three times with ethyl acetate, the reunited organic layers were washed with brine, dried over magnesium sulfate, filtered and the solvent was removed under reduced pressure. The product was purified by silica gel chromatography (T/CHX, 95/05, v/v, UV) to afford **2t** (160 mg, 94%) as a translucid solid. M.p. 99-100°C. ^{1}H NMR (500 MHz, $CDCl_3$) δ 8.37 (s, 2H), 8.11 – 7.98 (m, 2H), 7.65 – 7.47 (m, 2H), 4.16 (s, 2H), 3.88 (s, 3H), 3.85 (s, 3H), 2.29 (s, 3H). ^{13}C {^{1}H} NMR (126 MHz, $CDCl_3$) δ 159.3, 150.9, 150.8, 150.7, 133.1, 128.5, 127.2, 126.5, 126.17, 126.12, 125.7, 122.6, 122.5, 62.4, 61.7, 27.4, 12.9. HRMS (ESI+) calcd. for $C_{18}H_{18}BrN_2O_2$: 373.0546. Found: 373.0552 ($M+H^+$).

5-((1,4-dimethoxy-3-methylnaphthalen-2-yl)methyl)-2-((trimethylsilyl)ethynyl)pyrimidine (2v).

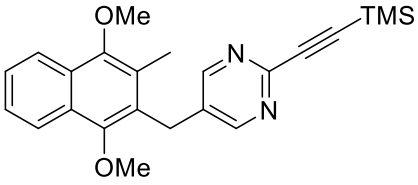

In a flame dried tube compound **2t** (100 mg, 0.27 mmol, 1 equiv.) was dissolved in triethylamine (8.5 mL) at 25°C under argon. Subsequently, were added in the following order dichlorobis(triphenylphosphine)palladium(II) (11.9 mg, 0.02 mmol, 0.05 equiv.), copper iodide (6.4 mg, 0.03 mmol, 0.1 equiv.) and ethynyl(trimethyl)silane (0.14 mL, 1.02 mmol, 3 equiv.). The mixture was stirred at 70°C for 24h. The brown solution turns rapidly into a darker one. The reaction mixture allowed to return at 25°C then

it was quenched with a 1:1 brine:water mixture and the crude of the reaction was extracted three times with ethyl acetate. Reunited organic layers were washed with water, dried over magnesium sulfate, filtered and the solvent was removed under reduced pressure. The crude was purified by silica gel chromatography (CHX/EtOAc, 8/2, v/v, UV) to afford **2v** (104 mg, 99%) as a brown oil. ^{1}H NMR (400 MHz, $CDCl_3$) δ 8.49 (s, 2H), 8.13 – 8.03 (m, 2H), 7.58 – 7.47 (m, 2H), 4.21 (s, 2H), 3.85 (s, 3H), 3.85 (s, 3H), 2.26 (s, 3H), 0.27 (s, 9H). ^{13}C {^{1}H} NMR (126 MHz, $CDCl_3$) δ 156.9, 150.9, 150.8, 150.4, 132.8, 128.4, 127.2, 126.4, 126.3, 125.9, 125.8, 122.6, 122.4, 102.4, 93.8, 62.4, 61.5, 28.0, 12.8, 1.1. HRMS (ESI+) calcd. for $C_{23}H_{27}N_2O_2Si$: 391.1836. Found: 391.1816 ($M+H^+$).

5-((1,4-dimethoxy-3-methylnaphthalen-2-yl)methyl)-2-ethynylpyrimidine (2w).

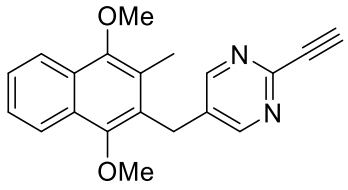

Compound **2v** (323.8 mg, 0.83 mmol, 1 equiv.) was dissolved in tetrahydrofuran (4.15 mL). Then a solution of tetrabutylammonium fluoride (602 mg, 1.91 mmol, 2.3 equiv.) in tetrahydrofuran (4.15 mL) was added dropwise to the original solution and the reaction was stirred during 2h at 25°C. The reaction was quenched with concentrate solution of ammonium chloride (10 mL) and was extracted three times with ethyl acetate. Reunited organic layers were washed with water, dried over magnesium sulfate, filtered and the solvent was removed under reduced pressure. The crude was purified by silica gel chromatography (CHX/EtOAc, 95/05, v/v, UV) to afford **2w** (163.3 mg, 62%) as a brown oil. ^{1}H NMR (400 MHz, $CDCl_3$) δ 8.50 (s, 2H), 8.18 – 7.96 (m, 2H), 7.61 – 7.44 (m, 2H), 4.21 (s, 2H), 3.87 (s, 3H), 3.85 (s, 3H), 3.07 (s, 1H), 2.27 (s, 3H). ^{13}C {^{1}H} NMR (126 MHz, $CDCl_3$) δ 157.1, 150.9, 150.8, 150.0, 133.3, 128.5, 127.2, 126.4, 126.2, 126.0, 125.8, 122.6, 122.5, 81.9, 75.4, 62.4, 61.6, 28.1, 12.9. HRMS (ESI+) calcd. for $C_{20}H_{19}N_2O_2$: 319.1441. Found: 319.1432 ($M+H^+$).

Preparation of the ionic liquid for the diazo-transfer reaction.

1-methyl-2-oxopyrrolidin-1-ium hydrogen sulfate.

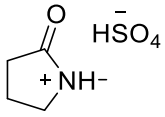

N-methyl-pyrrolidone (10 g, 101 mmol, 1 equiv.) was dissolved in DCM (162 mL). H_2SO_4 (5.4 mL, 101 mmol, 1 equiv.) was added dropwise within 10 min at 0°C, and the mixture was stirred for 4h at 25°C. The solvent was then removed under reduced pressure and the crude was dried under vacuum for 10h to afford a colorless oil (20 g, quantitative) in accordance to the literature data[134]. ^{1}H NMR (400 MHz, DMSO-d_6) δ 11.29 (s, 1H), 3.12 (d, J = 14.1 Hz, 2H), 2.46 (s, 3H), 2.00 (t, J = 8.1 Hz, 2H), 1.78 – 1.61 (m, 2H).

Synthesis of probe 13 and 16.

2-methyl-3-(4-nitrobenzyl)naphthalene-1,4-dione (14).

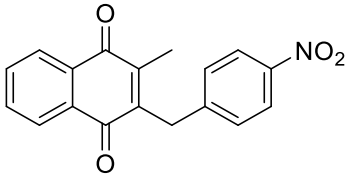

Menadione (500 mg, 2.9 mmol, 1 equiv.) and 4-nitrophenylacetic acid (1.05 g, 5.81 mmol, 2 equiv.) were dissolved in acetonitrile (44.9 mL) and water (14.9 mL). The mixture was heated to 85°C and silver nitrate (172.6 mg, 1.0 mmol, 0.35 equiv.) with ammonium persulfate (861.4 mg, 3.8 mmol, 0.35 equiv.) were added. The reaction was stirred for 4h at 85°C in the dark. The solvent was removed in vacuum and then extracted three times with ethyl acetate. Reunited organic layers were washed with water, dried over magnesium sulfate, filtered and the solvent was removed under reduced pressure. The crude oil was purified by silica gel chromatography (T/CHX, 7/3, v/v, UV) to afford **14** (839.2 mg, 94%) as a yellow solid (contains a small impurity). M.p. 153-154°C. ^{1}H NMR (400 MHz, $CDCl_3$) δ 8.22 – 8.03 (m, 4H), 7.79 – 7.61 (m, 2H), 7.44 – 7.31 (m, 2H), 4.13 (s, 2H), 2.26 (s, 3H). ^{13}C {^{1}H} NMR (101 MHz, $CDCl_3$) δ 185.1, 184.5, 146.8, 145.9, 145.3, 143.9, 133.9, 133.8,

132.2, 131.9, 129.5, 126.7, 126.6, 124.1, 32.6, 13.6. HRMS (ESI+) calcd. for $C_{18}H_{14}NO_4$: 308.0917. Found: 308.0923 ($M+H^+$).

2-(4-aminobenzyl)-3-methylnaphthalene-1,4-dione (15).

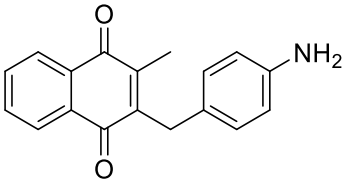

Compound **14** (276 mg, 0.9 mmol, 1 equiv.) was dissolved in ethanol (14 mL) and ethyl acetate (14 mL). Then palladium on carbon (95.6 mg, 0.09 mmol, 0.1 equiv.) was added. The mixture was degassed with dihydrogen three times then the reaction was stirred at 25°C for 16h under dihydrogen. The solution was filtered through celite, rinsed with ethyl acetate and the filtrate was concentrated under vacuum. The solid was dissolved in acetone (10 mL) and stirred at open air during 6 days. The crude was extracted three times with ethyl acetate. Reunited organic layers were washed with water, dried over magnesium sulfate, filtered and the solvent was removed under reduced pressure. The crude oil was purified by silica gel chromatography (CHX/EtOAc, 8/2, v/v, UV) to afford **15** (187.8 mg, 75%) as an orange solid. M.p. 55-57°C. ^{1}H NMR (400 MHz, $CDCl_3$) δ 8.08 (ddt, J = 6.0, 3.2 Hz, 2H), 7.68 (dd, J = 5.7, 3.3 Hz, 2H), 7.06 – 6.96 (m, 2H), 6.65 – 6.55 (m, 2H), 3.91 (s, 2H), 3.58 (s, 2H), 2.25 (s, 3H). ^{13}C {^{1}H} NMR (101 MHz, $CDCl_3$) δ 185.7, 184.9, 146.0, 144.9, 144.0, 133.54, 133.50, 132.3, 132.2, 129.7, 128.0, 126.6, 126.3, 115.5, 31.7, 13.3. HRMS (ESI+) calcd. for $C_{18}H_{16}NO_2$: 278.1175. Found: 278.1179 ($M+H^+$).

2-(4-azidobenzyl)-3-methylnaphthalene-1,4-dione (16).

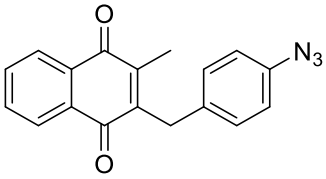

Compound **15** (100 mg, 0.36 mmol, 1 equiv.) was ground in a mortar using a pestle with 1-methyl-2-oxopyrrolidin-1-ium hydrogen sulfate (284.4 mg, 1.44 mmol, 4 equiv.) and water (0.7 mL) for 1 min. Then sodium nitrite (62.2 mg, 0.9 mmol, 2.5 equiv.) was added and the mixture was ground for 10 min. Finally, sodium azide (58.6 mg, 0.9 mmol, 2.5 equiv.) was added to the diazonium salt and grinding continued for 5 min until gas evolution completely stopped. An orange precipitated was formed. The crude was extracted three times with ethyl acetate. Reunited organic layers were washed with water, dried over magnesium sulfate, filtered and the solvent was removed under reduced pressure. The crude was purified by silica gel chromatography (CHX/EtOAc, 8/2, v/v, UV) to afford **16** (90.3 mg, 83%) as an orange solid. M.p. 60-62°C. ^{1}H NMR (400 MHz, $CDCl_3$) δ 8.09 (dt, J = 6.0, 3.2 Hz, 2H), 7.70 (dd, J = 5.8, 3.3 Hz, 2H), 7.26 – 7.18 (d, 2H), 6.98 – 6.89 (d, 2H), 4.00 (s, 2H), 2.25 (s, 3H). ^{13}C {^{1}H} NMR (101 MHz, $CDCl_3$) δ 185.4, 184.8, 145.1, 144.5, 138.4, 134.9, 133.7, 132.2, 132.1, 130.1, 126.6, 126.5, 119.4, 32.0, 13.4. HRMS (ESI+) calcd. for $C_{18}H_{14}N_3O_2$: 304.1080. Found: 304.1071 ($M+H^+$).

4,4,5,5-tetramethyl-2-(3-nitro-4-(trifluoromethyl)phenyl)-1,3,2-dioxaborolane (9).

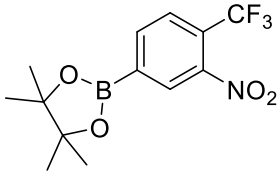

In a sealed tube 4-bromo-2-nitro-1-(trifluoromethyl)benzene (1 g, 3.7 mmol, 1 equiv.) and bis(pinacolato)diboron (2 g, 8.15 mmol, 2.2 equiv.) were added. Afterwards, dimethylformamide (18.5 mL) was transferred to the flask. To the prepared mixture, potassium acetate (2.18 g, 22.2 mmol, 6 equiv.) and (1,1'-bis(diphenylphosphino)ferrocene)palladium(II) dichloride (0.16 g, 0.2 mmol, 0.06 equiv.) were quickly added, the tube was sealed and the mixture was heated to 110°C for 16h. After cooling down to 25°C, the black mixture was filtered through a silica and celite pad, washed with ethyl acetate. The crude was extracted three times with ethyl acetate. Reunited organic layers were washed with water, dried over magnesium sulfate, filtered and the solvent was removed under reduced pressure. The crude was purified by silica gel chromatography (CHX/EtOAc, 9/1, v/v, UV) to afford to afford **9** (656 mg, 55.8%) as a greenish solid (with B_2pin_2 residue). M.p. 120-122°C. ^{1}H NMR (400 MHz,

$CDCl_3$) δ 8.23 (s, 1H), 8.09 (dt, J = 7.8, 1.0 Hz, 1H), 7.79 (d, J = 7.8 Hz, 1H), 1.35 (s, 12H). ^{19}F {^1H} NMR (377 MHz, $CDCl_3$) δ -60.23. ^{13}C {^1H} NMR (101 MHz, $CDCl_3$) δ 147.8, 138.6, 130.6, 127.2 (q, J = 5.1 Hz), 125.5 (q, J = 34.0 Hz), 122.1 (q, J = 273.5 Hz), 85.2, 24.9. HRMS (ESI) not found.

2-(3-amino-4-(trifluoromethyl)benzyl)-3-methylnaphthalene-1,4-dione (12).

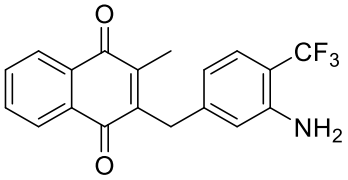

Compound **11** (297 mg, 0.79 mmol, 1 equiv.) was dissolved in ethanol (12.3 mL) and ethyl acetate (12.3 mL). Then palladium on carbon (84.22 mg, 0.08 mmol, 0.1 equiv.) was added. The mixture was degassed with dihydrogen three times then the reaction was stirred at 25°C for 16h under dihydrogen. The solution was filtered through celite, rinsed with ethyl acetate and the filtrate was concentrated under vacuum. The solid was dissolved in acetone (4.4 mL) and stirred at open air during 6 days. The crude was extracted three times with ethyl acetate. Reunited organic layers were washed with water, dried over magnesium sulfate, filtered and the solvent was removed under reduced pressure. The crude oil was purified by silica gel chromatography (CHX/EtOAc, 8/2, v/v, UV) to afford **12** (226 mg, 82.7%) as a yellow-orange solid. M.p. 75-78°C. ^1H NMR (400 MHz, $CDCl_3$) δ 8.13 – 8.03 (m, 2H), 7.76 – 7.66 (m, 2H), 7.31 (d, J = 8.1 Hz, 1H), 6.69 – 6.61 (m, 1H), 6.58 (s, 1H), 4.13 (s, 2H), 3.95 (s, 2H), 2.23 (s, 3H). ^{19}F {^1H} NMR (377 MHz, $CDCl_3$) δ -62.44. ^{13}C {^1H} NMR (101 MHz, $CDCl_3$) δ 185.3, 184.7, 144.9, 144.8 (q, J = 2.0 Hz), 144.6, 143.4, 133.7 (d, J = 1.7 Hz), 132.2, 132.1, 125.1 (q, J = 273.1 Hz), 127.1 (q, J = 5.1 Hz), 126.6, 126.5, 118.1, 117.0, 112.3 (q, J = 30.3 Hz), 32.3, 13.5. HRMS (ESI+) calcd. for $C_{19}H_{15}F_3NO_2$: 346.1049. Found: 346.1043 ($M+H^+$).

2-(3-azido-4-(trifluoromethyl)benzyl)-3-methylnaphthalene-1,4-dione (13).

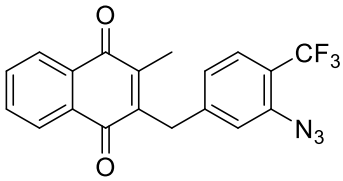

Compound **12** (50 mg, 0.14 mmol, 1 equiv.) was ground in a mortar with 1-methyl-2-oxopyrrolidin-1-ium hydrogen sulfate (114 mg, 0.58 mmol, 4 equiv.) and water (0.3 mL) for 1 min. Then sodium nitrite (25 mg, 0.36 mmol, 2.5 equiv.) was added and the mixture was ground for 10 min. Finally, sodium azide (23.5 mg, 0.36 mmol, 2.5 equiv.) was added to the diazonium salt and grinding continued for 5 min until gas evolution completely stopped. A yellow orange precipitated was formed. The crude was extracted three times with ethyl acetate. Reunited organic layers were washed with water, dried over magnesium sulfate, filtered and the solvent was removed under reduced pressure. The crude was purified by silica gel chromatography (T/CHX with 1% AcOH, 8/2, v/v, UV) to afford **13** (20 mg, 37%) as a yellow solid. M.p. 111-113°C. ^1H NMR (400 MHz, $CDCl_3$) δ 8.10 (ddd, J = 6.1, 5.2, 3.3 Hz, 2H), 7.79 – 7.69 (m, 2H), 7.51 (d, J = 8.1 Hz, 1H), 7.19 (s, 1H), 7.04 (d, J = 8.0 Hz, 1H), 4.08 (s, 2H), 2.28 (s, 3H). ^{19}F {^1H} NMR (377 MHz, $CDCl_3$) δ -61.64. ^{13}C {^1H} NMR (101 MHz, $CDCl_3$) δ 185.2, 184.6, 144.8, 144.72, 144.70, 144.5, 143.3, 133.6, 132.1, 131.9, 126.9 (q, J = 5.1 Hz), 126.5, 126.4, 125.9 (q, J = 273.4 Hz), 117.9, 116.9, 112.2 (q, J = 30.3 Hz), 32.2, 13.3. HRMS (ESI+) calcd. for $C_{19}H_{13}F_3N_3O_2$: 372.0954. Found: 372.0944 ($M+H^+$).

Synthesis of β-N-heteoaromatic-bMDs via Negishi cross-coupling.

2-((1,4-dimethoxy-3-methylnaphthalen-2-yl)methyl)-5-(trifluoromethyl)pyrimidine (2m).

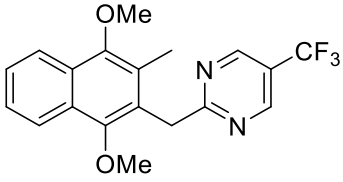

In a flame dried balloon was charged magnesium (24.15 mg, 0.92 mmol, 2.3 equiv.) and lithium chloride (21.98 mg, 0.52 mmol, 1.3 equiv.). Then a 1 M solution of zinc chloride (59.79 mg, 0.44 mmol, 1.1 equiv.) in dry tetrahydrofuran was added. A solution of compound **1** (100 mg, 0.4 mmol, 1 equiv.) in dry tetrahydrofuran (1 mL) was added and the reaction mixture was stirred at 25°C for 2h. To a solution of 2-chloro-5-(trifluoromethyl)pyrimidine (87.36 mg, 0.48 mmol, 1.2 equiv.) in dry tetrahydrofuran (1 mL) was added successively the previous mixture

and tetrakis(triphenylphosphine)palladium (23.04 mg, 0.02 mmol, 0.05 equiv.) under argon. The mixture was stirred at 80°C for 24h. After cooling down, the reaction mixture was diluted with ethyl acetate and quenched with concentrate solution of ammonium chloride. The phases were separated and the aqueous layer was extracted with ethyl acetate. The crude was extracted three times with ethyl acetate. Reunited organic layers were washed with water, dried over magnesium sulfate, filtered and the solvent was removed under reduced pressure. The crude was purified by silica gel chromatography (CHX/EtOAc, 9/1, v/v, UV) to afford **2m** (62.4 mg, 43.18%) as a light yellow solid, in accordance to the literature[132]. ^{1}H NMR (400 MHz, $CDCl_3$) δ 8.89 (s, 2H), 8.08 (dddd, J = 6.7, 4.6, 2.6, 0.7 Hz, 2H), 7.55 – 7.46 (m, 2H), 4.69 (s, 2H), 3.91 (s, 3H), 3.87 (s, 3H), 2.27 (s, 3H). ^{19}F {^{1}H} NMR (377 MHz, $CDCl_3$) δ -62.31.

2-((1,4-dimethoxy-3-methylnaphthalen-2-yl)methyl)-5-(trifluoromethyl)pyridine (2l).

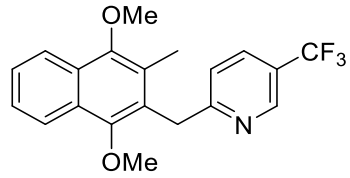

In a flame dried balloon was charged magnesium (0.22 g, 8.48 mmol, 2.3 equiv.) and lithium chloride (0.20 g, 4.79 mmol, 1.3 equiv.). Then a 1 M solution of zinc chloride (0.55 g, 4.056 mmol, 1.1 equiv.) in dry tetrahydrofuran was added. A solution of compound **1** (0.92 g, 3.69 mmol, 1 equiv.) in dry tetrahydrofuran (9.25 mL) was added and the reaction mixture was stirred at 25°C for 2h. To a solution of 2-bromo-5-(trifluoromethyl)pyridine (1 g, 4.42 mmol, 1.2 equiv.) in dry tetrahydrofuran (9.25 mL) was added successively the previous mixture and tetrakis(triphenylphosphine)palladium (0.21 g, 0.18 mmol, 0.05 equiv.) under argon. The mixture was stirred at 80°C for 24h. After cooling down, the reaction mixture was diluted with ethyl acetate and quenched with concentrate solution of ammonium chloride. The phases were separated and the aqueous layer was extracted with ethyl acetate. The crude was extracted three times with ethyl acetate. Reunited organic layers were washed with water, dried over magnesium sulfate, filtered and the solvent was removed under reduced pressure. The crude was purified by silica gel chromatography (CHX/EtOAc, 9/1, v/v, UV) to afford **2l** (702 mg, 52.7%) as a yellow oil, in accordance to the literature[132]. ^{1}H NMR (400 MHz, $CDCl_3$) δ 8.82 (s, 1H), 8.15 – 8.04 (m, 2H), 7.75 – 7.66 (m, 1H), 7.54 – 7.47 (m, 2H), 7.08 (d, J = 7.6 Hz, 1H), 4.52 (s, 2H), 3.90 (s, 3H), 3.87 (s, 3H), 2.28 (s, 3H). ^{19}F {^{1}H} NMR (377 MHz, $CDCl_3$) δ -62.22.

General procedure for the oxidative deprotection.

1,4-dimethoxy-3-benzylmenadione derivate (1 equiv.) was dissolved in stirring acetonitrile (0.08 M). Then, at room temperature, CAN (2.1 equiv.) dissolved in water (0.25 M) was added drop by drop. The mixture was stirred at 25°C during 1h. Then after TLC analysis showed complete conversion, the aqueous layer was extracted three times with dichloromethane. Combined organic layers were dried over magnesium sulfate, filtered and the solvent was removed under reduced pressure. Purification by silica gel chromatography was performed using the adequate eluent.

2-((2-ethynylpyrimidin-5-yl)methyl)-3-methylnaphthalene-1,4-dione (3v).

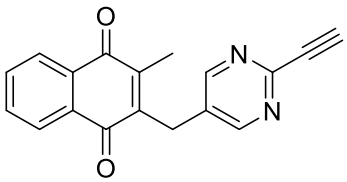

Eluant (CHX/EtOAc, 8/2, v/v, UV), yellow solid, 72% yield. M.p. 160-162°C. ^{1}H NMR (500 MHz, $CDCl_3$) δ 8.63 (s, 2H), 8.13 – 7.99 (m, 2H), 7.81 – 7.61 (m, 2H), 3.99 (s, 2H), 3.09 (s, 1H), 2.28 (s, 3H). ^{13}C {^{1}H} NMR (126 MHz, $CDCl_3$) δ 184.8, 184.3, 157.4, 150.4, 145.2, 142.8, 134.1, 133.9, 132.1, 131.8, 131.4, 126.7, 81.7, 75.9, 27.9, 13.6. HRMS (ESI+) calcd. for $C_{18}H_{13}N_2O_2$: 289.0971. Found: 289.0967 ($M+H^+$).

2-methyl-3-(3-nitro-4-(trifluoromethyl)benzyl)naphthalene-1,4-dione (11).

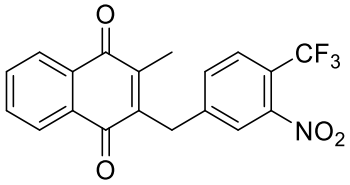

Eluant (CHX/EtOAc, 8/2, v/v, UV), yellow solid, 82% yield. M.p. 155-158°C. ^{1}H NMR (400 MHz, $CDCl_3$) δ 8.21 – 8.04 (m, 2H), 7.79 – 7.69 (m, 4H), 7.59 (ddt, J = 7.2, 1.7, 0.9 Hz, 1H), 4.14 (s, 2H), 2.28 (s, 3H). ^{19}F {^{1}H} NMR (377 MHz, $CDCl_3$) δ -59.88. ^{13}C {^{1}H} NMR (101 MHz, $CDCl_3$) δ 184.8, 184.4, 145.6, 144.8, 143.0, 134.1, 134.0, 132.7, 132.1, 131.8, 128.4 (q, J = 5.2 Hz), 126.8, 126.7, 125.1, 122.1 (q, J = 274.0 Hz), 122.0 (q, J = 34.0 Hz), 32.4, 13.7. HRMS (ESI+) calcd. for $C_{19}H_{13}F_3NO_4$: 376.0791. Found: 376.0791 ($M+H^+$).

2-methyl-3-((5-(trifluoromethyl)pyrimidin-2-yl)methyl)naphthalene-1,4-dione (3m).

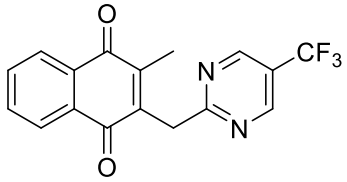

Eluant (CHX/EtOAc, 8/2, v/v, UV), yellow solid, 47% yield, in accordance to the literature[132]. ^{1}H NMR (400 MHz, $CDCl_3$) δ 8.86 (s, 2H), 8.16 – 8.02 (m, 2H), 7.75 – 7.65 (m, 2H), 4.46 (s, 2H), 2.21 (s, 3H). ^{19}F {^{1}H} NMR (377 MHz, $CDCl_3$) δ -62.38.

2-methyl-3-((5-(trifluoromethyl)pyridin-2-yl)methyl)naphthalene-1,4-dione (3l).

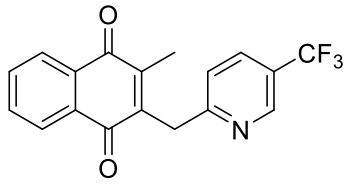

Eluant (CHX/EtOAc, 9/1, v/v, UV), yellow solid, 14% yield, in accordance to the literature[132]. ^{1}H NMR (400 MHz, $CDCl_3$) δ 8.72 (s, 1H), 8.14 – 8.02 (m, 2H), 7.86 – 7.78 (m, 1H), 7.74 – 7.62 (m, 2H), 7.46 – 7.38 (m, 1H), 4.27 (s, 2H), 2.30 (s, 3H). ^{19}F {^{1}H} NMR (377 MHz, $CDCl_3$) δ -62.36.

1.6 Chapitre III:

1.6.1 Travaux préliminaires

General procedure (A) for the acidic condensation between substituted α-tetralone and substituted salicylaldehyde by *in situ* HCl generation.

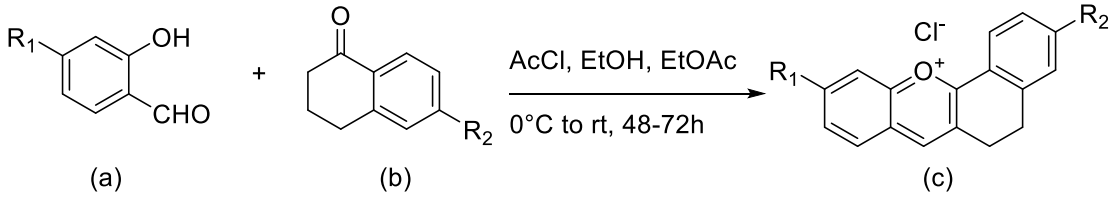

Acetyl chloride (50 equiv.) was added dropwise to ice-cold EtOH (80 equiv.) solution. HCl gas was thus produced *in situ*. Meanwhile, a solution of the corresponding salicylaldehyde (a) (1 equiv.) and the corresponding 3,4-dihydronaphthalen-1(2H)-one (α-tetralone) (b) (1 equiv.) was prepared in dry EtOAc (~ 0.07 M). After 15-30 min, the substrate solution was added dropwise to the HCl solution and the mixture was allowed to reach 25°C and stirred for 48h - 72h. The mixture was then evaporated, ice-cold EtOAc was added, and the resulting solid was filtered and washed several times with ice-cold EtOAc. The product (c) was dried under reduced pressure to give the corresponding dye. When indicate, the product was further purified by column chromatography on silica gel.

General procedure (B) for the acidic condensation between substituted α-tetralone and substituted salicylaldehyde with aqueous HCl in formic acid.

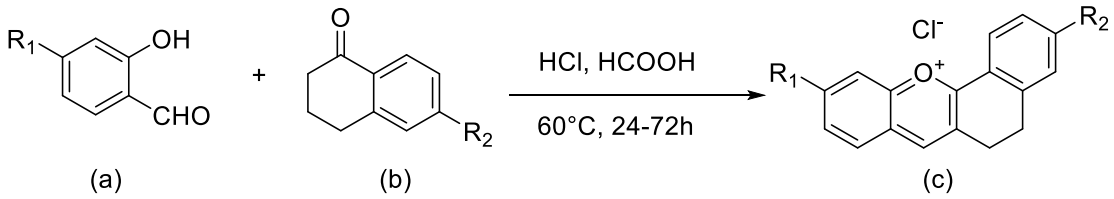

(a) (b) (c)

The substituted 3,4-dihydronaphthalen-1(2H)-one (α-tetralone) (b) (1 equiv.) and the corresponding 2-hydroxybenzaldehyde (a) (1 equiv.) were solubilized in formic acid (35 equiv.) containing 10% concentrated hydrochloric acid (37%). The reaction mixture was stirred at 60°C for 24h - 72h. The colour change of the reaction mixture was visible within a few minutes. At the end of the reaction, the solvents were evaporated to dryness. When indicate, the product was further purified by column chromatography on silica gel. If necessary, additional chromatography and/or recrystallization from methanol/ethyl acetate was performed. The final compound (c) was dried under vacuum on a Schenk line.

Synthesis of directly substituted azido-flavyliums.

6-azido-3,4-dihydronaphthalen-1(2H)-one (20).

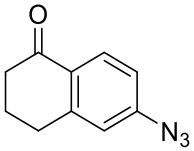

6-amino-3,4-dihydronaphthalen-1(2H)-one (500 mg, 3.1 mmol, 1 equiv.) was ground in a mortar with 1-methyl-2-oxopyrrolidin-1-ium hydrogen sulphate (979 mg, 12.4 mmol, 4 equiv.) and H_2O (6.2 mL) for 1 min. $NaNO_2$ (535 mg, 7.7 mmol, 2.5 equiv.) was then added and the mixture was ground for 10 min with periodic grinding using a pestle. NaN_3 (504 mg, 7.7 mmol, 2.5 equiv.) was then added in portions to the diazonium salt and grinding continued for 5 min until gas evolution had completely ceased. Azide formation started immediately after the addition of NaN_3 and the volume of the reaction mixture increased due to the formation of nitrogen gas. The crude mixture was then washed with H_2O and extracted with EtOAc. The organic phases were combined, washed twice with water and brine, dried over magnesium sulphate and filtered. The solvent was removed by evaporation under reduced pressure. The crude was purified by silica gel chromatography (CHX/EtOAc, 8/2, v/v, UV) to afford a brownish oil, **20** (542.7 mg, 93.5%) in accordance with the literature[155]. ^{1}H NMR (400 MHz, $CDCl_3$) δ 7.95 (d, J = 8.4 Hz, 1H), 6.86 (dd, J = 8.5, 2.3 Hz, 1H), 6.81 – 6.74 (m, 1H), 2.87 (t, J = 6.1 Hz, 2H), 2.57 (dd, J = 7.3, 5.8 Hz, 2H), 2.07 (d, J = 6.5 Hz, 2H). IR ν_{max} (cm^{-1}): 3468, 2108 (N_3), 1672 (C=O), 1275.

3-azidophenol (21).

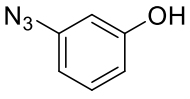

3-aminophenol (500 mg, 4.6 mmol, 1 equiv.) was ground in a mortar with 1-methyl-2-oxopyrrolidin-1-ium hydrogen sulphate (3.61 g, 18.4 mmol, 4 equiv.) and H_2O (15.3 mL) for 1 min. Then $NaNO_2$ (790 mg, 11.5 mmol, 2.5 equiv.) was added and the mixture was ground for 10 min with periodic grinding using a pestle. Then, NaN_3 (745 mg, 11.5 mmol, 2.5 equiv.) was added portion wise to the diazonium salt, and grinding continued for 5 min until gas evolution completely stopped. The formation of azide began immediately after NaN_3 addition, and the reaction mixture volume increased due to the evolution of nitrogen gas. The mixture was washed out with H_2O and extracted with EtOAc. The organic layers were combined and washed with brine twice, dried over magnesium sulfate and filtered. The solvent was removed under reduced pressure, and the crude was purified by silica gel chromatography (CHX/EtOAc, 8/2, v/v, UV) to afford a brownish oil, **21** (396 mg, 65%) in accordance with the literature[156]. ^{1}H NMR (400 MHz, DMSO-d_6) δ 9.76 (s, 1H), 7.20 (t, J = 8.0 Hz, 1H),

6.60 (dd, *J* = 8.0, 2.0 Hz, 1H), 6.54 (dd, *J* = 7.9, 2.0 Hz, 1H), 6.47 (t, *J* = 2.2 Hz, 1H). IR ν_{max} (cm^{-1}): 3337 (OH), 2106 (N_3), 1590, 1485.

4-azido-2-hydroxybenzaldehyde (20).

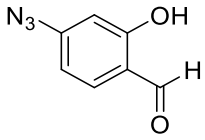

Compound **21** (381.5 mg, 2.8 mmol, 1 equiv.), $MgCl_2$ (806.4 mg, 8.5 mmol, 3 equiv.), CH_2O (593.4 mg, 19.8 mmol, 7 equiv.) were added to a solution of dry MeCN (10.9 mL) with 1 g of molecular sieves 3 Å. Then, TEA (1.5 mL, 10.7 mmol, 3.8 equiv.) was added and the mixture was stirred for 24h at 80°C leading to a yellow mixture. The reaction was quenched with 2 M HCl and stirred for 10 min. The mixture was extracted with EtOAc. The combined organic layers were washed with brine twice, dried over magnesium sulfate, filtered and the solvent was removed under reduced pressure. The crude was purified by silica gel chromatography (CHX/EtOAc, 9/1, v/v, UV) to afford a yellow solid, **20** (204 mg, 44%), in accordance with the literature[157]. ^{1}H NMR (400 MHz, MeOD) δ 9.92 (s, 1H), 7.69 (d, *J* = 8.4 Hz, 1H), 6.71 (dd, *J* = 8.4, 2.1 Hz, 1H), 6.59 (d, *J* = 2.1 Hz, 1H).

3-azido-5,6-dihydrobenzo[c]xanthen-12-ium chloride (23).

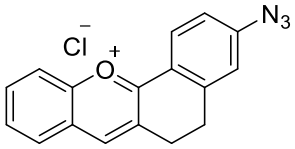

Following general procedure (A), acetyl chloride (10.3 mL, 144.9 mmol, 50 equiv.) was added to EtOH (13.5 mL, 231.9 mmol, 80 equiv.) at 0°C for 30 min. Compound **20** (542.7 mg, 2.9 mmol, 1 equiv.) and salicylaldehyde (354 mg, 2.9 mmol, 1 equiv.) in dry EtOAc (39.6 mL) were added and stirred for 72h. After purification by silica gel chromatography (DCM/MeOH, 10/0 to 7/3, v/v, UV) an orange solid, **23** (489.4 mg, 54%), was obtained. M.p. = 115-117°C. ^{1}H NMR (400 MHz, DMSO-d_6) δ 9.35 (s, 1H), 8.56 (d, *J* = 9.2 Hz, 1H), 8.42 (d, *J* = 8.6 Hz, 1H), 8.33 – 8.19 (m, 2H), 7.97 (t, *J* = 7.6 Hz, 1H), 7.43 (dq, *J* = 4.6, 2.3 Hz, 2H), 3.30 (d, *J* = 7.5 Hz, 2H), 3.21 (t, *J* = 7.2 Hz, 2H). ^{13}C {^{1}H} NMR (101 MHz, DMSO-d_6) δ 159.8, 152.8, 144.9, 142.9, 133.8, 125.9, 124.7, 120.9, 120.6, 119.3, 114.5, 109.1, 107.9, 105.1, 104.8, 18.9, 18.2. IR ν_{max} (cm^{-1}): 3011, 2662, 2111 (N_3), 1563, 1417. HRMS (ESI+) calcd. for $C_{17}H_{12}N_3O$: 274.0975. Found: 274.0973 (M^+).

Optical properties of 23: λ_{abs} = 454 nm, λ_{em} = 512 nm, ε = 3.22 (10^4 $M^{-1}.cm^{-1}$), Φ_{rel} = photosensitive, Stockes shift = 2500 cm^{-1}, Brightness = photosensitive, Solvent = Water pH 7.41 (0.1 M NaCl).

3-azido-10-(diethylamino)-5,6-dihydrobenzo[c]xanthen-12-ium chloride (24).

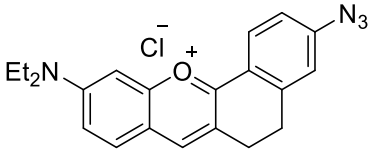

Following general procedure (A), acetyl chloride (3.8 mL, 53.4 mmol, 50 equiv.) was added to EtOH (5 mL, 85.5 mmol, 80 equiv.) at 0°C for 30 min. Compound **20** (200 mg, 1.1 mmol, 1 equiv.) and 4-(diethylamino)-2-hydroxybenzaldehyde (206.5 mg, 1.1 mmol, 1 equiv.) in dry EtOAc (39.6 mL) were added and stirred for 72h. After purification by silica gel chromatography (DCM/MeOH, 10/0 to 7/3, v/v, UV), a dark purple solid, **24** (175 mg, 43%), was obtained. M.p. = 198-200°C. ^{1}H NMR (400 MHz, MeOD) δ 8.54 (s, 1H), 8.28 (d, *J* = 8.5 Hz, 1H), 7.91 (d, *J* = 9.4 Hz, 1H), 7.47 (dd, *J* = 9.4, 2.4 Hz, 1H), 7.26 – 7.20 (m, 2H), 7.17 (d, *J* = 2.2 Hz, 1H), 3.77 (q, *J* = 7.2 Hz, 4H), 3.13 (d, *J* = 3.0 Hz, 4H), 1.36 (t, *J* = 7.1 Hz, 6H). ^{13}C {^{1}H} NMR (101 MHz, MeOD) δ 163.8, 160.4, 157.7, 149.6, 148.0, 145.7, 133.3, 128.9, 124.4, 122.5, 120.7, 120.3, 119.9, 119.5, 96.8, 47.2, 27.9, 26.0, 12.8. IR ν_{max} (cm^{-1}): 3403, 2100 (N_3), 1636, 1402. HRMS (ESI+) calcd. for $C_{21}H_{21}N_4O$: 345.1709. Found: 345.1714 (M^+).

10-azido-3-(dimethylamino)-5,6-dihydrobenzo[c]xanthen-12-ium chloride (25).

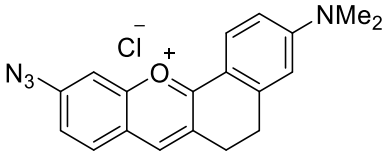

Following general procedure (A), acetyl chloride (2.1 mL, 29.3 mmol, 50 equiv.) was added to EtOH (2.7 mL, 46.8 mmol, 80 equiv.) and the mixture was stirred at 0°C for 30 min. 6-(dimethylamino)-1,2,3,4-tetrahydronaphthalen-1-one (110.8 mg, 0.6 mmol, 1 equiv.) and compound **22** (95.5 mg, 0.6 mmol, 1 equiv.) in dry EtOAc (8 mL) were added and stirred 72h. After purification by silica gel chromatography (DCM/MeOH, 10/0 to 7/3, v/v, UV) a purple solid, **25** (172.1 mg, 83.3%). M.p. = 169-172°C. ^{1}H NMR (400 MHz, MeOD) δ 8.17 (s, 1H), 8.14 (s, 1H), 7.82 (d, J = 8.6 Hz, 1H), 7.50 (d, J = 2.0 Hz, 1H), 7.26 (dd, J = 8.5, 2.1 Hz, 1H), 6.98 (dd, J = 9.4, 2.6 Hz, 1H), 6.79 (d, J = 2.5 Hz, 1H), 3.32 (s, 6H), 3.12 (m, 4H). ^{13}C {^{1}H} NMR (101 MHz, MeOD) δ 168.9, 159.3, 155.6, 150.9, 148.3, 142.9, 132.9, 131.6, 129.3, 121.4, 120.6, 115.3, 114.4, 112.7, 108.3, 41.1, 28.6, 27.6. IR ν_{max} (cm^{-1}): 3039, 2118 (N_3), 1586, 1135. HRMS (ESI+) calcd. for $C_{19}H_{17}ON_4$: 317.1397. Found: 317.1408 (M^+).

3-(dimethylamino)-10-(4-(4-(3-methyl-1,4-dioxo-1,4-dihydronaphthalene-2-carbonyl)phenyl)-1H-1,2,3-triazol-1-yl)-5,6-dihydrobenzo[c]xanthen-12-ium chloride (25-1).

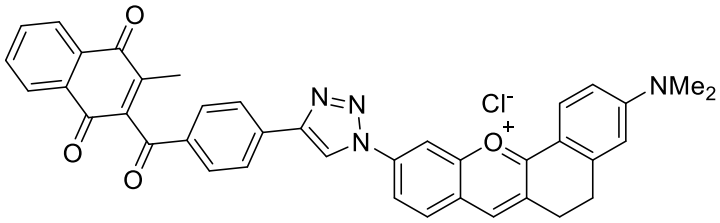

Probe 1 (25.5 mg, 0.08 mmol, 1 equiv.) and **25** (30 mg, 0.08 mmol, 1 equiv.) was solubilized in acetonitrile (12 mL) under argon. Three cycles argon/vaccum were done and $Cu(MeCN)_4BF_4$ (26.7 mg, 0.08 mmol, 1 equiv.) was added. The mixture was stirred 48h at 25°C in the dark under argon. Acetonitrile was removed under reduced pressure and purification by silica gel chromatography (DCM/MeOH, 9/1, v/v, UV) to afford **25-1** (20.9 mg, 37.6%) as a dark violet solid (contains a small impurity even after a second purification). ^{1}H NMR (400 MHz, $CDCl_3$) δ 8.32 (s, 1H), 8.23 – 8.16 (m, 1H), 8.11 – 8.06 (m, 2H), 8.04 – 7.88 (m, 4H), 7.88 – 7.69 (m, 3H), 7.55 – 7.35 (m, 2H), 6.83 – 6.72 (m, 1H), 6.64 – 6.57 (m, 1H), 6.38 (dd, J = 7.6, 2.6 Hz, 1H), 3.10 (s, 3H), 3.09 – 3.04 (m, 3H), 3.01 – 2.87 (m, 4H), 2.10 (s, 3H).

3-(4-(4-(3-methyl-1,4-dioxo-1,4-dihydronaphthalene-2-carbonyl)phenyl)-1H-1,2,3-triazol-1-yl)-5,6-dihydrobenzo[c]xanthen-12-ium chloride (23-1).

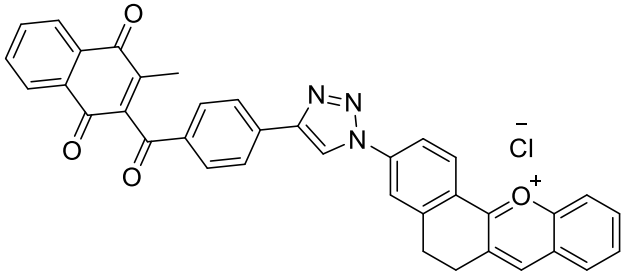

Probe 1 (40 mg, 0.13 mmol, 1 equiv.) was solubilized in water (0.65 mL) and tert-butanol (0.65 mL) under argon. Compound **23** (41.2 mg, 0.13 mmol, 1 equiv.) was added, protect the flask from light with aluminum foil. From a 1 M stock solution of copper sulfate and sodium ascorbate the correct amount was directly add (13 µL, 0.1 equiv.). The mixture was stirred under argon and every 1h an additional 0.2 eq. of the stock solution was added up to 1.1 eq. in total. After 16h of reaction time at 25°C, the reaction mixture was extracted with dichloromethane and wash with water, dry over $MgSO_4$, filter and solvent were removed under reduced pressure. The purification was performed by silica gel chromatography to afford **23-1** as a purple solid (DCM/MeOH, 95/05, v/v, UV) to afford (19.1 mg, 23.5%). M.p. = 114-119°C. ^{1}H NMR (400 MHz, $CDCl_3$) δ 8.46 – 7.35 (m, 17H), 3.18 – 2.92 (m, 4H), 2.10 (s, 3H). ^{13}C NMR (101 MHz, $CDCl_3$) δ 193.2, 184.9, 183.6, 177.2, 156.5, 155.7, 147.4, 144.3, 141.7, 138.2, 135.9, 135.5, 134.4, 134.3, 133.7, 132.1, 131.7, 130.1, 129.2, 126.9, 126.6, 126.4, 126.1, 125.6, 125.2, 123.7, 120.0, 118.75, 118.69, 118.1, 117.4, 27.4, 18.9, 13.8. HRMS (ESI+) calcd. for $C_{37}H_{24}N_3O_4$: 574.1761. Found: 574.1721 ($M+H^+$).

3-amino-5,6-dihydrobenzo[c]xanthen-12-ium chloride (23_{red}).

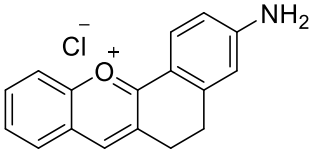

Following general procedure (B), 6-amino-3,4-dihydronaphthalen-1(2H)-one (67.8 mg, 0.4 mmol, 1 equiv.) and salicylaldehyde (42 µL, 0.4 mmol, 1 equiv.) were dissolved in 5.55 mL of formic acid solution containing 10% concentrated HCl (35 eq). The solution was then stirred at 60°C for 48h. After evaporation of the solvent, the crude product was purified on a silica column using the same eluent (DCM/MeOH, 9/1, v/v, UV). The compound **23_{red}** (105.3 mg, 93%) was obtained as a dark red powder. **23_{red}** is thermosensitive and decomposes at temperature above 40°C under reduced pressure. ^{1}H NMR (400 MHz, DMSO-d_6) δ 8.53 (s, 1H), 8.41 (s, 1H), 8.19 (d, J = 9.0 Hz, 1H), 7.97 – 7.83 (m, 2H), 7.67 – 7.59 (m, 1H), 6.87 (d, J = 9.1 Hz, 1H), 6.67 (s, 1H), 3.06 (m, 2H), 2.97 (m, 2H). ^{13}C {^{1}H} NMR (101 MHz, DMSO-d_6) δ 167.1, 160.2, 152.3, 150.5, 141.5, 134.1, 132.8, 129.0, 128.8, 127.5, 122.3, 117.4, 116.2, 113.0, 112.6, 40.2, 39.9, 39.7, 39.5, 39.3, 39.1, 38.9, 26.7, 26.0. HRMS (ESI+) calcd. for $C_{17}H_{14}NO$: 248.1070. Found: 248.1069 (M^+).

Optical properties of 23_{red}: λ_{abs} = 495 nm, λ_{em} = 556 nm, ε = 2.28 (10^4 $M^{-1}.cm^{-1}$), Φ_{rel} = 0.095, Stockes shift = 2220 cm^{-1}, Brightness = 2170, Solvent = Water pH 7.41 (0.1 M NaCl).

1.6.2 Article 3

Synthesis of the parent dye 2.

6-(ethylamino)-3,4-dihydronaphthalen-1(2H)-one (3).

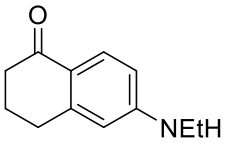

To a solution of 6-amino-3,4-dihydronaphthalen-1(2H)-one (3 g, 18.6 mmol, 1 equiv.) in dry DMF (25 mL) was added portion-wise Cs_2CO_3 (12.1 g, 37.2 mmol, 1.2 equiv.) under argon atmosphere at 25°C. The resulting mixture was stirred for 15 min. Ethyl iodide (1.6 mL, 20.5 mmol, 1.1 equiv.) was then added carefully and the resulting mixture was stirred for 18h at 50°C. The reaction was quenched by adding 1 M HCl aqueous solution and the organic layers were combined, washed with water and dried over anhydrous $MgSO_4$. After filtration, the solvent was removed under reduced pressure and the residue was purified by column chromatography (CHX/EtOAc, 9/1 to 7/3, v/v, UV) to afford **3** (1.4 g, 39%) as an orange solid, in accordance with the literature[158]. ^{1}H NMR (400 MHz, $CDCl_3$) δ 7.89 (d, J = 8.6 Hz,1H), 6.46 (dd, J = 8.6, 2.2 Hz, 1H), 6.30 (d, J = 2.3 Hz, 1H), 3.22 (m, J = 7.2 Hz, 2H), 2.84 (t, J = 6.0 Hz, 2H), 2.55 (t, J = 6.4 Hz, 2H), 2.06 (q, 2H), 1.27 (t, J = 7.2 Hz, 3H). ^{13}C {^{1}H} NMR (101 MHz, $CDCl_3$) δ 196.9, 152.4, 147.2, 129.7, 123.0, 111.4, 109.7, 38.9, 38.0, 30.5, 23.6, 14.8.

10-(diethylamino)-3-(ethylamino)-5,6-dihydrobenzo[c]xanthen-12-ium chloride (2).

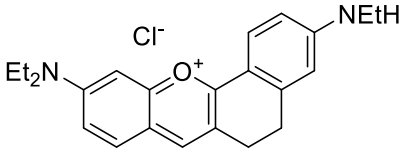

Following general procedure (B) **3** (99 mg, 0.5 mmol, 1 equiv.) and 4-(diethylamino)-2-hydroxybenzaldehyde (101 mg, 0.5 mmol, 1 equiv.) were solubilized in formic acid (6.9 mL) containing 10% of concentrated HCl (0.5 mL, 18.3 mmol, 35 equiv.). The mixture was stirred at 60°C for 72h. Solvents were removed under reduced pressure and the crude was purified by silica gel chromatography (DCM/MeOH, 9/1, v/v, UV) to afford a black solid, **2** (158 mg, 79%). ^{1}H NMR (500 MHz, DMSO-d_6) δ 8.29 (s, 1H), 8.08 (t, br, J = 5.5 Hz, 1H), 8.00 (d, J = 8.9 Hz, 1H), 7.73 (d, J = 9.2 Hz, 1H), 7.16 (dd, J = 9.2, 2.6 Hz, 1H), 7.08 (d, J = 2.1 Hz, 1H), 6.76 (dd, J = 9.0, 2.2 Hz, 1H), 6.61 (d, J = 2.1 Hz, 1H), 3.59 (q, J = 7.0 Hz, 4H), 3.27 (q, J = 7.0 Hz, 2H), 2.92 (s, 4H), 1.24 – 1.18 (3t, 9H).

^{13}C {^{1}H} NMR (126 MHz, DMSO-d_6) δ 164.7, 163.0, 156.5, 155.6, 153.2, 144.2, 130.7, 120.2, 114.8, 114.6, 112.8, 95.9, 44.8, 37.1, 27.1, 25.1, 14.1, 12.4. HRMS (ESI+) calcd. for $C_{23}H_{27}N_2O$: 347.2118. Found: 347.2113 (M^+). Activity: IC_{50} = 1770 nM, *Pf*K1 (**2**).

Optical properties of 2: λ_{abs} = 594 nm, λ_{em} = 633 nm, ε = 3.49 (10^4 $M^{-1}.cm^{-1}$), Φ_{rel} = 0.23, Stokes shift = 1034 cm^{-1}, Brightness = 8030, Solvent = Water pH 7.41 (0.1 M NaCl).

Synthesis of the flavylium dye bearing a short PEG-1-azido chain (F1).

Oxybis(ethane-2,1-diyl)*bis*(4-methylbenzenesulfonate) (4).

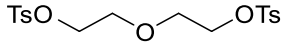

To a solution of 2,2'-oxybis(ethan-1-ol) (4.5 mL, 47.1 mmol, 1 equiv.) in DCM (47 mL) was added TsCl (18 g, 94.2 mmol, 2 equiv.). Then KOH (21 g, 376.9 mmol, 8 equiv.) was added to the mixture at 0°C portion-wise. The mixture was let stirred from 0°C to 25°C for 16h. 100 mL of water was added, and the crude was extracted three times with DCM. The organic layers were combined and washed with water and brine twice, dried over magnesium sulfate, filtered and the solvent was removed under reduced pressure. The desired product was obtained as a white solid, **4** (16.5 g, 84.8%), in accordance with the literature[159]. ^{1}H NMR (400 MHz, $CDCl_3$) δ 7.83 – 7.73 (m, 4H), 7.40 – 7.29 (m, 4H), 4.16 – 4.04 (m, 4H), 3.67 – 3.57 (m, 4H), 2.45 (s, 6H).

1-azido-2-(2-azidoethoxy)ethane (5).

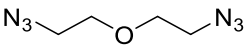

Compound **4** (4 g, 9.6 mmol, 1 equiv.) was dissolved in dry DMF (96 mL). Then NaN_3 (1.4 g, 21.2 mmol, 2.2 equiv.) was added slowly to the mixture. The reaction mixture was allowed to reach 60°C and was stirred for 24h. The solvent was removed under reduced pressure and the crude was extracted three times with EtOAc. The organic layers were combined and washed with water and brine, dried over magnesium sulfate, filtered and the solvent was removed under reduced pressure. The desired product was obtained as a colourless oil, **5** (70 mg, 46.4%), in accordance with the literature[160]. ^{1}H NMR (400 MHz, $CDCl_3$) δ 3.69 (t, J = 5.0 Hz, 4H), 3.41 (t, J = 5.0 Hz, 4H). IR ν_{max} (cm^{-1}): 2869, 2089 (N_3), 1441, 1283, 1125, 924.

2-(2-azidoethoxy)ethan-1-aminium chloride (6).

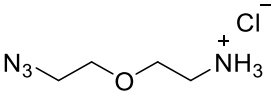

Compound **5** (700 mg, 4.4 mmol, 1 equiv.) was solubilized in EtOAc (35.8 mL) with a 1 M HCl solution (7.2 mL) to create an emulsion. Then a solution of triphenylphosphine (1.2 g, 4.5 mmol, 1 equiv.) in EtOAc (5.6 ml) was added dropwise over 1h. The mixture was stirred for 16h at 25°C. A solution of 1 M HCl was added, and the organic phase was extracted with water. The aqueous layer was washed three times with EtOAc and then evaporated. The desired product was obtained as an orange oil, **6** (640.7 mg, 85.8%), in accordance with the literature[161]. ^{1}H NMR (400 MHz, $CDCl_3$) δ 8.29 (s, 3H), 3.84 (s, 2H), 3.72 (t, J = 4.6 Hz, 2H), 3.50 (t, J = 4.5 Hz, 2H), 3.27 (s, 2H), 2.89 (s, 1H). IR ν_{max} (cm^{-1}): 3392 (NH_2), 2877, 2104 (N_3), 1607, 1283, 1109.

5-oxo-5,6,7,8-tetrahydronaphthalen-2-yl trifluoromethanesulfonate (7).

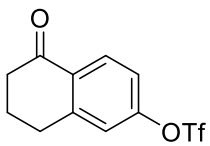

6-hydroxy-3,4-dihydronaphthalen-1(2H)-one (2.5 g, 15.4 mmol, 1 equiv.) was solubilized in DCM (12.5 mL) with pyridine (2.5 mL, 30.8 mmol, 2 equiv.). The mixture was then cooled to 0°C and triflic anhydride (3.1 mL, 18.5 mmol, 1.2 equiv.) was added dropwise. The mixture was stirred at 25°C for 2h. The crude was quenched with 1 M HCl and extracted with EtOAc. The organic layer was then washed with saturated Na_2CO_3, dried over magnesium sulfate, filtered and the solvent was removed under reduced pressure. The desired product was obtained as a yellow oil, **7** (4.5 g, 99.6%), in accordance with the literature[162]. ^{1}H NMR (400 MHz, $CDCl_3$) δ 8.13 (d, J = 8.4 Hz, 1H), 7.22 – 7.14 (m, 2H), 3.02 (t, J = 6.1 Hz, 2H), 2.69

(dd, *J* = 7.4, 5.8 Hz, 2H), 2.18 (tt, *J* = 6.7, 5.6 Hz, 2H). ^{19}F {^{1}H} NMR (377 MHz, $CDCl_3$) *δ* -72.83. ^{13}C {^{1}H} NMR (101 MHz, $CDCl_3$) *δ* 196.5, 152.5, 147.2, 132.5, 130.2, 121.5, 119.8, 120.1 (q, *J* = 34.5 Hz), 38.9, 29.9, 23.1. HRMS (ESI+) calcd. for $C_{11}H_{10}F_3O_4S$: 295.0246. Found: 295.0235 ($M+H^+$).

6-((2-(2-azidoethoxy)ethyl)amino)-3,4-dihydronaphthalen-1(2H)-one (8).

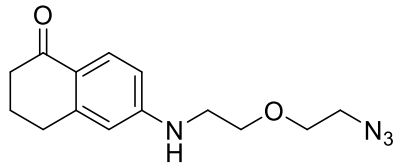

In a flame-dried balloon, under argon, was added first palladium diacetate (6.7 mg, 0.03 mmol, 0.1 equiv.) then BINAP (28 mg, 0.04 mmol, 0.15 equiv.) and finally cesium carbonate (488.9 mg, 1.5 mmol, 5 equiv.). The mixture was degassed with argon three times. A solution of compound **7** (88.3 mg, 0.3 mmol, 1 equiv.) and compound **6** (100 mg, 0.6 mmol, 2 equiv.) in toluene (2.9 mL) was added. The mixture was stirred at 100°C for 3h. The resulting crude was cooled, filtered on celite, washed with DCM and the solvent were removed under reduced pressure. The crude was purified by silica gel chromatography (CHX/EtOAc, 7/3 to 0/10, v/v, UV) to afford an orange oil, **8** (54.6 mg, 66.3%). ^{1}H NMR (400 MHz, $CDCl_3$) *δ* 7.88 (d, *J* = 8.6 Hz, 1H), 6.48 (dd, *J* = 8.6, 2.4 Hz, 1H), 6.33 (d, *J* = 2.4 Hz, 1H), 4.64 (s, 1H), 3.73 – 3.66 (m, 4H), 3.41 – 3.34 (m, 4H), 2.83 (t, *J* = 6.1 Hz, 2H), 2.53 (t, *J* = 6.1 Hz, 2H), 2.10 – 2.00 (m, 2H). ^{13}C {^{1}H} NMR (101 MHz, $CDCl_3$) *δ* 196.9, 152.2, 147.1, 129.6, 123.3, 111.5, 110.1, 70.3, 69.4, 50.7, 42.8, 38.9, 30.4, 23.5. IR ν_{max} (cm^{-1}): 3347, 2935, 2098 (N_3), 1656, 1583, 1279. HRMS (ESI+) calcd. for $C_{14}H_{18}N_4O_2$: 297.1328. Found: 297.1316 ($M+Na^+$).

3-((2-(2-azidoethoxy)ethyl)amino)-10-(diethylamino)-5,6-dihydrobenzo[c]xanthen-12-ium chloride (F1).

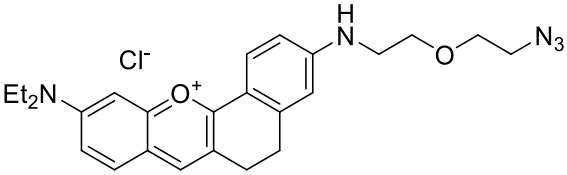

Following general procedure (A), acetyl chloride (3.9 mL, 54.7 mmol, 50 equiv.) was added to EtOH (5.1 mL, 87.5 mmol, 80 equiv.) and stirred at 0°C for 30 min. Compound **8** (300 mg, 1.1 mmol, 1 equiv.) and 4-(diethylamino)-2-hydroxybenzaldehyde (232.6 mg, 1.2 mmol, 1.1 equiv.) in dry EtOAc (14.9 mL) was added. The mixture was stirred for 72h and gave after purification by silica gel chromatography (DCM/MeOH, 10/0 to 6/4, v/v, UV) a purple solid, **F1** (428 mg, 83.6%). M.p. = 132-134°C. ^{1}H NMR (500 MHz, MeOD) *δ* 8.11 (s, 1H), 8.02 (d, *J* = 8.9 Hz, 1H), 7.67 (d, *J* = 9.2 Hz, 1H), 7.15 (dd, *J* = 9.2, 2.5 Hz, 1H), 7.02 – 6.98 (m, 1H), 6.76 (dd, *J* = 8.9, 2.3 Hz, 1H), 6.62 (d, *J* = 2.2 Hz, 1H), 3.74 – 3.68 (m, 4H), 3.63 (q, *J* = 7.1 Hz, 4H), 3.51 (t, *J* = 5.3 Hz, 2H), 3.42 – 3.38 (m, 2H), 2.98 (s, 4H), 1.30 (t, *J* = 7.1 Hz, 6H). ^{13}C {^{1}H} NMR (101 MHz, $CDCl_3$) *δ* 166.4, 158.3, 157.4, 155.2, 145.4, 131.9, 121.5, 116.4, 116.1, 114.8, 96.9, 71.1, 70.3, 51.8, 46.5, 43.9, 28.6, 26.6, 12.9. IR ν_{max} (cm^{-1}): 3188, 2972, 2113 (N_3), 1610, 1156. HRMS (ESI+) calcd. for $C_{25}H_{30}O_2N_5$: 432.2394. Found: 432.2387 (M^+). Activity: IC_{50} = 1343 nM, *Pf*NF54 (**F1**).

Optical properties of F1 λ_{abs} = 593 nm, λ_{em} = 633 nm, ε = 4.55 (10^4 $M^{-1}.cm^{-1}$), Φ_{rel} = 0.236, Stokes shift = 1070 cm^{-1}, Brightness = 10920, Solvent = Water pH 7.41 (0.1 M NaCl).

Synthesis of flavylium dyes bearing a PEG-2-azido chain (F2).

6-((2-(2-(2-chloroethoxy)ethoxy)ethyl)amino)-3,4-dihydronaphthalen-1(2H)-one (9).

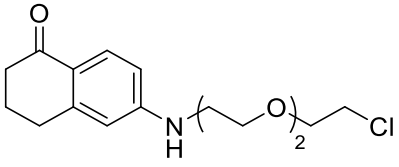

1,2-bis(2-chloroethoxy)ethane (1.9 g, 10.2 mmol, 1.1 equiv.) was dissolved in MeCN (61.9 ml) then DIPEA (9.7 ml, 55.8 mmol, 6 equiv.) and NaI (2.8 g, 18.6 mmol, 2 equiv.) were added. Compound 6-amino-3,4-dihydronaphthalen-1(2H)-one (1.5 g, 9.3 mmol, 1 equiv.) was then added to the reaction mixture (yellow solution) which was stirred for 48h at reflux. The mixture was then diluted in EtOAc, and the organic layers were washed 3 times with 1 M HCl

and brine, dried over magnesium sulphate, filtered and the solvent removed under reduced pressure. The crude was purified by silica gel chromatography (CHX/EtOAc, 6/4, v/v, UV) to afford an orange oil, **9** (472 mg, 16.3%). ^{1}H NMR (400 MHz, $CDCl_3$) δ 7.89 (d, J = 8.6 Hz, 1H), 6.49 (dd, J = 8.6, 2.4 Hz, 1H), 6.34 (d, J = 2.6 Hz, 1H), 3.80 – 3.57 (m, 10H), 3.37 (t, J = 5.2 Hz, 2H), 2.83 (t, J = 6.1 Hz, 2H), 2.55 (dd, J = 7.2, 5.8 Hz, 2H), 2.06 (dd, J = 5.6, 2.4 Hz, 2H). ^{13}C {^{1}H} NMR (101 MHz, $CDCl_3$) δ 196.9, 152.4, 147.1, 129.7, 123.2, 111.6, 110.1, 71.5, 70.7, 70.4, 69.4, 42.9, 42.9, 38.9, 30.4, 23.6. HRMS (ESI+) calcd. for $C_{16}H_{22}NO_3Cl$: 334.1180. Found: 334.1881 ($M+Na^+$).

6-((2-(2-(2-azidoethoxy)ethoxy)ethyl)amino)-3,4-dihydronaphthalen-1(2H)-one (1).

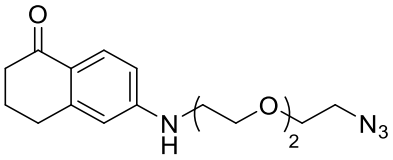

Compound **9** (560 mg, 1.8 mmol, 1 equiv.) was dissolved in dry DMF (3.4 mL), and NaN_3 (116.8 mg, 1.8 mmol, 1 equiv.) was then added slowly. The mixture was stirred and heated under reflux for 30h. The yellowish/brownish mixture was then mixed with water and extracted with EtOAc. The organic layers were combined, washed with brine, dried over magnesium sulfate, filtered and the solvent was removed under reduced pressure. The crude was purified by silica gel chromatography (CHX/EtOAc, 6/4, v/v, UV) to afford a brown oil, **1** (347.3 mg, 61%). ^{1}H NMR (400 MHz, $CDCl_3$) δ 7.85 (d, J = 8.6 Hz, 1H), 6.46 (dd, J = 8.7, 2.4 Hz, 1H), 6.30 (d, J = 2.2 Hz, 1H), 4.73 (s, 1H), 3.70 – 3.62 (m, 8H), 3.37 – 3.31 (m, 4H), 2.80 (t, J = 6.1 Hz, 2H), 2.51 (t, J = 6.8 Hz, 2H), 2.06 – 2.00 (m, 2H). ^{13}C {^{1}H} NMR (101 MHz, $CDCl_3$) δ 196.9, 152.4, 147.1, 129.7, 123.3, 111.6, 110.1, 70.8, 70.5, 70.3, 69.5, 50.8, 42.9, 38.9, 30.4, 23.6. IR ν_{max} (cm^{-1}): 3345, 2865, 2097 (N_3), 1585, 1280. HRMS (ESI+) calcd. for $C_{16}H_{23}N_4O_3$: 319.1765. Found: 319.1758 ($M+H^+$).

3-((2-(2-(2-azidoethoxy)ethoxy)ethyl)amino)-10-(diethylamino)-5,6-dihydrobenzo[c]xanthen-12-ium chloride (F2).

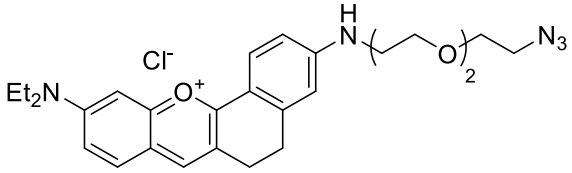

Following general procedure (A), acetyl chloride (2.2 mL, 31.4 mmol, 50 equiv.) was added to EtOH (2.9 mL, 50.2 mmol, 80 equiv.) and stirred at 0°C for 30 min. Compound **10** (200 mg, 0.6 mmol, 1 equiv.) and 4-(diethylamino)-2-hydroxybenzaldehyde (121.4 mg, 0.6 mmol, 1 equiv.) in dry EtOAc (8.6 mL) were added, stirred for 72h and gave after purification by silica gel chromatography (DCM/MeOH, 9/1, v/v, UV) a purple solid, **F2** (224.1 mg, 69.7%). M.p. = 151-153°C. ^{1}H NMR (400 MHz, MeOD) δ 8.08 (s, 1H), 7.98 (d, J = 8.9 Hz, 1H), 7.65 (d, J = 9.2 Hz, 1H), 7.13 (dd, J = 9.2, 2.5 Hz, 1H), 7.00 – 6.95 (m, 1H), 6.73 (dd, J = 9.0, 2.3 Hz, 1H), 6.58 (d, J = 2.3 Hz, 1H), 3.72 (t, J = 5.3 Hz, 2H), 3.70 – 3.66 (m, 5H), 3.66 – 3.57 (m, 5H), 3.47 (t, J = 5.3 Hz, 2H), 3.37 (dd, J = 5.5, 4.3 Hz, 2H), 2.96 (s, 4H), 1.30 (t, J = 7.1 Hz, 6H). ^{13}C {^{1}H} NMR (101 MHz, MeOD) δ 166.7, 158.5, 157.5, 155.3, 145.6, 131.9, 130.6, 121.7, 116.5, 116.2, 114.9, 96.9, 71.6, 71.1, 70.4, 51.7, 46.5, 43.9, 28.7, 26.8, 12.8. IR ν_{max} (cm^{-1}): 3212, 2869, 2097 (N_3), 1611, 1257. HRMS (ESI+) calcd. for $C_{27}H_{34}N_5O_3$: 476.2656. Found: 476.2639 (M^+). Activity: IC_{50} = 348 nM, *Pf*NF54 (**F2**).

Optical properties of F2: λ_{abs} = 594 nm, λ_{em} = 663 nm, ε = 1.76 (10^4 $M^{-1}.cm^{-1}$), Φ_{rel} = 0.224, Stockes shift = 1110 cm^{-1}, Brightness = 3940, Solvent = Water pH 7.41 (0.1 M NaCl).

Synthesis of the flavylium dye bearing a PEG-3-azido chain (F3).

6-(12-chloro-4,7,10-trioxa-1-azadodecan-1-yl)-1,2,3,4-tetrahydronaphthalen-1-one (10).

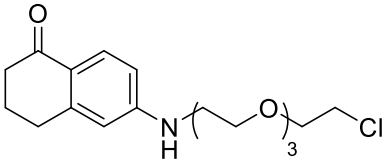

1-chloro-2-(2-(2-(2-chloroethoxy)ethoxy)ethoxy)ethane (1.5 mL, 7.7 mmol, 1.1 equiv.) was dissolved in MeCN (46.4 mL). DIPEA (7.3 mL, 41.8 mmol, 6 equiv.) and NaI (2.1 g, 13.9 mmol, 2 equiv.) were then added. Following addition of 6-amino-1,2,3,4-tetrahydronaphthalen-1-one (1.1 g, 6.9 mmol, 1 equiv.), the yellow mixture was stirred for 72h under reflux. The mixture was then diluted in EtOAc, the organic layers were combined, washed 3 times with HCl 1 M and brine, dried over magnesium sulfate, filtered and the solvent was removed under reduced pressure. The crude was purified by silica gel chromatography (CHX/EtOAc, 8/2, v/v, UV) to give **10** as an orange solid (598 mg, 24%). M.p. = 132-135°C. ^{1}H NMR (400 MHz, $CDCl_3$) δ 7.82 (d, 1H), 6.44 (dd, J = 8.6, 2.4 Hz, 1H), 6.28 (d, J = 2.4 Hz, 1H), 3.72 – 3.54 (m, 12H), 3.31 (t, J = 5.2 Hz, 2H), 3.20 (td, J = 6.8, 5.6 Hz, 2H), 2.77 (dt, J = 9.7, 6.0 Hz, 2H), 2.50 (dd, J = 7.2, 5.8 Hz, 2H), 2.04 – 1.93 (m, 2H). ^{13}C {^{1}H} NMR (126 MHz, $CDCl_3$) δ 196.8, 152.4, 147.0, 129.4, 122.7, 111.4, 109.8, 72.5, 71.8, 70.5, 70.3, 61.3, 42.7, 38.7, 30.2, 23.4, 2.9. HRMS (ESI+) calcd. for $C_{18}H_{27}ClNO_4$: 356.1623. Found: 356.1611 ($M+H^+$).

6-(12-azido-4,7,10-trioxa-1-azadodecan-1-yl)-1,2,3,4-tetrahydronaphthalen-1-one (11).

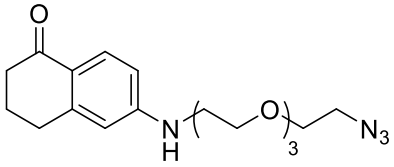

Compound **10** (420 mg, 1.2 mmol, 1 equiv.) was dissolved in dry DMF (3.2 mL). NaN_3 (92.1 mg, 1.42 mmol, 1.2 equiv.) was then slowly added. The mixture was stirred and heated under reflux for 48h. The yellowish/brownish mixture was mixed with water and extracted with EtOAc. The combined organic layers were washed with water and brine, dried over magnesium sulfate, filtered and the solvent was removed under reduced pressure. The crude was purified by silica gel chromatography (CHX/EtOAc, 5/5 to 0/10, v/v, UV) give a brown oil, **11** (397.8 mg, 93%). ^{1}H NMR (400 MHz, $CDCl_3$) δ 7.85 (d, J = 8.7 Hz, 1H), 6.45 (dd, J = 8.7, 2.4 Hz, 1H), 6.30 (d, J = 2.3 Hz, 1H), 4.75 (t, J = 5.5 Hz, 1H), 3.72 – 3.59 (m, 12H), 3.39 – 3.29 (m, 4H), 2.80 (t, J = 6.1 Hz, 2H), 2.56 – 2.48 (m, 2H), 2.03 (d, J = 6.4 Hz, 2H). ^{13}C {^{1}H} NMR (126 MHz, $CDCl_3$) δ 196.8, 152.4, 147.0, 129.5, 122.9, 111.5, 109.8, 70.7, 70.66, 70.63, 70.4, 70.0, 69.2, 50.7, 42.8, 38.8, 30.3, 23.5. IR ν_{max} (cm^{-1}): 3347, 2866, 2096 (N_3), 1585, 1281. HRMS (ESI+) calcd. for $C_{18}H_{26}N_4NaO_2$: 385.1846. Found: 385.1852 ($M+Na^+$).

3-((2-(2-(2-(2-azidoethoxy)ethoxy)ethoxy)ethyl)amino)-10-(diethylamino)-5,6-dihydrobenzo[c]xanthen-12-ium chloride (F3).

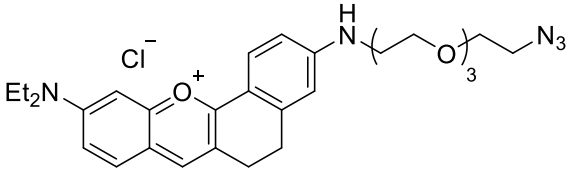

Following general procedure (A), acetyl chloride (0.9 mL, 12.5 mmol, 50 equiv.) was added to EtOH (1.2 mL, 20 mmol, 80 equiv.) and stirred at 0°C for 30 min. **11** (90.5 mg, 0.2 mmol, 1 equiv.) and 4-(diethylamino)-2-hydroxy-benzaldehyde (53.1 mg, 0.3 mmol, 1.1 equiv.) in dry EtOAc (8.6 mL) were added. The mixture was stirred for 72h and gave after purification by silica gel chromatography (DCM/MeOH, 7/3, v/v, UV) a purple solid, **F3** (95.7 mg, 68.9%). M.p. = 134-136°C. ^{1}H NMR (500 MHz, $CDCl_3$) δ 8.87 (t, J = 5.9 Hz, 1H), 7.96 (s, 1H), 7.88 (d, J = 9.0 Hz, 1H), 7.62 (d, J = 9.1 Hz, 1H), 6.97 (s, 1H), 6.90 (dd, J = 9.1, 2.4 Hz, 1H), 6.70 (dd, J = 2.6, 0.8 Hz, 1H), 3.79 (t, J = 6.0 Hz, 2H), 3.68 – 3.61 (m, 10H), 3.57 – 3.50 (m, 6H), 3.37 – 3.32 (m, 2H), 2.94 – 2.85 (m, 4H), 1.28 (t, J = 7.1 Hz, 6H). ^{13}C {^{1}H} NMR (126 MHz, $CDCl_3$) δ 165.2, 157.4, 156.7, 153.1, 142.7, 130.6, 120.9, 114.3, 114.0, 113.1, 96.1, 70.7, 70.6, 70.0, 69.4, 50.8, 45.5, 43.1, 27.9, 26.2, 12.6. IR ν_{max} (cm^{-1}): 3354, 2921, 2101 (N_3), 1601, 1095. HRMS (ESI+) calcd. for $C_{29}H_{38}N_5O_4$: 520.2918. Found: 520.2927 (M^+). Activity: IC_{50} = 1042 nM, *Pf*NF54 (**F3**).

Optical properties of F3: λ_{abs} = 594 nm, λ_{em} = 634 nm, ε = 7.49 (10^4 $M^{-1}.cm^{-1}$), Φ_{rel} = 0.265, Stokes shift = 1110 cm^{-1}, Brightness = 19850, Solvent = Water pH 7.41 (0.1 M NaCl).

1.6.3 Introduction

Synthesis of the flavylium-DBCO probe F2-DBCO.

***Tert*-butyl-(2-(2-(2-aminoethoxy)ethoxy)ethyl)carbamate (26).**

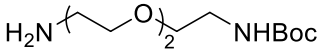

To a solution of 1,8-diamino-3,6-dioxaoctane (1 mL, 7 mmol, 6 equiv.) in DCM (7 mL) was added dropwise at 25°C, Boc_2O (254.3 mg, 1.2 mmol, 1 equiv.) in DCM (2.3 mL). The mixture was stirred for 16h at 25°C. The solvent was removed under reduced pressure and extracted with DCM. The combined organic layers were washed with $NaHCO_3$, dried over magnesium sulfate, filtered and the solvent was removed under reduced pressure. The desired product was obtained as a yellow oil, **26** (280 mg, 96.8%). ^{1}H NMR (400 MHz, $CDCl_3$) *δ* 5.15 (s, 1H), 3.58 (s, 4H), 3.50 (dt, *J* = 12.0, 5.2 Hz, 4H), 3.28 (q, *J* = 5.4 Hz, 2H), 2.84 (t, *J* = 5.2 Hz, 2H), 1.55 (s, 2H), 1.41 (s, 9H). ^{13}C {^{1}H} NMR (101 MHz, $CDCl_3$) *δ* 156.1, 79.3, 73.6, 70.3, 53.5, 41.9, 40.5, 28.5. HRMS (ESI+) calcd. for $C_{11}H_{25}N_2O_4$: 249.1809. Found: 249.1813 ($M+H^+$).

***Tert*-butyl-(2-(2-(2-((5-oxo-5,6,7,8-tetrahydronaphthalen-2-yl)amino)ethoxy)ethoxy)ethyl)carbamate (28).**

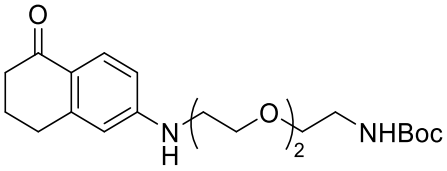

$Pd(OAc)_2$ (75 mg, 0.3 mmol, 0.1 equiv.), BINAP (310 mg, 0.5 mmol, 0.15 equiv.) and Cs_2CO_3 (1.5 g, 4.7 mmol, 1.4 equiv.) were mixed together under argon. Then a solution of **27** (1 g, 3.4 mmol, 1 equiv.) and compound **26** (1 g, 4 mmol, 1.2 equiv.) in toluene (32.9 mL) was added. The mixture was stirred at 100°C for 20h under argon. The crude was cooled down and was filtered over a celite pad, rinse with DCM and the solvent were removed under educed pressure. The crude was purified by silica gel chromatography (CHX/EtOAc, 5/5 to 0/10, v/v, UV) to afford a yellow oil, **28** (625.4 mg, 47.5%). ^{1}H NMR (400 MHz, $CDCl_3$) *δ* 7.89 (d, *J* = 8.7 Hz, 1H), 6.49 (dd, *J* = 8.6, 2.4 Hz, 1H), 6.33 (d, *J* = 2.4 Hz, 1H), 4.97 (s, 1H), 4.67 (s, 1H), 3.73 – 3.68 (m, 3H), 3.63 (d, *J* = 4.6 Hz, 4H), 3.55 (td, *J* = 5.6, 3.7 Hz, 3H), 3.40 – 3.29 (m, 4H), 2.83 (t, *J* = 6.1 Hz, 2H), 2.55 (dd, *J* = 7.2, 5.8 Hz, 2H), 2.09 – 2.02 (m, 2H), 1.44 (s, 9H). ^{13}C {^{1}H} NMR (101 MHz, $CDCl_3$) *δ* 196.9, 156.1, 147.1, 129.7, 111.5, 110.0, 70.5, 70.4, 69.4, 42.9, 38.9, 30.4, 28.5, 23.6. HRMS (ESI+) calcd. for $C_{21}H_{32}N_2O_5Na$: 415.2203. Found: 415.2192 ($M+Na^+$).

2-(2-(2-((5-oxo-5,6,7,8-tetrahydronaphthalen-2-yl)amino)ethoxy)ethoxy)ethan-1-aminium chloride (29).

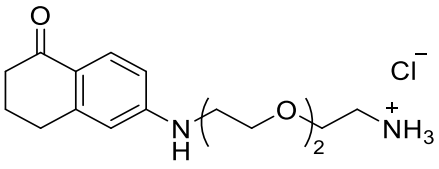

Compound **28** (625 mg, 1.6 mmol, 1 equiv.) was treated with TFA (3.8 mL, 50.7 mmol, 31.8 equiv.). The mixture was stirred for 1h at 25°C. The solvent was removed under reduced pressure, diluted and evaporated three times in MeOH and three times in $CHCl_3$. The solid was washed with ice cooled Et_2O and then dried. The desired product was obtained as a dark yellow oil, **29** (694.9 mg, quantitative). ^{1}H NMR (500 MHz, $CDCl_3$) *δ* 8.06 (s, 3H), 7.75 (d, *J* = 8.7 Hz, 1H), 6.81 (s, 2H), 6.48 (d, *J* = 8.5 Hz, 1H), 6.34 (s, 1H), 3.69 – 3.54 (m, 8H), 3.30 (t, *J* = 5.2 Hz, 2H), 3.09 (s, 2H), 2.75 (t, *J* = 6.2 Hz, 2H), 2.47 (t, *J* = 6.5 Hz, 2H), 2.03 – 1.88 (t, *J* = 6.4 Hz,

2H). ^{13}C {^{1}H} NMR (126 MHz, $CDCl_3$) δ 197.7, 152.2, 147.6, 129.5, 122.9, 112.1, 110.4, 70.0, 69.0, 66.6, 43.2, 39.6, 38.6, 30.1, 23.3. IR ν_{max} (cm^{-1}): 3356 (NH_2), 2939, 1673, 1581, 1125. HRMS (ESI+) calcd. for $C_{16}H_{25}N_2O_3$: 293.1859. Found: 293.1849 (M^+).

3-((2-(2-(2-ammonioethoxy)ethoxy)ethyl)amino)-10-(diethylamino)-5,6-dihydrobenzo[c]xanthen-12-ium chloride (30).

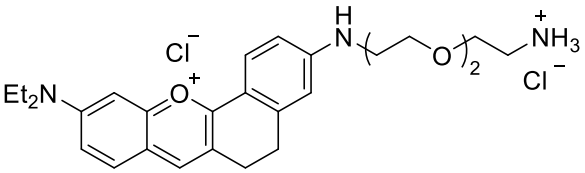

Following general procedure (A), acetyl chloride (1.8 mL, 24.6 mmol, 50 equiv.) was stirred in EtOH (2.3 mL, 39.4 mmol, 80 equiv.) at 0°C for 30 min. Compound **29** (200 mg, 0.5 mmol, 1 equiv.) and 4-(diethylamino)-2-hydroxybenzaldehyde (104.6 mg, 0.5 mmol, 1.1 equiv.) in dry EtOAc (6.7 mL) was added, stirred for 72h to give after purification by silica gel chromatography (DCM/MeOH, 10/0 to 4/6, v/v, UV) a purple solid, **30** (150.9 mg, 58.7%). M.p. = 89-91°C. ^{1}H NMR (400 MHz, MeOD) δ 8.19 (s, 1H), 8.10 (d, J = 8.9 Hz, 1H), 7.72 (d, J = 9.2 Hz, 1H), 7.20 (dd, J = 9.2, 2.5 Hz, 1H), 7.05 (dd, J = 2.6, 0.8 Hz, 1H), 6.82 (dd, J = 9.0, 2.3 Hz, 1H), 6.67 (d, J = 2.3 Hz, 1H), 3.72 – 3.64 (m, 10H), 3.53 (t, J = 5.4 Hz, 2H), 3.13 – 3.10 (m, 2H), 3.01 (s, 4H), 1.31 (t, J = 7.1 Hz, 6H). ^{13}C {^{1}H} NMR (101 MHz, $CDCl_3$) δ 166.8, 158.6, 157.5, 155.4, 145.8, 131.9, 130.7, 121.8, 116.6, 116.3, 115.0, 97.0, 71.5, 71.4, 70.4, 67.9, 58.3, 49.5, 46.4, 43.8, 40.7, 28.7, 26.8, 18.4, 12.7. IR ν_{max} (cm^{-1}): 3367 (NH_2), 2923, 1610, 1398, 1260. HRMS (ESI+) calcd. for $C_{27}H_{36}N_3O_3$: 450.2751. Found: 450.2768 (M^+).

Optical properties of 30: λ_{abs} = 593 nm, λ_{em} = 633 nm, ε = 2.37 (10^4 $M^{-1}.cm^{-1}$), Φ_{rel} = 0.22, Stokes shift = 1065 cm^{-1}, Brightness = 5258, Solvent = Water pH 7.41 (0.1 M NaCl).

8-((2-(2-(2-(6-(2-azatricyclo(10.4.0.0⁴,⁹)hexadeca-1(12),4(9),5,7,13,15-hexaen-10-yn-2-yl)-6-oxohexanamido)ethoxy)ethoxy)ethyl)amino)-3-(diethylamino) (F2-DBCO).

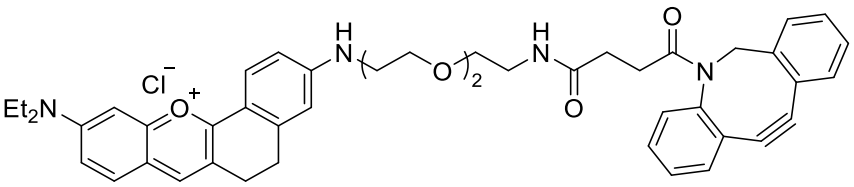

Compound **30** (30 mg, 0.06 mmol, 1.1 equiv.) and 4-(2-azatricyclo(10.4.0.0⁴,⁹)hexadeca-1(16),4,6,8,12,14-hexaen-10-yn-2-yl)-4-oxobutanoic acid (17.4 mg, 0.05 mmol, 1 equiv.) were solubilized in DMF (0.4 mL), HBTU (23.7 mg, 0.06 mmol, 1.2 equiv.) and DIPEA (0.04 mL, 0.3 mmol, 5 equiv.) were then added. The mixture was stirred at 25°C for 48h. The solvent was removed under reduced pressure and the residue was purified by silica gel chromatography (DCM/MeOH, 10/0 to 8/2, v/v, UV) to afford a purple solid, **F2-DBCO** (20.9 mg, 50%). M.p. = 125-127°C. ^{1}H NMR (400 MHz, $CDCl_3$) δ 7.99 (d, J = 8.9 Hz, 1H), 7.96 (s, 1H), 7.65 – 7.62 (m, 1H), 7.60 (d, J = 9.2 Hz, 1H), 7.52 – 7.46 (m, 2H), 7.42 – 7.32 (m, 2H), 7.33 – 7.25 (m, 2H), 7.22 (td, J = 7.0, 1.7 Hz, 1H), 6.96 (dd, J = 9.2, 2.5 Hz, 1H), 6.83 (d, J = 2.4 Hz, 1H), 6.66 (dd, J = 9.0, 2.3 Hz, 1H), 6.45 (d, J = 2.2 Hz, 1H), 5.13 (dd, J = 13.9, 4.6 Hz, 2H), 3.74 – 3.56 (m, 8H), 3.43 (d, J = 5.2 Hz, 4H), 3.31 (d, J = 5.3 Hz, 4H), 2.94 – 2.88 (m, 4H), 2.40 (ddd, J = 14.7, 8.5, 5.9 Hz, 2H), 2.18 (dt, J = 15.0, 6.1 Hz, 2H), 1.94 (dt, J = 16.9, 6.1 Hz, 2H), 1.30 (t, J = 7.2 Hz, 6H). ^{13}C {^{1}H} NMR (126 MHz, $CDCl_3$) δ 172.5, 172.4, 165.6, 162.7, 157.3, 155.9, 153.9, 151.5, 148.2, 144.5, 132.4, 131.0, 129.6, 128.9, 128.8, 128.4, 128.3, 127.9, 127.2, 125.6, 123.3, 122.5, 120.6, 115.3, 115.0, 114.8, 114.2, 108.1, 96.2, 70.7, 70.3, 69.8, 69.1, 55.7, 45.8, 43.1, 39.3, 38.8, 36.6, 31.5, 30.4, 27.8, 25.9, 12.7. HRMS (ESI+) calcd. for $C_{46}H_{49}N_4O_5$: 737.3697. Found: 737.3713 (M^+). Activity: IC_{50} = 506 nM, *Pf*NF54 (**F2-DBCO**).

Optical properties of F2-DBCO: λ_{abs} = 601 nm, λ_{em} = 633 nm, ε = 2.06 (10^4 $M^{-1}.cm^{-1}$), Φ_{rel} = 0.26, Stockes shift = 841 cm^{-1}, Brightness = 5200, Solvent = Water pH 6.9 (0.1 M NaCl).

1.6.4 Article 4

General procedure (C) for the CuAAC click reaction.

The alkyne (1 equiv.) and the azide (1 equiv.) were solubilized in MeCN (~ 0.015 M) under argon. The solution was then degassed three times with argon. Meanwhile, a fresh stock solution of $Cu(MeCN)_4BF_4$ and bathocuproin were prepared in MeCN. A mixture of 0.1 equivalent of copper(I)/ligand was added with a final concentration of MeCN not exceeding 0.01 M. The conversion was followed by TLC and if needed additional portions of copper(I)/ligand were added until completion of the reaction. The mixture was stirred at 25°C under argon until full conversion, then evaporated and purified by silica gel chromatography using the adequate eluent system to afford the targeted click adduct.

Synthesis of flavylium-PEG-1-bMD systems F1-10 and F1-1.

10-(diethylamino)-3-((2-(2-(4-(4-(1,4-dimethoxy-3-methyl-2-naphthoyl)phenyl)-1H-1,2,3-triazol-1-yl)ethoxy)ethyl)amino)-5,6-dihydrobenzo[c]xanthen-12-ium chloride (F1-10).

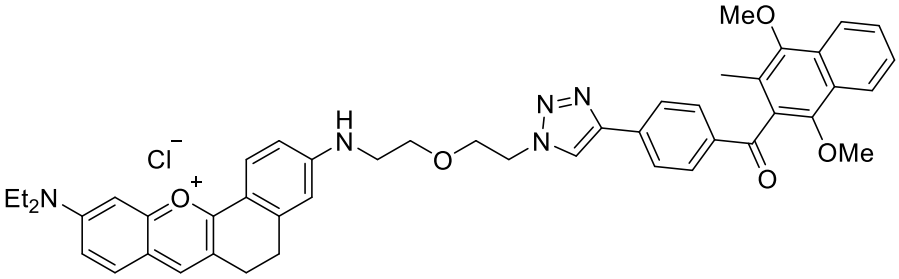

Following general procedure (C), compound **10** (40 mg, 0.1 mmol, 1 equiv.) and compound **F1** (50 mg, 0.1 mmol, 1 equiv.) were solubilized in MeCN (~ 0.015 M), then 0.2 equivalent in total of copper ($Cu(MeCN)_4BF_4$) and ligand (bathocuproin) were added. The mixture was stirred for 16h at 25°C under argon in the dark and gave after purification by silica gel chromatography (DCM/MeOH, 10/0 to 90/10, v/v, UV) a purple solid **F1-10** (46 mg, 53.9%). M.p. = 146-148°C. ^{1}H NMR (400 MHz, $CDCl_3$) δ 8.29 (s, 1H), 8.29 (s, 1H), 8.16 – 8.07 (m, 1H), 8.07 – 7.98 (m, 1H), 7.89 (d, *J* = 8.3 Hz, 2H), 7.84 – 7.73 (m, 3H), 7.62 – 7.44 (m, 3H), 6.88 (dd, *J* = 9.2, 2.4 Hz, 1H), 6.77 (d, *J* = 2.3 Hz, 1H), 6.69 – 6.59 (m, 2H), 6.44 (s, 1H), 4.62 (t, *J* = 5.0 Hz, 2H), 3.91 (t, *J* = 5.0 Hz, 2H), 3.89 (s, 3H), 3.78 (s, 3H), 3.68 (t, *J* = 5.0 Hz, 2H), 3.53 (q, *J* = 7.1 Hz, 4H), 3.37 (q, *J* = 5.2 Hz, 2H), 2.83 – 2.69 (m, 4H), 2.17 (s, 3H), 1.26 (t, *J* = 7.1 Hz, 6H). ^{13}C {^{1}H} NMR (101 MHz, $CDCl_3$) δ 196.9, 165.4, 156.9, 156.3, 153.6, 150.5, 149.2, 146.3, 143.8, 136.4, 136.3, 131.1, 130.7, 130.2, 129.4, 127.25, 127.20, 126.2, 125.9, 123.6, 123.1, 122.7, 122.5, 120.5, 114.8, 114.6, 113.6, 96.1, 69.0, 63.6, 61.7, 50.2, 45.6, 42.9, 27.5, 25.9, 12.9, 12.6. HRMS (ESI+) calcd. for $C_{47}H_{48}O_5N_5$: 762.3650. Found: 762.3629 (M^+). Activity: IC_{50} = 241 nM, *Pf*NF54 (**F1-10**).

Optical properties of F1-10: λ_{abs} = 608 nm, λ_{em} = 639 nm, ε = 3.71 (10^4 $M^{-1}.cm^{-1}$), Φ_{rel} = 0.23, Stockes shift = 800 cm^{-1}, Brightness = 8600, Solvent = Water pH 7.41 (0.1 M NaCl) + 10% DMSO.

10-(diethylamino)-3-((2-(2-(4-(4-(3-methyl-1,4-dioxo-1,4-dihydronaphthalene-2-carbonyl)phenyl)-1H-1,2,3-triazol-1-yl)ethoxy)ethyl)amino)-5,6-dihydrobenzo[c]xanthen-12-ium chloride (F1-1).

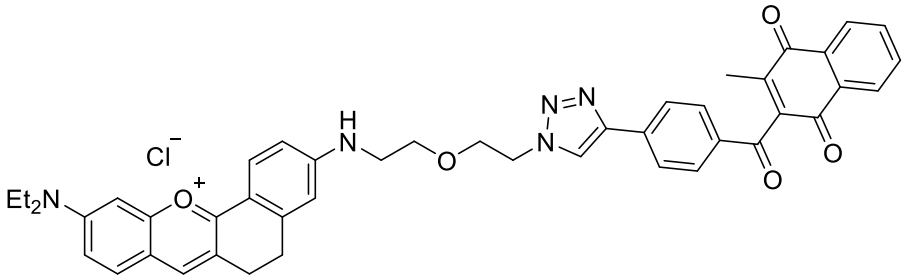

Following general procedure (C), **probe 1** (18 mg, 0.06 mmol, 1 equiv.) and compound **F1** (27 mg, 0.06 mmol, 1 equiv.) were solubilized in MeCN (~ 0.015 M), then a 0.2 equivalent in total of copper ($Cu(MeCN)_4BF_4$) and ligand (bathocuproin) were added. The mixture was stirred for 16h at 25°C under argon in the dark and gave after purification by silica gel chromatography (DCM/MeOH, 10/0 to 90/10, v/v, UV) a purple solid **F1-1** (20.6 mg, 46.5%). M.p. = 129-131°C. ^{1}H NMR (400 MHz, $CDCl_3$) δ 8.37 (s, 1H), 8.20 – 8.13 (m, 1H), 8.08 – 8.00 (m, 1H), 7.93 (d, *J* = 8.2 Hz, 2H), 7.83 (s, 1H), 7.78 (dd, *J* = 7.2, 3.1 Hz, 3H), 7.61 (s, 1H), 7.52 (d, *J* = 9.1 Hz, 1H), 6.92 (dd, *J* = 9.1, 2.4 Hz, 1H), 6.84 (d, *J* = 2.3 Hz, 1H), 6.67 – 6.56 (m, 2H), 6.36 (s, 1H), 4.60 (t, *J* = 5.0 Hz, 2H), 3.94 (t, *J* = 4.9 Hz, 2H), 3.71 (t, *J* = 4.9 Hz, 2H), 3.55 (q, *J* = 7.1 Hz, 4H), 3.39 (q, *J* = 5.3 Hz, 2H), 2.82 (t, *J* = 7.5 Hz, 2H), 2.68 (d, *J* = 7.7 Hz, 2H), 2.01 (s, 3H), 1.28 (t, *J* = 7.1 Hz, 6H). ^{13}C {^{1}H} NMR (126 MHz, $CDCl_3$) δ 193.3, 184.8, 183.7, 165.5, 156.9, 156.4, 153.6, 145.9, 144.5, 144.0, 143.5, 137.2, 134.5, 134.4, 134.3, 132.1, 131.7, 130.6, 129.8, 126.9, 126.4, 126.1, 123.5, 120.7, 114.7, 114.5, 113.6, 96.4, 69.3, 68.7, 50.2, 45.6, 42.8, 27.6, 25.9, 13.7, 12.6. HRMS (ESI+) calcd. for $C_{45}H_{42}O_5N_5$: 732.3180. Found: 732.3166 (M^+). Activity: IC_{50} = 396 nM, *Pf*NF54 (**F1-1**).

Optical properties of F1-1: λ_{abs} = 601 nm, λ_{em} = 633 nm, ε = 2.28 (10^4 $M^{-1}.cm^{-1}$), Φ_{rel} = 0.013, Stokes shift = 840 cm^{-1}, Brightness = 300, Solvent = Water pH 7.41 (0.1 M NaCl) + 10% DMSO.

Synthesis of flavylium-PEG-2-bMD systems F2-10 and F2-1.

2-methyl-3-(4-(1-(2-(2-(2-((5-oxo-5,6,7,8-tetrahydronaphthalen-2-yl)amino)ethoxy)ethoxy)ethyl)-1H-1,2,3-triazol-4-yl)benzoyl)naphthalene-1,4-dione (3).

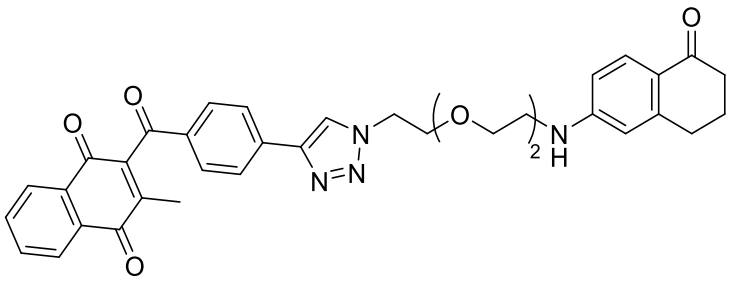

Following general procedure (C**), probe 1** (30 mg, 0.1 mmol, 1 equiv.) and **2** (32 mg, 0.1 mmol, 1 equiv.) were solubilized in MeCN (~ 0.015 M). 1 equivalent in total of copper ($Cu(MeCN)_4BF_4$) and ligand (bathocuproin) were then added. The mixture was stirred for 48h at 25°C under argon and gave after purification by silica gel chromatography (DCM, UV) a brown solid **3** (60 mg, 97.1%). M.p. = 145-147°C. ^{1}H NMR (400 MHz, $CDCl_3$) δ 8.18 – 8.12 (m, 1H), 8.06 – 8.00 (m, 2H), 7.92 (s, 4H), 7.83 (d, *J* = 8.6 Hz, 1H), 7.80 – 7.69 (m, 2H), 6.43 (dd, *J* = 8.6, 2.4 Hz, 1H), 6.27 (d, *J* = 2.3 Hz, 1H), 4.58 (dd, *J* = 5.5, 4.5 Hz, 2H), 3.91 (dd, *J* = 5.5, 4.4 Hz, 2H), 3.68 – 3.53 (m, 6H), 3.30 (d, *J* = 5.0 Hz, 2H), 2.78 (t, *J* = 6.1 Hz, 2H), 2.51 (dd, *J* = 7.2, 5.8 Hz, 2H), 2.05 (s, 3H), 2.04 – 1.97 (m, 2H). ^{13}C {^{1}H} NMR (101 MHz, $CDCl_3$) δ 196.8, 193.1, 184.8, 183.5, 152.2, 147.1, 144.3, 144.1, 136.6, 135.0, 134.3, 134.2, 131.9, 131.6, 129.9, 129.6, 126.8, 126.5, 126.1, 123.2, 122.3, 111.5, 109.9, 70.6, 70.3, 69.4, 69.3, 50.5, 42.7, 38.8, 30.3, 23.5, 13.7. HRMS (ESI+) calcd. for $C_{36}H_{35}N_4O_6$: 619.2551. Found: 619.2543 ($M+H^+$).

10-(diethylamino)-3-((2-(2-(2-(4-(4-(3-methyl-1,4-dioxo-1,4-dihydronaphthalene-2-carbonyl)phenyl)-1H-1,2,3-triazol-1-yl)ethoxy)ethoxy)ethyl)amino)-5,6-dihydrobenzo[c]xanthen-12-ium chloride (F2-1).

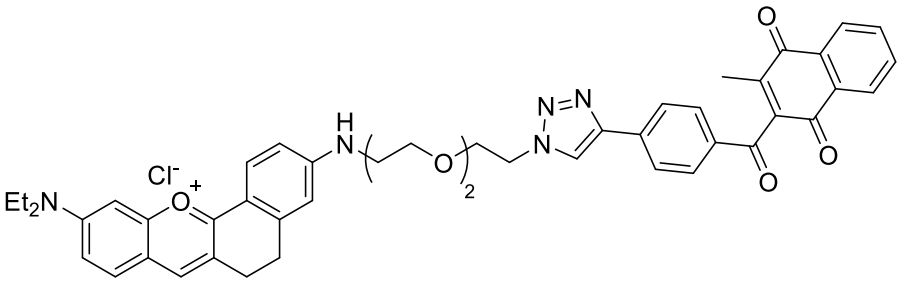

Following general procedure (A), acetyl chloride (0.12 mL, 1.6 mmol, 50 equiv.) and EtOH (0.15 mL, 2.6 mmol, 80 equiv.) were stirred at 0°C for 30 min. **4** (20 mg, 0.03 mmol, 1 equiv.) and 4-(diethylamino)-2-hydroxybenzaldehyde (8 mg, 0.03 mmol, 1.1 equiv.) in dry EtOAc (0.44 mL) were added. The mixture was stirred 72h at 25°C and gave after purification by silica gel chromatography (DCM/MeOH, 99/1, v/v, UV) a dark blue solid, **F2-1** (18.7 mg, 71.2%). M.p. = 166-168°C. ^{1}H NMR (400 MHz, $CDCl_3$) δ 8.37 (s, 1H), 8.17 – 8.11 (m, 1H), 8.02 – 7.97 (m, 1H), 7.96 – 7.84 (m, 4H), 7.80 (d, *J* = 8.7 Hz, 2H), 7.76 (ddd, *J* = 6.8, 4.8, 1.8 Hz, 2H), 7.62 – 7.57 (m, 1H), 7.54 (d, *J* = 9.2 Hz, 1H), 6.92 (dd, *J* = 9.2, 2.4 Hz, 1H), 6.81 (d, *J* = 2.4 Hz, 1H), 6.65 (dd, *J* = 9.0, 2.3 Hz, 1H), 6.52 (t, *J* = 5.5 Hz, 1H), 6.46 (s, 1H), 4.62 (t, *J* = 5.2 Hz, 2H), 3.95 (t, *J* = 5.2 Hz, 2H), 3.74 – 3.60 (m, 6H), 3.55 (q, *J* = 7.2 Hz, 4H), 3.37 (q, *J* = 5.4 Hz, 2H), 2.93 – 2.77 (m, 4H), 2.00 (s, 3H), 1.29 (t, *J* = 7.2 Hz, 6H). ^{13}C {^{1}H} NMR (101 MHz, $CDCl_3$) δ 193.2, 184.9, 183.6, 165.6, 157.0, 156.3, 153.6, 146.1, 144.5, 144.0, 143.8, 137.2, 134.6, 134.4, 134.3, 132.0, 131.6, 130.7, 129.9, 129.7, 129.2, 126.8, 126.4, 126.1, 123.3, 120.7, 114.9, 114.6, 113.8, 96.3, 70.5, 70.4, 69.3, 68.9, 50.3, 45.7, 43.2, 27.7, 26.3, 25.9, 13.7, 12.6. HRMS (ESI+) calcd. for $C_{47}H_{46}N_5O_6$: 776.3443. Found: 776.3435 (M^+). Activity: IC_{50} = 314 nM, *Pf*NF54 (**F2-1**).

Optical properties of F2-1: λ_{abs} = 605 nm, λ_{em} = 640 nm, ε = 4.37 (10^4 $M^{-1}.cm^{-1}$), Φ_{rel} = 0.022, Stokes shift = 900 cm^{-1}, Brightness = 1000, Solvent = Water pH 7.41 (0.1 M NaCl) + 10% DMSO.

6-((2-(2-(2-(4-(4-((1,4-dimethoxy-3-methylnaphthalen-2-yl)methyl)phenyl)-1H-1,2,3-triazol-1-yl)ethoxy)ethoxy)ethyl)amino)-3,4-dihydronaphthalen-1(2H)-one (4).

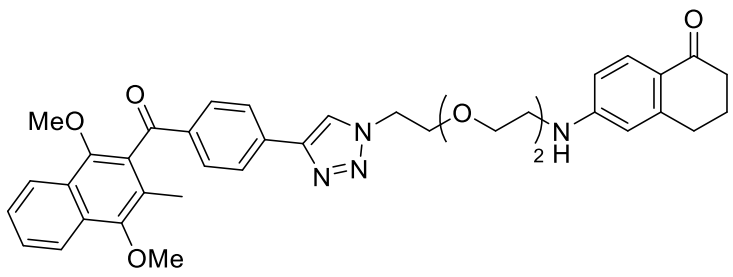

Following general procedure (C), compound **10** (30 mg, 0.1 mmol, 1 equiv.) and compound **2** (28.9 mg, 0.1 mmol, 1 equiv.) were solubilized in MeCN (~ 0.015 M). 1 equivalent in total copper ($Cu(MeCN)_4BF_4$) and ligand (bathocuproin) were then added. The mixture was stirred for 16h at 25°C under argon and gave after purification by silica gel chromatography (DCM, UV) a white solid **4** (44 mg, 74.7%). M.p. = 112-114°C. ^{1}H NMR (400 MHz, $CDCl_3$) δ 8.19 – 8.02 (m, 2H), 7.99 (s, 1H), 7.93 – 7.80 (m, 5H), 7.63 – 7.46 (m, 2H), 6.45 (dd, *J* = 8.6, 2.4 Hz, 1H), 6.27 (d, *J* = 2.4 Hz, 1H), 4.65 – 4.53 (m, 3H), 3.94 – 3.87 (m, 5H), 3.81 (s, 3H), 3.65 – 3.54 (m, 6H), 3.30 (q, *J* = 5.2 Hz, 2H), 2.79 (t, *J* = 6.1 Hz, 2H), 2.52 (dd, *J* = 7.2, 5.8 Hz, 2H), 2.22 (s, 3H), 2.02 (dd, *J* = 5.6, 1.9 Hz, 2H). ^{13}C {^{1}H} NMR (101 MHz, $CDCl_3$) δ 196.8, 152.2, 150.5, 149.3, 147.1, 146.6, 136.8, 135.9, 131.0, 130.4, 129.6, 129.5, 127.3, 127.2, 126.1, 125.8, 123.7, 123.2, 122.7, 122.5, 122.0, 111.5, 110.0, 70.6, 70.3, 69.5, 69.4, 63.7, 61.6, 50.5, 42.8, 38.9, 30.3, 23.5, 12.9. HRMS (ESI+) calcd. for $C_{38}H_{41}N_4O_6$: 649.3021. Found: 649.3020 ($M+H^+$).

10-(diethylamino)-3-((2-(2-(2-(4-(4-(1,4-dimethoxy-3-methyl-2-naphthoyl)phenyl)-1H-1,2,3-triazol-1-yl)ethoxy)ethoxy)ethyl)amino)-5,6-dihydrobenzo[c]xanthen-12-ium chloride (F2-10).

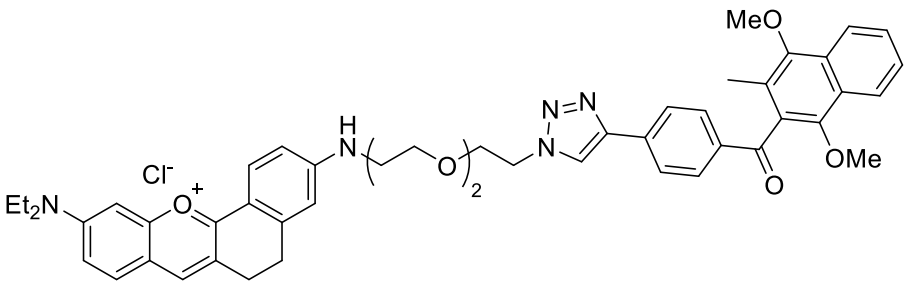

Following general procedure (A), acetyl chloride (0.16 mL, 2.3 mmol, 50 equiv.) and EtOH (0.2 mL, 3.7 mmol, 80 equiv.) were stirred at 0°C for 30 min. Compound **3** (30 mg, 0.05 mmol, 1 equiv.) and 4-(diethylamino)-2-hydroxybenzaldehyde (9 mg, 0.05 mmol, 1.1 equiv.) in dry EtOAc (0.63 mL) were added. The mixture was stirred for 72h and gave after purification by silica gel chromatography (DCM/MeOH, 99/1, v/v, UV) a dark purple solid, **F2-10** (25.9 mg, 66.3%). M.p. = 112-114°C. HRMS (ESI+) calcd. for $C_{49}H_{52}N_5O_6$: 806.3912. Found: 806.3915 (M^+). NMR gives no results because of its low resolution and the high line-broadening. Activity: IC_{50} = 331 nM, *Pf*NF54 (**F2-10**).

Optical properties of F2-10: λ_{abs} = 603 nm, λ_{em} = 639 nm, ε = 4.32 (10^4 $M^{-1}.cm^{-1}$), Φ_{rel} = 0.3, Stokes shift = 935 cm^{-1}, Brightness = 13000, Solvent = Water pH 7.41 (0.1 M NaCl) + 10% DMSO.

Synthesis of flavylium-PEG-3-bMD systems F3-10 and F3-1.

6-((2-(2-(2-(2-(4-(4-(1,4-dimethoxy-3-methyl-2-naphthoyl)phenyl)-1H-1,2,3-triazol-1-yl)ethoxy)ethoxy)ethoxy)ethyl)amino)-3,4-dihydronaphthalen-1(2H)-one (7).

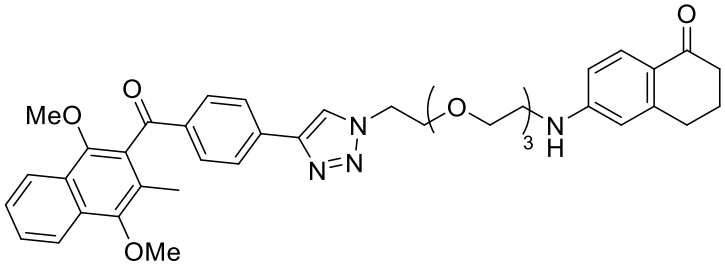

Following general procedure (C), compound **10** (33.1 mg, 0.1 mmol, 1 equiv.) and compound **5** (40 mg, 0.1 mmol, 1 equiv.) were solubilized in MeCN (~ 0.015 M). 0.3 equivalent in total copper ($Cu(MeCN)_4BF_4$) and ligand (bathocuproin) were then added. The mixture was stirred for 16h at 25°C under argon, evaporated, extracted in DCM. The combined organic phases were washed with water and brine twice, dried over magnesium sulfate, filtered and the solvent was removed under reduced pressure. The crude mixture was engaged in the next reaction without further purification.

10-(diethylamino)-3-((2-(2-(2-(2-(4-(4-(1,4-dimethoxy-3-methyl-2-naphthoyl)phenyl)-1H-1,2,3-triazol-1-yl)ethoxy)ethoxy)ethoxy)ethyl)amino)-5,6-dihydrobenzo[c]xanthen-12-ium chloride (F3-10).

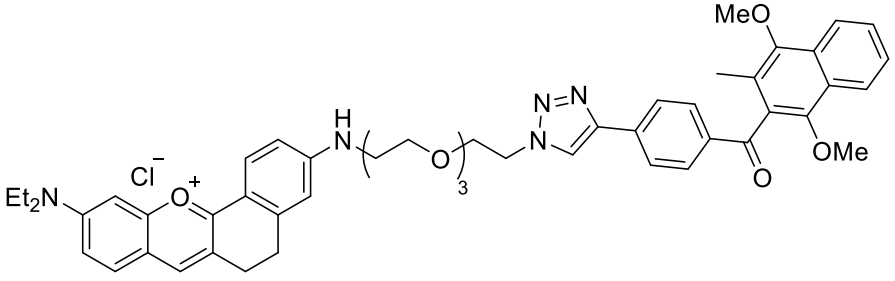

Following general procedure (A), acetyl chloride (0.4 mL, 6 mmol, 50 equiv.) and EtOH (0.48 mL, 9.6 mmol, 80 equiv.) were stirred at 0°C for 30 min. **7** (83.2 mg, 0.1 mmol, 1 equiv.) and 4-(diethylamino)-2-hydroxybenzaldehyde (25.5 mg, 0.1 mmol, 1.1 equiv.) in dry EtOAc (1.6 mL) were added. The mixture was stirred for 72h and gave after purification

by silica gel chromatography (DCM/MeOH, 10/0 to 7/3, v/v, UV) a purple powder, **F3-10** (33.5 mg, 31.4%). M.p. = 127-129°C. ^{1}H NMR (500 MHz, $CDCl_3$) δ 8.34 (s, 1H), 8.22 (t, *J* = 5.8 Hz, 1H), 8.12 (dt, *J* = 8.5, 1.0 Hz, 1H), 8.05 (dt, *J* = 8.2, 1.0 Hz, 1H), 7.97 – 7.87 (m, 3H), 7.86 – 7.78 (m, 3H), 7.63 – 7.48 (m, 4H), 6.89 (ddd, *J* = 12.8, 9.1, 2.5 Hz, 1H), 6.72 (dd, *J* = 10.8, 2.4 Hz, 1H), 4.62 (t, *J* = 5.0 Hz, 2H), 3.96 – 3.91 (m, 2H), 3.89 (s, 3H), 3.79 (s, 3H), 3.74 (t, *J* = 5.6 Hz, 2H), 3.65 – 3.60 (m, 8H), 3.54 – 3.50 (m, 4H), 3.43 (q, *J* = 5.7 Hz, 2H), 2.90 – 2.78 (m, 4H), 2.20 (s, 3H), 1.27 (t, *J* = 7.2 Hz, 6H). ^{13}C {^{1}H} NMR (126 MHz, $CDCl_3$) δ 196.9, 165.3, 157.1, 156.8, 156.7, 153.2, 150.5, 149.2, 146.3, 142.8, 136.4, 136.3, 131.1, 130.6, 130.2, 129.4, 127.3, 127.2, 126.1, 125.9, 123.7, 122.9, 122.7, 122.5, 120.8, 114.4, 114.1, 113.2, 96.2, 70.7, 70.69, 70.65, 70.59, 70.55, 70.51, 70.1, 69.4, 69.1, 63.6, 63.2, 61.6, 50.8, 50.4, 45.5, 43.2, 27.8, 26.1, 15.4, 12.9, 12.6. HRMS (ESI+) calcd. for $C_{51}H_{56}N_5O_7$: 850.4174. Found: 850.4150 (M^+). Activity: IC_{50} = 318 nM, *Pf*NF54 (**F3-10**).

Optical properties of F3-10: λ_{abs} = 602 nm, λ_{em} = 639 nm, ε = 4.64 (10^4 $M^{-1}.cm^{-1}$), Φ_{rel} = 0.29, Stokes shift = 960 cm^{-1}, Brightness = 13600, Solvent = Water pH 7.41 (0.1 M NaCl) + 10% DMSO.

2-methyl-3-(4-(1-(2-(2-(2-(2-((5-oxo-5,6,7,8-tetrahydronaphthalen-2-yl)amino)ethoxy)ethoxy)ethoxy)ethyl)-1H-1,2,3-triazol-4-yl)benzoyl)naphthalene-1,4-dione (6).

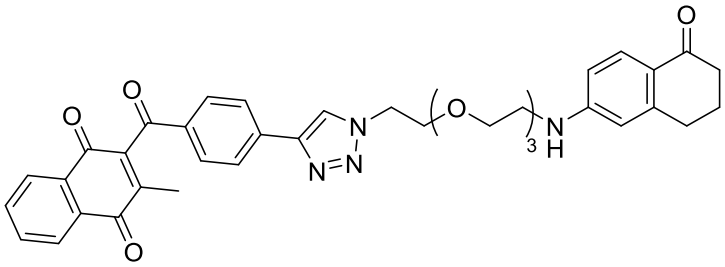

Following general procedure (C), **probe 1** (36.5 mg, 0.1 mmol, 1 equiv.) and compound **5** (40 mg, 0.1 mmol, 1 equiv.) were solubilized in MeCN (~ 0.015 M). 0.3 equivalent in total copper ($Cu(MeCN)_4BF_4$) and ligand (bathocuproin) were then added. The mixture was stirred for 16h at 25°C under argon, evaporated, extracted in DCM. The combined organic phases were washed with water and brine twice, dried over magnesium sulfate, filtered and the solvent was removed under reduced pressure. The crude mixture was engaged in the next reaction without any further purification.

10-(diethylamino)-3-((2-(2-(2-(2-(4-(4-(3-methyl-1,4-dioxo-1,4-dihydronaphthalene-2-carbonyl)phenyl)-1H-1,2,3-triazol-1-yl)ethoxy)ethoxy)ethoxy)ethyl)amino)-5,6-dihydrobenzo[c]xanthen-12-ium chloride (F3-1).

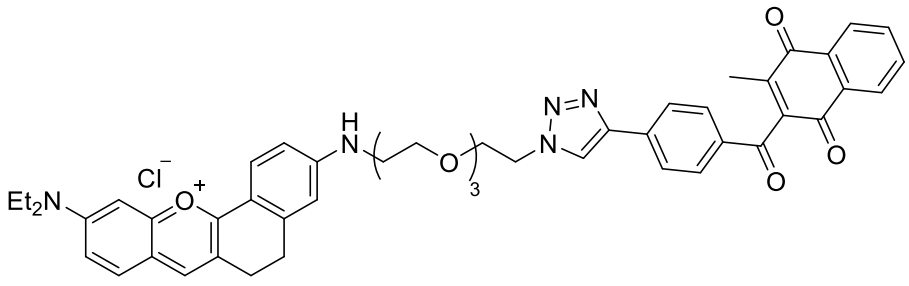

Following general procedure (A), acetyl chloride (0.6 mL, 5.3 mmol, 50 equiv.) and EtOH (0.5 mL, 8.5 mmol, 80 equiv.) were stirred at 0°C for 30 min. **6** (70.9 mg, 0.1 mmol, 1 equiv.) and 4-(diethylamino)-2-hydroxybenzaldehyde (22.7 mg, 0.1 mmol, 1.1 equiv.) in dry EtOAc (1.5 mL) were added. The mixture was stirred for 72h and gave after purification by silica gel chromatography (DCM/MeOH, 10/0 to 7/3, v/v, UV) a purple powder, **F3-1** (36.2 mg, 39.4%). M.p. = 120-122°C. ^{1}H NMR (500 MHz, $CDCl_3$) δ 8.80 (t, *J* = 5.6 Hz, 1H), 8.50 (s, 1H), 8.14 – 8.09 (m, 1H), 8.02 – 7.98 (m, 1H), 7.97 – 7.89 (m, 3H), 7.88 – 7.82 (m, 3H), 7.80 – 7.71 (m, 3H), 7.52 (d, *J* = 9.1 Hz, 1H), 6.87 (dd, *J* = 9.1, 2.4 Hz, 1H), 6.72 (d, *J* = 2.4 Hz, 1H), 4.65 (t, *J* = 5.0 Hz, 2H), 3.94 (t, *J* = 5.0 Hz, 2H), 3.74 (t, *J* = 5.7 Hz, 2H), 3.65 – 3.59 (m, 8H), 3.54 – 3.49 (m, 4H), 3.43 (q, *J* = 5.6 Hz, 2H), 2.88 – 2.75 (m, 4H), 2.00 (s, 3H), 1.26 (t, *J* = 7.1 Hz, 6H). ^{13}C {^{1}H} NMR (126 MHz, $CDCl_3$) δ 193.1, 184.8, 183.5,

165.2, 157.2, 156.6, 153.1, 145.9, 144.4, 143.9, 142.5, 137.2, 134.6, 134.3, 134.2, 131.9, 131.6, 130.4, 129.8, 126.8, 126.4, 126.1, 123.4, 120.8, 114.2, 113.9, 113.0, 96.3, 70.6, 70.5, 70.4, 69.4, 69.1, 50.4, 45.5, 43.2, 27.7, 26.1, 13.7, 12.6. HRMS (ESI+) calcd. for $C_{49}H_{50}N_5O_7$: 820.3704. Found: 820.3736 (M^+). Activity: IC_{50} = 296 nM, *Pf*NF54 (**F3-1**).

Optical properties of F3-1: λ_{abs} = 604 nm, λ_{em} = 637 nm, ε = 3.63 (10^4 $M^{-1}.cm^{-1}$), Φ_{rel} = 0.067, Stockes shift = 860 cm^{-1}, Brightness = 2400, Solvent = Water pH 7.41 (0.1 M NaCl) + 10% DMSO.

1.7 Chapitre IV:

1.7.1 Article 5

Synthesis of precursors.

2-(azidomethyl)-1,4-dimethoxy-3-methylnaphthalene (1).

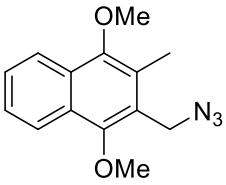

Compound 2-(chloromethyl)-1,4-dimethoxy-3-methylnaphthalene (500 mg, 2 mmol, 1 equiv.) was dissolved in dry DMF (9.9 mL) under argon. Sodium azide (389 mg, 6 mmol, 3 equiv.) was then slowly added. The reaction mixture was stirred for 16h under argon at 70°C under reflux. The mixture was mixed with water and extracted with ethyl acetate. The aqueous phase was extracted three times with ethyl acetate, dried over magnesium sulphate and the solvent was removed under vacuum. The crude was purified by silica gel chromatography (CHX/EtOAc, 95/5, v/v, UV) to **1** as a colorless oil (501.5 mg, 97.7%). ^{1}H NMR (400 MHz, $CDCl_3$) *δ* 8.12 – 8.07 (m, 2H), 7.57 – 7.47 (m, 2H), 4.63 (s, 2H), 3.97 (s, 3H), 3.89 (s, 3H), 2.48 (s, 3H). ^{13}C {^{1}H} NMR (101 MHz, $CDCl_3$) *δ* 151.9, 150.6, 129.3, 127.1, 126.9, 126.4, 125.9, 124.1, 123.0, 122.5, 63.6, 61.6, 46.9, 12.5. IR ν_{max} (cm^{-1}): 2937.05, 2089.76 (N_3), 1679.04. HRMS (ESI+) calcd. for $C_{14}H_{15}N_3NaO_2$: 280.1056. Found: 280.1052 ($M+Na^+$).

2-(azidomethyl)-3-methyl-1,4-dihydronaphthalene-1,4-dione (9).

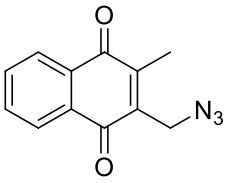

Compound **1** (1.5 g, 5.8 mmol, 1 equiv.) was solubilized in acetonitrile (70 mL). A solution of CAN (7 g, 12.8 mmol, 2.2 equiv.) prepared in water (23.4 mL) was then added, and the mixture was stirred at 25°C for 1h The organic solvent was removed under reduced pressure, then extracted three times with DCM, washed with water, dried over magnesium sulphate, and the solvent was removed under vacuum. The desired product **9** was obtained as a yellow solid (1.24 g, 93.6%). M.p. 97-99°C. ^{1}H NMR (400 MHz, $CDCl_3$) *δ* 8.20 – 7.98 (m, 2H), 7.79 – 7.65 (m, 2H), 4.39 (s, 2H), 2.26 (s, 3H). ^{13}C {^{1}H} NMR (101 MHz, $CDCl_3$) *δ* 185.0, 184.1, 146.9, 139.5, 134.04, 134.01, 132.1, 131.7, 126.7, 126.7, 45.4, 13.1. IR ν_{max} (cm^{-1}): 3303.31, 2088.55 (N_3), 1656.76. HRMS (ESI+) calcd. for $C_{12}H_9N_3NaO_2$: 250.0587. Found: 250.0589 ($M+Na^+$).

1,4-dimethoxy-3-methyl-2-naphthaldehyde (3).

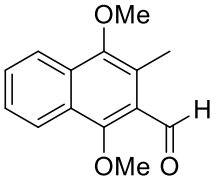

Compound 1,4-dimethoxy-2-methyl-naphthalene (1 g, 4.9 mmol, 1 equiv.) was dissolved in dichloromethane (7 mL) at 0°C under argon. Titanium tetrachloride (0.6 mL, 5.4 mmol, 1.1 equiv.) was then added slowly under argon, followed by dichloromethyl methyl ether (0.5 mL, 5.4 mmol, 1.1 equiv.). The brown mixture was

stirred under argon at 0°C for 2h. The reaction was then carefully quenched with water, and the mixture was stirred for 10 min until it turned white/green. The crude was extracted with ethyl acetate, washed with brine, dried over magnesium sulphate, filtered and evaporated. The desired compound **3** was obtained quantitatively (1.15 g, 100%) as a yellow green solid. ^{1}H NMR (400 MHz, $CDCl_3$) δ 10.73 (s, 1H), 8.26 – 8.04 (m, 2H), 7.77 – 7.47 (m, 2H), 4.07 (s, 3H), 3.87 (s, 3H), 2.65 (s, 3H). IR ν_{max} (cm^{-1}): 2935.92, 1681.69 (C=O), 1347.22. HRMS (ESI+) calcd. for $C_{14}H_{15}O_3$: 231.1016. Found: 231.1018 ($M+H^+$). In agreement with a previously published method[163].

1-(1,4-dimethoxy-3-methylnaphthalen-2-yl)-3-(trimethylsilyl)prop-2-yn-1-ol (4).

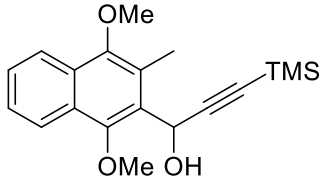

Trimethylsilylacetylene (0.22 mL, 1.5 mmol, 1.8 equiv.) was solubilized in anhydrous THF (4.3 mL) under argon in a dry balloon, then butyllithium (0.8 mL, 1.3 mmol, 1.5 equiv.) was added dropwise at 0°C. The resulting mixture was stirred at 0°C for 30 min. **3** (200 mg, 0.9 mmol, 1 equiv.) was dissolved in anhydrous THF (4.35 mL) and the alkyne was added to this mixture, which was then stirred to 25°C for 2h. The mixture was quenched with water and extracted three times with EtOAc, dried over magnesium sulphate. The solvent was then removed under vacuum. The desired product **4** was obtained in pure and quantitative form as a yellow oil. ^{1}H NMR (400 MHz, $CDCl_3$) δ 8.12 – 8.00 (m, 2H), 7.57 – 7.45 (m, 2H), 5.98 (d, J = 5.2 Hz, 1H), 4.07 (s, 3H), 3.88 (s, 3H), 2.59 (s, 3H), 0.16 (s, 9H). ^{13}C {^{1}H} NMR (101 MHz, $CDCl_3$) δ 150.7, 150.2, 129.9, 128.8, 127.1, 126.6, 125.8, 125.4, 122.5, 105.9, 90.5, 63.2, 61.5, 60.1, 12.4. HRMS (ESI+) calcd. for $C_{19}H_{24}KO_3Si$: 367.1126. Found: 367.1140 ($M+K^+$).

(3-(1,4-dimethoxy-3-methylnaphthalen-2-yl)prop-1-yn-1-yl)trimethylsilane (5).

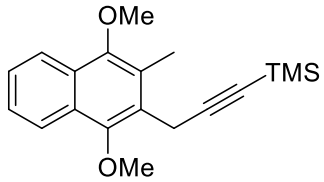

To a solution of **4** (50 mg, 0.15 mmol, 1 equiv.) in DCM (3 mL) at 0°C were successively added triethylsilane (37 µL, 0.2 mmol, 1.5 equiv.) and $BF_3.Et_2O$ (29 µL, 0.2 mmol, 1.5 equiv.). The mixture was stirred at 0°C for 30 min. The dark red mixture was quenched with water and the crude was extracted three times with DCM, dried over magnesium sulphate, and the solvent was removed under vacuum. The desired product **5** was obtained in pure and quantitative form as a dark yellow oil (42.4 mg, 89.1%). ^{1}H NMR (400 MHz, $CDCl_3$) δ 8.10 – 8.06 (m, 2H), 7.51 – 7.45 (m, 2H), 3.99 (s, 3H), 3.90 (s, 3H), 3.80 (s, 2H), 2.53 (s, 3H), 0.12 (s, 9H). ^{13}C {^{1}H} NMR (101 MHz, $CDCl_3$) δ 150.3, 149.8, 128.1, 127.3, 126.8, 126.5, 126.1, 125.6, 122.5, 122.3, 104.8, 84.9, 62.7, 61.6, 18.3, 12.5. HRMS (ESI+) calcd. for $C_{19}H_{24}KO_2Si$: 351.1177. Found: 351.1195 ($M+K^+$).

1,4-dimethoxy-2-methyl-3-(prop-2-yn-1-yl)naphthalene (2).

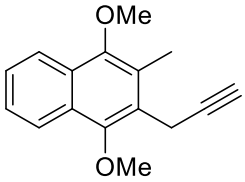

To a solution of **5** (35 mg, 0.1 mmol, 1 equiv.) dissolved in methanol (0.9 mL), was added K_2CO_3 (77.4 mg, 0.56 mmol, 5 equiv.). The mixture was stirred at 25°C for 3h. The dark mixture was filter, rinsed with DCM and evaporated. The crude was extracted three times with DCM and water, dried over magnesium sulphate, solvent was removed under vacuum. The crude was purified by silica gel chromatography (CHX/DCM, 6/4, v/v, UV) to afford **2** as a yellow oil (17.4 mg, 64.6%). ^{1}H NMR (400 MHz, $CDCl_3$) δ 8.11 – 8.01 (m, 2H), 7.55 – 7.45 (m, 2H), 3.99 (s, 3H), 3.89 (s, 3H), 3.76 (d, J = 2.7 Hz, 2H), 2.53 (s, 3H), 2.01 (t, J = 2.7 Hz, 1H). ^{13}C {^{1}H} NMR (101 MHz, $CDCl_3$) δ 150.5, 149.9, 128.2, 127.3, 126.6, 126.2, 126.1, 125.7, 122.5, 122.3, 82.5, 68.7, 62.7, 61.6, 16.8, 12.4. HRMS (ESI) calcd. for $C_{16}H_{16}O_2$: 240.1143. Found: 240.1145 (M).

2-methyl-3-(prop-2-yn-1-yl)-1,4-dihydronaphthalene-1,4-dione (10).

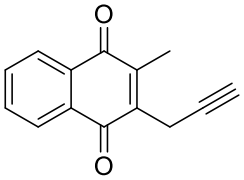

2 (313 mg, 1.3 mmol, 1 equiv.) was solubilized in MeCN (15.6 mL). A solution of CAN (1.6 g, 2.9 mmol, 2.2 equiv.) in water (5.2 mL) was then added. The mixture was stirred at 25°C for 1h. The organic solvent was removed under reduced pressure, extracted three times with DCM, washed with water, dried over magnesium sulphate, and the solvent was removed under vacuum. The desired product **10** was isolated as a yellow solid (260.3 mg, 95%). M.p. = 112-114°C. ^{1}H NMR (400 MHz, $CDCl_3$) δ 8.21 – 8.04 (m, 2H), 7.77 – 7.65 (m, 2H), 3.58 (dd, *J* = 2.9, 0.7 Hz, 2H), 2.31 (s, 3H), 2.00 (t, *J* = 2.8 Hz, 1H). ^{13}C {^{1}H} NMR (101 MHz, $CDCl_3$) δ 185.1, 183.4, 145.3, 141.3, 133.8, 133.7, 132.2, 132.0, 126.7, 126.6, 79.4, 69.4, 16.1, 13.1. HRMS (ESI+) calcd. for $C_{14}H_{11}O_2$: 211.0753. Found: 211.0754 ($M+H^+$).

Synthesis of 1,2,3-[TRZ-methyl]-menadiones.

1-((1,4-dimethoxy-3-methylnaphthalen-2-yl)methyl)-4-(trimethylsilyl)-1H-1,2,3-triazole (α6).

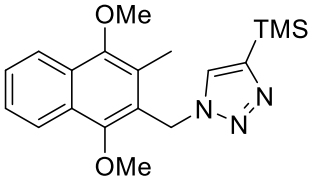

1 (50 mg, 0.2 mmol, 1 equiv.) was solubilized in MeCN (2.3 mL). Trimethylsilylacetylene (55 µL, 0.4 mmol, 2 equiv.) was then added under argon. Finally, $Cu(MeCN)_4BF_4$ (30.5 mg, 0.1 mmol, 0.5 equiv.) was added and the mixture was stirred at 50°C under argon for 72h. The conversion was monitored by TLC (CHX/EtOAc, 7/3, v/v, UV). The crude was then evaporated, extracted three times with ethyl acetate, dried over magnesium sulphate and the solvent was removed under vacuum. The crude was purified by silica gel chromatography (CHX/EtOAc, 7/3 to 0/10, v/v, UV) to afford **α6** as a light yellow oil (65 mg, 94.1%). ^{1}H NMR (400 MHz, $CDCl_3$) δ 8.16 – 8.05 (m, 2H), 7.55 (dqd, *J* = 9.7, 6.8, 1.6 Hz, 2H), 7.39 (s, 1H), 5.79 (s, 2H), 3.95 (s, 3H), 3.85 (s, 3H), 2.37 (s, 3H), 0.25 (s, 9H). ^{13}C {^{1}H} NMR (101 MHz, $CDCl_3$) δ 151.9, 150.8, 146.7, 129.5, 128.7, 127.2, 126.6, 126.1, 123.5, 122.9, 122.6, 63.2, 61.6, 45.7, 12.3, -1.0. HRMS (ESI+) calcd. for $C_{19}H_{26}N_3O_2Si$: 356.1789. Found: 356.1794 ($M+H^+$).

1-((1,4-dimethoxy-3-methylnaphthalen-2-yl)methyl)-1H-1,2,3-triazole (α7).

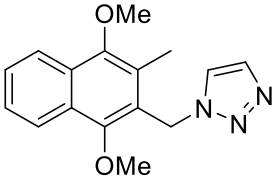

To a solution of **α6** (63.4 mg, 0.2 mmol, 1 equiv.) in THF (3.5 mL) was added at 25°C a 1 M TBAF solution in THF (0.5 mL, 0.5 mmol, 3 equiv.). The crude mixture was stirred at 25°C for 16h. The grey mixture was hydrolyzed with saturated aqueous ammonium chloride and extracted three times with ethyl acetate, dried over magnesium sulphate, and the solvent was removed under vacuum. The crude was purified by silica gel chromatography (CHX/EtOAc, 7/3 to 0/10, v/v, UV) to afford **α7** as a light yellow solid (33.4 mg, 66.1%). M.p. = 111-113°C. ^{1}H NMR (400 MHz, $CDCl_3$) δ 8.14 – 8.05 (m, 2H), 7.65 (s, 1H), 7.60 – 7.50 (m, 2H), 7.49 (s, 1H), 5.79 (s, 2H), 3.94 (s, 3H), 3.84 (s, 3H), 2.36 (s, 3H). ^{13}C {^{1}H} NMR (101 MHz, $CDCl_3$) δ 151.9, 150.9, 129.6, 127.3, 127.0, 126.4, 126.2, 123.2, 122.9, 122.6, 63.2, 61.6, 46.3, 12.3. HRMS (ESI+) calcd. for $C_{16}H_{18}N_3O_2$: 284.1393. Found: 284.1395 ($M+H^+$).

2-((1H-1,2,3-triazol-1-yl)methyl)-3-methylnaphthalene-1,4-dione (α8).

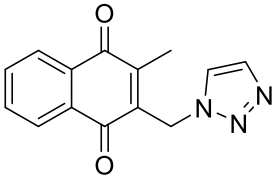

To a stirred solution of **α7** (33.4 mg, 0.1 mmol, 1 equiv.) and tetrabutylammonium iodide (87.1 mg, 0.2 mmol, 2 equiv.) in dry DCM (17.4 mL) was added dropwise boron trichloride (0.7 mL, 0.7 mmol, 6 equiv.) at -78°C. The reaction mixture was then allowed to reach 25°C and stirred for 16h. The yellow reaction mixture was quenched with water and extracted three times with DCM, dried over magnesium sulphate, and the solvent was removed under vacuum. The crude was purified by silica gel chromatography (DCM, UV) to afford **α8** as an orange solid (12 mg, 40.2%). M.p. 79-81°C. ^{1}H NMR (400 MHz, $CDCl_3$) δ 8.46 (s, 1H), 8.22 (d, J = 1.4 Hz, 1H), 8.16 – 8.05 (m, 2H), 7.82 – 7.77 (m, 2H), 5.77 (s, 2H), 2.51 (s, 3H). ^{13}C {^{1}H} NMR (101 MHz, $CDCl_3$) δ 183.89, 183.82, 150.6, 135.7, 134.9, 134.5, 132.1, 131.4, 131.1, 128.5, 127.3, 126.8, 48.4, 13.7. HRMS (ESI+) calcd. for $C_{14}H_{12}N_3O_2$: 254.0924. Found: 254.0923 ($M+H^+$).

General procedure for CuAAC click reaction.

Procedure [a]. The azide **9** (1 equiv.) or the alkyne **10** (1 equiv.) was mixed with the corresponding crude of alkyne or azide (1.2 equiv.) in THF (70% of 0.02 M). A solution of sodium ascorbate (0.4 equiv.) and $CuSO_4$ (0.2 equiv.) prepared in water (30% of 0.02 M) was then added. The mixture was stirred at 25°C for 16h. The organic solvent was removed under reduced pressure, extracted three times with DCM, washed with water, dried over magnesium sulphate, and the solvent was removed under vacuum. The crude was purified by silica gel chromatography using the appropriate eluent (see below). All the yields are calculated in two steps, since the alkyne or azide are not purified.

2-(4-((3-methyl-1,4-dioxo-1,4-dihydronaphthalen-2-yl)methyl)-1H-1,2,3-triazol-1-yl)ethyl4-methylbenzenesulfonate (β25).

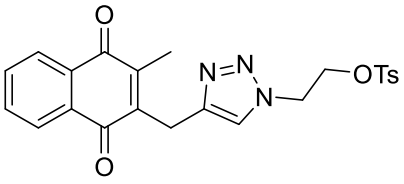

With **12**, eluent (CHX/EtOAc, 8/2 to 6/4, v/v, UV), yellow solid, 42.6% yield. M.p. = 87-89°C. ^{1}H NMR (500 MHz, $CDCl_3$) δ 8.06 (dt, J = 6.2, 3.3 Hz, 2H), 7.71 – 7.67 (m, 2H), 7.66 – 7.62 (m, 2H), 7.44 (s, 1H), 7.27 (d, J = 8.1 Hz, 2H), 4.55 (t, J = 5.2 Hz, 2H), 4.35 (t, J = 5.2 Hz, 2H), 4.04 (s, 2H), 2.41 (s, 3H), 2.32 (s, 3H). ^{13}C {^{1}H} NMR (126 MHz, $CDCl_3$) δ 184.1, 183.3, 144.4, 143.9, 143.5, 142.3, 132.6, 132.5, 131.1, 131.0, 130.9, 129.0, 126.8, 125.4, 125.3, 122.1, 66.5, 47.9, 22.5, 20.6, 12.1. HRMS (ESI+) calcd. for $C_{23}H_{22}N_3O_5S$: 452.1314. Found: 452.1275 ($M+H^+$).

***Tert*-butyl 4-((1-((3-methyl-1,4-dioxo-1,4-dihydronaphthalen-2-yl)methyl)-1H-1,2,3-triazol-4-yl)methyl)piperazine-1-carboxylate (α17).**

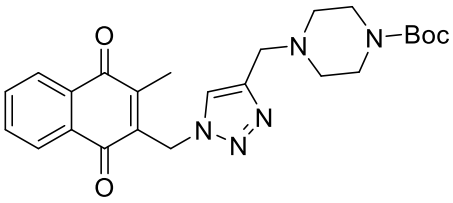

With **63**, eluent (EtOAc/MeOH, 10/0 to 8/2, v/v, UV), orange solid, 61.6% yield. M.p. = 97-99°C. ^{1}H NMR (500 MHz, $CDCl_3$) δ 8.13 – 8.06 (m, 2H), 7.76 – 7.72 (m, 2H), 7.66 (s, 1H), 5.54 (s, 2H), 3.64 (s, 2H), 3.40 (t, J = 5.1 Hz, 4H), 2.45 (s, 3H), 1.42 (s, 9H). ^{13}C {^{1}H} NMR (126 MHz, $CDCl_3$) δ 184.7, 184.0, 154.8, 148.7, 144.0, 138.2, 134.3, 134.2, 132.2, 131.5, 126.9, 126.7, 123.9, 79.8, 53.3, 52.7, 45.0, 28.5, 13.4. HRMS (ESI+) calcd. for $C_{24}H_{30}N_5O_4$: 452.2292. Found: 452.2305 ($M+H^+$).

2-methyl-3-((4-((oxetan-3-yloxy)methyl)-1H-1,2,3-triazol-1-yl)methyl)naphthalene-1,4-dione (α30).

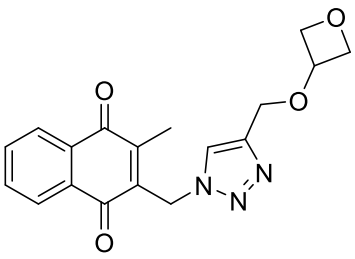

With **67**, eluent (EtOAc, v/v, UV), yellow solid, 51.7% yield. M.p. = 122-124°C. ^{1}H NMR (500 MHz, $CDCl_3$) δ 8.12 – 8.05 (m, 2H), 7.76 – 7.71 (m, 3H), 5.55 (s, 2H), 4.73 – 4.65 (m, 3H), 4.56 – 4.53 (m, 2H), 4.52 (s, 2H), 2.45 (s, 3H). ^{13}C {^{1}H} NMR (126 MHz, $CDCl_3$) δ 184.6, 183.9, 148.6, 144.5, 138.1, 134.3, 134.2, 132.1, 131.4, 126.9, 126.6, 123.9, 78.7, 72.3, 62.4, 45.1, 13.3. HRMS (ESI+) calcd. for $C_{18}H_{17}N_3NaO_4$: 362.1111. Found: 362.1106 ($M+Na^+$).

2-methyl-3-((4-(morpholinomethyl)-1H-1,2,3-triazol-1-yl)methyl)naphthalene-1,4-dione (α31).

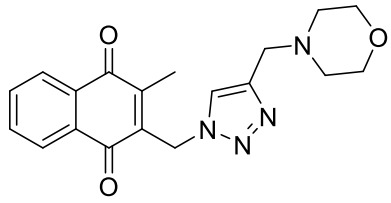

With **62**, eluent (EtOAc/MeOH, 10/0 to 8/2, v/v, UV), yellow solid, 29.9% yield. M.p. = 127-129°C. ^{1}H NMR (500 MHz, $CDCl_3$) δ 8.09 (ddt, *J* = 7.0, 5.5, 3.7 Hz, 2H), 7.74 (dd, *J* = 5.8, 3.3 Hz, 2H), 7.67 (s, 1H), 5.54 (s, 2H), 3.71 – 3.65 (m, 4H), 3.63 (s, 2H), 2.57 – 2.46 (m, 4H), 2.44 (s, 3H). ^{13}C {^{1}H} NMR (126 MHz, $CDCl_3$) δ 184.7, 184.0, 148.6, 143.9, 138.2, 134.3, 134.1, 132.2, 131.5, 126.9, 126.6, 123.9, 66.8, 53.6, 53.4, 44.9, 13.3. HRMS (ESI+) calcd. for $C_{19}H_{21}N_4O_3$: 353.1608. Found: 353.1611 ($M+H^+$).

***Tert*-butyl ((1-((3-methyl-1,4-dioxo-1,4-dihydronaphthalen-2-yl)methyl)-1H-1,2,3-triazol-4-yl)methyl)carbamate (α16).**

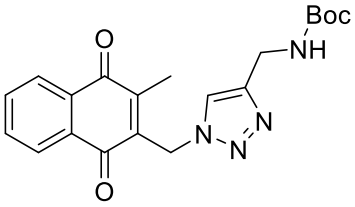

With **69**, eluent (CHX/EtOAc, 2/8, v/v, UV), orange solid, 54% yield. M.p. = 105-107°C. ^{1}H NMR (400 MHz, $CDCl_3$) δ 8.10 – 8.04 (m, 2H), 7.75 – 7.69 (m, 2H), 7.66 (s, 1H), 5.52 (s, 2H), 5.13 (s, 1H), 4.33 (d, *J* = 5.8 Hz, 2H), 2.41 (s, 3H), 1.39 (s, 9H). ^{13}C NMR (101 MHz, $CDCl_3$) δ 184.7, 183.8, 155.9, 148.5, 145.5, 138.2, 134.2, 134.1, 132.1, 131.4, 126.8, 126.6, 122.9, 44.9, 36.2, 28.4, 13.3. HRMS (ESI+) calcd. for $C_{20}H_{22}N_4NaO_4$: 405.1533. Found: 405.1533 ($M+Na^+$).

2-((4-((dibenzylamino)methyl)-1H-1,2,3-triazol-1-yl)methyl)-3-methylnaphthalene-1,4-dione (α28).

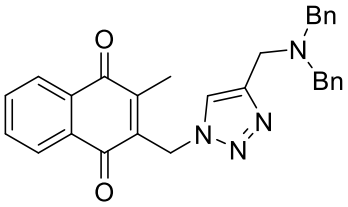

With **70**, eluent (CHX/EtOAc, 7/3, v/v, UV), orange oil, 8.3% yield. ^{1}H NMR (400 MHz, $CDCl_3$) δ 8.11 – 8.05 (m, 2H), 7.75 – 7.69 (m, 2H), 7.62 (s, 1H), 7.39 – 7.36 (m, 4H), 7.32 – 7.27 (m, 4H), 7.22 – 7.18 (m, 2H), 5.53 (s, 2H), 3.72 (s, 2H), 3.59 (s, 4H), 2.45 (s, 3H). ^{13}C {^{1}H} NMR (101 MHz, $CDCl_3$) δ 184.7, 183.9, 148.4, 145.4, 139.3, 138.3, 134.2, 134.0, 132.1, 131.5, 128.9, 128.3, 127.0, 126.8, 126.6, 123.8, 57.8, 48.1, 44.9, 13.3. HRMS (ESI+) calcd. for $C_{29}H_{27}N_4O_2$: 463.2128. Found: 463.2136 ($M+H^+$).

2-(4-((3-methyl-1,4-dioxo-1,4-dihydronaphthalen-2-yl)methyl)-1H-1,2,3-triazol-1-yl)acetonitrile (β26).

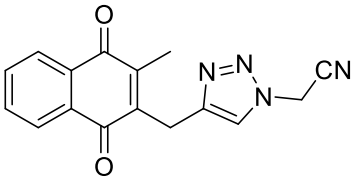

With **60**, eluent (CHX/EtOAc, 6/4, v/v, UV), orange solid, 26.8% yield. M.p. = 112-114°C. ^{1}H NMR (400 MHz, $CDCl_3$) δ 8.11 – 7.96 (m, 2H), 7.70 – 7.65 (m, 2H), 7.64 (s, 1H), 5.27 (s, 2H), 4.08 (s, 2H), 2.34 (s, 3H). ^{13}C {^{1}H} NMR (101 MHz, $CDCl_3$) δ 185.1, 184.5, 145.9, 145.4,

142.9, 133.8, 133.7, 132.2, 131.9, 126.6, 126.4, 122.6, 112.7, 37.5, 23.7, 13.3. HRMS (ESI+) calcd. for $C_{16}H_{13}N_4O_2$: 293.1033. Found: 293.1036 ($M+H^+$).

2-((4-((4,4-difluoropiperidin-1-yl)methyl)-1H-1,2,3-triazol-1-yl)methyl)-3-methylnaphthalene-1,4-dione (α32).

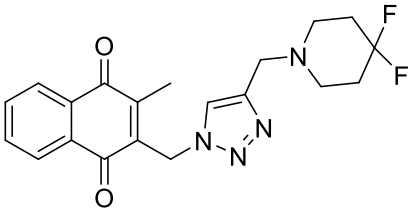

With **64**, eluent (EtOAc/MeOH, 95/5, v/v, UV), orange oil, 25.1% yield. ^{1}H NMR (400 MHz, $CDCl_3$) δ 8.09 (td, J = 6.0, 3.3 Hz, 2H), 7.74 (dd, J = 5.8, 3.3 Hz, 2H), 7.65 (s, 1H), 5.54 (s, 2H), 3.66 (s, 2H), 2.58 (t, J = 5.8 Hz, 4H), 2.45 (s, 3H), 2.01 – 1.90 (m, 4H). ^{19}F {^{1}H} NMR (377 MHz, $CDCl_3$) δ -98.13. ^{13}C {^{1}H} NMR (101 MHz, $CDCl_3$) δ 184.7, 184.0, 148.6, 144.5, 138.2, 134.3, 134.2, 132.2, 131.5, 126.9, 126.6, 123.8, 52.5, 49.9 (t, J = 5.4 Hz), 45.0, 33.9 (t, J = 23.1 Hz), 13.3. HRMS (ESI+) calcd. for $C_{20}H_{21}O_2N_4F_2$: 387.1627. Found: 387.1635 ($M+H^+$).

***Tert*-butyl 4-((1-((3-methyl-1,4-dioxo-1,4-dihydronaphthalen-2-yl)methyl)-1H-1,2,3-triazol-4-yl)methyl)piperazine-1-carboxylate (α34).**

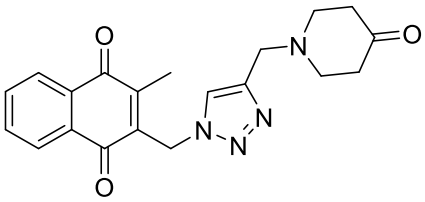

With **65**, eluent (EtOAc/MeOH, 9/1, v/v, UV), orange oil, 16.9% yield. ^{1}H NMR (400 MHz, $CDCl_3$) δ 8.14 – 8.06 (m, 2H), 7.75 (dd, J = 5.8, 3.3 Hz, 2H), 7.70 (s, 1H), 5.56 (s, 2H), 3.76 (s, 2H), 2.80 (t, J = 6.1 Hz, 4H), 2.46 (s, 3H), 2.44 (t, J = 6.1 Hz, 4H). ^{13}C {^{1}H} NMR (101 MHz, $CDCl_3$) δ 208.8, 184.7, 184.1, 148.7, 144.4, 138.2, 134.3, 134.2, 132.2, 131.5, 126.9, 126.7, 123.9, 52.8, 52.4, 45.1, 41.2, 13.4. HRMS (ESI+) calcd. for $C_{20}H_{21}O_3N_4$: 365.1608. Found: 365.1610 ($M+H^+$).

2-methyl-3-((4-(thiazolidin-3-ylmethyl)-1H-1,2,3-triazol-1-yl)methyl)naphthalene-1,4-dione (α21).

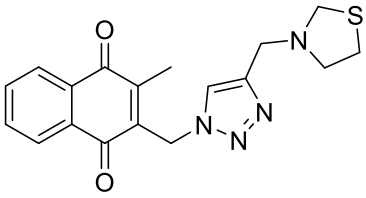

With **66**, eluent (EtOAc/MeOH, 9/1, v/v, UV), orange oil, 21.8% yield, contains a small impurity. ^{1}H NMR (400 MHz, $CDCl_3$) δ 8.10 (dt, J = 5.8, 3.6 Hz, 2H), 7.75 (dd, J = 5.8, 3.3 Hz, 2H), 7.71 (s, 1H), 5.56 (s, 2H), 4.07 (s, 2H), 3.65 (s, 2H), 3.09 (t, J = 6.6 Hz, 2H), 2.95 (t, J = 6.5 Hz, 2H), 2.46 (s, 3H). ^{13}C {^{1}H} NMR (101 MHz, $CDCl_3$) δ 184.8, 184.0, 148.7, 145.7, 138.2, 134.3, 134.2, 132.2, 131.5, 126.9, 126.7, 123.7, 60.5, 57.5, 48.0, 45.0, 29.5, 13.4. HRMS (ESI+) calcd. for $C_{18}H_{19}O_2N_4S$: 355.1223. Found: 355.1230 ($M+H^+$).

2-methyl-3-((1-(2-morpholinoethyl)-1H-1,2,3-triazol-4-yl)methyl)naphthalene-1,4-dione (β37).

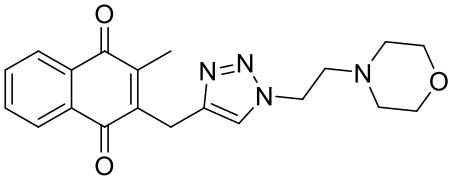

With **53**, eluent (EtOAc/MeOH, 9/1, v/v, UV), orange oil, 11.9% yield. ^{1}H NMR (400 MHz, $CDCl_3$) δ 8.10 – 8.04 (m, 2H), 7.70 (dd, J = 5.8, 3.3 Hz, 2H), 7.51 (s, 1H), 4.38 (t, J = 6.4 Hz, 2H), 4.08 (s, 2H), 3.67 – 3.60 (t, 4H), 2.77 (t, J = 6.4 Hz, 2H), 2.47 – 2.42 (t, 4H), 2.37 (s, 3H). ^{13}C {^{1}H} NMR (101 MHz, $CDCl_3$) δ 185.3, 184.7, 145.1, 144.3, 143.8, 133.7, 133.6, 132.3, 132.0, 126.6, 126.3, 122.9, 66.9, 57.9, 53.6, 47.5, 23.8, 13.3. HRMS (ESI+) calcd. for $C_{20}H_{23}O_3N_4$: 367.1760. Found: 367.1764 ($M+H^+$).

2-methyl-3-((1-(2-(thiazolidin-3-yl)ethyl)-1H-1,2,3-triazol-4-yl)methyl)naphthalene-1,4-dione (β22).

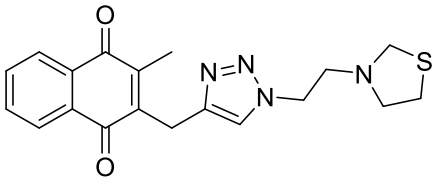

With **55**, eluent (EtOAc/MeOH, 9/1, v/v, UV), yellow solid, 5.7% yield, not stable leads to degradation after few hours. ^{1}H NMR (400 MHz, $CDCl_3$) δ 8.21 – 8.16 (m, 2H), 7.55 – 7.46 (m, 2H), 6.68 (s, 1H), 3.94 (s, 2H), 3.41 – 3.36 (m, 2H), 2.86 – 2.83 (m, 2H), 2.80 – 2.75 (m, 4H), 2.48 (s, 3H).

2-methyl-3-((1-(2-(4-oxopiperidin-1-yl)ethyl)-1H-1,2,3-triazol-4-yl)methyl)naphthalene-1,4-dione (β40).

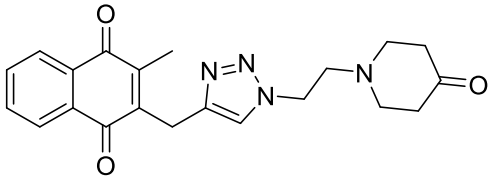

With **56**, eluent (EtOAc/MeOH, 9/1, v/v, UV), orange solid, 35.7% yield. M.p. = 109-111°C. ^{1}H NMR (400 MHz, $CDCl_3$) δ 8.08 – 7.97 (m, 2H), 7.70 – 7.64 (m, 2H), 7.53 (s, 1H), 4.42 (t, J = 6.3 Hz, 2H), 4.07 (s, 2H), 2.90 (t, J = 6.3 Hz, 2H), 2.75 (t, J = 6.0 Hz, 4H), 2.37 (d, J = 7.0 Hz, 7H). ^{13}C {^{1}H} NMR (101 MHz, $CDCl_3$) δ 208.2, 185.2, 184.6, 145.0, 143.6, 133.7, 133.6, 132.2, 131.9, 126.5, 126.2, 56.5, 53.1, 48.3, 41.2, 23.8, 13.2. HRMS (ESI+) calcd. for $C_{21}H_{22}O_3N_4Na$ 401.1584. Found: 401.1579 ($M+Na^+$).

2-((1-(2-(4,4-difluoropiperidin-1-yl)ethyl)-1H-1,2,3-triazol-4-yl)methyl)-3-methylnaphthalene-1,4-dione (β38).

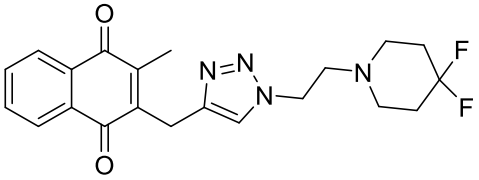

With **57**, eluent (EtOAc/MeOH, 9/1, v/v, UV), orange solid, 49.1% yield. M.p. = 110-112°C. ^{1}H NMR (400 MHz, $CDCl_3$) δ 8.05 (ddd, J = 9.3, 6.2, 3.3 Hz, 2H), 7.70 – 7.66 (m, 2H), 7.50 (s, 1H), 4.37 (t, J = 6.3 Hz, 2H), 4.07 (s, 2H), 2.81 (t, J = 6.2 Hz, 2H), 2.55 (t, J = 5.7 Hz, 4H), 2.36 (s, 3H), 1.91 (tt, J = 13.6, 5.7 Hz, 4H). ^{19}F {^{1}H} NMR (377 MHz, $CDCl_3$) δ -98.08, -98.34. ^{13}C {^{1}H} NMR (101 MHz, $CDCl_3$) δ 185.3, 184.6, 145.0, 143.7, 133.7, 133.6, 132.2, 131.9, 126.5, 126.3, 56.6, 50.1, 50.1, 50.0, 48.1, 34.2, 34.0, 33.8, 23.8, 13.2. HRMS (ESI+) calcd. for $C_{21}H_{23}F_2O_2N_4$: 401.1779. Found: 401.1783 ($M+H^+$).

***Tert*-butyl 4-(2-(4-((3-methyl-1,4-dioxo-1,4-dihydronaphthalen-2-yl)methyl)-1H-1,2,3-triazol-1-yl)ethyl)piperazine-1-carboxylate (β18).**

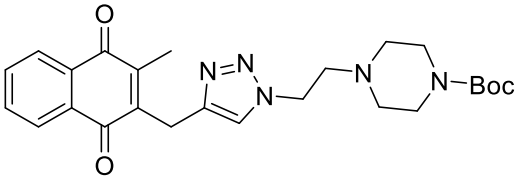

With **58**, eluent (EtOAc/MeOH, 9/1, v/v, UV), orange oil, 71.3% yield. ^{1}H NMR (400 MHz, $CDCl_3$) δ 8.11 – 8.02 (m, 2H), 7.71 – 7.67 (m, 2H), 7.50 (s, 1H), 4.38 (t, J = 6.4 Hz, 2H), 4.08 (s, 2H), 3.37 (t, J = 5.1 Hz, 4H), 2.78 (t, J = 6.4 Hz, 2H), 2.40 (t, J = 4.9 Hz, 4H), 2.37 (s, 3H), 1.45 (s, 9H). ^{13}C {^{1}H} NMR (101 MHz, $CDCl_3$) δ 185.3, 184.7, 154.8, 145.1, 144.3, 143.8, 133.7, 133.6, 132.3, 132.1, 126.6, 126.3, 122.9, 79.9, 57.6, 53.0, 47.8, 28.5, 23.8, 13.3. HRMS (ESI+) calcd. for $C_{25}H_{32}O_4N_5$: 466.2440. Found: 466.2449 ($M+H^+$).

Procedure [b]. Azide **9** (1 equiv.) or alkyne **10** (1 equiv.) was mixed with the corresponding alkyne or azide (1.5 equiv.) in DCM (0.1 M) under argon. $Cu(MeCN)_4BF_4$ (0.4 equiv.) was then added. The mixture was stirred at 40°C under argon for 16h. The organic solvent was removed under reduced pressure, extracted three times with DCM, washed with water, dried over magnesium sulphate, and the solvent

was removed under vacuum. The crude was purified by silica gel chromatography using the appropriate eluent (see below).

2-((1-benzyl-1H-1,2,3-triazol-4-yl)methyl)-3-methylnaphthalene-1,4-dione (β13).

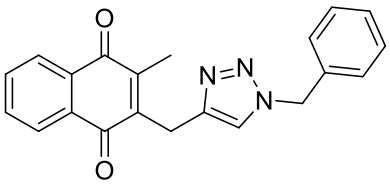

With **59**, eluent (CHX/EtOAc, 6/4, v/v, UV), yellow solid, 91% yield. M.p. = 115-117°C. ^{1}H NMR (400 MHz, $CDCl_3$) δ 8.09 – 7.95 (m, 2H), 7.70 – 7.65 (m, 2H), 7.35 – 7.31 (m, 3H), 7.24 – 7.21 (m, 2H), 5.43 (s, 2H), 4.04 (s, 2H), 2.33 (s, 3H). ^{13}C {^{1}H} NMR (101 MHz, $CDCl_3$) δ 185.2, 184.5, 145.1, 144.8, 143.5, 134.7, 133.6, 133.5, 132.2, 131.9, 129.1, 128.7, 128.1, 126.5, 126.3, 122.0, 54.1, 23.7, 13.2. HRMS (ESI+) calcd. for $C_{21}H_{17}O_2N_3Na$: 366.1213. Found: 366.1191 ($M+Na^+$).

2-((4-(2-hydroxypropan-2-yl)-1H-1,2,3-triazol-1-yl)methyl)-3-methylnaphthalene-1,4-dione (α27).

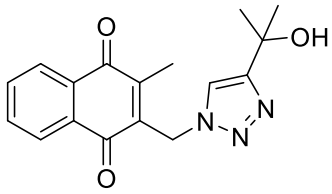

With 3-methyl-butynol, eluent (CHX/EtOAc, 8/2 to 0/10, v/v, UV), yellow solid, 91% yield. M.p. = 113-115°C. ^{1}H NMR (400 MHz, $CDCl_3$) δ 8.20 – 8.00 (m, 2H), 7.77 – 7.69 (m, 2H), 7.62 (s, 1H), 5.53 (s, 2H), 2.45 (s, 3H), 1.59 (s, 6H). ^{13}C {^{1}H} NMR (101 MHz, $CDCl_3$) δ 184.8, 184.0, 148.7, 138.2, 134.3, 134.1, 132.2, 131.5, 126.9, 126.7, 44.9, 30.5, 13.3. HRMS (ESI+) calcd. for $C_{17}H_{18}N_3O_3$: 312.1343. Found: 312.1334 ($M+H^+$).

2-((4-(hydroxymethyl)-1H-1,2,3-triazol-1-yl)methyl)-3-methylnaphthalene-1,4-dione (α29).

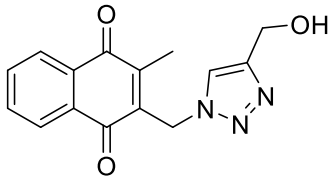

With 2-propyn-1-ol, eluent (EtOAc, UV), yellow solid, 42% yield. M.p. = 109-111°C. ^{1}H NMR (500 MHz, $CDCl_3$) δ 8.21 – 8.01 (m, 2H), 7.82 – 7.62 (m, 3H), 5.56 (s, 2H), 4.75 (s, 2H), 2.46 (s, 3H). ^{13}C {^{1}H} NMR (126 MHz, $CDCl_3$) δ 184.6, 183.9, 148.5, 147.6, 138.1, 134.2, 134.1, 132.1, 131.4, 126.8, 126.6, 122.8, 56.6, 44.9, 13.2. HRMS (ESI+) calcd. for $C_{15}H_{14}N_3O_3$: 284.1029. Found: 284.1031 ($M+H^+$).

Procedure [c]. Azide **9** (1 equiv.) or alkyne **10** (1 equiv.) was mixed with the corresponding alkyne (2 equiv.) or azide respectively (1.5 equiv.) in DCM (0.1 M) under argon. $Cu(MeCN)_4BF_4$ (0.4 equiv.) and bathocuproine (0.4 equiv.) were then added. The mixture was stirred at 40°C under argon for 72h. The organic solvent was removed under reduced pressure, extracted three times with DCM, washed with water, dried over magnesium sulphate, and the solvent was removed under vacuum. The crude was purified by silica gel chromatography using the appropriate eluent (see below).

2-((1-(2-hydroxyethyl)-1H-1,2,3-triazol-4-yl)methyl)-3-methylnaphthalene-1,4-dione (β36).

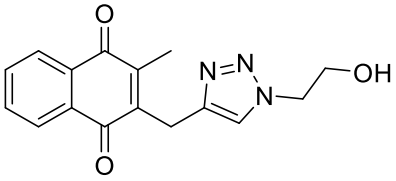

With **11**, eluent (CHX/EtOAc, 8/2 to 0/10, v/v, UV), yellow solid, 45.5% yield. M.p. = 102-104°C. ^{1}H NMR (500 MHz, $CDCl_3$) δ 8.12 – 8.03 (m, 2H), 7.72 – 7.67 (m, 2H), 7.50 (s, 1H), 4.46 – 4.36 (m, 2H), 4.10 (s, 2H), 4.05 (q, J = 5.2 Hz, 2H), 2.38 (s, 3H). ^{13}C {^{1}H} NMR (126 MHz, $CDCl_3$) δ 185.3, 184.7, 145.2, 143.6, 133.8, 133.6, 132.3, 132.1, 126.6, 126.4, 61.4, 52.6, 23.8, 13.3. HRMS (ESI+) calcd. for $C_{16}H_{16}N_3O_3$: 298.1186. Found: 298.1183 ($M+H^+$).

2-methyl-3-((4-(trimethylsilyl)-1H-1,2,3-triazol-1-yl)methyl)naphthalene-1,4-dione (α14).

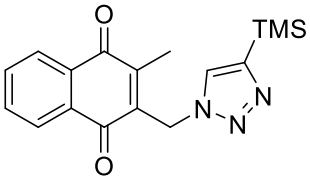

With trimethylsilylacetylene, eluent (CHX/EtOAc, 8/2 to 6/4, v/v, UV), yellow solid, 56.5% yield. M.p. = 117-119°C. ^{1}H NMR (500 MHz, $CDCl_3$) δ 8.11 – 8.05 (m, 2H), 7.75 – 7.70 (m, 2H), 7.67 (s, 1H), 5.57 (s, 2H), 2.47 (s, 3H), 0.28 (s, 9H). ^{13}C {^{1}H} NMR (126 MHz, $CDCl_3$) δ 184.8, 184.1, 148.6, 146.8, 138.5, 134.2, 134.1, 132.2, 131.5, 129.9, 126.8, 126.6, 44.3, 13.4, -1.0. HRMS (ESI+) calcd. for $C_{17}H_{20}N_3O_2Si$: 326.1319. Found: 326.1335 ($M+H^+$).

Procedure [d]. Azide **9** (1 equiv.) was mixed with the corresponding alkyne (2 equiv.) in MeCN (0.01 M) under argon. $Cu(MeCN)_4BF_4$ (0.1 equiv.) and bathocuproine (0.1 equiv.) were then added. The mixture was stirred under reflux at 80°C under argon for 72h. The organic solvent was removed under reduced pressure, extracted three times with DCM, washed with water, dried over magnesium sulphate, and the solvent was removed under vacuum. The crude was purified by silica gel chromatography using the appropriate eluent (see below).

2-((4-(bromomethyl)-1H-1,2,3-triazol-1-yl)methyl)-3-methylnaphthalene-1,4-dione (α23).

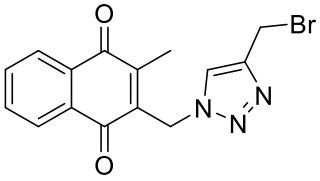

With 3-bromopropyne, eluent (CHX/EtOAc, 8/2 to 3/7, v/v, UV), yellow solid, 6% yield, contains a small impurity. M.p. = 93-95°C. ^{1}H NMR (500 MHz, $CDCl_3$) δ 8.14 – 8.08 (m, 2H), 7.79 (s, 1H), 7.75 (dd, *J* = 5.8, 3.3 Hz, 2H), 5.55 (s, 2H), 4.53 (s, 2H), 2.47 (s, 3H). ^{13}C {^{1}H} NMR (126 MHz, $CDCl_3$) δ 184.7, 184.1, 148.8, 138.0, 134.4, 134.2, 132.2, 131.5, 126.9, 126.7, 45.2, 21.6, 13.4. HRMS (ESI+) calcd. for $C_{15}H_{13}BrN_3O_2$: 346.0186. Found: 346.0168 ($M+H^+$).

General procedure for TFA deprotection.

The Boc-protected 1,2,3-[TRZ-methyl]-menadione (1 equiv.) was solubilized in DCM (0.03 M) and then TFA was added (32 equiv.). The mixture was stirred at 25°C for 1h. The organic solvent was removed and the crude was dissolved in MeOH and dried under vacuum. This procedure was repeated three times. The same procedure was then carried out with $CHCl_3$.

2-methyl-3-((4-(piperazin-1-ylmethyl)-1H-1,2,3-triazol-1-yl)methyl)naphthalene-1,4-dione (α19).

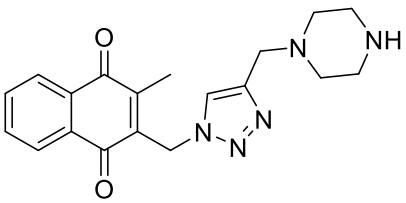

From **α17**, the pure product was obtained quantitatively as a TFA salt, orange solid. M.p. = 125-127°C. ^{1}H NMR (400 MHz, MeOD) δ 8.20 (s, 1H), 8.08 – 7.94 (m, 2H), 7.81 – 7.67 (m, 2H), 5.64 (s, 2H), 4.36 (s, 2H), 3.51 – 3.45 (m, 4H), 3.41 (dd, *J* = 6.9, 3.8 Hz, 4H), 2.36 (s, 3H). ^{13}C {^{1}H} NMR (101 MHz, MeOD) δ 185.8, 184.9, 149.5, 139.3, 135.2, 135.1, 133.5, 132.9, 127.5, 127.3, 58.3, 46.5, 43.6, 41.7, 18.4, 13.1. HRMS (ESI+) calcd. for $C_{19}H_{22}N_5O_2$: 352.1770. Found: 352.1768 ($M+H^+$).

2-((4-(aminomethyl)-1H-1,2,3-triazol-1-yl)methyl)-3-methylnaphthalene-1,4-dione (α15).

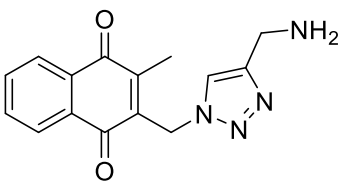

From **α16**, the pure product was obtained quantitatively as a TFA salt, brown solid. M.p. = 127-129°C. ^{1}H NMR (500 MHz, MeOD) δ 8.17 (s, 1H), 7.95 (dq, *J* = 7.1, 4.1 Hz, 2H), 7.72 (dt, *J* = 6.3, 3.0 Hz, 2H), 5.62 (s, 2H), 4.27 (s, 2H), 2.33 (s, 3H). ^{13}C {^{1}H} NMR (126 MHz, MeOD) δ

185.7, 184.7, 149.3, 141.2, 139.2, 135.2, 135.1, 133.2, 132.6, 127.4, 127.2, 126.4, 46.3, 35.4, 13.1. HRMS (ESI+) calcd. for $C_{15}H_{15}N_4O_2$: 283.1189. Found: 283.1196 ($M+H^+$).

2-methyl-3-((1-(2-(piperazin-1-yl)ethyl)-1H-1,2,3-triazol-4-yl)methyl)naphthalene-1,4-dione (β20).

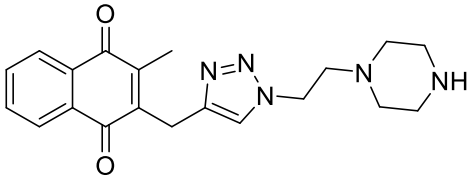

From **β18**, the pure product was obtained quantitatively as a TFA salt, brown solid. M.p. = 85-87°C. ^{1}H NMR (400 MHz, MeOD) δ 8.07 – 8.01 (m, 2H), 7.85 (s, 1H), 7.78 – 7.72 (m, 2H), 4.55 (t, J = 6.1 Hz, 2H), 4.07 (s, 2H), 3.25 – 3.21 (m, 4H), 3.05 (t, J = 6.1 Hz, 2H), 2.90 – 2.82 (m, 4H), 2.24 (s, 3H). ^{13}C {^{1}H} NMR (101 MHz, MeOD) δ 186.2, 185.4, 146.1, 145.6, 144.4, 134.8, 134.8, 133.5, 133.3, 127.2, 127.1, 124.8, 57.6, 50.4, 48.1, 44.4, 24.1, 13.1. HRMS (ESI+) calcd. for $C_{20}H_{24}O_2N_5$: 366.1924. Found: 366.1921 ($M+H^+$).

Synthesis of 1,2,4-TRZ-, 3-nitro-1,2,4-TRZ- and 2-nitroimidazole-menadiones.

General procedure for SN_2 with 2-(chloromethyl)-1,4-dimethoxy-3-methylnaphthalene.

2-(chloromethyl)-1,4-dimethoxy-3-methylnaphthalene (1 equiv.) was dissolved in MeCN (0.05 M). Then the nucleophile (2.5 equiv.) with TEA (3 equiv.) was slowly added. The reaction mixture was stirred under reflux at 80°C for 16h. The organic solvent was removed under reduced pressure, extracted three times with DCM, washed with water, dried over magnesium sulphate, and solvent was removed under vacuum. The crude was purified by silica gel chromatography using the appropriate eluent (see below).

1-((1,4-dimethoxy-3-methylnaphthalen-2-yl)methyl)-1H-1,2,4-triazole (42).

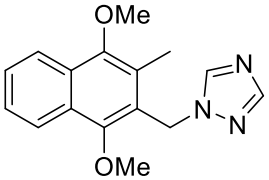

With 1H-1,2,4-triazole, eluent (CHX/EtOAc, 3/7, v/v, UV), white solid, 39.8% yield. M.p. = 115-117°C. ^{1}H NMR (400 MHz, $CDCl_3$) δ 8.19 – 8.04 (m, 2H), 7.97 (s, 1H), 7.93 (s, 1H), 7.64 – 7.45 (m, 2H), 5.58 (s, 2H), 3.93 (s, 3H), 3.86 (s, 3H), 2.38 (s, 3H). ^{13}C {^{1}H} NMR (101 MHz, $CDCl_3$) δ 152.1, 151.8, 150.9, 129.6, 127.3, 127.1, 126.2, 126.2, 122.9, 122.9, 122.6, 63.2, 61.7, 46.0, 12.4. HRMS (ESI+) calcd. for $C_{16}H_{18}O_2N_3$: 284.1393. Found: 284.1402 ($M+H^+$).

1-((1,4-dimethoxy-3-methylnaphthalen-2-yl)methyl)-3-nitro-1H-1,2,4-triazole (45).

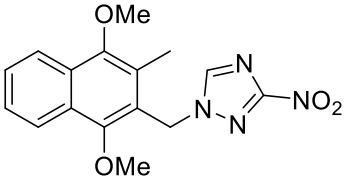

With 3-nitro-1,2,4-triazole, eluent (CHX/EtOAc, 8/2 to 4/6, v/v, UV), yellow oil, 50.4% yield. ^{1}H NMR (400 MHz, MeOD) δ 8.58 (s, 1H), 8.06 – 7.97 (m, 2H), 7.57 – 7.40 (m, 2H), 5.68 (s, 2H), 3.93 (s, 3H), 3.80 (s, 3H), 2.41 (s, 3H). ^{13}C {^{1}H} NMR (101 MHz, MeOD) δ 153.6, 151.9, 147.2, 130.8, 128.3, 128.1, 127.3, 127.1, 123.8, 123.5, 123.4, 63.5, 61.9, 48.3, 12.6. HRMS (ESI+) calcd. for $C_{16}H_{16}O_4N_4Na$: 351.1064. Found: 351.1071 ($M+Na^+$).

1-((1,4-dimethoxy-3-methylnaphthalen-2-yl)methyl)-2-nitro-1H-imidazole (46).

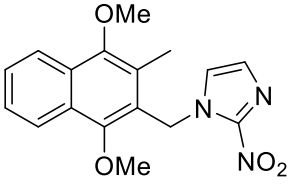

With 2-nitroimidazole, eluent (CHX/EtOAc, 8/2 to 4/6, v/v, UV), yellow oil, 78.9% yield. ^{1}H NMR (400 MHz, $CDCl_3$) δ 8.18 – 8.01 (m, 2H), 7.60 – 7.45 (m, 2H), 6.95 (d, J = 1.2 Hz, 1H), 6.61 (d, J = 1.2 Hz, 1H), 5.79 (s, 2H), 3.86 (s, 3H), 3.85 (s, 3H), 2.24 (s, 3H). ^{13}C {^{1}H} NMR (101 MHz, $CDCl_3$) δ 152.3, 150.9, 145.2, 129.6, 128.2, 127.4, 126.9, 126.3, 125.6, 124.2, 122.8, 122.5, 122.0, 63.1, 61.5, 45.9, 11.9. HRMS (ESI+) calcd. for $C_{17}H_{17}O_4N_3Na$: 350.1111. Found: 350.1115 ($M+Na^+$).

General procedure for the oxidative demethylation.

Boron trichloride (6 equiv.) was added dropwise at -78°C to a stirred solution of the protected substituted menadione and tetrabutylammonium iodide (2 equiv.) in dry DCM (0.007 M). The reaction mixture was then allowed to heat to 25°C and stirred for 16h. The yellow reaction mixture was quenched with water and the crude was extracted three times with DCM, dried over magnesium sulphate, and the solvent was removed under vacuum. The crude was purified by silica gel chromatography using the appropriate eluent.

2-((1H-1,2,4-triazol-1-yl)methyl)-3-methylnaphthalene-1,4-dione (41).

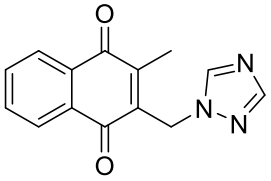

From **42**, eluent (CHX/EtOAc, 8/2 to 0/10, v/v, UV), orange solid, 20.9% yield. M.p. = 129-131°C. ^{1}H NMR (400 MHz, $CDCl_3$) δ 9.33 (s, 1H), 8.55 (s, 1H), 8.19 – 8.08 (m, 3H), 7.81 – 7.76 (m, 2H), 5.52 (s, 2H), 2.51 (s, 3H). ^{13}C {^{1}H} NMR (101 MHz, $CDCl_3$) δ 184.0, 183.8, 149.8, 145.9, 142.9, 135.5, 134.8, 134.6, 132.1, 131.1, 127.2, 127.1, 47.5, 13.7. HRMS (ESI+) calcd. for $C_{14}H_{12}O_2N_3$: 254.0924. Found: 254.0928 ($M+H^+$).

2-methyl-3-((3-nitro-1H-1,2,4-triazol-1-yl)methyl)naphthalene-1,4-dione (43).

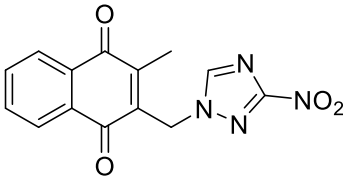

From **45**, eluent (CHX/EtOAc, 8/2 to 5/5, v/v, UV), yellow solid, 25.7% yield, very low solubility in deuterated solvent no ^{13}C NMR spectra was obtained. M.p. = 132-134°C. ^{1}H NMR (400 MHz, acetone-d_6) δ 8.79 (s, 1H), 8.13 – 7.99 (m, 2H), 7.92 – 7.81 (m, 2H), 5.68 (s, 2H), 2.44 (s, 3H). HRMS (ESI+) calcd. for $C_{14}H_{10}O_4N_4Na$: 321.0594. Found: 321.0591 ($M+Na^+$).

2-methyl-3-((2-nitro-1H-imidazol-1-yl)methyl)naphthalene-1,4-dione (44).

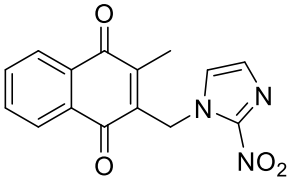

From **46**, eluent (CHX/EtOAc, 8/2 to 0/10, v/v, UV), orange solid, 14.6% yield. M.p. = 132-134°C. ^{1}H NMR (400 MHz, $CDCl_3$) δ 8.16 – 8.04 (m, 2H), 7.79 – 7.74 (m, 2H), 7.17 (d, J = 1.2 Hz, 1H), 7.12 (d, J = 1.2 Hz, 1H), 5.68 (s, 2H), 2.33 (s, 3H). ^{13}C {^{1}H} NMR (101 MHz, $CDCl_3$) δ 184.4, 183.8, 148.4, 138.1, 134.4, 134.4, 132.0, 131.6, 128.6, 126.9, 126.8, 126.1, 45.3, 13.4. HRMS (ESI+) calcd. for $C_{15}H_{12}O_4N_3$: 298.0822. Found: 298.0845 ($M+H^+$).

Oxidation of 1,2,3-[TRZ-methyl]-menadione by UV-irradiation.

Reactions were irradiated with a 350 nm light generated by eight RPR-3500A lamps of 200 W with a photochemical reactor for 72h at a distance of 3 cm from the light source.

2-(1-benzyl-1H-1,2,3-triazole-4-carbonyl)-3-methylnaphthalene-1,4-dione (β51).

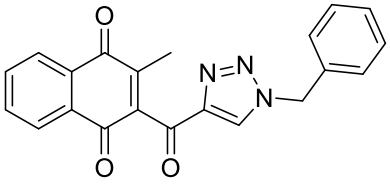

In a tube was dissolved in a mixture of propan-2-ol (0.74 mL) and DCM (0.92 mL), followed by **β13** (55 mg, 0.16 mmol, 1 equiv.). The mixture was bubbled in O_2 for 5 min, then stirred under O_2 pressure at 16°C for 72h under UV irradiation. The solvent was removed under vacuum and purified by silica gel chromatography (CHX/EtOAc, 8/2, v/v, UV) to afford **β51** (15.6 mg, 27.2%) as orange solid. M.p. = 115-117°C. ^{1}H NMR (400 MHz, $CDCl_3$) δ 8.17 – 8.11 (m, 2H), 8.08 – 8.03 (m, 1H), 7.78 – 7.73 (m, 2H), 7.43 (dd, J = 5.1, 2.0 Hz, 2H), 7.35 – 7.32 (m, 2H), 5.58 (s, 2H), 2.10 (s, 3H). ^{13}C {^{1}H} NMR (101 MHz, $CDCl_3$) δ 187.2, 185.1, 183.4, 147.5, 144.2, 143.8, 134.2, 134.1,

133.2, 132.1, 131.8, 129.6, 129.6, 128.8, 126.8, 126.5, 126.4, 54.8, 13.7. HRMS (ESI+) calcd. for $C_{21}H_{16}N_3O_3$: 358.1186. Found: 358.1183 ($M+H^+$).

1.7.2 Article 6

2-bromo-3,5-dimethylbenzene-1,4-diol (10).

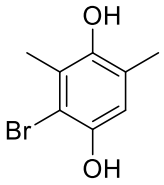

2,6-dimethylbenzoquinone (0.5 g, 3.7 mmol, 1 equiv.) was solubilized in Et_2O (45.8 mL), then a solution of $Na_2S_2O_4$ (4.8 g, 27.5 mmol, 7.5 equiv.) in water (45.8 mL) was added dropwise. The mixture was stirred 1h at 25°C. The crude was extracted three times with DCM, washed with water, dried over magnesium sulphate, solvent was removed under vacuum. The white solid was directly engaged in the next following step. The crude was solubilized in acetonitrile (16.1 mL) and NBS (0.65 g, 3.62 mmol, 1.07 equiv.) was added. The mixture was stirred 16h at 25°C. Organic solvent was removed under reduced pressure and was purified by silica gel chromatography (CHX/EtOAc, 7/3, v/v, UV) to obtain **10** (290.9 mg, 36.5%) as a white solid. ^{1}H NMR (400 MHz, $CDCl_3$) δ 6.72 (s, 1H), 5.14 (s, 1H), 4.30 (s, 1H), 2.34 (s, 3H), 2.20 (s, 3H). In accordance with a previous published method[149].

2-bromo-1,4-dimethoxy-3,5-dimethylbenzene (11).

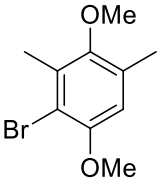

Compound **10** (290 mg, 1.34 mmol, 1 equiv.) was solubilized in acetone (13.4 mL) then K_2CO_3 (1.66 g, 12 mmol, 9 equiv.) and Me_2SO_4 (0.76 mL, 8 mmol, 6 equiv.) were added. The mixture was stirred under reflux 60°C for 4h. A 1 M NaOH aqueous solution was added, the organic solvent was removed under reduced pressure then extracted three times with DCM, washed with water, dried over magnesium sulphate and solvent was removed under vacuum. The yellow oil was directly engaged in the next reaction. ^{1}H NMR (400 MHz, $CDCl_3$) δ 6.60 (s, 1H), 3.85 (s, 3H), 3.66 (s, 3H), 2.37 (s, 3H), 2.27 (s, 3H). In accordance with a previous published method[149].

2-bromo-3,5-dimethylcyclohexa-2,5-diene-1,4-dione (18).

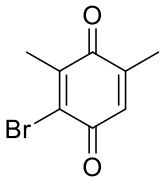

To a solution of 2,6-dimethylbenzoquinone (1 equiv.) in DCM (0.36 M), a solution of bromine (1.05 equiv.) in DCM (1.26 M) was added dropwise at 0°C. The mixture was stirred for 2h at 25°C, when DIPEA (1 equiv.) was added. The mixture was stirred for 3h at 25°C and poured into water. Water was added and extracted three times with DCM, washed with water, dried over magnesium sulphate, solvent was removed under vacuum. The crude was purified by silica gel chromatography (T, UV) to obtain **18** as an orange solid (47.5%). ^{1}H NMR (400 MHz, $CDCl_3$) δ 6.76 (q, J = 1.6 Hz, 1H), 2.24 (s, 3H), 2.08 (d, J = 1.6 Hz, 3H). ^{13}C {^{1}H} NMR (101 MHz, $CDCl_3$) δ 184.3, 179.9, 146.1, 145.7, 136.0, 133.2, 16.9, 16.6. HRMS (ESI+) calcd. for $C_8H_8BrO_2$: 214.9702. Found: 214.9709 ($M+H^+$). In accordance with a previous published method[164].

2-bromo-3,5-dimethyl-6-(4-(trifluoromethyl)benzyl)cyclohexa-2,5-diene-1,4-dione (20).

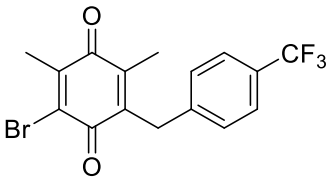

The compound **18** (1 equiv.) and 4-(trifluomethylphenyl)acetic acid (2 equiv.) were dissolved in a mixture of acetonitrile (0.06 M) and water (0.2 M). Then $AgNO_3$ (0.35 equiv.) and ammonium persulfate (1.3 equiv.) were added in the reaction mixture. The yellow mixture was protected from light and stirred under reflux for 3h. Organic solvent was

removed under reduced pressure then extracted three times with DCM, washed with water, dried over magnesium sulphate, solvent was removed under vacuum. The crude was purified by silica gel by silica gel chromatography (T/CHX, 7/3, v/v, UV), to obtain **20** as a yellow solid (65.7%). M.p. = 67-69°C. ^{1}H NMR (400 MHz, $CDCl_3$) δ 7.52 (d, J = 8.1 Hz, 2H), 7.30 (d, J = 7.9 Hz, 2H), 3.97 (s, 2H), 2.24 (s, 3H), 2.15 (s, 3H). ^{19}F {^{1}H} NMR (377 MHz, $CDCl_3$) δ -62.53. ^{13}C {^{1}H} NMR (101 MHz, $CDCl_3$) δ 184.6, 179.3, 146.3, 142.5, 141.9, 141.8 (q, J = 1.6 Hz), 135.7, 129.14 (q, J = 24.2 Hz), 129.06, 125.8 (q, J = 3.8 Hz), 124.3 (q, J = 279.6 Hz), 32.9, 17.3, 13.3. HRMS (ESI+) calcd. for $C_{16}H_{12}O_2BrF_3Na$: 394.9865. Found: 394.9860 ($M+Na^+$).

1-bromo-2,5-dimethoxy-4,6-dimethyl-3-(4-(trifluoromethyl)benzyl)benzene (22).

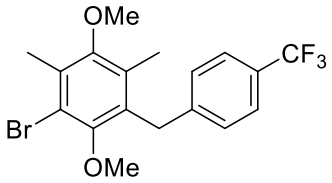

The compound **20** (1 equiv.) was solubilized in MeOH (0.26 M) then a solution of $SnCl_2$ (2.5 equiv.) in 37% HCl (4.12 equiv.) was added dropwise and the mixture was stirred 30 min at 25°C until the solution came back yellowish. Most of the solvent was evaporated under vacuum, the white precipitate was rinsed with water. The powder was dissolved in acetone (0.26 M) and dry over magnesium sulfate. Under argon dimethyl sulfate (5 equiv.) was added to the previous mixture then a solution of KOH (5 equiv.) in MeOH (1 M) was added dropwise. When the addition was completed the mixture was stirred under reflux 60°C during 3h. A 20% KOH aqueous solution (10 mL) was added to the mixture and organic solvent was removed under reduced pressure then extracted three times with DCM, washed with water, dried over magnesium sulphate, solvent was removed under vacuum. The crude was purified by silica gel chromatography (T/CHX, 5/5, v/v, UV) to obtain **22** as a colorless oil (73.6%). ^{1}H NMR (400 MHz, $CDCl_3$) δ 7.49 (d, J = 8.1 Hz, 2H), 7.20 (d, J = 8.2 Hz, 2H), 4.15 (s, 2H), 3.69 (s, 3H), 3.66 (s, 3H), 2.40 (s, 3H), 2.08 (s, 3H). ^{19}F {^{1}H} NMR (377 MHz, $CDCl_3$) δ -62.34. ^{13}C {^{1}H} NMR (101 MHz, $CDCl_3$) δ 154.0, 152.2, 144.5 (q, J = 1.4 Hz), 131.6, 130.9, 130.5, 129.2, 128.45, 128.44 (q, J = 24.5 Hz), 128.3, 125.5 (q, J = 3.7 Hz), 124.4 (q, J = 276 Hz), 118.3, 61.2, 60.5, 33.3, 16.9, 12.9. HRMS (ESI+) calcd. for $C_{18}H_{18}BrO_2F_3$: 402.0437. Found: 402.0418 ($M+H^+$).

General procedure of the metalation and borylation of the protected bromo-benzoquinone.

A solution of *n*-BuLi (1.2 equiv.) (1.6 M in hexanes) was added dropwise to a stirred solution of the corresponding protected bromo-benzoquinone (1 equiv.) in anhydrous THF (0.17 M) under argon at -78°C. The mixture was stirred at -78°C for 5 min and then triisopropyl borate (2.5 equiv.) was added dropwise at -78°C. The mixture was stirred back to 25°C for 16h. Quench with HCl 1 M an extracted three times with EtOAc, washed with water, dried over magnesium sulphate, solvent was removed under vacuum. The crude was purified by silica gel chromatography with the adequate solvent.

(3,6-dimethoxy-2,4-dimethylphenyl)boronic acid (12).

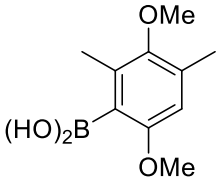

With compound **11**, eluent (CHX/EtOAc, 6/4, v/v, UV), white solid, 54% yield over two steps. ^{1}H NMR (400 MHz, $CDCl_3$) δ 6.58 (s, 1H), 5.83 (s, 2H), 3.83 (s, 3H), 3.65 (s, 3H), 2.48 (s, 3H), 2.31 (s, 3H). In accordance with a previous published method[149].

(2,5-dimethoxy-4,6-dimethyl-3-(4-(trifluoromethyl)benzyl)phenyl)boronic acid (24).

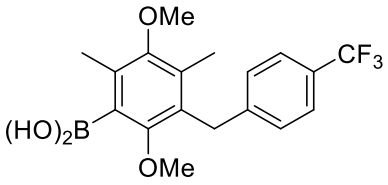

With compound **22**, eluent (CHX/EtOAc, 5/5, v/v, UV), white solid, 45.5% yield, contains a small impurity. M.p. = 115-117°C. ^{1}H NMR (400 MHz, $CDCl_3$) δ 7.49 (d, J = 8.1 Hz, 2H), 7.18 (d, J = 8.0 Hz, 2H), 5.93 (s, 2H), 4.08 (s, 2H), 3.65 (s, 3H), 3.62 (s, 3H), 2.44 (s, 3H), 2.11 (s, 3H). ^{19}F {^{1}H} NMR (377 MHz, $CDCl_3$) δ -62.32. ^{13}C {^{1}H} NMR (101 MHz, $CDCl_3$) δ 159.3, 154.2, 144.8 (q, J = 1.5 Hz), 135.9, 134.1, 129.0, 128.5 (q, J = 24.5 Hz), 128.4, 128.4, 125.4 (q, J = 3.8 Hz), 124.4 (q, J = 276 Hz), 62.7, 60.1, 32.4, 15.6, 13.1. HRMS (ESI+) calcd. for $C_{18}H_{19}BO_4F_3$: 367.1334. Found: 367.1331 ($M+H^+$).

General procedure of the oxidative demethylation of the protected benzoquinone.

The corresponding protected benzoquinone (1 equiv.) was solubilized in acetonitrile (0.08 M) then a solution of CAN (2.2 equiv.) in water (0.24 M) was added. The mixture was stirred 1h at 25°C. Organic solvent was removed under reduced pressure then extracted three times with DCM, washed with water, dried over magnesium sulphate, solvent was removed under vacuum. The crude was purified by silica gel chromatography with the adequate solvent.

(2,4-dimethyl-3,6-dioxocyclohexa-1,4-dien-1-yl)boronic acid (6).

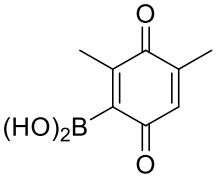

With compound **12**, no purification, yellow solid, 91.5% yield. ^{1}H NMR (400 MHz, $CDCl_3$) δ 7.00 (s, 2H), 6.60 (q, J = 1.6 Hz, 1H), 2.41 (s, 3H), 2.07 (d, J = 1.6 Hz, 3H). In accordance with a previous published method[149].

(2,4-dimethyl-3,6-dioxo-5-(4-(trifluoromethyl)benzyl)cyclohexa-1,4-dien-1-yl)boronic acid (27).

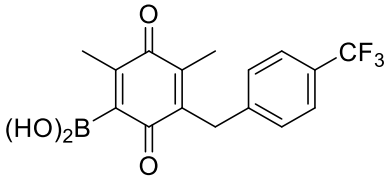

With compound **24**, eluent (T/CHX, 7/3, v/v, UV), yellow solid, 63.8% yield, with the same small impurity as observed for **24**. M.p. = 89-91°C. ^{1}H NMR (400 MHz, $CDCl_3$) δ 7.53 (d, J = 8.2 Hz, 2H), 7.28 (d, J = 7.8 Hz, 2H), 6.77 (s, 2H), 3.91 (s, 2H), 2.40 (s, 3H), 2.13 (s, 3H). ^{19}F {^{1}H} NMR (377 MHz, $CDCl_3$) δ -62.51. ^{13}C {^{1}H} NMR (101 MHz, $CDCl_3$) δ 193.8, 188.0, 157.5 (q, J = 1.5 Hz), 143.2, 142.9, 128.94, 128.91, 128.8 (q, J = 24.5 Hz), 125.8 (q, J = 4.0 Hz), 32.1, 15.7, 13.1. HRMS (ESI+) calcd. for $C_{16}H_{13}BO_4F_3$: 337.0864. Found: 337.0866 ($M+H^+$).

General procedure of the Diels-Alder cycloaddition reaction.

The corresponding boronic acid (1 equiv.) was solubilized in DCM (0.07 M), then at -20°C was added (3E/Z)-4-methoxybuta-1,3-diene (3 equiv.), the mixture was stirred 1h at -20°C. Water was added and the crude was extracted three times with DCM, washed with water, dried over magnesium sulphate, solvent was removed under vacuum. The crude was purified by silica gel chromatography with the adequate solvent.

(±)-3,4a-dimethyl-4a,5-dihydronaphthalene-1,4-dione (13).

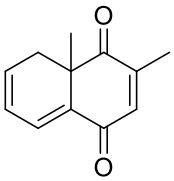

With compound **12**, eluent (CHX/EtOAc, 8/2, v/v, UV), yellow oil, 52.6% yield. ^{1}H NMR (400 MHz, $CDCl_3$) δ 7.06 (dt, J = 5.3, 1.1 Hz, 1H), 6.78 (q, J = 1.5 Hz, 1H), 6.33 – 6.18 (m, 2H), 2.64 – 2.56 (m, 2H), 2.06 (d, J = 1.5 Hz, 3H), 1.23 (s, 3H). In accordance with a previous published method[149].

(±)-3,4a-dimethyl-2-(4-(trifluoromethyl)benzyl)-4a,5-dihydronaphthalene-1,4-dione (2).

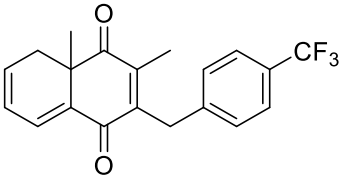

With compound **27**, eluent (CHX/EtOAc, 9/1, v/v, UV), yellow oil, 58.7% yield. ^{1}H NMR (400 MHz, $CDCl_3$) δ 7.52 (d, J = 8.1 Hz, 2H), 7.30 (d, J = 8.0 Hz, 2H), 7.15 (dd, J = 5.3, 1.2 Hz, 1H), 6.35 – 6.19 (m, 2H), 4.10 – 3.91 (m, 2H), 2.63 (dd, J = 4.6, 1.6 Hz, 2H), 2.12 (s, 3H), 1.21 (s, 3H). ^{19}F {^{1}H} NMR (377 MHz, $CDCl_3$) δ -62.48. ^{13}C {^{1}H} NMR (101 MHz, $CDCl_3$) δ 201.0, 184.4, 147.9, 144.9, 142.4 (q, J = 1.6 Hz), 134.3, 133.6, 131.0, 128.9, 128.8 (q, J = 24 Hz), 125.7 (q, J = 3.7 Hz), 124.3 (q, J = 279.6 Hz), 123.6, 44.2, 32.6, 32.2, 25.2, 14.3. HRMS (ESI+) calcd. for $C_{20}H_{18}O_2F_3$: 347.1253. Found: 347.1255 ($M+H^+$).

Références bibliographiques

(1) By-Nc-Sa, C. World Malaria Report 2023.
(2) Phillips, M. A.; Burrows, J. N.; Manyando, C.; Van Huijsduijnen, R. H.; Van Voorhis, W. C.; Wells, T. N. C. Malaria. *Nat. Rev. Dis. Primer* **2017**, *3* (1), 17050. https://doi.org/10.1038/nrdp.2017.50.
(3) Markus, M. B. The Hypnozoite Concept, with Particular Reference to Malaria. *Parasitol. Res.* **2011**, *108* (1), 247–252. https://doi.org/10.1007/s00436-010-2072-y.
(4) Baker, D. A. Malaria Gametocytogenesis. *Mol. Biochem. Parasitol.* **2010**, *172* (2), 57–65. https://doi.org/10.1016/j.molbiopara.2010.03.019.
(5) Bozdech, Z.; Llinás, M.; Pulliam, B. L.; Wong, E. D.; Zhu, J.; DeRisi, J. L. The Transcriptome of the Intraerythrocytic Developmental Cycle of Plasmodium Falciparum. *PLoS Biol.* **2003**, *1* (1), e5. https://doi.org/10.1371/journal.pbio.0000005.
(6) Gardner, M. J.; Hall, N.; Fung, E.; White, O.; Berriman, M.; Hyman, R. W.; Carlton, J. M.; Pain, A.; Nelson, K. E.; Bowman, S.; Paulsen, I. T.; James, K.; Eisen, J. A.; Rutherford, K.; Salzberg, S. L.; Craig, A.; Kyes, S.; Chan, M.-S.; Nene, V.; Shallom, S. J.; Suh, B.; Peterson, J.; Angiuoli, S.; Pertea, M.; Allen, J.; Selengut, J.; Haft, D.; Mather, M. W.; Vaidya, A. B.; Martin, D. M. A.; Fairlamb, A. H.; Fraunholz, M. J.; Roos, D. S.; Ralph, S. A.; McFadden, G. I.; Cummings, L. M.; Subramanian, G. M.; Mungall, C.; Venter, J. C.; Carucci, D. J.; Hoffman, S. L.; Newbold, C.; Davis, R. W.; Fraser, C. M.; Barrell, B. Genome Sequence of the Human Malaria Parasite Plasmodium Falciparum. **2002**, *419*.
(7) Kawada, H.; Ohashi, K.; Dida, G. O.; Sonye, G.; Njenga, S. M.; Mwandawiro, C.; Minakawa, N. Insecticidal and Repellent Activities of Pyrethroids to the Three Major Pyrethroid-Resistant Malaria Vectors in Western Kenya. *Parasit. Vectors* **2014**, *7* (1), 208. https://doi.org/10.1186/1756-3305-7-208.
(8) Hemingway, J.; Ranson, H.; Magill, A.; Kolaczinski, J.; Fornadel, C.; Gimnig, J.; Coetzee, M.; Simard, F.; Roch, D. K.; Hinzoumbe, C. K.; Pickett, J.; Schellenberg, D.; Gething, P.; Hoppé, M.; Hamon, N. Averting a Malaria Disaster: Will Insecticide Resistance Derail Malaria Control? *The Lancet* **2016**, *387* (10029), 1785–1788. https://doi.org/10.1016/S0140-6736(15)00417-1.
(9) Protopopoff, N.; Matowo, J.; Malima, R.; Kavishe, R.; Kaaya, R.; Wright, A.; West, P. A.; Kleinschmidt, I.; Kisinza, W.; Mosha, F. W.; Rowland, M. High Level of Resistance in the Mosquito Anopheles Gambiae to Pyrethroid Insecticides and Reduced Susceptibility to Bendiocarb in North-Western Tanzania. *Malar. J.* **2013**, *12* (1), 149. https://doi.org/10.1186/1475-2875-12-149.
(10) Stanisic, D. I.; Good, M. F. Malaria Vaccines: Progress to Date. *BioDrugs* **2023**, *37* (6), 737–756. https://doi.org/10.1007/s40259-023-00623-4.
(11) Ouattara, A.; Barry, A. E.; Dutta, S.; Remarque, E. J.; Beeson, J. G.; Plowe, C. V. Designing Malaria Vaccines to Circumvent Antigen Variability. *Vaccine* **2015**, *33* (52), 7506–7512. https://doi.org/10.1016/j.vaccine.2015.09.110.
(12) *RTS,S/AS01 vaccine (Mosquirix™): an overview*. https://www.tandfonline.com/doi/epdf/10.1080/21645515.2019.1669415?needAccess=true (accessed 2024-05-25).
(13) Neafsey, D. E.; Juraska, M.; Bedford, T.; Benkeser, D.; Valim, C.; Griggs, A.; Lievens, M.; Abdulla, S.; Adjei, S.; Agbenyega, T.; Agnandji, S. T.; Aide, P.; Anderson, S.; Ansong, D.; Aponte, J. J.; Asante, K. P.; Bejon, P.; Birkett, A. J.; Bruls, M.; Connolly, K. M.; D'Alessandro, U.; Dobaño, C.; Gesase, S.; Greenwood, B.; Grimsby, J.; Tinto, H.; Hamel, M. J.; Hoffman, I.; Kamthunzi, P.; Kariuki, S.; Kremsner, P. G.; Leach, A.; Lell, B.; Lennon, N. J.; Lusingu, J.; Marsh, K.; Martinson, F.; Molel, J. T.; Moss, E. L.; Njuguna, P.; Ockenhouse, C. F.; Ogutu, B. R.; Otieno, W.; Otieno, L.; Otieno, K.; Owusu-Agyei, S.; Park, D. J.; Pellé, K.; Robbins, D.; Russ, C.; Ryan, E. M.; Sacarlal, J.; Sogoloff, B.; Sorgho, H.; Tanner, M.; Theander, T.; Valea, I.; Volkman, S. K.; Yu, Q.; Lapierre, D.; Birren, B. W.; Gilbert, P. B.; Wirth, D. F. Genetic Diversity and Protective Efficacy of the RTS,S/AS01 Malaria Vaccine. *N. Engl. J. Med.* **2015**, *373* (21), 2025–2037. https://doi.org/10.1056/NEJMoa1505819.
(14) White, N. J. Qinghaosu (Artemisinin): The Price of Success. *Science* **2008**, *320* (5874), 330–334. https://doi.org/10.1126/science.1155165.
(15) *Total synthesis of qinghaosu | Journal of the American Chemical Society*. https://pubs.acs.org/doi/10.1021/ja00341a054 (accessed 2024-05-26).
(16) Eckstein-Ludwig, U.; Webb, R. J.; Van Goethem, I. D. A.; East, J. M.; Lee, A. G.; Kimura, M.; O'Neill, P. M.; Bray, P. G.; Ward, S. A.; Krishna, S. Artemisinins Target the SERCA of Plasmodium Falciparum. *Nature* **2003**, *424* (6951), 957–961. https://doi.org/10.1038/nature01813.
(17) Haynes, R. K.; Chan, W. C.; Lung, C.-M.; Uhlemann, A.-C.; Eckstein, U.; Taramelli, D.; Parapini, S.; Monti, D.; Krishna, S. The Fe2+-Mediated Decomposition, PfATP6 Binding, and Antimalarial Activities of Artemisone and Other Artemisinins: The Unlikelihood of C-Centered Radicals as Bioactive Intermediates. *ChemMedChem* **2007**, *2* (10), 1480–1497. https://doi.org/10.1002/cmdc.200700108.
(18) Mesén-Ramírez, P.; Bergmann, B.; Elhabiri, M.; Zhu, L.; Thien, H. von; Castro-Peña, C.; Gilberger, T.-W.; Davioud-Charvet, E.; Bozdech, Z.; Bachmann, A.; Spielmann, T. The Parasitophorous Vacuole Nutrient Channel Is Critical for Drug Access in Malaria Parasites and Modulates the Artemisinin

Resistance Fitness Cost. *Cell Host Microbe* **2021**, *29* (12), 1774-1787.e9. https://doi.org/10.1016/j.chom.2021.11.002.
(19) Phyo, A. P.; Nkhoma, S.; Stepniewska, K.; Ashley, E. A.; Nair, S.; McGready, R.; ler Moo, C.; Al-Saai, S.; Dondorp, A. M.; Lwin, K. M.; Singhasivanon, P.; Day, N. P.; White, N. J.; Anderson, T. J.; Nosten, F. Emergence of Artemisinin-Resistant Malaria on the Western Border of Thailand: A Longitudinal Study. *The Lancet* **2012**, *379* (9830), 1960–1966. https://doi.org/10.1016/S0140-6736(12)60484-X.
(20) Balikagala, B.; Fukuda, N.; Ikeda, M.; Katuro, O. T.; Tachibana, S.-I.; Yamauchi, M.; Opio, W.; Emoto, S.; Anywar, D. A.; Kimura, E.; Palacpac, N. M. Q.; Odongo-Aginya, E. I.; Ogwang, M.; Horii, T.; Mita, T. Evidence of Artemisinin-Resistant Malaria in Africa. *N. Engl. J. Med.* **2021**, *385* (13), 1163–1171. https://doi.org/10.1056/NEJMoa2101746.
(21) Das, S.; Saha, B.; Hati, A. K.; Roy, S. Evidence of Artemisinin-Resistant Plasmodium Falciparum Malaria in Eastern India. *N. Engl. J. Med.* **2018**, *379* (20), 1962–1964. https://doi.org/10.1056/NEJMc1713777.
(22) Woodward, R. B.; Doering, W. E. The Total Synthesis of Quinine. *J. Am. Chem. Soc.* **1945**, *67* (5), 860–874. https://doi.org/10.1021/ja01221a051.
(23) Coban, C. The Host Targeting Effect of Chloroquine in Malaria. *Curr. Opin. Immunol.* **2020**, *66*, 98–107. https://doi.org/10.1016/j.coi.2020.07.005.
(24) Wellems, T. E.; Plowe, C. V. Chloroquine-Resistant Malaria. *J. Infect. Dis.* **2001**, *184* (6), 770–776. https://doi.org/10.1086/322858.
(25) Wani, W. A.; Jameel, E.; Baig, U.; Mumtazuddin, S.; Hun, L. T. Ferroquine and Its Derivatives: New Generation of Antimalarial Agents. *Eur. J. Med. Chem.* **2015**, *101*, 534–551. https://doi.org/10.1016/j.ejmech.2015.07.009.
(26) Dubar, F.; Slomianny, C.; Khalife, J.; Dive, D.; Kalamou, H.; Guérardel, Y.; Grellier, P.; Biot, C. The Ferroquine Antimalarial Conundrum: Redox Activation and Reinvasion Inhibition. *Angew. Chem. Int. Ed.* **2013**, *52* (30), 7690–7693. https://doi.org/10.1002/anie.201303690.
(27) Nixon, G. L.; Moss, D. M.; Shone, A. E.; Lalloo, D. G.; Fisher, N.; O'Neill, P. M.; Ward, S. A.; Biagini, G. A. Antimalarial Pharmacology and Therapeutics of Atovaquone. *J. Antimicrob. Chemother.* **2013**, *68* (5), 977–985. https://doi.org/10.1093/jac/dks504.
(28) *Methylene blue as an antimalarial agent*. https://doi.org/10.1179/135100003225002899.
(29) Müller, T.; Johann, L.; Jannack, B.; Brückner, M.; Lanfranchi, D. A.; Bauer, H.; Sanchez, C.; Yardley, V.; Deregnaucourt, C.; Schrével, J.; Lanzer, M.; Schirmer, R. H.; Davioud-Charvet, E. Glutathione Reductase-Catalyzed Cascade of Redox Reactions To Bioactivate Potent Antimalarial 1,4-Naphthoquinones – A New Strategy to Combat Malarial Parasites. *J. Am. Chem. Soc.* **2011**, *133* (30), 11557–11571. https://doi.org/10.1021/ja201729z.
(30) Blank, O.; Davioud-Charvet, E.; Elhabiri, M. Interactions of the Antimalarial Drug Methylene Blue with Methemoglobin and Heme Targets in Plasmodium Falciparum: A Physico-Biochemical Study. *Antioxid. Redox Signal.* **2012**, *17* (4), 544–554. https://doi.org/10.1089/ars.2011.4239.
(31) Müller, S. Redox and Antioxidant Systems of the Malaria Parasite Plasmodium Falciparum. *Mol. Microbiol.* **2004**, *53* (5), 1291–1305. https://doi.org/10.1111/j.1365-2958.2004.04257.x.
(32) Ehrhardt, K.; Deregnaucourt, C.; Goetz, A.-A.; Tzanova, T.; Gallo, V.; Arese, P.; Pradines, B.; Adjalley, S. H.; Bagrel, D.; Blandin, S.; Lanzer, M.; Davioud-Charvet, E. The Redox Cycler Plasmodione Is a Fast-Acting Antimalarial Lead Compound with Pronounced Activity against Sexual and Early Asexual Blood-Stage Parasites. *Antimicrob. Agents Chemother.* **2016**, *60* (9), 5146–5158. https://doi.org/10.1128/aac.02975-15.
(33) *Antimalarial NADPH-Consuming Redox-Cyclers As Superior Glucose-6-Phosphate Dehydrogenase Deficiency Copycats*. https://doi.org/10.1089/ars.2014.6047.
(34) Manickam, M.; Boggu, P. R.; Cho, J.; Nam, Y. J.; Lee, S. J.; Jung, S.-H. Investigation of Chemical Reactivity of 2-Alkoxy-1,4-Naphthoquinones and Their Anticancer Activity. *Bioorg. Med. Chem. Lett.* **2018**, *28* (11), 2023–2028. https://doi.org/10.1016/j.bmcl.2018.04.060.
(35) Ravichandiran, P.; Masłyk, M.; Sheet, S.; Janeczko, M.; Premnath, D.; Kim, A. R.; Park, B.; Han, M.; Yoo, D. J. Synthesis and Antimicrobial Evaluation of 1,4-Naphthoquinone Derivatives as Potential Antibacterial Agents. *ChemistryOpen* **2019**, *8* (5), 589–600. https://doi.org/10.1002/open.201900077.
(36) Dulo, B.; Phan, K.; Githaiga, J.; Raes, K.; De Meester, S. Natural Quinone Dyes: A Review on Structure, Extraction Techniques, Analysis and Application Potential. *Waste Biomass Valorization* **2021**, *12* (12), 6339–6374. https://doi.org/10.1007/s12649-021-01443-9.
(37) Patel, O. P. S.; Beteck, R. M.; Legoabe, L. J. Antimalarial Application of Quinones: A Recent Update. *Eur. J. Med. Chem.* **2021**, *210*, 113084. https://doi.org/10.1016/j.ejmech.2020.113084.
(38) Salmon-Chemin, L.; Lemaire, A.; De Freitas, S.; Deprez, B.; Sergheraert, C.; Davioud-Charvet, E. Parallel Synthesis of a Library of 1,4-Naphthoquinones and Automated Screening of Potential

Inhibitors of Trypanothione Reductase from *Trypanosoma Cruzi*. *Bioorg. Med. Chem. Lett.* **2000**, *10* (7), 631–635. https://doi.org/10.1016/S0960-894X(00)00056-1.
(39) Weiss, C. R.; Moideen, S. V.; Croft, S. L.; Houghton, P. J. Activity of Extracts and Isolated Naphthoquinones from Kigelia Pinnata against Plasmodium Falciparum. *J. Nat. Prod.* **2000**, *63* (9), 1306–1309. https://doi.org/10.1021/np000029g.
(40) Davioud-Charvet, E.; Delarue, S.; Biot, C.; Schwöbel, B.; Boehme, C. C.; Müssigbrodt, A.; Maes, L.; Sergheraert, C.; Grellier, P.; Schirmer, R. H.; Becker, K. A Prodrug Form of a Plasmodium Falciparum Glutathione Reductase Inhibitor Conjugated with a 4-Anilinoquinoline. *J. Med. Chem.* **2001**, *44* (24), 4268–4276. https://doi.org/10.1021/jm010268g.
(41) Biot, C.; Bauer, H.; Schirmer, R. H.; Davioud-Charvet, E. 5-Substituted Tetrazoles as Bioisosteres of Carboxylic Acids. Bioisosterism and Mechanistic Studies on Glutathione Reductase Inhibitors as Antimalarials. *J. Med. Chem.* **2004**, *47* (24), 5972–5983. https://doi.org/10.1021/jm0497545.
(42) Bauer, H.; Fritz-Wolf, K.; Winzer, A.; Kühner, S.; Little, S.; Yardley, V.; Vezin, H.; Palfey, B.; Schirmer, R. H.; Davioud-Charvet, E. A Fluoro Analogue of the Menadione Derivative 6-[2‘-(3‘-Methyl)-1‘,4‘-Naphthoquinolyl]Hexanoic Acid Is a Suicide Substrate of Glutathione Reductase. Crystal Structure of the Alkylated Human Enzyme. *J. Am. Chem. Soc.* **2006**, *128* (33), 10784–10794. https://doi.org/10.1021/ja061155v.
(43) *The Redox Cycler Plasmodione Is a Fast-Acting Antimalarial Lead Compound with Pronounced Activity against Sexual and Early Asexual Blood-Stage Parasites*. https://doi.org/10.1128/aac.02975-15.
(44) Feng, L.; Lanfranchi, D. A.; Cotos, L.; Cesar-Rodo, E.; Ehrhardt, K.; Goetz, A.-A.; Zimmermann, H.; Fenaille, F.; Blandin, S. A.; Davioud-Charvet, E. Synthesis of Plasmodione Metabolites and 13C-Enriched Plasmodione as Chemical Tools for Drug Metabolism Investigation. *Org. Biomol. Chem.* **2018**, *16* (15), 2647–2665. https://doi.org/10.1039/C8OB00227D.
(45) Cichocki, B. A.; Donzel, M.; Heimsch, K. C.; Lesanavičius, M.; Feng, L.; Montagut, E. J.; Becker, K.; Aliverti, A.; Elhabiri, M.; Čėnas, N.; Davioud-Charvet, E. Plasmodium Falciparum Ferredoxin-NADP+ Reductase-Catalyzed Redox Cycling of Plasmodione Generates Both Predicted Key Drug Metabolites: Implication for Antimalarial Drug Development. *ACS Infect. Dis.* **2021**, *7* (7), 1996–2012. https://doi.org/10.1021/acsinfecdis.1c00054.
(46) Bielitza, M.; Belorgey, D.; Ehrhardt, K.; Johann, L.; Lanfranchi, D. A.; Gallo, V.; Schwarzer, E.; Mohring, F.; Jortzik, E.; Williams, D. L.; Becker, K.; Arese, P.; Elhabiri, M.; Davioud-Charvet, E. Antimalarial NADPH-Consuming Redox-Cyclers As Superior Glucose-6-Phosphate Dehydrogenase Deficiency Copycats. *Antioxid. Redox Signal.* **2015**, *22* (15), 1337–1351. https://doi.org/10.1089/ars.2014.6047.
(47) Nawrat, C. C.; Moody, C. J. Quinones as Dienophiles in the Diels–Alder Reaction: History and Applications in Total Synthesis. *Angew. Chem. Int. Ed.* **2014**, *53* (8), 2056–2077. https://doi.org/10.1002/anie.201305908.
(48) Nicolaou, K. C.; Snyder, S. A.; Montagnon, T.; Vassilikogiannakis, G. The Diels-Alder Reaction in Total Synthesis. *Angew. Chem. Int. Ed.* **2002**, *41* (10), 1668–1698. https://doi.org/10.1002/1521-3773(20020517)41:10<1668::AID-ANIE1668>3.0.CO;2-Z.
(49) Corey, E. J. Catalytic Enantioselective Diels-Alder Reactions: Methods, Mechanistic Fundamentals, Pathways, and Applications. *Angew. Chem. Int. Ed.* **2002**, *41* (10), 1650–1667. https://doi.org/10.1002/1521-3773(20020517)41:10<1650::AID-ANIE1650>3.0.CO;2-B.
(50) Rodo, E. C.; Feng, L.; Jida, M.; Ehrhardt, K.; Bielitza, M.; Boilevin, J.; Lanzer, M.; Williams, D. L.; Lanfranchi, D. A.; Davioud-Charvet, E. A Platform of Regioselective Methodologies to Access Polysubstituted 2-Methyl-1,4-Naphthoquinone Derivatives: Scope and Limitations. *Eur. J. Org. Chem.* **2016**, *2016* (11), 1982–1993. https://doi.org/10.1002/ejoc.201600144.
(51) Lanfranchi, D. A.; Cesar-Rodo, E.; Bertrand, B.; Huang, H.-H.; Day, L.; Johann, L.; Elhabiri, M.; Becker, K.; Williams, D. L.; Davioud-Charvet, E. Synthesis and Biological Evaluation of 1,4-Naphthoquinones and Quinoline-5,8-Diones as Antimalarial and Schistosomicidal Agents. *Org. Biomol. Chem.* **2012**, *10* (31), 6375–6387. https://doi.org/10.1039/C2OB25812A.
(52) Morin, C.; Besset, T.; Moutet, J.-C.; Fayolle, M.; Brückner, M.; Limosin, D.; Becker, K.; Davioud-Charvet, E. The Aza-Analogues of 1,4-Naphthoquinones Are Potent Substrates and Inhibitors of Plasmodial Thioredoxin and Glutathione Reductases and of Human Erythrocyte Glutathione Reductase. *Org. Biomol. Chem.* **2008**, *6* (15), 2731–2742. https://doi.org/10.1039/B802649C.
(53) Meanwell, N. A. A Synopsis of the Properties and Applications of Heteroaromatic Rings in Medicinal Chemistry. In *Advances in Heterocyclic Chemistry*; Elsevier, 2017; Vol. 123, pp 245–361. https://doi.org/10.1016/bs.aihch.2016.11.002.
(54) *Electrochemical Properties of Substituted 2-Methyl-1,4-Naphthoquinones: Redox Behavior Predictions*. https://doi.org/10.1002/chem.201403703.

(55) Trometer, N.; Roignant, M.; Davioud-Charvet, E. Efficient Multigram-Scale Synthesis of 7-Substituted 3-Methyltetral-1-Ones and 6-Fluoromenadione. *Org. Process Res. Dev.* **2022**, *26* (4), 1152–1164. https://doi.org/10.1021/acs.oprd.1c00421.
(56) Amaral, S. P.; Fernandez-Villamarin, M.; Correa, J.; Riguera, R.; Fernandez-Megia, E. Efficient Multigram Synthesis of the Repeating Unit of Gallic Acid-Triethylene Glycol Dendrimers. *Org. Lett.* **2011**, *13* (17), 4522–4525. https://doi.org/10.1021/ol201677k.
(57) Trometer, N.; Cichocki, B.; Chevalier, Q.; Pécourneau, J.; Strub, J.-M.; Hemmerlin, A.; Specht, A.; Davioud-Charvet, E.; Elhabiri, M. Synthesis and Photochemical Properties of Fluorescent Metabolites Generated from Fluorinated Benzoylmenadiones in Living Cells. *J. Org. Chem.* **2023**, acs.joc.3c00620. https://doi.org/10.1021/acs.joc.3c00620.
(58) Anderson, J. M.; Kochi, J. K. Silver(II) Complexes in Oxidative Decarboxylation of Acids. *J. Org. Chem.* **1970**, *35* (4), 986–989. https://doi.org/10.1021/jo00829a026.
(59) Urgin, K.; Jida, M.; Ehrhardt, K.; Müller, T.; Lanzer, M.; Maes, L.; Elhabiri, M.; Davioud-Charvet, E. Pharmacomodulation of the Antimalarial Plasmodione: Synthesis of Biaryl- and N-Arylalkylamine Analogues, Antimalarial Activities and Physicochemical Properties. *Molecules* **2017**, *22* (1), 161. https://doi.org/10.3390/molecules22010161.
(60) Dombrowski, A. W.; Gesmundo, N. J.; Aguirre, A. L.; Sarris, K. A.; Young, J. M.; Bogdan, A. R.; Martin, M. C.; Gedeon, S.; Wang, Y. Expanding the Medicinal Chemist Toolbox: Comparing Seven C(Sp2)–C(Sp3) Cross-Coupling Methods by Library Synthesis. *ACS Med. Chem. Lett.* **2020**, *11* (4), 597–604. https://doi.org/10.1021/acsmedchemlett.0c00093.
(61) Henry, N.; Enguehard-Gueiffier, C.; Thery, I.; Gueiffier, A. One-Pot Dual Substitutions of Bromobenzyl Chloride, 2-Chloromethyl-6-Halogenoimidazo[1,2-a]Pyridine and -[1,2-b]Pyridazine by Suzuki–Miyaura Cross-Coupling Reactions. *Eur. J. Org. Chem.* **2008**, *2008* (28), 4824–4827. https://doi.org/10.1002/ejoc.200800544.
(62) Ishiyama, T.; Murata, M.; Miyaura, N. Palladium(0)-Catalyzed Cross-Coupling Reaction of Alkoxydiboron with Haloarenes: A Direct Procedure for Arylboronic Esters. *J. Org. Chem.* **1995**, *60* (23), 7508–7510. https://doi.org/10.1021/jo00128a024.
(63) *Direct C−H Radical Alkylation of 1,4-Quinones*. https://doi.org/10.1002/ejoc.202100452.
(64) Donzel, M.; Elhabiri, M.; Davioud-Charvet, E. Bioinspired Photoredox Benzylation of Quinones. *J. Org. Chem.* **2021**, *86* (15), 10055–10066. https://doi.org/10.1021/acs.joc.1c00814.
(65) Trometer, N.; Pecourneau, J.; Feng, L.; Navarro-Huerta, J. A.; Lazarin-Bidóia, D.; de Oliveira Silva Lautenschlager, S.; Maes, L.; Fortes Francisco, A.; Kelly, J. M.; Meunier, B.; Cal, M.; Mäser, P.; Kaiser, M.; Davioud-Charvet, E. Synthesis and Anti-Chagas Activity Profile of a Redox-Active Lead 3-Benzylmenadione Revealed by High-Content Imaging. *ACS Infect. Dis.* **2024**, *10* (5), 1808–1838. https://doi.org/10.1021/acsinfecdis.4c00137.
(66) *Redox Polypharmacology as an Emerging Strategy to Combat Malarial Parasites*. https://doi.org/10.1002/cmdc.201600009.
(67) Görner, H. Photoreduction of Nitro-1,4-Naphthoquinones in Solution. *J. Photochem. Photobiol. Chem.* **2011**, *224* (1), 135–140. https://doi.org/10.1016/j.jphotochem.2011.09.016.
(68) Cotos, L.; Donzel, M.; Elhabiri, M.; Davioud-Charvet, E. A Mild and Versatile Friedel–Crafts Methodology for the Diversity-Oriented Synthesis of Redox-Active 3-Benzoylmenadiones with Tunable Redox Potentials. *Chem. – Eur. J.* **2020**, *26* (15), 3314–3325. https://doi.org/10.1002/chem.201904220.
(69) Swift, R. P.; Rajaram, K.; Elahi, R.; Liu, H. B.; Prigge, S. T. Roles of Ferredoxin-Dependent Proteins in the Apicoplast of Plasmodium Falciparum Parasites. *mBio* **2022**, *13* (1), e03023-21. https://doi.org/10.1128/mbio.03023-21.
(70) *Uncovering the essential genes of the human malaria parasite Plasmodium falciparum by saturation mutagenesis*. https://doi.org/10.1126/science.aap7847.
(71) Lichtman, J. W.; Conchello, J.-A. Fluorescence Microscopy. *Nat. Methods* **2005**, *2* (12), 910–919. https://doi.org/10.1038/nmeth817.
(72) Ding, C.; Ren, T. Near Infrared Fluorescent Probes for Detecting and Imaging Active Small Molecules. *Coord. Chem. Rev.* **2023**, *482*, 215080. https://doi.org/10.1016/j.ccr.2023.215080.
(73) Acuña-Rodriguez, J. P.; Mena-Vega, J. P.; Argüello-Miranda, O. Live-Cell Fluorescence Spectral Imaging as a Data Science Challenge. *Biophys. Rev.* **2022**, *14* (2), 579–597. https://doi.org/10.1007/s12551-022-00941-x.
(74) Helmchen, F.; Denk, W. Deep Tissue Two-Photon Microscopy. *Nat. Methods* **2005**, *2* (12), 932–940. https://doi.org/10.1038/nmeth818.
(75) *Design of Organic Molecules with Large Two-Photon Absorption Cross Sections*. https://doi.org/10.1126/science.281.5383.1653.
(76) Berezin, M. Y.; Achilefu, S. Fluorescence Lifetime Measurements and Biological Imaging. *Chem. Rev.* **2010**, *110* (5), 2641–2684. https://doi.org/10.1021/cr900343z.

(77) Sauer, M.; Heilemann, M. Single-Molecule Localization Microscopy in Eukaryotes. *Chem. Rev.* **2017**, *117* (11), 7478–7509. https://doi.org/10.1021/acs.chemrev.6b00667.
(78) Jiang, G.; Liu, H.; Liu, H.; Ke, G.; Ren, T.-B.; Xiong, B.; Zhang, X.-B.; Yuan, L. Chemical Approaches to Optimize the Properties of Organic Fluorophores for Imaging and Sensing. *Angew. Chem. Int. Ed.* **2024**, *63* (11), e202315217. https://doi.org/10.1002/anie.202315217.
(79) Zhu, H.; Fan, J.; Du, J.; Peng, X. Fluorescent Probes for Sensing and Imaging within Specific Cellular Organelles. *Acc. Chem. Res.* **2016**, *49* (10), 2115–2126. https://doi.org/10.1021/acs.accounts.6b00292.
(80) Beija, M.; Afonso, C. A. M.; Martinho, J. M. G. Synthesis and Applications of Rhodamine Derivatives as Fluorescent Probes. *Chem. Soc. Rev.* **2009**, *38* (8), 2410–2433. https://doi.org/10.1039/B901612K.
(81) Pina, F.; Melo, M. J.; Laia, C. A. T.; Parola, A. J.; Lima, J. C. Chemistry and Applications of Flavylium Compounds: A Handful of Colours. *Chem. Soc. Rev.* **2012**, *41* (2), 869–908. https://doi.org/10.1039/C1CS15126F.
(82) Khoo, H. E.; Azlan, A.; Tang, S. T.; Lim, S. M. Anthocyanidins and Anthocyanins: Colored Pigments as Food, Pharmaceutical Ingredients, and the Potential Health Benefits. *Food Nutr. Res.* **2017**.
(83) Trouillas, P.; Sancho-García, J. C.; De Freitas, V.; Gierschner, J.; Otyepka, M.; Dangles, O. Stabilizing and Modulating Color by Copigmentation: Insights from Theory and Experiment. *Chem. Rev.* **2016**, *116* (9), 4937–4982. https://doi.org/10.1021/acs.chemrev.5b00507.
(84) Elhabiri, M.; Figueiredo, P.; Toki, K.; P. Figueiredo, K. T.; Brouillard, R. Anthocyanin–Aluminium and –Gallium Complexes in Aqueoussolution. *J. Chem. Soc. Perkin Trans. 2* **1997**, No. 2, 355–362. https://doi.org/10.1039/A603851D.
(85) Basílio, N.; Pina, F. Chemistry and Photochemistry of Anthocyanins and Related Compounds: A Thermodynamic and Kinetic Approach. *Molecules* **2016**, *21* (11), 1502. https://doi.org/10.3390/molecules21111502.
(86) Roque, A.; Lodeiro, C.; Pina, F.; Maestri, M.; Dumas, S.; Passaniti, P.; Balzani, V. Multistate/Multifunctional Systems. A Thermodynamic, Kinetic, and Photochemical Investigation of the 4'-Dimethylaminoflavylium Compound. *J. Am. Chem. Soc.* **2003**, *125* (4), 987–994. https://doi.org/10.1021/ja0287276.
(87) Cruz, L.; Basílio, N.; Mateus, N.; De Freitas, V.; Pina, F. Natural and Synthetic Flavylium-Based Dyes: The Chemistry Behind the Color. *Chem. Rev.* **2022**, *122* (1), 1416–1481. https://doi.org/10.1021/acs.chemrev.1c00399.
(88) Sun, Y.; Sun, P.; Li, Z.; Qu, L.; Guo, W. Natural Flavylium-Inspired Far-Red to NIR-II Dyes and Their Applications as Fluorescent Probes for Biomedical Sensing. *Chem. Soc. Rev.* **2022**, *51* (16), 7170–7205. https://doi.org/10.1039/D2CS00179A.
(89) *A Ratiometric Fluorescent Probe for Biological Signaling Molecule H2S: Fast Response and High Selectivity*. https://doi.org/10.1002/chem.201300455.
(90) Liu, J.; Sun, Y.-Q.; Wang, P.; Zhang, J.; Guo, W. Construction of NIR and Ratiometric Fluorescent Probe for Hg2+ Based on a Rhodamine-Inspired Dye Platform. *The Analyst* **2013**, *138* (9), 2654. https://doi.org/10.1039/c3an00061c.
(91) Wang, C.; Chi, W.; Qiao, Q.; Tan, D.; Xu, Z.; Liu, X. Twisted Intramolecular Charge Transfer (TICT) and Twists beyond TICT: From Mechanisms to Rational Designs of Bright and Sensitive Fluorophores. *Chem. Soc. Rev.* **2021**, *50* (22), 12656–12678. https://doi.org/10.1039/D1CS00239B.
(92) Wang, Y.; Yang, X.-F.; Zhong, Y.; Gong, X.; Li, Z.; Li, H. Development of a Red Fluorescent Light-up Probe for Highly Selective and Sensitive Detection of Vicinal Dithiol-Containing Proteins in Living Cells. *Chem. Sci.* **2016**, *7* (1), 518–524. https://doi.org/10.1039/C5SC02824H.
(93) *Locked-flavylium fluorescent dyes with tunable emission wavelengths based on intramolecular charge transfer for multi-color ratiometric fluorescence imaging - Chemical Communications (RSC Publishing)*. https://pubs.rsc.org/en/content/articlelanding/2015/cc/c5cc01242b (accessed 2023-05-12).
(94) Jiang, W.; Chen, H.; Pan, Y.; Lin, W. A Long-Wavelength Fluorescent Turn-on Probe for Video Detection of Biological Thiols in Living Cells. *Anal. Methods* **2015**, *7* (10), 4168–4172. https://doi.org/10.1039/C5AY00737B.
(95) Xu, L.; He, X.; Ma, P.; Liu, X.; Zhang, F.; Sun, Y.; Song, D.; Wang, X. A Water-Soluble Fluorescent Probe for the Sensitive Detection of Endogenous Alkaline Phosphatase in Living Cells. *Dyes Pigments* **2018**, *159*, 584–589. https://doi.org/10.1016/j.dyepig.2018.07.023.
(96) Lin, X.; Chen, Y.; Wang, S.; Liu, K.; Kong, F. Construction of a Novel Cell-Trappable Fluorescent Probe for Hydrogen Sulfide (H2S) and Its Bio-Imaging Application. *Anal. Bioanal. Chem.* **2019**, *411* (27), 7127–7136. https://doi.org/10.1007/s00216-019-02090-9.
(97) Li, Z.; Gao, J.; Guo, Z.; Zhao, H.; Liu, L.; Wang, M.; Zhang, P.; Chen, G.; Li, X.; Wei, C. Monitoring the Fluctuation of H2S in Insulin-Resistant HepG2 Cells and Diabetic Mice with a Dual-

Locked NIR Fluorescent Probe. *Sens. Actuators B Chem.* **2022**, *353*, 131141. https://doi.org/10.1016/j.snb.2021.131141.
(98) Liu, X.; Lei, H.; Hu, Y.; Fan, X.; Zhang, Y.; Xie, L.; Huang, J.; Cai, Q. A Turn-on Fluorescent Nanosensor for H2S Detection and Imaging in Inflammatory Cells and Mice. *Spectrochim. Acta. A. Mol. Biomol. Spectrosc.* **2023**, *297*, 122739. https://doi.org/10.1016/j.saa.2023.122739.
(99) Ruiz-Castillo, P.; Buchwald, S. L. Applications of Palladium-Catalyzed C–N Cross-Coupling Reactions. *Chem. Rev.* **2016**, *116* (19), 12564–12649. https://doi.org/10.1021/acs.chemrev.6b00512.
(100) Ma, D.; Cai, Q.; Zhang, H. Mild Method for Ullmann Coupling Reaction of Amines and Aryl Halides. *Org. Lett.* **2003**, *5* (14), 2453–2455. https://doi.org/10.1021/ol0346584.
(101) *Recent Progress in the Use of Vilsmeier-Type Reagents*. https://www.tandfonline.com/doi/epdf/10.1080/00304948.2010.513911?needAccess=true (accessed 2024-06-08).
(102) Liu, X.; Qiao, Q.; Tian, W.; Liu, W.; Chen, J.; Lang, M. J.; Xu, Z. Aziridinyl Fluorophores Demonstrate Bright Fluorescence and Superior Photostability by Effectively Inhibiting Twisted Intramolecular Charge Transfer. *J. Am. Chem. Soc.* **2016**, *138* (22), 6960–6963. https://doi.org/10.1021/jacs.6b03924.
(103) Grimm, J. B.; English, B. P.; Chen, J.; Slaughter, J. P.; Zhang, Z.; Revyakin, A.; Patel, R.; Macklin, J. J.; Normanno, D.; Singer, R. H.; Lionnet, T.; Lavis, L. D. A General Method to Improve Fluorophores for Live-Cell and Single-Molecule Microscopy. *Nat. Methods* **2015**, *12* (3), 244–250. https://doi.org/10.1038/nmeth.3256.
(104) Gomes, A.; Fernandes, E.; Lima, J. L. F. C. Use of Fluorescence Probes for Detection of Reactive Nitrogen Species: A Review. *J. Fluoresc.* **2006**, *16* (1), 119–139. https://doi.org/10.1007/s10895-005-0030-3.
(105) Yin, J.; Zhan, J.; Hu, Q.; Huang, S.; Lin, W. Fluorescent Probes for Ferroptosis Bioimaging: Advances, Challenges, and Prospects. *Chem. Soc. Rev.* **2023**, *52* (6), 2011–2030. https://doi.org/10.1039/D2CS00454B.
(106) Agard, N. J.; Prescher, J. A.; Bertozzi, C. R. A Strain-Promoted [3 + 2] Azide−Alkyne Cycloaddition for Covalent Modification of Biomolecules in Living Systems. *J. Am. Chem. Soc.* **2004**, *126* (46), 15046–15047. https://doi.org/10.1021/ja044996f.
(107) Tornøe, C. W.; Christensen, C.; Meldal, M. Peptidotriazoles on Solid Phase: [1,2,3]-Triazoles by Regiospecific Copper(I)-Catalyzed 1,3-Dipolar Cycloadditions of Terminal Alkynes to Azides. *J. Org. Chem.* **2002**, *67* (9), 3057–3064. https://doi.org/10.1021/jo011148j.
(108) Rostovtsev, V. V.; Green, L. G.; Fokin, V. V.; Sharpless, K. B. A Stepwise Huisgen Cycloaddition Process: Copper(I)-Catalyzed Regioselective "Ligation" of Azides and Terminal Alkynes. *Angew. Chem.* **2002**, *114* (14), 2708–2711. https://doi.org/10.1002/1521-3757(20020715)114:14<2708::AID-ANGE2708>3.0.CO;2-0.
(109) Huisgen, R. 1,3-Dipolar Cycloadditions. Past and Future. *Angew. Chem. Int. Ed. Engl.* **1963**, *2* (10), 565–598. https://doi.org/10.1002/anie.196305651.
(110) Meldal, M.; Tornøe, C. W. Cu-Catalyzed Azide−Alkyne Cycloaddition. *Chem. Rev.* **2008**, *108* (8), 2952–3015. https://doi.org/10.1021/cr0783479.
(111) Dommerholt, J.; Rutjes, F. P. J. T.; Van Delft, F. L. Strain-Promoted 1,3-Dipolar Cycloaddition of Cycloalkynes and Organic Azides. In *Cycloadditions in Bioorthogonal Chemistry*; Vrabel, M., Carell, T., Eds.; Topics in Current Chemistry Collections; Springer International Publishing: Cham, 2016; pp 57–76. https://doi.org/10.1007/978-3-319-29686-9_4.
(112) Meldal, M.; Diness, F. Recent Fascinating Aspects of the CuAAC Click Reaction. *Trends Chem.* **2020**, *2* (6), 569–584. https://doi.org/10.1016/j.trechm.2020.03.007.
(113) Scinto, S. L.; Bilodeau, D. A.; Hincapie, R.; Lee, W.; Nguyen, S. S.; Xu, M.; Am Ende, C. W.; Finn, M. G.; Lang, K.; Lin, Q.; Pezacki, J. P.; Prescher, J. A.; Robillard, M. S.; Fox, J. M. Bioorthogonal Chemistry. *Nat. Rev. Methods Primer* **2021**, *1* (1), 30. https://doi.org/10.1038/s43586-021-00028-z.
(114) Rigolot, V.; Biot, C.; Lion, C. To View Your Biomolecule, Click inside the Cell. *Angew. Chem. Int. Ed. n/a* (n/a). https://doi.org/10.1002/anie.202101502.
(115) Bilodeau, D. A.; Margison, K. D.; Serhan, M.; Pezacki, J. P. Bioorthogonal Reactions Utilizing Nitrones as Versatile Dipoles in Cycloaddition Reactions. *Chem. Rev.* **2021**, *121* (12), 6699–6717. https://doi.org/10.1021/acs.chemrev.0c00832.
(116) Porte, K.; Riberaud, M.; Châtre, R.; Audisio, D.; Papot, S.; Taran, F. Bioorthogonal Reactions in Animals. *ChemBioChem* **2021**, *22* (1), 100–113. https://doi.org/10.1002/cbic.202000525.
(117) Porte, K.; Riomet, M.; Figliola, C.; Audisio, D.; Taran, F. Click and Bio-Orthogonal Reactions with Mesoionic Compounds. *Chem. Rev.* **2021**, *121* (12), 6718–6743. https://doi.org/10.1021/acs.chemrev.0c00806.

(118) Zhou, Z.; Fahrni, C. J. A Fluorogenic Probe for the Copper(I)-Catalyzed Azide−Alkyne Ligation Reaction: Modulation of the Fluorescence Emission via ^{3} (n,Π*) − (π,Π*) Inversion. *J. Am. Chem. Soc.* **2004**, *126* (29), 8862–8863. https://doi.org/10.1021/ja049684r.
(119) Sivakumar, K.; Xie, F.; Cash, B. M.; Long, S.; Barnhill, H. N.; Wang, Q. A Fluorogenic 1,3-Dipolar Cycloaddition Reaction of 3-Azidocoumarins and Acetylenes. *Org. Lett.* **2004**, *6* (24), 4603–4606. https://doi.org/10.1021/ol047955x.
(120) Carlson, J. C. T.; Meimetis, L. G.; Hilderbrand, S. A.; Weissleder, R. BODIPY–Tetrazine Derivatives as Superbright Bioorthogonal Turn-on Probes. *Angew. Chem. Int. Ed.* **2013**, *52* (27), 6917–6920. https://doi.org/10.1002/anie.201301100.
(121) Shieh, P.; Dien, V. T.; Beahm, B. J.; Castellano, J. M.; Wyss-Coray, T.; Bertozzi, C. R. CalFluors: A Universal Motif for Fluorogenic Azide Probes across the Visible Spectrum. *J. Am. Chem. Soc.* **2015**, *137* (22), 7145–7151. https://doi.org/10.1021/jacs.5b02383.
(122) Fu, H.; Li, Y.; Sun, L.; He, P.; Duan, X. Ratiometric Fluorescence Azide–Alkyne Cycloaddition for Live Mammalian Cell Imaging. *Anal. Chem.* **2015**, *87* (22), 11332–11336. https://doi.org/10.1021/acs.analchem.5b02612.
(123) Wen, Y.; Liu, K.; Yang, H.; Li, Y.; Lan, H.; Liu, Y.; Zhang, X.; Yi, T. A Highly Sensitive Ratiometric Fluorescent Probe for the Detection of Cytoplasmic and Nuclear Hydrogen Peroxide. *Anal. Chem.* **2014**, *86* (19), 9970–9976. https://doi.org/10.1021/ac502909c.
(124) Cichocki, B. A.; Khobragade, V.; Donzel, M.; Cotos, L.; Blandin, S.; Schaeffer-Reiss, C.; Cianférani, S.; Strub, J.-M.; Elhabiri, M.; Davioud-Charvet, E. A Class of Valuable (Pro-)Activity-Based Protein Profiling Probes: Application to the Redox-Active Antiplasmodial Agent, Plasmodione. *JACS Au* **2021**, *1* (5), 669–689. https://doi.org/10.1021/jacsau.1c00025.
(125) Deng, H.; Lei, Q.; Wu, Y.; He, Y.; Li, W. Activity-Based Protein Profiling: Recent Advances in Medicinal Chemistry. *Eur. J. Med. Chem.* **2020**, *191*, 112151. https://doi.org/10.1016/j.ejmech.2020.112151.
(126) Cox, P. A.; Leach, A. G.; Campbell, A. D.; Lloyd-Jones, G. C. Protodeboronation of Heteroaromatic, Vinyl, and Cyclopropyl Boronic Acids: pH–Rate Profiles, Autocatalysis, and Disproportionation. *J. Am. Chem. Soc.* **2016**, *138* (29), 9145–9157. https://doi.org/10.1021/jacs.6b03283.
(127) Davies, M. W.; Johnson, C. N.; Harrity, J. P. A. Synthesis of Novel Quinone Boronic Ester Derivatives via a Highly Regioselective Cr-Mediated Benzannulation Reaction and Their Application in Pd-Catalyzed Coupling Processes. *J. Org. Chem.* **2001**, *66* (10), 3525–3532. https://doi.org/10.1021/jo010098f.
(128) Oka, N.; Yamada, T.; Sajiki, H.; Akai, S.; Ikawa, T. Aryl Boronic Esters Are Stable on Silica Gel and Reactive under Suzuki–Miyaura Coupling Conditions. *Org. Lett.* **2022**, *24* (19), 3510–3514. https://doi.org/10.1021/acs.orglett.2c01174.
(129) Villar, L.; Orlov, N. V.; Kondratyev, N. S.; Uria, U.; Vicario, J. L.; Malkov, A. V. Kinetic Resolution of Secondary Allyl Boronates and Their Application in the Synthesis of Homoallylic Amines. *Chem. – Eur. J.* **2018**, *24* (61), 16262–16265. https://doi.org/10.1002/chem.201804395.
(130) Fleury-Brégeot, N.; Oehlrich, D.; Rombouts, F.; Molander, G. A. Suzuki–Miyaura Cross-Coupling of Potassium Dioxolanylethyltrifluoroborate and Aryl/Heteroaryl Chlorides. *Org. Lett.* **2013**, *15* (7), 1536–1539. https://doi.org/10.1021/ol400320q.
(131) Giroux, A. Synthesis of Benzylic Boronates via Palladium-Catalyzed Cross-Coupling Reaction of Bis(Pinacolato)Diboron with Benzylic Halides. *Tetrahedron Lett.* **2003**, *44* (2), 233–235. https://doi.org/10.1016/S0040-4039(02)02566-2.
(132) Uteuliyev, M. M.; Shu, L.; Richards, S. J.; Warkentin, A. A.; Davis, D. Naphthoquinone Derivatives for Treatment of Oxidative Stress Disorders, December 17, 2020. https://patentscope.wipo.int/search/en/detail.jsf?docId=WO2020252414 (accessed 2023-05-15).
(133) Bräse, S.; Gil, C.; Knepper, K.; Zimmermann, V. Organic Azides: An Exploding Diversity of a Unique Class of Compounds. *Angew. Chem. Int. Ed.* **2005**, *44* (33), 5188–5240. https://doi.org/10.1002/anie.200400657.
(134) Hajipour, A. R.; Mohammadsaleh, F. Preparation of Aryl Azides from Aromatic Amines in *N* -Methyl-2-Pyrrolidonium Bisulfate. *Org. Prep. Proced. Int.* **2011**, *43* (5), 451–455. https://doi.org/10.1080/00304948.2011.613695.
(135) De Lourdes G. Ferreira, M.; Pinheiro, L. C. S.; Santos-Filho, O. A.; Peçanha, M. D. S.; Sacramento, C. Q.; Machado, V.; Ferreira, V. F.; Souza, T. M. L.; Boechat, N. Design, Synthesis, and Antiviral Activity of New 1H-1,2,3-Triazole Nucleoside Ribavirin Analogs. *Med. Chem. Res.* **2014**, *23* (3), 1501–1511. https://doi.org/10.1007/s00044-013-0762-6.

(136) Xu, Z.; Zhao, S.-J.; Liu, Y. 1,2,3-Triazole-Containing Hybrids as Potential Anticancer Agents: Current Developments, Action Mechanisms and Structure-Activity Relationships. *Eur. J. Med. Chem.* **2019**, *183*, 111700. https://doi.org/10.1016/j.ejmech.2019.111700.
(137) Gholampour, M.; Ranjbar, S.; Edraki, N.; Mohabbati, M.; Firuzi, O.; Khoshneviszadeh, M. Click Chemistry-Assisted Synthesis of Novel Aminonaphthoquinone-1,2,3-Triazole Hybrids and Investigation of Their Cytotoxicity and Cancer Cell Cycle Alterations. *Bioorganic Chem.* **2019**, *88*, 102967. https://doi.org/10.1016/j.bioorg.2019.102967.
(138) Coulidiati, T. H.; Dantas, B. B.; Faheina-Martins, G. V.; Gonçalves, J. C. R.; do Nascimento, W. S.; de Oliveira, R. N.; Camara, C. A.; Oliveira, E. J.; Lara, A.; Gomes, E. R.; Araújo, D. A. M. Distinct Effects of Novel Naphtoquinone-Based Triazoles in Human Leukaemic Cell Lines. *J. Pharm. Pharmacol.* **2015**, *67* (12), 1682–1695. https://doi.org/10.1111/jphp.12474.
(139) Xu, Z. 1,2,3-Triazole-Containing Hybrids with Potential Antibacterial Activity against Methicillin-Resistant Staphylococcus Aureus (MRSA). *Eur. J. Med. Chem.* **2020**, *206*, 112686. https://doi.org/10.1016/j.ejmech.2020.112686.
(140) Xu, Z.; Zhang, S.; Song, X.; Qiang, M.; Lv, Z. Design, Synthesis and in Vitro Anti-Mycobacterial Evaluation of Gatifloxacin-1H-1,2,3-Triazole-Isatin Hybrids. *Bioorg. Med. Chem. Lett.* **2017**, *27* (16), 3643–3646. https://doi.org/10.1016/j.bmcl.2017.07.023.
(141) Reis, R. C. F. M.; dos Santos, E. G.; Benedetti, M. D.; Reis, A. C. C.; Brandão, G. C.; Silva, G. N. da; Diniz, L. A.; Ferreira, R. S.; Caldas, I. S.; Braga, S. F. P.; Souza, T. B. de. Design and Synthesis of New 1,2,3-Triazoles Derived from Eugenol and Analogues with in Vitro and in Vivo Activity against Trypanosoma Cruzi. *Eur. J. Med. Chem.* **2023**, *258*, 115622. https://doi.org/10.1016/j.ejmech.2023.115622.
(142) Hassan, N. W.; Sabt, A.; El-Attar, M. A. Z.; Ora, M.; Bekhit, A. E.-D. A.; Amagase, K.; Bekhit, A. A.; Belal, A. S. F.; Elzahhar, P. A. Modulating Leishmanial Pteridine Metabolism Machinery via Some New Coumarin-1,2,3-Triazoles: Design, Synthesis and Computational Studies. *Eur. J. Med. Chem.* **2023**, *253*, 115333. https://doi.org/10.1016/j.ejmech.2023.115333.
(143) Singh, A.; Gut, J.; Rosenthal, P. J.; Kumar, V. 4-Aminoquinoline-Ferrocenyl-Chalcone Conjugates: Synthesis and Anti-Plasmodial Evaluation. *Eur. J. Med. Chem.* **2017**, *125*, 269–277. https://doi.org/10.1016/j.ejmech.2016.09.044.
(144) Gogoi, K.; Baishya, G.; Saikia, B.; Barua, N.; Dohutia, C.; Verma, A.; Prakash, A. Antimalarial Activity of a Novel Series of Artemisinin-Derived 1, 2, 3-Triazole Dimers. *Asian Pac. J. Trop. Med.* **2019**, *12* (5), 195. https://doi.org/10.4103/1995-7645.259240.
(145) Pertino, M. W.; F. de la Torre, A.; Schmeda-Hirschmann, G.; Vega, C.; Rolón, M.; Coronel, C.; Rojas de Arias, A.; Leal López, K.; Carranza-Rosales, P.; Viveros Valdez, E. Synthesis, Trypanocidal and Anti-Leishmania Activity of New Triazole-Lapachol and nor-Lapachol Hybrids. *Bioorganic Chem.* **2020**, *103*, 104122. https://doi.org/10.1016/j.bioorg.2020.104122.
(146) Erasmus, C.; Aucamp, J.; Smit, F. J.; Seldon, R.; Jordaan, A.; Warner, D. F.; N'Da, D. D. Synthesis and Comparison of in Vitro Dual Anti-Infective Activities of Novel Naphthoquinone Hybrids and Atovaquone. *Bioorganic Chem.* **2021**, *114*, 105118. https://doi.org/10.1016/j.bioorg.2021.105118.
(147) Menozzi, C. A. C.; França, R. R. F.; Luccas, P. H.; Baptista, M. dos S.; Fernandes, T. V. A.; Hoelz, L. V. B.; Sales Junior, P. A.; Murta, S. M. F.; Romanha, A.; Galvão, B. V. D.; Macedo, M. de O.; Goldstein, A. da C.; Araujo-Lima, C. F.; Felzenszwalb, I.; Nonato, M. C.; Castelo-Branco, F. S.; Boechat, N. Anti-Trypanosoma Cruzi Activity, Mutagenicity, Hepatocytotoxicity and Nitroreductase Enzyme Evaluation of 3-Nitrotriazole, 2-Nitroimidazole and Triazole Derivatives. *Molecules* **2023**, *28* (22), 7461. https://doi.org/10.3390/molecules28227461.
(148) Chem Biol Drug Des - 2018 - Leite - New 1 2 3-triazole-based Analogues of Benznidazole for Use against Trypanosoma Cruzi (1).Pdf.
(149) Redondo, M. C.; Veguillas, M.; Ribagorda, M.; Carreño, M. C. Control of the Regio- and Stereoselectivity in Diels–Alder Reactions with Quinone Boronic Acids. *Angew. Chem. Int. Ed.* **2009**, *48* (2), 370–374. https://doi.org/10.1002/anie.200803428.
(150) Veguillas, M.; Redondo, M. C.; García, I.; Ribagorda, M.; Carmen Carreño, M. Synthesis of Benzo- and Naphthoquinonyl Boronic Acids: Exploring the Diels–Alder Reactivity. *Chem. – Eur. J.* **2010**, *16* (12), 3707–3719. https://doi.org/10.1002/chem.200902796.
(151) Snyder, C.; Chollet, J.; Santo-Tomas, J.; Scheurer, C.; Wittlin, S. In Vitro and in Vivo Interaction of Synthetic Peroxide RBx11160 (OZ277) with Piperaquine in Plasmodium Models. *Exp. Parasitol.* **2007**, *115* (3), 296–300. https://doi.org/10.1016/j.exppara.2006.09.016.
(152) Desjardins, R. E.; Canfield, C. J.; Haynes, J. D.; Chulay, J. D. Quantitative Assessment of Antimalarial Activity in Vitro by a Semiautomated Microdilution Technique. *Antimicrob. Agents Chemother.* **1979**, *16* (6), 710–718. https://doi.org/10.1128/AAC.16.6.710.
(153) Human Malaria Parasites in Continuous Culture. **1976**.

(154) Pathak, R.; Vandayar, K.; van Otterlo, W. A. L.; Michael, J. P.; Fernandes, M. A.; de Koning, C. B. The Synthesis of Angularly Fused Polyaromatic Compounds by Using a Light-Assisted, Base-Mediated Cyclization Reaction. *Org. Biomol. Chem.* **2004**, *2* (23), 3504. https://doi.org/10.1039/b412932f.
(155) Kumpina, I.; Brodyagin, N.; MacKay, J. A.; Kennedy, S. D.; Katkevics, M.; Rozners, E. Synthesis and RNA-Binding Properties of Extended Nucleobases for Triplex-Forming Peptide Nucleic Acids. *J. Org. Chem.* **2019**, *84* (21), 13276–13298. https://doi.org/10.1021/acs.joc.9b01133.
(156) Pirali, T.; Gatti, S.; Di Brisco, R.; Tacchi, S.; Zaninetti, R.; Brunelli, E.; Massarotti, A.; Sorba, G.; Canonico, P. L.; Moro, L.; Genazzani, A. A.; Tron, G. C.; Billington, R. A. Estrogenic Analogues Synthesized by Click Chemistry. *ChemMedChem* **2007**, *2* (4), 437–440. https://doi.org/10.1002/cmdc.200600192.
(157) Demeter, O.; Fodor, E. A.; Kállay, M.; Mező, G.; Németh, K.; Szabó, P. T.; Kele, P. A Double-Clicking Bis-Azide Fluorogenic Dye for Bioorthogonal Self-Labeling Peptide Tags. *Chem. – Eur. J.* **2016**, *22* (18), 6382–6388. https://doi.org/10.1002/chem.201504939.
(158) CN107141840A.Pdf.
(159) Keegstra, E. M. D.; Zwikker, J. W.; Roest, M. R.; Jenneskens, L. W. A Highly Selective Synthesis of Monodisperse Oligo(Ethylene Glycols). *J. Org. Chem.* **1992**, *57* (24), 6678–6680. https://doi.org/10.1021/jo00050a065.
(160) Bonger, K. M.; van den Berg, R. J. B. H. N.; Heitman, L. H.; IJzerman, A. P.; Oosterom, J.; Timmers, C. M.; Overkleeft, H. S.; van der Marel, G. A. Synthesis and Evaluation of Homo-Bivalent GnRHR Ligands. *Bioorg. Med. Chem.* **2007**, *15* (14), 4841–4856. https://doi.org/10.1016/j.bmc.2007.04.065.
(161) Takeuchi, T.; Takahashi, N.; Ishi, K.; Kusayanagi, T.; Kuramochi, K.; Sugawara, F. Antitumor Antibiotic Fostriecin Covalently Binds to Cysteine-269 Residue of Protein Phosphatase 2A Catalytic Subunit in Mammalian Cells. *Bioorg. Med. Chem.* **2009**, *17* (23), 8113–8122. https://doi.org/10.1016/j.bmc.2009.09.050.
(162) Ogura, R.; Satoh, K.; Kiuchi, W.; Kato, K.; Ikeuchi, K.; Suzuki, T.; Tanino, K. Two-Step Method for Constructing a Quaternary Carbon Atom with a Geminal Divinyl Group from a Ketone. *Org. Lett.* **2022**, *24* (28), 5040–5044. https://doi.org/10.1021/acs.orglett.2c01799.
(163) Nyland, R. L.; Luo, M.; Kelley, M. R.; Borch, R. F. Design and Synthesis of Novel Quinone Inhibitors Targeted to the Redox Function of Apurinic/Apyrimidinic Endonuclease 1/Redox Enhancing Factor-1 (Ape1/Ref-1). *J. Med. Chem.* **2010**, *53* (3), 1200–1210. https://doi.org/10.1021/jm9014857.
(164) Yu, D.; Ji, R.; Sun, Z.; Li, W.; Liu, Z.-Q. Electrochemical Chlorination and Bromination of Electron-Deficient CH Bonds in Quinones, Coumarins, Quinoxalines and 1,3-Diketones. *Tetrahedron Lett.* **2021**, *86*, 153514. https://doi.org/10.1016/j.tetlet.2021.153514.

Université de Strasbourg

EDSC École Doctorale des Sciences Chimiques

Baptiste DUPOUY

Optimisation de dérivés 3-benzylmenadiones antiparasitaires rédox-actifs et conception de sondes moléculaires cliquables et/ou photoréactives

Para Frap

cnrs

Résumé

Les maladies parasitaires, notamment le paludisme dû au parasite *P. falciparum*, font face à une résistance croissante aux médicaments actuels. L'objectif de cette thèse a été de poursuivre le développement de composés rédox-actifs antiparasitaires, notamment les 3-benz(o)ylménadiones (bMD), dont la molécule-phare, la plasmodione, a montré une activité puissante *in vitro* mais faible *in vivo*. En effet, ses propriétés physicochimiques ne sont pas adaptées à un traitement oral efficace, et ses cibles biologiques restent à confirmer. L'un des objectifs était donc de concevoir des outils chimiques pour identifier les cibles selon une stratégie de profilage de protéines (AfBPP) couplée à de l'imagerie bioorthogonale parasitaire. En combinant des sondes cliquables bMDs avec une famille de fluorophores bioinspirés, les flavyliums, ces outils moléculaires ont également permis de créer des pro-fluorophores flavylium-bMD rédox-actifs. Parallèlement, pour améliorer la biodisponibilité et optimiser l'activité antiparasitaire des bMDs, des groupements β-pyridine et β-pyrimidine ont été introduits via une stratégie de couplage. En outre, deux nouvelles séries ont été synthétisées : i) des triazole-bMD hybrides en utilisant la chimie clique et, ii) des pro-drogues non-quinoniques de la plasmodione fonctionnalisées par un méthyle angulaire métabolisable par le parasite.

Mots-clés: chimie clique, fluorophore flavylium, *N*-hétéroaromatique, 3-benz(o)ylménadione.

Résumé en Anglais

Parasitic diseases, particularly malaria caused by the *P. falciparum* parasite, are facing increasing resistance to current drugs. The aim of this thesis was to pursue the development of antiparasitic redox-active compounds, in particular 3-benz(o)ylmenadiones (bMD), whose lead compound, plasmodione, has shown potent activity *in vitro* but weak activity *in vivo*. Its physico-chemical properties are not yet appropriate for effective oral treatment, and its biological targets have yet to be elucidated. One of the objectives was therefore to develop chemical tools for target identification using a protein profiling strategy (AfBPP) coupled with parasite bioorthogonal imaging. By combining clickable bMDs probes with a family of bioinspired fluorophores, the flavyliums, these molecular tools led to the development of redox-active flavylium-bMD pro-fluorophores. At the same time, to improve both the bioavailability and the antiparasitic activity of the bMDs, β-pyridine and β-pyrimidine groups were introduced via a coupling strategy. In addition, two new series were synthesized: i) triazole-bMD hybrids using click chemistry and, ii) non-quinone based plasmodione pro-drugs functionalized with an angular methyl that can be metabolized by the parasite.

Keywords: click chemistry, flavylium fluorophore, *N*-heteroaromatics, 3-benz(o)ylmenadione.